Yuri Shunin Stefano Bellucci Alytis Gruodis Tamara Lobanova-Shunina

# Nonregular Nanosystems

Theory and Applications



## **Lecture Notes in Nanoscale Science and Technology**

Series Editors
Zhiming M Wang, Chengdu, China
Andreas Waag, Braunschweig, Germany
Greg Salamo, Fayetteville, USA
Naoki Kishimoto, Tsukuba, Ibaraki, Japan
Stefano Bellucci, Frascati RM, Italy
Young June Park, Seoul, Korea (Republic of)

Yuri Shunin • Stefano Bellucci • Alytis Gruodis Tamara Lobanova-Shunina

### Nonregular Nanosystems

Theory and Applications



Yuri Shunin Institute of Solid State Physics University of Latvia Riga, Latvia

Alytis Gruodis Faculty of Physics Vilnius University Vilnius, Lithuania Stefano Bellucci Frascati National Laboratory National Institute of Nuclear Physics Frascati, Italy

Tamara Lobanova-Shunina Faculty of Mechanical Engineering Riga Technical University Riga, Latvia

ISSN 2195-2159 ISSN 2195-2167 (electronic)
ISBN 978-3-319-69166-4 ISBN 978-3-319-69167-1 (eBook)
https://doi.org/10.1007/978-3-319-69167-1

Library of Congress Control Number: 2017957644

#### © Springer International Publishing AG 2018

This work is subject to copyright. All rights are reserved by the Publisher, whether the whole or part of the material is concerned, specifically the rights of translation, reprinting, reuse of illustrations, recitation, broadcasting, reproduction on microfilms or in any other physical way, and transmission or information storage and retrieval, electronic adaptation, computer software, or by similar or dissimilar methodology now known or hereafter developed.

The use of general descriptive names, registered names, trademarks, service marks, etc. in this publication does not imply, even in the absence of a specific statement, that such names are exempt from the relevant protective laws and regulations and therefore free for general use.

The publisher, the authors and the editors are safe to assume that the advice and information in this book are believed to be true and accurate at the date of publication. Neither the publisher nor the authors or the editors give a warranty, express or implied, with respect to the material contained herein or for any errors or omissions that may have been made. The publisher remains neutral with regard to jurisdictional claims in published maps and institutional affiliations.

Printed on acid-free paper

This Springer imprint is published by Springer Nature
The registered company is Springer International Publishing AG
The registered company address is: Gewerbestrasse 11, 6330 Cham, Switzerland

#### **Preface**

A tremendous shift in the emphasis of interests in physics and chemistry of condensed matter towards nanoscale systems has shaken the scientific community in recent years. Experimental research technologies in physical and chemical laboratories all over the world have considerably expanded, with fundamental studies of new classes of materials and phenomena occupying a prominent place. New features of nanomaterials have become a core challenge for theoretical physics, condensed matter physics, computational methods and modelling.

The 1950s–1960s can be considered as the period of emergence of interest in amorphous solids. Since that time, the molecular structure of liquids, amorphous semiconductors, polymer solutions, magnetic phase transitions, electrical and optical properties of liquid metals, the glassy state of matter, disordered alloys, metal vapours and many other systems have provoked scientific and technological inquisitiveness. Brilliant advances in the field of crystalline solids, both in theory and technology, have inspired the desire to obtain the same results in electronics by means of even more efficient technological processes. One example is the effort to replace the relatively long crystal growth process with thin-film deposition or the rapid cooling of melts.

At the same time, the problem of morphological repeatability of the created materials is highly important. Significant interest in disordered materials was justified by the practically proven determinant role of the so-called short-range order with a characteristic size of  $10^{-8}$ – $10^{-9}$  m. Indeed, the electronic structures of amorphous and crystalline solids are very similar. Thus, amorphous silicon, as a basic structure, has become the foundation for the development of optoelectronics and solar cells.

New technological breakthroughs can be associated with research on carbon nanotubes. Scientific and practical interest in these nanostructures was initiated by Sumio Iijima in 1991 (**1991** *Nature* **354**(6348)). However, the key fundamental works of L.V. Radushkevich and V.M. Lukyanovich (**1952** *J Phys Chem* **16**(1) 89, USSR) with clear images of 50 nm diameter tubes should also be mentioned. Furthermore, the works of A. Oberlin, M. Endo and T. Koyama (**1976** *Journal of* 

vi Preface

Crystal Growth 32(3) 335) followed in which hollow tubes of rolled up graphite sheets synthesized by a chemical vapour-growth technique were observed.

Significant progress was associated with the discovery of graphene by Kostya Novoselov and Andre Geim (2004 Novoselov K S, Geim A K et al. *Science* 306 (5696) 666–9, *Nobel Prize in Physics* 2010). And again, the first theoretical and technological achievements were connected with 'ideal', i.e. regular, structures with typical dimensions ~1 nm.

Other regular carbon-based structures were also researched, for example, fullerenes (*buckyballs*) which were first generated in 1985 by Harold Kroto, James R Heath, Sean O'Brien, Robert Curl and Richard Smalley (**1985** Kroto H W et al. *Nature* **318** (6042) 162–3) at Rice University.

Similar regular nanosystems were created on a non-carbon basis, e.g. BCN nanotubes (1994), boron nitride nanotubes, a polymorph of boron nitride (1994–1995), DNA nanotubes (2004–2005), gallium nitride nanotubes (2003), silicon nanotubes (2000), inorganic nanotubes/tungsten(IV) sulphide nanotubes (1992), membrane nanotubes (2008), titania nanotubes (2008), etc.

Two-dimensional materials also received intensive development. Starting with graphene (2004), further research turned up graphyne, borophene, germanene, silicene, stanene, phosphorene, molybdenite, single-atom metal layers of palladium and rhodium, etc.

However, it soon became clear that to realize the unique physical and chemical properties of new materials, their functionalization was necessary. It implied, for example, the creation and use of various interfaces, with new nanophenomena corresponding to new non-regular nanostructures. Moreover, nanoeffects with the participation of biological nano-objects open the way for the realization of catalytic reactions and, accordingly, the creation of new nanoscale devices. In this case, we encounter nanophenomena in irregular nanosystems, which is the subject of many sections of this book.

At present, applied and commercial interest encompasses carbon nanotubes, graphene, dendrimers. fullerenes. nanofibers, nanocellulose. nanodiamonds, nanowires and quantum dots (silicon oxide nanoparticles). Interest also focuses on a wide range of nanoparticles, namely, aluminium oxide, antimony tin oxide, bismuth oxide, cerium oxide, cobalt oxide, copper oxide, gold, iron oxide, magnesium oxide, manganese oxide, nanosilver, nickel, titanium dioxide, zirconium oxide and zinc oxide, as well as other nanomaterials including nanoprecipitated calcium carbonate, graphene and carbon quantum dots, hydroxyapatite nanoparticles, palladium/phosphorene, C<sub>2</sub>N, carbon nitride, germanene, graphdiyne, graphane, hexagonal boron nitride, molybdenum disulphide (MoS<sub>2</sub>), rhenium disulphide (ReS<sub>2</sub>), diselenide (ReSe<sub>2</sub>), silicene, stanene/tinene and tungsten diselenide.

Within the format of the present book, the authors consider it necessary to discuss the social and technological challenges of nanotechnology. Although advances in the fields of nanoscience and nanotechnology have resulted in thousands of consumer products that have already migrated from laboratory benches onto store shelves and e-commerce websites, the general public often lacks

Preface vii

awareness and understanding of the basic properties, and sometimes even the existence, of nanotechnologies and their implications for the consumption of nanoproducts. Areas of research at the intersection of nanotechnology and biotechnology, including food, healthcare and environmental issues, elicit complex debates within society today. Moreover, current developments in scientific and technological research raise a number of ethical questions and the potential for fragmenting of responsibility. Therefore, one of the chapters of the book (Chap. 11) is devoted to nanomaterial consumers, managers, education practitioners, students—researchers, manufacturers, work health and safety practitioners and other interested people who need to understand the benefits and hazards of engineered nanomaterials.

It is clear that to discuss all of the problems and results of scientific research in physics and chemistry of irregular systems within one book is practically impossible. However, the concept of non-regularity can be fundamental for a deeper understanding of the key properties of nanoscale systems. Structural imperfections of nanomaterials, and the non-stationary nature of many nanoprocesses, determine the functionality of potential nanoscale devices.

There is hope that many specific materials and observed phenomena will allow us to grasp the general theoretical and mathematical principles of a unified theory.

Some reliable and attractive theoretical results, for example, related to models of perfect nanostructures such as carbon nanotubes, graphene, fullerenes, etc., do not solve the problems of the general theory of non-regular nanosystems associated with their diverse interfaces and the specific tasks of their functionalization.

Apparently, the theory of non-regular nanosystems should be considered as part of the general theory of disordered systems, which itself has not yet developed as a unified theory and contains a multitude of phenomenological constructions.

This book focuses on specific verified results obtained by instruments of theoretical physics, computer simulations and the analysis of experiments. However, some results should be considered tentative. The ways of creating new unique nanodevices are very complex and consist of numerous stages. A new nanophenomenon does not always give way to a new nanodevice.

Our goal also extends to showing the connection of phenomena in non-regular nanosystems with the basic characteristics of various theoretical model systems. In this context, we discuss the limitations of theoretical models as well. In some cases, excessive idealizations that simplify the mathematical description can lead to inexplicable artefacts and imaginary false coincidences with experiments. References to the specific results of numerous studies do not claim to be complete, because the data of experiments are too numerous, sometimes contradictory, and since the conditions of the experimental protocols are not always comparable and require special attention and analysis.

The present book is not a textbook. However, the reader will find consistently outlined subjects of the educational value, which have been methodologically verified by the experience of presenting university lectures at different levels and making reports at international conferences.

It may be impossible in the theory of non-regular disordered systems to find such a powerful principle as the Bloch theorem in regular condensed materials.

viii Preface

Descriptions of the type of scaling theory, percolation theory or similarity theory are not free from essential empirical parameters and can hardly fulfil the role of a universal theoretical tool in the case of non-regular systems. One can only rely on the search for adequate topological transformations of regular morphological systems into non-regular ones. Obviously, this is not a trivial task.

The materials for the book are selected based on many years of scientific work of the authors and their numerous topical researches. For a comfortable comprehension of the content, the insights into the standard university course in theoretical physics will be enough for the reader. Some sections of the book are conceptual in nature and address specialists covering a wide profile in the fields of nanotechnology and nanoelectronics. However, many theoretical and experimental research results lie in the plane of mixed scientific trends. Unfortunately, the bibliography of any book can never reflect all of the relevant literature to date. The bibliography is huge and the rate of its growth is ruthless in relation to the author of any book on such a dynamic topic. We apologize in advance to any colleague whose publication we did not cite.

The conceptual approaches to the content of this book have evolved over the past few years. This is a generalization of a long-term research experience of the authors and their continual scientific cooperation with colleagues coming from the *Institute of Solid State Physics, University of Latvia* (Riga, Latvia), *Avionics Institute of Riga Technical University* (Riga, Latvia), *Faculty of Physics, Vilnius University* (Vilnius, Lithuania) and *Laboratori Nacionali di Frascati INFN* (Frascati-Rome, Italy). Obviously, participation in numerous international conferences, workshops and seminars enriched knowledge and experience; allowed putting the necessary accents in the direction of nanotechnology development; and simply gave pleasure in sharing ideas with colleagues. At the same time, this book is undoubtedly the authors' views on the problems under consideration.

The authors are also indebted to the technical editor of the book, *Natalia Burlutskaya*, and express their warm gratitude for her assistance in many practical problems that had to be resolved in a timely manner and which made it possible to bring this publication to print.

On behalf of the authors Yuri Shunin

#### **Contents**

1	Intro	duction to Non-regular Nanosystems	1
2	Gene	eral Approach to the Description of Fundamental	
	Prop	erties of Disordered Nanosized Media	7
	2.1	Introduction	7
	2.2	Correlation of Atomic and Electronic Structures	10
	2.3	Order and Disorder	13
	2.4	Concepts of Modelling Atomic Nanostructures	18
	2.5	Concepts of Nanoporous and Nanocomposite Materials	22
		2.5.1 Nanoporous Materials	23
		2.5.2 Aerogels	25
		2.5.3 Nanocomposites	26
	2.6	Scaling in Functional Nanomedia	26
	2.7	Concluding Remarks	28
	Refer	rences	28
3	Poter	ntials and Electronic Structure Calculations	
	of No	on-regular Nanosystems	33
	3.1	Introduction	33
	3.2	Atomic Potential Functions	33
		3.2.1 Construction of Atomic Potential Functions	34
	3.3	'Crystalline' Potentials	39
	3.4	Potentials of Charged Defects	41
	3.5	Electronic Structure and Total Energy: Atoms,	
		Molecules and Nanoclusters	44
	3.6	Interatomic Interaction Potentials and Force Calculations	49
	3.7	Multiple Scattering Theory and Effective Media	
		Approach	50
		3.7.1 Methods of Electronic Structure Calculation	
		of Non-regular Condensed Materials	51

x Contents

		3.7.2	Non-regular Condensed Medium: 'Liquid Metal' Model	54		
		3.7.3	Model	34		
		3.1.3	Approach	59		
		3.7.4	Scattering on the General Type Potential	60		
	3.8	Monoatomic Nanosystems: Nano-Si, Nano-Se				
	2.0	3.8.1	Production of Nanosilicon	62		
		3.8.2	Nanosilicon: Calculations of Electronic Structure	64		
		3.8.3	Selenium Versus Nano-selenium	66		
		3.8.4	Nano-selenium: Calculations of Electronic			
			Structure	68		
	3.9	Nanoc	ompounds: Nanochalcogenides	69		
		3.9.1	Binary and Ternary Chalcogenide Glassy			
			Systems	71		
	Refer	ences		74		
4	Scatt	ering Pr	ocesses in Nanocarbon-Based Nanointerconnects	77		
•	4.1	Non-regularities in Nanointerconnects				
	1.1	4.1.1	Scattering Processes in Nanocarbon-Based	, 0		
		1.1.1	Nanointerconnects	80		
	4.2	Electro	onic Structure Calculations of Nanocarbon-Based			
	Interfaces					
	4.3		omagnetics of CNT and Graphene-Based Systems	81 86		
		4.3.1	'Liquid Metal' Model for CNT–Metal Junction:			
			CNT–Ni case	86		
		4.3.2	Model of 'Effective Bonds' for Simulations			
			of CNT–Me and GNR–Me Junctions	88		
		4.3.3	SWCNT and SL and ML GNR Simulations	89		
		4.3.4	Parametric Calculations of CNT–Me			
			Interconnect Resistances	96		
		4.3.5	Resistance MWCNT–Me Junctions	96		
		4.3.6	Current Loss Between the Adjacent Shells			
			Inside the MWCNT	100		
		4.3.7	Resistances and Capacitances of SL GNR-Me,			
			ML GNR–Me Interconnects	106		
		4.3.8	Frequency Properties of CNT–Me and GNR–Me			
			Interconnects	107		
	<b>D</b> 0	4.3.9	Concluding Remarks	110		
	Refer	ences		112		
5	Surfa	ce Nano	physics: Macro-, Meso-, Micro-			
		lano-app	proaches	115		
	5.1		e: Thermodynamics, Anisotropy	115		
	5.2		al and Chemical Adsorption, Adsorption Kinetics	120		
	5.3	Gibbs	Adsorption Isotherms	126		

Contents xi

	5.4		gen Adsorption	132
	5.5	Electro	onic Structure of Surface	133
	5.6	Surface	e Plasmon Resonance	140
	5.7	Interac	tion of Light and Nanoparticle	141
	5.8	Nanosl	hells	144
	5.9	Organi	c-Nonorganic Interfaces	145
	Refer	ences		145
6	Class	ification	and Operating Principles of Nanodevices	147
	6.1		fication	147
		6.1.1	Correlations of the Fundamental Properties	
			of Non-regular Materials	147
		6.1.2	Nanosensoring Paradigm	150
	6.2	Physic	al Nanosensors	152
	6.3	Chemi	cal Nanosensors	163
	6.4	Bio-na	nosensors	165
	6.5	Memor	ry Nanodevices	167
	6.6	Biomo	lecular Rotary Machines	177
	6.7	Nanotr	ransducers	178
		6.7.1	Optical Nanotransducers	180
		6.7.2	Mechanical Nanotransducers	182
		6.7.3	Electrochemical Nanotransducers	182
		6.7.4	Magnetic Nanotransducers	185
	6.8		erogels and Nanofoams	187
		6.8.1	Introduction to Aerogels	187
		6.8.2	Aerogels Forms and Characterization	189
		6.8.3	Aerogels Commercialization	191
		6.8.4	Functionalization	192
	6.9		mposites	193
		6.9.1	Biocomposite Concepts and Definitions	193
		6.9.2	Bio-nanocomposites from Renewable Resources	193
		6.9.3	Bio-nanocomposite Applications	197
	Refer	ences		199
7			phene Growth: Growing, Quality Control,	
			ansion and Chiral Dispersion	207
	7.1		ima Method for Growing CNTs and Graphene	207
		7.1.1	Arc Discharge	207
			Purification	209
	7.2		scharge and Induced Non-regularities	210
	7.3		Ablation and Self-Organization of Matter	212
		7.3.1	Laser Ablation	212
		7.3.2	Chemical Vapour Deposition	214
	7.4		ations of Growth: Sporadic and Stimulated	215
		7.4.1	CNT Growth Mechanism	215
		7.4.2	The Tip-Growth Mechanism	216

xii Contents

		7.4.3	The Base-Growth Mechanism	216
		7.4.4	Several Control Strategies	218
		7.4.5	Quality Control	219
	7.5	Graphe	ne Growth and Technological Defects	221
		7.5.1	Defects in Graphene	222
	7.6	Simula	tion of Magnetically Stimulated CVD CNT Growth	224
		7.6.1	Research Motivation	225
		7.6.2	CNT Growth in the Chemical Vapour Deposition	
			Process Based on Metal Nanoparticles	228
		7.6.3	CVD Process Analysis	229
		7.6.4	Advantages of CVD	231
		7.6.5	CNT Precursors	233
		7.6.6	CNT Growth Control	233
		7.6.7	Magnetically Stimulated CNT CVD Growth	
			on Fe–Pt Catalysts	235
		7.6.8	Effective Bonds Model for CNT-Fe-Pt	
			Interconnect Electromagnetic Properties	235
		7.6.9	$CNT$ - $Fe_xPt_{1-x}$ Interconnect Formation	237
		7.6.10	Magnetic Properties of Fe–Pt Alloys	240
		7.6.11	Magnetically Stimulated CNT Growth	241
		7.6.12	Model of CVD CNT Growth with the	
			Probabilistically Predefined Morphology	243
	Refere	nces		245
8	Grank	one Ful	llerenes, Carbon Nanotubes: Electronic	
U			Carbon Nanotubes. Electronic	253
	8.1		: Allotropic Forms	253
	8.2		Derivatives: Formation of Electronic System	263
	8.3		ne Electronic Structure	265
	8.4		es for Nanotubes (n,0), Nanotubes (n,n)	268
	8.5		bes: Electronic Angular Momentum	200
	0.5		in-Dependent Properties	272
	8.6		bes of the Metal Type and of the Semiconductor	212
	0.0			274
	8.7		stry of Nanotubes: Catalysis and Toxicity	276
	8.8		duence of Defects on Electrical, Mechanical	270
	0.0		ermal Properties of Graphene	279
	8.9		ed Nanocarbon Systems	280
				282
				202
9	Spintr		d Nanomemory Systems	287
	9.1	o . m	ronament Fundamentals	287
			ransport Fundamentals	
	9.1	Magnet	toresistance Nanodevices	290

Contents xiii

	9.3	Magnetic Disorder and Spin Transport	293
		9.3.1 Magnetic Disorder in Fe–Pt Nanodrops	294
	9.4	Concluding Remarks	305
	Refere	ences	305
10	Nanos	ensor Systems Simulations	309
	10.1	Physical and Chemical Nanosensors	310
		10.1.1 Conductivity as a Tool of Nanosensor Systems	310
	10.2	Bio-nanosensors: Polymer Nanoporous Model Structures	315
		10.2.1 Biosensor Model Testing and Experimental Results	316
	10.3	Nanocomposite-Based Nanosensoring Devices	320
		10.3.1 Real-Time Polymer Nanocomposite-Based	
		Physical Nanosensors	320
		10.3.2 Models of CNT- and GNR-Based Nanocomposites	324
		10.3.3 Simulation of Stress- and Temperature-Induced	
		Resistance of Carbon-Based Nanocomposite	
		Sensors: Results and Discussions	327
	10.4	Concluding Remarks	331
	Refere	ences	333
11	Nanot	echnology Application Challenges: Nanomanagement,	
		isks and Consumer Behaviour	337
	11.1	Consumer Insights into Nanotechnology: <i>Introduction to</i>	
		Rational Consumerism and Consumer Behaviour	337
	11.2	Nanoscience and Nanotechnology: What Is Special About	
		'Nano' and Why Should Consumers Be Informed?	339
	11.3	Basic Categories of Nanotechnology-Based Consumer	
		Products on the Market and Consumer Awareness	343
	11.4	Towards an Open Dialogue with Consumers on the Benefits	
		and Risks of Nanotechnology-Engaged Products	357
	11.5	New Technologies and Responsible Scientific Consumption	
		in Constructing Consumer Identity	363
	11.6	Knowledge Management as a Means of Social Change:	
		Who Needs Nanotechnology Education?	366
	11.7	Convergence of Science, Technology and Society:	
		Nano-Bio-Info-Cogno-Socio-Humanosciences	
		and Technologies – A Way to NBICSH Society	371
	11.8	Global Citizenship Competence: The Vision	
		for Educational Change	376
	11.9	Nanochallenges: Nanomanagement, Nanoeducation,	
		Nanothinking and Public Participatory Technology	
		Assessment (pTA)	378
		11.9.1 Nanomanagement: Risks Versus Benefits	380
		11.9.2 Nanoeducation and the Global Consciousness	383

xiv Contents

	11.9.3	Nanothinking as an Educational Concept	
		of the Twenty-First Century	385
	11.9.4	Public Participatory Technology Assessment	
		(pTA) in Risk Management	387
11.10	Conclu	ding Remarks	389
Refere	nces		392
ndex			397

## **Chapter 1 Introduction to Non-regular Nanosystems**

Physics of non-regular nanosystems is a branch of physics dealing with nanoagents – nanoparticles when their non-regular nanosized morphological characteristics predefine the nature and essence of physical phenomenon (nanophenomenon). In particular, multiple technological interfaces of nanoparticles with morphogically regular systems denote a creation of micro- or mesostructures with essential nanodimensional effects (e.g. in various schemes of functionalization of nanocarbon systems, viz. CNTs, GNRs GNFs, carbon-based nanoaerogels and nanofoams, etc.). Such nanosystems should also be considered as non-regular.

Non-regularities characterize surface nanointeractions (surface area, interaction quality, distribution of nanoagents of influence) and various nanointerconnects when essentially expected and unexpected effects of nanophenomena, nanosensoring and nanomaterials' functionality take place. As a result, these effects will define prospective qualities of future consumer nanoproducts and nanodevices.

A special class of non-regular nanophenomena concerns the interaction of large carbon-based macromolecule assemblies of different chemical qualities, the interaction boundaries of which are sporadically changed. A utilitarian interest to nanocarbon systems is explained by their suitability to become pertinent materials that are beneficial for the integration with biomaterials or biological systems since carbon is the chemical basis of all known living systems on Earth.

What we consider under *regularity* and *non-regularity* in the context of the presented book:

Regular nanosystems – are systems with morphologically ordered structures characterized by any type of spatial symmetry and at least one nanosized dimension (parameter).

Non-regular nanosystems – are systems comprising nanoscale morphological traits (characteristics) when there is no spatial symmetry of characteristics for the nano-, micro- and mesolevels in a steady state, or their spatial symmetry is broken by transients (nonsteady processes), or the systems are intensely functionalized at the nano- and micro-levels. Non-regular systems should also

1

comprise technologically defective nanostructures (bending, vacancies, doping and various types of disordering), both organic and inorganic.

Nanophysics is a part of physics that combines experimental and theoretical methods of material and radiation studies at the nanoscale level. It also describes major physical approaches to the study of nanoobjects and their behaviours, which are important for the consideration of nanophenomena. Nanoobjects and nanosystems being a combination of nano-, micro-, meso- and macrostructures demand a thorough description using classical and quantum approaches. The key points of full-scale analysis include:

- Nanoobject morphology (atomic structures, symmetry, chirality, etc.)
- Electronic, magnetic and optical parameters
- · Electric conductivity
- Heat behaviour and heat transfer parameters
- Force interactions of various qualities
- · Chemical and biochemical activities

The second chapter – General approach to the description of fundamental properties of disordered nanosized media – is devoted to basic conceptions of disordered atomic structures. Correlations of atomic, electronic and phononic properties are discussed taking into account the scaling effects in nanosized media. The chapter also addresses concepts of atomic structures for modelling nanoporous and nanocomposite materials.

The third chapter – *Potentials and electronic structure calculations of non-regular nanosystems* – focuses on general approaches to the calculations of electronic structure in nanosized systems using multiple scattering theory and effective media approximation. This approach allows providing a full-scale modelling of nanosized structures in various cases of host media (from vacuum to crystalline cases).

The fourth chapter – Scattering processes in nanocarbon based nanointerconnects – considers surfaces and interfaces where nanophenomena are very variable and usually take place in conditions of disordered media. Nanoagents (nanoparticles) change the local electronic structure and magnetic states of the host matter. It means that simulations and ab initio calculations cannot use the atomic structure symmetry. In general, the most favourable way to model disordered systems is the self-consistent effective medium approach, including various approximations and simplifications, for example, the (CPA) Coherent Potential Approximation. The multiple scattering theory as the main tool of our numerical research in composition with the EMA provides methods for modelling electronic and magnetic properties including electronic and spin transport in the nanosurface area. It is also important for simulation of novel carbon-based nanomemory devices.

The fifth chapter – *Surface nanophysics: macro-, meso-, micro- and nanoapproaches* – deals with the description of the surface phenomena. According to the classical description, a surface can be treated as a two-dimensional manifold;

thus, several thermodynamic assumptions should be used in order to model the surface interactions. Anisotropy in crystallography, determination of optical pathway, belongs to the well-known classical assumptions (problems of a surface potential). The surface tension anisotropy and the formation of order-disorder phenomenon on a surface – these two tasks contain the physical part of material organization. Otherwise, several additional assumptions are useful in nanoscience: pseudo-three-dimensional surface in order to involve a microstructure determined by micro-crystallites on a surface. This approach is used for the description of the processes of physical and chemical adsorption on a surface by means of macro- and micro-levels. In particular, the task of hydrogen adsorption on a surface is important in the field of fuel cells. Adsorption and desorption of reactants onto the surface must be analysed in the field of surface reactions. Characteristics of adsorption processes (adsorption enthalpy, crystallographic specifications, nature of adsorption, saturation, concurrent kinetics, etc.) are related and predetermined by the electronic structure of the surface. The formation of nanoshells is analysed using two approaches: structural (as a surface phenomenon) and electronic (as minimized electronic interactions). In several research models, the physical fundamentals are described: atomic ionization experiments, Auger emission spectroscopy, taking into account the model structure (isolated atoms, atom clusters, molecular clusters, supermolecules and crystals). As a novel research method, surface plasmon resonance together with classical non-invasive methods is important in material sciences. Due to high sensitiveness of research objects, interaction of light and nanoparticles must be used of non-invasive type such as Raman scattering, surface plasmon resonance and Auger emission spectroscopy.

The sixth chapter – Classification and operating principles of nanodevices – presents a review of fruitful applications of surface nanophysics phenomena and nanodevices. Problems of precise metrology, environment monitoring and security, medical applications, and so on demand a creation of wide classes and families of nanosensors. Challenges in the development of artificial intelligence systems are directed to the integration and functionalization of nanosystems where nanosensors and nanotransducers play the decisive role. Carbon-based integrated nanosystems are vitally important for prosthetics and various implants creation to contribute to the quality of the human life enhancement. The results of functionalized nanodevice modelling are presented as an essential part of the considered topic.

The seventh chapter – CNTs and graphene growth: growing, quality control, thermal expansion, and chiral dispersion – is devoted to the structure control problems. The well-known Iljima method for growing carbon nanotubes is analysed from the chemical position. Using the arc discharge technique, several operating methods allow us to control the quality and quantity of growth in the disordered environment. Laser ablation methods for the surface forming, control and adsorbate filling are offered. In general, all methods of nanocarbon systems growth are sporadic and lead to a large dispersion of key parameters. It means that additional efforts should be applied to divide, distribute and group the growth output for experimental applications and commercial use. That is why we have to look for more predictable and controlled growth processes. The factors of stimulated

(electrically, magnetically) and controlled growth in CVD type processes are also considered. The analysis of experimental results and computer simulations allow determining the limitations in the creation of predefined nanocarbon systems' morphologies (chirality, spatial composition).

The eighth chapter – *Graphene, fullerenes and carbon nanotubes: electronic subsystem* – is devoted to the description of carbon compounds, starting from catalysis and finishing with electronic/conducting models. Many allotropic forms (diamond, graphite, black carbon, graphene, buckminsterfullerene, nanotubes, etc.) are analysed from the electronic point of view. The formation of an electronic system is dependent on the spatial arrangement of carbon atoms in a molecular derivative or a molecule. Zone formation for indexed nanotubes is explained in terms of reaction coordinate, which is important for the following explanation of conducting properties for both types of nanotubes: metallic-like and semiconductor-like. The main part of electronic properties of nanotubes could be explained using the electronic angular momentum model. Spin-dependent properties in conducting are illustrated by experiments as well as theoretical considerations. Defected nanocarbon system has also found their part of attention in the chapter.

The ninth chapter – *Spintronics and nanomemory systems* – describes spintronic models of nanomemory devices, considers spin transport mehanisms and spins correlations in disordered nanomagnetics. Magnetoresistance phenomena with disordered nanocarbon inclusions for nanomemory devices are also considered by the authors.

The tenth chapter -Nanosensor systems simulations - addresses basic principles of nanosensoring. Models and simulations of physical, chemical, bio-nanosensors, nanocomposite and nanoporous (nanotrack) based nanosensoring devices are illustrated and discussed in the chapter.

eleventh chapter Nanotechnology application nanomanagement, nanorisks, and consumer behaviour: Nanoeducation and nanothinking - provides a deeper insight into scientific consumerism related to nanotechnology, nanotechnology-enhanced goods and nanocarbon systems application. Consciously or unconsciously, the term 'nanotechnologies' is firmly entering the life of every consumer-citizen of the global community designating both relatively simple nanomaterials and goods that have already entered the market and very complex technologies that are supposed to change radically the future of mankind. The unique properties of nanotechnology applications suggest potential to solve some of the most pressing social and business challenges, but they come with uncertainties and risks as all new technologies. Taking advantage of technological progress and preventing adverse side effects require analysis, evaluation and guidance to ensure technology development in ways that benefit wider consumer society and every individual consumer on the planet. Unfortunately, general public lacks understanding and awareness of the basic properties, and sometimes even the existence of nanotechnologies and their implications linked to the consumption of nanoproducts. Moreover, a generally sceptical attitude among society groups prevails towards new technologies.

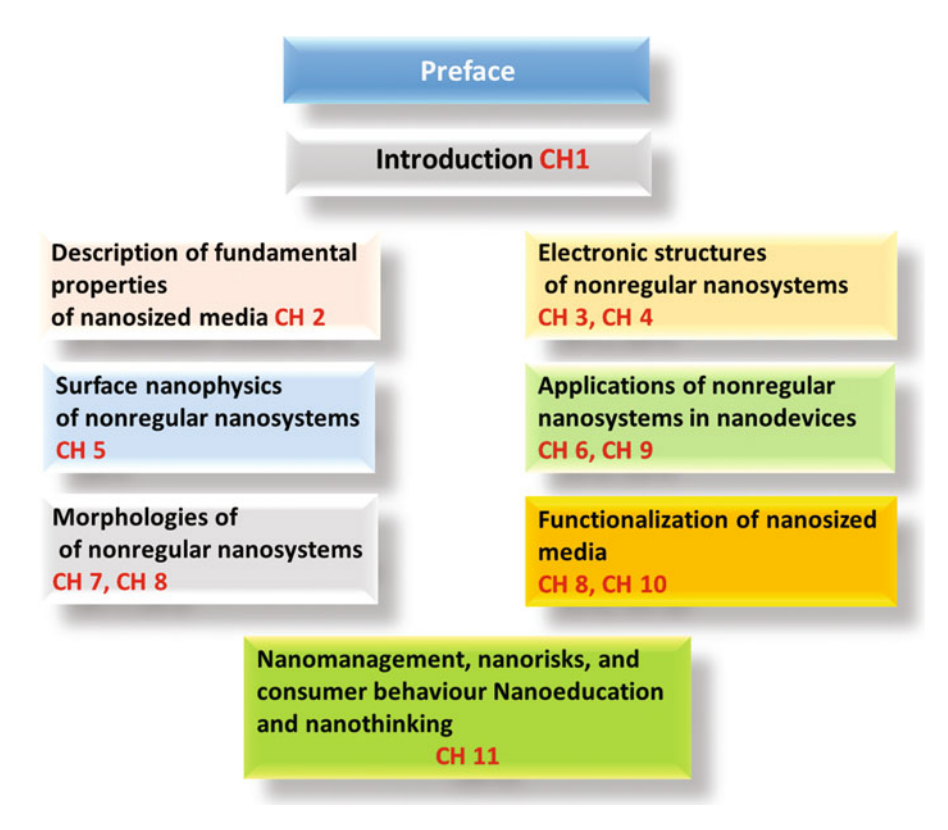


Fig. 1.1 The book structure by chapters

The general lack of public knowledge about nanoproducts that are already on the market in a full swing is likely to bring irrational and erroneous, potentially harmful, results. Therefore, modern technology requires educated workforce and responsible consumers and hence imperative for educated population. Our mission has a focus on introducing changes into the higher education curriculum to eliminate gaps in scientific knowledge of potential nanoscientists and nanoconsumers and to foster an active approach to developing responsible scientific consumption practices to explore these questions and to reflect on the place of new technologies in the spheres of every individual and in the global society.

This chapter is intended for nanomaterial consumers, managers, education practitioners, students-researchers, manufacturers, work health and safety practitioners and other interested people who do not have a background in technical sciences but who need to understand the benefits and hazards of engineered nanomaterials and require guidance on managing risks associated with these.

Figure 1.1 shows the emphases of the book by chapters. We hope that this will facilitate the readers to find the material of special interest to them.

## Chapter 2 General Approach to the Description of Fundamental Properties of Disordered Nanosized Media

#### 2.1 Introduction

Non-regularities characterize surface nanointeractions (surface area, interaction quality, distribution of nanoagents of influence) and various nanointerconnects when essentially expected and unexpected effects of nanophenomena, nanosensoring and nanomaterials' functionality take place. As a result, these effects will define prospective qualities of future consumer nanoproducts and nanodevices.

A special class of non-regular nanophenomena concerns the interaction of large carbon-based macromolecule assemblies of different chemical qualities, where the interaction boundaries of which are sporadically changed. A utilitarian interest to nanocarbon systems is explained by their suitability to become pertinent materials that are beneficial for the integration with biomaterials or biological systems since carbon is the chemical basis of all known living *systems* on Earth.

Regular nanosystems – are systems with morphologically ordered structures characterized by any type of spatial symmetry and at least one nanosized dimension (parameter).

Non-regular nanosystems – are systems comprising nanoscale morphological traits (characteristics) when there is no spatial symmetry of characteristics for the nano-, micro- and meso-levels in a steady state, or their spatial symmetry is broken by transients (nonsteady processes), or the systems are intensely functionalized at the nano- and micro-levels. Non-regular systems should also comprise technologically defective nanostructures (bending, vacancies, doping and various types of disordering), both organic and inorganic.

Nanophysics is a part of physics that combines experimental and theoretical methods of material and radiation studies at the nanoscale level. It also describes major physical approaches to the study of nanophenomena behaviours, which are important for the consideration of nanophenomena. Nanophects and

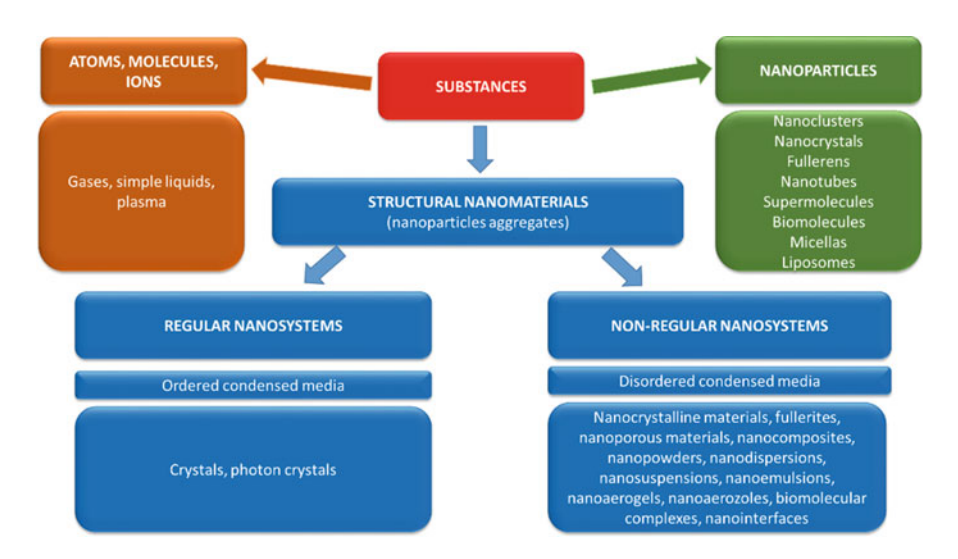


Fig. 2.1 Structural classification of nanomaterials

nanosystems being a combination of nano-, micro-, meso- and macrostructures demand a thorough description using classical and quantum approaches.

It is reasonable to start the classification of nanoobjects from the concept of 'matter' which is presented systematically in the periodic table. Properties of matter determine functional peculiarities of created materials for practical tasks. (see Fig. 2.1). Materials serve to carry out production activities or other activities, for example, related to the solution of health problems or environmental problems.

It is generally believed that objects of the nanoworld are objects whose characteristic dimensions lie in the range of 1–100 nm, i.e. characterized by nm scale (1–100 nm) at least in one dimension. The main feature of nanoobjects is that, due to their small size, they exhibit special properties.

In many cases, these special properties can also be manifested when the size of nanoobjects exceeds the conventionally established limit of 100 nm by 10 times, which forms functional mesostructures. Nanomaterials, as well as ordinary materials, can be in various aggregate states. Thus, 'nano' means usually the scale of nanophenomena, but not simply the characteristic sizes of functionalized nanodevices.

In practice, the most common are solid-state nanomaterials. Well-known features of nanomaterials are structural synergetics, new structural symmetries, new types of phase interfaces, high surface catalytic activity and dimensional effects in nanoparticle aggregates.

Our comments in Fig. 2.1 start with the definition of *nanoparticles* [1] as atomic and molecular aggregates – nanoclusters – particles between 1 and 100 nm in size. Morphologically ordered *nanoclusters* create *nanocrystals*. *Fullerenes* are carbon molecules formations in the form of a hollow sphere, ellipsoid, tube and many other

2.1 Introduction 9

shapes. Spherical fullerenes are also referred to as buckminsterfullerenes (buckyballs) [2].

*Nanotubes* are nanometer-scale tube-like structures. Nanotubes are kinds of nanoparticles and can serve as pipes through which other nanoparticles can be channelled [3]. *Supermolecules* are host molecules with functional molecules – inclusions, e.g. hydrogen-bonded acetic acid dimers [4].

Biomolecules are molecules that are presented in living organisms, including large macromolecules, such as proteins, carbohydrates, lipids and nucleic acids, as well as small molecules such as primary metabolites, secondary metabolites and natural products [5, 6]. *Micelles* are aggregates of surfactant molecules dispersed in a liquid colloid [7]. *Liposomes* are spherical vesicles having at least one lipid bilayer. The liposome can be used as a vehicle for administration of nutrients and pharmaceutical drugs [8].

Talking about structural nanomaterials, we should regard classical crystals as a 'marginal' form of ideally composed and fully identical ordered nanoclusters. This definition will allow us to treat all structures in key terms of nanosystems. First of all, we note the concepts of regular and non-regular systems that include structural and physical regularity extents and then ordered and disordered condensed media that include topological and morphological aspects.

The next candidates into this group are *photonic crystals* (1D,2D,3D) being periodic optical nanostructures that affect the motion of photons in much the same way that ionic lattices affect electrons in solids [9].

Talking about non-regular nanosystems, we can mention *nanocrystalline materials* – the general class of materials consisting of nanocrystals [10]. *Fullerites* are the solid-state manifestation of fullerenes and related compounds and materials [11].

Ceramic-matrix nanocomposites (CNC) are the group of composites where the main part of the volume is occupied by a ceramic, i.e. a chemical compound from the group of oxides, nitrides, borides, silicides, etc. In most cases, ceramic-matrix nanocomposites encompass a metal as the second component [12]. Metal matrix nanocomposites (MNC) can also be defined as reinforced metal matrix composites. This type of composites can be classified as continuous and noncontinuous reinforced materials [13]. Polymer nanocomposites (PNC) consist of a polymer or copolymer having nanoparticles or nanofillers dispersed in the polymer matrix. These may be of different shapes (e.g. platelets, fibres, spheroids), but at least one dimension must be in the range of 1–50 nm [14, 15].

Nanoporous materials consist of a regular organic or inorganic framework supporting a regular, porous structure. The size of the pores is generally 100 nm or smaller [16]. Nanoaerogels are nanoporous materials with nanosized walls [17]. Nanopowders are solid powders of nanoparticles, often containing micronsized nanoparticle agglomerates. These agglomerates can be redispersed using, for example, ultrasonic processing. Nanoparticle dispersions – nanodispersions – are suspensions of nanoparticles in water or organic solvents. These dispersions can be diluted with suitable (compatible) solvents [18, 19]. Nanosuspensions are colloidal dispersions of nanosized drug particles stabilized bv surfactants [20]. *Nanoemulsions* consist of liquid nanodrops distributed within the other liquid [21].

Nanoaerosols consist of nanoparticles and nanodroplets that freely propagate in a gas medium [22]. *Biomolecular complex*, also called macromolecular complex or biomacromolecular complex, is any biological complex made of more than one molecule of protein, RNA, DNA, lipids and carbohydrates. The interactions between these biomolecules are non-covalent [23]. Various *nanointerfaces* for nanotechnology and nanodevices play an essential role in growing nanotubes, catalytic activities and nanointerconnect fundamental properties [24–26].

#### 2.2 Correlation of Atomic and Electronic Structures

Disordered condensed matter is a general case of non-regular condensed nanosystems. This is an extremely wide class of materials, including amorphous substances, glasses, crystals with a high concentration of defects or spin disordering (spin glasses), composites, porous materials, gels, etc.

As a rule, they are united by a strong atomic-electron correlation at the nanoscale level. Using the term 'disordered condensed medium (or system)', most often we have in mind structural 'nano-faults' compared to crystals that are accepted as a standard of perfection and full order. The state of a disordered condensed medium is considered to be metastable, which does not correspond to the minimum of the total energy, which in time will be transformed into a stable crystalline state.

However, the relaxation time of such a process can be very large. General ideas about disordered condensed media almost immediately reveal difficulties in describing of their fundamental properties. Non-regularities of qualitative and quantitative nature do not allow the active use of periodic functions, periodic boundary conditions and the group theory.

Thus, many theoretical concepts used in the theory of crystalline solids are ineffective. In particular, the inability to apply the Bloch theorem and to establish boundary conditions of the Born-Karman type forces us to seek alternative approaches that somehow reduce to the concept of an effective medium as a boundary condition simulating the absence of long-range order in a disordered system.

The features of the short- and medium-range orders, as a rule, can be taken into account accurately, because they are reduced to the calculation of finite sums. However, the variety of realizations of these scale orders in specific local atomic configurations nullifies this certainty. Here, a statistical approach is required to describe macroscopic characteristics. The notions of short-, medium- and long-range orders also require a clarification in view of the noticeable progress in the development of new classes of nanomaterials.

As to the general direction in the study and modelling of fundamental properties of non-regular condensed media, such as characteristics of atomic and electronic structures, vibrational spectra and conductivity, usually it is based on a cluster approach. The essence of the latter is as follows: non-regular condensed solids are mentally divided into elementary fragments of the atomic structure – *nanoclusters*.

The statistical characteristics of this set determine the integral properties of the entire substance as a whole. Based on this approach, it is possible to formulate various versions of the effective medium method, which differs only in the way of averaging the local characteristics by the volume of matter. The genesis of the cluster approach is based on a number of fundamental experiments, for example, on the electronic properties of disordered chalcogenides, performed in the 1950–1960s at the Leningrad Physical and Technical Institute.

To explain these properties Ioffe and Regel [27] have formulated a hypothesis about the decisive role of short-range order, which corresponds to the nanoscale effect. Futher investigations are shown in the topological similarity of crystalline and noncrystalline materials. This quality leads to closeness of their physical and chemical characteristics. This quality also outlines nanoscale responsibility for all fundamental properties.

For the first time the theory fundamentals of disordered condensed state of matter were consequently described by Gubanov [28]. The next essential steps of conception development were made by Mott and Davis [29], Lifshitz et al. [30], Ziman [31], Feltz [32] (1983), Bonch-Bruevich et al. [33], Zvyagin [34], Cutler [35], Regel and Glazov [36], Shklovski and Efros [37], Ehrenreich and Schwartz [38], Klinger [39]) and Marshall [40]. Certainly, this is not an exhaustive list of the scientific works of 1960–1990, when we can review and consider as nanoscale physics and nanotechnology elements.

Comprehensive experimental studies of photo- and radiation-stimulated changes in optical properties in amorphous chalcogenides make it possible to speak of a completely determined correlation of the features of the atomic structure and the electronic spectrum. In addition, it is known that various external influences (radiation, light, pressure, heating, etc.) lead to a change in the short-range order in these and other amorphous semiconductor materials [29]. The analysis of published data in [42, 43] allows revealing one more side of the qualitative picture of the correlation being discussed.

For a significant part of the covalent compounds, the dependence of the band gap  $E_g$  on their density  $\rho_m$ , which is the integral parameter of the atomic structure, is described by an empirical relationship  $E_g \approx 5.36 - 0.79 \rho_m$ , where  $\rho_m$  is the material density in g/cm<sup>3</sup>. This dependence is a manifestation of the known quantum-mechanical result of removing the degeneracy when the electronic subsystem is compacted. A similar tendency is demonstrated by many covalent compounds under high-pressure compressions [44], when metallization of properties (decrease of  $E_g$ ) is observed.

The above-mentioned considerations allow formulating a semi-quantitative model of structurally optical correlations for the explanation of the interrelated photoinduced changes in the atomic structure and electronic spectrum in the region of the fundamental absorption edge in chalcogenide materials.

#### Note

Photoinduced changes in the atomic structure in the context of the foregoing are due to the thermal heating of the structure of the supposed 'pixel' of optical recording. This leads to a change in the local nanoscale properties in the density of electronic states and the refractive index due to a change in the local mass density. It is known that in the case of such traditional nanoobjects as, for example, nanotubes, their bending leads to a change in the local electronic density of states [46]. This effect can be used for the development of pressure nanosensors.

It is noteworthy that among a number of theoretical models that explain the features of the edge of fundamental absorption in the materials, Urbach's empirical rule occupies a prominent place:

$$\kappa(\omega) = \kappa_0 \exp\left[-\gamma \left(E_g - \hbar\omega\right)/kT\right],\tag{2.1}$$

which is valid for  $\kappa \approx 10^2 - 10^4 \text{cm}^{-1}$ , and a power-law dependence of the type:

$$k(\omega)\hbar\omega = B(\hbar\omega - E_g), \tag{2.2}$$

for  $k > 10^4 \text{cm}^{-1}$ . The deviations from (2.1) and (2.2) in chalcogenides are noted in [29, 32].

However, the relations (2.1) and (2.2) serve as the basis for determining  $E_g$  from the frequency dependences of the absorption curves. The analysis (2.1) and (2.2) shows that the relative change in the absorption coefficient will be determined by the relations:

$$\frac{\delta \kappa}{\kappa} = -\left(\frac{\gamma}{kT}\right) \delta E_g,\tag{2.3}$$

and

$$\frac{\delta \kappa}{\kappa} = -\left[\frac{2}{\hbar \omega (\hbar \omega - E_g)}\right] \delta E_g. \tag{2.4}$$

On the other hand, as it was already indicated, decreasing  $E_g$  via the hydrostatic compression P takes place (typical dependence of  $E_g$  via pressure P looks as follows:  $E_g = E_g(0) + \alpha P$ , where for many chalcogenides  $\alpha < 0$  [47].

Assuming that an increase in pressure leads to a decrease in the average interatomic distances in matter, it is possible to relate the width of the energy gap  $E_g$  and the distance d between the adjacent neighbours in the linear approximation by the relation:

$$E_g = E_{g0} + b(d - d_0), (2.5)$$

where  $E_{g0}$  and  $d_0$  are the width of the energy gap and the interatomic distance before the action on the substance, respectively. In the case of photoinduced processes, the changes in  $\delta E_g$  and  $\delta d$  are usually small, which makes the approximation acceptable in the vicinity of any  $d_0$ . Further we obtain:

2.3 Order and Disorder 13

$$\frac{\delta \kappa}{\kappa} = -\left(\frac{\gamma b}{kT}\right) \delta d,\tag{2.6}$$

or

$$\frac{\delta \kappa}{\kappa} = -\left[\frac{2b}{\hbar \omega (\hbar \omega - E_g)}\right] \delta d, \qquad (2.7)$$

where  $\delta d$  is the interatomic distance change. This model allows explaining the mechanism of structural-optical correlations in amorphous chalcogenide films [41].

In [45], particularly, it has been demonstrated that a change in the width of the energy gap of a chalcogenide film  $\Delta E_g$  and a change in the refractive index are stipulated by a change of its thickness  $\Delta d$ . It is assumed that  $\Delta d$  is proportional to  $\delta d$ . A more general analysis of the effect of external influences on the optical properties of amorphous semiconductors is possible with the aid of:

$$\left(\frac{\partial E_g}{\partial P}\right) = \frac{\binom{\partial E_g}{\partial T}_P}{\left[\binom{\partial V}{\partial T}_P\binom{\partial P}{\partial V}_T\right]},$$
(2.8)

where the typical temperature dependence is usually described by a linear law  $E_g = E_g(0) - \beta T$  [48]. However, in this case, it is necessary to know the thermodynamic properties of materials, which require a separate study of complex computer modelling [49]. Topological and morphological character is absolutely required.

The basic achievement of nanotechnology refers not only to the development of traditional nanosized and non-regular structures but also to the creation of new short-range structures such as nanotubes, fullerenes and thin-film nanoribbons, which should be considered more regular. This also applies to nanostructured chalcogenide glasses discussed here in connection with photoinduced processes (see also, Tanaka [50]).

#### 2.3 Order and Disorder

Of course, one should determine the place of non-regular nanosystems within the general concepts of disordered condensed media. These concepts in the scientific literature are ambiguous, namely, (1) nanoobjects can be considered taking into account only their nanosized parameters for which the conditional boundaries of possible changes are established; and (2) nanoobjects are characterized by special properties, which are manifested by the nanodimensions inherent in them.

Nanomaterials should be divided into two main groups: (1) nanoparticles as self-sufficient nanobjects and (2) nanostructured materials as complex structural objects saturated with various embedded (included also by technological processes) nanoparticles. We consider non-regular nanostructured materials from the point

of view of their internal structural correlation, which ultimately determines their local and integral fundamental properties. Moreover, determining the correlation lengths is decisive. The correlation length acts as the base scaling factor of a nanomaterial.

It is reasonable to connect the characteristic lengths of the correlation  $L_{\rm cor}$  of the fundamental properties with the concepts of a short-range order  $L_{\rm sro}$ , medium-range order  $L_{\rm mro}$  and long-range order  $L_{\rm lro}$ . In many cases, the degree of ordering of atomic structures can be estimated from the thin structure of the radial distribution curves. In the case of liquids and many glasses, we can observe one really pronounced peak.

For ideal crystals  $L_{\rm lro}$  will be close to the characteristic size of a crystalline sample. We can find cases of different types of ordering, for example, a total magnetic spin disorder in perfectly ordered regular structures. We define disorder as a certain violation of the order of a fully ordered system, expressed in the absence of correlation of the physical quantity describing this system at distances that determine the scale of the disorder.

It is necessary to consider in more detail the degrees of ordering.

Short-Range Order SRO is the order due to the correlation function of local physical quantities  $f(\mathbf{r})$ , which is noticeably manifested at distances of  $|\mathbf{r}_2 - \mathbf{r}_1| \approx L_{\rm SRO} - 0.1$ –0.5 nm and becomes insignificant when  $|\mathbf{r}_2 - \mathbf{r}_1| > L_{\rm SRO}$ . In the scales of a solid, the distance  $L_{\rm SRO}$  is of order of 1–3 coordination spheres radii magnitude. A correlation of local physical quantities (parameters) of a disordered material  $f(\mathbf{r})$  means a noticeable difference from zero of the mean values of the type  $\langle f(\mathbf{r}_1)f(\mathbf{r}_2)\rangle$ . Talking about SRO, we have in mind only a structural SRO. Namely, the talk is about the identity of the positions of atoms in the material in the neighbourhood of an arbitrarily chosen atom in the region of  $L_{\rm SRO}$  size. However, some more subtle characteristics (for example, spin orientation) are ignored and cannot be obtained by traditional methods of structure research. Correlation of fluctuations in the density of material  $\Delta \rho_m(\mathbf{r})$  on a scale  $L_{\rm SRO}$  determines the identity of atoms arrangement. However, according to another parameter, the correlation can be absent.

**Medium-Range Order** MRO is the order, due to the correlation of physical parameters, which is noticeably manifested at distances  $|\mathbf{r}_2 - \mathbf{r}_1| \approx L_{\text{MRO}} - 0.5-5.0$  nm and becomes insignificant when  $|\mathbf{r}_2 - \mathbf{r}_1| > L_{\text{MRO}}$  does not necessarily indicate the presence of SRO. For example, in complex amorphous compounds of the type  $A_x B_{1-x-y} C_y$ , the structural MRO characteristic for them does not allow judging about their SRO.

**Long-Range Order** LRO is the order due to the correlation of parameters, which manifests itself at distances  $|\mathbf{r}_2 - \mathbf{r}_1| \approx L_{LRO} \rightarrow \infty$ , where  $L_{LRO}$  is the characteristic size of the system. SRO and MRO can absent. LRO is a characteristic, for example, for the electron subsystem of superconductors, where long-range correlations exist.

Thus, the quantities  $L_{SRO}$ ,  $L_{MRO}$ ,  $L_{LRO}$  are the scales (radii, lengths) of the correlation of physical parameters, characterizing the degree of order of the

2.3 Order and Disorder 15

material. In this case, the correlation can take place for one of any physical quantity and be absent for another.

**Perfect Order** PO is the order caused by a noticeable non-vanishing correlation of all physical quantities, which manifests itself at any distances within the system.

The correlation function is a measure of the order in a system, as characterized by a mathematical correlation function. Correlation functions describe how microscopic variables, such as spin and density, at different positions are related. More specifically, correlation functions quantify how microscopic variables covariate with one another across space and time. A classic example of such spatial correlations is in ferro- and antiferromagnetic materials, where the spins prefer to align parallel and antiparallel with their nearest neighbours, respectively.

The general definition of a correlation function is the canonical ensemble (thermal) average of the scalar product of two random variables,  $x_1$  and  $x_2$ , at positions R and R+r and times t and  $t+\tau$  [51]:

$$G(r,\tau) = \langle x_1(R,t) \cdot x_2(R+r,t+\tau) \rangle - \langle x_1(R,t) \rangle \cdot \langle x_2(R+r,t+\tau) \rangle.$$

Here, the brackets  $\langle \dots \rangle$  indicate the above-mentioned thermal average. The main idea is to evaluate the characteristic correlation length  $L_{\rm cor}$ , when the correlation function begins the essential decline. For example, in magnetic spin systems in the case of time-equal correlation function  $G(r) = \langle x_1(R) \cdot x_2(R+r) \rangle - \langle x_1(R) \rangle \cdot \langle x_2(R+r) \rangle$ .

Even in a magnetically disordered phase, spins at different positions are correlated, i.e. if the distance r is very small (compared to a certain length scale  $L_{\rm cor}$ ), the interaction between the spins will cause them to be correlated. The alignment that would naturally arise as a result of the interaction between spins is destroyed by thermal effects. At high temperatures, exponentially decaying correlations are observed with the increasing distance, with the correlation function being given asymptotically by  $G(r) \approx \frac{1}{r^{d-2+\eta}} \exp\left(\frac{-r}{L_{\rm cor}}\right)$ , where r is the distance between spins, d is the dimension of the system and  $\eta$  is the critical exponent. At high temperatures, the correlation decays to zero exponentially with the distance between the spins.

One of the important directions in the study of the atomic structure of amorphous materials is a quantitative evaluation of the degree of order. In practice, the criteria based on comparing the disordered structure with its crystal analogue are often used. But not always such an analogue exists. In some cases, we can use the general Stevels criterion [32, 52, 64, 65], which is free from this drawback. In particular, the repeatability number represents the probability of finding an atom in an atomic structure similar to the initial atom in a certain direction and through a predetermined interval. The repeatability number is calculated as follows:

$$(RN)_{r_0} = \frac{3}{4\pi r_0^3} \int_0^{r_0} CRS(r) 4\pi r^2 dr, \qquad (2.9)$$

characterizing the structure as a whole, where  $CRS(r) = (\sum_i N_i ACR_i)/(\sum_i N_i)$  is the coefficient of repeatability in space within a sphere of radius r,  $ACR = (\sum_i n_i CLR_i)/(\sum_i N_i)$ 

 $(\sum_i n_i)$  is the average weighted repeatability factor,  $CLR_i$  is the coefficient of linear repetition, equal to the number of atoms in the *i*-th direction on the  $n_i$ -th step, related to the number of steps n. For ideal crystals RN = 1 and for amorphous and non-regular solids RN = 0 [64].

It should also be noted that in itself the arrangement of atoms does not characterize the degree of ordering. In this sense, the knowledge of the exact coordinates of atoms in the structure  $R_1, R_2, ..., R_i$  ... is useless. The use of the apparatus of many-particle distribution functions  $g(1, 2, ..., s) = n(1, 2, ..., s)n^3$  is more productive. Here n(1, 2, ..., s) is the multiple-particle probability density, and n is the average particle density [31, 53].

Further we introduce the pair correlation function (the 'pairs' distribution function):

$$g(1,2) = g(\mathbf{R}_{12})n^{-1}\delta(\mathbf{R}_{12} - \mathbf{I}), \tag{2.10}$$

which in the case of an isotropic medium looks like:

$$g(\mathbf{R}_{12}) = g(R) = n^{-1}N(l)\delta(R-l),$$
 (2.11)

where l is the lattice vector and N(l) is the number of lattice vectors of the same length l.

To describe simple liquids, we introduce a three-particle correlation function (the distribution of 'triangles'):

$$g(1,2,3) = n^{-2}\delta(\mathbf{R}_{12} - \mathbf{l})\delta(\mathbf{R}_{13} - \mathbf{l}).$$
 (2.12)

In this case, the superposition approximation of Bogoliubov–Born–Green–Kirkwood–Yvon (BBGKY) is usually used [53]:

$$g(1,2,3) \approx g(1,2)g(2,3)g(3,1),$$
 (2.13)

which allows us to close the chain of Bogoliubov equations for equilibrium distribution functions of the type:

$$\frac{1}{kT}\nabla_{1}\ln(g(1,2,\ldots,s)) = \nabla_{1}g(1,2,\ldots,s) + \frac{n}{g(1,2,\ldots,s)} \int_{V_{s}} g(1,2,\ldots,s+1)\Phi(1,s+1)dV_{s}.$$
(2.14)

However, to describe an amorphous solid or non-regular disordered system, three-point distribution functions are not sufficient. Moreover, the technical difficulties of the next stage significantly increased. In particular, to calculate four-point distribution functions, we can use the so-called 'over-superposition' approximation [54]:

2.3 Order and Disorder 17

$$g(1,2,3,4) = \frac{g(1,2,3)g(1,2,4)g(1,3,4)g(2,3,4)}{g(1,2)g(1,3)g(1,4)g(2,3)g(2,4)g(3,4)}.$$
 (2.15)

Using the representation of many-particle functions developed in statistical physics through many-particle interaction potentials:

$$g(1, 2, \dots, N) = \exp\left(-\frac{1}{kT}\Phi(1, 2, \dots, N)\right),$$
 (2.16)

we come to the necessity to reproduce the latter. Most practical, from the point of view of practical modelling, many-particle potentials are represented in the pair interaction approximation:

$$\Phi(1,2,\ldots,N) \cong \frac{1}{2} \sum_{i,j} \Phi(i,j).$$
(2.17)

As it has been mentioned earlier, the pair distribution function, which is calculated by the formula:

$$g(1,2) \cong C \int_{V_3} \dots \int_{V_N} \exp\left(-\frac{1}{2kT} \sum_{i,j} \Phi(i,j)\right) dV_3 \dots dV_N, \qquad (2.18)$$

is practically measurable.

The approximation of the pair interaction is satisfactory for gases, wherein:

$$g(1,2) = C\exp\left(-\frac{1}{kT}\Phi(1,2)\right).$$
 (2.19)

However, if we assume that the averaged interaction energy  $\overline{\Phi}(1,2)$ , which takes into account the interaction with other atoms of the system, is known, then:

$$g(1,2) \equiv \exp\left(-\frac{1}{kT}\overline{\Phi}(1,2)\right). \tag{2.20}$$

and the scope of such a ratio is greatly expanded.

The function  $\overline{\Phi}(1,2)$  is analogous to one electronic crystal potential in the problem of the electronic spectrum in the one-electron approximation (see Chap. 3). Based on the pair distribution function, the total correlation function  $h(R) \equiv g(R) - 1$  is determined. Then the order parameter of the system (the characteristic scale of the system) can be defined as the correlation length L, when for some R > Lh(R) = 0. In more details, such an approach to the estimation of the degree of ordering is analysed in [32, 34], where, particularly, the characteristic scale of a disordered system of  $A_xB_{I-x}$  type, depending on the composition of X, is investigated. The system is regarded as a superposition of statistically independent sublattices X and X. The corresponding mass densities X and X are approximated by step

functions of different intensities. In this case, the effective correlation length of the system is given by the ratio  $L_{AB}(x) = C(x^{1/3} + (1-x)^{1/3})^{-1}$ , where C is the structure constant.

Further modelling efforts should be directed, first of all, to the reproduction of pair distribution functions and comparison of the latter with the experiment and, secondly, to the evaluation of the macroparameters of the material. For example, an entropy evaluation can be presented by the equation:

$$\begin{split} \frac{S}{Nk} &= -\frac{1}{2}n \int g(1,2) \ln (g(1,2)) dV_2 \\ &-\frac{1}{6}n^2 \iint g(1,2,3) \ln \left\{ \frac{g(1,2,3)}{g(1,2)g(1,3)g(2,3)} \right\} dV_2 dV_3. \end{split} \tag{2.21}$$

It is essential to calculate also the total energy, free energy, pressure, compressibility, etc. Really, this direction is connected with the construction of the material thermodynamics.

It should also be noted that the small correlation radii of the distribution functions of low order g(1,2), g(1,2,3) and g(1,2,3,4), which can actually be taken into account, restrict the integration regions in (2.21) by small cluster volumes. Then, the cluster integrals only sum up and give the entropy evaluation of the entire material. This is especially important for the modelling of non-regular nanoscale structures.

#### 2.4 Concepts of Modelling Atomic Nanostructures

The main theoretical efforts in modelling atomic structures of non-regular condensed materials are directed toward the construction of structural models, the study of their topological properties and evaluation of their nano-, micro- and macrophysical properties. Simulation of properties of a non-regular disordered material usually begins with a probable model of the atomic structure. At the first stage, purely qualitative and speculative views are usually used. Figure 2.2 summarizes the classification of condensed materials by the type of spatial disorder, from the point of view of topology and morphology as well as topological structures.

In this sense, a disorder is imposed on a spatial structure (ordered or disordered) on any parameter. For example, a magnetic disorder means a spin disorder in a spatially regular lattice (spin glasses of spin glasses – magnetic nanosystems). Such a disorder can also be represented in a non-regular lattice. However, in this case we will also have to consider the non-regularity factor. Small distortions of a regular atomic structure, as a rule, preserve the topology of a crystal (or rather, a regular object). This is a fairly common idea of disorder.

But it should be noted that such lattices are not physically stable and should quickly relax to a regular structure corresponding to a minimum of the total energy.

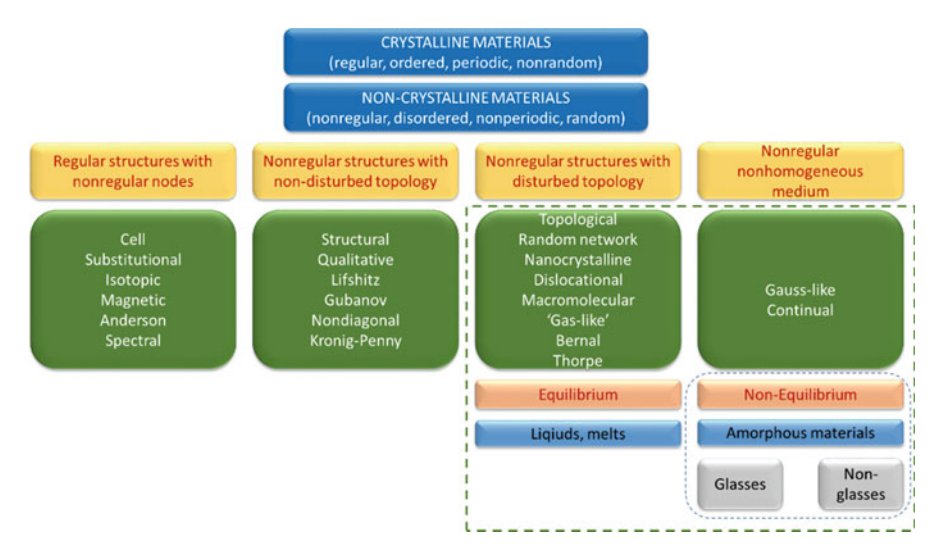
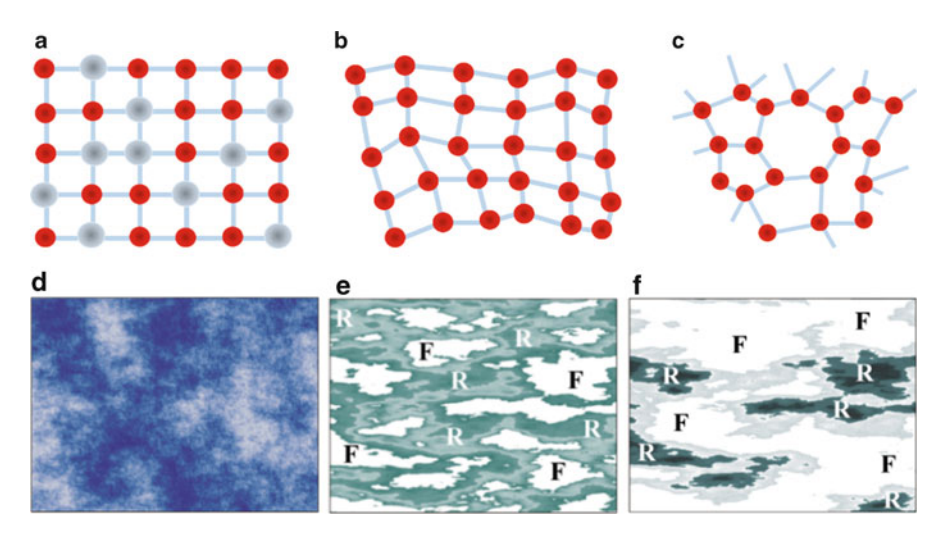


Fig. 2.2 Classification of condensed materials based on spatial disorder criterion

However, there are non-regular structures with a higher degree of disorder, which cannot be transformed into a regular analogue by a continuous topological transformation.

Restoring the broken topology of the structure requires significant energy costs, since this requires the breaking of atomic bonds. Such structures essentially remain nanosystems. In addition, non-regular lattices with broken topology are very stable and can exist for a long time. In this sense, they can be considered as a certain phase state of matter. Typical classic examples are glasses, which can crystallize. However, the times of crystallization (relaxation) are great. There are also models of disorder, which generally ignore any structure and develop the concept of a continuous medium. They are based on some special random distributions of mass densities (for example, Gaussian) or potential energy.

Using the concept of perfect order, the concepts of disorder can be divided into four classes: (1) disorder in spatially regular lattices, (2) disorder of spatially non-regular lattices with the topology of the crystal, (3) disorder of spatially non-regular lattices with broken topology and (4) disorder of the 'continuous medium' type without a lattice. Some types of disorder are presented in Fig. 2.3. *The disorder in regular lattices* can be considered as a cell disorder when the physical properties of the unit cells of the structural matrix are not identical and vary randomly (Fig. 2.3a). *The disorder in non-regular lattices* with the preserved topology of the crystal in comparison with the first class is characterized by a small displacement of the lattice sites relatively to the 'correct' positions, which leads to translational non-periodicity of the physical characteristics (Fig. 2.3b). *The disorder in non-regular lattices* with broken topology is associated with irreversible structural changes (in comparison with reversible structures of the second class), which may be accompanied by other violations of local physical characteristics.



**Fig. 2.3** Types of disorder: (a) quantitative; (b) positional; (c) topological; (d) continual; (e) Thorpe-amorphous solid; (f) Thorpe-polymer glass

The topological disorder (Fig. 2.3c) is the most characteristic. It refers to disordered systems, when the perfect order cannot be restored by a continuous topological transformation. Thus, the topological disorder in this sense is topologically irreversible, since it is characterized by a random structure. The most constructive content has the model of Thorpe disorder [55] (Fig. 2.3e, f). Thorpe model declares topologically disordered networks, containing, for example, large and small rings, which, in turn, cause the presence of rigid (rigid, R) and non-rigid (floppy, F) regions in the structure. The ratio of these areas defines a disordered material either (1) as a polymeric glass – with a lack of hardness regions – or (2) as an amorphous solid, with their excess. The disorder of an inhomogeneous continuous medium is based on the structureless concept of matter, where the distribution functions of mass or potential energy are random and continuous. For example, continual disorder (Fig. 2.3d) considers a disordered system as a continuous medium (continuum approximation). The microstructure of the medium is ignored because it is assumed that the wavelengths of the perturbations considered in the medium are greater than the characteristic detail sizes.

It is essentially relevant to analyse the order level for nanoporous and nanocomposite materials and control their technological repeatability, which normally consist of nanoparticles (e.g. CNTs, GRNs, fullerenes). A special attention should be paid to various interfaces and interconnects in the host material space. At present, the range of nanoparticles has significantly expanded (BN nanotubes,  $TiO_2$ -based nanotubes, etc.).

It would seem that the perfect experimental methods of visualization and detection of properties of nanomaterials should give full information on their atomic and nanostructure. However, the information, as a rule, is indirect and in many cases describes the properties of the surface.

Table 2.1 Basic methods of structural and chemical analysis of nanostructures

Method	Resolution
High-resolution transmission electron microscopy (HRTEM)	High resolution till 0.1 nm
Scanning electron microscopy (SEM)	Resolution (probe diameter) -51000 nm
Auger electron spectroscopy (AES)	Electronic beam – 0.13 κ <sub>3</sub> B, scanning depth 0.53.0 nm, resolution – till 50 nm
Secondary ion mass spectrometry	Scattered secondary ions analysis, resolution depth 1–10 nm
Laser microprobe analysis	Laser pulse radiation, evaporation of tested nanomaterial, pulse duration – <30 ns diameter of laser beam 100500 nm. Low accuracy of detection of composition of tested nanomaterial (~30%)
X-ray methods: X-ray structural analysis and X-ray phase analysis	Nanocrystals, nanocrystallites, study of orientations and distances of crystalline planes distributions
Scanning probe methods	Metrological precise 3D information (distribution map) about surface properties of tested nanosample, resolution – 1–10 nm
Scanning tunnelling microscopy (STM)	Voltage between a probe and a sample электрического (1–10 V). Tunnelling current is about 1–10 nA and, resolution along (x,y)-plane is about 0.1 nm, along the z-axis till 0.001 nm. However the tested material should be a good conductor. Conditions: vacuum and low temperatures (about 50100 K). For resolution about 1 nm, these conditions are not obligatory
Scanning probe microscopy (SPM)	Visualization of nanostructures, wide range of external operation conditions: high and low temperature, vacuum, liquid and controlled gas medium. It is possible to observe surface processes dynamics. Surface resolution is about 1 nm
Atomic force microscopy (AFM)	The detection of the surface is based on controlled changes of interaction force of probe needle with the sample surface. Resolution on (x,y)-plane is about 1 nm, along the z-axis till 0.1 nm
Magnetic force microscope (MFM)	A variant of ( <i>AFM</i> ), however, a probe needle is prepared from ferromagnetic material. Resolution is about 1050 nm
Near-field scanning optical microscopy (NFSOM)	NFSOM use as a probe detector a light waveguide. Resolution is about 10 nm
Photoacoustic spectroscopy (PA)	PA use in combination of a laser photoacoustic spectroscopy and methods of indention for detection of internal stresses in nanostructural materials
Surface control of nanosurfaces	Control of properties of functionalized nanosurfaces, nanostructural covers, control of nanohardness

For the experimental study of nanoscale materials, the same methods can be used, practically the same as for the study of crystalline materials. Still, it is necessary to take into account the resolution of the methods, since surfaces with

dimensions smaller than 200 nm are subjected to the study. The main methods of structural and chemical analysis are presented in Table 2.1 [56].

Thus, experimental structural studies of non-regular condensed materials do not provide detailed information about the local atomic structure (exact coordinates of atoms, lengths and bond angles) and the structure of nanoclusters. Reliably, in the averaged form, it is possible to obtain structural information in the form of *radial distribution curves of atoms* (RDCA). Comparing the intensity and position of the RDCA peaks can give information about the conservation of short-range order and average order and to estimate the necessary correlation lengths. Perhaps, this is the only criterion for the technological comparison of serial nanomaterials. At the same time, obtaining probable local characteristics of the atomic and nanocluster structures is inevitably connected with its modelling. In this case, each version of the model is built on the structural units and relationships that are specific to particular classes of nanomaterials. Among the models of structures grouped by the method of their production, we can distinguish:

- 1. Obtained by introducing any structural perturbations into ideally ordered structures (crystals), for example, models of 'nanocrystallites', 'hot solid' disorder, dislocations and random packing [31, 57]
- 2. Obtained by randomly located 'hard' spheres or other structural units including models of tight packing of hard spheres (Bernal liquid models) [31, 58, 59] and models of random close-packed structural units, taking into account the features of the short-range order of the simulated structures [58]
- 3. Constructed from the 'ball and spoke models' [60, 61], in which fluctuations in the parameters of the structure for a given coordination (viz. fluctuations of lengths and bond angles) are within a few percent of the equilibrium values (Polk models)
- 4. Constructed from the 'first principles' using numerical simulation and, e.g. the theoretical apparatus of molecular dynamics [62] in the pair interaction approximation (as a rule) using the model potentials which are selected from physical considerations
- 5. Obtained by topological mapping onto a three-dimensional Euclidean space of a set of close-packed polyhedra completely filling a space with a higher dimension and a given coordination of the modelled structure [57]

#### 2.5 Concepts of Nanoporous and Nanocomposite Materials

Special attention of technologists and manufacturers attract nanoporous and nanocomposite materials.

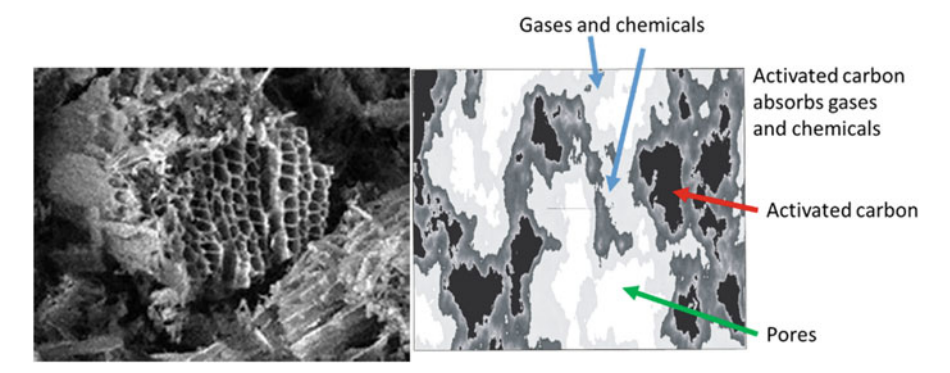


Fig. 2.4 Activated carbon and sorbent model

#### 2.5.1 Nanoporous Materials

Nanoporous materials consist of a regular organic or inorganic network supporting a regular, porous structure. The size of the pores is generally 1–100 nanometers. Most nanoporous materials can be classified as bulk materials or membranes. Activated carbon (see Fig. 2.4) and large group of various zeolites (e.g. see Fig. 2.5) are bulk nanoporous materials. The reduction of pore sizes in nanomaterials leads to new capabilities for filtering and sorption of various chemical elements.

Cell membranes can be thought of as nanoporous membranes. There are many natural nanoporous materials, but artificial materials can also be manufactured. One method of doing so is to combine polymers with different melting points, so that upon heating one polymer degrades. A nanoporous material with consistently sized pores has the property of letting only certain substances pass through while blocking others. Nanoporous materials, in accordance with *IUPAC* (International Union of Pure and Applied Chemistry), are subdivided into three categories [63]: *microporous materials* (0.2–2 nm), *mesoporous materials* (2–50 nm) and *macroporous materials* (50–1000 nm).

The zeolites present a popular group of minerals for collectors and an important group of minerals for industrial and other purposes (see Table 2.2). They combine rarity, beauty, complexity and unique crystal habits. Typically forming in the cavities (or vesicles) of volcanic rocks, zeolites are the result of very low-grade metamorphism. The zeolites are framework silicates consisting of interlocking tetrahedrons of  $SiO_4$  and  $AlO_4$ . In order to be a zeolite, the ratio (Si + Al)/O must equal to 1/2. The alumino-silicate structure is negatively charged and attracts the positive cations that reside within.

Zeolites are characterized by their ability to lose and absorb water without damage to their crystal structures. The large channels explain the consistent low specific gravity of these minerals. Zeolites have many useful purposes. They can perform ion exchange, filtering, odour removal, chemical sieve and gas absorption



Clinoptilolite fuctionalities:

- ✓ Removal of ammonia
- ✓ Removal of iron
- ✓ Removal of manganese
- ✓ Mechanical filtration down to particle size of 5 micron
- ✓ Removal of odour in water

Fig. 2.5 Natural zeolite (clinoptilolite) granulated mineral

Table 2.2 Zeolites groups

Sample zeolite formulas	Mineral name general formula
Analcime	Na <sub>16</sub> [Al <sub>16</sub> Si <sub>32</sub> O <sub>96</sub> ]·16H <sub>2</sub> O
Chabazite	(Ca <sub>0.5</sub> ,Na,K) <sub>4</sub> [Al <sub>4</sub> Si <sub>8</sub> O <sub>24</sub> ]·12H <sub>2</sub> O
Clinoptilolite	(Na,K)6[Al6Si30O72]·20H2O
Erionite	$K_2(Na,Ca_{0.5})_8[Al_{10}Si_{26}O_{72}]\cdot 28H_2O$
Heulandite	(Na,K)Ca <sub>4</sub> [Al <sub>9</sub> Si <sub>27</sub> O <sub>72</sub> ]·24H <sub>2</sub> O
Laumontite	Ca <sub>4</sub> [Al <sub>8</sub> Si <sub>16</sub> O <sub>48</sub> ]·18H <sub>2</sub> O
Mesolite	Na <sub>16</sub> Ca <sub>16</sub> [Al <sub>48</sub> Si <sub>72</sub> O <sub>240</sub> ]·64H <sub>2</sub> O
Scolecite	Ca <sub>8</sub> [Al <sub>16</sub> Si <sub>24</sub> O <sub>80</sub> ]·24H <sub>2</sub> O
Stilbite	NaCa <sub>4</sub> [A <sub>19</sub> Si <sub>27</sub> O <sub>72</sub> ]·30H <sub>2</sub> O

tasks. The most well-known use of zeolites is as water softeners. Calcium in water can cause it to be 'hard' and capable of forming stable salts, contamination and other problems. Zeolites charged with much less destructive sodium ions can allow hard water to pass through its structure and exchange calcium for sodium ions. This process is reversible. In a similar way, zeolites can absorb ions and molecules and thus act as a filter for odour control, toxin removal and chemical sieve.

Zeolites can have water in their structures removed by heat with the basic structure left intact. Then other solutions can be pushed through the structure, and zeolites can act as a delivery system for a new fluid. This process has applications in medicine, livestock feeds and other types of research. Zeolites added to livestock feed have been shown to absorb toxins that are harmful and even fatal to the growth of animals, while the basic structure of zeolites is biologically neutral (see Fig. 2.5 and Table 2.3).

Generally, we can consider one component porous material as a mixture of substance and emptiness. In the case of porous metals, we deal with the percolation matrix. However, one component system cannot include finite metal clusters. Really it is the infinite cluster, and we cannot talk about the percolation threshold x. Considering a two-component mixture, we can observe two percolation transitions at different values of x, which corresponds to the formation of an infinite cluster for each of the two components.

Function	Description
Catalysis	Catalysts for several important reactions involving organic molecules. The reactions can take place within the pores of the zeolite, which allows a greater degree of product control
Gas separation	The porous structure of zeolites can be used to 'sieve' molecules having certain dimensions and allow them to enter the pores. The porous structure provides polymerization of semiconducting materials and conducting polymers to produce materials having unusual physical and electrical attributes
Ion exchange	Hydrated cations within the zeolite pores are bound loosely to the zeolite framework and can readily exchange with other cations when in aqueous media. It is possible to remove radioactive ions from contaminated water

Table 2.3 Main uses for zeolites in industry

Pores are important for capacitive energy storage as, in general terms, more pores mean a larger surface area for *physical adsorption*, which, in turn, leads to higher storage capacity. Traditional porous carbon, once made, has a set volume with fixed pores randomly scattered inside and outside. It is not really possible to readjust the structure and jam more porous carbon in the same amount of space without crumpling a fraction of the pores that are especially crucial for capacitive energy storage. Nanofoams are a class of nanostructured, porous materials, foams, containing a significant population of pores with diameters less than 100 nm. Bryce Tappan at Los Alamos National Laboratory discovered a technique for producing *metal nanofoams* by igniting pellets of energetic metal bis(tetrazolato)amine complexes in 2006. Nanofoams of iron, cobalt, nickel, copper, silver and palladium have been prepared through this technique.

#### 2.5.2 Aerogels

Aerogel is a synthetic porous ultralight material derived from a gel, in which the liquid component of the gel has been replaced by a gas. Aerogels are one example of nanofoams.

The result is a solid with extremely low density and low thermal conductivity. Nicknames include 'frozen smoke', 'solid smoke', 'solid air' or 'blue smoke' owing to its translucent nature and the way light scatters in the material. It feels like fragile expanded polystyrene (Styrofoam) to touch. Aerogel was first created by Samuel Stephens Kistler in 1931. Aerogels are produced by extracting the liquid component of a gel through supercritical drying. This allows the liquid to be slowly dried off without causing the solid matrix in the gel to collapse from capillary action, as would happen with conventional evaporation. The first aerogels were produced from silica gels. Kistler's later work involved aerogels based on alumina, chromia and tin dioxide. Carbon aerogels were first developed in the late 1980s.

Scale	Functionality
<5 nm	Catalytic activity
<20 nm	Making a hard magnetic material soft
<50 nm	Refractive index changes
<100 nm	Achieving superparamagnetism, mechanical strengthening or restricting matrix
	dislocation movement

**Table 2.4** Functionality of nanocomposites via nanoscale

#### 2.5.3 Nanocomposites

Nanocomposite is defined as a multiphase material with inclusions of 1D, 2D or 3D nanoscale (about 10–100 nm) component. Nanoinclusions can be nanolayers divided by distances about tens of nm within the host matrix of nanocomposite.

The mechanical, electrical, thermal, optical, electrochemical, catalytic properties of the nanocomposite will differ markedly from that of the component materials. Nanoscale limits for these functionality effects presented in Table 2.4.

There are three basic morphological groups of nanocomposites as presented in Table 2.5.

#### 2.6 Scaling in Functional Nanomedia

Many nanodevices using the advantages of nanophenomena are highly integrated structures called mesostructures (100–1000 nm), e.g. nanomemory and nanosensor systems. This provides an opportunity for human health correction and enhancement by using adequate dimensions of the corresponding nanodevices (See Fig. 2.6). Thus, 'nano' means usually the scale of nanophenomena, but not simply the characteristic sizes of functionalized nanodevices.

Analysing Fig. 2.6, we should point out the *top-down approach*, when nanocomponents are obtained using larger, externally controlled tools from the microscale, microcontact printing, imprint lithography or direct-write dip-pen nanolithography. This approach is able to obtain nanoscale components with atomic precision.

The bottom-up approach builds up smaller components into more complex assemblies. Molecular manufacturing, i.e. the process of assembling nanodevices molecule by molecule, exemplifies a bottom-up approach.

*The bio-hybrid approach* uses biological components as building blocks of integrated nanodevices for the creation of biosensors, nanoactuators, etc.

Nanocomposite	
group	Properties
Ceramic-matrix	The main part of the volume is occupied by a ceramic (oxides, nitrides, borides, silicides, etc.). Ceramic-matrix nanocomposites use a metal as the second component. These nanocomposites demonstrate improving their optical, electrical, magnetic, tribological, corrosion-resistance and other protective properties
Metal matrix	Metal matrix nanocomposites are reinforced metal matrix composites. This type of composites can be classified as continuous and noncontinuous reinforced materials. One of the more important nanocomposites is <i>carbon nanotube metal matrix composites</i> , which is an emerging new material that is being developed to take advantage of the high tensile strength and electrical conductivity of carbon nanotube materials
Polymer-matrix	Polymer host matrix filled by nanoparticles. Qualities of polymer matrix and nanoinclusions are responsible for nanocomposite functionality. Thin films

ment), which rely on polymer nanocomposites

made of polymer nanocomposites will enable the future development of multifunctional small-scale devices (i.e. sensor, actuator, medical equip-

Table 2.5 Technologically important nanocomposite groups

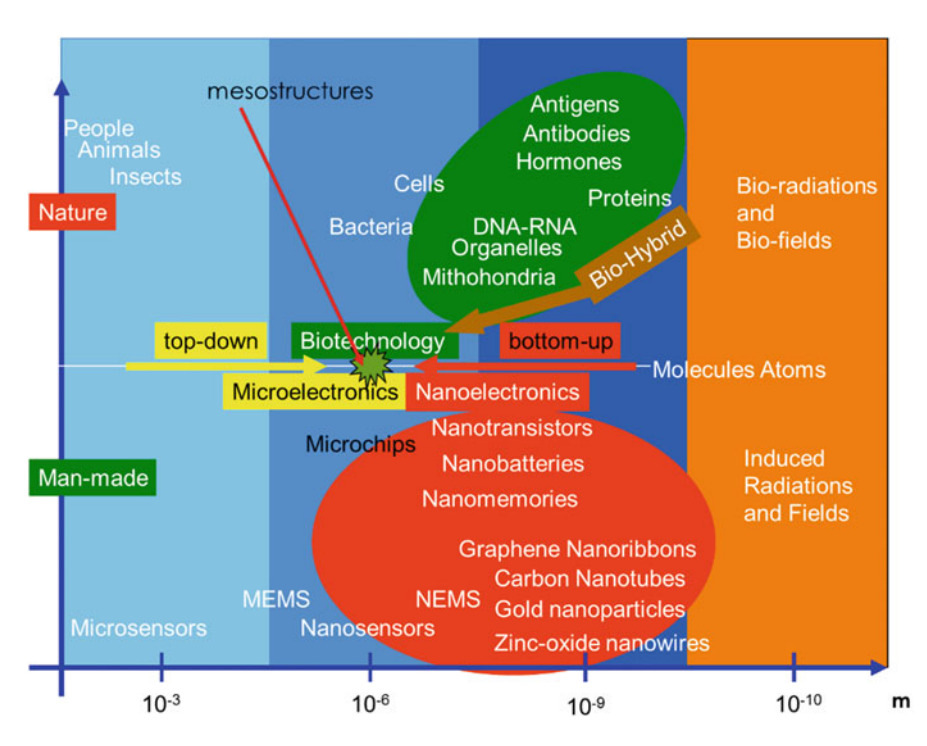


Fig. 2.6 Comparative scales of particular nanotechnology objects

#### 2.7 Concluding Remarks

Nanomaterials are fundamental to the creation of nanosystems for specific functional purposes (see Fig. 2.7 and Table 2.6). According to the principle of their functioning, they can be divided into electronic, optical and mechanical.

The functioning of electronic nanosystems is based on the transformation of optical signals, magnetic signals and chemical signals to electrical signals and vice versa, as well as mechanical ones to the transformation of mechanical motion. Nanosystems of certain types constitute the corresponding branches of nanosystems engineering, namely, nanoelectronics, nanooptics and nanomechanics. The development of various types of nanosystems is closely interlinked, which leads to the creation of more complex integrated nanosystems, such as nano-optoelectronic, nanoelectromechanical, nano-optomechanical and nano-optoelectromechanical systems.

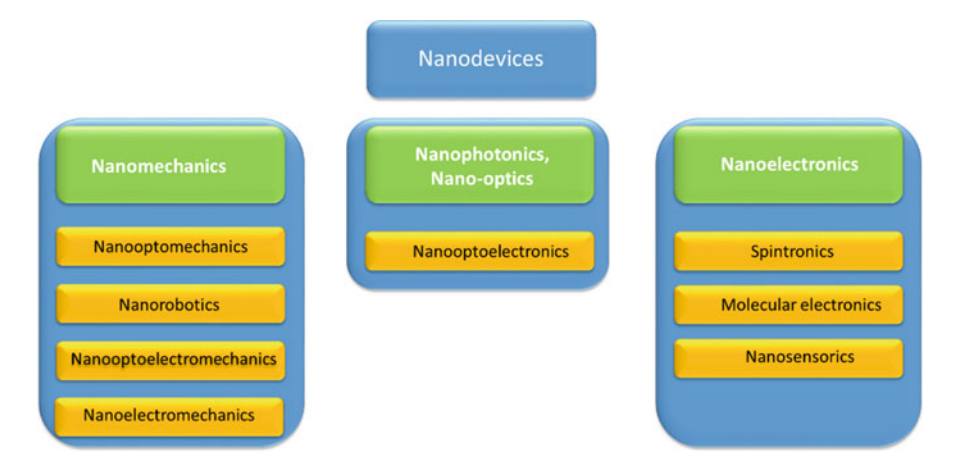


Fig. 2.7 Classification of functionalized nanosystems

Table 2.6	Functional	groups o	f integrated	nanodevices

Functionality	Properties
Nanophotonics or nanooptics	Light impact on the nm-scale materials, interaction of nanometer-scale objects with light (wavelengths from 300 to 1200 nm)
Nanomechanics	Mechanical (elastic, thermal and kinetic) properties of physical systems at the nm scale
Nanoelectronics	Nanoelectronic component development, in particular, for actual recent CMOS technology generations (10–20 nm nodes), development of spintronics, molecular electronics and nanosensorics

References 29

#### References

 Buzea C, Pacheco I I, Robbie K 2007 Nanomaterials and nanoparticles: Sources and toxicity Biointerphases 2(4) MR17–71

- 2. Iijima S 1980 Direct observation of the tetrahedral bonding in graphitized carbon black by high resolution electron microscopy *Journal of Crystal Growth* 50(3) 675–83
- 3. Raduhkevich L V, Luckyanovich V M **1952** On carbon structure under thermal decomposition on Fe contact *J Phys. Chem.* **26** 88–95 (*in Russian*)
- 4. Lehn J-M 1995 Supramolecular Chemistry VCH ISBN 3-527-29311-6
- Walter P, Alberts, B, Johnson, A S, Lewis J, Raff M C, Roberts K 2008 Molecular Biology of the Cell (5th edition, Extended version) New York: Garland Science
- 6. Slabaugh M R, Seager S L **2007** Organic and Biochemistry for Today (6th ed.) Pacific Grove: Brooks Cole
- 7. Nicolai T, Colombani O, Chassenieux Ch **2010** Dynamic polymeric micelles versus frozen nanoparticles formed by block copolymers *Soft Matter* **6**(14) 3111–8
- 8. Torchilin V **2006** Multifunctional nanocarriers *Advanced Drug Delivery Reviews* **58** (14) 1532–55
- Yablonovitch E 1987 Inhibited Spontaneous Emission in Solid-State Physics and Electronics Physical Review Letters 58(20) 2059–62
- Talapin D V 2012 Nanocrystal solids: A modular approach to materials design MRS Bulletin 37 63–71
- 11. Blank V **1998** Ultrahard and superhard phases of fullerite C<sub>60</sub>: Comparison with diamond on hardness and wear *Diamond and Related Materials* **7**(2–5) 427–31
- 12. Zhang S, Sun D, Fu Y, Du H **2003** Recent advances of superhard nanocomposite coatings: a review *Surf. Coat. Technol.* **167**(2–3) 113–9
- Silvestre N 2013 State-of-the-art Review on Carbon Nanotube Reinforced Metal Matrix Composites International Journal of Composite Materials 3(6A) 28–44
- 14. Manias E 2007 Nanocomposites: Stiffer by design Nature Materials 6(1) 9-11
- 15. Lang X Y, Zhang G H, Lian J S, Jiang Q 2006 Size and pressure effects on glass transition temperature of poly (methyl methacrylate) thin films *Thin Solid Films* 497(1–2) 333–7
- 16. Nanoporous Materials: Science and Engineering 2004 Eds G Q Lu and X S Zhao Series on Chemical Engineering Imperial College Press 912p
- 17. Aegerter M A, Leventis N, Koebel M M 2011 Aerogels Handbook Springer publishing
- Weibel A, Bouchet R, Boulc'h, F, Knauth P 2005 The Big Problem of Small Particles: A Comparison of Methods for Determination of Particle Size in Nanocrystalline Anatase Powders Chem. Mater. 17 2378–85
- 19. Hilding J, Grulke E A, Zhang Z G, Lockwood F **2003** Dispersion of Carbon Nanotubes in Liquids *J Dispersion Science and Technology* **24**(1) 1–41
- Shid R L, Dhole Sh.N, Kulkarni N, Shid S L 2013 Nanosuspension: A Review Int. J. Pharm. Sci. Rev. Res. 22(1) 98–106
- Solans C, Izquierdo P, Nolla J, Azemar N, Garcia-Celma M J 2005 Nano-emulsions Current Opinion in Colloid & Interface Science 10(3–4) 102–10
- Bogdan A, Bucket M I., Japuntich D 2014 Nano-Sized Aerosol Classification, Collection and Analysis—Method Development Using Dental Composite Materials *Journal of Occupational* and Environmental Hygiene 11(7) 415–26
- 23. Moore P B **2012** How Should We Think About the Ribosome? *Annual Review of Biophysics* **41** (1) 1–19
- Zhang Zhi-cheng, Xu Biao, Wang Xun 2014 Engineering nanointerfaces for nanocatalysis Chem. Soc. Rev. 43 7870–86
- 25. Shunin Yu, Bellucci S, Zhukovskii Yu, Gopeyenko V, Burlutskaya N, Lobanova-Shunina T 2015 Nanocarbon electromagnetics in CNT-, GNR- and aerogel-based nanodevices: models and simulations Computer Modelling & New Technologies 19(1A) 35–42

- 26. Shunin Yu N, Zhukovskii Yu F, Gopeyenko V I, Burlutskaya N, Lobanova-Shunina T, Bellucci S 2012 Simulation of electromagnetic properties in carbon nanotubes and graphene-based nanostructures J. Nanophotonics 6(1) 061706–16
- Ioffe A F, Regel A R 1960 Non-crystalline, amorphous, and liquid electronic semiconductors *Prog. Semicond.* 4 237–91
- 28. Gubanov A I **1963** *Quantum electronic theory of amorphous conductors* (Moscow:Nauka) 264p (in Russian)
- 29. Mott N F, Davis E A **1971** Electronic Processes in Non-Crystalline Materials (Oxford: Clarendon-Press) 437p
- 30. Lifshitz I M, Gredeskul S A, Pastur L A **1986** Introduction to the theory of disordered systems (Moscow:Mir) 360p (in Russian); Lifshitz, I M, Gredeskul, S A, Pastur, L A **1988** Introduction to the theory of disordered systems (New York:Wiley)
- 31. Ziman J M **1979** Models of Disorder. The Theoretical Physics of Homogeneously Disordered Systems (New York :JohnWilley & Sons)
- 32. Feltz A **1983** *Amorphe und glasartige anorganische Festkörper* (Berlin: Akademie-Verlag); Feltz A 1986 *Amorphous and glassy inorganic solids* (Moscow:Mir) (*in Rusian*); Feltz A **1993** *Amorphous Inorganic Materials and Glasses* (Weinheim:Wiley-VCH Verlag GmbH)
- 33. Bonch-Bruevich V L, Zvyagin I P, Kaiper R, Mironov A G, Enderlain R, Esser B 1981 Electron Theory of Disordered Semiconductors (Moscow:Nauka) 383p (in Rusian)
- 34. Zvyagin I P **1984** Kinetic phenomena in disordered semiconductors Moscow: MSU) 192p (in Rusian)
- 35. Cutler M **1977** *Liquid semiconductors* (Oxford : Elsevier Science)
- 36. Regel A P, Glazov V M 1980 Physical properties of electronic melts (Moscow: Nauka) (in Russian)
- 37. Shklovski B I, Efros A L **1979** Electronic properties of doped semiconductor (Moscow:Nauka) (in Russian); Shklovski B I, Efros A L **1984** Electronic properties of doped semiconductors (Heidelberg:Springer)
- 38. Ehrenreich H, Schwartz L M **1976** The Electronic Structure of Alloys *Phys Rev B. Solid State* **31** 149–286
- 39. Klinger M I 1988 Glassy disordered systems: topology, atomic dynamics and localized electron states *Phys.Rep.* 165 275–397
- Marshall J M 1983 Carrier diffusion in amorphous semiconductors Rep.Progr.Phys. 46 1235–82
- 41. Shvarts K K **1986** *Physics of optical recording in isolators and semiconductors* (Riga:Zinatne) (in Russian)
- 42. Shunin Yu N, Shvarts K K Atomic and electronic structure of disordered semiconductors Preprint: Institute of Physics Academy of Sciences of Latvia **LAFI-154** (Riga-Salaspils:IP) 97 p (in Russian)
- 43. Shunin Yu N, Shvarts K K **1990** Modelling of radiation stimulated processes in disordered semiconductors *Izv AN LSSR ser fiz i tehn nauk* No 2 38–56 (*in Russian*)
- 44. *The Structure and Properties of Matter* **1982** Ed T Matsubara. (Berlin-Heidelberg-N.-Y.: Springer Verlag)
- 45. Shvarts K K, Pirogov F V, Shunin Yu N, Teteris J A 1987 Photoinduced structural changes in amorphous chalcogenides *Cryst. Latt. Def. and Amorph. Mat.* 17 133–8
- 46. Shunin Yu N, Zhukovskii Yu F, Gopeyenko V I, Burlutskaya N Yu, Bellucci S 2012 Properties of CNT- and GNR-Metal Interconnects for Development of New Nanosensor Systems In: Nanodevices and Nanomaterials for Ecological Security, Series: NATO Science for Peace Series B Physics and Biophysics, eds. Yu.Shunin, A. Kiv (Springer Verlag, Heidelberg) 237–62
- 47. Physical and chemical properties of semiconductors 1978 Handbook (Moscow:Nauka) (in Russian)
- Ridley B K 1982 Quantum processes in semiconductors (N-Y. Oxford University Press) 1<sup>st</sup>-5<sup>th</sup> edtions 1982, 1988, 1993, 1999, 2013

References 31

 Shunin Yu N, Schwartz K K 1997 Correlation between electronic structure and atomic configurations in disordered solids In: Computer Modelling of Electronic and Atomic Processes in Solids, Eds R C Tennyson and A E Kiv (Dodrecht/Boston/London: Kluwer Acad. Publisher) 241–57

- Tanaka K 2003 Nanostructured chalcogenide glasses Journal of Non-Crystalline Solids 326–327 21–8
- Sethna J P 2011 Statistical Mechanics: Entropy, Order Parameters, and Complexity (Oxford: Clarendon Press) 215–40
- 52. Owen A E **1973** Preparation of amorphous materials and the glassformation In: *Electronic and structural properties of amorphous semiconductors* Eds P C Le Comber, J Mort (London-N. Y.:Ac.Press)
- 53. Kuni F M 1981 Statisticheskaia fizika i termodinamika (Moskva:Nauka) (in Russian)
- Fisher I Z, Kopeliovich B Ja 1960 On precision of superpositional approach in liquid theory Dokl Akad Nauk SSSR 133 1392–5
- Thorpe M F 1985 Rigidity percolation In: *Physics of Disordered Materials* Eds.D.Adler, H Fritzsche, R.Ovshinsky (N.-Y.-London: Ac.Press) 55–61
- Akzhigitova O F, Tarasov R V, Makarova L V 2014 Research methods and equipment in nanotechnologies *Modern scientific researches and innovation* No.5 http://web.snauka.ru/ issues/2014/05/34627
- 57. Topological disordered in condensed matter 1983 Ed F Yonezawa and T Ninomiya (Berlin-Heidelberg-N.-Y.-Tokyo: Springer Verlag)
- 58. Bernal J D 1964 The structure of Liquids Proc.Roy.Soc.A. 280 299-322
- 59. Ishikawa T **1975** The Assembly of Hard Spheres as a structure models of amorphous iron *phys. stat.sol.* (a) **29** 293–302
- Greaves G N, Davis E A 1974 A continuous random network model with threefold coordination *Phys.Mag.* 29 1201–6
- Connel C A N, Temkin R J 1974 Modelling the structure of amorphous tetrahedrally coordinated semiconductors *Phys.Rev.* B 9 5323–33
- 62. Wooten F, Winer K, Weaire D **1985** Computer generation of structural models of amorphous Si and Ge *Phys.Rev.Lett.* **54** 1392–5
- 63. Compendium of Chemical Terminology. Gold Book 2014 Version 2.3.3 International Union of Pure and Applied Chemistry IUPAC 2014-02-24
- 64. Scholze H **1991** *Glass. Nature, structure and properties* (N-Y-Berlin-Heidelberg-London-Paris-Tokyo-Hong Kong Barcelona: Springer-Verlag)
- 65. Stevels J M 1948 Progress in the Theory of the Physical Properties of Glass Elsevier Amsterdam

# Chapter 3 Potentials and Electronic Structure Calculations of Non-regular Nanosystems

#### 3.1 Introduction

Any ab initio calculations of physical characteristics of condensed materials, associated with the electron and phonon subsystems, require the calculations or construction of potentials (potential functions) that take into account simulated effects. Moreover, this concerns not only the electronic structure of the material sample as a whole but also local or spatially limited structural defects in it. The first step on the way to obtaining potentials is to calculate the electronic spectrum of a sample considering it as a quantum mechanical object. However, some simplifying approximations are necessary. In these cases, one-electron approximation is practically preferable, when the motion of each electron of the system is considered in the averaged field of nuclei and other electrons. The averaged field takes into account both the pure Coulomb interaction of the charged particles of the system and the exchange-correlation effects in the electronic subsystem. In the simplest version of such an approximation, the dynamics of the lattice of a rigid body (adiabatic approximation) is neglected, and only the stationary approach is considered. However, even for such an option, the problem of calculating the electronic spectrum of a non-regular condensed system is very problematic.

#### 3.2 Atomic Potential Functions

Consider the methodology of calculations in the case of isolated neutral atoms. There are two classes of problems that can be distinguished in quantum mechanics.

The first class includes eigenvalue problems, when resulting from the solution of the Schrödinger equation  $Hu_i = \varepsilon_i u_i$  one-electron wave functions  $u_i$  and the corresponding values of the energies of one-electron states  $\varepsilon_i$  are sought. This is usually a self-consistent procedure, since the exact form of the potential function is

not known and can be obtained in the process of iteration on the basis of some starting *seeding* potential. Boundary conditions of wave functions provide the 'natural' property of their vanishing at the infinity. Namely, wave functions go to zero at the infinity or on the sample boundaries (as an approximation). In this case, as is known, a discrete energy spectrum is obtained. Then, based on the wave functions obtained, wave functions of many-electron states and the corresponding basis are formed.

The second class of stationary problems includes scattering problems, when, for example, a plane electron wave is scattered by a potential  $V(\mathbf{r})$  and the Schrodinger equation:

$$(\Delta + k^2)\psi_k(\mathbf{r}) = V(\mathbf{r})\psi_k(\mathbf{r}) \tag{3.1}$$

is solved under boundary conditions corresponding to the scattered wave, for example:

$$\psi_{\mathbf{k}} \to \exp(i\mathbf{k}\mathbf{r}) + f(\theta, \varphi)\exp(ikr)/r,$$
 (3.2)

where the solution is sought as a superposition of the original plane wave  $\exp(i\mathbf{kr})$  and a spherical scattered wave dependent on scattering  $\theta$  and azimuth angles  $\varphi$ .

Initially, it was assumed that such a statement of the problem is reasonable only for positive energies  $k^2 = \varepsilon > 0$ . However, subsequently this approach was successfully used for negative energy states of atoms and molecules and was formed as a cluster multiple scattering method for calculating the electronic structure of complex molecules and impurities in solids (see, e.g. [1]). Later, these principles were used to construct various calculation schemes suitable for disordered solids. More details of the scattering problem concerning the calculation of the electronic properties of disordered semiconductors are considered, for example, in [2].

Knowledge of the right potential  $V(\mathbf{r})$  is highly desirable, but not always necessary. It is enough to simulate the so-called pseudopotential. This is due to the fact that in most practical operation cases of electronic devices, the deep electronic states of condensed systems are passive.

#### 3.2.1 Construction of Atomic Potential Functions

It is intuitively clear that the potential function of an isolated atom (or potential) is an element of the potential function of any condensed system. However, the latter cannot be obtained by a simple superposition. Therefore, a detailed analysis of the factors determining the atomic potential is required. There is a group of methods that make it possible to calculate the potential as a result of solving the eigenvalue problem. These methods are based on the Hartree approach, which proposed a one-electron equation for the spin-orbitals  $u_i$  of the wave function of the i-th electron in an atom.

The solution of the Schrödinger equation, which should be solved with an electronic spectrum of atoms, molecules and solids (both ordered and disordered), usually uses the non-relativistic approximation and requires the knowledge of the self-consistent potential (self-consistent potential energy) of an electron in the field of nuclei and other electrons to come to the one-electron problem. As a rule, such a potential is unknown or known only for some particular cases. For free (isolated) atoms, one can perform a self-consistent procedure of the Hartree–Fock–Slater type [1] and find the self-consistent potential of the atom, as well as the corresponding wave functions in the one-electron approximation. Such a calculation reduces to the numerical integration of a system of differential equations of the type:

$$\left[ -\nabla_{1}^{2} + V_{C}(1) + V_{Xi}(1) \right] u_{i}(1) = \varepsilon_{i} i_{i}(1), \tag{3.3}$$

where  $-\nabla_1^2$  is the kinetic energy operator (in **Ry**-Rydberg units) and  $V_C(1)$  is the Coulomb potential energy of the electron at point 1 due to its interaction with the nucleus and other electrons of the system. For an atom with a charge number Z:

$$V_C(1) = -\frac{2Z}{r} + \sum_j n_j \int u_j^*(2)u_j(2)g_{12}dV_2, \tag{3.4}$$

where  $u_j^*(2)u_j(2)$  is the density of the electron charge of j-th orbital at the point 2,  $g_{12}=2/r_{12}$ ,  $r_{12}$  is the distance between points 1 and 2 and  $n_j$  is the number of the orbital filling (0 or 1). The term  $V_{Xi}(1)=-n_i\int u_i^*(2)u_i(2)g_{12}dV_2$  takes into account that the electron on the i-th orbital does not interact with itself. The integration is carried out over the entire volume of the atom. The total charge density by Hartree is  $\rho(1)=\sum_i n_i u_i^*(1)u_i(1)$ . In this case, the one-electron functions included in the known determinant total wave function [1]  $\Psi=\frac{1}{\sqrt{N!}}\det\|\mathbf{u}_{k_1}(1),\mathbf{u}_{k_2}(2),\ldots,\mathbf{u}_{k_N}(N)\|$  with  $k_i=1,2,\ldots,N$  are varied and mini-

mize the total energy of the atom. The use of such wave functions in the variational procedure leads to the Hartree–Fock equation:

$$\left[ -\nabla_1^2 + V_c(1) \right] u_i(1) - \sum_j n_j \int u_j^*(2) u_i(2) g_{12} dV_2 u_j(1) = \varepsilon_i u_i(1).$$
 (3.5)

However, the set of spin-orbitals in the Hartree–Fock method, which minimizes the total energy, is ambiguous, and the value  $\varepsilon_i$  in the Hartree method becomes the matrix  $\varepsilon_{ij}$ . It is possible to choose orbitals which diagonalize  $\varepsilon_{ij}$ .

Slater rewrote Eq. (3.5) in the following way:

$$\left[ -\nabla_{1}^{2} + V_{C}(1) + V_{XiHF}(1) \right] u_{i}(1) = \varepsilon_{i} u_{i}(1), \tag{3.6}$$

where

$$V_{XiHF} = -\frac{\sum_{j} n_{j} \int u_{i}(1)u_{j}^{*}(2)u_{j}(1)u_{i}(2)g_{12}dV_{2}}{u_{i}^{*}(1)u_{i}(1)},$$
(3.7)

is the exchange-correlation term.

The charge that creates the potential is called the exchange-correlation charge, or the 'Fermi hole'. The Fermi hole moves together with the electron and is a metal surrounding electron-like sphere, from which the electron charge is eliminated. The size of the Fermi hole can be estimated, knowing the local density of the electron charge, namely,  $r_s = [3\rho/4\pi]^{-1/3}$ , which is also called the Wigner radius  $r_s$ . Note, that in the electronic theory of metals [3], the parameter  $r_s$  uniquely characterizes the state of the electronic subsystem. In the limit case  $r_s \to 0$ , the kinetic energy  $k^{2\sim}1/r_s^2$  dominates over the energy of the electron–electron Coulomb interaction  $\sim 1/r_s$ . For  $r_s \to \infty$  the electron gas density is small, and the electrons are localized, forming Wigner lattice. Under the transition to  $r_s \neq 0$ , quantum effects and the longrange exchange interaction are switched on.

Then, the total energy of the electron subsystems per one electron looks like:

$$\varepsilon = \frac{E}{N} = \left( -\frac{1.792}{r_s} + \frac{2.65}{r_s^{3/2}} - \frac{0.73}{r_s^2} - \dots \right), Ry.$$
 (3.8)

The Hartree–Fock equation, which is well applicable to atoms, turns out to be of little use for solids because of a rather complicated exchange-correlation term. Slater proposed to replace  $V_{XiHF}$  by the weighted average values with weights corresponding to the probability of finding the electron in position 1 of the *i-th* spin-orbitals:

$$[V_{XiHF}]_{AV} = \frac{\sum_{i\uparrow,j\uparrow} n_i n_j \int u_i^*(1) u_j^*(2) u_j(1) u_i(2) g_{12} dV_2}{\sum_{k\uparrow} n_k u_k^*(1) u_k(1)},$$
(3.9)

where  $\uparrow(\downarrow)$  is the position of the spin 'up' (down). The formula for electrons with the spin  $\uparrow$  for a gas of free electrons is as follows:

$$[V_{XiHF}]_{AV} = -6[3\rho \uparrow (1)/4\pi]^{1/3} = V_{XS}(1). \tag{3.10}$$

The formula for electrons with the spin \( \) looks similar.

As a result, a self-consistent field method based on the equation:

$$\left[-\nabla_1^2 + V_C(1) + V_{XS}(1)\right] u_{i\uparrow}(1) = \varepsilon_i u_{i\uparrow}(1) \tag{3.11}$$

has been developed.

It was widely used in various calculations of the electronic structure of atoms. In particular, such calculations were performed by Herman and Skillman [4] for all atoms of the periodic system. An introduction of the statistical exchange-correlation potential (3.9) is convenient for calculations because of its locality. However, the price that has to be paid for this relative simplicity is expressed in a noticeable discrepancy between the total atomic energies calculated by successive Hartree–Fock method and Hartree–Fock–Slater method used. It was also found that if we introduce the statistical exchange-correlation term into the expression for the total energy and then apply the variational principle, then we obtain the exchange-correlation potential as  $(2/3)V_{XS}(1)$ . Therefore, in the future, the statistical approximation started to be used in the form:

$$V_{X\alpha}(1) = \alpha V_{XS}(1) = -6\alpha (3\rho/8\pi)^{1/3}, \tag{3.12}$$

where  $\alpha$  is a certain coefficient, which is usually calculated from the condition that the total Hartree–Fock and Hartree–Fock–Slater energies are identical in the so-called  $X\alpha$ -approximation. The physical details of the coefficient can be elucidated by means of a many-electron theory.

Note that  $\alpha$  is a function of the Wigner correlation radius  $r_s$ . If we take into account the inhomogeneity in the distribution of the electron density and perform the gradient expansion  $\rho(\mathbf{r})$  on powers  $\nabla \rho$  at the vicinity of the mean electron density  $\rho_0$ , then, up to terms of the second order, one can obtain:

$$V_{XS}^{H}(1) = \frac{2}{3}V_{XS}(1) + \frac{2\pi}{(3\pi^{2})^{4/3}} \left[ \frac{4}{3} \left( \frac{\nabla \rho}{\rho} \right)^{2} - 2\frac{\nabla^{2}\rho}{\rho} \right] \rho^{-1/3}.$$
 (3.13)

The expediency of such a form of the exchange-correlation potential is discussed below. The analysis, carried out in [5–7], makes it possible to use the analytical potential of Gaspar [8, 9] for potentials modelling:

$$V^{G}(r) = -\frac{2Z}{r} \cdot \frac{\exp(-\lambda r/\mu)}{(1 + Ar/\mu)},\tag{3.14}$$

where  $\lambda = 0.1837$ ,  $\mu = 0.8853Z^{-1/3}$ , A = 1.05, which is a successful approximation of the self-consistent potential function  $V_C(1) + V_{Xi}(1)$  of the Hartree method in a wide range of numbers Z. Thus, in (3.14), only the electrostatic interaction of electrons with the nucleus and with each other is taken into account, but the exchange-correlation interaction is not taken into consideration in any way. If we separate the electron part of the potential from the nucleon (nuclear) part, then, using the Poisson equation, it is possible to restore the 'realistic' density of the electron charge:

$$\rho(r) = \Delta_r V_e / 8\pi, \tag{3.15}$$

where  $\Delta_r$  is the radial part of Laplace operator,  $V_e(r) = \frac{2Z}{r} - V^G(r)V_e(r) = 2Z/r - V^G(r)$ . Further, using the exchange-correlation correction in the form (3.12), we obtain the potential of the atom:

$$V_{\rm at}(r) = V^G(r) + V_{X\alpha}(r).$$
 (3.16)

A comparison with the self-consistent calculations of Herman–Skillman potentials [4] for  $\alpha = 1$  gives good results [5–7]. For numerical calculations, it is convenient to introduce the designation  $f(r) = \exp(-\lambda r/\mu)/(1 + Ar/\mu)$ .

Then, 
$$V^G(r) = -\frac{2Z}{r}f(r)$$
.

Further, after transformations we obtain:

$$f'(r) = \lambda_{\mu} f(r) - A_{\mu} f(r), f''(r) = -(\lambda_{\mu} + A_{\mu}) f'(r) + A_{\mu}^{2} f(r), \rho(r) = -\Delta_{r} V^{G}(r)$$
$$= -Z f''(r) / 4\pi r$$

where

$$\lambda_{\mu} = \lambda/\mu, A_{\mu} = (A/\mu)(1 + Ar/\mu)^{-1}.$$

It can also be seen that the total charge of the atom is:

$$Q = \int_{0}^{\infty} \rho(r) 4\pi r^{2} dr = -\int_{0}^{\infty} Zr f''(r) dr = -Z.$$

The exchange-correlation correction in the form (3.12), which contains an implicit dependence on the charge number Z, creates great difficulties in constructing the 'crystalline' potentials of complex compounds. These difficulties can be circumvented by introducing a more complicated exchange-correlation correction (3.13) in the form:

$$V_{X\alpha\beta} = [\alpha + \beta G(\rho)]V_{XS}, \tag{3.17}$$

where 
$$\alpha = 0.67$$
,  $\beta \cong 0.003$ ,  $G(\rho) = \frac{4}{3} \left(\frac{\nabla \rho}{\rho}\right)^2 - 2\frac{\nabla^2 \rho}{\rho}$  and  $V_{XS} = -6[3\rho/8\pi]^{1/3}$ .

Thus, at the cost of introducing a new adjustable parameter, we can achieve the constancy of  $\alpha$  and  $\beta$ . To ensure a better convergence of numerical calculations, we can write:

$$V_{X\alpha\beta} = \alpha \left[ 1 + th \left( \frac{\beta}{\alpha} G(\rho) \right) \right] V_{XS},$$
 (3.18)

where analytic properties of the function th(x) are used.

Applying the previously introduced notation, we can obtain:

$$\begin{split} \nabla_{r}\rho &= Z\big(f'''-f''/r\big)/4\pi r,\\ \rho'' &= Z\big(f^{iv}-2f'''/r+2f''/r^2\big)/4\pi r,\\ \nabla^{2}\rho &= Zf^{iv}/4\pi r,\\ f''' &= -2A_{\mu}^{3}f(r)+2A_{\mu}^{2}f'(r)-\big(\lambda_{\mu}+A_{\mu}\big)f''(r),\\ f^{iv} &= 6A_{\mu}^{4}f(r)-6A_{\mu}^{3}f'(r)+3A_{\mu}^{2}f''(r)-\big(\lambda_{\mu}+A_{\mu}\big)f'''(r). \end{split}$$

Thus,  $G(\rho)$  and, consequently,  $V_{X\alpha\beta}$  can be expressed in the analytical form, which is very important for numerical simulations.

A comparison of the analytical potentials (3.16) with the self-consistent calculations of Herman–Skillman potentials [4] for  $\alpha = 1$  provides good results in a wide range of charge numbers [5–7] and is shown in Fig. 3.1.

The exchange-correlation corrections of the form  $V_{X\alpha}$  (3.12) and  $V_{X\alpha\beta}$  (3.18), which yielded close values throughout the entire range of the  $\alpha$  parameter variations, have also been thoroughly investigated. In addition, the inclusion of analytical potentials of the type (3.16) in the scheme of self-consistent calculations of atoms ensures fast convergence. The calculation efficiency is widely confirmed [2].

#### 3.3 'Crystalline' Potentials

Using the procedure for constructing the potentials of atoms and the superposition principle, we can develop a technique for calculating crystalline potentials. Moreover, for slightly correlated systems such as liquids, this procedure is as follows:

$$V_C(r) = V^G(r) + V^G(a - r),$$
 (3.19)

$$\rho_{\rm cr}(r) = \rho(r) + \rho(a - r),$$
(3.20)

$$V_{\text{exch}}(r) = -6\alpha [3\rho_{\text{cr}}(r)/8\pi]^{1/3}, \tag{3.21}$$

$$V_{\rm cr}(r) = V_C(r) + V_{\rm exch}(r), \tag{3.22}$$

where *a* is the distance to the nearest neighbouring atom smeared in the vicinity of the selected 'central' one. Following this logic, it is also possible to construct crystalline potentials which are necessary for the realization of the scattering problem in the cluster approach. Then, the Coulomb part of the potential and the electron density are obtained, as above, based on the principle of superposition of the corresponding factors of individual atoms, namely:

$$V_C(\mathbf{r}) = V^G(\mathbf{r}) + \sum_{\gamma, n_{\gamma}} V_{\gamma}^G(\mathbf{r} - \mathbf{R}_{n_{\gamma}}^{\gamma}), \tag{3.23}$$

$$\rho_{\rm cr}(\mathbf{r}) = \rho(\mathbf{r}) + \sum_{\gamma, n_{\gamma}} \rho_{\gamma} \left( \mathbf{r} - \mathbf{R}_{n_{\gamma}}^{\gamma} \right), \tag{3.24}$$

where  $\gamma$  is the type of atom and  $n_{\gamma}$  is the number of atoms neighbours.

Then the crystalline potential is calculated:

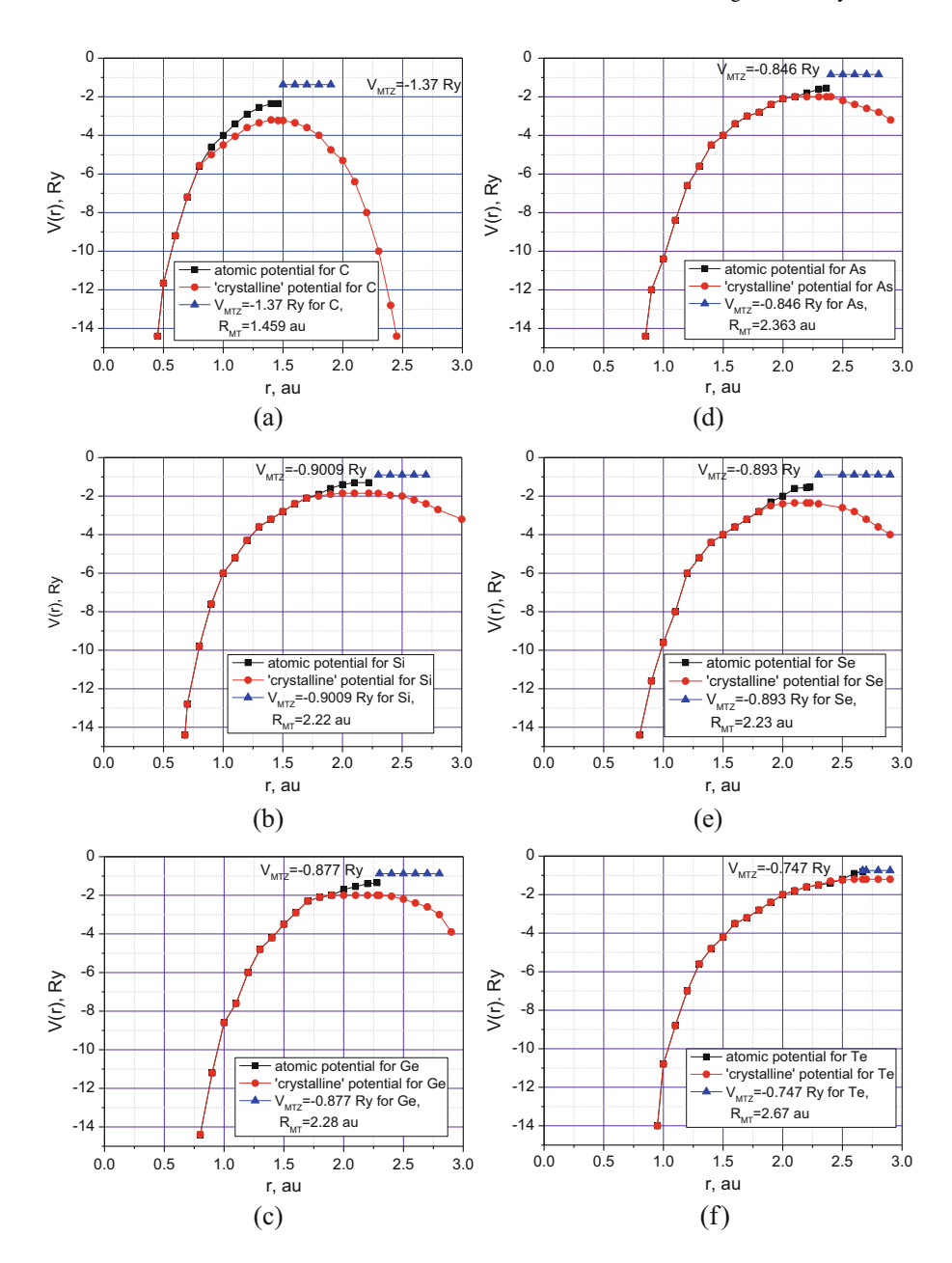


Fig. 3.1 Potentials (a, b, c, d, e, f): atomic potentials, crystalline potentials, MT-zero levels

$$V_{\rm cr}(\mathbf{r}) = V_C(\mathbf{r}) + V_{\rm exch}(\mathbf{r}), \tag{3.25}$$

where

$$V_{\rm exch}(\mathbf{r}) = -6\alpha [3\rho_{\rm cr}(\mathbf{r})/8\pi]^{1/3}.$$
 (3.26)

For binary and more complex compounds, the exchange-correlation correction  $V_{X\alpha\beta}$  (3.18) should be used. Applying the known MT-approximation of the potentials  $V_{\rm cr}$  and  $\rho_{\rm cr}$ , these functions are averaged over the surface of the MT-sphere, and then the spherically symmetric MT-potential of a single scatterer is constructed:

$$V_{\rm MT}(r) = V_{\rm cr}(r) - V_{\rm MTZ}, \tag{3.27}$$

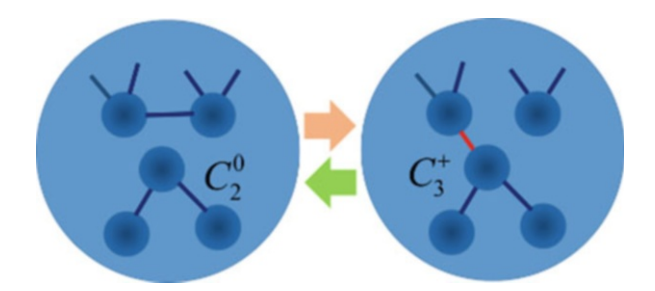
where  $V_{\rm MTZ}=-2/R_{\rm MT}$ , e.g. for monoelemental covalent materials,  $R_{\rm MT}$  is the MT-radius and  $V_{\rm MTZ}=-2\left(x1/R_{\rm MT}^A+(1-x)1/R_{\rm MT}^B\right)$  for binary materials  $A_xB_{1-x}$ , where  $R_{\rm MT}^A$  and  $R_{\rm MT}^B$  are radii of the corresponding MT-spheres [2, 11, 12].

#### 3.4 Potentials of Charged Defects

An important direction in the calculation of the electronic structure of non-regular nanosystems is the modelling of defects of various natures. However, since any defect formation is ultimately associated with a local transfer of the electron charge, the simulation itself is reduced to constructing a local defect potential which takes this transfer into account. Such a procedure is considered using the example of modelling of bonds switching in chalcogenides in the processes of photo- and radiation-stimulated transformations in the atomic structure (see Fig. 3.2). Typical applications of photoinduced structural transformations in chalcogenide glasses are presented in Table 3.1.

Chalcogenide glasses and corresponding nanosystems include group XVI chalcogen elements of the periodic table: {O}, S, Se, Te, {Po}. Chalcogenides are considered to be alloys of chalcogens and elements of groups III, IV, V, VI, e.g. As<sub>2</sub>S<sub>3</sub>, GeSe<sub>2</sub>, Ge<sub>2</sub>Sb<sub>2</sub>Te<sub>5</sub>, etc., but glass-forming materials are characterized by wide composition ranges. Atomic coordination of chalcogenide glasses is

**Fig. 3.2** Typical transformations of chalcogenide charged defects



Materials	Devices	Process
Photoresists	Vidicons	Holography
Photonic crystals	Diffractive elements DVD RW discs	Thermoplastic recording
Integral optics		Xerography

Table 3.1 Photoinduced structural transformations in chalcogenide glasses

described by the '8-N rule' (N = no. of valence electrons): chalcogens ( $\{O\}$ , S, Se) = 2 (N = 6) (Te) = 2 (3 dative), pnictogens (P, As, Sb) = 3 (N = 5), tetragens (Si, Ge) = 4 (N = 4) and halogens (Cl, Br, I) = 1 (N = 7).

In the framework of *Phillips–Thorpe constraint theory*, we can assume that a glass structure is a *continuous network* (CN) with  $r_i$  of constituent elements i, and for the average coordination number of CN  $\langle r \rangle = \sum_i x_i r_i$ , where  $x_i$  and  $r_i$  are the

mole fraction and the coordination number, respectively, referring to each species i in the glass. The *bond-stretching constraint* is  $\langle r \rangle/2$ , and the *bond-bending constraint* is  $2\langle r \rangle - 3$ . The average number of atomic constraints in a system can be expressed as  $n = \frac{\langle r \rangle}{2} + (2\langle r \rangle - 3)$ , where  $\langle r \rangle$  is the average coordination number of atoms in the system. The total number of constraints is  $n_{\text{tot}} = \frac{5\langle r \rangle}{2} - 3$ . For 3D this critical value  $\langle r_{\text{cr}} \rangle = 12/5 = 2.4$  is called the rigidity percolation threshold, because, at this composition, rigid structures percolate throughout the glass, leading to an isostatic network [13].

Fundamental reasons of photo-transformations in chalcogenides and, as a result, their high photosensitivity are as follows:

- Bandgap photons excite electrons from the top of the VB i.e. lone-pair electrons.
- Optical excitation can cause changes in weak van der Waals 'intermolecular' interactions.
- Low atomic coordination number of chalcogens favours local structural rearrangements without necessarily breaking covalent bonds.
- Similar (~octahedral 3/4-fold) coordination geometry of a-/c-phases in *telluride* glasses → ps/ns changes.

Photo- and radiation-induced changes are responsible for local structural changes in chalcogenide systems and can be explained by local nanosized defect transformations [14–16].

Street and Mott [48] proposed a model of dangling bonds, with the combination of positively and negatively charged dangling bonds  $D^+$  and  $D^-$  having, respectively, no and two spin-paired electrons, energetically favoured over the neutral dangling bond  $D^0$  with one unpaired electron. This defect-based version of the negative-U model was developed by Kastner et al. [49] for the case of a-Se, with a singly coordinated, negatively charged selenium  $(C_1^-)$  and a threefold coordinated, positively charged site  $(C_3^+)$  emerging as the most likely equilibrium defect configurations. Moreover, for the study of dangling bonds, the general negative-U model was developed by Anderson [50] and later by Karpov et al. [51] based on the

self-localization of electron (and hole) pairs (SLEP). Charged defects analysis is primary for the explanation of photo- and radiation-induced local nanosized transformations in chalcogenide systems [17–19] including corresponding nanomemory materials [20].

The idea of modelling is to correct the outer part of the non-defect electronic cloud [21]. For this purpose, s- and p-like orbitals are used:

$$\varphi_s(\mathbf{r}) = C_s \exp(-r/r_0) Y_{00}(\mathbf{r}), \tag{3.28}$$

$$\varphi_p(\mathbf{r}) = C_p \exp(-r/r_0) Y_{1m}(\mathbf{r}), \tag{3.29}$$

where  $C_s$  and  $C_p$  are the normalization coefficients,  $r_0$  is the characteristic covalent radius and m = -1,0,1. Then, the radial densities of the electron charge are represented as:

$$\rho_s(r) = C_s' \exp\left(\frac{-2r}{r_0}\right),\tag{3.30}$$

$$\rho_p(r) = C_p' r^2 \exp\left(\frac{-2r}{r_0}\right),\tag{3.31}$$

where  $C_s' = 4/r_0^3$  and  $C_p' = 4/3r_0^5$  are calculated using the normalization condition  $\int_{-\infty}^{\infty} \rho(r) 4\pi r^2 dr = 1.$ 

The corresponding contributions to the potentials are calculated as:

$$V(r) = \frac{2}{r} \int_{0}^{r} \rho(r') 4\pi r'^{2} dr', \qquad (3.32)$$

i.e.

$$V_{s}(r) = -\frac{2}{r} \left\{ 1 - \exp\left(\frac{-2r}{r_{0}}\right) \left[ \frac{1}{2!} \left(\frac{2r}{r_{0}}\right)^{2} + \frac{1}{1!} \left(\frac{2r}{r_{0}}\right)^{1} + \frac{1}{0!} \left(\frac{2r}{r_{0}}\right)^{0} \right] \right\}, \quad (3.33)$$

$$V_{p}(r) = -\frac{2}{r} \left\{ 1 - \exp\left(\frac{-2r}{r_{0}}\right) \times \left[ \frac{1}{4!} \left(\frac{2r}{r_{0}}\right)^{4} + \frac{1}{3!} \left(\frac{2r}{r_{0}}\right)^{3} + \frac{1}{2!} \left(\frac{2r}{r_{0}}\right)^{2} + \frac{1}{1!} \left(\frac{2r}{r_{0}}\right)^{1} + \frac{1}{0!} \left(\frac{2r}{r_{0}}\right)^{0} \right] \right\}. \quad (3.34)$$

Then, finally, the Coulomb part of the defect potential can be presented in the form:

$$V_C(r) = V^G(r) - n_s V_s(r) - n_p V_p(r), (3.35)$$

where  $n_s$  and  $n_p$  (( $\geq$ ,  $\leq$ 0)) are numbers of added or removed s- and p-electrons. Further, the potential (3.35) is included into the general scheme for building potentials. A more general approach related to the potentials that do not possess spherical symmetry is considered in [21, 22], where some aspects of the generalization of the MT-approximation are studied.

### 3.5 Electronic Structure and Total Energy: Atoms, Molecules and Nanoclusters

The problem of calculating the total energy of a large condensed system (crystal, disordered material) is one of the oldest in theory. Usually, this problem is reduced to the calculation of the binding energy of a large condensed system, namely, the cohesive energy  $E_{\rm coh} = E_{\rm tot}^{\rm at} - E_{\rm tot}^{\rm sys}/N$ , where  $E_{\rm tot}^{\rm at}$  is the total energy of its atoms and  $E_{\rm tot}^{\rm sys}$  is the total energy of the system under consideration. In this connection, it is possible to single out problems of calculation of the total energy of atoms, molecules, macromolecules, nanoclusters, nanocrystals, large non-regular disordered condensed systems and, finally, crystals. Each of these problems has its own peculiarities.

Note that the total energy of atoms arises as a natural result of self-consistent calculations of their electronic spectra [1]. It is practically impossible to realize this calculation self-consistently of the total energy for large quantum systems. At the same time, the calculation of the total energy is very important, because any change of states in the electron and phonon subsystems of a large quantum system (crystal, disordered solid) leads to a change in the value of its total energy. Local and total phase transitions, in particular, are also accompanied by a change in the total energy, and its estimates are of fundamental importance for understanding the features of structural and other transformations under the influence of radiation and electromagnetic radiation on functional materials. Local phase transitions, for example, take place in the processes of optical recording of information in nanocrystalline and amorphous semiconductor films [2, 23, 24].

The total energy, as a fundamental characteristic, comprehensively characterizes the functional material as a physical object with all possible elementary excitations in it, including, as a rule, many problems of exciting the electronic and phonon subsystems, as well as their interaction [3, 25, 26]. The most natural way to estimate the total energy of large quantum system is apparently based on the formalism of the functional electron charge density  $\rho(\mathbf{r})$  [27, 28]. The total energy as a density functional for the ground state of a multielectron system in the presence of an external potential can be presented in the form:

$$E_{\text{tot}}[V_{\text{EXT}}, \rho] = E_{\text{ee}}[V_{\text{EXT}}, \rho] = T[\rho] + \int d\mathbf{r} V_{\text{EXT}}(\mathbf{r}) \rho(\mathbf{r}) + \frac{1}{2} \int d\mathbf{r} \int d\mathbf{r}' \frac{\rho(\mathbf{r})\rho(\mathbf{r}')}{|\mathbf{r} - \mathbf{r}'|} + E_{\text{XC}}[\rho],$$
(3.36)

where the kinetic energy, the energy of interaction of the electron gas with the external potential, the energy of the electron–electron interaction and the exchange-correlation energy are summed up. There are three main problems of this general formula (3.36) using:

- 1. The finding of  $\rho(\mathbf{r})$  that minimizes the functional  $E_{\text{tot}}[V_{\text{EXT}}, \rho]$
- 2. The estimation of the kinetic energy functional  $T[\rho(\mathbf{r})]$
- 3. The estimation of the exchange-correlation energy functional

A consistent but very laborious way of calculation was proposed by Kohn and Sham [27, 28]. On the basis of the solution of a system of one-electron equations for varying wave functions of fictitious noninteracting electrons:

$$\{-\nabla^2 + V_{KS}[\rho(\mathbf{r})]\}\varphi_i(\mathbf{r}) = \varepsilon_i\varphi_i(\mathbf{r}), \tag{3.37}$$

where  $\varphi_j$  and  $\varepsilon_j$  are one-particle eigenfunctions and eigenvalues and  $V_{\rm KS}[\rho(\mathbf{r})]$  is the integrally differential of potential:

$$V_{\text{KS}}[\rho(\mathbf{r})] = V_{\text{EXT}}(\mathbf{r}) + \int d\mathbf{r}' \frac{\rho(\mathbf{r}')}{|\mathbf{r} - \mathbf{r}'|} - \frac{\partial E_{xc}[\rho(\mathbf{r}')]}{\partial \rho(\mathbf{r})} = V_{\text{EXT}}(\mathbf{r}) + V_{C}[\rho(\mathbf{r})] + V_{\text{XC}}[\rho(\mathbf{r})],$$
(3.38)

where  $V_C$  is the Coulomb potential and  $V_{\rm XC}$  is the exchange-correlation potential. Then,  $\rho({\bf r})$  is determined in a self-consistent manner similar to the procedure in the Hartree–Fock–Slater method. The kinetic energy of the many-electron system is calculated as:

$$T[\rho] = \sum_{j} \langle \varphi_{j} | \varepsilon_{j} - V_{KS}[\rho] | \varphi_{j} \rangle. \tag{3.39}$$

Further, the local density approximation is usually used, consisting of a slowly varying  $\rho(\mathbf{r})$ ; hence, we can assume:

$$E_{\rm XC}[\rho] \cong \int d\mathbf{r} \rho(\mathbf{r}) \varepsilon_{\rm XC}[\rho(\mathbf{r})],$$
 (3.40)

where  $\varepsilon_{\rm XC}[\rho({\bf r})]$  is the exchange-correlation energy per electron of density $\rho({\bf r})$  of a homogeneous electron gas. The corresponding exchange-correlation potential is then represented in the form of  $V_{\rm XC} = \partial E_{\rm XC}/\partial \rho$ .

We can meet various representations for  $E_{\rm XC}$ . In this case, we only note the way of finding in the form:

$$\varepsilon_{\rm XC} = \varepsilon_{\rm X} + \varepsilon_{\rm C},$$
 (3.41)

taking into account:

$$\varepsilon_X = -0.9164/r_S,\tag{3.42}$$

$$\varepsilon_C = \begin{cases} -0.2846/(1 + 1.9529r_S^{1/2} + 0.3334r_S, & \text{if } r_S \ge I, \\ -0.0960 + 0.0622 & \text{ln } r_S - 0.0232r_S + 0.004r_S & \text{ln } r_S, & \text{if } r_S < I, \end{cases}$$
(3.43)

where  $r_S$  is Wigner radius. Then, the exchange-correlation potential is obtained in the form:

$$V_{\rm XC} = \varepsilon_{\rm XC} - \frac{r_S}{3} \frac{d\varepsilon_{\rm XC}}{dr_S}.$$
 (3.44)

The Eqs. (3.41, 3.42 and 3.43) make it possible to distinguish 'pure' exchange and correlation and can be included in the simulation design scheme. However, if we use Slater's statistical approximation, we will get:

$$\varepsilon_{\rm XC} = \frac{3}{4}\rho(\mathbf{r})V_{\rm XC}(\mathbf{r}),\tag{3.45}$$

where:

$$V_{\rm XC} = \alpha V_{\rm XS} = V_{X\alpha} = -6\alpha (3\rho(\mathbf{r})/8\pi)^{1/3}, \ (2/3 \le \alpha \le 1).$$

Consequently, in (3.45), the exchange and correlation are not distinguishable. This feature, in a certain sense, is the lack of statistical approximation.

The model of the atom in the statistical approximation of the distribution of the electron charge is based on the fact that the electron subsystem of an atom is considered in the field of its nucleus as an 'electron liquid', i.e. as an electron gas with the 'included' exchange-correlation interaction.

The approximation, however, is that the electronic subsystem is considered locally free. This means that at each point in space  $\mathbf{r}$  the electron of the subsystem is regarded as a plane electron wave. Then the total energy of the atom can be presented as a function of the electron charge density  $\rho(\mathbf{r})$ :

$$E[\rho(\mathbf{r})] = \int \frac{3}{5} (3\pi^2)^{2/3} \rho^{5/3}(\mathbf{r}) d\mathbf{r} + \int \rho(\mathbf{r}) v_n(\mathbf{r}) d\mathbf{r} + \frac{1}{2} \int \rho(\mathbf{r}) v_e(\mathbf{r}) d\mathbf{r} + \int \rho(\mathbf{r}) v_x[\rho(\mathbf{r})] d\mathbf{r},$$
(3.46)

where  $v_n$ ,  $v_e$  and  $v_x$  are the corresponding electron–nucleon, electron–electron and exchange-correlation interaction potentials. Assuming that, on the average, the charge of an electron of an atom is distributed in a spherically symmetric manner with respect to the nucleus is possible to represent (3.46) in the form:

Atom	$E_{\text{tot}}, Ry$	$E_{\text{tot}}^{\text{XF}}, Ry [1, 29]$
Ne	-264.904	-257.067
Si	-571.258	-577.638
P	-679.411	-681.297
S	-786.024	-794.923
Аг	-1036.516	-1053.635
Ge	-4188.585	-4150.718
As	-4712.566	-4468.256
Se	-5019.476	-4799.731
Xe	-5563.094	-5504.111

**Table 3.2** Total energies of the ground states of atoms

$$E[\rho(r)] = \int \left[ \frac{3}{5} (3\pi^2)^{2/3} \rho^{5/3}(r) + \frac{1}{2} \rho(r) V_e(r) - \rho(r) \frac{2Z}{r} - \frac{9}{2} \alpha \left( \frac{3}{8\pi} \right)^{1/3} \rho^{4/3}(r) \right] 4\pi r^2 dr.$$
(3.47)

Table 3.2 shows the energies of the ground states of atoms calculated according to formula (3.47) (see [22, 23]) in comparison with the results of self-consistent calculations [1, 29]. In [22], the detailed numerical studies of various contributions to the total energy are given,  $E_{\text{tot}} = T_e + U_{\text{en}} + U_{\text{ee}} + U_{\text{xc}}$ , where  $T_e$  is the total kinetic energy of the electron charge,  $U_{\text{en}}$  is the energy of interaction of the electron gas with the nucleus,  $U_{\text{ee}}$  is the energy of the interelectronic interaction and  $U_{\text{xc}}$  is the energy of the exchange-correlation interaction.

Note that the discrepancy of evaluations by the analytical relationship (3.47) of  $E_{\rm tot}$  with self-consistent calculations does not exceed 5%. This procedure can also be used to calculate the total energy of more complex systems (e.g. molecules, nanoclusters, etc.). The necessary condition in this case is the construction of realistic electron charge density functions  $\rho(\mathbf{r})$  and one-electron potentials of the above-mentioned systems  $V(\mathbf{r})$  based on the superposition principle. The ability to calculate the total energy of nanoclusters is fundamental. For disordered systems, this is extremely important, since such systems are represented by a set of nanoclusters which are close in their properties, geometry and morphology. The size of such a nanocluster is estimated by the characteristic order parameter L. In fact, this is a quasi-translational 'symmetry' with a 'period'.

As for complex composite systems (e.g. binary compounds  $A_xB_{1-x}$ ), such large clusters are formed of basic structural units or small (basic) clusters characterizing the system at the level of short-range order.

This approach in consideration of the atomic structure was used in calculations of the density of electronic states  $As_xSe_{1-x}$ ,  $Sb_xSe_{1-x}$  and  $As_xS_{1-x}$  [14, 30–32]. The calculations of the total energy are performed in different ways of computing the electronic structure of polyatomic complexes, since the total energy is a self-consistent parameter [1]. However, in most cases the calculation approaches use the concept of the density functional [33]. The difference is only

in the value of the electronic charge, which is included in the core part, and the remainder of it, which is responsible for the interatomic interaction.

To calculate the total energy of the cluster:

$$E^{\rm CL} = E_{\rm ion} + E_{\rm ee}[V_{\rm ext}, \rho], \tag{3.48}$$

where  $E_{\text{ion}}$  and  $E_{\text{ee}}$  are the internuclear and electronic parts of the total energy; it is necessary to use cluster sums for the electron density:

$$\rho^{\mathrm{CL}}(\mathbf{r}, \mathbf{R}_1, \dots \mathbf{R}_N) = \sum_{i} \rho^{i}(\mathbf{r} - \mathbf{R}_i), \tag{3.49}$$

and potentials:

$$V_{\text{EXT}}^{\text{CL}}(\mathbf{r}, \mathbf{R}_1, \dots \mathbf{R}_N) = 2 \sum_{i} \frac{Z_i}{|\mathbf{r} - \mathbf{R}_i|},$$
(3.50)

$$V_{\text{ee}}^{\text{CL}}(\mathbf{r}, \mathbf{R}_1, \dots \mathbf{R}_N) = \sum_{i} V_e^{i}(\mathbf{r} - \mathbf{R}_i). \tag{3.51}$$

Taking into account that all significant changes in the system are related to the outer ('core') part of the electron cloud, it is advisable to introduce a certain version of the MT-approximation into the calculation scheme. Cutting out the 'core parts' of  $\rho^{\rm CL}$ ,  $V_{\rm EXT}^{\rm CL}$  and  $V_{\rm ee}^{\rm CL}$  by the 'MT-spheres', and considering them spherically symmetric inside the 'MT-spheres', we get:

$$E^{\text{CL}} = \sum_{i} E_{i}^{\text{MT}} + \sum_{i \neq i} \frac{Z_{i}' Z_{j}'}{|\mathbf{R}_{i} - \mathbf{R}_{j}|} + T_{e}' + U_{\text{en}}' + U_{\text{ee}}' + U_{\text{xc}}',$$
(3.52)

where  $T_e'$ ,  $U'_{\rm en}$ ,  $U'_{\rm ee}$  and  $U'_{\rm xc}$  are analogues of corresponding quantities  $T_e$ ,  $U_{\rm en}$ ,  $U_{\rm ee}$  and  $U_{\rm xc}$ .

However, it must be taken into account that in this case the integration of functions without spherical symmetry over the interstitial space is performed, i.e. triple integrals of the type  $\Omega^{-1}\int F(\vec{r})d\vec{r}$  are computed.  $E[\rho(\mathbf{r})]$  is found according to the procedure (3.47) when integrating over the volume of the 'MT-sphere'.

The excess charge of the core  $Z'=Z-\int_0^{R_{\rm MT}}\overline{\rho^{\rm CL}({\bf r})}4\pi r^2 dr$ , where  $\overline{\rho^{\rm CL}({\bf r})}$  is the density of the electron charge, averaged over the spherical layers. In this case, the radius  $R_{\rm MT}$  may not coincide with the analogous one for the potentials [2.5–7] because Z should be equal to the number of valence electrons of a given atom.

The total energy of the whole system can be considered as  $E_{\mathrm{tot}}^{\mathrm{sys}} \cong \sum_{i} E_{\mathrm{tot},i}^{\mathrm{CL}} + E_{\mathrm{rest}}$ . Especially when it comes to local (intra-cluster) changes  $\Delta E_{\mathrm{tot}}^{\mathrm{sys}} \cong \Delta \sum_{i} E_{\mathrm{tot},i}^{\mathrm{CL}}$  in the total energy of the non-perturbing 'rest medium'.

### 3.6 Interatomic Interaction Potentials and Force Calculations

The calculation of the dynamic properties of solids is based on the knowledge of the forces  $\mathbf{F}_i$  acting on the corresponding ions with coordinates  $\mathbf{R}_i$ .

Then, for the cluster we have:

$$\mathbf{F}_{i} = -\nabla_{\mathbf{R}_{i}} E^{\mathrm{CL}} = 2 \sum_{i \neq j} \frac{Z_{i}^{\prime} Z_{j}^{\prime} (\mathbf{R}_{i} - \mathbf{R}_{j})}{|\mathbf{R}_{i} - \mathbf{R}_{j}|} - \nabla_{\mathbf{R}_{i}} E_{\mathrm{ee}} = \mathbf{F}_{i}^{\mathrm{ion}} + \mathbf{F}_{i}^{\mathrm{el}}.$$
(3.54)

Significant problems arise with the evaluation of the second term, which has a complex structure, since according to (3.49, 3.50 and 3.51)  $\rho^{\rm CL}$ ,  $V_{\rm EXT}^{\rm CL}$  and  $V_{\rm ee}^{\rm CL}$  are functions of the positions of the ions  ${\bf R}_i$ . Consequently, each value of the number  $T_e^{'}$ ,  $U_{\rm en}^{'}$ ,  $U_{\rm en}^{'}$ ,  $U_{\rm ee}^{'}$  and  $U_{\rm xc}^{'}$  will contain their gradients  $\nabla_{{\bf R}_i}(...)$ . Then it is possible to write:

$$\mathbf{F}_{i}^{\text{el}} = -\int d\mathbf{r} \frac{\partial V_{\text{EXT}}(\mathbf{r}, \mathbf{R})}{\partial \mathbf{R}_{i}} \rho(\mathbf{r}, \mathbf{R}) - \int d\mathbf{r} V_{\text{EXT}}(\mathbf{r}, \mathbf{R}) \frac{\partial \rho(\mathbf{r}, \mathbf{R})}{\partial \mathbf{R}_{i}} = -\int d\mathbf{r} \frac{\partial V_{\text{EXT}}(\mathbf{r}, \mathbf{R})}{\partial \mathbf{R}_{i}} \rho(\mathbf{r}, \mathbf{R}) - \int d\mathbf{r} \frac{\delta E_{\text{ee}}}{\delta \rho} \frac{\partial \rho(\mathbf{r}, \mathbf{R})}{\partial \mathbf{R}_{i}} = \mathbf{F}_{i}^{\text{el}(1)} + \mathbf{F}_{i}^{\text{el}(2)},$$
(3.55)

where  $V_{\text{EXT}}(\mathbf{r}, \mathbf{R})$  is the 'external' 'crystalline' potential and  $\mathbf{R} = {\mathbf{R}_i}$  is a set of coordinates of atoms.

Forces in the electron-ion system, which do not contain density gradients of the type  $\nabla_{\mathbf{R}_i}\rho$ , together represent the so-called Hellmann–Feynman force  $\mathbf{F}_i^{\mathrm{HF}} = \mathbf{F}_i^{\mathrm{ion}} + \mathbf{F}_i^{\mathrm{el}(1)}$ , which takes into account the classical electrostatic interaction and is determined only by the potential gradients. In our case:

$$\mathbf{F}_{i}^{\text{el}(1)} = -\int \frac{\partial}{\partial \mathbf{R}_{i}} \sum_{i \neq j} \frac{2Z_{i}}{|\mathbf{R}_{i} - \mathbf{R}_{j}|} \rho^{\text{CL}}(\mathbf{r}, \mathbf{R}_{1}, \dots \mathbf{R}_{N}) d\mathbf{r} + \frac{1}{2} \int \frac{\partial}{\partial \mathbf{R}_{i}} V_{\text{ee}}^{\text{CL}}(\mathbf{r}, \mathbf{R}_{1}, \dots \mathbf{R}_{N}) d\mathbf{r},$$
(3.56)

where analytical functions are used. The force  $\mathbf{F}_i^{\text{el}(2)}$  that is usually found from the Schrödinger equation by the variation Kohn–Sham procedure [27, 28] can also be obtained directly using analytical functions. In a simpler version of the evaluation of force characteristics, and following the general rules of potential modelling, we can write down the potential of the pair interaction:

$$\Phi(R) = \int \rho_1(r) V_2(R - r) 4\pi r^2 dr, \qquad (3.57)$$

and the interaction force:

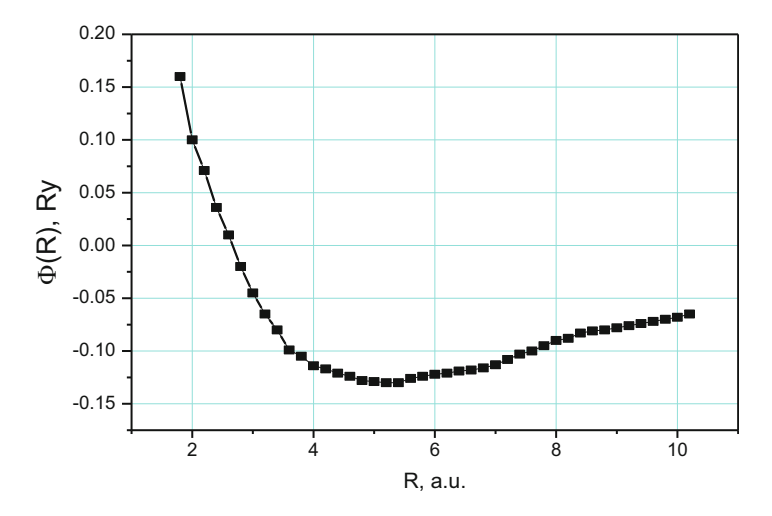


Fig. 3.3 Model potential of pair interaction of Se atoms

$$F(R) = -d\Phi/dR = \int \rho_1(r)[dV_2(R-r)/dR]4\pi r^2 dr,$$
 (3.58)

where  $\rho_1(r)$  is the density of the electron charge of atom 1 (central) and  $V_2(R-r)$  is the potential of atom 2 or 'quasi-atom' 2, which, in fact, expresses the potential of the 'rest medium' (i.e. crystalline potential) [15]. Figure 3.3 shows the model potential of the pair interaction for Se calculated on the basis of (3.57).

## 3.7 Multiple Scattering Theory and Effective Media Approach

The absence of a structural periodicity of disordered materials makes it difficult to describe their electronic structure in general. The main difficulty is to set the boundary conditions that would be adequate for physical conditions with a limited fragment of the structure, namely, a cluster. In fact, the only reasonable possibility in this case is to use various modifications of boundary conditions of the 'effective medium' type, which is the carrier of the disorder property of matter in the far field. The features of the near and middle orders, as a rule, are taken into account in detail.

The experience of numerical calculations shows that a significant increase in the size of the considered fragment of the structure, at which boundary conditions can be neglected in general, is not effective and requires a lot of computer time. In addition, macroscopic physical quantities in disordered materials do not depend on the detailed configurations of atoms and are obtained by averaging over the set of possible configurations. The averaged information about the structure is contained in paired and many-particle distribution functions. This fact is a formal basis for

statistical averaging of other physical quantities, and the calculation of large structural fragments has no practical meaning.

Another aspect of the problem is the formal (i.e. mathematical) implementation of the cluster approach using any version of the concept of an effective medium.

In this sense, there are two basic possibilities: (1) the *tight-binding approxima*tion using one or another standard basic set of wave functions and (2) the *nearly* free electron approximation, which is usually based on the scattering theory and uses the Bessel functions as a key set.

#### 3.7.1 Methods of Electronic Structure Calculation of Nonregular Condensed Materials

As it has already been mentioned, the problem of effectively calculating the electronic properties of structurally disordered substances can be solved in different ways of approximation of the effective medium, which differ from each other by the method of approximate averaging of the total perturbation series for one-electron Green's functions (see, e.g. [34]). Thus, for example, in the stationary case, when the system is characterized by a Hamiltonian:

$$H = H_0 + H_1, (3.59)$$

where  $H_0$  is the Hamiltonian of non-perturbed system,  $H_1$  is the perturbation and the corresponding Green's functions are given by the resolvents:

$$G_0(z) = (z - H_0)^{-1},$$
 (3.60)

$$G(z) = (z - H)^{-1},$$
 (3.61)

and the perturbation series for G(z) is as follows:

$$G = G_0 + G_0 H_1 G_0 + G_0 H_1 G_0 H_1 G_0 + \dots = G_0 + G_0 H_1 G.$$
(3.62)

Next, we introduce the transition T-matrix T(z), in which all perturbation effects  $H_1$  are automatically taken into account, that is:

$$H_1G = TG_0,$$
 (3.63)

which yields from (3.62):

$$G = G_0 + G_0 TG_0. (3.64)$$

Naturally, the introduction of T(z) itself does not solve the problem of the spectrum of the perturbed system but only shifts the emphasis in this problem and allows us to rewrite a number of perturbations (3.62) in the form:

$$T = H_1 + H_1 GT. (3.65)$$

Further, taking into account a specific nature of the disordered system, the configurational averaging of the Green's function in (3.64) is performed. Details of the averaging procedure are determined by the properties of the disordered system itself. In accordance with (3.62) and (3.64), the following averaging possibilities arise:

$$\langle G \rangle = G_0 + G_0 \langle H_1 G \rangle \tag{3.66}$$

and

$$\langle G \rangle = G_0 + G_0 \langle T \rangle G_0. \tag{3.67}$$

The assumption  $\langle H_1G \rangle \cong \langle H_1 \rangle \langle G \rangle$  in (3.66) leads to the so-called virtual crystal approximation.

In the case of  $\langle H_1 \rangle = \varepsilon$ , we obtain:

$$\langle G(E) \rangle = (E - H_0 - \varepsilon)^{-1} = (E - \langle H \rangle)^{-1}. \tag{3.68}$$

Actually,  $\langle G(H) \rangle$  is calculated as  $\langle G(\langle H \rangle) \rangle$  and only leads to a shift of the energy scale by  $\varepsilon$ . This shift can be eliminated by selecting  $H_0 = \langle H \rangle$  and  $H_1 = H - \langle H \rangle$ . Then, we obtain  $\langle G \rangle = G_0$ .

The possibility associated with averaging, according to (3.67), considers  $T = f(\{t_m\})$  as a function of the individual T-matrices of the individual nodes m. Then, if we assume:

$$\langle T \rangle = f(\langle t_m \rangle), \tag{3.69}$$

we get the *average T-matrix approximation*. In this case, the shift of the spectrum occurs on a complex energy-dependent quantity, i.e. similarly to (3.68), we have:

$$\langle G(E) \rangle = (E - H_0 - \Sigma(E))^{-1},$$
 (3.70)

where, for example, in the case of a single-site approximation, we obtain:

$$\Sigma = \frac{\langle t_{m} \rangle}{1 + \langle t_{m} \rangle G_{0}(m, m)},\tag{3.71}$$

More consistently, the concept of an effective medium is carried out in the coherent potential approximation (CPA), where an unknown effective Hamiltonian  $H_e$  of some effective medium with unknown complex energy-dependent eigenvalues  $\Sigma$  is immediately introduced. Then, in the expansion (3.64), instead, we use the effective Green's function  $G_e = (E - H_e)^{-1}$ . Then

$$G = G_e + G_e T' G_e, \tag{3.72}$$

where

$$T' = H_1' + H_1' G_e T', (3.73)$$

$$H_1' \equiv H - H_e. \tag{3.74}$$

Following the well-known definitions, the Green's function averaged over the configuration is calculated as:

$$\langle G(z) \rangle = \left\langle (z - H)^{-1} \right\rangle = \left( z - H_0 - \sum_{z} (z) \right)^{-1}.$$
 (3.75)

Specify further the definition of the Hamiltonian of the system in the following way:

$$H = (H_0 + V_e(z)) + (V - V_e(z)) = H_e + H_1', \tag{3.76}$$

where V is the potential of the then studied material and  $V_e(z)$  is the energy-dependent effective potential. By averaging in (3.72), we obtain:

$$\langle G(z) \rangle = G_e + G_e \langle T' \rangle G_e,$$
 (3.77)

$$\sum (z) = z - H_0 - \left[ \langle G(z) \rangle \right]^{-1} = V_e + \langle T' \rangle (1 + G_e \langle T' \rangle)^{-1}, \tag{3.78}$$

provided:

$$\langle T(z)\rangle = 0, (3.79)$$

allows finding  $\Sigma(z)$ . The condition (3.79) implies the *coherent potential approximation* (CPA), which under the given conditions is the simplest and is equivalent to the choice  $\langle G \rangle = G_e$ .

Table 3.3 [22] presents the main calculation methods associated with the concept of an effective medium.

Moreover, a virtual crystal approximation might not be totally reliable, because in this case the role of the effective medium is fulfilled simply by the real averaged potential. The moment and the recursive methods are reduced to the calculation of G(z) and the partial densities of different groups of atoms in the system, which is equivalent to the G(z) moment expansion in the form of the density of states of different orders or continued fractions.

The problem of these methods is the convergence of the expansions. The unreasonable breakdown of such expansions leads to unphysical results. An effective medium is not explicitly present here too. As a rule, these approximations are considered in the tight-binding formalism. Here, the long-standing tradition in the band calculations of crystals is affected. Another direction, based on the concept of nearly free electrons, is usually based on the previously mentioned MT-model of scattering potentials. The spherical symmetry of such potentials is a strong simplification of reality, which gives quite good results in many cases.

Approximation	Contributors
Quasi-crystalline approximation – QCA	M Lax (1951, 1952)
	J M Ziman (1966)
	F Cyrot-Lackmann (1966)
Self-consistent quasi-crystalline approximation – SQCA	B L Gyorffy (1970)
	M Watable (1971)
	J Korringa, R L Mills (1972)
Self-consistent single-site approximation – SSSA	L Schwartz, N Ehrenreich (1917)
	Y Ishida, F Yonezawa (1973)
	B Movaghar et al. (1974)
Coherent potential approximation – CPA	P Soven (1967) F Yonezawa (1968)
Effective medium approximation – EMA	L Roth (1974)

**Table 3.3** Methods of electronic structure calculations using effective medium concepts

However, there are also approaches that generalize the MT-model and correct the spherical symmetry of the potentials by taking into account the effects of asymmetry [22–24]. Table 3.4 presents some methods for calculating the electronic structure using the MT-approximation of potentials. These methods are based on the well-known formalism of the KKR method (Korringa–Kohn–Rostoker) [35]. There is also a synthetic direction that combines the advantages of the strong-coupling approximation and MT-model representations (the MTO method of localized MT-orbitals – LMTO) [36].

### 3.7.2 Non-regular Condensed Medium: 'Liquid Metal' Model

The simplest idea about a disordered solid is to treat the latter as an ensemble of non-regularly located atomic spheres. It is clear that such a system will be characterized mainly by a pair function of the distribution of atoms. Correlation functions of a higher order have not a decisive significance. Such a model treats a non-regular disordered solid as a liquid [2, 5–7]. It can be a good model for metal and semiconductor metals and, in some cases, glasses of high homogeneity. The developed cluster approach [2, 6, 7] in the case of considering the electronic properties of the aforementioned type of condensed matter, leads to a study of the behaviour of the trial electron wave in the system 'monatomic cluster + rest medium' (Fig. 3.4a). In this case, the potential of a single scatterer, enclosed in a cluster volume, takes into account the averaging of the nearest environment from the first coordination sphere. Within the framework of this model, the influence of the nearest neighbour located at the distance *a* is taken into account. Thus, the potential of a single bond is constructed. This potential plays the role of the crystalline potential of the material being modelled.

Approximation	Objects	Contributors
Quasi-crystalline approximation	Liquid metals	J M Ziman (1966) J Lloyd (1967)
Quasi-crystalline approximation	Transition metals	P W Andersen, W L McMillan (1967)
Self-consistent single-site approximation	Disordered alloys Cu-Ni	L Schwartz, H Ehrenreich (1971)
Concept of finite clusters	Amorphous C, Si, Ge	J Keller (1971) T C McGill, J Klima (1972)
Modified quasi-crystalline approximation	Disordered metal substitutional alloys, liquid metals	L Schwartz et al., (1975)
Self-consistent single-site approximation	Liquid metals	J Bethel, J L Beeby (1977)
Single-site approximation of effective medium	Liquid metals	W John, W Keller (1977)
Coherent potential approximation on the basis of the concept of finite clusters	Amorphous Si	S Yoshino, M Inoue, M Oka- zaki (1975)
Coherent potential approximation on the basis of the concept of finite clusters	Amorphous semiconductors, Si, Ge, As, Te, Se, Sb, binary chalcogenides, nanocarbon, nano-Si, nano-Se	Yu Shunin (1981–2014)

Table 3.4 Methods of electronic structure calculations using MT-approximation

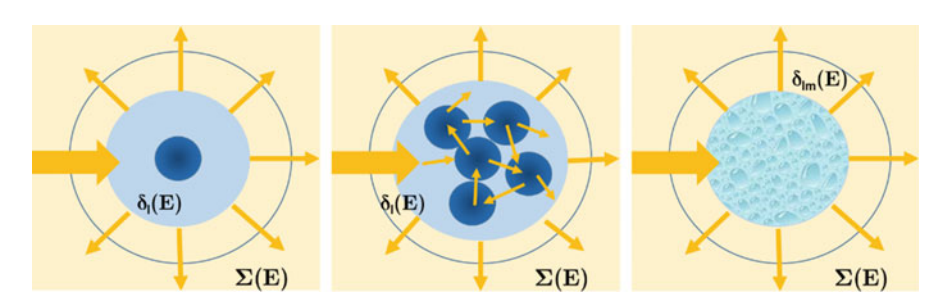
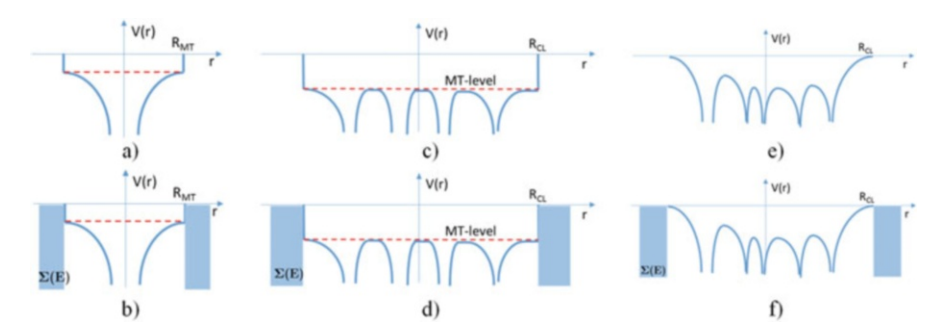


Fig. 3.4 The general scheme of the calculation method for the electronic structure based on the theory of multiple scattering and the coherent potential approximation of an atomic cluster as a group of MT-potentials embedded into effective medium; (a) 'liquid metal' model; (b) a polyatomic cluster of predefined atomic structure; (c) a polyatomic cluster with a potential function of a general form.  $\Sigma(E)$  is the coherent potential of an effective medium

The next step is based on the crystalline potential of the MT-approximation, according to (3.27); also see Fig. 3.5a–f. The radius of the MT-sphere is chosen equal to a half of the distance to the nearest neighbour [1–3, 5].

The potential (3.27) should be used for the numerical integration of the radial Schrödinger equation (see, e.g. [37]):



**Fig. 3.5** Potential models in the scattering problem for electronic structure calculations of various non-regular disordered materials: (a) MT-potential in vacuum; (b) a group of MT-potentials in vacuum; (c) a general potential in vacuum; (d) a cluster with MT-potential in the effective medium; (e) a cluster of MT-potentials in the efficient medium; (f) a cluster with potential of general form in the effective medium.  $R_{\rm MT}$  is the radius of the MT-potential;  $R_{\rm CL}$  is the radius of the cluster.

$$\frac{1}{r^2} \frac{d}{dr} \left( r^2 \frac{dR_l}{dr} \right) + \left[ \kappa^2 - \frac{l(l+1)}{r^2} - V(r) \right] R_l = 0$$
 (3.80)

and the calculation of logarithmic derivatives  $\gamma_l = \frac{R'_l(r)}{R_l(r)}\Big|_{R_{\rm MT}}$ , where  $R_l(r)$  are the radial wave functions. Then, based on the known relationship, phase shifts  $\delta$  are

radial wave functions. Then, based on the known relationship, phase shifts  $\delta_l$  are calculated [37]:

$$tg\,\delta_l = \frac{\kappa j_l'(\kappa R_{\rm MT}) - \gamma_l j_l(\kappa R_{\rm MT})}{\kappa n_l'(\kappa R_{\rm MT}) - \gamma_l n_l(\kappa R_{\rm MT})},$$

where  $j_l(\kappa r)$  and  $n_l(\kappa r)$  are the Bessel and Neumann functions,  $\kappa = \sqrt{E}$ .

The numerical integration of the Schrödinger Eq. (3.80) was carried out by the Runge–Kutta method. The peculiarity of the algorithm is the fact that the integration interval  $(0, R_{\text{MT}})$  is divided into two parts. For the small r in the neighbourhood of the singularity of the atomic potential, the solution of (3.80) is sought in the form  $R_l = r^l f(r)$ , and the equation of the function f(r) has the form:

$$f'' + \frac{2}{r}(l+1)f' + \left[\kappa^2 - V(r)\right]f = 0.$$
 (3.81)

The solution of (3.81) must be regular near the singularity of the potentials. For large r, regions of a weak potential change, the Eq. (3.80) itself is integrated. The solutions in these two regions are sewn together for a small r. The text of the numerical integration programme for the Schrödinger equation, as well as the entire software package for calculation of logarithmic derivatives  $\gamma_l$  and phase shifts  $\delta_l$  (see, also, Fig. 3.6), is presented in [38–40].

Further, taking into account the spherical symmetry of the potentials (3.27), the radial part of the Green's function is represented in the form:

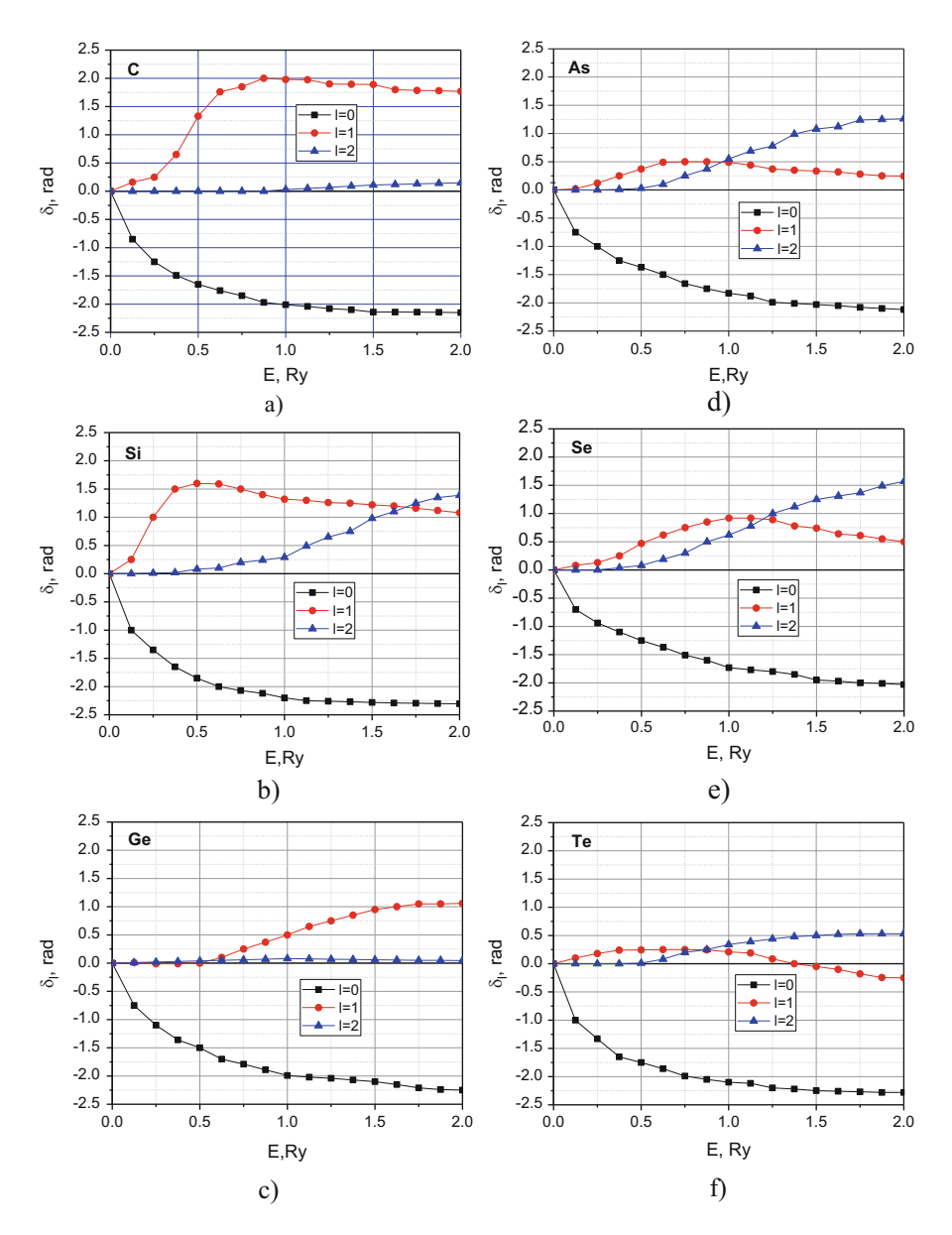


Fig. 3.6 Calculated phase shifts for C, Si, Ge, As, Se and Te scatterers

$$G_l(r, r') = kF_l(kr_>)J_l(kr_<),$$
 (3.82)

where  $r_{>}$  and  $r_{<}$  are the larger and smaller of  $\{r, r^{'}\}$ .

The function  $J_l(kr) = \cos \delta_l j_l(kr) - \sin \delta_l n_l(kr)$  corresponds to a free electron wave, satisfying the radial Schrödinger equation for  $r > R_{\rm MT}$ . In order to take into

account the effect of the damping of the electron wave in the far field and the dispersion properties of the effective medium, we must look for  $F_l = N_l + A_l J_l$ , where  $N_j = \cos \delta_l n_l(kr) + \sin \delta_l j(kr)$  also satisfies the Schrodinger equation, and  $A_l$  is the complex self-consistent coefficient.

As it can be seen, when  $A_l = i$ ,  $F_l = \exp(i\delta_l)h_l^{(+)}(kr)$ , where  $h_l^{(+)}(kr)$  is the Hankel function describing the outgoing wave with asymptotic behaviour  $\sim \exp(ikr)/r$  at  $r \to \infty$ . Further, based on the constructed Green's function, the density of electronic states is calculated:

$$\rho(E) = \frac{2}{\pi} \text{Im} SpG(\mathbf{r}, \mathbf{r}'; E), \tag{3.83}$$

which, for the monatomic cluster embedded into the effective medium, gives the following expression [2, 6, 7]:

$$\rho(E) = \frac{2}{\pi} \sum_{l} (2l+1) \left[ \frac{d\delta_{l}}{dE} - R_{C}^{2} J_{l}^{2} \sqrt{E} \frac{\partial \gamma_{l}(E, R_{C})}{\partial E} \right] \text{Im} A_{l},$$
 (3.84)

where  $R_C$  is the radius of the cluster sphere and  $\gamma_l(E,R_C)$  is the logarithmic derivative at the cluster boundary. Using the self-consistency condition for the coherent potential approximation:

$$\int \langle \mathbf{k} \mid \tilde{t} \mid \mathbf{k}' \rangle d\Omega_{\mathbf{k}} = 0; \tag{3.85}$$

within the framework of this model, we obtain the dispersion equation:

$$\sum_{l} (2l+1)\tilde{t}(K) = \frac{1}{K} \sum_{l} (2l+1) \exp(i\delta_{l}) \sin \delta_{l}(K, R_{c}) = 0,$$
 (3.86)

where  $\tilde{t}(K)$  is the *t*-matrix of the effective medium and K is the radial part of the complex wave vector **K**of the scattered electron wave  $\Psi_E = A \exp(i \mathbf{K} \mathbf{r})$ , the damping of which simulates the absence of long-range order in the system. Complex phase shifts  $\delta_l(K, R_C)$  and logarithmic derivatives  $\gamma_l(K, R_C)$  on the boundary of the cluster are determined in the same way as it was done for the MT-sphere:

$$tg \,\delta_l(K, R_c) = \frac{Kj_l'(KR_c) - \gamma_l j_l(KR_c)}{Kn_l'(KR_c) - n_l j_l(KR_c)}, \tag{3.87}$$

and

$$\gamma_l(k, R_c) = \frac{k \left[\cos \delta_l j_l'(kR_c) - \sin \delta_l n_l'(kR_c)\right]}{\cos \delta_l j_l(kR_c) - \sin \delta_l n_l(kR_c)}.$$
(3.88)

The self-consistent parameter  $A_l$  is then determined from the equation:

$$k\left[\frac{N_l'(kR_c) + A_l J_l'(kR_c)}{N_l + A_l J_l}\right] = K \frac{h_l^{(+)} \prime (KR_c)}{h_l^{(+)} (KR_c)}.$$
 (3.89)

Numerous calculations for amorphous and nanocrystalline C, Si, Ge, As, Se and Te were carried out based on this model [2, 6, 7].

# 3.7.3 A Model of a Non-regular Material in the Cluster Approach

The cluster approximation developed in [2, 6, 7, 30–32] consists in considering the structure of the investigated material as a finite cluster embedded into the effective medium (effective energy-dependent potential (see Fig. 3.5)). At first, the atomic structure at the level of the near order and, if required, medium order (e.g. for binary, ternary and more complicated nanocompounds) is postulated.

Then, the construction of crystalline potentials with respect to a given atomic structure is carried out. Various models of crystalline potentials are presented in Fig. 3.6b—e. Further, the MT-approximation of the crystalline potentials is introduced. The MT-approximation symmetrizes crystalline potentials. The scattering problem for individual MT-potentials is solved, and the corresponding phase shifts are found. The cluster of MT-potentials is embedded into the effective complex potential, which is calculated self-consistently. The procedure for constructing MT-potentials is based on the relations (3.23, 3.24, 3.25, 3.26 and 3.27).

Passing to the system of MT-potentials, from the point of view of scattering theory, it becomes inconvenient and cumbersome to use realistic potentials with a complex relief. Therefore, this approach uses a non-local shell energy-dependent pseudopotential:

$$\left\langle \mathbf{r}_{\alpha}|V_{\alpha}|\mathbf{r}_{\alpha}'\right\rangle = \sum_{\mathrm{lm}} A_{\mathrm{lm}}^{\alpha}(E) \frac{\delta\left(|\mathbf{r}_{\alpha}'| - R_{\mathrm{MT}}^{\alpha}\right)}{\left(R_{\mathrm{MT}}^{\alpha}\right)^{2}} \frac{\delta\left(|\mathbf{r}_{\alpha}'| - R_{\mathrm{MT}}^{\alpha}\right)}{\left(R_{\mathrm{MT}}^{\alpha}\right)^{2}} Y_{\mathrm{lm}}(\mathbf{r}_{\alpha}') Y_{\mathrm{lm}}(\mathbf{r}_{\alpha}'), \quad (3.90)$$

where  $r_{\alpha}$  is the radius vector of the position of the atom. The coefficients  $A_{lm}^{\alpha}$  are selected in such a way as to provide the same scattering properties as for a realistic potential. The calculation of the density of electronic states is based on the Lloyd formula [41–43] for the integral density of states:

$$N(E) = -\frac{2}{\pi} \ln \det ||G(E)||, \tag{3.91}$$

where  $G = G_e + G_e t_e G_e$  and  $G_e$  is the unperturbed Green's function and t is the matrix of the effective medium. The density of electronic states of a cluster in an effective medium is calculated by the formula:

$$\rho(E) = \frac{2}{\pi} \Delta [\text{Im ln det} || Z(E) - H'(K) / H(K) ||] / \Delta E, \tag{3.92}$$

where Z(E) are the structural energy-dependent cluster constants,  $H(K) = \delta_{ll'}\delta_{mm'}h_l^{(1)}(kR_c)$ ,  $h_l^{(1)}$  is the Hankel function of the 1st kind and  $R_c$  is the radius of the cluster. The self-consistency condition in the framework of the coherent potential approximation in this case is as follows:

$$\mathbf{Sp}t_e(K,E) = 0, (3.93)$$

where:

$$t_e(K,E) = \frac{Z(E)J(K) - J'(K)}{Z(E)H(K) - H'(K)} - \frac{1}{iK},$$
(3.94)

and

$$J(K) = \delta_{ll'} \delta_{mm'} j_l(KR_c). \tag{3.95}$$

#### 3.7.4 Scattering on the General Type Potential

The problem of electron scattering in a field of the general form potential  $V(\mathbf{r})$  leads to finding a solution of Eq. (3.1) that satisfies the boundary condition of the scattered wave. The wave function expansion in terms of partial waves  $\Psi(\mathbf{r}) = \sum_{L} (g_L(r)/r)Y_L(\mathbf{r})$  gives a system of coupled ordinary differential equations in relation to radial wave functions  $g_L$  [44, 45]:

$$-\frac{d^2}{dr^2}g_L + \frac{l(l+1)}{r^2}g_L + \sum_L W_{LL'}(r)g_{L'}(r) = Eg_L(r), \tag{3.96}$$

where  $W_{\mathrm{LL'}}(r) = \int Y_L^*(r) V(r) Y_{L'}(r) d\Omega_r$  are the potential moments. The analysis carried out in [21, 22] demonstrates the decoupling of the system of Eq. (3.96), which is reduced to the uncoupled equation set:

$$-\frac{d^2}{dr^2}g_L + \frac{l(l+1)}{r^2}g_L + W_{LL}(r)g_L = Eg_L.$$
 (3.97)

The potential of a general form used as a scatterer can be considered either as a nonspherically symmetric potential of the atom or as a potential of a cluster region with a complex topography of the potential function (see, Fig. 3.6c, f). Numerical simulation was performed for Si nanoclusters embedded in 'vacuum' (1, 5, 17-atomic clusters [22]). To construct the potential, it is necessary to take into

account a number of features that distinguish Si, as a semiconductor with a covalent bond, from well-studied ionic compounds. If in ionic compounds the valence electrons are localized near the atomic cores, then in covalent ones valence electrons are distributed in the interstitial space with a high degree of heterogeneity. The maximum density of the electron charge is observed along the bond line of the neighbouring atoms. Such a charge distribution can be interpreted as a homopolar covalent bond. Simulation of this bond is possible in two ways, namely, by (1) cutting off the core part of the electron charge and redistribution of the valence charge along the bond direction and (2) introducing into the Hamiltonian a term that describes the covalent interaction in explicit direct form. In this case, the spatial inhomogeneity of the electron charge density in the cluster volume was due to the superposition of the electron charge densities of the nearest atoms. The described procedure for reproducing the electron charge density of a cluster region with the subsequent construction of its potential based on the principles allows one to estimate the MT-approximation of potentials, where the complex form of the potential function in the interatomic region is replaced by its mean value-MT-zero.

In this sense, the model under consideration can be considered a generalized MT-approximation, since the MT-boundary here is moved on a considerable distance from the centre of the cluster.

Numerical integration of equations of the type (3.97) makes it possible to obtain T-matrix elements, then phase shifts  $\delta_L$ , which are related to the elements  $T_L$  by the known relation  $T_L = \exp(2i\delta_L) - 1$ . EDOS for the potentials under consideration can be written [12, 13]:

$$\rho(E) = \frac{k}{\pi} R_c^2 \sum_{L} \left[ \cos \delta_L j_l(kR_c) - \sin \delta_L n_l(kR_c) \right]^2 \frac{d\gamma_L(k,R_c)}{\Omega dE}, \tag{3.98}$$

where  $\Omega$  is the cluster volume.

Another way to calculate EDOS is related to direct computations of phase functions  $T_L$ , logarithmic derivatives and matrix elements of the T-matrix without direct calculations of wave functions  $g_L(r)$ . Using the well-known relations, we can obtain the equation for the phase transition function:

$$dT_L(r)/dr = -2ikr^2W_{LL}(r)\left[j_l(kr) + \frac{1}{2}T_L(r)h_l^{(1)}(kr)\right]^2,$$
 (3.99)

The initial condition for Eq. (3.99) corresponds to the situation when scattering does not occur. It means that the radius of action of the perturbing potential is zero and  $T_L(k,0) = 0$ . Taking into account the relations connecting scattering matrices definitions:  $T_L = S_L - 1 = \exp[2i\delta_i] - 1 = 2i \exp[i\delta_L] \sin \delta_L$ , we obtain equations for the phase functions  $S_L(r)$  of scattering or phase shifts  $\delta_L(r)$ :

$$dS_L(r)/dr = -\frac{1}{2}ikr^2W_{LL}\left[h_l^{(2)}(kr) + S_L(r)h_l^{(1)}(kr)\right]^2,$$
(3.100)

and

$$d\delta_L(r)/dr = -kr^2 W_{LL} [j_l(kr)\cos\delta_L(r) - n_l(kr)\sin\delta_L(r)]^2.$$
 (3.101)

The initial conditions for the Eqs. (3.100) and (3.101) are, respectively,  $S_L(k,0) = 1$  and  $\delta_L(k,0) = 0$ . A work with the Eqs. (3.99, 3.100 and 3.101) and, in particular, with the Eq. (3.101) presents notable advantages: (1) phase shifts  $\delta_L$  are obtained directly from the integration (3.101), which are then used to calculate the EDOS by the formula of type (3.98); (2) during the calculation it is easy to investigate the influence of the form of the potential function on the scattering properties of the potential region; and (3) Eq. (3.101) is a differential equation of the first order, and the computer time expenses are less than in the case of the radial Schrödinger equation integration. However, a serious obstacle in calculating software implementation by the method of phase functions is encountered due to nonlinearity of the differential equations for phase functions. For them, the convergence of various difference schemes and the optimal methods of their construction are poorly studied.

#### 3.8 Monoatomic Nanosystems: Nano-Si, Nano-Se

The successful application of the multiple scattering theory concept in the coherent potential approximation for monoelement nanomaterials with pronounced covalence C, Si, Ge, As, Se, Sb, Te is presented in [2, 6–8, 12, 24]. These materials represent, on the one hand, a wide range of elements of the periodic system, and, on the other hand, they have different coordination at the level of short-range order (the number of nearest neighbours for Se and Te-2, As and Sb-3, C, Si and Ge-4). The main task of modelling is the parametric study of the electronic structure of nanoparticles through the effect of the number of atoms in a nanocluster.

#### 3.8.1 Production of Nanosilicon

There are various ways of nanosilicon production which were developed mainly in the 2000s. Usually the method of plasma-chemical synthesis is used. The technology is as follows: silicon is introduced into argon plasma at the temperature about 6000 °C. It is evaporated, decomposing into separate atoms, and supersaturated vapour is formed. Then, the vapour is condensed and forms silicon nanoparticles of a spherical shape. In fact, nanostructures of 8–200 nm are assembled. Nanopowders of silicon are of undoubted interest for various fields of technology and industry, which begin to experience a great need for these materials because of their unique properties.

#### 3.8.1.1 Nanosilicon Applications

The change of condensation conditions allows, in certain limits, to control the properties of synthesized nanoparticles. The plasma flow is gradually cooled, the silicon atoms are captured and actually re-formed and the 'sought-for' nanostructures are 'assembled'. So, changing the synthesis modes (temperature, cooling rate, etc.), it is possible to control the process of growth of nanosilicon particles.

In particular, it is possible to obtain particles of nanocrystalline silicon of the necessary size (2–50 nm) and the most suitable spherical form. It is also possible to obtain hollow silicon nanospheres from 5 to 60 nm in diameter. Such materials are of great interest for applications in nanophotonics and catalysis. They can be used to create the so-called biological nanocapsules, placing the necessary substances in the internal volume. They can be in demand for the storage of various gases, including hydrogen. Varying the size of such nanospheres, it is possible to control their optical and electronic properties. Obtaining and researching silicon-containing nanoparticles, new properties with the different morphology and structural organization are very relevant.

The possibilities of applying nanosilicon are far from being limited. If, for example, a layer of particles of this chemical element with a thickness no more than 10 nm is applied to the surface of the solar battery, then the battery efficiency will increase by 5% (the main role is played by the effect of re-emission of ultraviolet light quanta). Plasma-chemical nanosilicon can be used in the development of a fundamentally new technology for cancer combating. Its essence lies in the fact that on the surface of spherical particles, oxygen is available. Its usual triplet state is biologically inert. But, if we bring it into an excited, singlet state, 'highlighting' the nanosilicon with a laser, it turns into the strongest oxidizer and literally burns cancer-infected cells, if, of course, the drug is delivered to the right place. Nanodispersed silicon powders have the ability to absorb ultraviolet radiation and are widely used for making sunscreen cosmetics.

#### 3.8.1.2 Other Nanosilicon Applications

*In agricultural production*, the use of nanosilicon improves the absorption of nitrogen, phosphorus and potassium by crops. Nano-transformed silicon stimulates growth processes and stress resistance of agricultural crops and accelerates the maturation process. The main function of silicon in plants can be called the increasing of the resistance level to any stresses and unfavourable conditions and the ability to withstand toxins.

In medical practice, nanosilicon:

• Creates electrical colloidal systems that have the property of 'sticking' to themselves viruses and pathogens that are dangerous to humans. Organic compounds of silicon are able to form bioelectric charged systems that adhere to pathogens (influenza, fungi, herpes, hepatitis, etc.) and neutralize them

- Plays a major role in the connective tissue components and bonds individual fibres of elastin and collagen
- Together with protein structures promotes the formation of enzymes, amino acids and hormones
- Affects the work of the nervous system and brains (improves the conductivity of nerve fibres and the function of certain structures of the brain and energizes the cerebellum, which is responsible for controlling and coordinating our movements and balance)
- Stimulates the activity of the immune system (increases resistance to viral and bacterial infections) and influences metabolic processes in erythrocytes, monocytes and lymphocytes
- Is an antioxidant that blocks the processes of peroxide and enzymatic oxidation
  of lipids, which in turn increases the protective functions of the epidermis and
  increases the resistance of nails and hair to the oxidative effects of free radicals
- Ensures the elasticity of the walls of the vessels and the ability to respond to brain commands to widen and narrow the vessels
- Prevents the penetration of cholesterol into the blood plasma and the deposition of lipids on the vessels walls

In the scientific community, nanosilicon evokes the keenest interest, including the actual creation of new morphological structures such as Si-fullerenes. In this case, nanosilicon becomes economically competitive in comparison with nanocarbon. To obtain nanosilicon is cheaper than nanocarbon, since silicon is presented in nature much wider. Silicon processing technologies are also well developed and very effective. Nanosilicon has many reasons to occupy an important niche in the knowledge-intensive industry and market in the nearest time.

#### 3.8.2 Nanosilicon: Calculations of Electronic Structure

Figure 3.7 shows cluster models of nanosilicon in the effective medium. Figure 3.8 shows EDOS curves and corresponding coherent potentials for 1-, 2- and 5-atomic silicon clusters.

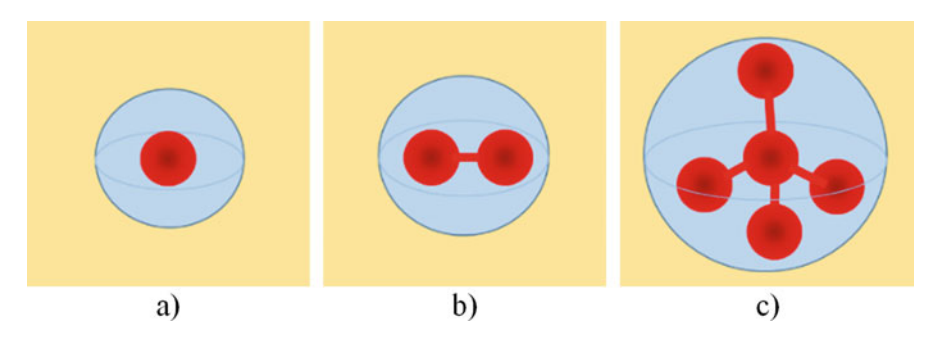
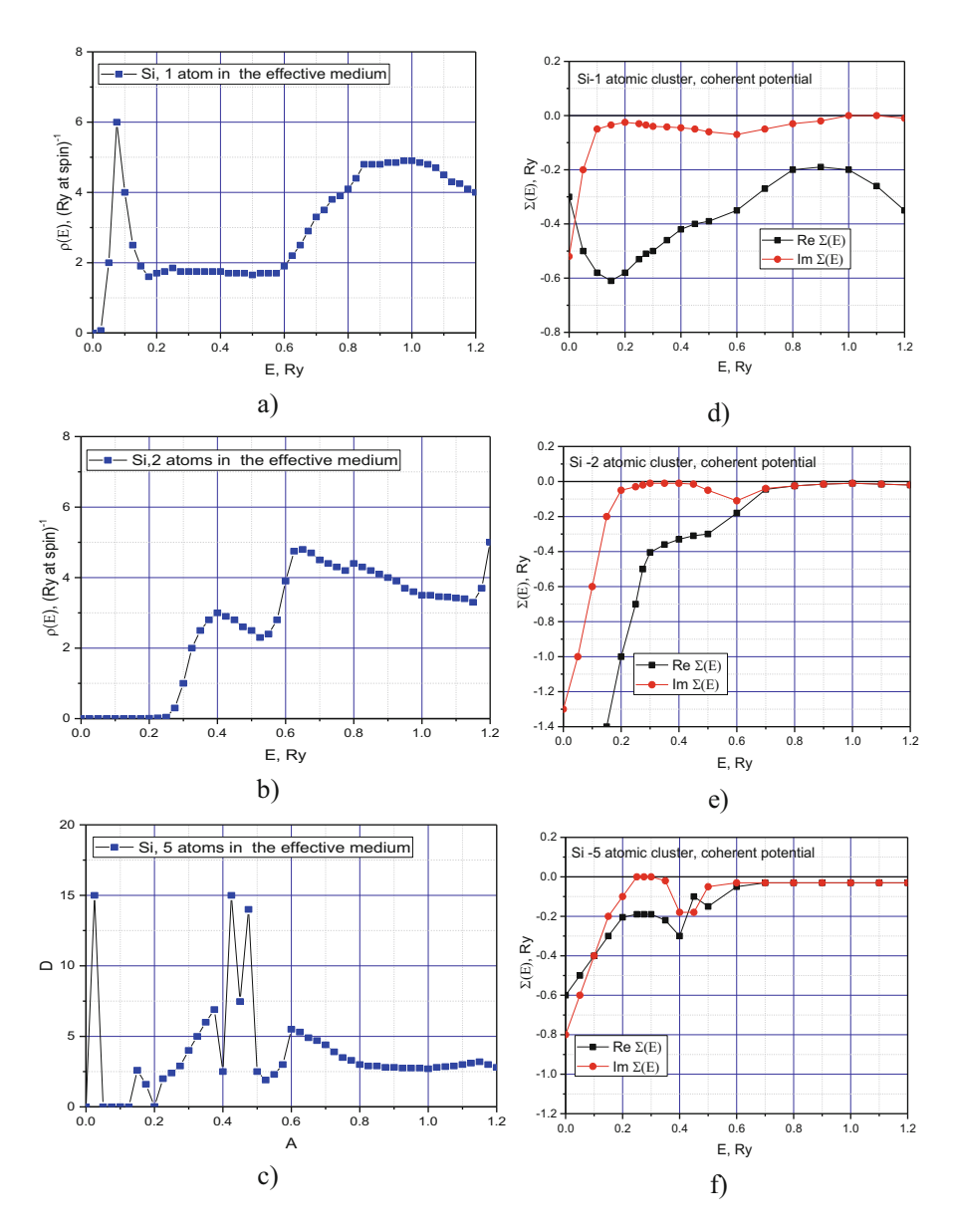


Fig. 3.7 Nanosilicon models: (a) 1-atomic cluster; (b) 2-atomic cluster; (c) 5-atomic cluster. Interatomic distance is 2.22 au



**Fig. 3.8** Modelling of nanocrystalline silicon:  $(\mathbf{a}, \mathbf{b}, \mathbf{c})$  – density of electronic states for 1-,2- and 5-atomic clusters;  $(\mathbf{d}, \mathbf{e}, \mathbf{f})$  – corresponding coherent potentials

Figures 3.9 and 3.10 represent the model and EDOS calculation results for PES 18-atomic cluster as a spherical nanoparticle of 15 nm in diameter, embedded into a 'vacuum'. Although a solid-state maximum exists in the vicinity  $E \sim 0.3 Ry$ , the degeneracy of the EDOS curve profile is generally observed. This fact can be

Fig. 3.9 Model of nanoparticle in 'vacuum', 18-atomic cluster, nanoparticle diameter is about 15 nm

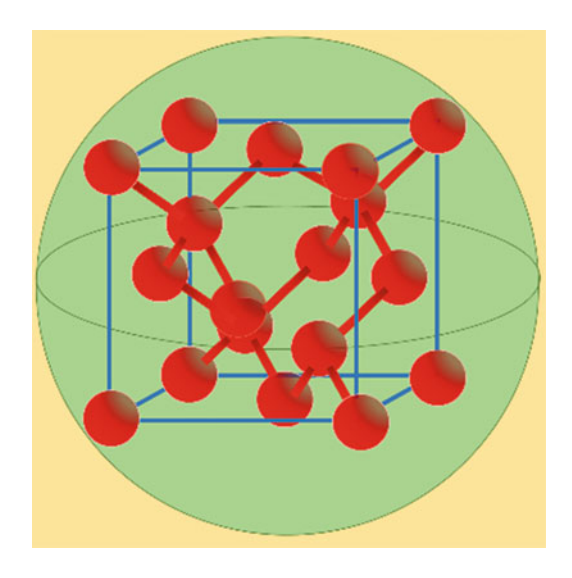
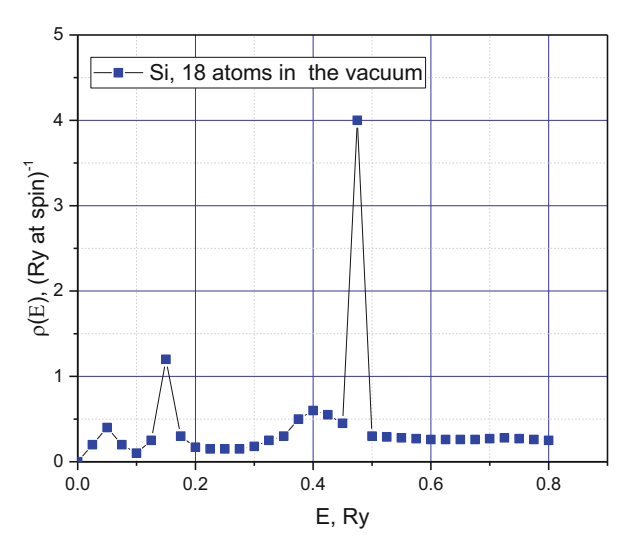


**Fig. 3.10** Typical density of electronic density of states of nanosilicon particle



attributed to a decrease in the symmetry of the atomic configuration (in comparison with the symmetry of the 5-atomic cluster).

#### 3.8.3 Selenium Versus Nano-selenium

Selenium (Se) was discovered by the outstanding Swedish chemist Jons Berzelius in 1817. Se is a fairly common microelement. Se is a non-metallic chemical

element, the element of the XVI group of the periodic table. In chemical activity and physical properties, it resembles *sulphur* and *tellurium*. Se appears in a number of allotropic forms: the most popular are *a red amorphous powder*, a red crystalline material and *a grey crystalline metal-like form called* metallic selenium. This last form conducts electricity better in the light than in the dark and is used in photocells. Se burns in air and is unaffected by water but dissolves in concentrated nitric acid and alkalis.

#### 3.8.3.1 General Se Applications

- Se has good photovoltaic and photoconductive properties, and it is used extensively in electronics, such as photocells, light meters and solar cells.
- The second largest use of selenium is in the glass industry: selenium is used to remove colour from glass, to give a red colour to glasses and enamels.
- The third main use, taking about 15%, is sodium selenite for animal feeds and food supplements.
- Se can also find applications in photocopying, in the toning of photographs. Its
  artistic use is to intensify and extend the tonal range of black and white
  photographic images.
- Other uses of selenium are in metal alloys such as lead plates used in storage batteries and in rectifiers to convert AC current in DC current. Selenium is used to improve the abrasion resistance in vulcanized rubbers. Some selenium compounds are added to antidandruff shampoos.

#### 3.8.3.2 Nano-selenium in the Environment

- Se is among the rarer elements on the surface of this planet and is rarer than silver. Selenium is present in the atmosphere as methyl derivatives. Non-combined Se is occasionally found, and there are around 40 known selenium-containing minerals, some of which can have as much as 30% selenium but all are rare and generally they occur together with sulphides of metals such as copper, zinc and lead.
- The main producing countries are Russia, the USA, Bolivia and Canada. Global
  industrial production of selenium is around 1500 tonnes a year, and about
  150 tonnes of Se are recycled from industrial waste and reclaimed from old
  photocopiers.
- Se occurs naturally in the environment. It is released through both natural processes and human activities. Well-fertilized agricultural soil generally has about 400 mg/ton since the element is naturally present in phosphate fertilizers and is often added as a trace nutrient. In its natural form as an element, selenium cannot be created or destroyed, but Se does have the ability to change form.

- The behaviour of Se in the environment strongly depends upon its interactions with other compounds and the environmental conditions at a certain location at a certain time.
- Se can accumulate in the body tissues of organisms and can then be passed up through the food chain.

#### 3.8.3.3 Health Effects of Nano-selenium

Humans may be exposed to selenium in several different ways:

- Se exposure takes place either through food or water or when we come in contact
  with soil or air that contains high concentrations of selenium. This is not very
  surprising, because selenium occurs naturally in the environment extensively
  and it is very widespread. The exposure to selenium mainly takes place through
  food, because selenium is naturally present in grains, cereals and meat.
- Humans need to absorb certain amounts of Se daily, in order to maintain good health. Food usually contains enough selenium to prevent disease caused by shortages.
- Se uptake through food may be higher than usual in many cases, because in the past many selenium-rich fertilizers have been applied on farmland.
- Se poisoning may become so severe in some cases that it can even cause death.
- Overexposure of selenium fumes may produce accumulation of fluid in the lungs, garlic breath, bronchitis, pneumonitis, bronchial asthma, nausea, chills, fever, headache, sore throat, shortness of breath, conjunctivitis, vomiting, abdominal pain, diarrhoea and enlarged liver. Se is an eye and upper respiratory irritant and a sensitizer. Overexposure may result in red staining of the nails, teeth and hair. Selenium dioxide reacts with moisture to form selenious acid, which is corrosive to the skin and eyes.

#### Se demonstrates:

- Three antigenic functions on hepatitis B
- Three antigenic functions on hepatitis C
- A magical liver protection ability being the natural killer of liver diseases

#### 3.8.4 Nano-selenium: Calculations of Electronic Structure

Cluster models of the nano-selenium are presented in Fig. 3.11.

The results of the EDOS modelling and the corresponding coherent potentials of nanocrystalline models (Fig. 3.11) are presented in Fig. 3.12. It is shown that the 3-atomic cluster reflects the electronic properties of amorphous selenium, and the 7-atomic cluster gives the main features of its nanocrystalline modification [6–8, 12]. The structural data used in the calculations corresponds to trigonal selenium.

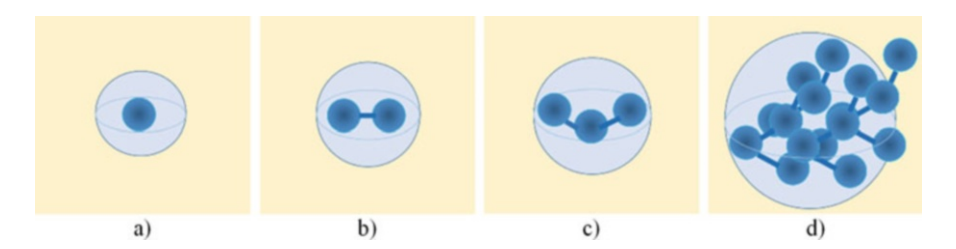


**Fig. 3.11** Nano-selenium models: (a) 1-atomic cluster; (b) 2-atomic cluster; (c) 3-atomic cluster; (d) 7-atomic cluster. Interatomic distance is 2239 a.u

The purpose of this numerical study is to find out at which level of a short-range order the crystalline properties begin to appear. The obtained data indicate that the second coordination sphere already sufficiently well determines the nanocrystalline properties. This is consistent, in particular, with the Ioffe–Regel hypothesis, about the decisive role of a short-range order in determining the electronic properties of non-regular disordered semiconductor materials.

#### 3.9 Nanocompounds: Nanochalcogenides

A fundamental difficulty in modelling electronic properties of the binary chalcogenide-type compounds is the reproduction of the composition characteristic x. Calculations have demonstrated that the short-range order at the level of the first coordination sphere of the atomic structure under consideration makes it possible to obtain the correct EDOS of monoelement amorphous and nanocrystalline semi-conductors. In fact, this means the essential role of nanoscale factors. This circumstance made it possible to apply a similar calculation scheme for binary chalcogenides. However, in this case, it is necessary to solve the problem of constructing 'crystalline' potentials of a binary compound for any x, which is for monoelemental materials looks relatively simple [2, 34]. However, if the problem of potentials can be considered technical, then the concept of the structure of a binary compound is nontrivial and cannot be based only on the level of a short-range order.

The atomic structure of the system for arbitrary x is a system with a medium order.

Namely, this level of the structural configuration can provide the reproduction of the atomic structure characteristic of a given 'x'. It should be taken into account that this is not a substitutional alloy with a regular matrix but a system with explicit topological disorder.

From the point of view of the cluster model developed in [2, 22, 23], the structure of a non-regular binary compound can be considered as a set of different basic clusters represented in a structural matrix with different statistical weights

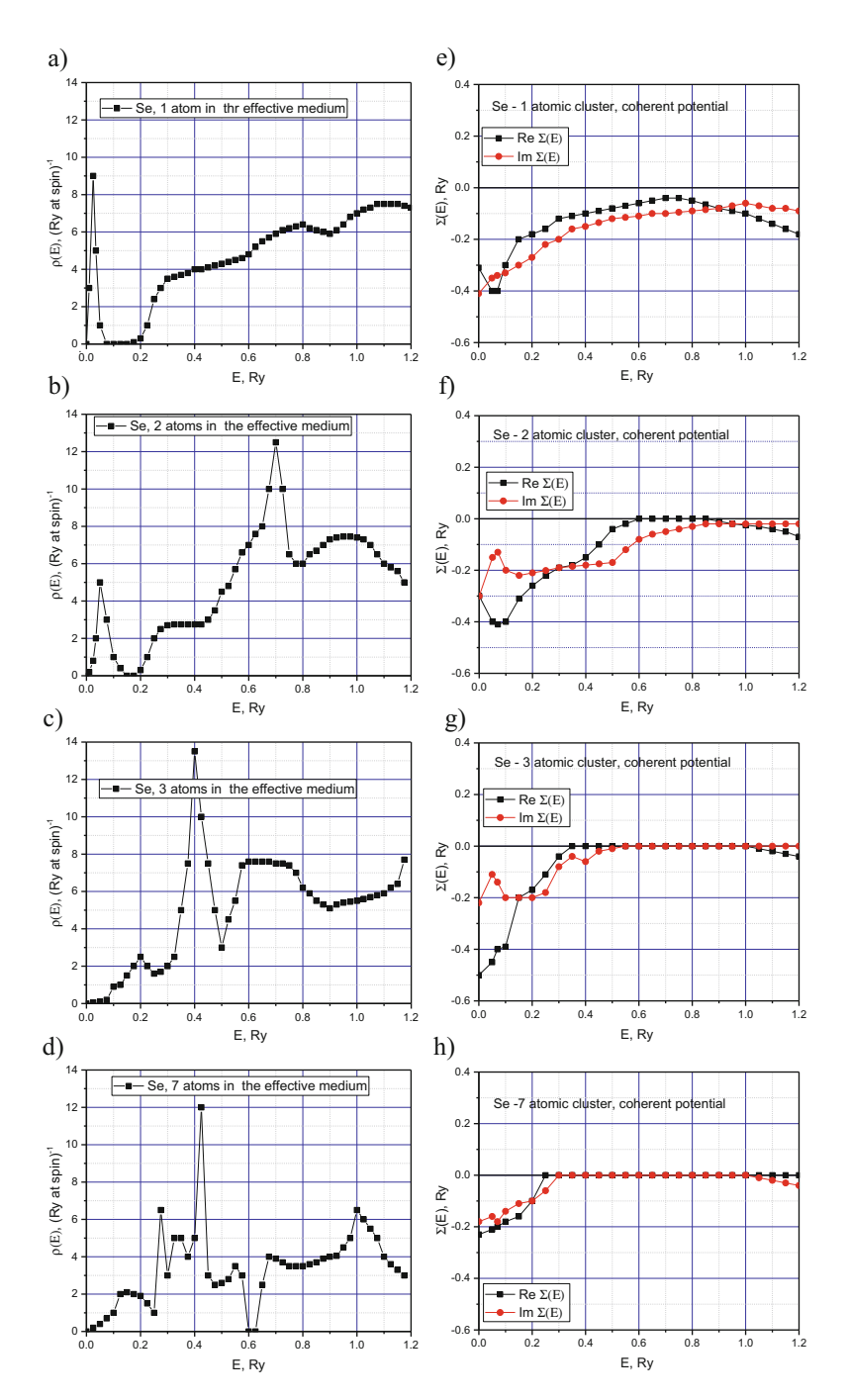


**Fig. 3.12** Modelling of nanocrystalline selenium:  $(\mathbf{a}, \mathbf{b}, \mathbf{c}, \mathbf{d})$  – density of electronic states for 1-, 2-, 3- and 7-atomic clusters;  $(\mathbf{e}, \mathbf{f}, \mathbf{g}, \mathbf{h})$  – corresponding coherent potentials

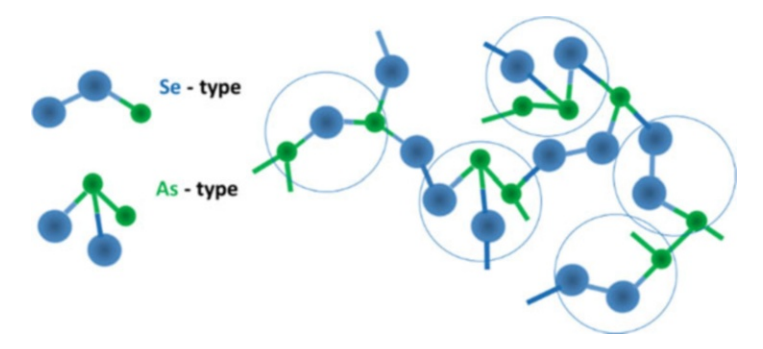


Fig. 3.13 Model of chalcogenide nanocrystalline material based on the concept of structural units: binary compound with As-type and Se-type structural units

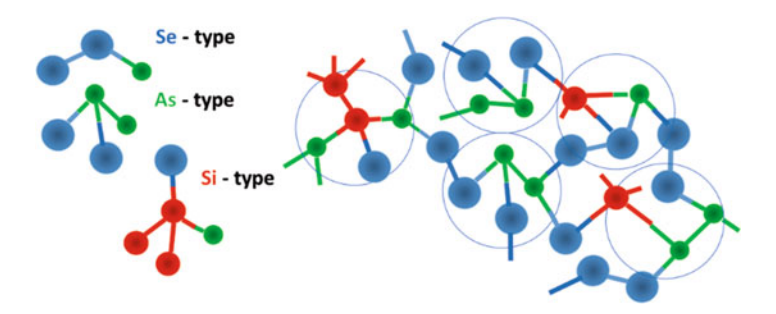


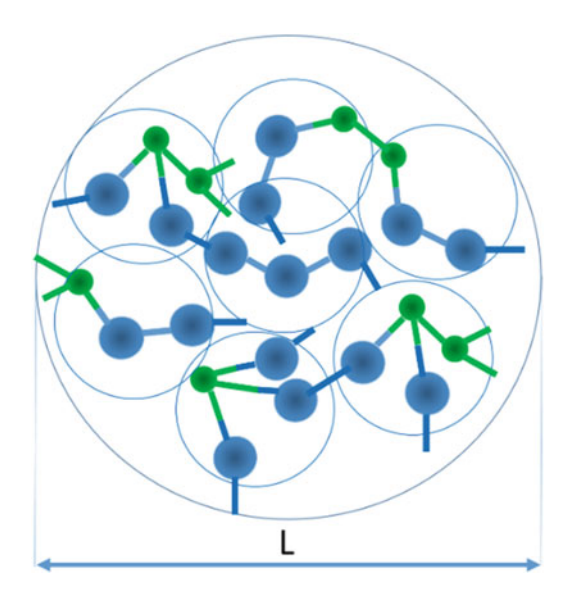
Fig. 3.14 Model of chalcogenide nanocrystalline material based on the concept of structural units: ternary compound with As-type, Se-type and Si-type structural units

(see Figs. 3.13 and 3.14) [23, 46] in an effective medium. It might seem, that it is possible to calculate simply a large cluster that takes into account the features of the atomic structure of the investigated composition  $A_xB_{1-x}$ . However, it is a very time-consuming calculation. Moreover, this calculation is not reasonable for essential contribution of a short-range order into EDOS. But, since the short-range order in the binary compound can vary significantly from node to node of the structural matrix of the nanocrystalline material, there is the statistics of the basic clusters that determines the final EDOS [23, 31, 32, 46] (Fig. 3.15).

#### 3.9.1 Binary and Ternary Chalcogenide Glassy Systems

The bandgap estimation in numerical modelling is based on the cluster model including the group of basic clusters (Se<sub>3</sub>, As<sub>4</sub>, AsSe<sub>3</sub>, As<sub>2</sub>Se<sub>2</sub>, As<sub>2</sub>Se, etc.) embedded into the effective medium with a complex potential in accordance with the CPA.

**Fig. 3.15** The model of the characteristic cluster structure of the non-regular chalcogenide system  $A_xB_{1-x}$ , L is the characteristic size (scale) of the system



The selection of a composition of clusters for the reproduction of a necessary predefined *x* is performed according to the relation:

$$As_x Se_{1-x} \sim \sum_{i=1}^{N} [As_{k_i} Se_{l_i}] \alpha_i, \qquad (3.102)$$

where  $[As_{k_i}Se_{l_i}]$  is the symbolic designation of the *i*-th basic cluster,  $k_i$  and  $l_i$  are the number of As- and Se-type atoms,  $\alpha_i$  is the weight coefficient of the *i*-th basic cluster and N is the number of basic clusters.

The averaging of physical characteristics, for example,  $\bar{E}_g$ , is performed by the formula:

$$\bar{E}_g = \left(\sum_{i=1}^N \alpha_i E_g^i\right) / \left(\sum_{i=1}^N \alpha_i\right). \tag{3.103}$$

The values  $E_g^i$  are obtained in the EDOS calculations for each basic *i*-th cluster, taking into account the mass density  $\rho_i$  determining the radius of the cluster  $R_{\text{CL}}^i$ . When selecting the composition of basic clusters, it is also necessary to take into consideration the chemical ordering in the system, that is, take into account the characteristic binding energies of As–As, Se–Se and As–Se (2.07, 2.14, 2, 26 eV, respectively).

This circumstance has a noticeable effect in the 'rare' composition at 0.45 < x < 0.66, where stronger As–Se bonds are more likely to occur. Combining the composition of basic clusters pursues the goal of reproducing the characteristic space topological invariant of the system  $As_xSe_{1-x}$ . Figure 3.16 and Table 3.5 illustrate the results of bandgap estimations for various cluster compositions.

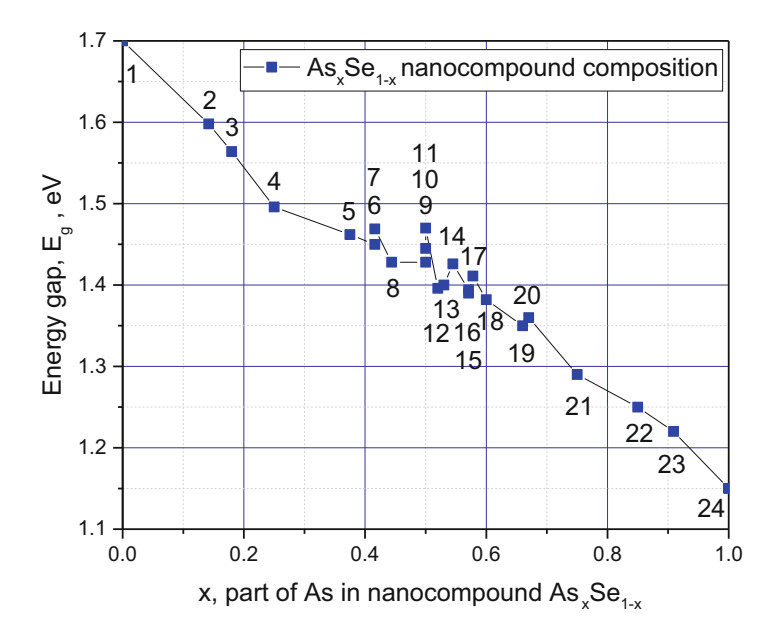


**Fig. 3.16** Energy gap of nanocrystalline  $As_xSe_{1-x}$  via the composition number x

The ambiguity of structural ordering in complex non-regular solids and nanocrystalline materials  $A_x B_{1-x}$  can be considered as their common property. The features of the short-range order in the neighbourhood of each node are, first of all, due to the physical conditions for the system preparation and, secondly, the principle of chemical ordering taking into account the 8-N rule and the values of the neighbouring atoms binding energies.

Reproduction of a given composition is possible in many ways. For example, at x=0.50, the increase in the cluster fraction of the As<sub>4</sub> and Se<sub>3</sub> type in the system leads to the increase in the bandgap (Fig. 3.16, point 11, = 1.47 eV) in comparison with the more equilibrium structure, where there are clusters of the As<sub>2</sub>Se<sub>2</sub> type (Point 9,  $E_g^i=1.428$  eV). Moreover, the first atomic configuration can be associated with freshly evaporated film and the second one with the annealed film. Then an estimation of the energy gap changes under the photoinduced transformation and gives the value of  $\Delta E_g \approx 0.04$ eV.

At subsequent light effects, we find  $\Delta E_g \approx 0.02 \mathrm{eV}$  (structural transitions:state 11  $\Leftrightarrow$  state 9). These estimations are generally in satisfactory agreement with data on photoinduced changes ( $\Delta E_g \approx 0.015 \mathrm{eV}$  for amorphous As<sub>2</sub>Se<sub>3</sub> [47]).

The developed cluster multicomponent model [24] using the cluster calculation method [10, 21–23, 30, 32, 46] allows performing energy estimations of the change in optical properties under induced structural changes. It should also be noted that the calculation data satisfactorily describe the general nature of the experimental dependence (see Fig. 3.16). The cluster approach to binary and more complex

	Cluster type	x	$E_g^i$ , eV
1	Se <sub>3</sub>	0.0	1.700
2	(Se <sub>3</sub> )(AsSe <sub>3</sub> )	0.142	1.598
3	(Se <sub>3</sub> )(AsSe <sub>3</sub> ) <sub>2</sub>	0.180	1.564
4	AsSe <sub>3</sub>	0.250	1.496
5	$(AsSe_3)(As_2Se_2)$	0.375	1.462
6	$(AsSe_3)(As_2Se_2)_2$	0.416	1.450
7	$(AsSe_3)_3(As_2Se_2)_3(As_2Se)_3 (Se_3)$	0.416	1.469
8	(AsSe3)2(As2Se2)(As2Se)2	0.444	1.428
9	As <sub>2</sub> Se <sub>2</sub>	0.500	1.428
10	$(As_4)(Se_3) (As_2Se_2)$	0.500	1.445
11	$(As_4)_3(Se_3)_4$	0.500	1.470
12	(As <sub>2</sub> Se <sub>2</sub> )(As <sub>2</sub> Se) <sub>2</sub> (Se <sub>3</sub> )(As <sub>4</sub> )(AsSe <sub>3</sub> )	0.520	1.396
13	$(As_4)_3 (Se_3)_4 (As_2Se_2)(As_2Se)_{12} (AsSe_3)_{12}$	0.530	1.400
14	(As4)(Se3) (As2Se2)	0.545	1.426
15	$(As_2Se_2)(As_2Se)$	0.571	1.394
16	$(As_4)_3(Se_3)_4 (As_2Se_2)_{12}$	0.571	1.390
17	$(AsSe_3)(As_2Se_2)(As_2Se)_2$	0.578	1.411
18	$(As_2Se_2)(As_2Se)$	0.600	1.382
19	$(As_4)(Se_3) (As_2Se_2)_3$	0.660	1.350
20	As <sub>2</sub> Se	0.670	1.360
21	$(As_4)(As_2Se)_2$	0.750	1.290
22	$(As_4)(As_2Se)$	0.850	1.250
23	$(As_4)_2(As_2Se)$	0.909	1.220
24	As <sub>4</sub>	1.0	1.150

**Table 3.5** Nanocrystalline  $As_xSe_{1-x}$  energy gap via the cluster composition

amorphous systems based on the proposed multiconfiguration model is rather general. It allows making  $E_g$  reasonable estimations for materials of the  $A_x^V B_{1-x}^{VI}$  -type. The more accurate are these estimations, the more carefully the calculations of electronic properties of the basic clusters occurring in these materials will be performed. It is worth noting that the cluster multicomponent model is indirectly confirmed by the results of photoemission measurements for  $As_2Se_3$ ,  $As_2S_3$  and  $As_2Te_3$ , which indicate that electronic spectra, for example, nanocrystalline  $As_2Se_3$  can be obtained by statistical mixing of electronic spectra of monoelements As and Se.

#### References

- Slater J C 1974 The self-consistent field for molecules and solids Vol 4 (New York-San Francisco-London-Mexico-Montreal-New-Delhi-Panama-Paris-San-Paulo-Singapore-Sydney-Tokyo-Toronto: McGraw-Hill Book Company)
- Shunin Yu N, Shvarts K K 1986 Calculation of the Electronic Structure in Disordered Semiconductors *Phys. Stat. Sol.* (b) 135 15–36

References 75

3. Kondratjev A C, Kuchma A E **1980** Electronic liquid of normal metals (Leningrad: Leningrad State University) (*in Russian*)

- Herman F, Skillman S 1997 Atomic Structure Calculations New York: Prentice Hall Englewood Cliffs
- 5. Shunin Yu N 1980 On the choice of 'crystalline' potential for MT-approximation *Izv AN LSSR*, ser fiz i the nauk No 6 76-79 (in Russian)
- 6. Shunin Yu N **1981** Calculation of the electronic density of states of amorphous semiconductors C, Si, Ge, As, Se and Te in the 'liquid metal' model. 1 Theory *Izv AN LSSR*, *ser fiz i the nauk* **2** 73–7 (*in Russian*)
- 7. Shunin Yu N **1981** Calculation of the electronic density of states of amorphous semiconductors C, Si, Ge, As, Se and Te in the 'liquid metal' model. 2 Results *Izv AN LSSR*, *ser fiz i the nauk* **2** 78–82 (*in Russian*)
- 8. Gaspar R 1952 Über ein analitisches Näharungsverfachren zur Bestimung von Eigenfunktionen und Energieeigenwerten von Atomelektronen. *Acta Phys. Acad. Sci. Hung.* 2, 151–178 (*in German*)
- 9. Gaspar R 1953 Über eine Approximation des Hartree-Fockschen Potential dürch eine universelle Potentialfunktion. *Acta Phys. Acad. Sci. Hung.* 3, 263–286 (*in German*)
- Shunin Yu N, Shvarts K K 1994 Electronic structure and conductivity of disordered binary semiconductors Tech. Phys. 39 1025–31
- 11. Shunin Yu N, Shvarts K K 1986 Cluster model and calculation of electronic structure of covalent solids *Zh Struct Chem* 27(6) 143–150.
- 12. Shunin Yu N, Shvarts K K, Sokol A A **1990** Scattering of electrons in disordered solids: theory and experiment *Izv AN LSSR* **4** 74–91 (*in Russian*)
- Thorpe M F 1983 Continuous Deformations in Random Networks J. Non-Cryst. Solids 57 355–70
- 14. Belykh A V, Efimov O M, Glebov L B, Matveev Yu A, Mekryukov A M, Mikhailov M D, Richardson K 1997 Photo-structural transformation of chalcogenide glasses under non-linear absorption of laser radiation *Journal of Non-Crystalline Solids* 213–214 330–5
- Owen A E, Firth A P, Ewen P J S 1985 Photo-induced structural and physico-chemical changes in amorphous chalcogenide semiconductors *Philosophical Magazine Part B* 52(3) 347–62
- Kokenyesi S, Beke D L, Sangunni K S, Takats V, Csik A, Daroczi L 2009 Photo-induced transformations in amorphous chalcogenide nano-multilayers *Journal of Materials Science: Materials in Electronics* 20(1) 107–10
- Adriaenssens G J, Stesmans A 2002 Gap states in chalcogenide glasses Journal of Optoelectronics and Advanced Materials 4(4) 837–42
- Malyovanik M, Kikineshi A, Messaddeq S H, Messaddeq Y, Ivan I, Ribeiro S J L 2004 Photoinduced transformations in chalcogenide composite layers *Journal of Non-Crystalline Solids* 348 144–8
- Kavetskyy T S 2013 Radiation-induced structural changes in chalcogenide glasses as revealed from Raman spectroscopy measurements Semiconductor Physics Quantum Electronics & Optoelectronics 16(1) 27–3
- Borisenko K B, Shanmugam Ja, Williams B A O, Ewart P, Gholipour B, Hewak D W, Hussain R, Ja'vorfi T, Siligardi G, Kirkland A I 2015 Photo-induced optical activity in phase-change memory materials Scientific Reports 5 (8770) 1–5
- 21. Shunin Yu N, Sokol A A **1988** Scattering of electronic waves on the general-type. 1. On the diagonality of T-matrix *Izv AN LSSR*, *ser fiz i the nauk* **1** 24–29 (*in Russian*)
- 22. Shunin Yu N, Shvarts K K **1989** Atomic and electronic structure of disordered semiconductors Preprint: Institute of Physics Academy of Sciences of Latvia LAFI-154 Riga-Salaspils: IP 97 p (in Russian)
- 23. Shunin Yu N, Shvarts K K **1990** Modelling of radiation stimulated processes in disordered semiconductors *Izv AN LSSR ser fiz i tehn nauk* **2** 38–56 (*in Russian*)
- 24. Shunin Yu N, Shvarts K K 1986 Cluster model and calculation of electronic structure of covalent solids J Structure Chem 27(6) 143–50 (in Russian)
- 25. Ziesche P, Lehmann G 1983 Ergebnisse in der Elektronentheorie der Metalle Akademie-Verlag Berlin

- 26. Rice T M, Hensel J C, Phillips T C, Thomas G A **1977** Electron-hole liquid in semiconductors *Solid State Physics* **32** London
- Srivastava C P, Weaire D 1987 The theory of the cohesive energies of solids Adv. Phys. 36 463–517
- Kohn W, Sham L J 1965 Self-consistent equations including exchange and correlation effects Phys. Rev. 140 A 1133–8
- 29. Clementi E, Roetti C 1974 Roothaan-Hartree-Fock Wave functions. Basis Functions and Their Coefficients for Ground and Certain Excited States Neutral and Ionized Atoms,  $Z \le 54$  Special Issue of Atomic Data and Nuclear Data Tables 14 177–478 Academic Press
- 30. Shvarts K K, Shotyuk O V, Kornelyuk V N, Shunin Yu N **1990** Irreversible photo- and radiation-induced processes in amorphous films of arsenic three sulfide *Izv AN LSSR ser fiz i tehn nauk* **1** 3–13 (*in Russian*)
- 31. Shvarts K K, Shunin Yu N, Teteris J A **1987** Photoinduced structural changes in amorphous chalcogenides and modelling *Izv AN LSSR ser fiz i tehn nauk* **4** 51–57 (*in Russian*)
- 32. Shvarts K K, Pirogov F V, Shunin Yu N, Teteris J A 1987 Photoinduced structural changes in amorphous chalcogenides *Cryst. Latt. Def. and Amorph. Mat.* 17 133–138
- Gonzales D J, Zoriota M L, Alonso J A 1983 Density functional of disordered solid alloys of nontransition metals *phys.stat.sol*. (b) 119 589–94
- 34. Economou E N **1983** *Green's functions in quantum physics* (Berlin-Heidelberg-N-Y-Tokyo: Springer Verlag)
- 35. Kohn W, Rostoker N **1954** Solution of Schrodinger's equation in periodic lattices with application to metallic lithium *Phys. Rev.* **94** 1111–20
- 36. Skriver H L **1983** *The Linear muffin tin orbital method* (Berlin, Springer Verlag)
- Landau L D, Lifshitz E M 1965 Quantum mechanics. Non-relativistic theory. Course of theoretical physics 2<sup>nd</sup> edition Institute of Physical Problems USSR Academy of Sciences (Oxford-London-Edinbourgh-N-Y-Paris-Frankfurt:Pergamon Press)
- Shunin Yu N 1982 Calculation of the density of electronic states of amorphous semiconductors.
   Calculation of phase shifts in the MT-approximation *Deposited Latvian NIINTI*, *Depon. Manuscripts* 9 Ref 543 21p
- 39. Shunin Yu N 1982 Calculation of the density of electronic states of amorphous semiconductors. 2. The liquid metal model *Deposited Latvian NIINTI*, *Depon. Manuscripts* 9 Ref 544 19p
- Shunin Yu N 1982 Calculation of the density of electronic states of amorphous semiconductors.
   Cluster model *Deposited Latvian NIINTI*, *Depon. Manuscripts* 9 Ref 545 43p
- 41. Lloyd P **1967** Wave propagation through an assembly of spheres. 2. Density of single-particle eigenstates *Proc. Phys. Soc.* **90** 207–16
- 42. Lloyd P **1967** Wave propagation through an assembly of spheres. 3. The density of states in a liquid *Proc. Phys. Soc.* **90** 217–31
- 43. Lloyd P, Smith P V **1972** Multiple scattering theory in condensed materials *Adv Phys* **21** 69–142
- 44. Calogero F 1967 Variable Phase Approach to Potential Scattering 35 Elsevier Science 322 p
- 45. Babikov V V **1976** Method of phase shifts in quantum mechanics Moscow: Nauka 287 p (in Russian)
- 46. Shunin Yu N, Shvarts K K **1989** Influence of composition on the electronic structure of amorphous As<sub>x</sub>Se<sub>1-x</sub>Phys and tech. semiconductors **23**(6) 1049–53 (in Russian)
- Tanaka K 1980 Reversible photostructural change: Mechanisms, properties and applications J Non-Cryst.Sol 35/36 1023–34
- 48. Street R A, Mott N F **1975** States in the Gap in Glassy Semiconductors *Physical Review Letters* **35**(19) 1293–6
- Kastner M, Adler D, Fritzsche H 1976 Valence-Alternation Model for Localized Gap States in Lone-Pair Semiconductors *Physical Review Letters* 37(22) 1504–7
- 50. Anderson P W 1975 Model for the Electronic Structure of Amorphous Semiconductors Physical Review Letters 34(15) 953–5
- 51. Karpov V G, Klinger M I, Ignat'ev F N **1983** Theory of the low-temperature anomalies in the thermal properties of amorphous structures *Sov. Phys. JETP* **57** 439–48 (*Zh. Eksp. Teor. Fiz.* **84** 760–75 *Russian*)

# Chapter 4 Scattering Processes in Nanocarbon-Based Nanointerconnects

In order to overcome disadvantages of contemporary microtechnology, the miniaturization of electronic devices, the integration level expansion and the increase of the operation frequencies and power density are required, including the use of adequate materials and innovative chip interconnects. Due to their unique physical properties, especially due to a ballistic mechanism of conductivity, carbon nanotubes (CNTs) attract a permanently growing technological interest, for example, as promising candidates for nanointerconnects in high-speed electronics. New possibilities for modern nanoelectronics open with novel 'marginal' forms of graphene – nanoflakes (GNFs) and nanoribbons (GNRs), which are comparable with CNTs – demonstrate a wasteless ballistic mechanism of conductivity. Graphene nanointerconnects are also important for nanotechnology. Full integration of graphene into conventional device circuitry would require a reproducible large-scale graphene synthesis that is compatible with conventional thin film technology.

The main aim of the current research is to implement advanced simulation models for a proper description of the electrical resistance for *end* contacts between CNTs and GNRs of different morphologies and metallic substrates of different nature [1]. An adequate description of nanotube chirality [2] is one of the key points for the proper simulations on electric properties of CNT-based nanoelectronic devices.

The resistance of contact between arbitrary CNT and metallic catalytic substrate can considerably exceed that observed separately in a nanotube and a metal [3]. The conductance between real metals and CNTs still occurs, but it is mainly due to the scattering processes, which are estimated to be rather weak [4]. We draw attention to these scattering phenomena in detail (e.g. [1]).

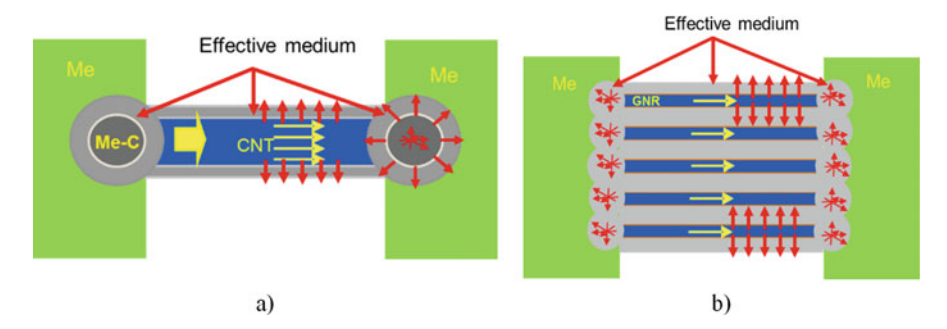


Fig. 4.1 Models of C-Me interconnects as prototypes of novel nanodevices: (a) CNT-Me interconnect; (b) multilayered GNR-Me interconnect

#### 4.1 Non-regularities in Nanointerconnects

Now the main attention is focused on the junctions of carbon nanotubes (CNTs) and graphene nanoribbons (GNR) with contacting metallic elements of a nanocircuit. These contact spaces are essentially *non-regular*. Numerical simulations on the conductance and resistance of these contacts are performed using the multiple scattering theory and the effective media cluster approach. We have simulated both single-walled (SW) and multiwalled (MW) CNTs and single-layered (SL) and multilayered (ML) GNRs with different morphology. Figure 4.1 represents the contacts of metal substrates with CNTs and GNRs, respectively, as prototype nanodevices. The contact regions (CNT–Me and GNR–Me) are the objects of a microscopic approach responsible for the main contribution to the resistance. Meanwhile, the resistances of nanotubes, nanoribbons and the metallic substrate per se may be considered as macroscopic parameters.

There are some important applications of CNTs- and GNRs-based interfaces with other materials for novel nanosensor devices. Usually, these devices are considered as integrated devices around  $10{\text -}50~\mu\text{m}^2$  in size. The fundamental electron devices are field-effect transistors (FETs) (see Fig. 4.2a), which are very sensitive to various external influences of different nature such as mechanical, chemical, electrical, magnetic, etc.

A field-effect transistor (FET) is *nano* in size, whose on/off threshold depends on the tube dimensions, shape and temperature, among others. A local deformation of CNT (GNR) creates a change in the on/off threshold voltage of the transistor. The electrical properties of carbon-based interconnects change under the influence of external factors. The advantage of CNTs and GNRs in comparison with bulk materials is due to their small size, high strength, high electrical and thermal conductivity and a large surface area. Unique physical properties of CNTs and GNRs and their various interconnects allow considering them as sensing nanomaterials in different kinds of sensors – pressure, flow, thermal, gas, optical, mass, position, stress, strain, chemical and biological sensors.

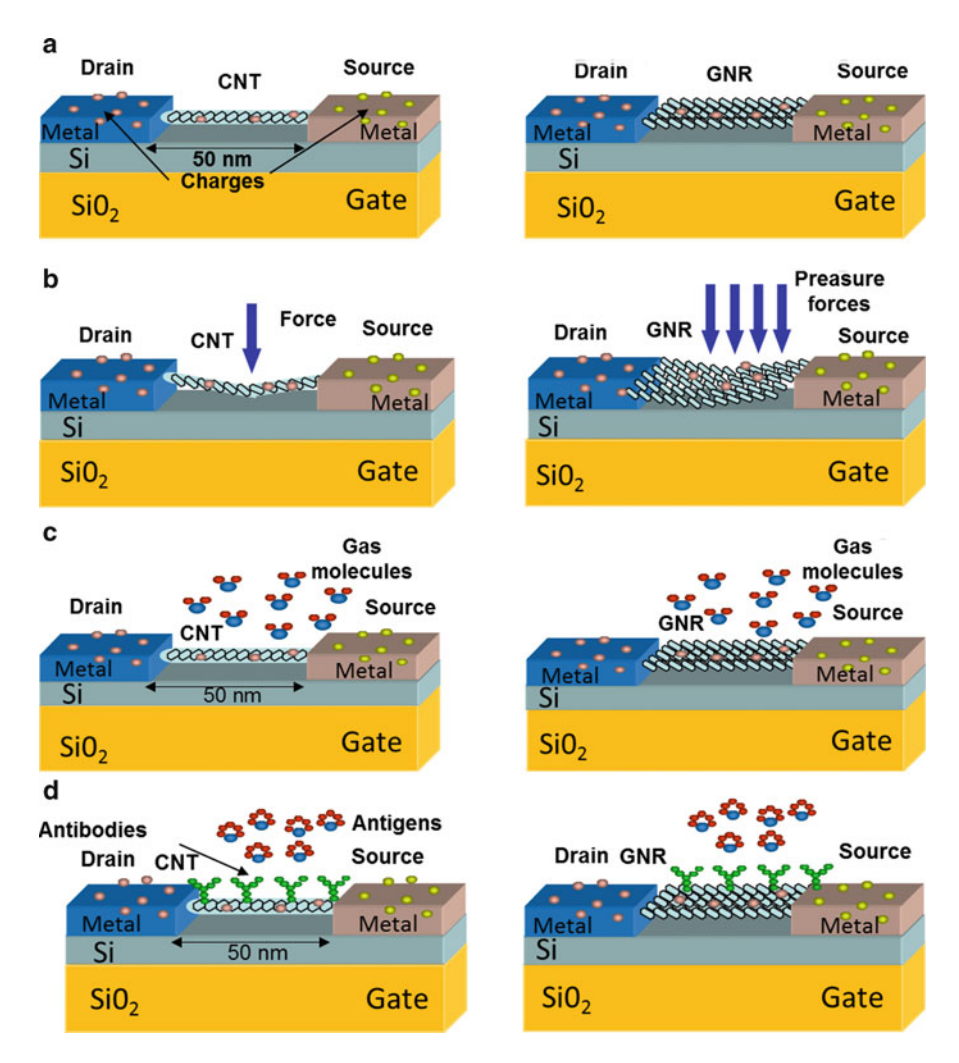


**Fig. 4.2** (a) The unperturbed field-effect transistors based on a CNT and GNR. CNT- or GNR-based FET is mainly composed of a corresponding semiconducting carbon material suspended over two electrodes. (b) *Physical nanosensors*: a conducting threshold can be altered when the tube or graphene ribbon is bent. (c) *Chemical nanosensors*: a conducting threshold can be altered when the amount of free charges on the tube of graphene ribbon surface is increased or decreased by the presence of donor or acceptor molecules of specific gases or composites. (d) *Biological nanosensors*: monitoring of biomolecular processes such as antibody/antigen interactions, DNA interactions, enzymatic interactions or cellular communication processes, among others

Taking into account specific physical properties of CNTs and GNRs metal interconnects, which are explained by the presence of 'dangling' chemical bonds, we should point out the expressed sensitivity of electric properties of interconnect space to chemical, electric and magnetic influences. Moreover, we can treat

interconnects as spaces with morphological non-regularities. Therefore, we also consider interconnects as a perspective group of nanosensors. The recent classification of nanosensors based on CNTs and GNRs considers three main groups: physical, chemical and biological [1] (see Fig. 4.2).

*Physical nanosensors* are used to measure magnitudes such as mass, pressure, force or displacement. The working principle is usually based on the fact that the electronic properties of both nanotubes and nanoribbons change when these are bent or deformed (Fig. 4.2b).

*Chemical nanosensors* are used to measure magnitudes such as the concentration of a particular gas, the presence of a specific type of molecules or the molecular composition of a substance (Fig. 4.2c).

*Biological nanosensors* are used to monitor biomolecular processes such as antibody/antigen interactions, DNA interactions, enzymatic interactions or cellular communication processes, among others (Fig. 4.2d).

The central point of research is the interconnect space, where *non-regularity* effects are very essential. This space determines also the conductivity of interfaces of nanodevices and integrated nanosystems.

## 4.1.1 Scattering Processes in Nanocarbon-Based Nanointerconnects

The electronic structure for CNT–Me and GNR–Me interconnects can be evaluated through the electronic density of states (DOS) for carbon–metal contact considered as a 'disordered alloy', where clusters containing both C and Me atoms behave as scattering centres. The computational procedure that we have developed for these calculations is based on the construction of cluster potentials and the evaluation of both scattering (S) and transfer (T) matrices [5]. The general model of multiple scattering using the effective media approximation (EMA) combined with the coherent potential approach (CPA) for condensed matter is based on the atomic cluster formalism. When using the CPA as EMA approximation, the resistance of the interconnect is evaluated through Kubo–Greenwood formalism [6–8] or, in the simplest cases, through Ziman model [9].

A general model of multiple scattering with the effective media approximation (EMA) for condensed matter based on the atomic cluster approach is presented in Fig. 4.3. So far, the cluster formalism has been successfully applied for metal Cu metal [5], as well as for semiconductors, both elemental (Ge and Si) and binary  $(As_xSe_{1-x} \text{ and } Sb_xSe_{1-x})$  [10, 11]. Special attention has been paid to the latter, since the concept of statistical weighing has been applied for the binary components in solid solutions.

We have developed structural models for CNT-Me and GNR-Me junctions, based on their precise atomistic structures, which take into account the CNT

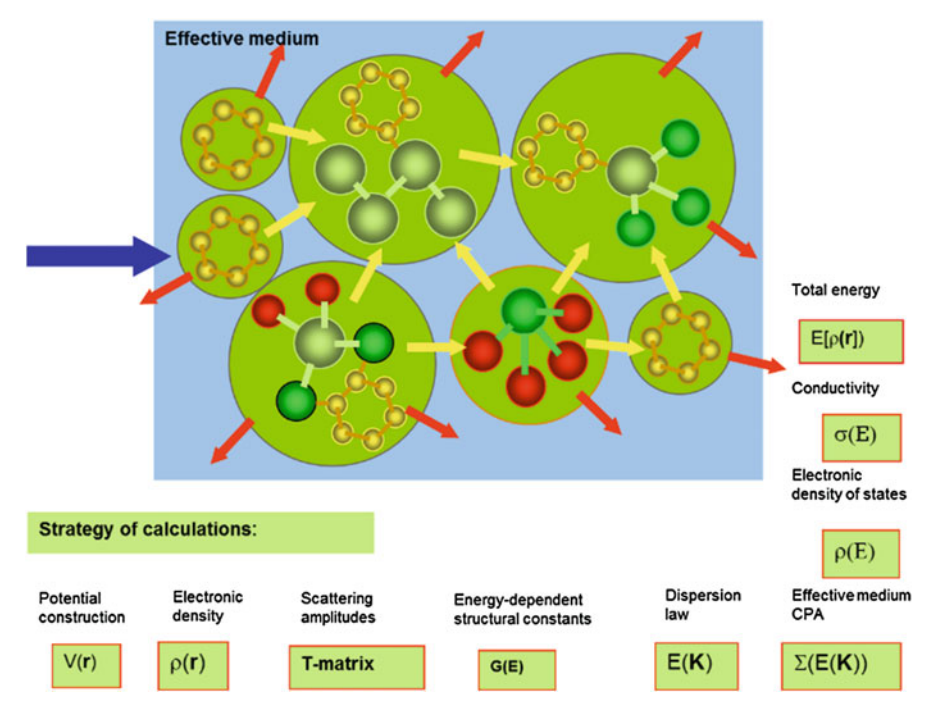


**Fig. 4.3** Multiple scattering problem for the system of clusters as multiple scattering model of condensed matter: strategy of calculations on fundamental properties of condensed medium described within the effective media approximation

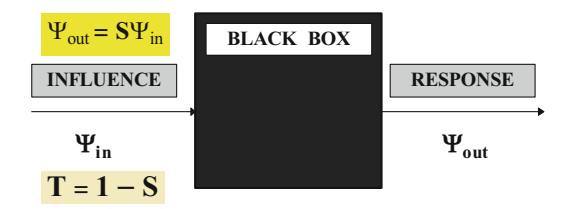
chirality effect and its influence on the interconnect resistance for Me (= Ni, Cu, Ag, Pd, Pt, Au) and predefined CNT (or GNR) geometry.

In the simplest cases, the electronic structure of CNT–Ni interconnects can be evaluated through the DOS for the C–Ni contact considered as a 'disordered alloy' [12]. In the current study, we have developed more complicated structural models of CNT–metal junctions based on a precise description of their atomistic structures. When estimating the resistance of a junction between a nanotube and a substrate, the main problem arises due to the influence of the nanotube chirality on the resistance of SW and MWCNT–Me interconnects (Me = Ni, Cu, Ag, Pd, Pt, Au) for a predefined CNT geometry.

# **4.2 Electronic Structure Calculations of Nanocarbon- Based Interfaces**

Resistivity can be considered as a scattering problem, where the current carriers participate in the transport, according to various mechanisms based on the presence of scattering centres (phonons, charge defects, structural defects, etc.), including a

**Fig. 4.4** The scattering paradigm: influence (*in*) and response (*out*)



pure elastic way, called ballistic (Matissien rule). The developed computational procedure is based on the construction of cluster potentials and the evaluation of the S- and T-matrices for scattering and transfer, respectively, [8, 10]. It allows us to realize the full-scale electronic structure calculations for condensed matter ('black box'), where influence means a set of electronic 'trial' energy-dependent wave functions  $\Psi_{\rm in}(\mathbf{r})$  and response  $\Psi_{\rm out}(\mathbf{r})$  gives a set of scattering amplitudes corresponding to possible scattering channels for any 'trial' energy. This allows us 'to decrypt' the electronic spectra of 'black box' [10, 12].

The scattering paradigm is presented in Fig. 4.4. This allows us to realize full-scale electronic structure calculations for condensed matter.

We consider a domain where the stationary solutions of the Schrödinger equation are known, and we label them as:

$$\psi_{\rm in}(\mathbf{r}) = \varphi_{\mathbf{k}}(\mathbf{r}) = \exp(i\mathbf{k}\mathbf{r}).$$
 (4.1)

The scattering of 'trial' waves, in the presence of a potential, yields new stationary solutions labelled as:

$$\psi_{\text{out}}(\mathbf{r}) = \psi_{\mathbf{k}}^{(\pm)}(\mathbf{r}) \tag{4.2}$$

for the modified Schrödinger equation  $\hat{H}\psi_{\mathbf{k}}^{(\pm)}(\mathbf{r}) = E\psi_{\mathbf{k}}^{(\pm)}(\mathbf{r})$ . An electronic structure calculation is considered here as a scattering problem, where the centres of scattering are identified with the atoms of clusters [1, 12].

The first step to modelling is the construction of potentials [12], both atomic and crystalline, which is based on analytical Gaspar's potential of screened atomic nucleus [13] and  $X\alpha$  and  $X\alpha\beta$  presentations for the electronic exchange and correlation, using the LDA (*local density approximation*).

Figure 4.5 shows both atomic and crystalline potentials for carbon as compared to the Hartree–Fock atomic potential. Then, we apply the so-called muffin-tin approximation (*MTA*) for potential models.

To obtain an electronic structure, the calculations of scattering properties are necessary, generally, in the form of *S*- and *T*-matrices (Fig. 4.3). These calculations start with the definition of the initial atomic structure to produce a medium for the solution of the scattering problem for a trial electronic wave. The results of the potential modelling and phase shifts in the framework of *MT*-approximation are presented elsewhere.

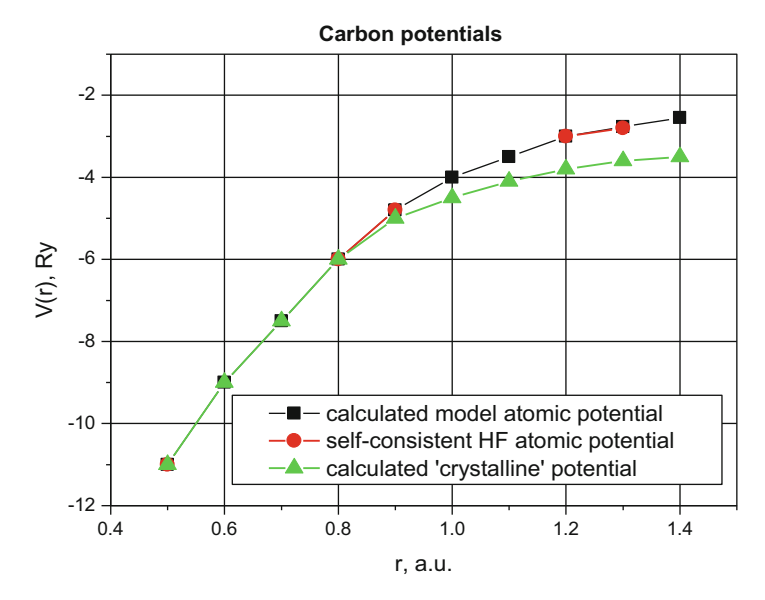


**Fig. 4.5** Analytical carbon potentials based on a simulation procedure as compared to the results of Hartree–Fock calculations [1]

The formalism used here for calculations on the electronic structure is based on the CPA, the multiple scattering theory and cluster approach. As a *first step*, we postulate the atomic structure at the level of short- and medium-range orders. As a *second step*, we construct a 'crystalline' potential and introduce the muffin-tin (*MT*)-approach. This is accomplished by using realistic analytical potential functions (e.g. [1, 8]).

The scattering paradigm for the simplest cases of spherically symmetrical potentials (elastic scattering) looks as follows:

$$\psi(\mathbf{r}) \to e^{\mathrm{i}kz} + f(\theta) \frac{e^{\mathrm{i}kr}}{r}$$
 ("liquid metal" model) (4.3)

and

$$\psi(\mathbf{r}) \to e^{\mathrm{i}kz} + f(\theta, \varphi) \frac{e^{\mathrm{i}kr}}{r}$$
 (spherical cluster model). (4.4)

Then, the electronic wave scattering problem is solved, and the energy dependence of the scattering properties for isolated MT-scatterers is obtained in the form of the phase shifts  $\delta_{lm}(E)$ , and the T-matrix of the cluster is found as a whole. The indices l and m arise, as a result of expansions of such functions as Bessel's functions  $j_l$ , Hankel's functions  $h_l$  and spherical harmonics  $Y_{lm}$ .

In general, the modelling of disordered materials represents them as a set of atoms or clusters immersed in an effective medium, with the dispersion  $E(\mathbf{K})$  and a

complex energy-dependent coherent potential  $\Sigma(E)$  found self-consistently in the framework of the CPA. The basic equations of this approach are:

$$\Sigma(E) = V_{\text{eff}} + \langle T \rangle (1 + G_{\text{eff}} \langle T \rangle)^{-1}, \tag{4.5}$$

$$G(E) = G_{\text{eff}} + G_{\text{eff}} \langle T \rangle G_{\text{eff}} = \langle G \rangle,$$
 (4.6)

$$\langle T(E, \mathbf{K}) \rangle = 0, \tag{4.7}$$

$$\Sigma(E) = V_{\text{eff}},\tag{4.8}$$

$$\langle G \rangle = G(E) = G_{\text{eff}},$$
 (4.9)

$$N(E) = -(2/\pi) \ln \left\{ \det \|G(E)\| \right\}. \tag{4.10}$$

Here < ... > denotes averaging;  $V_{\rm eff}$  and  $G_{\rm eff}$  are the potential and the Green's function of the effective medium, respectively;  $T(E, \mathbf{K})$ , the T-matrix of the cluster; and N(E), the integral density of the electronic states. Equation (4.7) can be re-presented in the form:

$$\langle T(E, \mathbf{K}) \rangle = \mathbf{Sp}T(E, \mathbf{K}) = \int_{\Omega_{\mathbf{K}}} \langle \mathbf{K} | T(E, \mathbf{K}) | \mathbf{K} \rangle d\Omega_{\mathbf{K}} = 0,$$
 (4.11)

where  $|\mathbf{K}\rangle = 4\pi \sum_{l,m} (\mathrm{i})^l j_l(kr) Y_{lm}^*(\mathbf{K}) Y_{lm}(\mathbf{r})$  is the one-electron wave function, **Sp** 

means the calculation of the matrix trace while the integration is performed over all angles of **K** inside the volume  $\Omega_{\mathbf{K}}$ . Equation (4.7) enables obtaining the dispersion relation  $E(\mathbf{K})$  of the effective medium. The DOS calculations have been performed using the relation:

$$\rho(E) = \frac{2}{\pi} \int \operatorname{Im} \{ \mathbf{SpG}(\mathbf{r}, \mathbf{r}', E) \} d\mathbf{r}, \tag{4.12}$$

where  $G(\mathbf{r}, \mathbf{r}', E) = \sum_{l,m} Y_{lm}(\mathbf{r}) Y_{lm}(\mathbf{r}') G_l(\mathbf{r}, \mathbf{r}')$  is the angular expansion of Green's function.

The paradigm of the scattering theory and the developed strategy of simulation of CNTs electronic properties use the generalized scattering condition for the low-dimensional atomic structures of the condensed matter:

$$\psi_{\mathbf{k}}^{(\pm)}(\mathbf{r}) \underset{r \to \infty}{\propto} \phi_{\mathbf{k}}(\mathbf{r}) + f_{\mathbf{k}}^{(\pm)}(\Omega) \frac{\exp(\pm ikr)}{r^{(d-1)/2}}, \tag{4.13}$$

where  $\Omega$  describes the integrated space in angular units while superscripts '+' and '-' label the asymptotic behaviour in terms of *d*-dimensional waves:

$$\frac{\partial \sigma_{a \to b}}{\partial Q} = \frac{2\pi}{\hbar v} \left| \langle \varphi_b | \hat{V} | \psi_a^+ \rangle \right|^2 \rho_d(E), \tag{4.14}$$

where d is the atomic structure dimension.

The calculations of conductivity are usually performed using Kubo-Greenwood formula [14]:

$$\sigma_{E}(\omega) = \frac{\pi \Omega}{4\omega} \int [f(E) - f(E + \hbar \omega)] |D_{E}|^{2} \rho(E) \rho(E + \hbar \omega) dE, \qquad (4.15)$$

where  $\omega$  is a real frequency parameter of Fourier transform for the time-dependent functions, f(E) is Fermi-Dirac distribution function,  $D_{E,E'} = \int_{\Omega} \Psi_{E'}^* \nabla \Psi_E d\mathbf{r}$ ,  $\Psi_E$ 

 $_{(\mathbf{K})} = A \exp(i\mathbf{K}\mathbf{r})$  and **K** is the complex wave vector of effective medium.

The dispersion function  $E(\mathbf{K})$  determines the properties of the wave function  $\Psi_E$  upon the isoenergy surface in **K**-space.

For static conductivity ( $\omega = 0$  and T = 0 K), Eq. (4.16) gives the Drude-like formula:

$$\sigma_{E(\mathbf{K})} = \frac{e^2 n^*}{m^*} \tau, \tag{4.16}$$

where  $n^*$  is the effective electron density with a relaxation time  $\tau \approx l/v_h$ , l(T) is the free path while a heat velocity is  $v_h = (3kT/m*)^{1/2}$ . The effective electron mass can be defined using the dispersion law:

$$m^* = \left(\partial^2 E / \partial K_R^2\right)^{-1},\tag{4.17}$$

where  $K_R$  is a modulus of the real part of the vector **K**.

There are some ideas to estimate the conductivity in static and frequency regimes taking into account the temperature effects. However, in the case of CNT (of GNR), we must consider not only the diffusive mechanism of conductivity but also the 'so-called' ballistic one. This is an evident complication in the interpretation of electrical properties of CNTs, GNRs and the related systems.

Usually two basic electron conductivity mechanisms in CNT-based structures are considered. The ballistic mechanism is engaged in electron transport within CNTs, while the collisional mechanism is characteristic of CNT-substrate interconnects. Hence the general conductivity  $\sigma_{\rm gen}$  is evaluated as follows:  $\sigma_{\rm gen}^{-1} = \sigma_{\rm coll}^{-1} + \sigma_{\rm ball}^{-1}$ . For pure CNTs, we clearly observe that  $\sigma_{\rm ball} \gg \sigma_{\rm coll}$ . The collisional contribution is basically connected with the specific morphology of interconnects space [14]. In the framework of multiple scattering theory formalism and effective medium approximation, we can evaluate both factors of conductivity.

# **4.3** Electromagnetics of CNT and Graphene-Based Systems

# 4.3.1 'Liquid Metal' Model for CNT-Metal Junction: CNT-Ni case

The term 'liquid metal' means the structural disorder of the substance involved; more precisely, only the nearest order (short-range order – SRO) is considered as it usually occurs in a liquid. It also means that the interatomic distance between the nearest neighbours (first coordination sphere) is fixed, whereas the angular coordinates are random. In the context of this model, the interconnect space C-Ni is considered as 'liquid' alloy  $C_xNi_{1-x}$ .

Both Figs. 4.6 and 4.7 depict the idealized images of contacts between CNTs and the Ni substrate.

The model in CPA approach (4.11) gives the dispersion law for the effective medium and the electronic density of states (EDOS, see Eq. (4.12)), where the argument **K** of dispersion function  $E(\mathbf{K})$  is a complex:  $\mathbf{K_R} + i\mathbf{K_I}$ . The 'mixed' dispersion law [12]:

$$E_{\mathrm{C-Ni}}(\mathbf{K_R}) = xE_{\mathrm{C}}(\mathbf{K_R}) + (1 - x)E_{\mathrm{Ni}}(\mathbf{K_R}) \tag{4.18}$$

means configurationally averaged state of the electronic structure within the interconnect space with a variable extent of disorder. The 'liquid metal' alloy model can be used for evaluating mixed effective mass  $m^*_{\text{C-Ni}}(E)$  (see Eq. (4.17)). Taking into account the spectral dependence of the effective mass  $m^*(E)$  and estimating the spectral resistivity  $\rho_x(E) = 1/\sigma_x(E)$ , and following Eq. (4.16), we can estimate the average layer resistivity  $\rho_{x,\text{av}}$  as follows:

**Fig. 4.6** Fragment of interconnects between the Ni substrate and C nanotubes

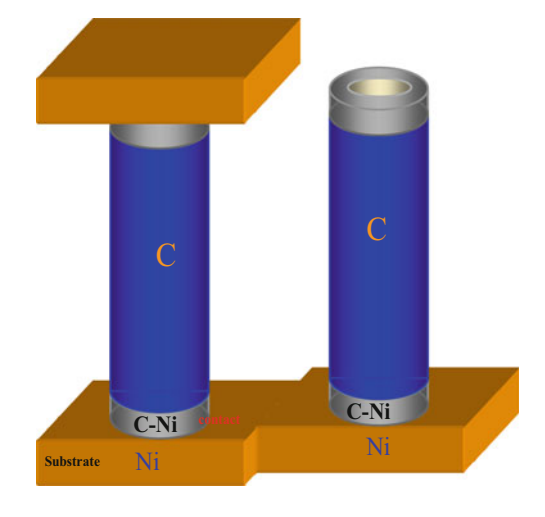


**Fig. 4.7** Model of CNT–Ni interconnect as a disordered alloy

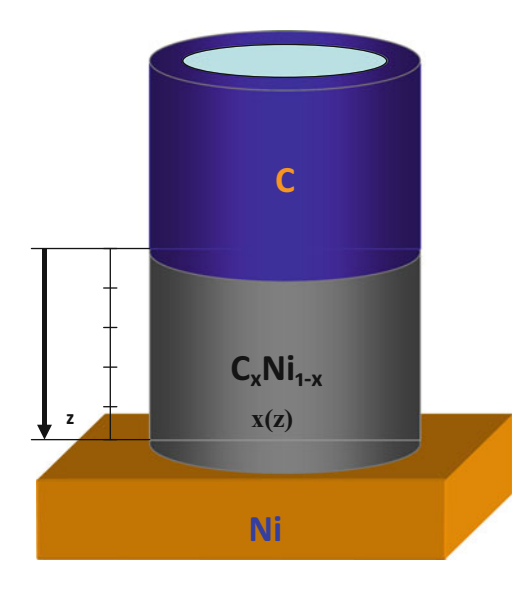


**Table 4.1** Dependence of specific resistivity  $\rho(x)$  on alloy composition (x)

No.	x	Layer resistivity $C_x Ni_{1-x}$ , $\rho(x)$ , $10^2$ Ohm'nm
1	0.00	0.807
2	0.10	0.813
3	0.20	0.821
4	0.30	0.833
5 6	0.40	0.849
6	0.50	0.871
7	0.60	0.905
8	0.70	0.962
9	0.80	1.081
10	0.90	1.458
11	1.00	8.231

$$\rho_{x,\text{av}} = \frac{\int_0^{E_{\text{fin}}} \rho_x(E) dE}{E_{\text{fin}}},\tag{4.19}$$

where  $E_{\rm fin}$  is the width of the conduction band and x(z) is the stoichiometry coefficient depending on the coordinate z of the ring layer (Fig. 4.7). The dependence of specific resistivity on alloy composition is presented in Table 4.1.

The evaluation of resistance for the CNT–Ni contact gives ~105 kOhm for the nanotube with the internal and external radii  $-R_1 = 1.0$  nm and  $R_2 = 2.0$  nm, respectively.

Evidently, the results of the resistance evaluation for interconnect depend essentially on both the layer height  $l_0$  and the spectral integration parameter  $E_{\rm fin}$ , which is responsible for the electron transport of really activated *hot electrons*.

The 'liquid metal' model [12] does not operate with CNT chirality in the interconnect space. Limitations of chirality effects (e.g. chirality angle) in the CNT–Me junctions forced to develop a semiempirical model that considers the local atomic structure of the interconnect. For this aim, we have constructed a model of 'effective bonds' for the interconnect with a realistic atomic structure.

# 4.3.2 Model of 'Effective Bonds' for Simulations of CNT–Me and GNR–Me Junctions

The model of CNT–Me and GNR–Me nanointerconnects (Fig. 4.1) has been developed in the present research. Within the electronic transport formalism, it consists of two regions supporting two different electron transport mechanisms: *ballistic* (elastic) and *collisional* (non-elastic). These electron transport processes are simulated using the corresponding boundary conditions in the form of the effective medium. The CNT and GNR chiralities (*n*,*m*) are simulated by the corresponding orientation of the chirality vectors within the scattering medium. The most problematic areas for the proper simulation are CNT–Me and GNR–Me *end-type* junctions, where the atomic structural disorder (non-regularity) is observed and the conductivity mechanism is changed.

The influence of chirality on resistance in the vicinity of interconnect depends on the number of statistically realized bonds between the CNT (GNR) and the metal contact (e.g. Ni, Cu, Au, Ag, Pd, Pt).

Using the simulation models, presented earlier [1], we have determined the resistance for both (SW and MW) CNT–Me and (SL and ML) GNR–Me interconnects, based on the evaluation of the interface potential barriers and implementation of Landauer formula [14], which defines the integrated conductance:

$$I_G = \frac{2e^2}{h} \sum_{i=1}^{N} T_i = \left(\frac{1}{12.92(\text{kOhm})}\right) \sum_{i=1}^{N} T_i = 0.0774 \sum_{i=1}^{N} T_i.$$
 (4.20)

The chirality (m,n) is simulated by the corresponding orientation of carbon rings within the scattering medium (Fig. 4.8).

CNT interconnect configuration models for zigzag and armchair morphologies and active bond formation for computer simulations are presented in Figs. 4.9 and 4.10.

Figures 4.11, 4.12 and 4.13 demonstrate *end-type* contact formation.

In the case of *side-type* contact for GNR–Me interconnects, the number of effective bonds per contact square is quite high (see Fig. 4.14).

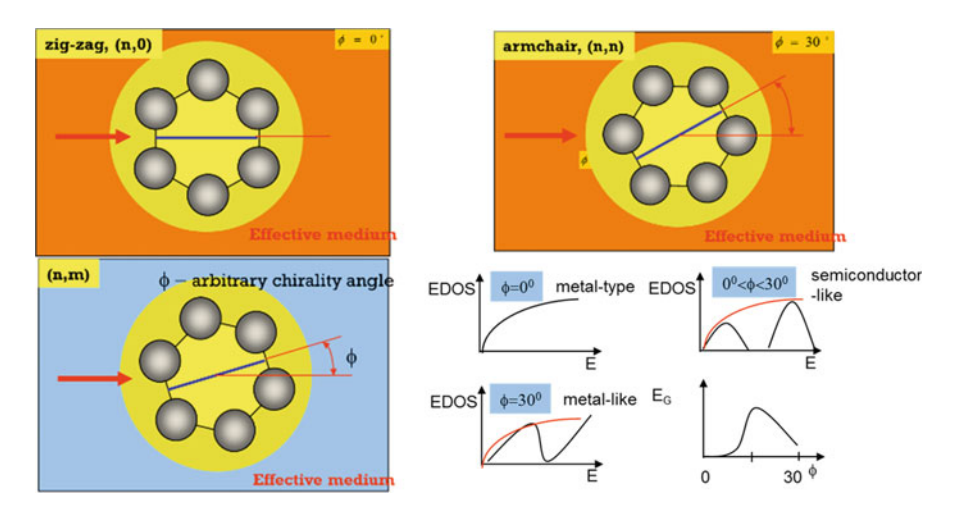


Fig. 4.8 Modelling of chirality: carbon ring rotation within CNT and GNR and the expected results

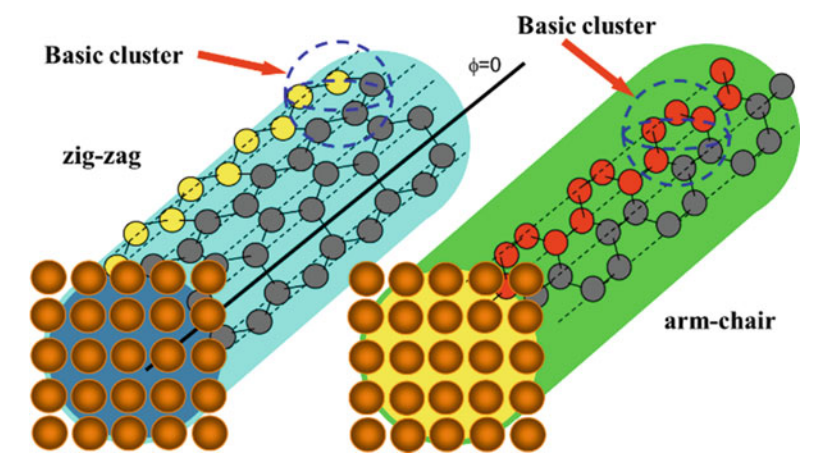


Fig. 4.9 CNT interconnect configuration model

#### 4.3.3 SWCNT and SL and ML GNR Simulations

Figures 4.11, 4.12 and 4.13 present a creation of C–Me 'effective bonds'. Substrates of *fcc*-metals are considered here [100]. It should also be emphasized that this is a probabilistic process when only more-or-less equilibrium bonds ('effective bonds') are formed at interatomic distances corresponding to the minimum total energies. The evaluation of a number of 'effective bonds' using Eq. (4.20) is principal for the number of 'conducting channels', since the conductance is proportional to the number of appeared 'effective bonds' within the CNT–Me interconnect.

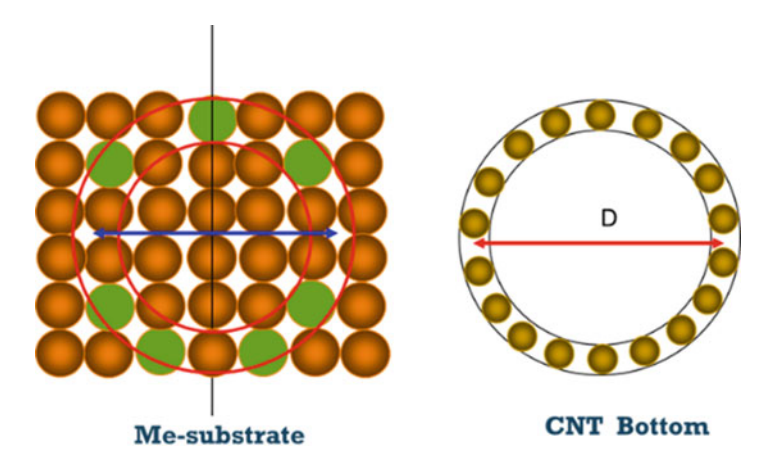


Fig. 4.10 Active bonds formation in the simulation of catalytic growth of CNT on the Me-substrate

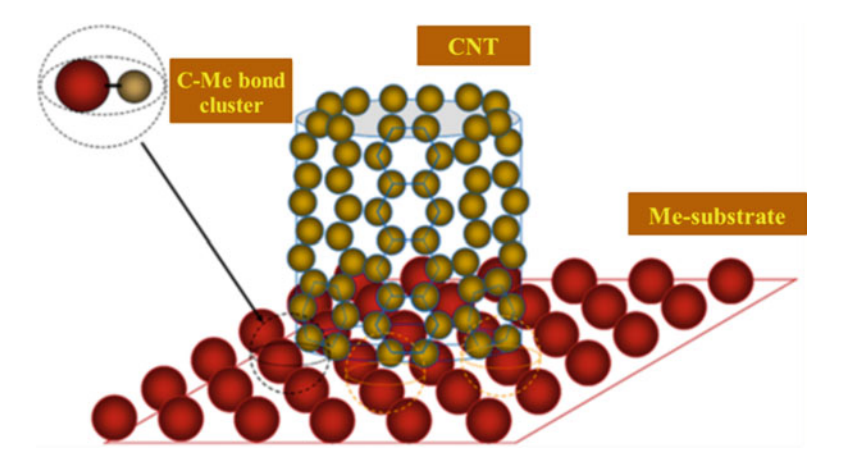


Fig. 4.11 CNT-Me interconnect formation model

The calculations of the 'effective bonds' capabilities lead to an estimate of the energy-dependent transparency coefficient of the potential barrier C–Me (Figs. 4.15 and 4.16). The scattering process for this potential barrier is regulated by the effect of 'thin film' for conductivity electrons, which leads to quantization in voltaic parameters (in the case of full transparency). The transmission (transparency) coefficient T for the barrier scattering problem (Fig. 4.16) is defined as:

$$T = \sqrt{\frac{E_2}{E_1}} \left( \frac{2\sqrt{E_1}}{\sqrt{E_1} + \sqrt{E_2}} \right)^2, \tag{4.21}$$

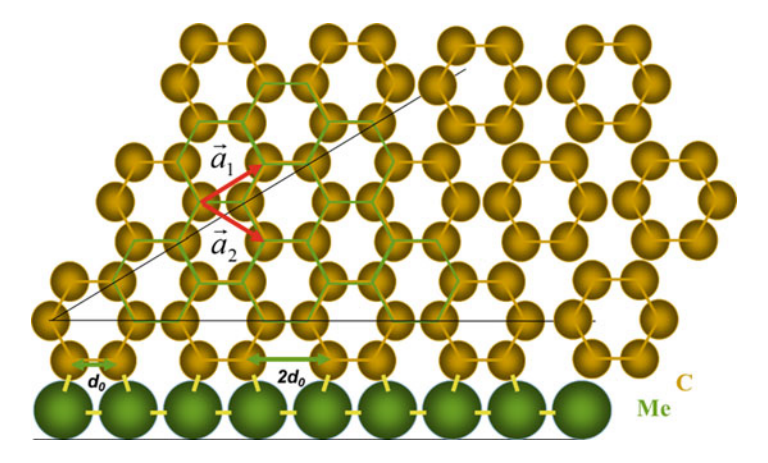


Fig. 4.12 Zigzag CNT-Ni interconnect formation

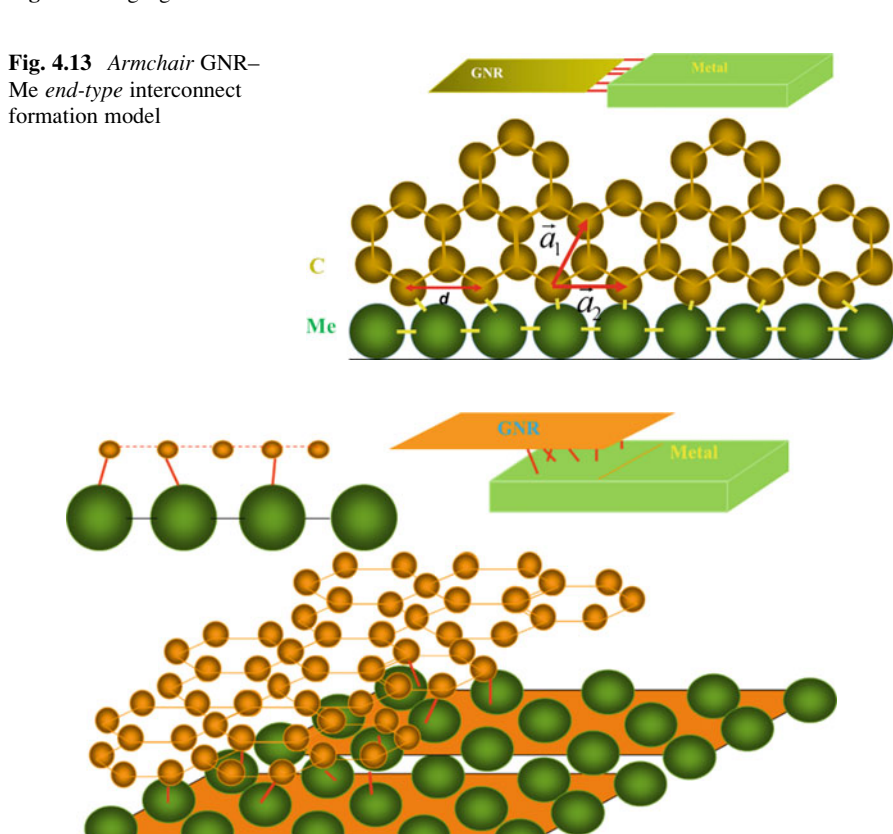


Fig. 4.14 GNR-Me side-type interconnect formation model

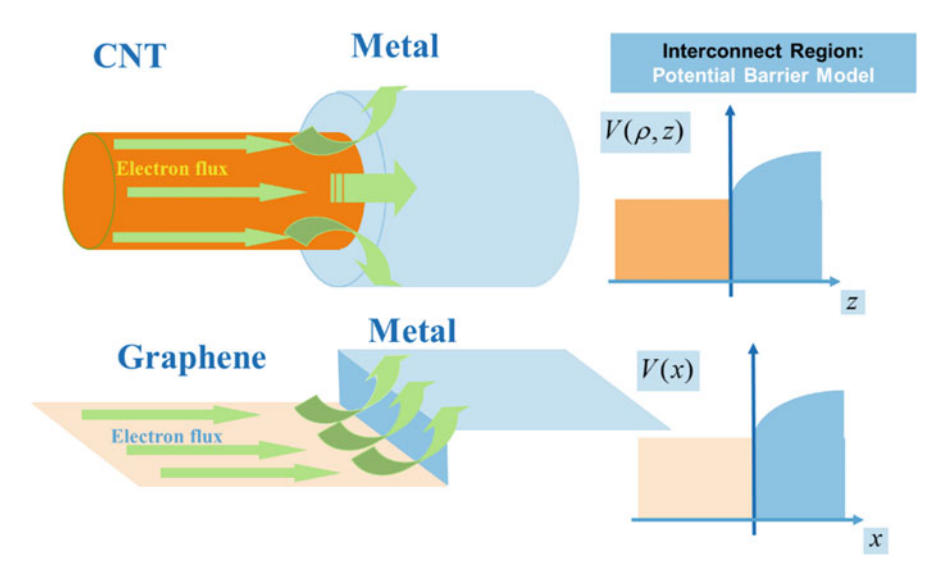


Fig. 4.15 Interconnect potential model for the scattering problem: CNT-Me, GNR-Me

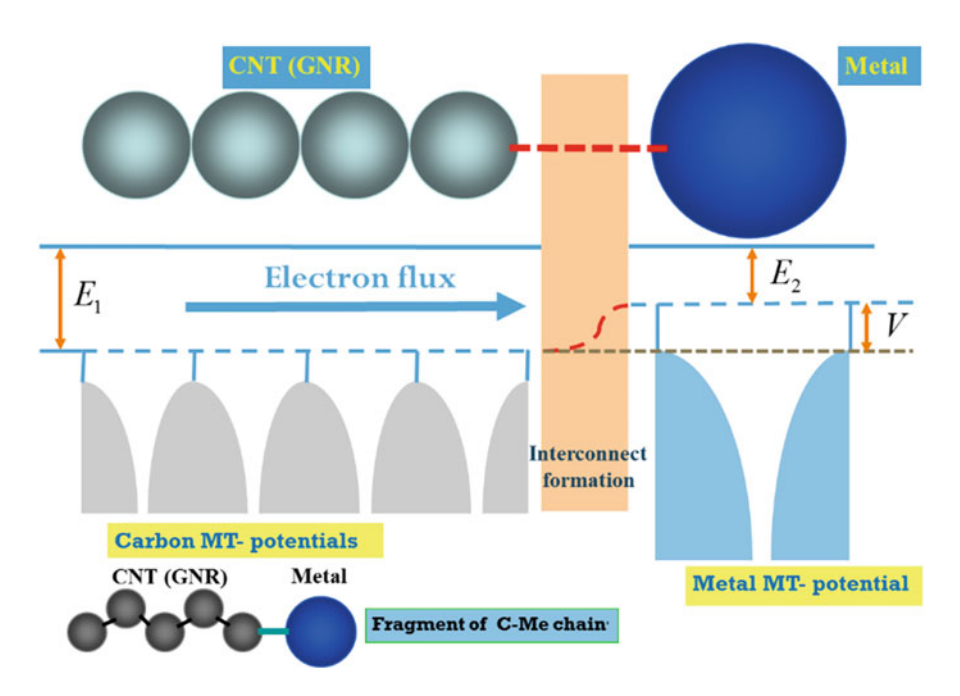


Fig. 4.16 Formation of a potential barrier for SWCNT-Me (SL GNR-Me) junction

Diameter	Chirality	Number of bonds	Modulus of chirality	Interconnect
(nm)	indices	in contact	vector (nm)	resistance (kOhm)
$_{\rm zigzag}, \phi = 0$	•			
1.010	C(13,0)	12	2.952	665,19
2.036	C(26,0)	24	6.394	333,33
5.092	C(65,0)	64	15.990	124,72
10.100	C(130,0)	129	32.002	61,87
20.360	C(260,0)	259	63.940	30,82
$_{\text{armchair}}, \phi = 30^{\circ}$				
0.949	C(7,7)	12	2.982	665,19
2.035	C(15,15)	28	6.391	205,71
5.021	C(37,37)	72	15.765	111,11
10.041	C(74,74)	146	31.531	54,79
20.084	C(128,128)	294	63.062	27,21
$_{\mathrm{C}(3m,m)},\phi=$	14°			
0.847	C(9,3)	3	2.66	2666,66
1.694	C(18,6)	5	5.32	1600,00
5.082	C(54,18)	16	15,96	500,00
10.16	C(108,36)	36	32.05	222,22
20.32	C(216,72)	80	64.10	100,00
$C(2m,m), \phi = 19^{\circ}$				
1.036	C(10,5)	5	3.254	1600,00
2.072	C(20,10)	9	6.508	888,88
4.973	C(48,24)	17	15.614	470,50
10.1528	C(98,49)	47	31.880	170,21
20.5128	C(198,99)	97	64.410	82,47

**Table 4.2** Resistances for SWCNT-Ni interconnects

where  $E_1$  and  $E_2$  are the corresponding electron energies. Evaluation of resistances of CNT–Ni junctions for various NT diameters and chiralities is presented in Table 4.2 (see also Figs. 4.17 and 4.18).

These resistances have been evaluated taking into account that only thermally activated electrons, i.e. a small part  $\Delta n$  of all quasi-free electrons n, participate in the conductance process with Fermi velocity  $v_F$ . This ratio can be evaluated as follows (see also Fig. 4.19):

$$\frac{\Delta n}{n} \approx \frac{\frac{1}{2}\rho(E_F(0)kT)}{\frac{2}{3}\rho(E_F(0))E_F(0)} = \frac{3}{4}\frac{kT}{E_F(0)},$$
(4.22)

where f(E) is Fermi–Dirac distribution function and  $\rho(E)$  is a DOS while kT = 0.0258 eV for T = 300 K.

Evaluations of thermalization effect for Ni, Pd and Au substrates are presented in Fig. 4.20.

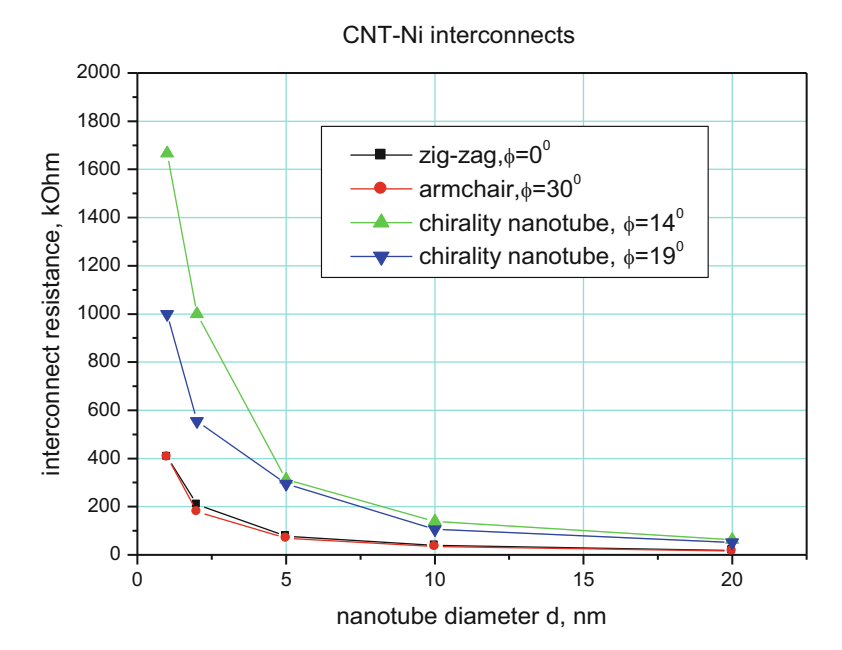


Fig. 4.17 CNT-Ni interconnect resistances via NT diameter

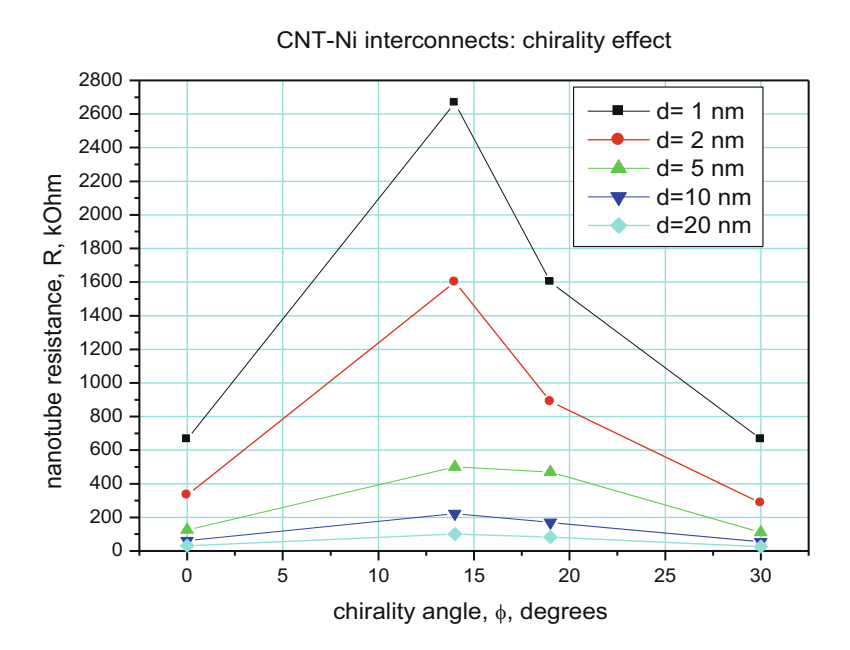
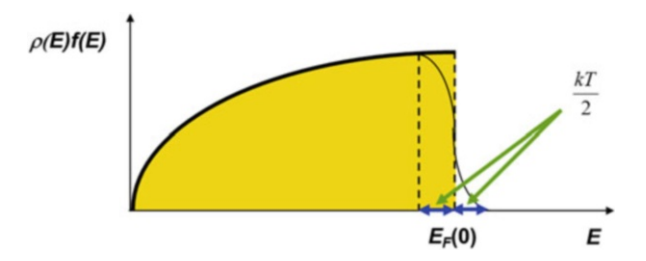
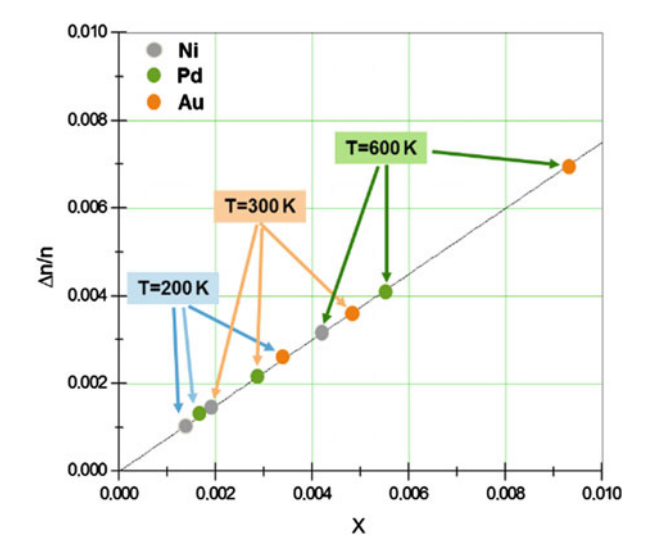


Fig. 4.18 CNT-Ni interconnect simulation: chirality effects

**Fig. 4.19** Hot electrons of conductivity: evaluation of thermalization factor



**Fig. 4.20** Thermalization effect in CNT-Ni, CNT-Pd and CNT-Au



$$\frac{\Delta n}{n} = \frac{3}{4} \frac{kT}{E_F(T)} \approx \frac{3}{4} \frac{kT}{E_F(0)} \frac{1}{1 - \left(\frac{\pi kT}{2\sqrt{3}E_F(0)}\right)^2},$$

$$x = \frac{kT}{E_F(0)}, \frac{\Delta n}{n} \approx 0,75 \frac{x}{1 - 0.82x^2}.$$

The role of thermally activated electrons is described by the scattering mechanism changing in the space of CNT–Me interconnect. The mean free path L in the CNT is of order  $10^2-10^4a_{\rm C}$ , where  $a_{\rm C}$  is a carbon covalent radius, which can be explained by the ballistic mechanism of electron transport within the energy channel of the CNT. At the vicinity of interconnect, we observe a drastic decrease of the electron mean free path down to  $1-2~a_{\rm C}$ . From the uncertainty condition  $\kappa L \approx 1$  (where  $L \sim a_{\rm C} \sim 2~a.u.$  is a free path), it is possible to evaluate Fermi electron wave number  $\kappa \propto \kappa_F \approx 1/a_{\rm C} \approx 0.5~{\rm a.u.}^{-1}$ . It means that  $E_F \sim 0.25~{\rm Ry}$ , i.e. a large increase of resistance, occurs in the interconnect space. In particular, the variation of the chirality angle  $\phi$  within the interconnect space leads to the fluctuation of the number of C–Me atomic bonds. In the case of  $0^\circ < \phi < 30^\circ$ , a certain number of

non-stable and non-equilibrium bonds can be created. Evidently, this leads to the decrease of interconnect conductance, which is well observed when performing variation of nanotube diameter (Fig. 4.17).

Specific results for chirality effect simulations are shown in Fig. 4.18, with the evident maximum of the resistance for  $\phi \approx 15^{\circ}$ , where a large number of non-equilibrium bonds is formed, with higher potential barriers and lower transparency.

# 4.3.4 Parametric Calculations of CNT–Me Interconnect Resistances

In the course of the study, parametric calculations of the effective numbers of bonds and resistances for Ni, Pd and Au CNT interconnects were performed, where CNT diameters varied from 1 to 22 nm and chirality angle from 0° to 30° (with the step of 5°) for two basic metal substrate orientations ([100] and [111]). The aim of these detailed simulations is to create approximation dependences and data base of interconnect compositions for various technological applications [15, 16]. Technologically, reasonable results of these simulations (Au–Me interconnect [100], [111]) are shown in Fig. 4.21.

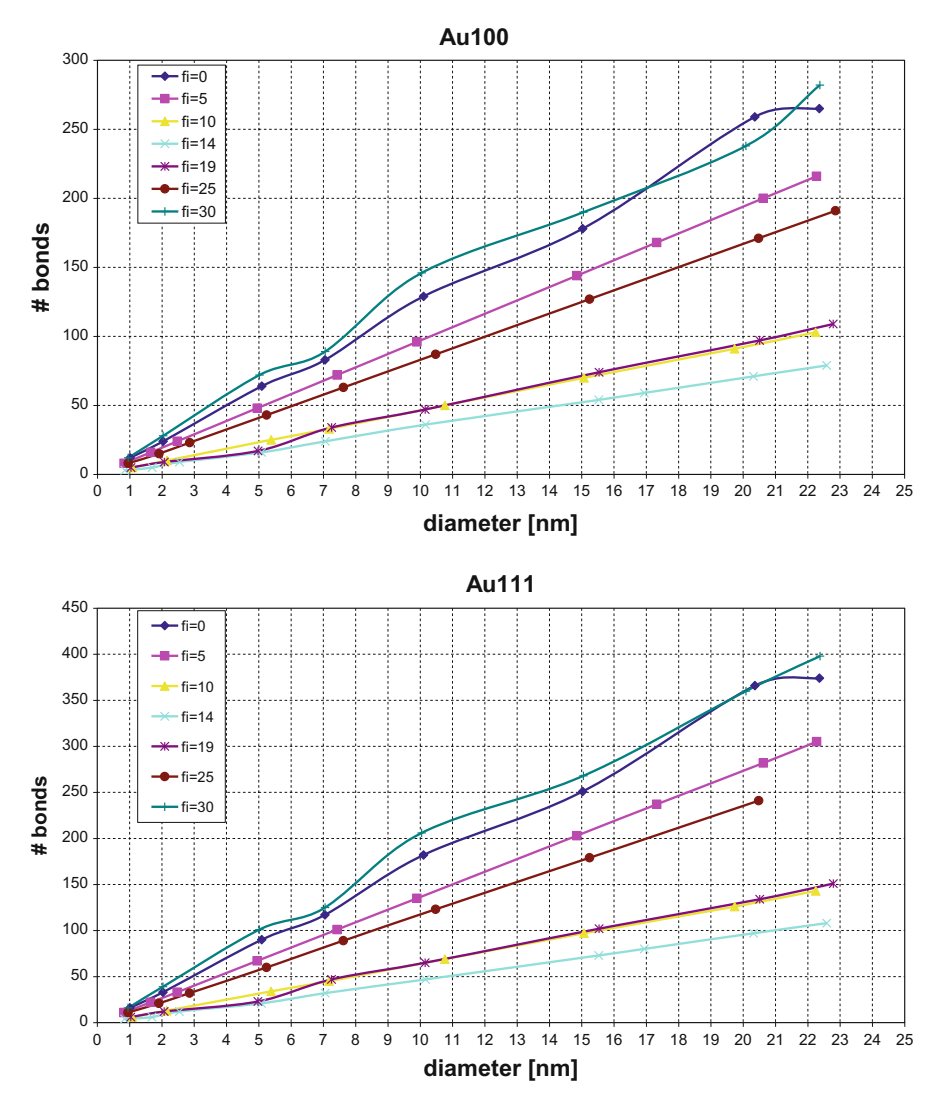
The dependence of the interconnect resistance on the number of effective bonds ( $R_{\text{interconnect}} \times N_{\text{eff. bonds}}$ ) is a constant value. In the case of CNT-Au interconnect ([100]), it equals approximately 4000 kOhm (Figs. 4.22 and 4.23).

Figure 4.24 shows the generalized results of simulations on resistance of junctions obtained for various metallic substrates. It is clear that Ag and Au substrates are more effective electrically while Ni appears much less appropriate substrate for interconnect, although it yields the most effective catalyst for CNT growth. On the other hand, the catalysts, which are usually used for the SWCNT growth (e.g. Fe, Co and Ni), have stronger bonds to the ends of SWCNTs than noble metals [16]; therefore, some compromise exists between electrical parameters and strengths of the interconnect bonding.

#### 4.3.5 Resistance MWCNT-Me Junctions

We have constructed atomistic model of MWCNTs which could fit into a porous alumina with the diameters of holes ~20 nm. In particular, a model of MWCNT with a predefined combination of *armchair* (ac) and zigzag (zz) shells is presented in Table 4.3 and Fig. 4.25.

Using the simulation models presented earlier, we have developed an 'effective bonds' model for MWCNT-Me junction resistance [12]. The results of these simulations are presented in Fig. 4.26. For MWCNT-Me junction, the integral



**Fig. 4.21** Results of parametric calculations of effective bonds via CNT diameter for CNT–Me interconnects: (a) Au[100]–CNT; (b) Au[111]–CNT; (c) Pd[100]–CNT; (d) Pd[111]–CNT; (e) Ni [100]–CNT; (f) Ni[111]–CNT

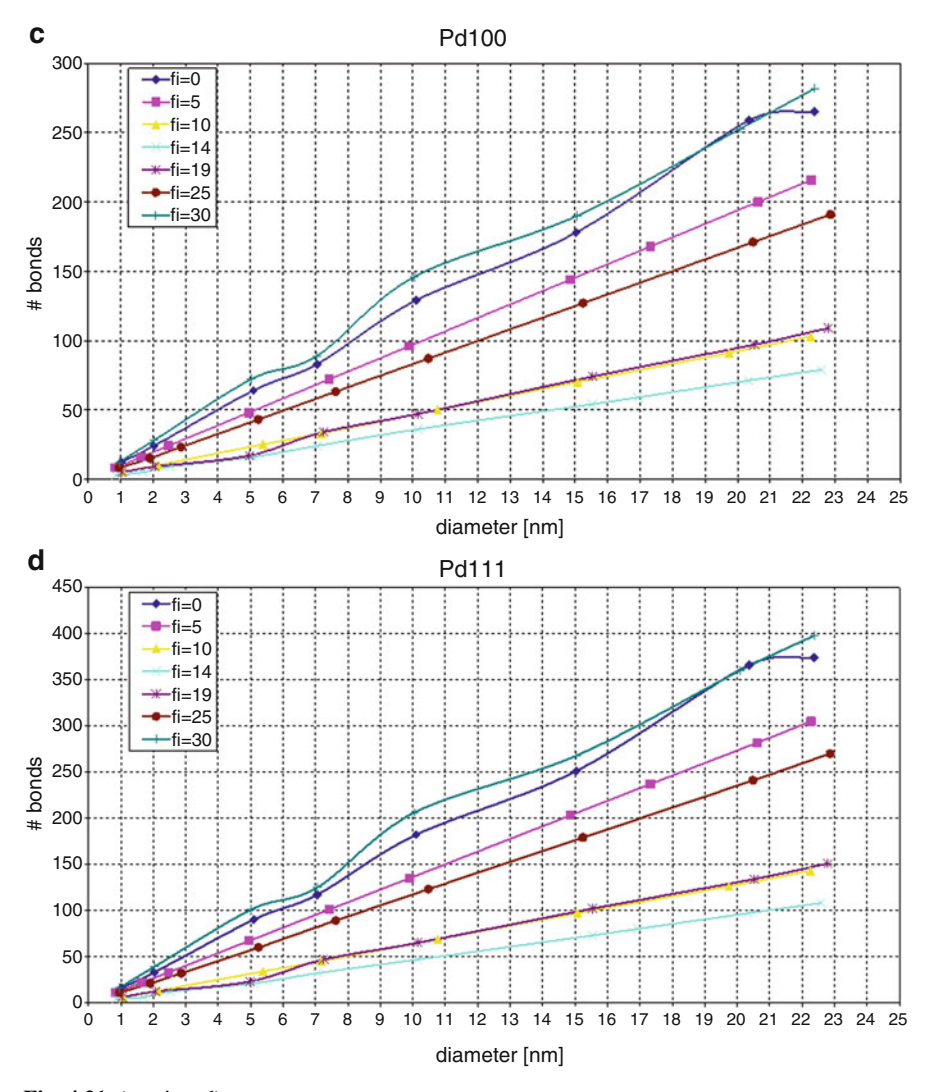


Fig. 4.21 (continued)

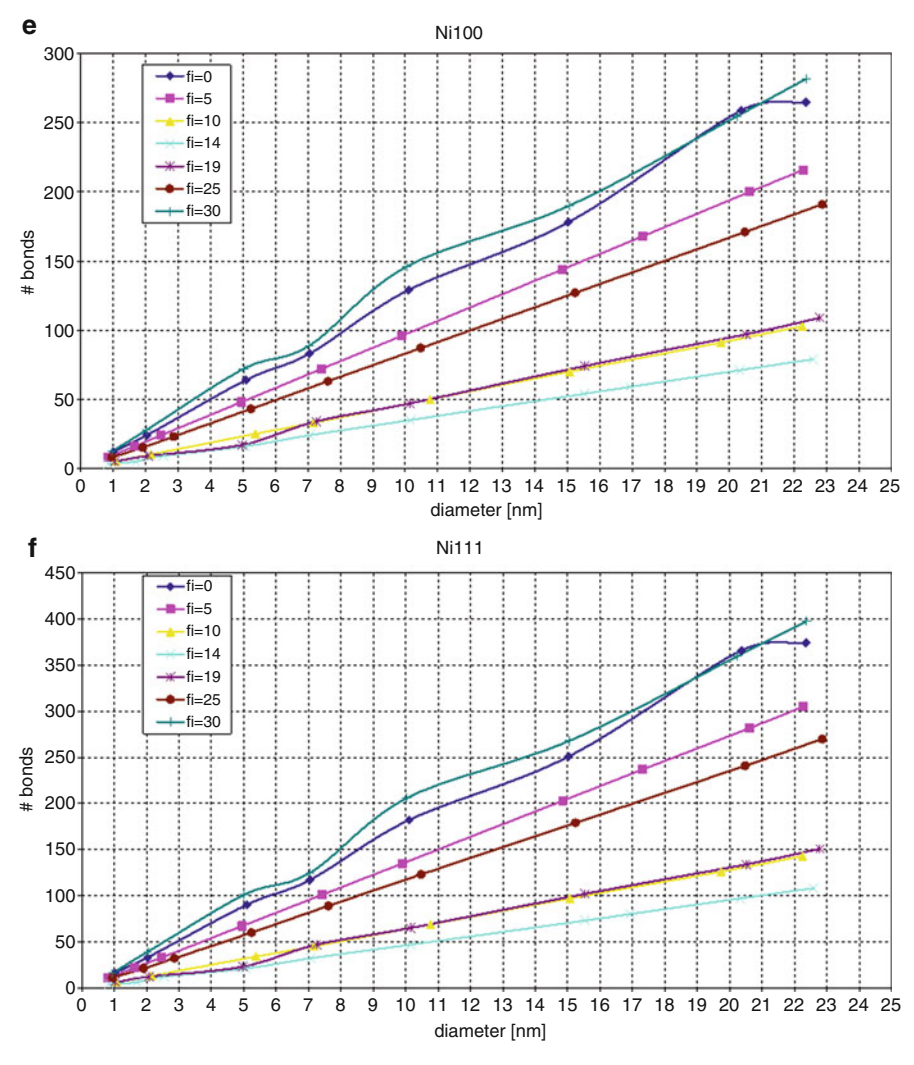


Fig. 4.21 (continued)

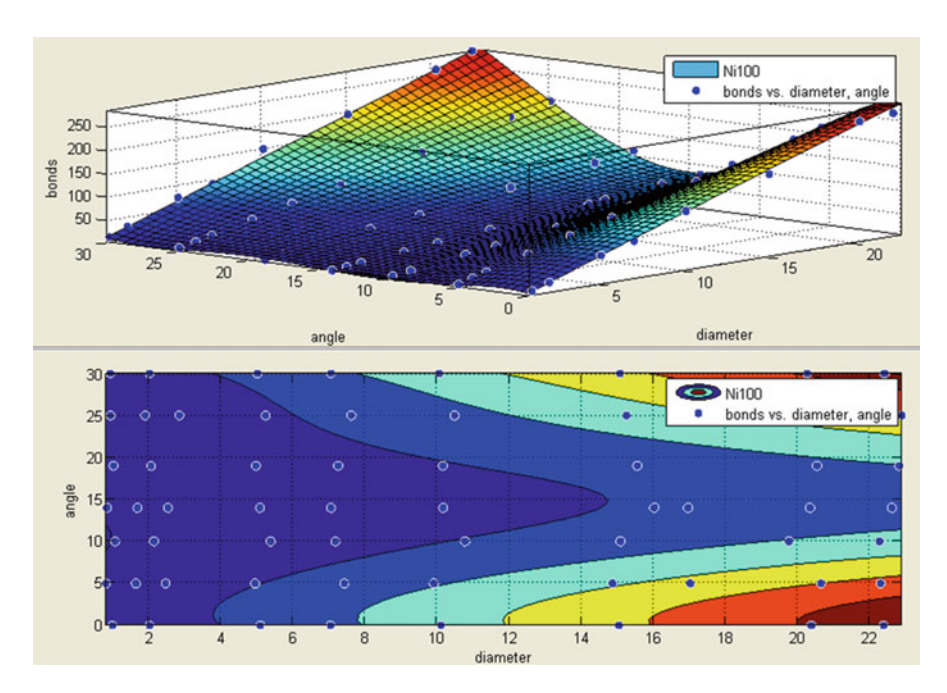


Fig. 4.22 3D-diagram of parametric calculations of effective bonds via CNT diameter for CNT-Ni interconnects

bonding with a corresponding substrate may be not as significant as in the case of SWCNTs, where a weak bonding can be fundamental. Figure 4.26 shows similar ratios of electric resistances for SWCNTs (Fig. 4.24), in favour of Au, Ag and Pt. It should be noted, that technological qualities of CNT–Me interfaces predefine the resulting resistance. In particular, experimental evaluations of CNT–Pt interconnect resistances for *side-type* and *end-type* contacts are 50 k $\Omega$  and 50–300 k $\Omega$ , correspondingly (see [17]).

## 4.3.6 Current Loss Between the Adjacent Shells Inside the MWCNT

Using the model of inter-shell potential within the MWCNT, the transparency coefficient has also been evaluated, which determines the possible 'radial current' losses. Figure 4.27 shows the inter-shell potential which is calculated using the developed realistic analytical potentials (see comments on the procedure of the potential construction, e.g. in [5]).

In Fig. 4.27, A is the electron emission energy, E is the electron energy and V is the height of the potential barrier between the nearest atoms in neighbouring

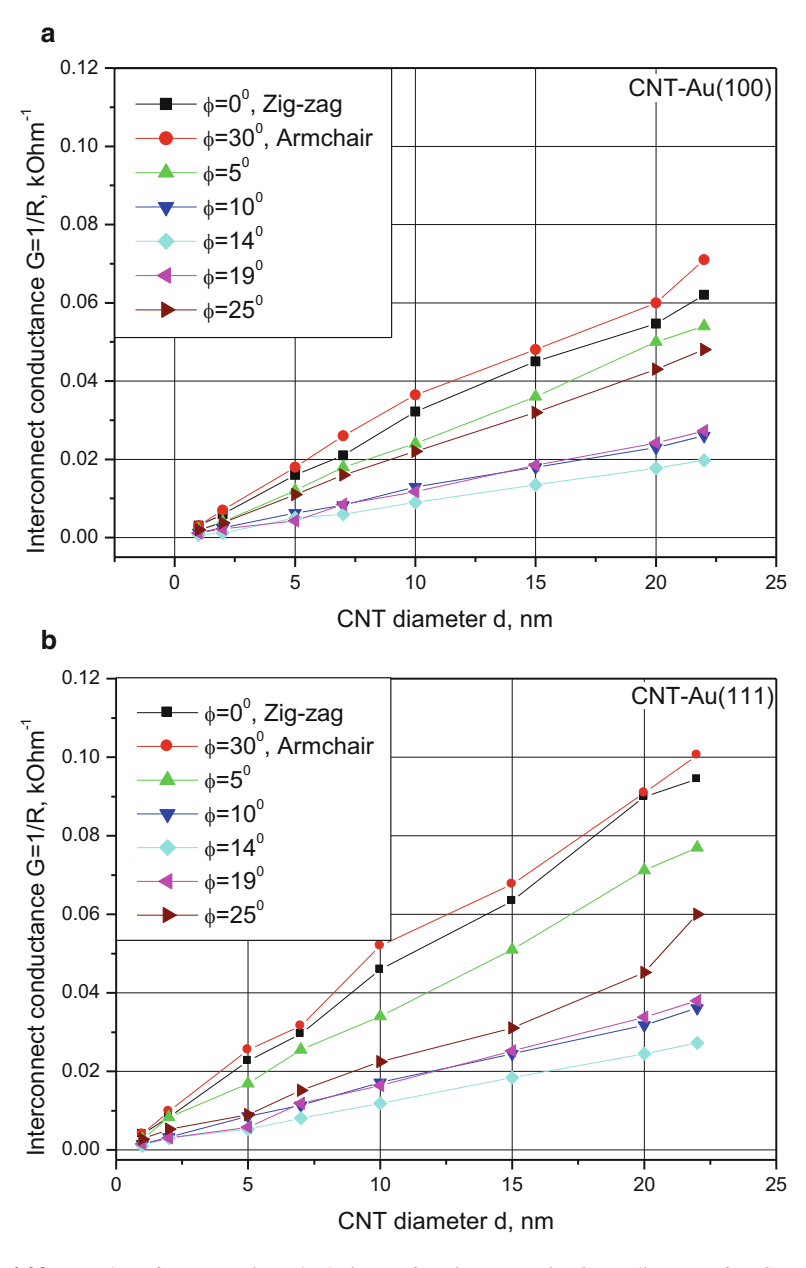


**Fig. 4.23** Results of parametric calculations of resistances via CNT diameter for CNT–Me interconnects: (a) Au[100]–CNT; (b) Au[111]–CNT; (c) Pd[100]–CNT; (d) Pd[111]–CNT; (e) Ni[100]–CNT; (f) Ni[111]–CNT

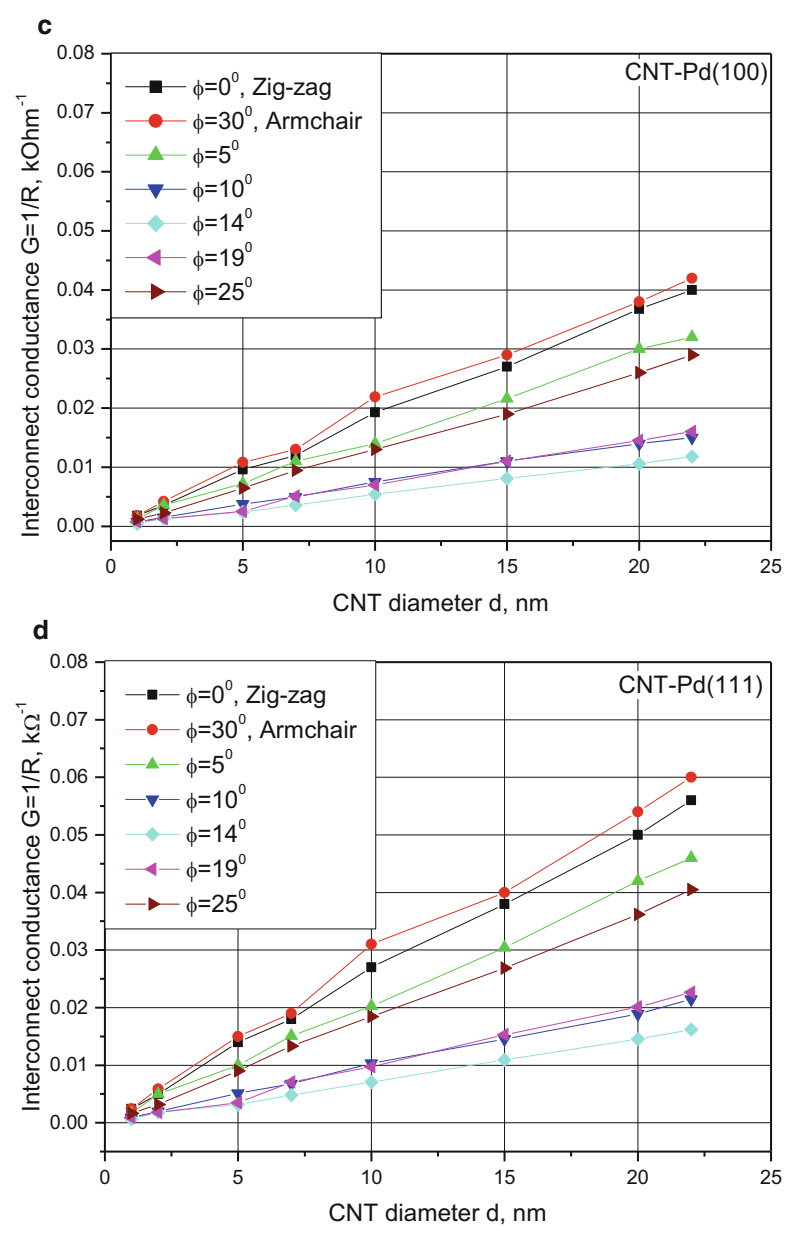


Fig. 4.23 (continued)

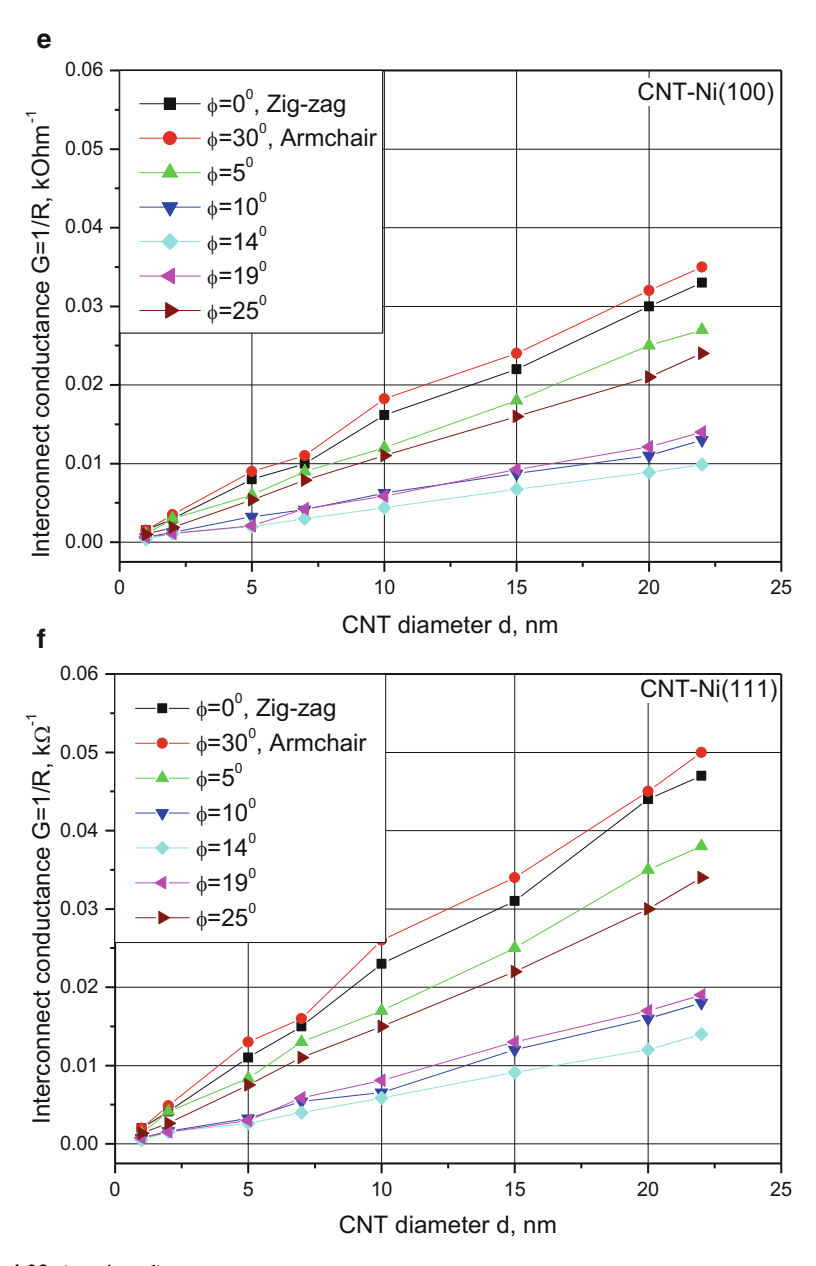


Fig. 4.23 (continued)

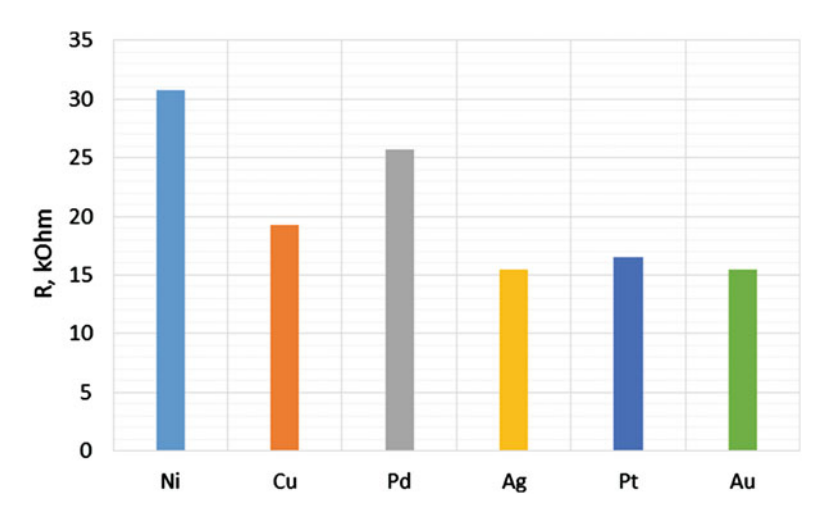


Fig. 4.24 Resistances of the zigzag-type SWCNT-Me interconnects for the CNT diameter ~1 nm

**Table 4.3** Details of the model for MWCNT–Me interconnects

Diameter of CNT shell (nm)	Chirality
12.88	(95,95) ac
13.54	(173,0) zz
14.24	(105,105) ac
14.87	(190,0) zz
15.58	(199,0) zz
16.27	(120,120) ac
16.99	(217,0) zz
17.69	(226,0) zz
18.44	(136,136) ac
19.18	(245,0) zz
19.88	(254,0) zz

nanotube shells. Thus, a radial transparency coefficient T for the two different energy ratios can be defined as follows:

$$E > V, T = \frac{4Ek_2^2}{\left(E - k_2^2\right)\sin^2 k_2 a + 4Ek_2^2}, k_2^2 = E - V, \tag{4.23}$$

$$E < V, T = \frac{4E\kappa_2^2}{(E - \kappa_2^2)sh^2\kappa_2 a + 4E\kappa_2^2}, k_2^2 = V - E,$$
 (4.24)

where  $k_2$  is the electron wave number in the case of above-barrier motion and  $\kappa_2$  is the same for under-barrier motion. For example, between the second and first shells (zz-ac case, Fig. 4.19) a=13.54–12.88=0.66 nm = 12.47 a.u. and  $T=3.469\cdot 10^{-6}$  per 1 bond.

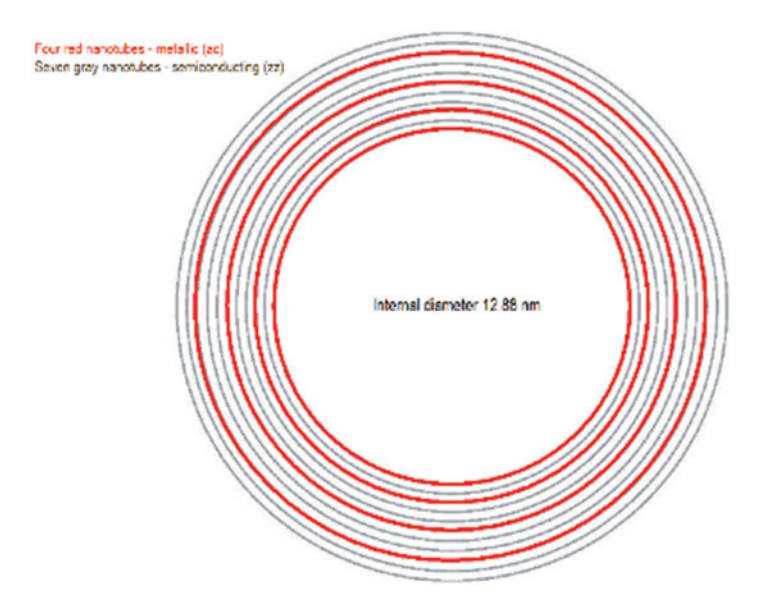


Fig. 4.25 Model of MWCNT with a predefined combination of armchair (ac) and zigzag (zz) shells

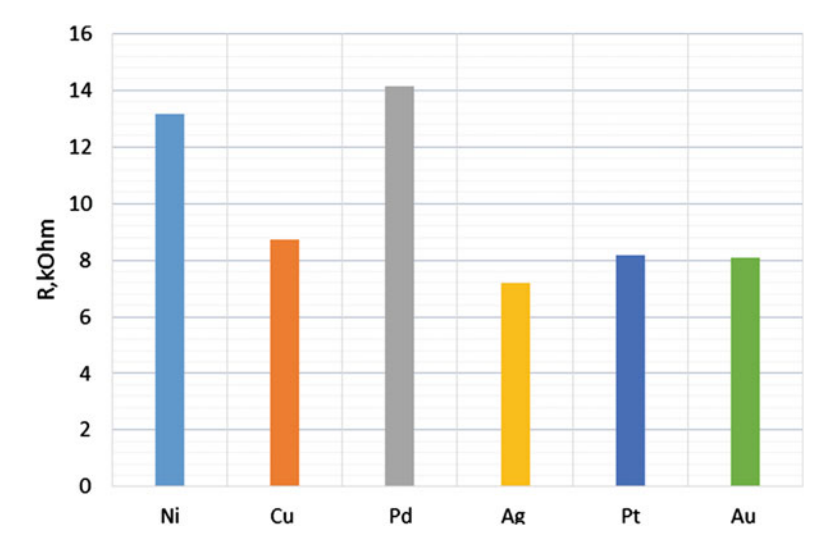
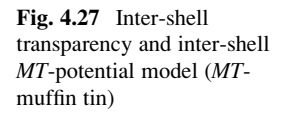
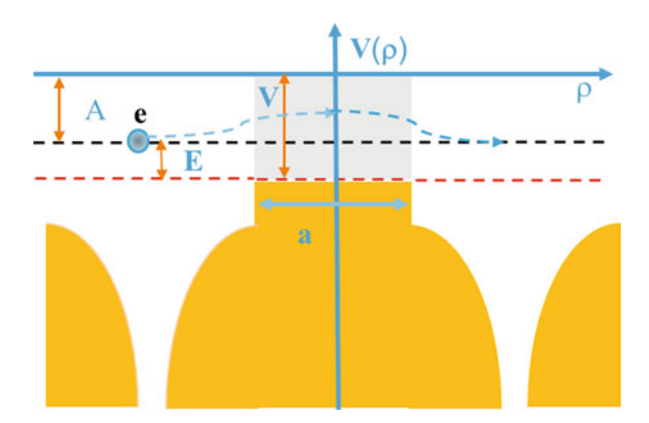


Fig. 4.26 Resistances of various MWCNT-Me interconnects





Clearly, the total radial conductance is proportional to T and the number of effective potential barriers. It is also clear that the 'radial current' losses (or, simply radial current) are similar to the Hall current due to the induced magnetic field of the basic axial current. A pure scattering mechanism is also possible. However, the radial conductance per CNT length depends on the morphology (chirality) of the nearest nanotubes, when the number of shortest effective barriers is varied in a probabilistic way. This also means that current–voltage parameters of MWCNTs can be less stable than in the case of SWCNTs. It has been found that inter-shell interactions, such as inter-shell tunnelling of electrons and Coulomb interactions, cause a reduction of the total MWCNT conductance [18–20].

## 4.3.7 Resistances and Capacitances of SL GNR–Me, ML GNR–Me Interconnects

Similar calculations of resistances and capacitances have been carried out for special configurations of SL GNR(zigzag)—Me interconnect and for ML GNR (zigzag)—Me interconnect (*end-type* contacts) (Figs. 4.28, 4.29, 4.30 and 4.31), which is essential, e.g. in case of planar technology in nanodevices design [15, 16, 23].

For cases of *side-type* contact, the number of effective bonds per contact square is essential. Figure 4.32 shows the conductance of GNR–Au interconnect via the depth 'y' of contact overlapping.

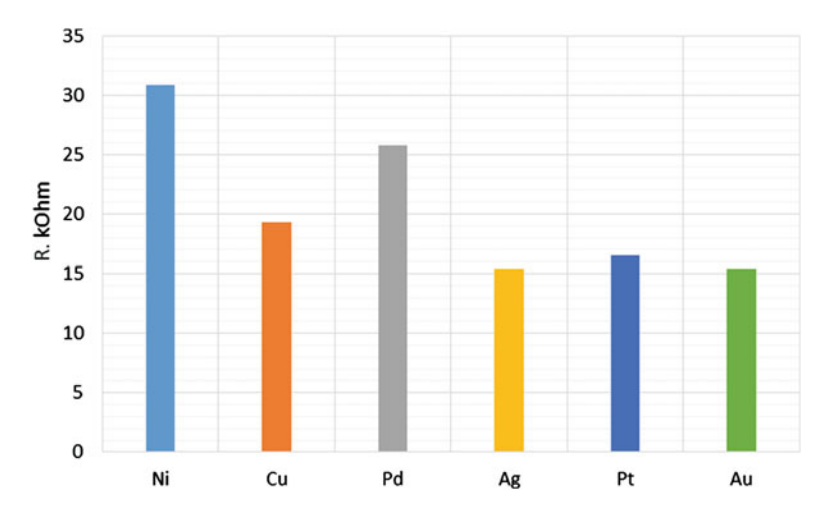


Fig. 4.28 Resistances of SL GNR(zigzag)—Me end-type interconnects. SL GNR-metal interconnect, width  $-125~\mathrm{nm}$ 

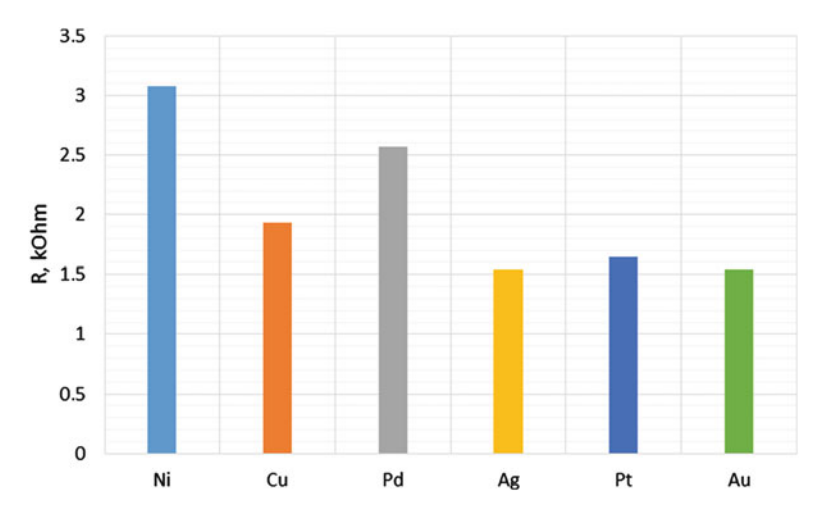


Fig. 4.29 Resistances of ML GNR(zigzag)—Me end-type interconnects. ML GNR-metal interconnect, width – 125 nm, 10 layers

# 4.3.8 Frequency Properties of CNT-Me and GNR-Me Interconnects

Figures 4.33 and 4.34 show parametric simulations of SWCNT (*zigzag*)—Au interconnect impedances Z via chiralities and curvatures. These results correlate with calculations in the framework of semiclassical approach of Maksimenko et al.

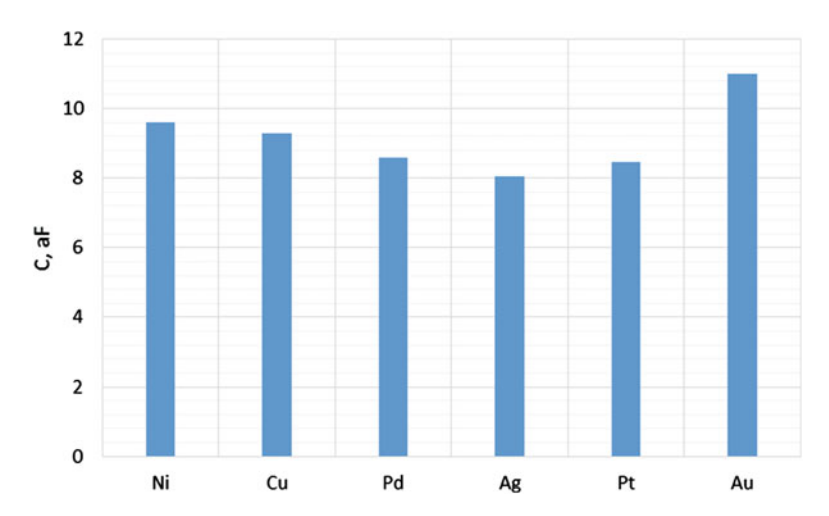


Fig. 4.30 Capacitances of SL GNR (zigzag)—Me end-type interconnects. SL GNR-metal interconnect, width – 125 nm

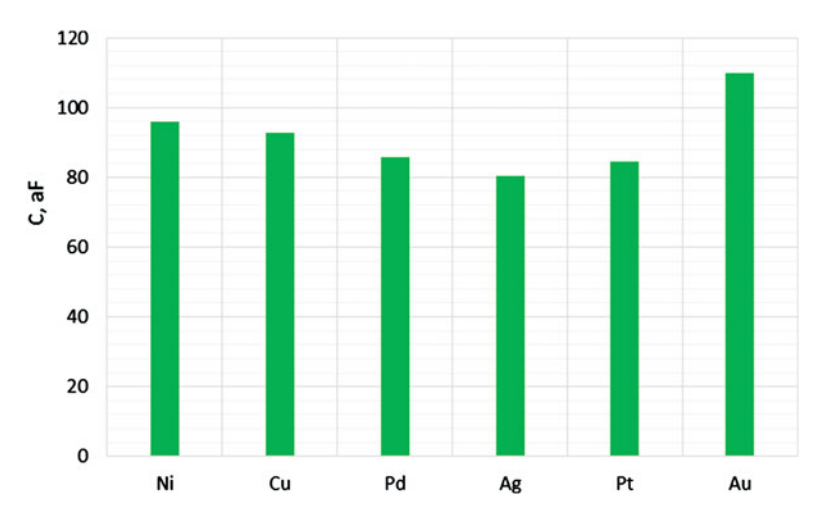


Fig. 4.31 Capacitances of ML GNR (zigzag)—Me end-type interconnects. ML GNR-metal interconnect, width – 125 nm, 10 layers

[21, 22], where the GHz-THz range has demonstrated essential changes of interconnect resistances.

Our calculations (see Fig. 4.35) have been also carried out for Au(100) and MWCNT(zigzag) with external diameter d=20 nm and are presented in Fig. 4.25. Evaluations of C–Au potential barrier gave for zigzag SWCNT–Au V=10.2297 Ev and the corresponding capacitance  $C_b \approx 11.45 \, aF$ . Using the evaluation of local single bond resistance (see Sect. 4.3.4):

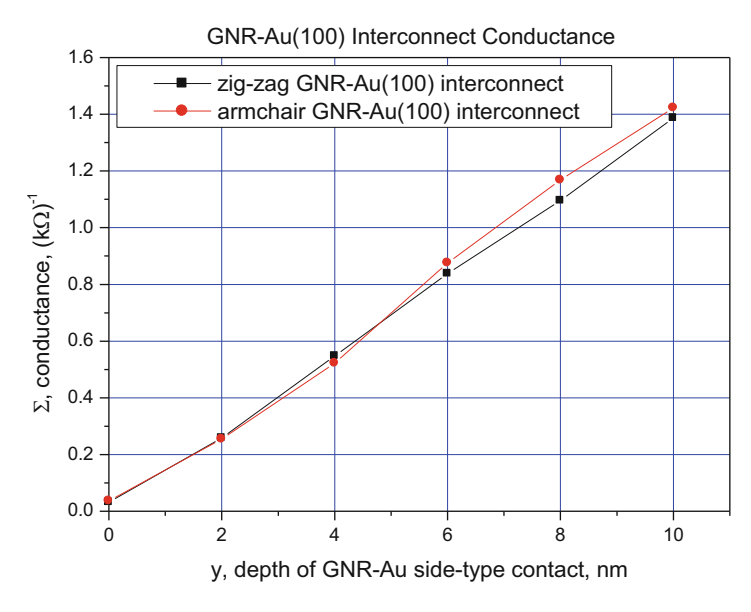


Fig. 4.32 Conductance of GNR-Au interconnect (*side-type* contact) via the depth 'y'-parameter of contact overlapping

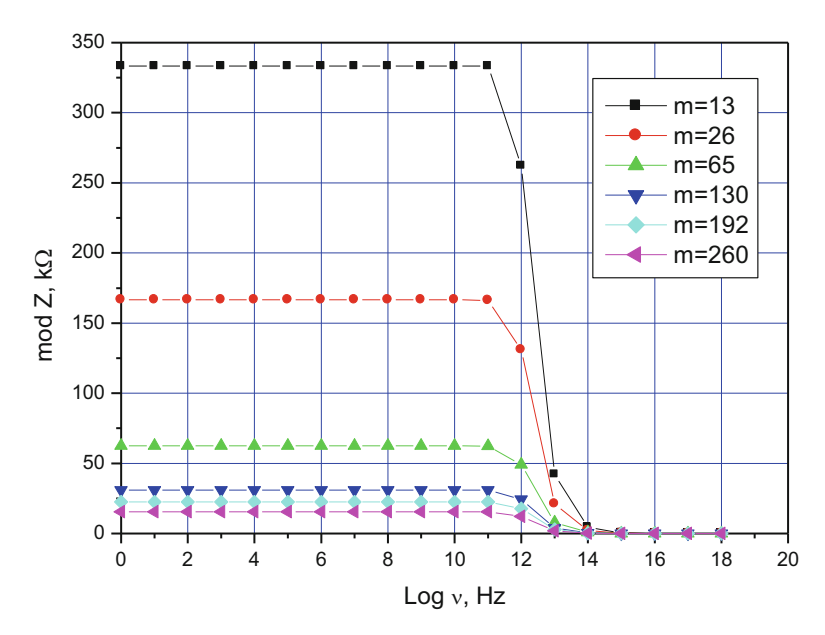


Fig. 4.33 SWCNT (zigzag)-Au(100) interconnect impedances via the frequency for various chiralities

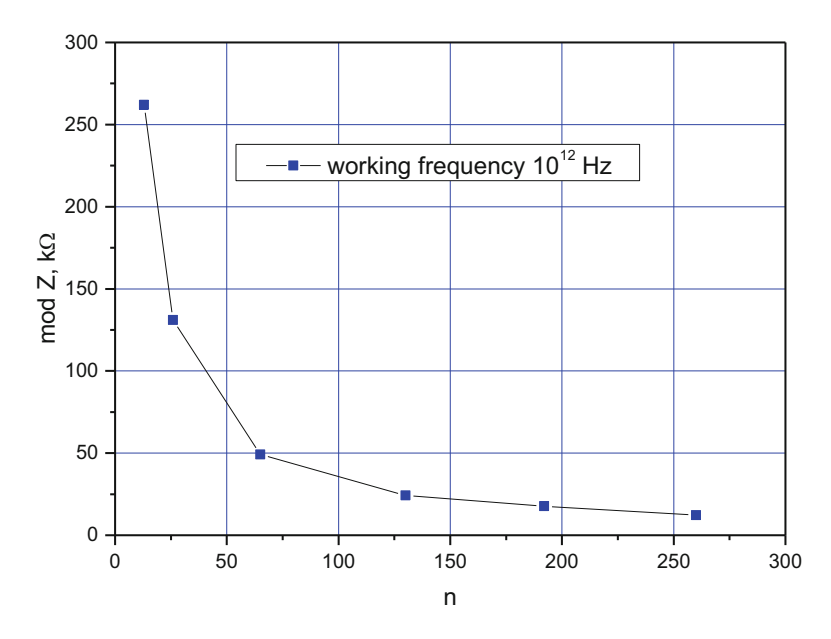


Fig. 4.34 SWCNT (zigzag)-Au(100) interconnect impedance via the curvature parameter (chirality index) n

$$\begin{split} R_b \approx 4000 \, k\Omega, \;\; \frac{1}{Z_{\mathrm{SINGLE}}} = & \frac{N_b}{R_b} + i\omega N_b C_b, \;\; \frac{1}{Z_{\mathrm{MULT}}} = \sum_{i=1}^N \left(\frac{N_{b,i}}{R_{b,i}} + i\omega N_{b,i} C_{b,i}\right), \\ |Z_{\mathrm{SINGLE}}| = & \frac{1}{\sqrt{\left(\frac{N_b}{R_b}\right)^2 + \left(N_b C_b\right)^2 \omega^2}} = & \frac{1}{\sqrt{\left(\frac{N_b}{R_b}\right)^2 + \left(2\pi N_b C_b\right)^2 \nu^2}}, \end{split}$$

where  $\omega$  is the cyclic frequency,  $N_b$  is the number of effective bonds,  $N_{b,i}$  is the number of effective bonds in particular CNT in the MWCNT tested morphology and N is the number of CNTs in MWCNT.

## 4.3.9 Concluding Remarks

Using the *effective bonds* model, we have predicted the resistivity of interconnects between a metal substrate and SW or MWCNTs (SL GNR or ML GNR). There also exists a qualitative compatibility of results obtained for CNT–Me junctions using both approaches considered in this research: (1) Ab initio *liquid metal* model and (2) semiempirical *effective bonds* model based on the Landauer relationship. At the same time, the latter results are quantitatively comparable with those measured experimentally, i.e. within the range of several up to 50 kOhm.

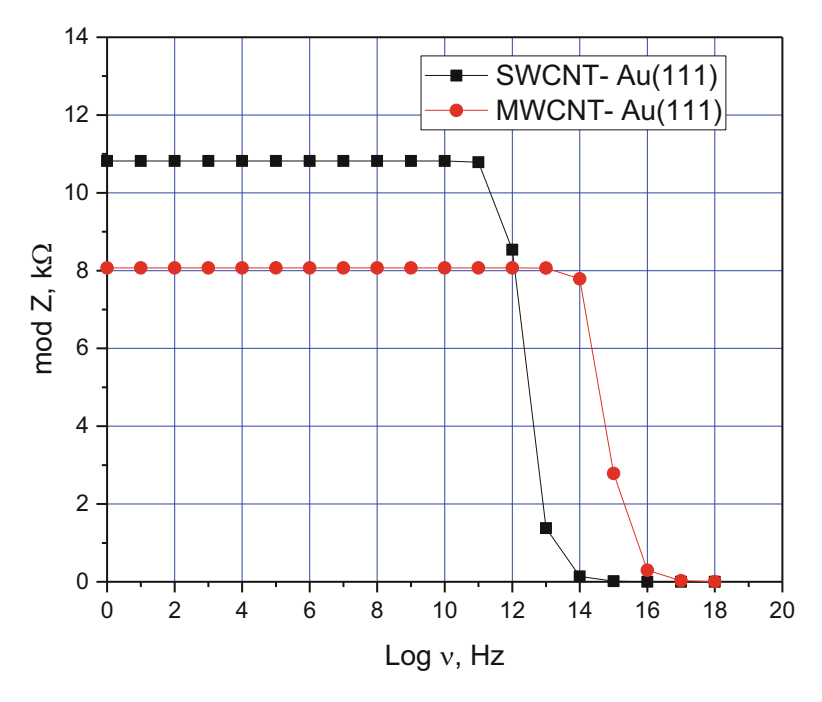


**Fig. 4.35** Interconnect impedances via the frequency for various for SWCNT-Au and MWCNT-Au: comparison connected with critical impedance changes

We have also developed the model of inter-shell interaction for MWCNTs, which allows estimating the transparency coefficient as an indicator of possible 'radial current' losses.

We have emphasized that conductance and other current-voltaic parameters depend on the morphology of the nearest shells in MWCNTs and ML GNRs, which leads to complications for technology and production of nanodevices with stable electric characteristics.

We are able now to create a database of CNT-metal and GNR-metal junction combinations taking into account a set of parameters, namely, the angle of chirality, the CNT diameter, the number of walls or layers, the type of metal substrate (Me) and the orientation of metal substrate (e.g.(100), (111) or (110)). Thus, we are able to forecast interconnect properties for various SW, MWCNT and SL and ML GNR configurations.

Potential nanosensor devices based on CNTs, GNRs and their interconnects are absolutely feasible and can be very effective for external influences of different nature. They can change the electron transport regime and promote the current losses. At the same time, the interconnect interfaces can also be sensitive to chemical adsorbents, electrical and magnetic fields, changing the properties of interconnect potential barrier and efficiency of conducting channels. All these mechanisms of nanosensoring are possible to simulate in the framework of the proposed models.

#### References

- Shunin Yu N, Zhukovskii Yu F, Gopeyenko V I, Burlutskaya N Yu, Bellucci S 2012 Properties
  of CNT- and GNR-Metal Interconnects for Development of New Nanosensor Systems In:
  Nanodevices and Nanomaterials for Ecological Security, Series: NATO Science for Peace
  Series B Physics and Biophysics Eds Yu Shunin and A Kiv (Springer Verlag: Heidelberg)
  237–62
- 2. Dresselhaus M S, Dresselhaus G, Eklund P C **1996** Science of Fullerenes and Carbon Nanotubes (Academic: San Diego)
- Tans S J, Verschueren R M, Dekker C 1998 Room-temperature transistor based on a single carbon nanotube Nature 393 49–52
- 4. Tersoff J 1999 Contact resistance of carbon nanotubes Appl. Phys. Lett. 74 2122-4
- Shunin Yu N, Schwartz K K 1997 Correlation between electronic structure and atomic configurations in disordered solids In: Computer Modelling of Electronic and Atomic Processes in Solids Eds R C Tennyson and A E Kiv Kluwer Acad. Publisher: Dordrecht/ Boston/London 241–57
- Shunin Yu N, Zhukovskii Yu F, Bellucci S 2008 Simulations of properties of carbon nanotubes using the effective media approach Computer Modelling & New Technologies 12(2) 66–77
- 7. Kubo R **1957** Statistical mechanical theory of irreversible processes. I. General theory and simple applications to magnetic and conduction problems *J. Phys. Soc. Jpn.* **12**, 570–86
- Shunin Yu N, Shvarts K K 1986 Calculation of the Electronic Structure in Disordered Semiconductors *Phys. Stat. Sol.* (b) 135 15–36
- 9. Ziman J M 1979 Models of Disorder Ch10 (Cambridge University Press, London, New York
- Shunin Yu N 1991 Simulation of atomic and electronic structures of disordered semiconductors Dr.Sc.Habil. Thesis (Phys&Math) Riga-Salaspils
- 11. Shunin Yu N, Shvarts K K **1990** Modelling of radiation stimulated processes in disordered semiconductors *Izv AN LSSR ser fiz i tehn nauk* No **2** 38–56 (*in Russian*)
- Shunin Yu N, Zhukovskii Yu F, Burlutskaya N Yu, Bellucci S 2011 Resistance simulations for junctions of SW and MW carbon nanotubes with various metal substrates Central European Journal of Physics 9(2) 519–29
- Gaspar R 1952 Über ein analitisches Näharungsverfachren zur Bestimung von Eigenfunktionen und Energieeigenwerten von Atomelektronen Acta Phys. Acad. Sci. Hung. 2 151–78; Gaspar R 1954 Über eine Approximation des Hartree-Fockschen Potential dürch eine universelle Potentialfunktion Acad. Sci. Hung. 3 263–86
- 14. Stone D, Szafer A 1988 What is measured when you measure a resistance? The Landauer formula revisited *IBM J. Res. Develop.* 32(3) 384–413
- 15. Shunin Yu N, Zhukovskii Yu F, Burlutskaya N, Gopeyenko V I, Bellucci S 2010 Theoretical Resistance Simulations For Junctions of SW and MW Carbon Nanotubes with Metal Substrates in Nanoelectronic Devices Computer Modelling And New Technologies 14(2) 7–19
- 16. Shunin Yu N, Zhukovskii Yu F, Gopejenko V I, Burlutskaya N, Bellucci S 2011 Ab Initio Simulations on Electric Properties for Junctions Between Carbon Nanotubes and Metal Electrodes Nanoscience and Nanotechnology Letters 3 816–25
- Ngo Q, Petranovic D, Krishnan Sh, Cassell A M, Ye Qi, Li Jun, Meyyappan M, Yang C Y 2004
   Electron transport through metal multiwall carbon nanotubes interfaces *IEEE Transactions on Nanotechnology* 3(2) 311–7
- 18. Uryu S **2004** Electronic states and quantum transport in double-wall carbon nanotubes *Phys. Rev.* B **69** 075402–12
- Lunde A M, Flensberg K, Jauho A-P 2005 Intershell resistance in multiwall carbon nanotubes: A Coulomb drag study *Phys. Rev. B* 71 125408-25
- Kordrostami Z, Sheikhi M H, Mohammadzadegan R 2008 Modeling Electronic Properties of Multiwall Carbon Nanotubes Fullerenes, Nanotubes, and Carbon Nanostructures 16(1) 66–77

References 113

21. Shuba M V, Slepyan G Ya, Maksimenko S A, Thomsen C, Lakhtakia A 2009 Theory of multiwall carbon nanotubes as waveguides and antennas in the infrared and the visible regimes *Phys. Rev.* B 79(15) 155403-17

- 22. Miano G, Forestiere C, Maffucci A, Maksimenko S A, Slepyan G Ya 2011 Signal propagation in carbon nanotubes of arbitrary chirality *IEEE Transactions on Nanotechnology* 10(1) 135–49
- 23. Shunin Yu N, Zhukovskii Yu F, Burlutskaya N, Bellucci S 2011 Theoretical Simulations on Electric Properties of CNT-Me and GNR-Me Interconnects Using Effective Media Approach Procedia Computer Science 7 343–5

# Chapter 5 Surface Nanophysics: Macro-, Meso-, Microand Nano-approaches

#### 5.1 Surface: Thermodynamics, Anisotropy

The surface represents a geometric set of points in accordance with strictly formulated rules. The most common use of this term is to denote a two-dimensional (2D) submanifold of the three-dimensional (3D) Euclidian space (xyz). In geometry, 2D collection of points represents a flat surface according to Eq. (5.1):

$$\alpha \cdot x + \beta \cdot y + \gamma \cdot z + \Delta = 0. \tag{5.1}$$

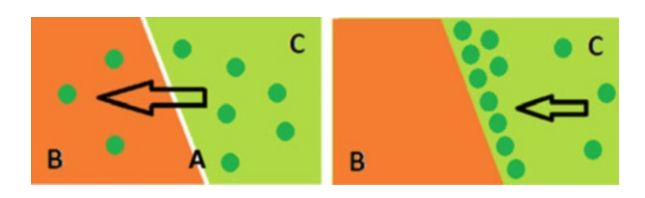
Quadratic, cubic, etc. equations describe the non-flat surfaces, which are important in many fields of natural sciences. The range of the surface could be expressed by the natural number (2,3) as well as by fractional (e.g. fractal surface).

In physics, a surface is a continuous boundary that separates a 3D space into two different subspaces. The phases of certain materials occur in the case when diffusion processes take place. Figure 5.1 represents a comparison of absorption and adsorption processes between two phases B and C. The absorption process represents the mixing of phase C into phase B: increasing the concentration of C-type particles in B volume without any chemical reaction. Gas particles penetrate the mass of a solid. Absorption processes in many cases are reversible, and it is possible to recover absorbed substance into the previous state. Substance B (liquid or gas) diffuses into liquid C to form a solution according to Fick's second law (1D form):

$$\frac{\partial c}{\partial t} = D \frac{\partial^2 c}{\partial t^2},\tag{5.2}$$

where c represents the concentration of substance B into C, x is the reaction coordinate (physical distance from the interaction point), and D is the diffusion coefficient related to the substance behaviour. At intermediate states, concentration of C-type particles increases in B volume, and it is a time-dependent process. After

**Fig. 5.1** Absorption and adsorption processes between phases *B* and *C*. *Left* – bulk phase *C* and absorbing phase *B*, *right* – bulk phase *C* and adsorbing phase *B* 



established equilibrium, concentration of *C*-type particles in *B* volume is uniform (time-independent and distance-independent).

Otherwise, adsorption occurs in case when particles (extracted from liquid solute or gas) accumulate or concentrate at the surface of solid forming heterogeneous surface (mass transfer process). Adsorbent (also called substrate) represents the solid where adsorption takes place (covering the surface), adsorbate represents the substance adsorbed on the surface of solid (short distance to surface), and adsorptive represents the substance before the adsorption process (long distance to surface). Thus, the generated high-energy interface is located at a short distance to low-energy adsorptive system:

ADSORBENT 
$$\leftarrow$$
 ADSORBATE  $\leftarrow$  ADSORPTIVE. (5.3)

Diffusion processes (or more generally mass transfer processes) as well as adhesion processes create the region of particle accumulation at the liquid–solid or gas–solid interface. Adsorbed substance B creates an atomic or molecular film. Limited quantities of substance (in many cases – very small) are adsorbed (in comparison to absorption). Adsorption is a surface phenomenon, and geometrical area of surface could be treated as the main parameter for modelling. Saturation of covering is also limited by the surface. Surfaces of solids always express the tendency to attract the additional particles due to the presence of surface energy. In microparticle assumption, unbalances residual forces represent driving forces for adsorption.

Let us assume the existence of two phases -B and C. Two different approaches are presented in Fig. 5.1. with two bulk phases B and C with volumes  $V_B$  and  $V_C$  and the interface between phases (surface A). Figure 5.2 represents the dependence of concentration c of the bulk phase on the distance to the surface d. In the near surrounding, the concentration c rapidly increases.

Adsorbate (a substance adsorbed on the surface) and adsorbent (a substance which creates the region of increased concentration of adsorbate) could be treated as two interacting materials (the so-called phases).

An idealized model (Gibbs model) could be used in some cases, where the thickness of the surface phase is negligible, and two phases – B and C – are divided by Gibbs dividing plane, the so-called ideal interface.

The real alternative model (Guggenheim model) represents a quasi 3D surface, and the thickness of the surface phase is equal to z. The interfacial region is extended and its volume is significant. Figure 5.3 represents Gibbs (ideal) interface vs Guggenheim (real) interface between phases B and C.

Fig. 5.2 Adsorption processes between phases B (surface) and C (bulk solution). Left – dependence of concentration c of bulk phase on distance to surface d. Right – bulk phase C and adsorbing phase B

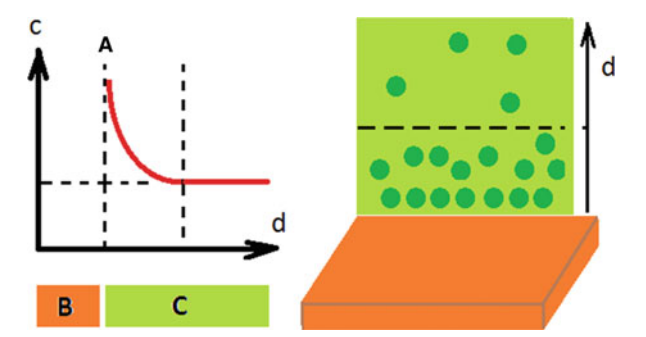
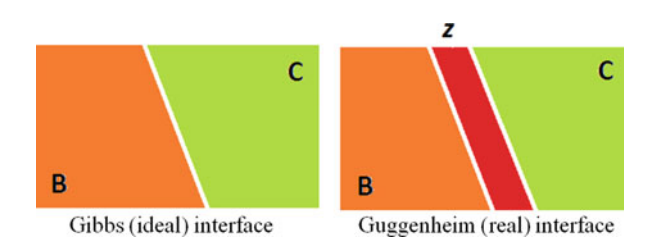


**Fig. 5.3** Surfaces between phases *B* and *C* 



Otherwise, Gibbs model as the first assumption allows interpreting the interface as ideally thin. The crystallographic surface as well as covered surface (thin film) and also the cell membrane may be considered similarly in the framework of the physical chemistry. The classical liquid surface can often be treated in the first assumption as a solid surface [1].

The adsorption processes must be analysed in two aspects: (1) thermodynamically, equilibrium of interfacial energy must be realized in the final phase of the processes; and (2) kinetically, the rate of adsorption process depends on the surface and substance behaviour as well as previously declared thermodynamic conditions.

Thermodynamically, many processes could be characterized through changes of arguments T and p, which results from Gibbs' free energy  $\Delta G$ :

$$\Delta G = \Delta H - T \Delta S,\tag{5.4}$$

where  $\Delta H$  represents the enthalpy and  $\Delta S$  is the entropy. For adsorption, decreasing of free energy takes place (in the case if T and p are constants). Adsorption as a spontaneous exothermic process is characterized by the negative Gibbs energy. The so-called condition of spontaneity arises from Eq. (5.5)

$$\Delta G = \Delta H - T \Delta S < 0, \tag{5.5}$$

when particles of the adsorbate are fixed on the surface of the adsorbent (adsorption process is finished) the translational motion of the adsorbate is strongly limited in comparison with the bulk phase. It means that the freedom of the adsorbate strongly decreases and the entropy becomes negative:

$$\Delta S < 0, \tag{5.6}$$

$$\Delta G = \Delta H - T[-\Delta S],\tag{5.7}$$

$$\Delta G = \Delta H + T \Delta S. \tag{5.8}$$

According to Eq. (5.8), enthalpy  $\Delta H$  should be negative, as determines the mentioned process as exothermic:

$$\Delta H < 0. \tag{5.9}$$

The so-called condition of exothermicity arises from Eq. (5.9).

Several parameters of Gibbs model will be described as the sum of partial parameters: total volume V, internal energy U, entropy S and number of particles of the i-th type  $N_i$ :

$$V = V_B + V_C, \tag{5.10}$$

$$U = U_B + U_C + U_A, (5.11)$$

$$S = S_B + S_C + S_A, (5.12)$$

$$N_i = N_{Ri} + N_{Ci} + N_{Ai}, (5.13)$$

where indexed parameters belong to the mentioned phases B and C as well as interface A. Now it is necessary to estimate the exact phase contribution. Let us assume the energy density for both homogeneous phases as internal energy per unit volume:  $u_B$  and  $u_C$ .

The total energy U could be expressed as follows:

$$U = u_B V_B + u_C V_C + U_A, (5.14)$$

where  $U_A$  represents an internal energy of interface A. Actually, the molecular amount at interfaces changes significantly. For i-th type of particles, molecular concentration represents the behaviour of two phases:  $c_{Bi}$  and  $c_{Ci}$ . According to Eq. (5.15), an additional quantity of particles is formed in two-phase system due to the interface is equal to  $N_{Ai}$ :

$$U_A = U - u_B V_B - u_C V_C, (5.15)$$

$$N_{Ai} = N - c_{Bi}V_B - c_{Ci}V_C. (5.16)$$

Now it is possible to determine the main parameter – interfacial excess  $\Gamma_i$ :

$$\Gamma_i = \frac{N_{Ai}}{A}.\tag{5.17}$$

In some cases, interfacial excess  $\Gamma_i$  could be treated as a molecular concentration on the surface (number of particles per unit area).

The Gibbs approach is known as the Gibbs dividing surface (GDS). Let us assume the existence of the solution: any substance dissolved in a certain solvent. The interface is determined by the point of position, where the surface excess of solvent particles becomes zero.

The main phenomena of the surface could be titled as physical stability of the surface as well as the presence of the surface free energy [2]. The classical task (how to estimate the surface energy) starts from a crystal interface (*macro*-approach).

Let us assume the crystal of volume V, which consists of N particles. Let us assume the internal energy U as a function of entropy S, which is predetermined by temperature T, pressure P and chemical potential  $\mu$ :

$$U = U(S, V, N), \tag{5.18}$$

$$dU = \left[\frac{\partial U}{\partial S}\right]_{VN} dS + \left[\frac{\partial U}{\partial V}\right]_{SN} dV + \left[\frac{\partial U}{\partial N}\right]_{VS} dN, \tag{5.19}$$

$$dU = TdS - PdV + mdN. (5.20)$$

In a specific case, if solid consists of one particle (N = 1), the chemical potential  $\mu = m$ , and Eq. (5.20) transforms to Euler equation for one particle (5.22):

$$U(IS, IV, IN) = IU(S, V, N),$$
 (5.21)

$$U = TS - PV + mN. (5.22)$$

For a conservative system, the particle energy U is a time-independent function:

$$\frac{dU}{dT} = 0, (5.23)$$

$$SdT - PdV + Ndm = 0. (5.24)$$

Equation (5.24) is called the Gibbs–Duhem equation.

Now it is necessary to evaluate the differences between macro- and microstructures. For large isotopic solids, the pressure inside is the same in all directions, but the pressure at the plane surface is anisotropic (anisotropy ratio is very high). It means that damaging the crystal surface (crystal cleavage along crystallographic planes) needs to consume additional energy which is proportional to the surface A. As a result, from Eq. (5.22), the additional member gA must be introduced, when the factor g is called the surface tension:

$$U = TS - PV + mN + gA, (5.25)$$

$$g = \frac{dU}{dA}. (5.26)$$

The surface tension is related to the surface formation energy when the main physical parameters (temperature T, volume V and the chemical potential of the particle m) are time independent. For microparticles, an additional condition must be established: the number of particles N does not change. The surface tension for a solid body corresponds to the gas pressure (two-dimensional analogue). The second term in Eq.  $(5.25) \ pdV$  represents the work by increasing the volume V. The pressure p is always directed from surface (in normal direction). If the surface

Pore size		Surface, %		Volume, %		
Macro		Negligible		30		
Meso		<5		<10		
Micro		>90		40 ÷ 50		
Nano		>95		100		
0.1 nm	Nanoscale	100 nm	Microscale	100 μm	Macroscale	1 mm
		2 μm	Mesoscale	20 μm		

Table 5.1 Size-scaled approaches in materials science

area A increases when the volume V remains constant, the surface of the elastic vector is oriented parallel to the surface.

Now it is possible to determine four different approaches in materials science concerning the surface phenomena (see Table 5.1). A geometric surface can cover some amount of chemical substances, or otherwise, chemical substance could be formed in a certain cube containing pores. Significance of the surface according to surface thermodynamics could be treated as negligible (in case of macro-subjects) or significant (in case of micro-subjects). For practical estimation, the value of diameter d allows attributing the particles or pores into four groups:  $d > 20 \ \mu \text{m} - \text{macropores}$ ,  $2 \ \mu \text{m} < d < 20 \ \mu \text{m} - \text{mesopores}$ ,  $800 \ \text{nm} < d < 2 \ \mu \text{m}$  micropores and  $d < 800 \ \text{nm} - \text{nanopores}$ .

The ideal geometric surface contains any kind of pores. On the contrary, real surfaces are in pores of dimensions of molecular size and bigger. The real surface phenomena include two factors: (1) covering or adsorption as a slow mass transfer and (2) bonding capacity of the adsorbate.

# 5.2 Physical and Chemical Adsorption, Adsorption Kinetics

Adsorption is a surface-based process where adhesion of molecules from gas or liquid to a surface occurs. Attraction of adsorbate molecules to an adsorbent surface is a spontaneous process. Adsorption can occur at all surfaces. This term was first used in 1881 by a German physicist Heinrich Kayser (1853–1940). For the adsorbent surface and adsorbate molecules, adsorption processes start with the reorientation of molecules in the near environment to the surface and finish with the strong or soft fixation of molecules by short distances too. At the final position, attractive and repulsive forces become balanced when adsorption occurs. After finishing all steps, the free energy of the system decreases.

The surface forces of an adsorbent (substrate) are unsaturated, and according to the mentioned condition, the concentration of particles in the proximity of a surface arises (deposition takes place). The adsorbent surface and adsorbate gas (or liquid) could be treated as a thermodynamic system characterized by the total energy.

Type	Definition
Van der Waals forces, London dispersion forces	PS
Inductive forces, dipole–dipole forces	PS, presence of significant induced dipole moment
Hydrogen bonding	Interactions between proton-donor group of adsorbate and nucleophilic polar surface of adsorbent
Covalent bonding	CS

Table 5.2 Nature of adsorption forces for physical (PS) and chemical (CS) adsorption

Two types of adsorption can be found in materials science: physical adsorption and chemical adsorption. Exchange adsorption is always regarded as a special case of adsorption, when the strong electrostatic forces attract the particles to charged sites on the surface. Table 5.2 represents the comparison of adsorption forces.

Physical adsorption (additional terms physisorption, van der Waals adsorption) occurs in the case if attracting forces are of van der Waals type only. Chemical adsorption (additional terms chemisorption, Langmuir adsorption, activated adsorption) occurs in the case if attracting forces are of similar strength in comparison with chemical bonds.

Inductive forces such as intermediate forces could make a major contribution to the total adsorption energy on several metals such as alumina. Surprisingly, but this contribution is negligible for silica.

Due to the weak bonding forces, physical adsorption is the reverse process: increasing temperature or decreasing pressure can reduce the adsorbed amount of adsorbate. Van der Waals interactions are significant at low temperatures only. The attraction of particles is not fixed to a specific area. Individuality of both types of particles (adsorbent and adsorbate) is preserved. According to that, adsorbate is relatively free to move from the surface or along the surface. Surface covering and surface dissipation are limited by thermal motion.

Otherwise, chemical adsorption is related to the creation of new chemical bonds while passing through the activation energy barrier. Due to unsatisfied vacancies of the surface and the existence of molecular fragments of the adsorbent, a solid surface can catalyze reactions. Table 5.3 represents a comparison of physical adsorption vs chemical adsorption processes.

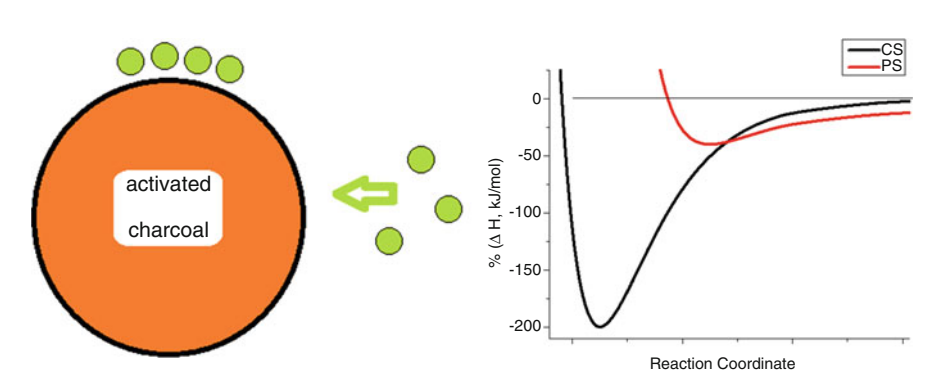
Figure 5.4 presents the gas adsorption scheme on activated charcoal. Also, potential energy diagram of physical (PS) and chemical (CS) adsorption is presented. The dependence contains a minimum, which predetermines the condition of a stable point.

As in the case of interaction between two molecules, adsorbate-adsorbent interactions could be modelled by means of Lennard-Jones (LJ) potential:

Exothermic

Tuble 5.5 Thysical (15) vs chemical (C5) at	asorption		
Different aspects of adsorbent (AT) and adsorbate (AE)			
Physisorption (PS)	Chemisorption (CS)		
Requiring of suitable <i>PT</i> conditions in any gas–solid system	Chemical bonding between AT and AE		
Relatively low temperature required	Wide interval of temperature is possible		
PS accelerates with decreasing of temperature	CS accelerates with increasing of temperature until extremum point, then decreases		
High pressure <i>P</i> favours PS, low pressure causes desorption	High pressure <i>P</i> is favourable, low pressure does not cause desorption		
No activation energy barrier	Activation energy takes place		
Equilibrium rapidly	Equilibrium slowly		
Reversible	Mostly irreversible		
Longer distance between AT and AE	Shorter distance between AT and AE		
Long range, weak bonding between AT and	Short range, strong bonding between AT and AE		
AE (van der Waals interactions)	(usually covalent)		
No decomposition of adsorbate	Possible breakage of adsorbate into radicals (or atoms) which will be bounded separately		
No significant MO overlap	MO overlap takes place		
No electron transfer	Electron transfer takes place		
No sharing of electrons	Sharing of electrons takes place		
No chemical reactions	Chemical reaction occurs		
PS begins as a monolayer	CS begins as a monolayer		
Multilayer or monolayer covering	Monolayer covering only		
Any canalization	Canalization of reactions		
Enthalpy in range [5 ÷ 50] kJ/mol	Enthalpy in range [40 ÷ 800] kJ/mol		
Dissociation energy up to 0.5 eV	Dissociation energy [1 ÷ 10] eV		

Table 5.3 Physical (PS) vs chemical (CS) adsorption



Exothermic

Fig. 5.4 Gas adsorption on activated charcoal (*left*). Energy diagram of physical (PS) and chemical (CS) adsorption

$$V_{L,J} = E \left[ \left[ \frac{R_m}{R} \right]^{12} - \left[ \frac{R_m}{R} \right]^6 \right], \tag{5.27}$$

where E represents the depth of the potential well, R is the distance between the particles, and  $R_m$  is the distance of minimal potential. Buckingham potential looking similar to LJ-potential contains repulsive part as an exponential function:

$$V_B = E \left[ \exp\left(-\frac{R_m}{R}\right) - \left[\frac{R_m}{R}\right]^6 \right]. \tag{5.28}$$

Near the equilibrium point and especially for chemical adsorption, Morse potential could be useful:

$$V_M = D_E[1 - \exp(-\alpha(R - R_m))]^2,$$
 (5.29)

$$\alpha = \sqrt{\frac{k}{2D_E}},\tag{5.30}$$

where  $D_E$  represents dissociation energy and k is the force constant at the minimum of the well.

In many cases, chemical adsorption and physical adsorption could occur at the same time but at different distances. CS always is dominating at short distances, in comparison to PS. At long distances, PS starts to dominate over CS.

Some differences between chemical adsorption and physical adsorption could be explained by energy exchange. Heat of adsorption,  $\Delta H$ , could be derived from Clausius—Chaperon equation:

$$\left[\frac{\partial \ln P}{\partial T}\right]_V = -\frac{\Delta H_{AD}}{RT^2}.\tag{5.31}$$

Especially for physical adsorption, enthalpy of adsorption  $H_{ADS}$  is approximately equal to enthalpy of condensation  $Q_{CON}$ :

$$\Delta H_{\rm ADS} \approx Q_{\rm CON}.$$
 (5.32)

For chemical adsorption, such two values can differ in orders. Tables 5.4 and 5.5 represent several structures with energies typical for process.

Many popular adsorbents are grouped into three classes:

- (i) Carbon-based compounds: activated carbon, graphite and graphene. Such materials are typically hydrophobic and non-polar.
- (ii) Oxygen-containing compounds: silica gel and zeolites. Such materials are typically hydrophilic and polar.
- (iii) Polymer-based compounds: functional polar groups in a porous polymer matrix. Figure 5.5 represents model of silica surface covered in different ways. Free hydroxyl and bounded hydroxyl on silica surface are the simplest

Process	Motion	Adsorbate/adsorbent	$\Delta H$ , kJ/mol
Physisorption	Condensation	N2/Fe	-6
Physisorption	Adsorption	N2/Fe	-10
Physisorption	Adsorption	N2/graphite	-12
Chemisorption	Adsorption	N2/Fe	-150

Table 5.4 Enthalpies of processes

Table 5.5 Physical (PS) vs chemical (CS) adsorption. Comparison on energies

Physisorption (PS)	Energy, kJ/mol	Chemisorption (CS)
	200 ÷ 400	Covalent bonding
	100 ÷ 200	Donor-acceptor interactions
	70 ÷ 150	CT interactions
Acid-base interaction with proton transfer	60 ÷ 80	
$\pi - \pi$ intermolecular complexes	30 ÷ 40	
Hydrogen bonding	<20	
Dipole-dipole interactions	10	
Van der Waals interactions	5	

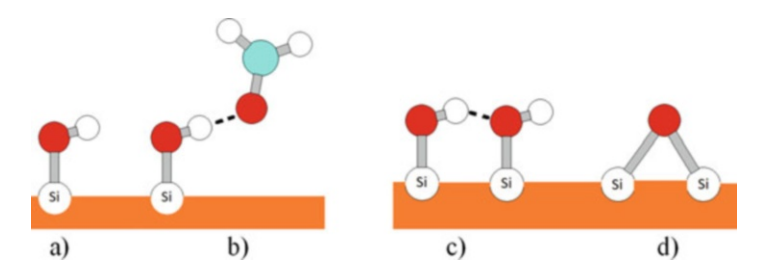


Fig. 5.5 Silica (Si) surface covered by hydroxyls [-OH]: (a) free hydroxyl; (b) bounded hydroxyl by [O = CH2]; (c) reactive and bound hydroxyl; (d) surface siloxane

case in layer formation. Otherwise, mixed bounding could create more stable structures when reactive and bound hydroxyl forms several bonds. In addition, 'molecular' structure, so-called surface siloxane, could form in special case.

Adsorption process could be characterized as cp dependency (amount or concentration of adsorbate on the adsorbent surface as function of adsorbate gas pressure p at constant temperature T).

This type of graph is called the adsorption isotherm. The reversible process as behaviour of two types of chemical reactions (adsorption and desorption at the same time) could be characterized by Eqs. (5.33) and (5.34):

ADSORBATE + ADSORBENT 
$$\rightarrow$$
 COVERED\_LAYER, (5.33)  
COVERED\_LAYER  $\rightarrow$  ADSORBATE + ADSORBENT. (5.34)

Chemisorption is always followed by charge transfer (CT) processes, in which adsorbate and adsorbent occur (reactant R and catalyst). Let us assume the existence of initial reaction of electron accepting:

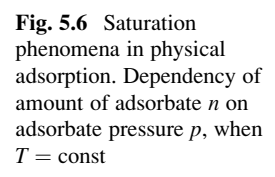
$$R + e^- \to R^-. \tag{5.35}$$

If the reactant R is placed outside the surface, a partial charge transfer between the reactant R and the catalyst could be formed (corresponds to a chemisorption bond). If the reactant R is placed on the surface, a complete charge transfer between the reactant R and the catalyst initiates the creation of a charged area (hole layer) following a flow of electrons. This process is called depletive chemisorption.

Equilibrium of both processes could be achieved at a certain temperature, but in the transition period, equilibrium will shift in the direction where the number of particles decreases. After saturation, the increase of pressure does not affect the covered amount of the adsorbent. Figure 5.6 represents the saturation phenomena in physical adsorption. Dependency of adsorbed amount of adsorbate on adsorbate pressure is not linear but becomes linear after saturation pressure *PS*. Figure 5.7 represents adsorption isobars for both processes: physical adsorption (PS) and chemical adsorption (CS).

Generally, four factors are significant to describe the phenomena of adsorption effect:

- 1. The nature of the adsorbent and adsorbate (molecular structure of gas and crystalline or polycrystalline structure of surface). Actually, vacant electronic states on the surface represent the additional potential. The possibility to catalyze many chemical reactions occurs due to the mentioned condition.
- 2. The surface area of the adsorbent. Geometrically, the area of 2D surface gives the smallest value. For metal clusters of different diameters, the surface area is more fractal than plane; the surface area increases (e.g. from 2 to 2.3). For smaller clusters, absorbance on surface interface increases significantly, in orders.
- 3. Temperature. Le Chatelier's principle (or the principle of response reactions) claims that any change in status quo of chemical substance prompts an opposing reaction in the responding system. Initially, the system must be presented at equilibrium, and any changes in temperature induce the readjustment processes to counteract the effect of the applied change. Finally, a new equilibrium is established. For adsorption as an exothermic process, it means that magnitude of adsorption increases when temperature decreases (case of physical adsorption). The rise of temperature can switch physical adsorption to chemical adsorption (passing to the activation barrier, formation of strong bonding).
- 4. Pressure. Increasing pressure, the adsorption reaction yield increases until a certain saturation level is exceeded (see Fig. 5.6). The decrease of pressure causes a reverse process desorption.



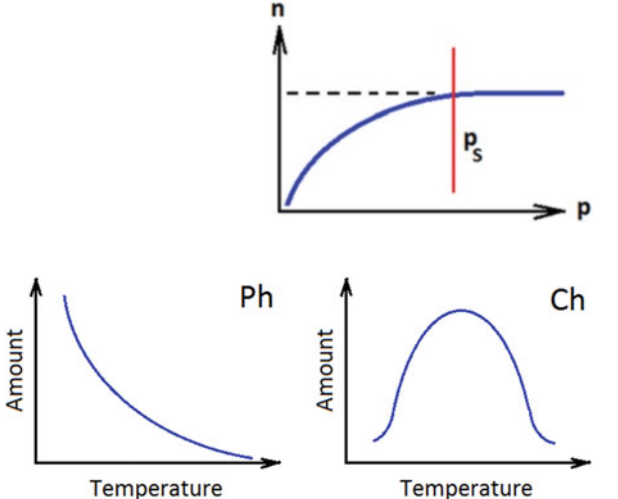


**Fig. 5.7** Adsorption isobars: dependencies of adsorbate amount on temperature. *Left*, physical adsorption (PS); *right*, chemical adsorption (CS)

Adsorption could be characterized through isotherms – dependency of the amount of the adsorbent on its pressure (in case of gas) or concentration (in case of liquid), when temperature is constant.

### 5.3 Gibbs Adsorption Isotherms

Now it is necessary to estimate a near-surface layer. Particles of substances may form several sub-layers as thin films in the processes of accumulation. Let us assume the existence of two-phase systems consisting of B and C – see previous Fig. 5.1. Separation of phases is obtained by the surface A (cross-sectional area of the dividing surface). Total Gibbs free energy of a system could be obtained as a sum:

$$G = G^B + G^C + G^A, (5.36)$$

where  $G^B$  and  $G^C$  represent Gibbs free energy of phase B and phase C, respectively, and  $G^A$  represents Gibbs free energy of a cross-sectional area (surface A) which separates the mentioned phases B and C.

Let us assume the existence of several homogeneous components (total number j) with the chemical potential  $\mu_i$  and concentration  $c_i$ . Each phase (phases B, C and interface A) could be characterized by Gibbs free energy for a phase:

$$G^{B} = U + pV - TS + \sum_{i=1}^{j_{B}} \mu_{i} n_{i}, \qquad (5.37)$$

$$G^{C} = U + pV - TS + \sum_{i=1}^{j_{C}} \mu_{i} n_{i},$$
 (5.38)

$$G^{A} = U + pV - TS + \sum_{i=1}^{j_{A}} \mu_{i} n_{i}, \qquad (5.39)$$

where pVT represents thermodynamic parameters: pressure, volume and temperature, U is the internal energy, and S is the entropy.

The total derivative according to Eq. (5.36) includes three types of factors:

$$dG = \sum_{B,C,A} [X_1 + X_2] + X_3, \tag{5.40}$$

where

$$X_1 = dU + pdV + V dp - TdS - SdT, (5.41)$$

$$X_2 = \sum_{i=1}^{j} \mu_i dn_i + \sum_{i=1}^{j} n_i d\mu_i,$$
 (5.42)

$$X_3 = Adg + gdA. (5.43)$$

Actually, gdA factor must be treated as negligible (in case of stable surface area). Factor g represents the surface tension.

All chemical or physical processes related to the covering of surfaces and creation of interface are reversible. According to the first law of thermodynamics, dU represents behaviour of heat energy Q and work W (non-pressure volume work, surface energy is considered):

$$dU = Q + W. (5.44)$$

In Eqs. (5.40) and (5.41) presented dU can be expressed as follows:

$$dU = Q + W = \sum_{B,C,A} [TdS - pdV - W].$$
 (5.45)

By substituting Eqs. (5.45, 5.46, 5.47, 5.48, 5.49 and 5.50):

$$dG = \sum_{B,C,A} \left[ Vdp - SdT + \sum_{i=1}^{j} \mu_i dn_i + \sum_{i=1}^{j} n_i d\mu_i \right] + Adg,$$
 (5.46)

$$dG = Vdp - SdT + \sum_{i=1}^{J} \mu_i dn_i.$$
 (5.47)

Properties of B, C phases and interface A are related by Eq. (5.48):

$$\sum_{i=1}^{j} n_{iB} d\mu_i + \sum_{i=1}^{j} n_{iC} d\mu_i + \sum_{i=1}^{j} n_{iA} d\mu_i + Adg = 0.$$
 (5.48)

Let us assume the phases B and C as bulk phases. Let us establish the equilibrium (T = const, p = const). First two members in Eq. (5.48) are negligible:

$$\sum_{i=1}^{j} n_{iB} d\mu_i = \sum_{i=1}^{j} n_{iC} d\mu_i \to 0.$$
 (5.49)

According to Eq. (5.49)

$$\sum_{i=1}^{j} n_{iA} d\mu_i + A dg = 0. (5.50)$$

The Gibbs isotherm equation (Eq. 5.50) is called the adsorption isotherm that related surface tension g of a solution with the concentration of the solute n.

Foo et al. [3] presented a great number of different models for researches. Table 5.6 represents several models of adsorption isotherms which are important from the historical point of view or due to real acceptance in the surface chemistry – advantages and disadvantages are pointed out.

Freundlich Adsorption Isotherm. In 1909, Herbert Freundlich derived a primitive empirical relation which allows predicting the adsorption capacity on adsorbate pressure. This model has been useful so far as the relation of the first order assumption. In the case when identity of solute is unknown, it is possible to postulate the deposition model as simple as possible: adsorbate forms a monomolecular layer on the surface.

The quantitative dependence of the adsorption capacity (the amount of deposited particles of substance) was related to the equilibrium pressure of the adsorbate *p*:

$$\frac{x}{m} = k \cdot p^{\frac{1}{n}},\tag{5.51}$$

$$\log\left[\frac{x}{m}\right] = \log k + \frac{1}{n}\log p,\tag{5.52}$$

where x is the mass of the adsorbate and m is the mass of the adsorbent. Constants k and n > 1 are characteristic for a particular gas and the surface (adsorbate and adsorbent, respectively). Equation (5.70) as a logarithmic dependence shows that the adsorbate amount increases slowly in comparison with pressure.

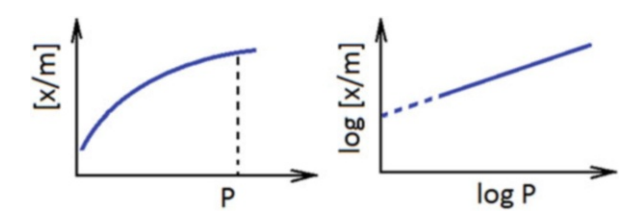
Figure 5.8 represents Freundlich isotherm, which explains idealized adsorption in first assumption as a linear dependence.

Slope n-1 is distributed practically in range  $[0.1 \div 0.5]$ . In a special case (at high pressure) if n-1=0, Eq. (5.70) becomes:

Advantages	Disadvantages
Monolayer on surface Any interactions betwadsorbate particles	
01	*
One-layer model	Empirical model, any physics
Three-layer model	Semi-empirical model
Complete description of interactions between	Big computer resources
adsorbate particles	required
	Monolayer on surface One-layer model Three-layer model Complete description of interactions between

Table 5.6 Physical (PS) vs chemical (CS) adsorption. Comparison on models

Fig. 5.8 Freundlich adsorption isotherms



$$\log\left[\frac{x}{m}\right] = \log k,\tag{5.53}$$

$$\frac{x}{m} = k = \text{const.} \tag{5.54}$$

Equation (5.54) expresses the process of adsorption independent of pressure. In the next case, if n - 1 = 1, Eq. (5.70) becomes:

$$\log\left[\frac{x}{m}\right] = \log k + \log p,\tag{5.55}$$

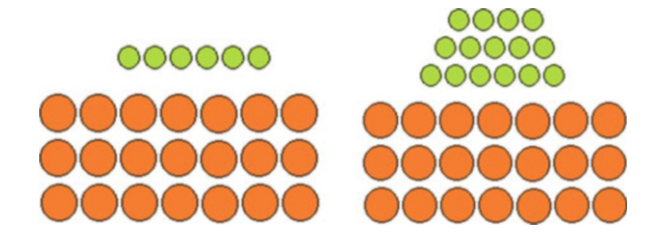
$$\frac{x}{m} = kp. (5.56)$$

Adsorption is pressure dependent. It is necessary to point out that the Freundlich isotherm correctly represents the adsorption capacity at equilibrium pressure of the adsorbate only at low pressure.

Langmuir Adsorption Isotherm. In 1916, Irving Langmuir (Nobel Prize winner in 1932) presented a simple model for the adsorption of substance onto simple surfaces. Let us assume ideal gas to be adsorbed on surface, and adsorbed molecules are fixed at surface (immobile). All adsorbate regions are identical energetically. This model is suitable when surface is homogeneous and uniform, and only monolayer adsorption occurs. Figure 5.9 represents the surface structure of Langmuir adsorption: adsorbate – monolayer. Interactions between adsorbed molecules are absent, and adsorbed and desorbed (free) molecules exist in equilibrium.

The presented model is suitable for the analysis of reaction mechanisms in chemisorption as well as physisorption [4]. According to the model, reaction yield is independent of the amount of the adsorbed substance. Heat of the adsorption is a constant.

**Fig. 5.9** Langmuir adsorption (adsorbate – monolayer) and BET adsorption (three-layer)



Let us assume the existence of the surface covered by adsorbate at pressure of adsorbate P. The total number of adsorption sites is equal to N, number of occupied sites -n. The fraction q of the surface (as covered by substance):

$$q = \frac{n}{N}. (5.57)$$

At equilibrium of adsorption and desorption processes:

$$k_A P(N-n) = k_D n ag{5.58}$$

The equilibrium constant  $K_{eq}$  is equal:

$$K_{\text{eq}} = \frac{k_A}{k_D} = \frac{n}{P(N-n)},$$
 (5.59)

where  $k_A$  and  $k_D$  are adsorption and desorption rate constants. From thermodynamics:

$$K_{\rm eq} = \exp\left[-\frac{\Delta H}{RT}\right],\tag{5.60}$$

where  $\Delta H$  represents heat of adsorption at standard pressure,  $P_{ST}$ , and temperature T. Equation (5.59) could be rewritten in the form of value q (see Eq. 5.57):

$$K_{\text{eq}} = \frac{n}{P(N-n)} = \frac{1}{P(\frac{N-n}{n})} = \frac{1}{P(\frac{N}{n}-1)} = \frac{1}{P(\frac{1}{q}-1)},$$
 (5.61)

$$q = \frac{K_{\text{eq}}P}{1 + K_{\text{eq}}P} = \frac{P}{K_{\text{eq}}^{-1} + P}.$$
 (5.62)

Taking into account Eq. (5.60):

$$q = \frac{P}{K_{\text{eq}}^{-1} + P} = \frac{P}{P_{ST} \exp\left[+\frac{\Delta H}{RT}\right] + P},$$
 (5.63)

$$n^{-1} = N^{-1} + [K_{eq}NP]^{-1},$$
 (5.64)

$$\frac{P}{V} = \frac{P}{V_m} + \frac{1}{\alpha V_m}. ag{5.65}$$

**BET**, **Brunauer–Emmett–Teller Adsorption Isotherm.** In 1938, Stephen Brunauer, Paul Hugh Emmett and Edward Teller published the first article about the BET theory [5]. Development of BET theory was related with the tasks of industry, especially in solid catalysis. BET theory applies to systems of multilayer physisorption and is useful in surface area determination. Figure 5.9 represents the surface structure of the BET adsorption when the three-layer covering is made. The BET theory usually utilizes an adsorbate that does not react chemically with the adsorbent.

Let us assume the volume of the adsorbed vapour V, the monolayer capacity  $V_m$ , both at the standard pressure,  $P_{ST}$ , and partial pressure of the adsorbate P, as well as the saturation vapour pressure of the adsorbate  $P_0$ . According to the first assumptions that Langmuir theory can be applied to each layer:

$$\frac{P}{V[P_0 - P]} = \frac{1}{V_m C} + \frac{(C - 1)P}{V_m C P_0}.$$
 (5.66)

The constant C is called the BET constant (adsorbate and adsorbent dependent), where  $\Delta H_A$  and  $\Delta H_L$  represent the heat of adsorption for the first and second layers, respectively:

$$C \approx \exp\left[\frac{\Delta H_A - \Delta H_L}{RT}\right]. \tag{5.67}$$

In case, if  $P_0 > P$ :

$$\frac{C-1}{C} \to 1. \tag{5.68}$$

The BET isotherm is transformed to the Langmuir isotherm:

$$\frac{P}{VP_0} = \frac{1}{V_m C} + \frac{P}{V_m P_0}. (5.69)$$

The BET method is one of the most frequently used in the surface science when the surface area of solids must be calculated from the data of physisorption of some gas.

#### 5.4 Hydrogen Adsorption

The problem of hydrogen storage belongs to one of the more complicated technical tasks of the contemporary humanity. Hydrogen as a source of energy could be suitable for many areas of technical activities. However, gas form storage is not safe; liquid form storage requires the cryogenic equipment (some sort of tank). Liquid hydrogen boils at around  $20.27 \text{ K } (-252.88 \,^{\circ}\text{C})$ .

There are two methods for the hydrogen storage: physical and chemical.

The physical storage could be organized as the behaviour of two physical processes: compressing under high pressure (700 bar) and/or liquefaction ( $<20~\mathrm{K}$ ) of molecular H<sub>2</sub>. All processes are reversible. Cryogenic equipment consists of the high-pressure pumps and well-isolated tanks.

Chemical storage is dissociative according to Eq. (5.70):

$$H_2 \to H + H. \tag{5.70}$$

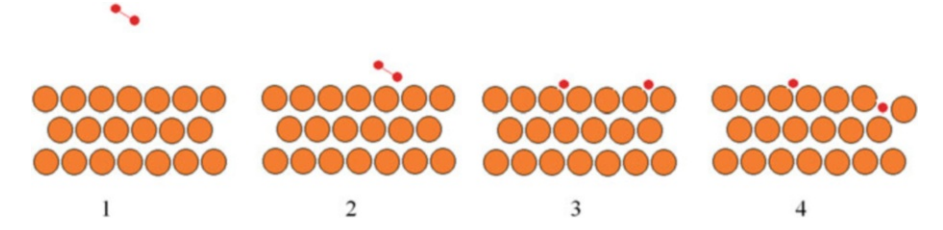
Decomposition of molecular hydrogen into the atomic one allows organizing the deposition of the substance onto an activated surface as well as following long-time storage. Processes of deposition can be both reversible (using metal hydrides as adsorbents) and nonreversible (hydrolysed fuel, decomposed fuel).

Figure 5.10 represents the general scheme of molecular hydrogen adsorption on a metal surface. Molecular hydrogen as adsorptive and adsorbate could be deposited on a metal surface (physical adsorption). The reaction yield is very low. But after the decomposition of molecular hydrogen, atomic hydrogen can be placed as an adsorbate directly on the surface (3) as well as into pores (4).

This way is preferable taking into consideration two circumstances. Thomas K [6] reported results of fuel cells useful for hydrogen storage for transport applications. Author discussed the tasks of adsorption of hydrogen on porous materials, ranging from activated carbons to metal organic framework materials. The advantage is formulated as follows: at temperature 77 K, up to 5 and 7.5 wt% of hydrogen can be stored on porous carbon and metal organic framework materials, respectively. Ströbel et al. [7] studied the hydrogen adsorption on carbon materials at ambient temperature. Hydrogen adsorption reached values of 1.5 wt.% at ambient temperature and 125 bars.

Generally, storage of solid-state materials could be realized through two interfaces: metal hydrides and porous materials. Metal hydrides, such as palladium hydride, TiFeH<sub>2</sub>, MgH<sub>2</sub>, LiAlH<sub>4</sub>, LiH, etc., could be used as storage media of low degree efficiency. Porous materials such as carbons, metal organic framework, porous polymers and zeolites are more prominent materials for storage media.

Bianco S et al. [8] reported the study of the hydrogen adsorption in several kinds of carbon nanotubes (CNT). Morphological microstructure and physical properties of CNT were examined in order to establish microstructure–process–property relationships. Several types of carbon nanotubes (SWCNT and five MWCNT) were examined using different methods, including Brunauer–Emmett–Teller



**Fig. 5.10** Four stages of hydrogen (red) adsorption on a metal surface. Molecular hydrogen as adsorptive (I) and an adsorbate (2) at long and short distances from the surface, respectively. Atomic hydrogen as an adsorbate near the surface (3 and 4)

(BET) analysis for the surface area. The experimental measurements demonstrate a direct correlation between the exposed surface area and adsorbed hydrogen capacity, which confirms their linear relationship observed previously. SWCNT with surface area density of  $800 \text{ m}^2/\text{g}$  has shown hydrogen storage of approximately 1.7 wt% at a pressure of 35 atm. Adsorption process seems to be perfectly reversible.

Meisner G P et al. [9] reported the previous results of novel synthesized carbon materials with microporous of high surface area. Specific surface area value was distinguished up to nearly 2000 m²/g and an excess hydrogen storage capacity of 4.2 wt% was observed. Authors claim that a strong correlation between the BET values of the specific surface area and the excess hydrogen adsorption capacity was observed.

#### 5.5 Electronic Structure of Surface

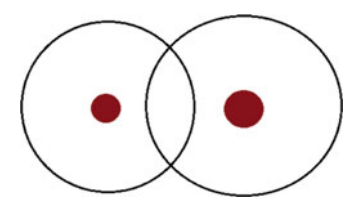
**The Molecular System.** First form of material complexation is a certain atomic or molecular system (molecule, dimer, cluster, etc). Electronic properties of molecular system could be established by solving the Schrödinger equation. The solution of the differential wave equation describes particle systems as well as macroscopic systems. The fundamental postulate of quantum mechanics claims that the wave function  $\Psi_0$  describes all energetic properties of the system.

The time-independent Schrödinger equation for a simple molecular system contains Hamilton operator  $\overset{\wedge}{H_0}$  which acts on a wave function  $\Psi_0(\mathbf{r})$  representing stationary state. Proportionality constant E represents energy of the mentioned stationary state:

$$\overset{\wedge}{H_0}\Psi_0(\mathbf{r}) = E \cdot \Psi_0(\mathbf{r}). \tag{5.71}$$

Hamiltonian  $\overset{\wedge}{H_0}$  includes Laplacian  $\Delta$  (as second derivative) and potential energy  $U_0(\mathbf{r})$  as simplest case of Coulomb expression. For one-dimensional case:

Fig. 5.11 Simplest molecular system: two protons and two electrons. Overlap of two  $\sigma$ -orbitals



$$\stackrel{\wedge}{H_0}(x) = -\frac{\hbar^2}{2m} \cdot \frac{\partial^2}{\partial x^2} + U_0(x). \tag{5.72}$$

The simplest equation of the wave function is presented below as a plane wave with the amplitude A, wave vector  $\mathbf{k}$  and angular frequency  $\omega$ :

$$\Psi_0(\mathbf{r},t) = A \cdot \exp[i(\mathbf{kr} - \omega t)]. \tag{5.73}$$

The solution of the Schrödinger equation for a molecular system depends on the properties of the model. One of the simplest systems is a hydrogen molecule  $H_2$  – a molecular system that consists of two protons and two electrons (see Fig. 5.11). In the framework of the molecular orbital (MO) as a linear combination of the atomic orbital (LCAO), the solution of the Schrödinger equation gives two and more possible states with different energies.

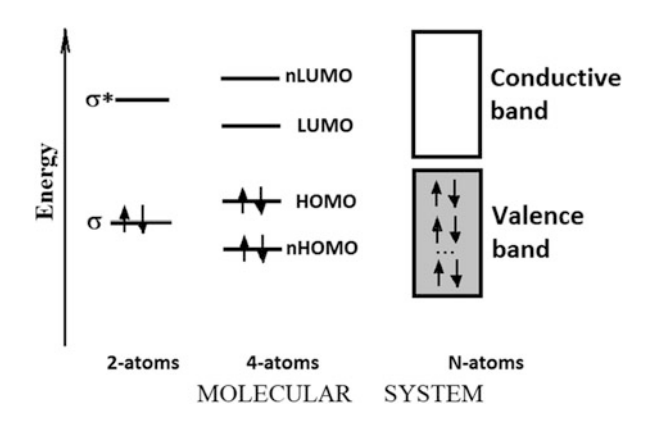
Figure 5.12 represents energy diagrams of the two-atom system, four-atom system and *N*-atom system. Such three systems could be treated as the main assumption of material organization starting from molecular. Practically evaporated molecular beam arranges on the surface in some periodicals. Formation of crystals is based on the lattice template.

Using the MO method, the number of stationary electronic states is equal to the number of electrons. According to the Pauli principle, one state could be populated by two electrons with different spins (presented by top-arrow and bottom-arrow). The two-atom two-electron system could be characterized by two electronic states, when the lowest is populated by both electrons with different spins ( $\sigma$ -state), and next is empty, virtual ( $\sigma * -$ -state).

The four-atom four-electron system could be characterized by four electronic states, when two lowest states are populated by four electrons (two pairs of electrons in state with different spins), and two highest states are empty, virtually. The highest occupied molecular orbital (HOMO) is related to the ionization energy, and the lowest unoccupied molecular orbital (LUMO) is related to the electron affinity. HOMO  $\rightarrow$  LUMO transition denotes the electronic excitation dynamics of the system.

According to the mentioned assumption, N-atom N-electron system contains N states, which are overlapped in bands: the valence band (corresponds to the occupied MO) and the conductive band (corresponds to the virtual MO). This approach looks similar to the crystal definition.

Fig. 5.12 Energy diagram of different molecular systems: two atoms, four atoms, N-atoms



Crystal and Surface. The second form of material complexation is a solid formed in the form of an ordered (monocrystalline), partially ordered (polycrystalline, film based, etc.) or disordered system. According to the definition, a crystal represents a certain realization of the spatial distribution of a molecular system according to the rules of periodicals. A surface represents a two-dimensional behaviour of geometric localization of atoms.

Let us assume the existence of a cubic crystal with the lattice constant a – see Fig. 5.13. Vector  $\mathbf{R}_{\mathbf{n}}$  describes the coordinates of nuclear related to the lattice vector in three-dimensional space:  $\mathbf{a}_i$ , i = 1,2,3. The factor  $n_i$  represents the natural number.

$$\mathbf{R_n} = \sum_{i=1}^{3} n_i \mathbf{a_i},\tag{5.74}$$

$$\mathbf{a_1} \to (a, 0, 0),$$
 (5.75)

$$\mathbf{a_2} \to (0, a, 0),$$
 (5.76)

$$\mathbf{a_3} \to (0, 0, a).$$
 (5.77)

To describe the potential energy  $U_1(\mathbf{r})$  of electrons in the crystal, operations of translation symmetry must be used. Vector  $\mathbf{r}$  describes the coordinates of electrons related to the nuclear according to the Born-Oppenheimer assumption:

$$U_1(\mathbf{r} + n_1\mathbf{a_1} + n_2\mathbf{a_2} + n_3\mathbf{a_3}) = U_1(\mathbf{r}). \tag{5.78}$$

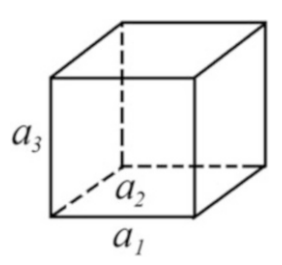
In the Schrödinger equation, Hamiltonian  $H_1$  includes Laplacian  $\Delta$  (as second derivate) and mentioned potential energy  $U_1(\mathbf{r})$ :

$$\stackrel{\wedge}{H_1} \Psi_1(\mathbf{r}) = E \cdot \Psi_1(\mathbf{r}), \tag{5.79}$$

$$\stackrel{\wedge}{H_1} \Psi_1(\mathbf{r}) = E \cdot \Psi_1(\mathbf{r}), \tag{5.79}$$

$$\stackrel{\wedge}{H_1} (x) = -\frac{\hbar^2}{2m} \cdot \frac{\partial^2}{\partial x^2} + U_1(x). \tag{5.80}$$

Fig. 5.13 Cubic crystal lattice with lattice vectors  $a_1, a_2, a_3$ 



Let us assume the existence of all electrons in the crystal as a behaviour of single isolated electrons (coordinate  $\mathbf{r}$ ) belonging to the nuclear ( $\mathbf{R}_{\mathbf{n}}$ ). The complicated equation of the wave function is presented below as a product of the coefficient c and the wave function of the isolated electron  $\phi(\mathbf{r} - \mathbf{R}_{\mathbf{n}})$ :

$$\Psi(\mathbf{r}) = \sum_{n} c(n_1, n_2, n_3) \phi(\mathbf{r} - \mathbf{R_n}). \tag{5.81}$$

In that case, the wave function of the isolated electron  $\phi$  must satisfy the Schrödinger equation, where s represents the energy of the stationary state of the isolated electron:

$$\stackrel{\wedge}{H_2} \phi(\mathbf{r} - \mathbf{R_n}) = \varepsilon \cdot \phi(\mathbf{r} - \mathbf{R_n}), \tag{5.82}$$

$$\stackrel{\wedge}{H_2} \phi(\mathbf{r} - \mathbf{R_n}) = \varepsilon \cdot \phi(\mathbf{r} - \mathbf{R_n}), \qquad (5.82)$$

$$\stackrel{\wedge}{H_2} (x) = -\frac{\hbar^2}{2m} \cdot \frac{\partial^2}{\partial x^2} + U_2(\mathbf{r} - \mathbf{R_n}). \qquad (5.83)$$

The potential electronic energy  $U_1(\mathbf{r})$  is expressed as the sum of potentials of isolated electrons and additional potentials  $\delta$ :

$$U_1(\mathbf{r}) = \sum_{n} U_2(\mathbf{r} - \mathbf{R_n}) + \delta.$$
 (5.84)

By solving the Schrödinger equation Eq. (5.79), assumptions of Born-von Karman type must be made. A crystal of infinity dimensions is divided into crystals of finite dimensions with N > 1 atoms. The condition of translational symmetry according to Eq. (5.78) must be applicable to coefficients  $c(n_1, n_2, n_3)$ :

$$c(n_1, n_2, n_3) = c(n_1 + N, n_2, n_3) = c(n_1, n_2 + N, n_3) = c(n_1, n_2, n_3 + N),$$
 (5.85)

$$c(n_1, n_2, n_3) = \exp[i(k_1n_1 + k_2n_2 + k_3n_3)a].$$
 (5.86)

After replacing, Eq. (5.81) becomes Eq. (5.87):

$$\Psi(\mathbf{r}) = \sum_{n} \left[ \exp[i(k_1 n_1 + k_2 n_2 + k_3 n_3) a] \right] \phi(\mathbf{r} - \mathbf{R_n}).$$
 (5.87)

The factor  $k_i$  represents the expression of the natural number  $0 \le u_i \le N$ :

$$k_i = \frac{2\pi}{Na} u_i. \tag{5.88}$$

Firstly, it is necessary to solve wave equations for isolated electrons and to receive the energy of the stationary state of the isolated electrons. Secondly, the equation Eq. (5.79) must be solved in any practical way using semi-empirical lattice atomic potentials. The solution of the Eq. (5.79) is presented below:

$$E = \varepsilon + \alpha + 2\beta(\cos n_1 a + \cos n_2 a + \cos n_3 a), \tag{5.89}$$

where  $\alpha$  represents the Coulomb integral and  $\beta$  represents the exchange integral. Analysing Eq. (5.100), it is easy to establish the minimum and maximum energy, in case of  $\cos \gamma = 1$  or  $\cos \gamma = -1$ :

$$E_{\text{max}} = \varepsilon + \alpha + 6\beta, \tag{5.90}$$

$$E_{\min} = \varepsilon + \alpha - 6\beta. \tag{5.91}$$

Energetically, the width of the zone W increases with the decreasing lattice constant a (due to increasing of exchange integral  $\beta$ ).

$$W = E_{\text{max}} - E_{\text{min}} = 12\beta. \tag{5.92}$$

Figure 5.14 represents the energy diagram of the isolated atom (single energy level) and atoms in crystal (many overlapped energy levels formed as zone). With  $N \to \infty$ , zone forms as quasi-continuous.

The task of forming the two-dimensional surface is related to the breaking of three-dimensional periodicity of the crystal. After mechanical motion, the absence of atoms initiates: (1) redistribution of the electronic charge inside the crystal and in the near-surface environment and (2) following the reformation of the damaged electronic states (formation of so-called surface states).

Let us assume the breaking operation of a cubic crystal  $(n_3 = 0)$  and arising of the surface (see Fig. 5.15). Vectors  $\mathbf{a_1}$  and  $\mathbf{a_2}$  are placed in a plane surface  $(n_3 = 0)$ . Vector  $\mathbf{R_p}$  describes the coordinates of any atom placed on the surface in a two-dimensional space:  $\mathbf{a}_i$ , i = 1,2. The factor  $n_i$  represents the natural number (1, 2, 3, etc.).

$$\mathbf{R}_{\mathbf{p}} = \sum_{i=1}^{2} n_i \mathbf{a_i}.\tag{5.93}$$

The condition of the translational symmetry according to Eq. (5.78) must be applicable to coefficients  $c(n_1, n_2, n_3)$ :

$$c(n_1, n_2, n_3) = c(n_1 \pm N, n_2, n_3) = c(n_1, n_2 \pm N, n_3).$$
 (5.94)

The condition for the surface  $n_3 = N$  must be present in form:

**Fig. 5.14** Energy diagram: energy levels of the isolated atom (IA) and atoms in the crystal (CR)

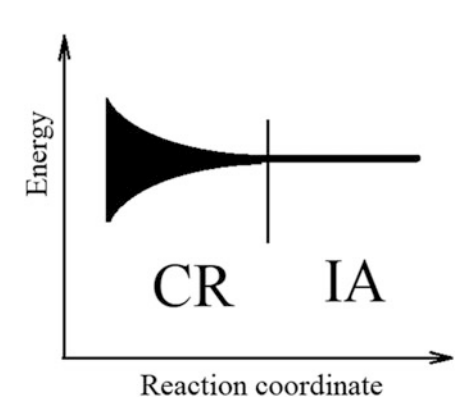
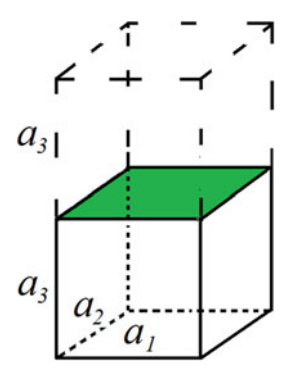


**Fig. 5.15** Plane surface of crystal lattice vectors  $a_1$ ,  $a_2$ 



$$c(n_1, n_2, N) = 0, (5.95)$$

$$c(n_1, n_2, n_3) = \exp[i(k_1n_1 + k_2n_2)a]\sin(N - n_3)k_3a.$$
 (5.96)

After replacing, Eq. (5.81) becomes Eq. (5.97):

$$\Psi(\mathbf{r}) = \sum_{n} \left[ \exp[i(k_1 n_1 + k_2 n_2) a] \right] \phi(\mathbf{r} - \mathbf{R_n}). \tag{5.97}$$

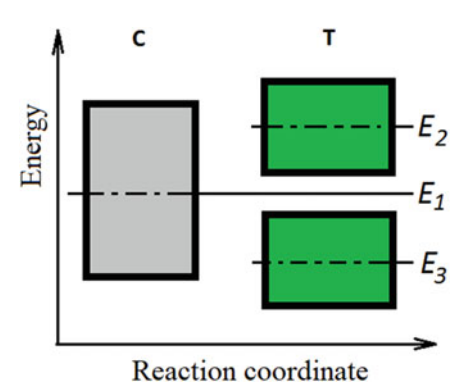
Solving the Schrödinger equation for the surface, the so-called Tamm states:

$$E_3 = \varepsilon + \alpha + 2\beta(\cos k_1 a + \cos k_2 a) + 2\beta \cosh \eta a, \tag{5.98}$$

$$E_3 = \varepsilon + \alpha + 2\beta(\cos k_1 a + \cos k_2 a) - 2\beta \cosh \eta a, \tag{5.99}$$

where  $\alpha$  represents the Coulomb integral and  $\beta$  represents the exchange integral. Figure 5.16 represents distributions of energy levels of atoms in the crystal (C) and atoms on the surface (T). The energetic width of the zone W increases with the decreasing lattice constant  $\alpha$  (due to increasing the exchange integral  $\beta$ ):

**Fig. 5.16** Energy diagram: energy levels of atoms in the crystal (C) and atoms on surface (T):  $E_1 = c + \alpha$ ,  $E_2 = c + \alpha + 2\beta \cosh \eta a$ ,  $E_3 = c + \alpha - 2\beta \cosh \eta a$ .



$$W = E_{\text{max}} - E_{\text{min}} = 2 \cdot 4\beta = 8\beta. \tag{5.100}$$

Local electronic states can be created on the surface of solids. There are three reasons why surface electronic states occur:

- Damage of the periodic potential of the crystalline lattice due to the atomic dislocations.
- 2. The presence of uncompensated covalent bands on the surface.
- Molecules or atoms of the adsorbate perturb the periodic potential created by the adsorbent in the lattice.

For the determination of the surface electronic states, two main assumptions are useful according to the presented model: the Tamm states and Shockley states. From the physical point of view, both models represent the same reality. The mathematical approach is different.

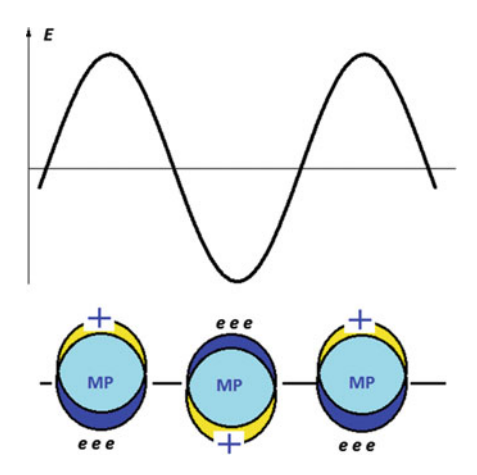
The Tamm states could be received by the following assumptions: (1) wave functions are of orbital-like type and (2) the tight-binding model for localized electrons. This method could be applied for semiconductors as well as for transition metals. The existence of the surface states was first shown by Igor Tamm in 1932.

The Shockley states could be received by the following assumptions: (1) wave functions are of crystal-like type and (2) the nearly free electron model. This method could be applied for narrow-gap semiconductors as well as many metals such as K, Al, etc.

Inglesfield [10] presented a very complete review of the electronic structure theory of clean metals and semiconductor surfaces. Effective methods how to solve the one-electron Schrödinger equation are described. Detailed calculations of the surface states of transition metals, s–p bonded metals and semiconductors are also explained and reviewed.

Zangwill [11] presented a detailed review of the surface electronics from different points of view: thermodynamic, crystallographic and phase transition. In addition, the review of Green [12] must be pointed out as one of significant classical reviews in the surface physics.

Fig. 5.17 Metal particles (MP) in electric field E: oscillations of E induce oscillations of electronic clouds



### 5.6 **Surface Plasmon Resonance**

Plasmon represents a collective oscillation of the plasma density at optical or near optical frequencies. According to this model, plasma must be treated as a free electron gas. Figure 5.17 represents metal particles (MP) in the electric field E when oscillations of E induce oscillations of electronic clouds. The surface plasmon resonance (SPR) is the basic method for the estimation of interactions between adsorbent (typically gold or silver) and adsorbate. The macro-surface or the surface of metal nanoparticles could be used for such purposes.

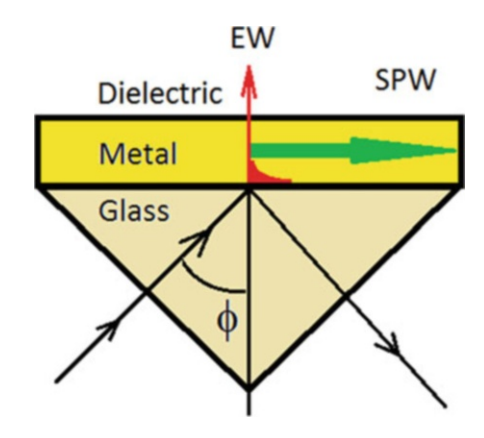
Figure 5.18 represents an experimental setup for the surface plasmon resonance (SPR) built up by the Kretschmann configuration. The glass prism is covered with a layer of Au (thickness  $45 \div 55$  nm). The metal layer is covered with a dielectric (sample to investigate). The incident light beam passes through the glass prism (incident angle  $\varphi$ ) and is reflected from the inner prism surfaces. If p-polarized light (the wavelength of the incident light  $\lambda$ ) accesses metal layer at the total reflection angle, the charge density oscillations on the metal layer (evanescent field) occur. The surface plasmon represents transverse magnetic waves. Three different environments are present in this experiment.  $\varepsilon_d$  and  $\varepsilon_m$  represent a complex dielectric constant of dielectrics and the metal.  $\varepsilon_p$  is a dielectric constant of the prism, when the refractive index of the prism $n_p = \varepsilon_p^2$ .

Gwon et al. [13] presented resonance conditions for SPR experiments. The propagating vector of the surface plasmon wave  $k_{\rm sp}$  and electromagnetic wave  $k_{\rm em}$  must be equal:

$$k_{\rm sp} = k_{\rm em},\tag{5.101}$$

$$k_{\rm sp} = k_{\rm em},$$
 (5.101)  
 $k_{\rm sp} = \frac{2\pi}{\lambda} \sqrt{\frac{\varepsilon_m \cdot \varepsilon_d}{\varepsilon_m + \varepsilon_d}},$  (5.102)

Fig. 5.18 Kretschmann configuration for SPR experiment. Surface plasmon wave (SPW) by *green* array, evanescence wave (EW) by *red* 



$$\varphi = \sin^{-1} \sqrt{\frac{\varepsilon_m \cdot \varepsilon_d}{\varepsilon_p (\varepsilon_m + \varepsilon_d)}}.$$
 (5.103)

The real SPR experiment could be organized using two techniques: (1) reflected beam changes intensity at the resonance angle (measuring of intensities at a fixed excitation wavelength); (2) resonance angle increases by the exciting metal layer covered by an active material (searching for the incidence angle at the lowest refraction index R).

The second way is more profitable:

- 1. Covering the surface of a sapphire prism by Au (thickness 50 nm).
- 2. Measuring the refractive index  $R_0$  at different UV beam incident angles  $\varphi$  in the range of  $[25 \div 45]^{\circ}$  background curve  $R_0 = R_0(\varphi)$ .
- 3. Covering metal surface by an active organic material.
- 4. Measuring the refractive index  $R_x$  at different UV beam incident angles  $\varphi$  in the range of  $[25 \div 45]^{\circ}$  sample curve $R_x = R_x(\varphi)$ .
- 5. The refractive index dependence on the incident angles  $\varphi$  contains the minimum at  $[36 \div 37]^{\circ}$ . A shift to higher angles for the active material takes place.

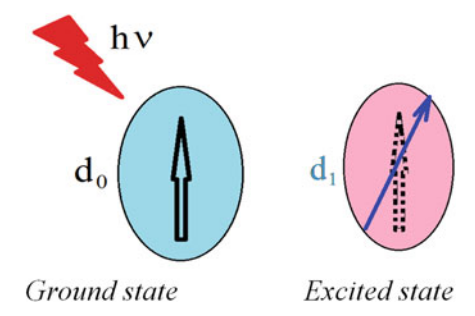
# 5.7 Interaction of Light and Nanoparticle

**The Molecular Approach.** Interaction of light and material could be understood using the approach of particle interaction. If the light absorption process is allowed, the main reaction could be written as follows:

$$R + h\nu \to R^* \to R + Q. \tag{5.104}$$

The reactant (molecule, dimer, cluster, etc.) R interacts with the light quantum  $h\nu$  and produces the reactant in the excited state  $R^*$ . After the internal conversion and different relaxation processes (luminescence, dark state depopulation, electron

Fig. 5.19 Schematic chart of material-light interactions (neutral  $\pi$ -conjugated molecule and light quantum  $h\nu$ ). Essential change of the molecular dipole moment:  $\mathbf{d_0} \rightarrow \mathbf{d_1}$  at transition from the ground state to the excited state



transfer, etc.), the reactant returns to the ground state through energy Q dissipation processes. Eq. (5.104) represents only the energy balance according to the law of energy conservation in isolated systems. Figure 5.19 represents schematic chart of material-light interactions when the neutral  $\pi$ -conjugated molecule interacts with the light quantum  $h\nu$ . If the molecule absorbs the quantum, an essential change of the molecular dipole moment must occur. Dipole moments of ground and excited states  $\mathbf{d_0}$  and  $\mathbf{d_1}$ , respectively, could be of different orientations or of different scalar values.

If the light absorption process is forbidden, scattering processes takes place. Any significant changes of the molecule dipole moment occur. Several processes are significant in materials science: vaporization of the medium, heat transfer to the medium and generation of particle cavitation on the media surface.

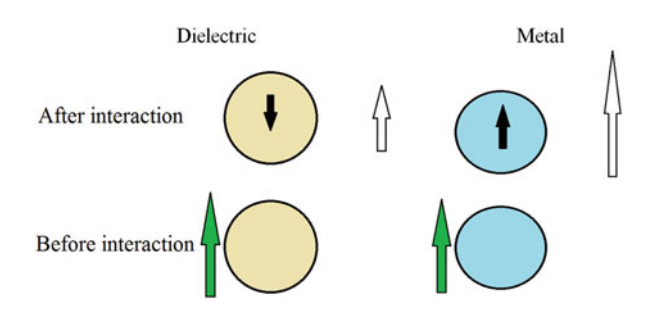
**The Nanoparticle Approach.** For particles, aspects related to quantum absorption are the same as in the case of molecules. If the light absorption process is allowed, the reaction according to Eq. (5.104) is realized. Otherwise, additional aspects related to the size of the particle (active nanosurface) sometimes are prior.

At the nanoscale, three types of nanoparticles could be accepted: (1) nanoparticles containing only several atoms; (2) small nanoparticles, diameter 1 nm < d < 100 nm; and (3) large nanoparticles (diameter d > 100 nm).

Figure 5.17 represents large metal particles (MP) in the electric field E when oscillations of E induce the oscillations of electronic clouds (plasmonic waves). Resonance conditions for such type oscillations could be distinguished in several ways. According to that, plasmonic nanoparticles could express higher reactivity in many scattering processes such as electron scattering, electron—phonon scattering, evaporation and melting of particle and fragmentation.

Figure 5.20 represents the scheme of interactions of light and a particle of a dielectric type and a metal type. Excitation could be produced by a light beam; the green arrow represents the vector of the incident electric field. The dielectric particle gives the response to the incident electric field by creating the induced dipole of the opposite direction. The metal particle gives the response to the incident electric field through oscillations of free electrons – the induced dipole in the same direction. Black arrows represent the vectors of induced dipoles. The vector of the resulting electric field after interaction (corresponds to the optical

Fig. 5.20 Interactions of light and dielectric particle (*left*) or metal particle containing free electrons (*right*). Incident electric field, *green arrow*; inner electric field (induced), *black arrow*; resulting electric field, *transparent arrow*: *green* + *black* → *transparent* 



response) is shown as a transparent arrow: for dielectric – a decreased length, for metal – an increased length. The directions of the resulting vector and the incident vector coincide.

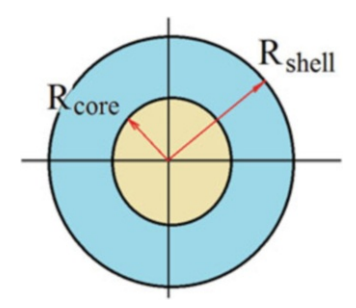
This effect could occur in macro-objects as well as in micro- or nanoobjects. A significant influence could be found only for nanoobjects. The Mie theory describes scattering processes of such type. The optical response for large metallic nanoparticles  $(d > \lambda)$  (near UV, VIS region) depends on the size of the particle (it means on the density of a free electron).

For small nanoparticles (diameter 1 nm < d < 100 nm), several physical characteristics such as the refraction index and dielectric permittivity dramatically change. Kubo [14] established the refraction index dependence on the particle size when the size of a particle (50 nm Ag, Au) is comparable to the de Broglie wavelength for the electron. Predictions according the Mie theory are generally acceptable, but not exact. If the size of a particle (0.5 nm Ag, Au) is comparable with the Fermi wavelength for the electron, simulations of physical properties by means of the Mie theory are inaccurate. Several popular structures such as  $Au_{25}$  nanorods and  $Au_{25}$  nanospheres are useful as fluorescent nanoclusters.

For nanoparticles containing only several atoms, the size effects predominate over the steady-state electronic effects [15]. The properties of metallic nanoparticles are similar to molecules. Cesca et al. [16] studied a non-resonant broadband energy-transfer mechanism using sub-nanometric Au nanoclusters. It was found that small Au nanoclusters are very efficient sensitizers for the luminescent emission of  $\mathrm{Er}^{(3+)}$  ions in silica. It was concluded that the short-range nature of the interaction coincides with the non-radiative energy-transfer mechanisms.

Kubo [14] in 1962 decided that the energy level distribution in metallic nanoclusters is of discrete type but not continuing one. According to Fig. 5.20, interactions of light and a metallic particle induce charge density redistributions in the volume of the particle and also on the particle surface. Response depends on the free electron concentration which is related to the free path length of the electron. If the size of the metallic nanoparticle is more than the free path length of the electron, then the light absorption processes are related to the transition dipole moment. If the size of the metallic nanoparticle is less than the free path length of the electron, the light absorption energy is inverse proportional to the particle diameter [17]. According to Kubo [14], the energetic level distribution in metallic

Fig. 5.21 Geometry of metallic nanoshell



nanoclusters is of discrete type due to one condition: the size of a nanoparticle is equal to the Fermi wavelength (the so-called de Broglie wavelength for electron at the Fermi energy).

#### 5.8 **Nanoshells**

A nanoshell represents a composite spherical nanoparticle which consists of a dielectric material covered by a thin Au shell (core and shell) [18]. Figure 5.21 represents a schematic chart geometry of metallic nanoshell. The sphere of radius  $R_{\text{core}}$  is covered by a metallic sphere of radius  $R_{\text{shell}}$ . The shell thickness t and nanoshell constant  $\alpha$  are the main geometric parameters, which characterize the physical properties related to the plasmon excitation:

$$t = R_{\text{shell}} - R_{\text{core}},\tag{5.105}$$

$$t = R_{\text{shell}} - R_{\text{core}}, \tag{5.105}$$

$$\alpha = \frac{t}{R_{\text{shell}}} = 1 - \frac{R_{\text{core}}}{R_{\text{shell}}}. \tag{5.106}$$

For practical purposes,  $R_{\rm shell} \approx 10$  nm,  $t \approx 5$  nm and  $\alpha = 0.5$ .

A quasiparticle of such a type, called a nanoshell plasmon, represents a derivative where oscillations of electrons of the core and the shell are summarized: electrons simultaneously oscillate in relation to all ions. According to that, optical resonance of these nanoshells can be varied in the region from midIR to near UV, depending on the dimension.

Pena et al. [19] presented the study of the nanoshells linear optical responses. The plasmon resonance of metal nanoshells displays geometric tunability controlled by the ratio of the shell thickness either to the core radius or to the total radius of the particle. Considering the final  $R_{\rm shell} \approx 20$  nm by varying  $\alpha$  parameter, several SPR peak positions can be shifted in the range of 510 ÷ 660 nm for Au,  $360 \div 560$  nm for Ag, and  $553 \div 655$  nm for Cu. Authors claim that the intensity and position of the SPR peak strongly depends on the ratio  $\alpha$ .

The advantages of metallic nanoshells are well-known in the area of biomedicine. Biocompatibility of nanoshells with tissues in vivo provides the specific applicability in the tumour therapy. Absorption and adsorption properties on References 145

demand could be realized for the targeted displacing of nanoshells inside the tumour cells and killing the selected cells using appropriate therapeutical methods. Paithankar et al. [20] described several medical therapies for the treatment of diseases including atherosclerosis and thrombosis. The use of inorganic silicagold nanoshells for various kinds of treatment is very prominent: core – SiO<sub>x</sub>, shell – Au,  $R_{\rm shell} \approx 150$  nm,  $t \approx 15$  nm and  $\alpha = 0.1$ . As excitation source infrared and red laser irradiation was used to thermally disrupt overactive sebaceous glands in the skin.

## 5.9 Organic-Nonorganic Interfaces

Polar molecular compounds represent a possibility to perform any conformational motion with the following charge transfer processes. After the external perturbation (laser light, current pulse, electron beam, etc.), electronic charge redistribution along the molecular axis is related to the occurrence of the transition dipole moment. Relaxation processes in a molecule are space limited (volume of a molecule) and time limited (up to several ns).

The possibility to manipulate the molecular charge distribution for informational purposes is strongly limited by the current contact problem: how to establish a true contact (in macro-approach resistiveless contact, in micro-approach junction according to the overlap of wave function).

Wang et al. [21, 22] studied the effect of metal-molecule contacts in molecular junctions and proposed a multibarrier tunnelling model. Sun et al. [23] presented an extensive review of the application of single molecules in electronics for the miniaturization purposes.

### References

- 1. Croxton C 1980 Statistical mechanics of the liquid surface (Wiley:Chichester)
- 2. Herring C 1951 Some theorems on the free energies of crystal surfaces Phys. Rev. 82 87
- 3. Foo K Y, Hameed B H **2010** Insights into the modeling of adsorption isotherm systems *Chemical Engineering Journal* **156**(1) 2–10
- Langmuir I 1916 The constitution and fundamental properties of solids and liquids. Part 1. Solids. J. Am. Chem. Soc. 38(11) 2221–95
- 5. Brunauer S, Emmett P, Teller E **1938** Adsorption of Gases in Multimolecular Layers *Journal* of the American Chemical Society **60**(2) 309–19
- Mark K T 2007 Hydrogen adsorption and storage on porous materials Catalysis Today 120 (3–4) 389–98
- Ströbel R, Jörissen L, Schliermann T, Trapp V, Schütz W, Bohmhammel K, Wolf G, Garche J
   1999 Hydrogen adsorption on carbon materials *Journal of Power Sources* 84(2) 221–4
- 8. Bianco S, Giorcelli M, Musso S, Castellino M, Agresti F, Khandelwal A, Lo Russo S, Kumar M, Ando Y, Tagliaferro A **2010** Hydrogen adsorption in several types of carbon nanotubes *J Nanosci Nanotechnol.* **10**(6) 3860–6

- Meisner G P, Hu Q 2009 High surface area microporous carbon materials for cryogenic hydrogen storage synthesized using new template-based and activation-based approaches Nanotechnology 20(20) 204023
- 10. Inglesfield J E 1982 Surface electronic structure. Rep. Prog. Phys. 45 224-84
- 11. Zangwill A 1996 Physics at Surfaces Cambridge university press
- 12. Solid State surface Science 1969 Ed. by M Green 1 (New York: Marcel Dekker)
- 13. Hyuk R G, Seong H L **2010** Spectral and Angular Responses of Surface Plasmon Resonance Based on the Kretschmann Prism Configuration *Materials Transactions* **51**(6) 1150–5
- Kubo R 1962 Electronic Properties of Metallic Fine Particles. I Journal of the Physical Society of Japan 17(6) 975–86
- Schaaff G, Knight G, Shafigullin M, Borkman R, Whetten R 1998 Isolation and selected properties of a 10.4 kda gold: glutathione cluster compound *Journal of Physical Chemistry B* 102(52) 10645–6
- Cesca T, Kalinic B, Michieli N, Maurizio C, Scian C, Devaraju G, Battaglin G, Mazzoldi P, Mattei G 2014 Energy-transfer from ultra-small Au nanoclusters to Er3+ ions: a short-range mechanism *Phys Chem Chem Phys* 16(29) 15158–63
- 17. Mizutani U 2001 Introduction of electron theory of metals Cambridge: university press
- 18. Loo C, Lin A, Hirsch L, Lee MH, Barton J, Halas N, West J, Drezek R **2004** Nanoshell-enabled photonics-based imaging and therapy of cancer *Technol Cancer Res Treat*. **3**(1) 33–40
- Pena O, Pal U, Rodriguez-Fernandez L, Crespo-Sosa A 2008 Linear optical response of metallic nanoshells in different dielectric media J. Opt. Soc. Am. B 25(8) 1371–9
- Paithankar D, Hwang B, Munavalli G, Kauvar A, Lloyd J, Blomgren R, Faupel L, Meyer T, Mitragotri S 2015 Ultrasonic delivery of silica-gold nanoshells for photo- thermolysis of sebaceous glands in humans: Nanotechnology from the bench to clinic *Journal of Controlled Release* 206 30–6
- Wang G, Kim T W, Lee H, Lee T 2007 Influence of Metal-Molecule Contacts on Decay Coefficients and Specific Contact Resistances in Molecular Junctions Phys. Rev. B 76 205320
- 22. Wang G, Kim T W, Jang Y H, Lee T 2008 Effects of Metal-Molecule Contact and Molecular Structure on Molecular Electronic Conduction in Nonresonant Tunneling Regime: Alkyl versus Conjugated Molecules J. Phys. Chem. C 112 13010–6
- Sun L, Diaz-Fernandez Y A, Gschneidtner T A, Westerlund F, Lara-Avila S, Moth-Poulsen K
   2014 Single-molecule electronics: from chemical design to functional devices *Chem. Soc. Rev.* 43 7378–411

# Chapter 6 Classification and Operating Principles of Nanodevices

### 6.1 Classification

# 6.1.1 Correlations of the Fundamental Properties of Non-regular Materials

The analysis of the principles of nanosensorics, nanomemory and energy nanotransducers is based on the study of various correlations of the fundamental properties of non-regular nanomaterials with the elements of functionalization.

Consider the general scheme of modelling of non-regular materials [1–4] (see Fig. 6.1). The cycle of full-scale self-consistent calculations begins with the specification of the atomic structure  $\left\{\mathbf{R}_i^{(0)}\right\}$  in the form of coordinates that fix the initial configuration. The potentials of the atoms must be known [1–4]. Then the statistical characteristics of the structure in the form of pair correlation functions g(R) or, in more detail, in the form of a number of many-particle correlation functions  $g(1,2), g(1,2,3), g(1,2,3,4), \ldots$  are estimated. The postulated atomic structure is divided into clusters, the electron charge density  $\rho_{\rm cr}$  is calculated, crystalline potentials  $V_{\rm cr}$  are built, and a self-consistent EDOS  $\rho(E)$  calculation is performed in the EMA-CPA framework. Then the total energy  $E_{\rm tot}^{(0)}[\rho(\mathbf{r})]$  is estimated as an electron charge density functional, which is minimized by the positions of atoms  $\{\mathbf{R}_i\}$ , and new positions  $\left\{\mathbf{R}_i^{(1)}\right\}$  of atoms are defined. And again, the cycle of calculations  $g^{(1)}(R) \to \rho^{(1)}(E) \to E_{\rm tot}^{(1)}$  is carried out.

This is the basic meaning of the correlations of the atomic and electronic structure of the material. After that, the total energies  $\left|E_{\rm tot}^{(1)}-E_{\rm tot}^{(0)}\right|=\Delta E$  are compared. It should be noted that in this formulation, the characteristics of the ground state of the system are estimated. If the convergence of the calculation cycle  $g(R) \rightarrow \rho(E) \rightarrow E_{\rm tot}$  is satisfactory with respect to a given value  $\Delta E$ , then it is possible to proceed to the calculations of dynamic characteristics, such as

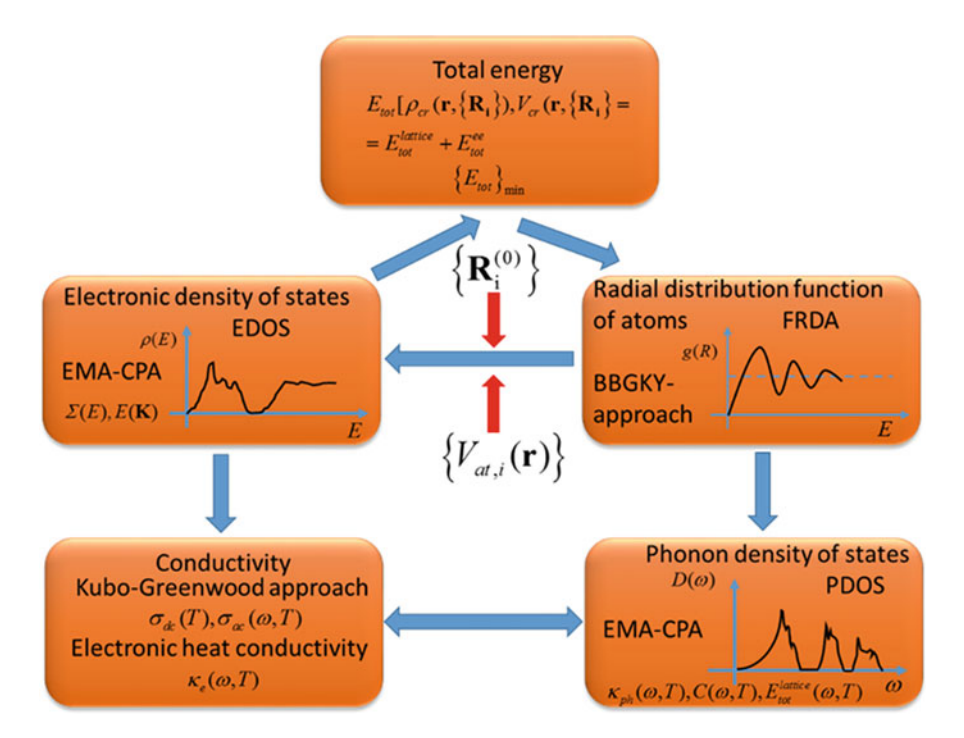


Fig. 6.1 Correlations of the fundamental properties of condensed non-regular materials

conductivity  $\sigma(\omega,T)$ , thermal conductivity  $\kappa(\omega,T)$ , heat capacity  $C(\omega,T)$  and lattice total energy  $E_{\rm tot}^{\rm lattice}(\omega,T)$ , taking into account the temperature factor introduced by means of the Fermi–Dirac and Bose–Einstein distribution functions.

Therefore, further ways of modelling are:

1. 
$$\rho(E) \to \sigma(\omega, T) \to \kappa_e(\omega, T)$$
;  
2.  $\{R_i\} \to g(R) \to D(\omega) \to \kappa^{\text{lattice}}(\omega, T) \to E_{\text{tot}}^{\text{lattice}}(\omega, T) \to C(\omega, T)$ .

We note that in accordance with the adiabatic approximation, the electron and phonon factors are separated. However, it is also necessary to keep in mind the requirement of mixed excitations modelling, for example, the estimation of the electron–phonon thermal conductivity or conductivity factor, which is also reflected in the modelling scheme (see Fig. 6.1). It is also worth mentioning the more subtle practically significant changes in EDOS caused by the magnetic field  $\mathbf{B}$ , which are significant for nanospintronics, namely,  $\rho_{\uparrow\downarrow}(E) \xrightarrow{\mathbf{B}_{\uparrow}} \rho_{\uparrow}(E)$  and  $\rho_{\uparrow\downarrow}(E) \xrightarrow{\mathbf{B}_{\downarrow}} \rho_{\downarrow}(E)$ . This is important for creating nanomemory devices.

However, the greatest practical values for creating nanosensors are correlations  $\rho(E) \to \sigma(\omega,T)$ . This means that EDOS-induced changes in the EDOS  $\rho(E)$  are reflected in the conductivity changes of the nanosensor sensing element. A typical example of a theoretical description of this kind is the Kubo–Greenwood approximation:

6.1 Classification 149

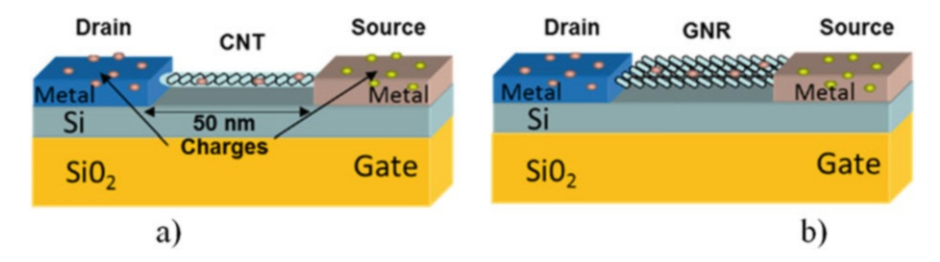


Fig. 6.2 Typical structure of a CNT-based FET (a) and GNR-based FET (b). The unperturbed field-effect transistors based on CNT and GNR are given CNT- or GNR-based FET which is mainly composed of a corresponding semiconducting carbon material suspended over two electrodes

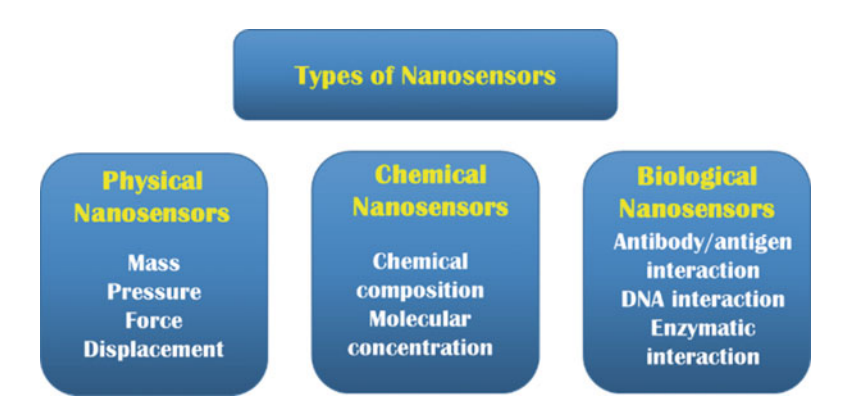


Fig. 6.3 Nanosensors types, which can be realized using FET-type technology

$$\sigma_E(\omega) = rac{2\pi e^2\hbar^2\Omega}{m^2\hbar\omega}\int \left[f(E) - f(E+\hbar\omega)\right] |D_F|^2 
ho(E) 
ho(E+\hbar\omega) dE,$$

where f(E) is the Fermi–Dirac function and  $\rho(E)$  is the EDOS.

Practically, the correlation  $\rho(E) \to \sigma(\omega, T)$  can be realized in FET-type nanodevices [5] (see Fig. 6.2), including sensing elements based on CNTs and GNRs. If it is necessary, CNTs and GNRs are provided with appropriate functional elements [6–10].

There are some important applications of CNT- and GNR-based interfaces with other materials for novel nanosensor devices. Usually, these devices are considered as integrated devices around 10–50 nm in size. The fundamental electron devices are field-effect transistors (FETs), which are very sensitive to various external influences of different nature such as mechanical, chemical, electrical, magnetic, etc. [5].

Variants of nanosensor realizations using FET-type nanodevices are presented in Fig. 6.3.

Source-drain current via gate voltage of typical CNT-based FET and GNR-based FET nanodevices is a monotonally growing function and sensitive on CNT or

GNR electrical properties and morphologies. Electrical properties of CNT and GNR are sensitive to the effects of various external influences, including mechanical, electromagnetic, chemical and biochemical factors, which induce charge transfer changes.

### 6.1.2 Nanosensoring Paradigm

A sensor represents a device or instrument that converts a physical, chemical or biochemical stimulus into a quantity measurable form. The stimulus can be expressed in different ways. A physical phenomenon, presented in the absence of certain material, can perturb some environment, and the mentioned perturbation must be received in 'understandable' form for data acquisition system (DAS).

As a rule, converters of different stimuli are constructed using the generalized scheme shown in Fig. 6.4. A flow of photons or particles must be directed to the sensor (in some cases using certain optics equipment for the flow concentration purposes), and a sensor gives the response understandable for the DAS. The presented chart demonstrates macro- and microconverters.

A nanosensor (NS) represents a device working at the nanoscale space by means of previously described principles. The main task of a nanosensor is to recognize the presence of nanoparticles (nanospheres of nanoscale diameter, the size order of  $10^{-9}$  m) and to create physical stimuli for translating to the macroscopic world (technically, to the data acquisition system).

In general, nanoparticles in the macroscopic world can drive the same surrounding information in comparison with macroactions. However, a miniaturization of devices or sensors increases the functionality and specificity and decreases the operating power. Such significant factors allow expanding the application area in biology: quantitative measurements in intracellular surrounding by negligible physical perturbation of the cell. In addition, the sensitivity of nanosensors can be in higher orders because of the insignificant resistance in electrical circuits.

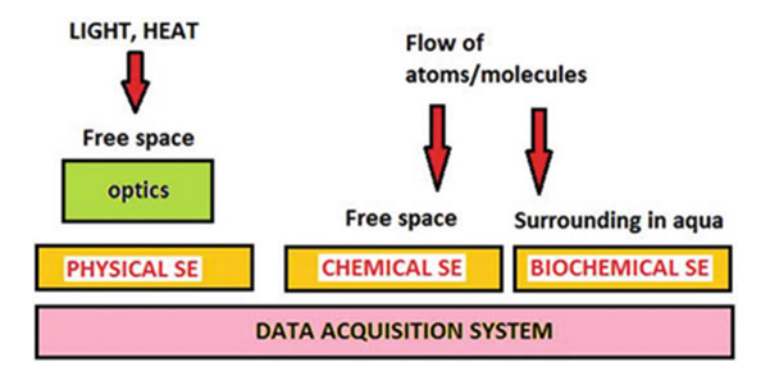


Fig. 6.4 Physical, chemical and biochemical sensors

6.1 Classification 151

An additional term *nanosensory point* is related to the nanosphere recognition. Three phenomena are important for the use of nanosensors: (1) small quantities of a sample could be recognized and analysed; (2) the physical limit of detection should be very low; and (3) in many cases, an intermediate reagent for detection is unnecessary (direct detection is possible). Nanosensors can be integrated into a practical macro device to continuously present the important current information on the chemical or biochemical parameters.

Another aspect of utilizing nanosensors is related to the surface/volume ratio (S/V) phenomena. When the size of a structure (atomic, molecular, macromolecular, cluster, policrystalic, etc.) decreases, the surface/volume ratio increases significantly. Two models – cubic and spherical – are available as the first approach models. For example, Table 6.1 represents the comparison of parameters related to the volume and surface.

Decreasing the cube edge from 3 to 1 (in arbitrary units), the surface/volume ratio increases from 2 to 6. For a spherical particle, the surface/volume ratio increases from 1 to 3 when the sphere radius decreases from 3 to 1. This example illustrates the influence of the nanosensor driving reactivity on the particle size. For practical purposes, a small nanosensor size realizes a fast reaction rate (according to the Arrhenius equation for a chemical reaction) – ensures fast information readout (physical measurement).

According to that, the surface phenomena (physisorption) start to predominate over the chemistry (bonding). In that case, particles display new energetic properties related to the size.

Nanorobots represent a separate class of nanosensors (NS) working in an autonomic regime. Table 6.2 represents a classification of nanosensors according to the recognition type. According to the stimulus recognition process, nanosensors can be divided into two groups: (1) NS with transducing mechanism and (2) NS with recognition mechanism.

In NS with a transducing mechanism, many processes in different areas of physics and chemistry can be involved: electrochemical (potentiometric, amperometric, ion conducting, etc.), optical (absorption, fluorescence, phosphorescence, polarization) and mass detection (acoustic wave). Practically, all sensors with

Cube edge (arbitrary units)	a=3	a=2	a=1
Sides (a)	3	2	1
Surface $(S = 6a^2)$	$6.3^2 = 54$	$6.2^2 = 24$	$6 \cdot 1^2 = 6$
Volume $(V = a^3)$	$3^3 = 27$	$2^3 = 8$	$1^3 = 1$
S/V = 6/a	2	3	6
Sphere radius (arbitrary units)	r=3	r=2	r = 1
Radius (r)	3	2	1
Surface $(S = 4\pi r^2)$	$4\pi \cdot 3^2 = 113.09$	$4\pi \cdot 2^2 = 50.24$	$4\pi \cdot 1^2 = 12.57$
Volume $(V = 1.33\pi r^3)$	$1.33\pi \cdot 3^3 = 113.09$	$1.33\pi \cdot 2^3 = 33.51$	$1.33\pi \cdot 1^3 = 4.19$
S/V = 3/r	1	1.5	3

Table 6.1 Cubic and spherical models of nanoparticle

Physical NS	Chemical NS	Biochemical NS
Displacement (size)	Atoms	Enzymatic interaction
Force (pressure)	Molecules	DNA interaction
Mass	Cations/anions	Tracers
Charge	Species	Antibody/antigen
Optical	Specificity	Cytotoxicity
Thermal	pH	Vitamins
		Cell/tissue

Table 6.2 Classification of nanosensors (NS) according to recognition type

transducing mechanism where mentioned processes are used belong to the group of physical NS.

In NS with a recognition mechanism, several sensitive processes from analytical chemistry (ion vaporization, volatile gases), biochemistry (DNA, enzymatic interaction, antibody/antigen) and macromolecular chemistry (cell/tissue recognition, vitamin recognition, cytotoxicity) are involved. Practically, all sensors with a recognition mechanism where mentioned processes are used belong to the group of chemical and biochemical NS.

Current NS devices are divided into two groups: nanocrystalline NS and nanostructured NS. Nanostructured NS are also divided into two groups: (1) polymerbased, such as pigment-conjugated, drug-conjugated dendrimers, micelles and nanoparticles, and (2) nonpolymer-based such as silica nanoparticles, classical porous silicon, metallic nanoparticles, single-walled and multiwalled carbon nanotubes, nanowires, nanoprobes and quantum dots. To manufacture nanosensors, three different technologies are possible: molecular self-assembly, bottom-up assembly and top-down lithography.

Hierold et al. [11] presented a very complete review of sensors at the nanoscale including device concepts, functional properties and realization type. Written in 2005, this review has not lost its importance nowadays. Nano-electromechanical sensors based on carbon nanotubes (CNTs) are described as multipurpose devices.

Nanosensoring as a paradigm started at the end of the twentieth century with the recent development of micro- and nanotechnologies. Mechanical, optical, fibre optical and nanoelectrode-based nanosensors are known from the 1990s. Fullerenes, nanocrystal and quantum dot-based nanosensors start to pervade from the 2000s. For biological experiments in vivo, new types of nanosensors such as DNA-based nanosensors and nanogap nanoparticles have been introduced purposefully.

# **6.2** Physical Nanosensors

Physical nanosensors aim to recognize a certain motion (kinematical translation or rotation, changes of pressure, wave, etc.) as well as a certain radiation and to generate a specific output signal. A certain motion can be flow based, diffusion

based, walkway based, etc. Electromagnetic radiation (gamma, X-ray, UV, visible, IR) can be recognized according to the standard procedure of interactions between light and material.

Here, a prototype of physical nanosensor will be demonstrated from the initial idea till the molecular realization.

After significant achievements in solid-state physics, molecular electronics started developing in 1970s. The possibility to use low-cost mass production of molecular devices that are suitable for light conversion, catalysis of chemical reactions and drug/medication synthesis stimulated a rapid growth of molecular electronics and utilization of molecular devices.

With the development of lasers operating in near IR region (invisible for human eyes), the problem of creating a light sensor was quite serious. Solid-state crystal-line detectors were manufactured to detect a sufficiently high flux density. An idea to use sensitive sensors for the detection of near IR radiation build-up by a polar molecular compound arises from multitasking experiments in chemical physics. Figure 6.5 represents a prototype of a physical sensor able to make the conversion from near IR to visible. For such a task, a polar molecular compound of the extreme stability with the well-expressed  $\pi$ -conjugated system must be found.

**DMABI.** Figure 6.6 represents N,N-dimethylamine benzylidene indan-1,3-dione (DMABI) as the prototype of a physical sensor. Two polar fragments, namely, indandione and diamino phenyl derivatives, are connected via the [>C = CH-] bridge. The  $\pi$ -conjugated system is displaced along the long molecular axis. According to crystallographic studies [12], the DMABI molecule is practically flat. According to quantum chemical studies [13–15], the DMABI molecule is flat in the ground electronic state and twisted through the mentioned [>C = CH-] junction in the excited electronic state.

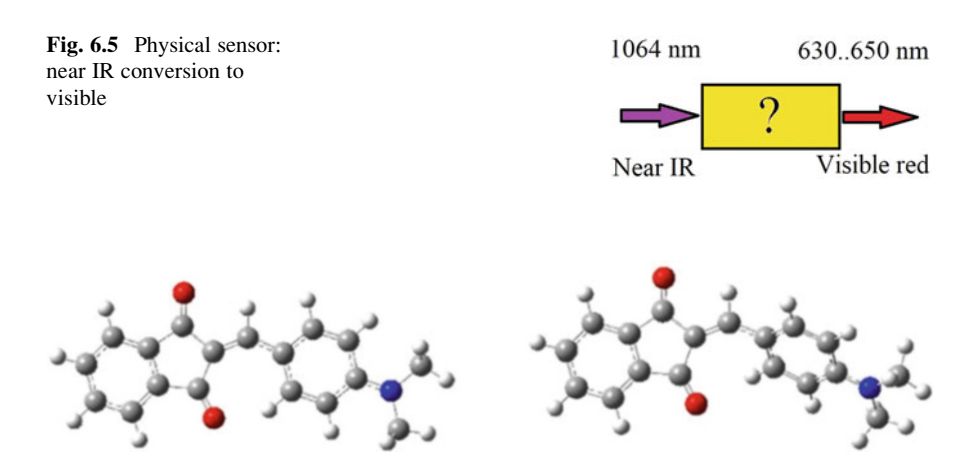


**Fig. 6.6** Prototype of physical sensor: N,N-dimethylamine benzylidene indan-1,3-dione (DMABI). Plane structure (*left* conformation) and twisted by [-C-C-] junction structure (*right* conformation)

As polar molecular compounds, DMABI crystalline derivatives  $(\alpha, \beta, \gamma)$  exhibit the red fluorescence at  $610 \div 680$  nm spectral region by the excitation into molecular absorption band at 488 nm wavelength (typical autolocalized excitons) and also by the excitation at 1064 nm wavelength (anti-Stokes luminescence), with the typical time  $8 \div 15$  ns [16, 17]. A luminescence of DMABI dissolved in different solvents and DMABI deposited as crystalline films as well as Langmuir–Blodget (LB) molecular films differs significantly [18, 19]. Stokes shift for DMABI dissolved in different solvents is equal to  $30 \div 50$  nm.

According to the quantum chemistry simulations (DMABI in flat conformation), an electronic charge redistribution was established for [HOMO]  $\rightarrow$  [LUMO] allowable transition (see Fig. 6.7 – from ground to first excited electronic state) and for [HOMO-1]  $\rightarrow$  [LU-MO + 1] forbidden transition (see Fig. 6.8 – from ground to second excited electronic state). Such two transitions represent the population of two spectroscopic states (first and second). For both transitions, an interfragmental charge redistribution takes place. Pure  $\pi \rightarrow \pi^*$ -type transition is allowed along the long molecular axis in flat conformation. This conformation is typical for crystalline modifications and polycrystalline films (strong ordered derivatives). Otherwise, in twisting conformation, two types of transitions –  $\pi \rightarrow \pi^*$  type and  $n \rightarrow \pi^*$  type – are mixed. A twisted conformation is allowed for LB films and solutions in the excited electronic state (non-ordered derivatives).

The indandione fragment contains two carbonyl [>C = O] fragments, which are the sources of two pairs of n-electron. Also, the benzylidene fragment contains dimethylamino [ $-N(CH_3)_2$ ] group, which is the sources of one pair of n-electron. For the electronic charge redistribution process, when the second excited electronic

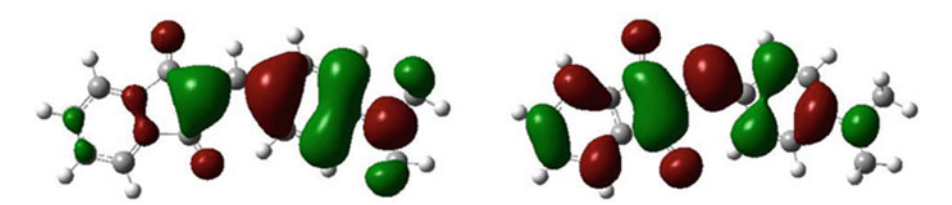


**Fig. 6.7** DMABI: ground and first excited electronic states. Electronic charge redistribution for [HOMO] → [LUMO] transition

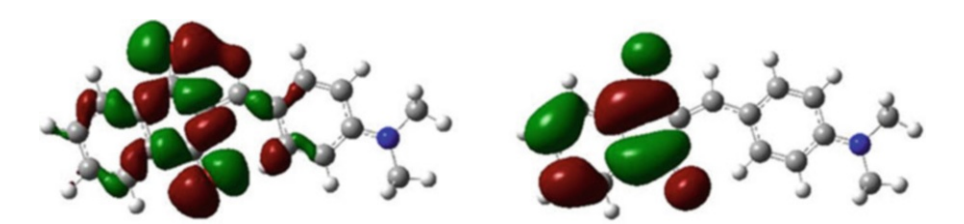
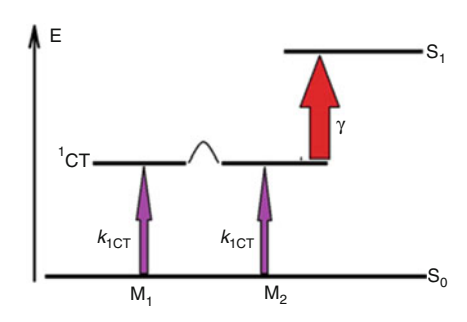


Fig. 6.8 DMABI: ground and second excited electronic states. Electronic charge redistribution for [HOMO-1]  $\rightarrow$  [LUMO + 1] transition

Fig. 6.9 DMABI: energy diagram of CT exciton interaction model



state is populated, a charge redistribution is localized in the indandione fragment  $(n \to \pi^*)$  transition is significant). Unfortunately, a transition of this type is forbidden for flat configuration. For a twisted configuration, a transition of  $n \to \pi$ \* type is partially allowed. In that case, n-electrons of carbonyls from indandione fragments take place in the charge redistribution process.

Generally, for a flat conformation,  $\pi \to \pi^*$  transition is allowed, but  $n \to \pi^*$ transition is forbidden. For a twisted conformation,  $\pi \to \pi^*$  transition is partially allowed, and  $n \to \pi^*$  transition is also partially allowed. A behaviour of two types charge redistribution allows receiving a spectral information related to the surroundings viscosity, polarity, etc.

Anti-Stokes red luminescence of strong ordered (crystalline) derivatives of DMABI shows quadratic dependence on the excitation intensity. At high excitation intensities, quadratic dependence changes to linear one. Figure 6.9 represents the energy diagram of CT exciton interaction model. Excitation of DMABI by IR quantum (1064 nm wavelength) means that population of <sup>1</sup>CT energy level (M<sub>1</sub> and M<sub>2</sub> molecular derivatives) takes place. The mentioned excitation is too low to populate  $S_1$  state.

The suggested bimolecular reaction can be explained as <sup>1</sup>CT singlet-singlet annihilation reaction rate constant  $\gamma$ :

$${}^{1}\mathrm{CT} + {}^{1}\mathrm{CT} \to S_{1}. \tag{6.1}$$

For bimolecular reaction, two kinetic equations are useful to describe the population of <sup>1</sup>CT and S<sub>1</sub> energy levels:

$$\frac{dn_{\text{CT}}}{dt} = I - k_1 n_{\text{CT}} - \gamma n_{\text{CT}}^2,$$

$$\frac{dn_S}{dt} = \gamma n_{\text{CT}}^2 - k_S n_S,$$
(6.2)

$$\frac{dn_S}{dt} = \gamma n_{\rm CT}^2 - k_S n_S,\tag{6.3}$$

where the intensity of IR laser pulse is denoted as I,  $k_1$  represents the linear decay constant of  ${}^{1}$ CT state and  $n_{CT}$  and  $n_{S}$  represent population densities of  ${}^{1}$ CT and  $S_{1}$ states. The solutions of differential equations Eq. (6.2) and Eq. (6.3) are presented below:

$$n_{\rm CT} = \frac{I}{k_1},\tag{6.4}$$

$$n_S = \frac{\gamma I^2}{k_S k_1^2} = \frac{I}{k_S} \frac{\gamma I}{k_1^2}.$$
 (6.5)

Now it is necessary to estimate the intensity. In case of:

$$\frac{\gamma I}{k_1^2} >> 1,\tag{6.6}$$

$$I \gg \frac{k_1^2}{\gamma},\tag{6.7}$$

$$\frac{\gamma I}{k_1^2} << 1,\tag{6.8}$$

$$I << \frac{k_1^2}{\gamma},\tag{6.9}$$

and the expression of population density of S state  $n_S$  according to Eq. (6.4) becomes shorter:

$$n_{\rm CT} = \frac{I}{k_1} \approx \sqrt{\frac{I}{\gamma}}.$$
 (6.10)

Equation (6.10) shows the possibility to switch the quadratic dependence to linear one and in case of:

$$\frac{\gamma I}{k_1^2} = 1, (6.11)$$

$$n_S = \frac{I}{k_S} \frac{\gamma I}{k_1^2} \approx \frac{I}{k_S}.$$
 (6.12)

The value  $\gamma$  was estimated of the order of  $10^{12}$  cm<sup>3</sup>·s<sup>-1</sup>, which is a typical value for excimer–excimer annihilation rate constant in organic molecular crystals.

The origin of  $^1\text{CT}$  state is related to the exciton–phonon interaction. The analysis of vibrational spectra of different DMABI derivatives [17] allows the estimating behaviour of fragmental motion: symmetric stretch [C = O] at 1698 cm<sup>-1</sup>, skeletal scissoring of indandione and benzylidene fragments at 612 cm<sup>-1</sup> and ring stretch deformation of benzylidene at 1663 cm<sup>-1</sup>. The mentioned vibrations are responsible for the occurrence of  $^1\text{CT}$  state, related with the charge separation in fragments. The occurrence of  $^1\text{CT}$  state is related to the charge redistribution during fragmental motion. In the case of symmetric stretch [C = O], the  $n \to \pi^*$ -type charge redistribution in carbonyl fragment takes place. In the case of skeletal scissoring of indandione and benzylidene fragments, the  $\pi \to \pi^*$ -type charge redistribution along the long molecular axis can be observed. The origin of self-trapped excitons was discussed in [19–21]. A detection limit of material can be established in order of 100  $\mu$ m.

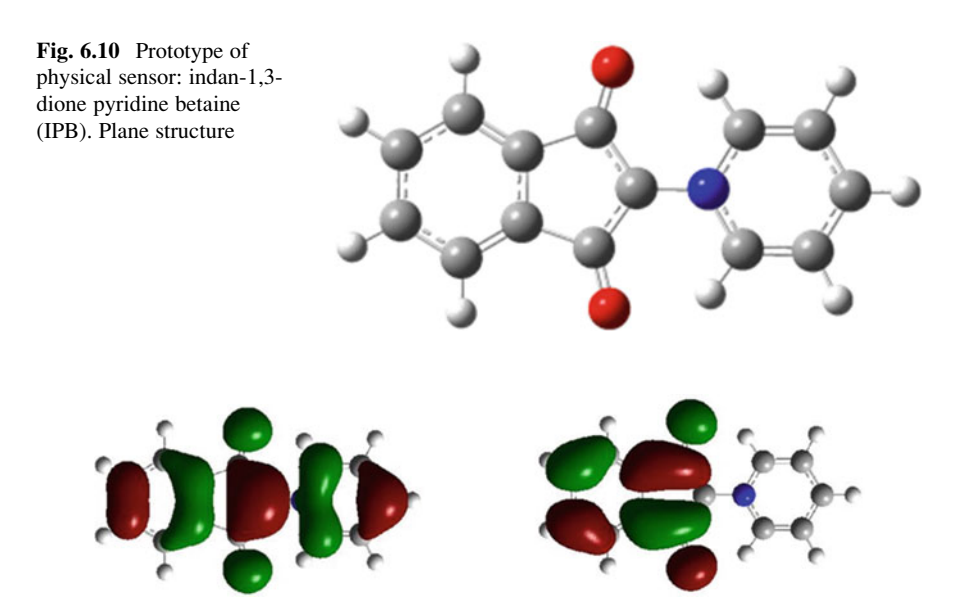


Fig. 6.11 IPB: electronic charge redistribution for [HOMO]  $\rightarrow$  [LUMO + 1] transition, belonging to ground and first excited electronic states, respectively

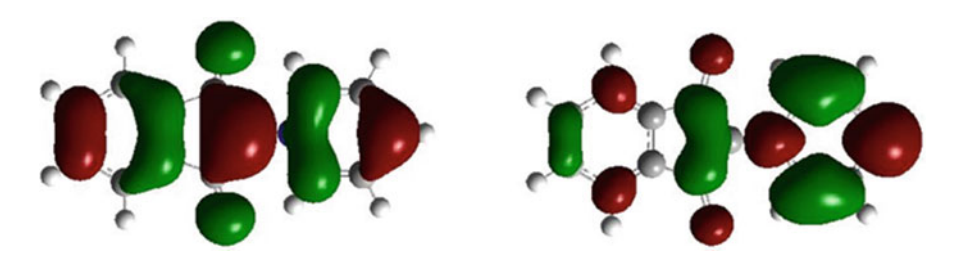


Fig. 6.12 IPB: electronic charge redistribution for [HOMO]  $\rightarrow$  [LUMO] transition, belonging to ground and second excited electronic states, respectively

*IPB*. Another prototype of molecular sensor can be realized using the polar molecular compound indan-1,3-dione pyridine betaine (IPB), presented in Fig. 6.10. IPB consists of two fragments – indan-1,3-dione and pyridine betaine – connected via [>C-N<] bridge. Both fragments are presented in plane surface, and this conformation is typical for ground and excited states.

According to quantum chemistry simulations [22] (IPB in flat conformation), an electronic charge redistribution has been established for [HOMO]  $\rightarrow$  [LUMO + 1] forbidden transition (see Fig. 6.11 – from ground to first excited electronic state) and for [HOMO]  $\rightarrow$  [LUMO] allowable transition (see Fig. 6.12 – from ground to second excited electronic states).

Such two transitions represent the population of two spectroscopic states (the first and second). For both transitions, an interfragmental charge redistribution

takes place. The pure  $\pi \to \pi^*$ -type transition is allowed along the long molecular axis in flat conformation. This conformation is typical for crystalline modifications, polycrystalline films and LB films and solutions. The interfragmental twist is forbidden.

Unique properties of IPB derivatives are related to dipole moment phenomena. Dipole moments of a molecule in the ground state and first excited state are equal to (+3.7) D and (-4.5) D, respectively. After excitation, the direction of the change in the dipole moment is opposite [22]. This circumstance is very important for the surface manipulation purposes, when a fabrication of layers through a self-organizing procedure occurs. Analysing the charge redistribution between the ground and first excited electronic states, it is easy to recognize the important asymmetry: the excited state is populated after the charge redistribution to the local indandione fragment.

As in the case of DMABI, the analysis of vibrational spectra of different IPB derivatives [23] allows estimating a behaviour of the fragmental motion: out of plane skeleton bend 151 cm<sup>-1</sup>, interfragmental stretch 305 cm<sup>-1</sup> and in-plane skeleton bend 146 cm<sup>-1</sup>.

From the chemical point of view, the IPB molecule and molecular derivatives including films, the Langmuir–Blodgett films, and molecular crystals are less stable in comparison with DMABI. The origin of self-trapped excitons has been discussed in [24].

Carbazole: Fluorene Compounds. Carbazole and fluorene compounds play a very important role in molecular electronics due to such circumstances: they are mechanically flexible, chemically stable at room temperature and electronically well  $\pi$ -conjugated. Carbazole as a tricyclic structure consists of nitrogen-containing pentaring and two six-membered benzene rings and belongs to the basic materials for the dye industry. Fluorene as a tricyclic structure consists of one pentaring and two six-membered benzene rings and belongs to a series of precursors in pharmaceutical industry.

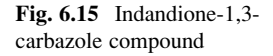
Figure 6.13 represents carbazole and fluorene structures. Molecular substitutes in positions 2 or 3 represent a possibility to drive the velocity of charge redistribution. A population of excited state for 2,7- and 3,6-substituted carbazole derivatives and simulations using quantum chemistry methods shows the overlap of different

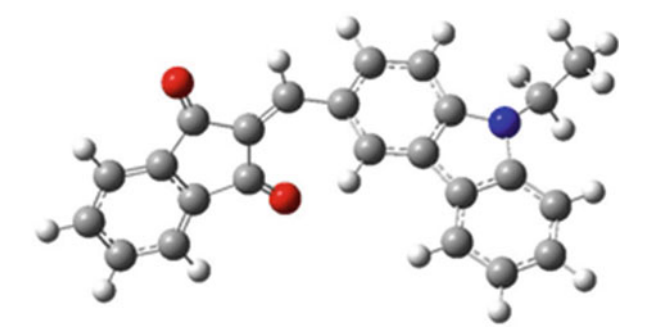


Fig. 6.13 Carbazole and fluorene compounds



Fig. 6.14 Triad formed from carbazoles connected in 2-7 positions





types of wave functions. For 3,6-substituted compounds, a partial charge localization in 3,6-bicarbazole core takes place; otherwise, for 2,7-substituted compounds, charge delocalization along the long axis is realized.

Baronas et al. [25] described the investigations of carbazole, namely, fluorene tetrads created using bicarbazole core with carbazole substitutes in 3–6 positions:

2-(9,9-diethyl-fluoren-2-yl)-6-[7-(9,9-diethylfluoren-2-yl)-9-(2-ethylhexyl)-3,4-dihydrocarbazol-3-yl]-9-(2-ethylhexyl) carbazole. A potential host material exhibits a large hole drift mobility (up to 10–3 cm2 V -1 s -1) in the solution processed amorphous films.

Tomkeviciene et al. [26] studied 2-, 2,7-substituted carbazole dimers and trimers as charge carrier transport materials. Triad of carbazoles with connections in 2–7 positions is presented in Fig. 6.14. 2,7-Di(9-carbazolyl)-9-(2-ethylhexyl) carbazole was found to show very high electron mobility ( $\mu_e = 2*10^{-3}$  cm<sup>2</sup> V<sup>-1</sup> s<sup>-1</sup> at an electric field of  $1.8\cdot10^5$  V cm<sup>-1</sup>) and reasonably high hole mobility ( $\mu_h = 8*10^{-4}$  cm<sup>2</sup> V<sup>-1</sup> s<sup>-1</sup> at an electric field of  $1.8\cdot10^5$  V cm<sup>-1</sup>). Dihedral angle between different carbazoles is equal to  $\approx$ 40°. Pyrene-substituted and naphthalimide-substituted fluorene and carbazole derivatives [27, 28] also express a low-energy barrier for intramolecular twisting in the ground and excited states.

Karpicz et al. [15] investigated indan-1,3-dione and carbazole-based (IDC) compounds with single and four covalently connected chromophores (see Fig. 6.15). An intramolecular charge distribution takes place. Two types of charge

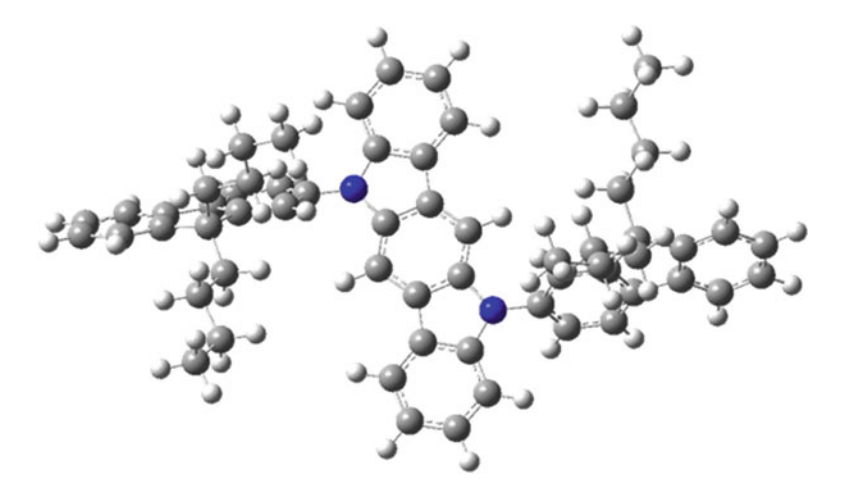


Fig. 6.16 Indolocarbazole derivative NN3

distribution  $(n \to \pi^*)$  and  $\pi \to \pi^*$ ) also are observed. Carbonyl fragments of indandione fragments are sources of *n*-type electrons, and carbazole fragments are acceptors.

Due to the molecule twisting, opening transitions to  $n \to \pi^*$  states, IDC chromophores in solutions express the ultra-fast excited state relaxation (time constant of about 2 ps, in solids and films, and about 300 ps in solid films).

Streckaitė et al. [29] studied the indole [3,2-b] carbazole derivatives. Figure 6.16 represents 5,11-bis(9-butyl-9H-carbazol-3-yl)-6-pentyl-5,11-dihydro-indolo[3,2-b] carbazole – NN3. Conformational motions of the substituents in solutions have been found to cause a significant acceleration of the non-radiative excited state relaxation.

Figure 6.17 represents the maps of electronic charge redistribution related to the transitions  $S_0 \to S_1$  and  $S_0 \to S_2$ . The population of spectroscopic state  $S_1$  is related to the allowed [HOMO]  $\to$  [LUMO] transition, while charge redistribution is localized in indole core.

Otherwise, a population of spectroscopic state  $S_2$  is related to the partially forbidden [HOMO-1]  $\rightarrow$  [LUMO + 1] transition, when a charge redistribution is delocalized from the indole core to carbonyl substitutes. A similar effect is presented for fluorene substitutes. According to this mechanism, substituents influence the radiative relaxation rates.

Figure 6.18 represents the total energy distributions of NN3 on reaction parameter  $\varphi$ , namely, the orientation dihedral angle between indole core and carbazole substitute.

The ground state  $S_0$ , first and second excited states  $S_1$  and  $S_2$  dependence contain minima at different  $\varphi$  value: for  $S_0$ , 75°, and for  $S_1$  and for  $S_2$ , 50°. Transition  $S_0 \to S_1$  is allowed: value of oscillator strength is quite high, about 0.1, but transition  $S_0 \to S_2$  is partially forbidden. It means that the absorption  $S_0 \to S_2$  is

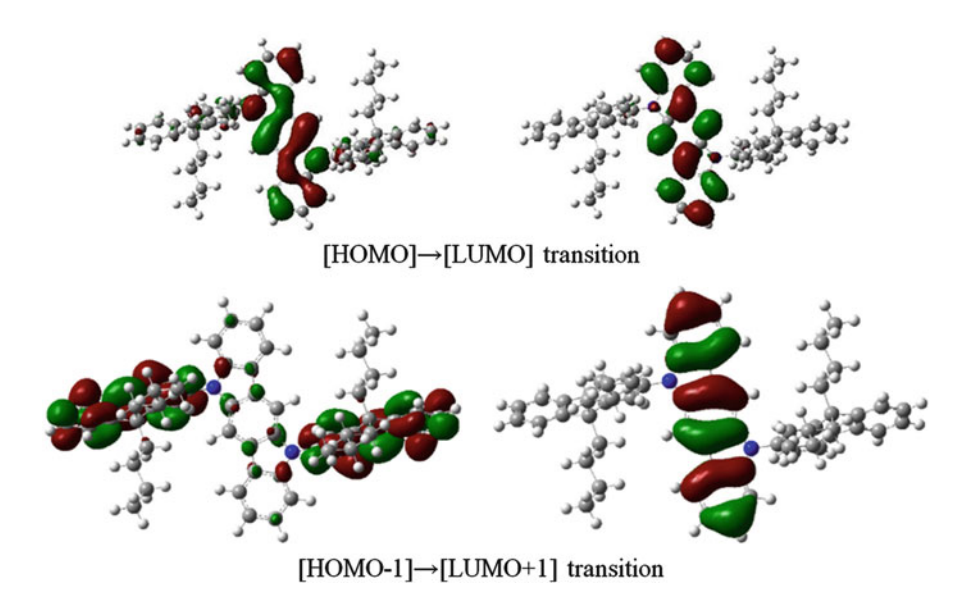


Fig. 6.17 Indolocarbazole derivative NN3. Maps of electronic charge redistribution related to the transitions  $S_0 \to S_1$  (top) and  $S_0 \to S_2$  (bottom)

related to the population of  $S_1$  state using internal conversion processes. The absorption occurs from the twisted configuration ( $\varphi = 75^{\circ}$ ). After excitation, the planarity of the molecule increases ( $\varphi \to 50^{\circ}$ ).

A twist to a more planar conformation may cause an acceleration of the non-radiative relaxation. A twist to the pure planar position ( $\varphi \to 0^{\circ}$ ) is forbidden due to the rotational barrier >0.2 eV. The green rectangle describes an energetically limited twist motion of carbazole-substituted groups in the range of  $45 \div 75^{\circ}$ .

Rimkus et al. [30] investigated spatial carbazole-type structures as a charge transport material. Figure 6.19 represents the structure of 8-alkyl-6,10-disubstituted 8H-16,17-epoxydinaphto[2,3-c:2,3-g] carbazoles (EDNC).

The V-shape geometry (meaning a broke planar structure) through bridging fragments of nitrogen, sulphur and oxygen heteroatom produces the extended  $\pi$ -electron system. Also, an alteration of the molecular structure with conjugated or nonconjugated side groups enables the tuning of ionization potential from 4.7 to 5.5 eV. This ensures hole drift mobility for thick films up to  $8 \cdot 10^{-4}$  cm<sup>2</sup> V<sup>-1</sup> s<sup>-1</sup> at 1 MV cm<sup>-1</sup>.

Physical nanosensors are nanoscale devices, which are able to control masses of small particles, local pressure, force and temperature changes. Usually, schemes of these devices are based on the corresponding electric responses.

**FET-Based Nanosensors.** Physical nanosensors are used to measure magnitudes such as mass, pressure, force or displacement. The working principle is usually based on the fact that the electronic properties of both nanotubes and nanoribbons

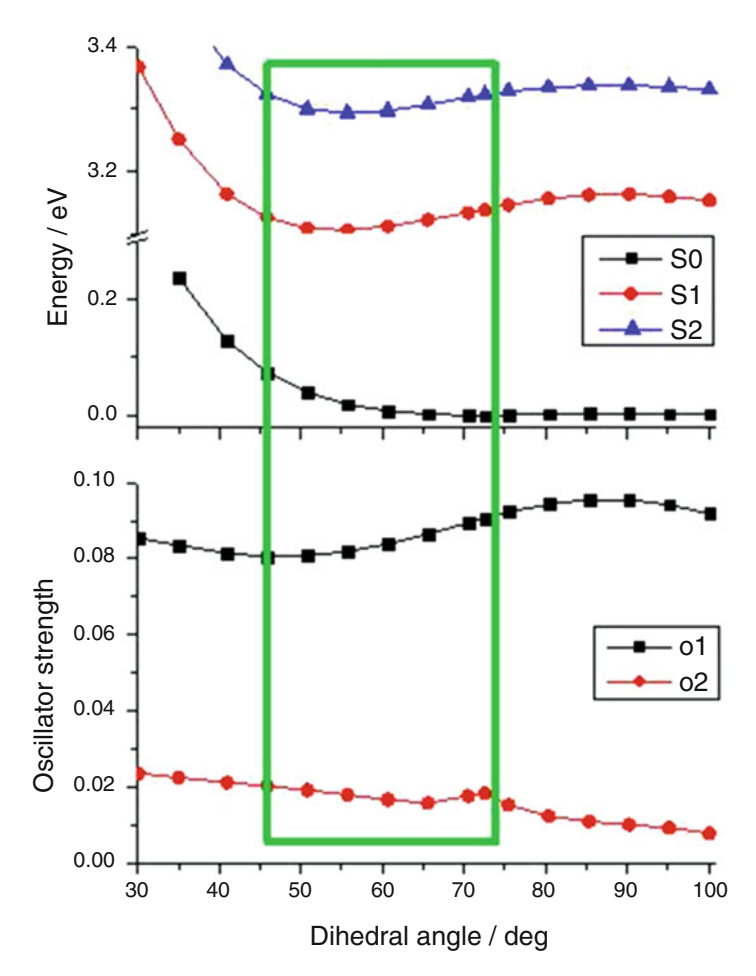


**Fig. 6.18** Diagrams of total energy distributions of indolocarbazole derivative NN3. Ground state  $S_0$  and the first and second excited states  $S_1$  and  $S_2$  dependence on orientation dihedral angle  $\varphi$  between indole core and carbazole substitute (top). The oscillator strength  $O_1$  and  $O_2$  dependence on orientation dihedral angle  $\varphi$  (bottom). Green rectangle describes energetically limited twist motion (in range  $45 \div 75^{\circ}$ )

change when these are bent or deformed. For example, CNTs (or GNRs) can be used to build a field-effect transistor (FET) nano in size, whose on/off threshold depends on the tube dimensions, shape and temperature, among others. A local deformation of the tube/ribbon creates a change in the on/off threshold voltage of the transistor (see Fig. 6.20 and [5]).

Starting from this simple principle, different types of nano-electromechanical systems (NEMSs) have been proposed in the literature with different applications, such as pressure nanosensors [31], force nanosensors [32] or displacement nanosensors [33].

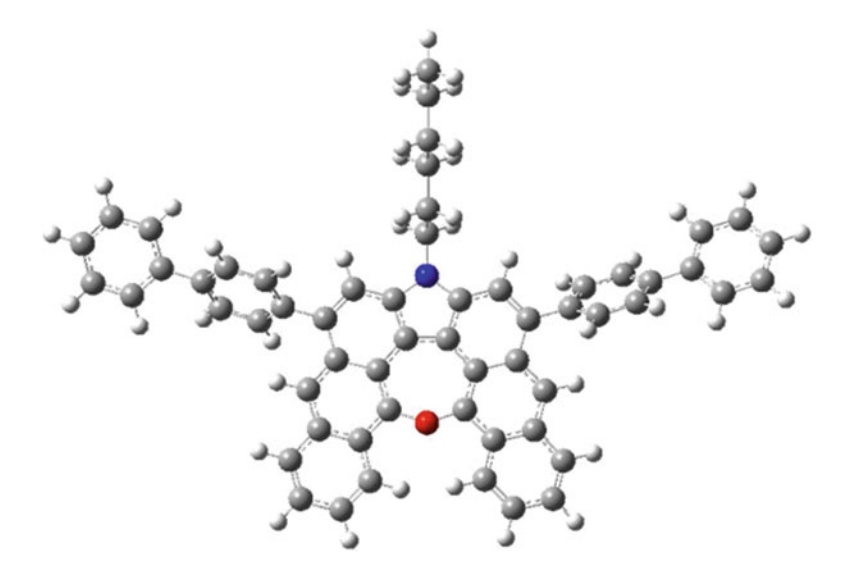


Fig. 6.19 8-alkyl-6,10-disubstituted 8H-16,17-epoxydinaphto[2,3-c:2,3-g] carbazoles (EDNC)

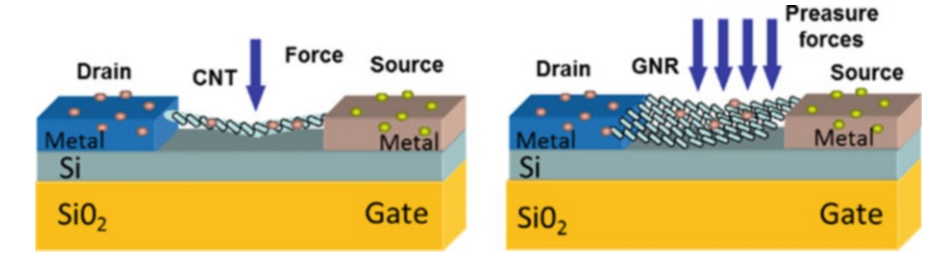
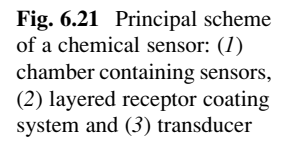


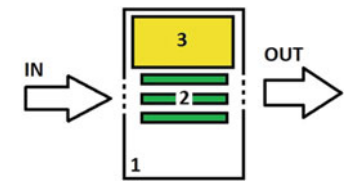
Fig. 6.20 Physical nanosensors: a conducting threshold can be altered when the tube (CNT) or graphene ribbon (GNR) is bent

### **6.3** Chemical Nanosensors

Chemical nanosensors are aimed at recognizing the unknown species of substances, for example, gaseous or liquid. The composition, concentration and presence of certain elements through the partial pressure in the form of chemical information should be generated and converted to a signal of another type (electrical, light, etc.). Different types of gases, including NO, NO<sub>2</sub>, CO, explosive gases H<sub>2</sub>, NH<sub>3</sub>, etc., are objects of recognition in the well-known project – the *electronic nose*.

Figure 6.21 represents a principal scheme of a chemical sensor. Two components (a recognition system as a receptor and an electronic system as a transducer) represent a chemical sensor. Requirements for chemical sensors are the following: (1) direct contact with analytes, (2) transformation of chemical (non-electric) information into electric one and (3) quick response without any delay.





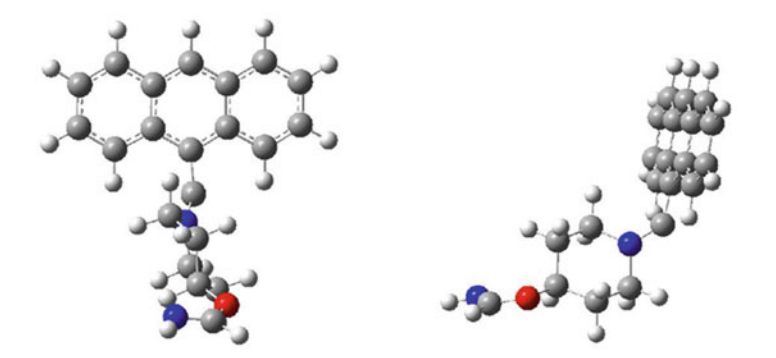


Fig. 6.22 Anthracene derivatives. Two projections

Molecular analytes such as explosive gases or poison gases must be pumped at the certain pressure through a chamber, containing sensor receptors (arrays IN and OUT). A layered receptor coating system must be selected according to the task. A layer of receptor can be manufactured for the selective respond to particular substances (analytes) or also to series of analytes. Metal lattice (Pd, Au, Ni, etc.) as well as polymer surface (poly-epoxy-propyl-X) changes its own properties after a physical contact to analytes. Main interaction processes useful for practical purposes are liquid–liquid extraction, ion exchange and surface adsorption.

Nowadays, transducers operate as amplifiers of an electric signal to a readable one. A response will be made by a transducer as a change of capacitance, conductance, light intensity, etc. Selectivity and sensitivity of the mentioned technique are distinguished on demand.

Sensors based on the photo-induced electron transfer (PET) effect are well known in photochemistry, physiology and medicine. De Silva et al. [34] observed basic principles of PET sensors when luminescence and PET effects are mixed together. A single-point receptor can be connected to a catalytically active peptide. Figure 6.22 represents a derivative constructed as a monoamine which is selective to a presence of protons in bonding distance [34].

The most sensitive materials for detection purposes are single-walled carbon nanotubes (SWCNT). Collins et al. [35] found a low barrier for detection of  $NO_2$  (200 ppm). Chopra et al. [36] investigated selectivity of SWCNT for  $O_2$ , Ar and  $N_2$ , and a low barrier at 100 ppm has been distinguished (ppm parts per million).

6.4 Bio-nanosensors 165

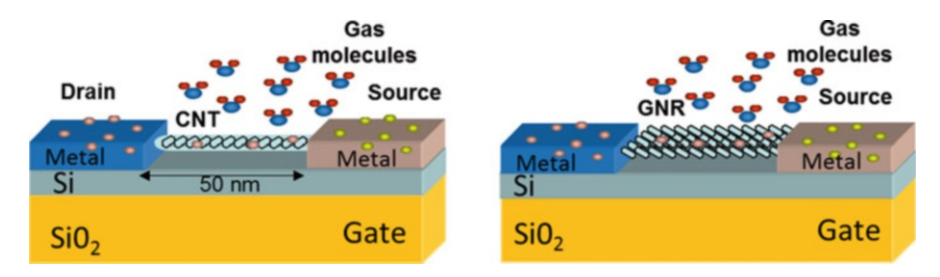


Fig. 6.23 Chemical nanosensors: a conducting threshold can be altered when the amount of free charges on the tube of graphene ribbon surface is increased or decreased by the presence of donor or acceptor molecules of specific gases or composites

Multiwalled carbon nanotubes (MWCNTs) in comparison with SWCNT show a lower barrier due to topological properties. Suehiro et al. [37] reported a detection of ammonia NH<sub>3</sub> of concentrations of 10 ppm.

**FET-Based Nanosensors.** Chemical nanosensors are used to measure magnitudes such as the concentration of a particular gas, the presence of a specific type of molecule or the molecular composition of a substance. The functioning of the most common type of chemical nanosensors is based on the fact that the electronic properties of CNTs and GNRs change when different types of molecules are adsorbed on their top, which locally increases or decreases the number of electrons able to move through the carbon lattice (see Fig. 6.23 and [5]).

Similarly to physical sensors, the presence of a specific type of molecules changes the on/off threshold voltage of the transistor when a nanotube or a nanoribbon is used in a transistor configuration. Various gas sensors based on nanotubes have been reported in the past few years. Modi et al. have developed a miniaturized gas ionization detector based on CNTs [38]. The sensor can be used in gas chromatography. Titania nanotubes have been incorporated in a wireless sensor network to detect hydrogen concentrations in the atmosphere [39]. Kong et al. have developed a chemical sensor based on nanotube molecular wires for the detection of gaseous molecules such as NO<sub>2</sub> and NH<sub>3</sub> in the environment [40].

### 6.4 Bio-nanosensors

Usually biosensors are constructed using three component schema:

**Bioreceptor** 
$$\rightarrow$$
 **transducer**  $\rightarrow$  **detector**. (6.13)

A bioreceptor is an active biological structure (enzyme, NA, cell, etc.) which interacts directly to certain chemical component or virus. If a physical contact occurs, the bioreceptor generates a response signal, which through a transducer excites a detector in order to create the measurable signal (in electric circuit).

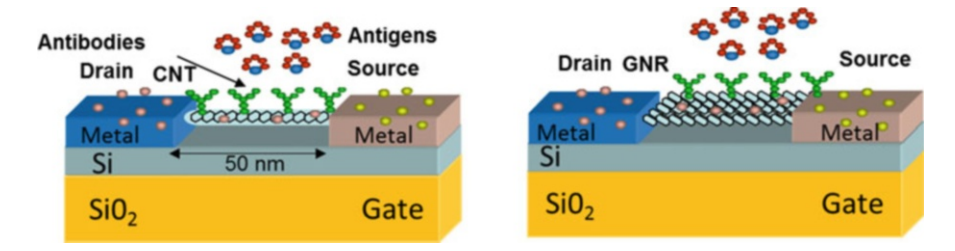


**Fig. 6.24** *Biological nanosensors*: monitoring of biomolecular processes such as antibody/antigen interactions, DNA interactions, enzymatic interactions or cellular communication processes, among others

Biosensors for measuring glucose in blood represent about 90% of global market. Possibility of such detection is organized using glucose dehydrogenase also glucose oxidase [41]. Some enzyme categories are useful for determined functions, for example, ligases, for joining of two molecules; isomerases, for intramolecular rearrangement; and transferases, for intermolecular transfer motion of molecular groups.

Barone et al. [42] reported a usage of single-walled carbon nanotube (SWNT) for beta-D-glucose recognition in strongly absorbing media. Two different mechanisms of signal transduction (fluorescence and charge transfer) have been used. Results demonstrate new opportunities for nanoparticle optical sensors.

Das et al. [43] presented the study of affinity-based biosensors in the framework of scaling laws. Several parameters of physical importance (implications of scaling on the response time, signal-to-noise ratio and dynamic range of biosensor) were analysed using stochastic differential methods and particularly Fokker–Planck equation. Authors claim that scaling down significantly reduces the achievable signal-to-noise ratio and dynamic range of biosensors (miniaturization phenomenon takes place).

**FET-Based Biological Nanosensors.** Biological nanosensors are used to monitor biomolecular processes such as antibody/antigen interactions, DNA interactions, enzymatic interactions or cellular communication processes, among others (Fig. 6.24 and [5]). A biological nanosensor is usually composed of (1) a biological recognition system or bioreceptor, such as an antibody, an enzyme, a protein or a DNA strain, and (2) a transduction mechanism, e.g. an electrochemical detector, an optical transducer or an amperometric, voltaic or magnetic detector [44].

Electrochemical biological sensors work in a similar way as chemical nanosensors, but in this case, the change might be in the electronic properties of a protein, for example, or of any other chemical composite that binds itself to the functionalized nanotube. A specific antigen that binds itself to an antibody stuck to the nanotube. A single-stranded DNA chain binds itself to another DNA chain, which has been attached to the nanotube [45]. There are commercial nanosensors based on this principle. They are able to detect lung cancer, asthma attacks,

different common viruses such as the influenza virus or the parasites responsible for malaria [46].

The second subtype of biological nanosensors is based on the use of noble metal nanoparticles and the excitation using optical waves of surface plasmons, i.e. coherent electron waves at the interfaces between these particles. Simply stated, the resonant frequency of the surface plasmons, resulting from light irradiation, changes when different materials are adsorbed on and in between the particles. This technique, known as localized surface plasmon resonance (LPSR), is the underlying principle behind many biological nanosensors [47].

**Polymer Ion Track-Based Bio-nanosensors** Since 1960s, it has been known that energetic (with tens of MeV or more) heavy (with atomic masses being usually larger than that of Ar) ion irradiation ('swift heavy ions', SHI) introduces very narrow (~ some nm) but long (typically  $10{\text -}100~\mu\text{m}$ ) parallel trails of damage in irradiated polymer foils, the so-called latent ion tracks. The damage shows up primarily by the formation of radiochemical reaction products. Whereas the smaller ones readily escape from the irradiated zone, thus leaving behind themselves nanoscopic voids, the larger ones tend to aggregate towards carbonaceous clusters. Thus, emerging structural disorder along the tracks modifies their electronic behaviour.

In particular, a complicated biochemical kinetics of basic reaction of glucose detection depends on track qualities (e.g. track creation mechanism, foil material properties), enzyme (GOx) distribution on the track surface, geometry of the etched track, etc. All these factors are the subject for the nearest special research. Moreover, the detailed kinetics of reaction is the object of 3D modelling to design the optimal geometry of nanosensor active space. This allows creating optimal nanosensors with the increased efficiency.

The newly created intrinsic free volume enables electrolytes to penetrate into the polymer, thus forming parallel liquid nanowires. In case of tracks penetration through all the foil, the conducting connections emerge between the front and back sides of the foil. The ion track technology is particularly intended to biosensing applications. In this case, the ion tracks are functionalized directly by attaching organic or bioactive compounds (such as enzymes) to their walls [48–51].

# 6.5 Memory Nanodevices

Memory could be defined as an equipment or device for storing a certain amount of information for retrieving purposes. This task physically must be realized by a storing of the system state. A realization of memory can be very different: mechanical, electromagnetic, etc. There are four basic groups of memory devices: resistive, ferroelectric, charge trapping and phase change. Many physical characteristics of a system such as position, capacitance, resistance and inductance can be realized for such purposes. A storing time depends on the material structure as well as of the state overload.

A macro-realization of memory is related to the rapid growth of computer implementation. Random access memory (RAM) in the form of integrated circuits plays the general role for direct access purposes. Dynamic RAM (DRAM) and older static RAM (SRAM) are constructed as the device suitable to store and retrieve the electronic state of several (from six) memory cells built up by *p-n-p* or *n-p-n* transistors (SRAM) or capacitors (DRAM). Charging and discharging of corresponding cell structures create the high-energy state and low-energy state (informational 1 and 0, TRUE and FALSE). Some sort of bistability of any parameter must be allowed for a certain system. Generally, a paradigm of bistability is typical for many dynamic systems, and the simple differential equation can illustrate the phenomena of presence of several energy states:

$$\frac{\partial z}{\partial t} = z(1 - z^2). \tag{6.14}$$

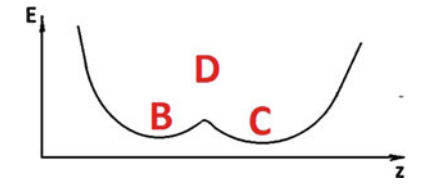
Figure 6.25 represents the illustration of bistability from the physical point of view. The distribution of the potential energy E on the reaction parameter z contains two local minima, B and C, which are separated by the energy barrier D. The solution of the mentioned Eq. (6.14) represents a triplet of states: z = 1, z = -1 (two minima, B and C, stable states) and z = 0 (local maximum, D, unstable state). The bistability must be realized via the macro-approach (macro-circuit) or via the micro-approach (atomic, molecular system).

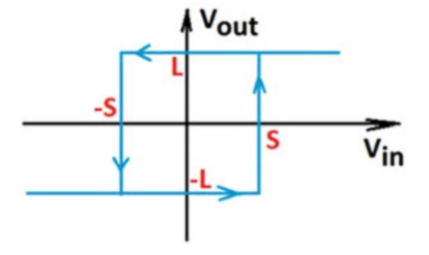
For example, the Schmitt trigger as a typical model of comparator circuit in macroelectronics is used as a model system. Figure 6.26 represents the energy diagram as the output voltage  $V_{\rm out}$  via the input voltage  $V_{\rm in}$ .

The output voltage levels L and -L represent the states for information storing (informational 1 and 0, TRUE and FALSE); the switching between states must be realized by manipulating input voltage levels S and -S. It means that Schmitt

**Fig. 6.25** Bistable system: distribution of potential energy *E* on reaction parameter *z*. Two local minima, B and C, are separated by energy barrier D

Fig. 6.26 Schmitt trigger: output voltage  $V_{\rm out}$  dependence on input voltage  $V_{\rm in}$ . S and L represent the voltage levels of input (switching) and output, respectively





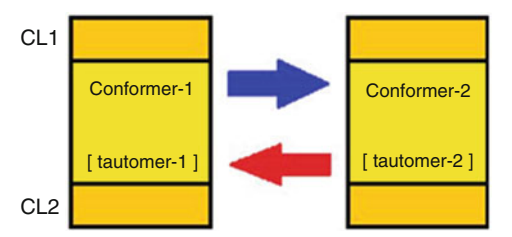


**Fig. 6.27** Sandwich-type structure includes two conducting layers (CL1 and CL2) and bistable molecular structure (two conformers or two tautomers). Switching between two states occurs after external perturbation

trigger converts an analogy input signal (range from -S and less until +S and more) to a digital one - only L and -L values without intermediates. A transfer function with a positive feedback is realized as hysteresis. It is necessary to point out that the metastable state (see Fig. 6.19, D) is not suitable for the storage realization.

Figure 6.27 represents a practical composition of sandwich-type structure, which includes two conducting layers (CL1 and CL2) and active material (solution or Langmuir–Blodget film) consisting of bistable molecular structure (two conformers or two tautomers). A switching between two states occurs after an external perturbation of tautomers. Two tautomers when the proton transfer occurs from carbonyl the amino fragment represent one of simplest bistable systems (see Fig. 6.27). Limitations of memory in macro-realization are the following: (1) in crystalline structures, significant fluctuations of excited state relaxation time take place; (2) during operating period, significant thermal gradients occur; and (3) applications in micro- and nanosized structures (e.g. in cell biology, etc.) are not possible.

**Molecular-Based Nanodevices.** Bistability in a molecular system or a single molecule can be realized in a very simple way: by exciting the system from ground to the lowest excited state. In case, when the molecule contains the well-organized  $\pi$ -electronic system, the excitation energy is order of several eV. In the case of  $\sigma$  transition, this energy arises up to  $\sim (5 \div 10)$  eV, and problems with the molecular stability occur. A decomposition of molecule into molecular fragments destroys the device. Also, the lowest excited state can be populated for several ns or ps only, and after that a molecule returns to the ground state. A switching of molecular behaviour (e.g. the creation of two tautomers through a proton transition, creation of two conformers by rotating two molecular fragments, etc.) realizes the idea of bistability in the ground electronic state. Two states (informational 1 and 0, TRUE and FALSE) can be realized for such a type of bistable molecule as, for example, low- and high-conductance states, respectively. A reason for reswitch could be induced by a laser pulse, by heating, by the occurrence of a redox reaction, by a mechanical deformation of a polymer, etc.

Franckevicius et al. [52] described the advanced research of the promesogenic unit containing the salicylidenimine chromophore groups. Figure 6.28 represents



Fig. 6.28 Proton transfer motion in carbonyl-amine system

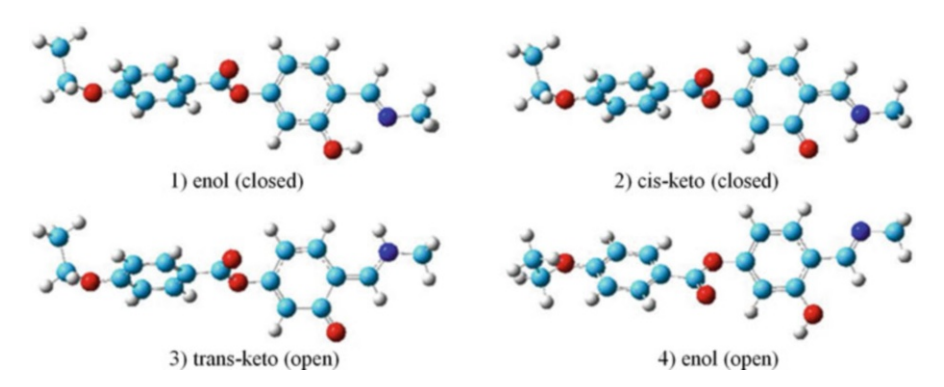


Fig. 6.29 Four tautomeric forms of 4-(4'-ethoxybenzoyloxy)salicylaldehyde chromophores

four tautomeric forms of 4-(4'-ethoxybenzoyloxy)salicylaldehyde chromophores which are the parts of PPI dendrimer chains.

Two forms – enol (1,4) and cis-keto (2,3) – can be formed by rotation about the phenyl long axis. Closed (1,2) and open (3,4) structures could be formed due to proton motion (related to oxygen or nitrogen). The closed form represents the more stable structure (of lowest total energy) due to hydrogen bonding (in enol (closed) structure [>C=O.H-N<] and cis-keto (closed) structure [>C=O..H-N<]) (see Fig. 6.29).

Such two circumstances predetermine the usage of the two most prominent structures: second, cis-keto (closed) and third, cis-keto (open). Figure 6.30 represents the charts of charge redistribution corresponding to  $S_0 \rightarrow S_1$  electronic transition from ground to excited electronic state. For the second cis-keto (closed) and third cis-keto (open) forms, the charge redistribution is delocalized along all molecules. Both fragments are included in the mixed but not pure CT process of  $\pi \rightarrow \pi^*$  and  $n \rightarrow \pi^*$  type. A twist of the fragment containing the nitrogen atom along the long axis is related to the creation of a new semi-ring (for cis-keto (closed)) and charge acceptor (electron donor) properties of the molecular fragment increases.

From the chemical point of view, the whole tautomeric structure must be stable and not reversible. In order to estimate a reversibility of structures, quantum chemical simulations have been carried out. Figure 6.31 represents the potential energy diagram (the ground state  $S_0$  and first excited state  $S_1$  energy dependence on reaction coordinate – the dihedral twisting angle  $\varphi$ ), which determines tautomeric structure. The rotation of phenyl substitutes along the long axis realizes occurrence of two tautomeric forms: second form cis-keto (closed),  $\varphi = 180^{\circ}$  and  $\varphi = -180^{\circ}$ ,

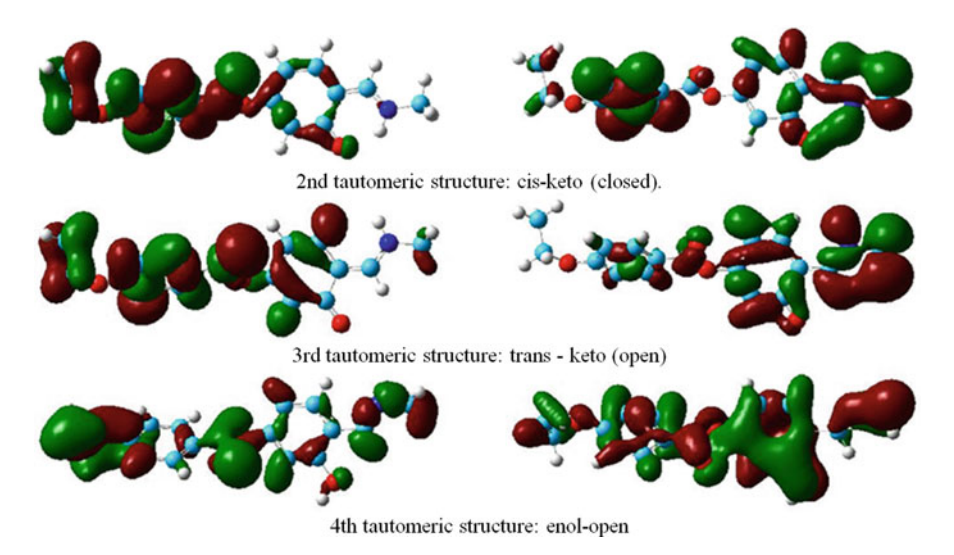
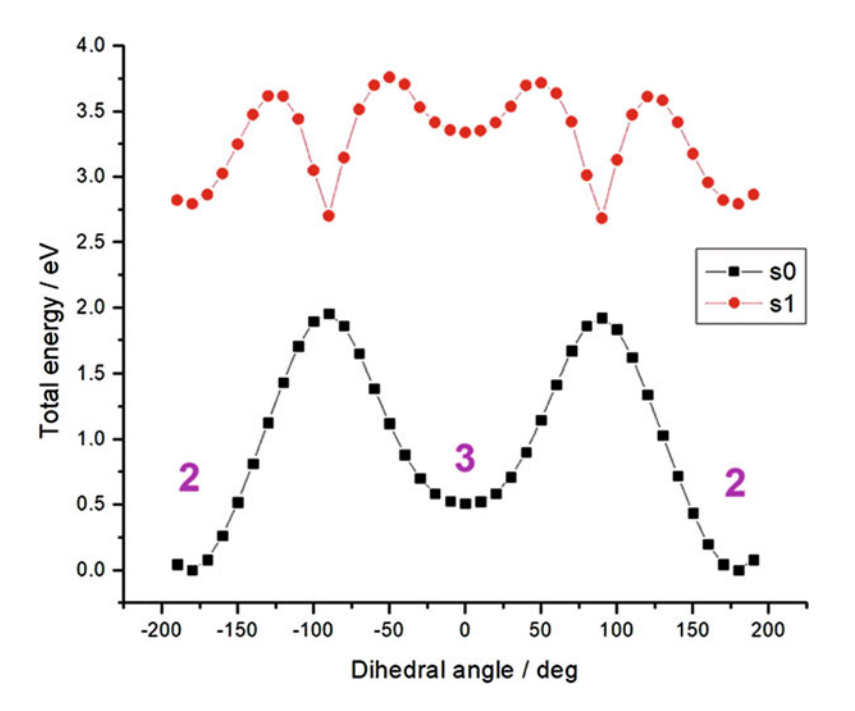


Fig. 6.30 Most important tautomeric structures: second, third and fourth. Charge redistribution corresponding to  $S_0 \rightarrow S_1$  electronic transition: from ground state (left) to excited state (right)



**Fig. 6.31** Potential energy diagram. Ground state  $S_0$  and first excited state  $S_1$  energy dependence on dihedral twisting angle which determines tautomeric structure: second form cis-keto (closed) or third form trans-keto (open)

or third form trans-keto (open),  $\varphi=0^\circ$ . The difference between ground state energies of such forms is equal >0.5 eV. The rotation barrier contains 2.0 eV, in comparison to kT factor for room temperature objects, which is equal to 0.03 eV. This means that both configurations – second form cis-keto (closed) and third form trans-keto (open) – can exist quite a long time in the ground state, and the transition from second to third can be made through the excited state only. A twist of molecular fragment occurs in the excited state only.

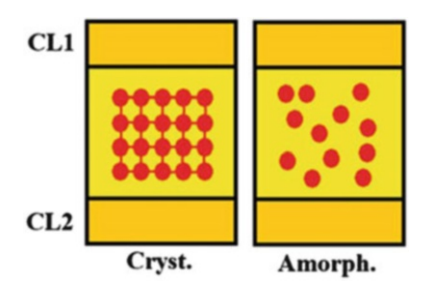
After excitation, the first excited state is populated after finishing internal conversion processes. A curve form of the ground state dependency and excited state dependency differs significantly. The presence of the minimum of the excited state dependency at  $\varphi=90\,^\circ$  realizes a possibility of relaxation to the ground state in a twisted configuration while the twisting continues until  $\varphi=0^\circ$ .

The presented model is presumptive and can be used by choosing materials of demand properties.

Kim et al. [53] demonstrated the non-volatile memory cell element as the transistor, namely, the resistor hybrid-type device consisting of a silicon transistor and a resistive polymer memory. Organic memory has been constructed using poly[(9,9-bis((60-(N,N,N-trimethylammonium)hexyl)polyfluorene-derivative 2,7-fluorene)-alt-(9,9-bis(2-(2methoxyethoxy) ethyl)-fluorene)] (WPFoxy-F). Actually, the authors claimed that the construction of difluorene derivative exhibits non-volatile memory properties. Zhao et al. [54] presented the active layer application built up by poly(9-vinylcarbazole) (PVK) with zinc oxide (ZnO). Cho et al. [55] presented the originally constructed organic-based device dioxide nanoparticles (TiO<sub>2</sub> NPs) embedded using titanium (9-vinylcarbazole) (PVK) film. The presented structure exhibits the bistable resistance states and unipolar non-volatile memory effect. Kim et al. [56] described the reversible switching performance of metal-organic-semiconductor (MOS) memory devices containing a polyfluorene-derivative single-layer film.

**Phase Change Nanodevices.** Phase change nanodevices are based on the idea to use phase change (PC) switching between stable material states, e.g. conduction states for the electrical memory, or a large difference of the refractive index for optical memory. A sandwich-type structure can be composed from two conducting layers (CL1 and CL2) and PC material inside (see Fig. 6.32). Crystalline and amorphous states of material can be received after an internal perturbation

Fig. 6.32 Sandwich-type structure includes two conducting layers (CL1 and CL2) and phase transition material



(e.g. current pulse or laser pulse). A phase transition from the crystalline to amorphous state is related to the significant increase of the resistance, a refraction index, etc. Restoration of the crystalline order can be made by another type of pulse (refers to the properties of the material). Laser pulse duration, pulse energy and pulse polarization can be titled as driving factors for advanced phase transitions (from ordered to non-ordered and back).

Warren et al. [57] described Ge<sub>2</sub>Sb<sub>2</sub>Te<sub>5</sub> (GST)-based phase change PC memory. Figure 6.33 represents phase transitions and the related state diagrams.

A crystalline state is stable with the temperature increasing from  $T_1$  to  $T_3$ . A volume of amount changes negligible (crystal heating process). After receiving the melting point at  $T_3$ , the volume increases drastically from  $V_3$  to  $V_4$  (melting process occurs). After some time, a disordered state forms from a crystalline state. During the starting fast cooling process (4–5–6), a volume decreases, but not drastically, and a stable amorphous state forms at the temperature  $T_6$ . Set operation (amorphous to crystalline) represents the phase change  $6 \rightarrow 1$  – the heating to  $500\,^{\circ}\text{C}$  – and the reset operation (crystalline to amorphous) represents the phase change  $1 \rightarrow 2 \rightarrow 3 \rightarrow 4 \rightarrow 5 \rightarrow 6$  – the heating to  $600\,^{\circ}\text{C}$  and fast cooling. Table 6.3 represents the scheme of memory state manipulation.

Nano-electromechanical (NEM) Switching Devices. A switch is an electrical equipment for manipulating of the electrical circuit. An interruption of current can be realized in several ways: significant increasing of conductivity or breaking the circuit. A mechanical degree of freedom (one, two, etc.) must be presented for a selecting mechanism of macroscale. Two-state logic schema can be realized by a spatial configuration of vibrating, rotating or generally moving objects (in micro- or macroscale).

**Fig. 6.33** Phase transitions and the related state diagrams. 1-2-3, crystal state;  $T_3$ , melting point; 3-4, melting process; 4-5, disordered state; 4-5-6, fast cooling; 6, stable amorphous state

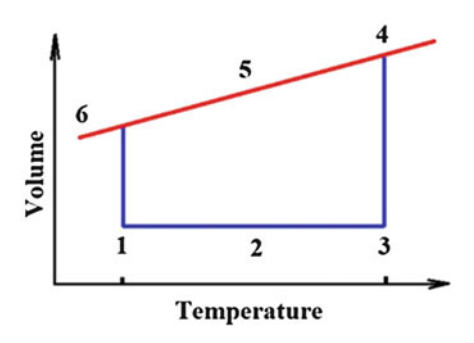


**Table 6.3** The scheme of memory state manipulation. Adapted according to [57]

Operation		Reset		Set	
Memory state	1	$\rightarrow$	0	$\rightarrow$	1
Phase	Crystalline	$\rightarrow$	Amorphous	$\rightarrow$	Crystalline
Temperature, °C		600		500	

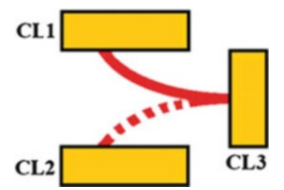


**Fig. 6.34** Nano-electromechanical (NEM) switch. Sandwich-type structure includes two conducting layers (CL1 and CL2) and polymer chain (red). Applying the potential to conducting layer CL3, polymer chain changes mechanical position from CL1 to CL2. Reversible process is allowed by the absence of the potential to CL3

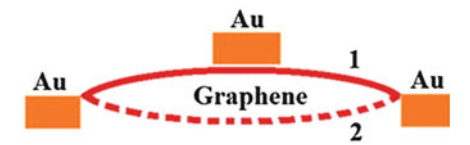


**Fig. 6.35** NEM switch realized as double-clamped graphene beam. Conducting layers are built up by Au. Graphene bend (first or second position) is related to a potential

A nano-electromechanical (NEM) switch can be realized using a nanoscale equipment when the switch motion could be applied by programming electrical signal. A low voltage operation is possible in the region of 1 V. For a special equipment, a low-temperature processing is possible. For one of the best examples in nanoelectronics, information reading and erasing times can be distinguished in the range of <6 ns.

Figure 6.34 represents the principal scheme of nano-electromechanical (NEM) switch. A polymer chain is placed in the space with a possibility at different conditions to touch conducting layers CL1 and CL2. Applying the potential to the conducting layer CL3, a polymer chain changes a mechanical position from CL1 to CL2. A reversible process is allowed by absence of potential to CL3.

Peschot et al. [58] analysed a chip functionality from the energy point of view. NEM relays are promising candidates for low-power applications due to very low switching voltages. Hwang et al. [59] analysed NEM switching device based on carbon nanotube (CNT) and Cu electrode. The energy dependences on *In–Out* processes showed the hysteresis loop that has been induced by the adhesion of the CNT on the Cu (interatomic interaction).

Wang et al. [60] studied graphene—metal static contacts by fabricating the transmission line model (TLM) pattern on a graphene nanoribbon (GNR) and dynamic contacts by GNR nano-electromechanical (GNEM) switches. They checked that all the dynamic contacts in GNEM switches show clear pull-in operations, which are not reversible.

Kulothungan et al. [61] reported the NEM switch as a double-clamped graphene band (see Fig. 6.35). The authors showed the possibility of achieving a pull-in voltage as low as 2 V. The presence or absence of the potential is related to a graphene bend (first or second position).

**Flash Memory Nanodevices.** Flash memory can be designed using two approaches: charge transfer material (organized at the sub-macro level) or using the circuits containing field-effect transistors. Firstly, the sandwich-type structure can be composed of two conducting layers (CL1 and CL2) and a material containing silicon nitride inside (see Fig. 6.36).

Polysilicon–oxide–nitride–oxide–silicon (SONOS) and titanium–aluminium–nitride–oxide–silicon (TANOS) are medium for the charge transfer (CT) realization, which can be performed using an insulating layer (operating potential from the conducting layer CL2).

Kim et al. [62] investigated polyfluorene-derivative polymer as the hole device. The device showed excellent resistive switching behaviours such as device-to-device switching uniformity and good retention times.

Secondly, the field-effect transistors using single-walled carbon nanotubes are known from the pioneering Tans publication [63, 64]. Martel et al. [65] reported the fabrication of field-effect transistors, as the multiwalled carbon nanotube device. Holes are dominated in the charge transport motion through the nanotubes.

Nanodevices of Memristor Type. Memristor or memory resistor represents a nonlinear electronic device. A resistance of memristor depends on history of current. Generally, a resistance depends on the amount of charge, which passes through it. When the voltage is turned off, the memristor must remember its state (as most recent resistance) until voltage is turned on again. The practical realization of memristor can be performed as follows. The sandwich-type structure is created in this case from two conducting layers (CL1 and CL2) and a layer of resistive oxide (see Fig. 6.37).

Fig. 6.36 Flash memory nanodevice: two conducting layers (CL1 and CL2) and silicon nitride inside

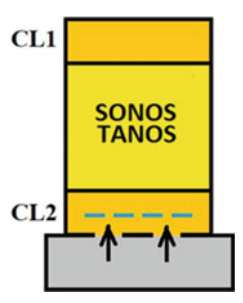


**Fig. 6.37** Memristor-type nanodevice: two conducting layers (CL1 and CL2) and resistive oxide inside

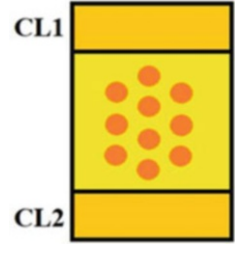
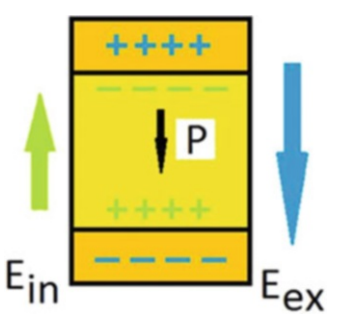


Fig. 6.38 Ferroelectric memristor: two conducting layers (CL1 and CL2) and ferroelectric material inside



The external voltage pulse drives the electronic state of device. FALSE state (0) corresponds to a high resistance state, TRUE state (1) – to a low resistance state. One of the oldest reports about  $\text{TiO}_2$  phenomena was published by Argal [66]. Thin films of anodized  $\text{TiO}_2$  can be made to switch between three distinct conductivity states.

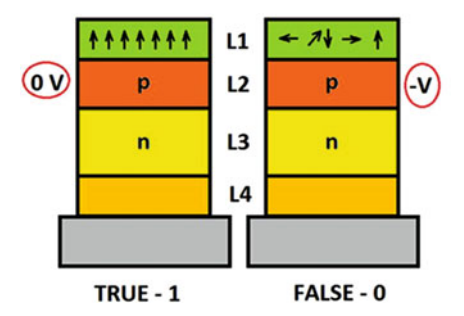
Alibart et al. [67] reported a novel device called firstly as nanoparticle organic memory field effect transistor (NOMFET). A device has been composed from organics and nanoparticle to exhibit the memristor properties. Additionally, a behaviour of a biological spiking synapse appears. Secondly, a name was expanded to a synapstor (synapse transistor).

**Ferroelectric Nanodevices.** This type of nanodevices belongs to a class of memristors, when a bistable ferroelectric material is used. Due to difficulties to perturb ferromagnetic material by an external source and to keep a material in the same crystalline phase (any phase transition of first or second type must occur!), polarization phenomena could be used. Figure 6.38 represents ferroelectric memristor: two conducting layers (CL1 and CL2) and ferroelectric material inside. A memory manipulation can be provided by applying a positive or negative voltage which switches the positive polarization states to negative (computational states FALSE '0' to TRUE '1'). A reversible action is allowed. Chanthbouala et al. [68] describe the practical implementation of the device with a speed 10 of *ns*.

**Spintronic Nanodevices.** Spintronic (or spin transport electronics) devices are driven by the processes of intrinsic electron spin and associated magnetic moment. A class of magnetic semiconductors represents a significant part of the spintronic system. Practical applications of a spintronic system are presented in Fig. 6.39.

Gallium manganese nitride magnetic layer (L1) is intended for spin manipulating purposes. A traditional pn junction (L2, L3 layers) is placed on a gallium nitride substrate (L4). A closed electric circuit must be organized through the pn junction. With the negative voltage, the concentration of holes in the p layer significantly decreases, and spins of manganese atoms (from L1 layer) become disoriented. The creation of state '0' is finished. With a zero voltage, the concentration of holes in the p layer significantly increases, and spins of manganese atoms become aligned due to the interaction of holes and manganese atoms. The creation of state '1' is finished.

Fig. 6.39 Spintronic system. L1, gallium manganese nitride magnetic layer; L2 and L3, pn junction; L4, gallium nitride substrate



#### 6.6 Biomolecular Rotary Machines

All biological systems represent various embodiments of molecular machines. Richard Feynman pointed out in his pioneering work [69] the idea about the biological cells organization through self-replication structures at the nanoscale.

All biological complexes as machines transduce the energy from one form to another (generally, from chemical to mechanical). A metabolic breakdown of glucose through the phosphorylation reaction can be treated as the main source of energy in cells. All organisms use the reaction of adenosine triphosphate ATP $^{4-}$  hydrolysis to ADP to drive the metabolic breakdown of glucose  $\mbox{\sc G}^{\circ}=-30.5$  kJ mol $^{-1}$ .

$$ATP^{4-} + H_2O \rightarrow ADP^{3-} + HPO_4{}^{2-} + H^+. \eqno(6.15)$$

Many molecular motors can be divided into several groups according to their biological importance.

- 1. *Nucleic acid motors*. DNA polymerase for the single-stranded DNA converting to the double-stranded DNA. RNA polymerase for transcription of RNA from the template.
- 2. *Rotary motors (proteins)*. They convert the chemical energy from ATP to the electrochemical potential energy of a proton gradient across a membrane.
- 3. Cytoskeletal motors. Myosin responsible for the muscle contraction.
- 4. Synthetic molecular motors.

Vicario et al. [70] reported the light-driven unidirectional molecular motor, where a fluorene core is connected through an alkene double bond [>C = C<] to helicene (pentaring substituted) (see Fig. 6.40). This system is titled as one of the fastest systems; rotation motion is realized by thermal helix inversion, when half-life of process is 0.005 s.

Katoono et al. [71] reported the propeller-shaped dynamic helicity, which was realized in a hexakis (phenylethynyl) benzene framework (see Fig. 6.41).

**Fig. 6.40** Synthetic molecular motor built up using fluorene core

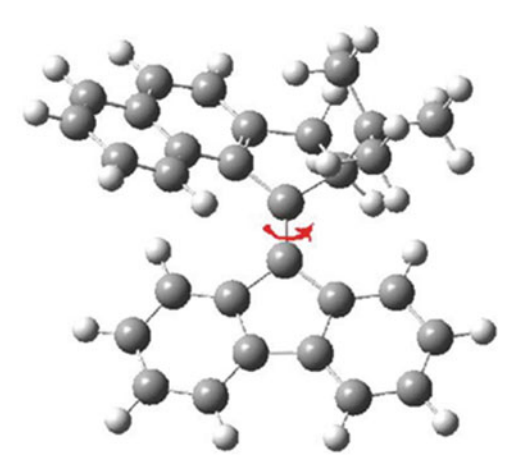
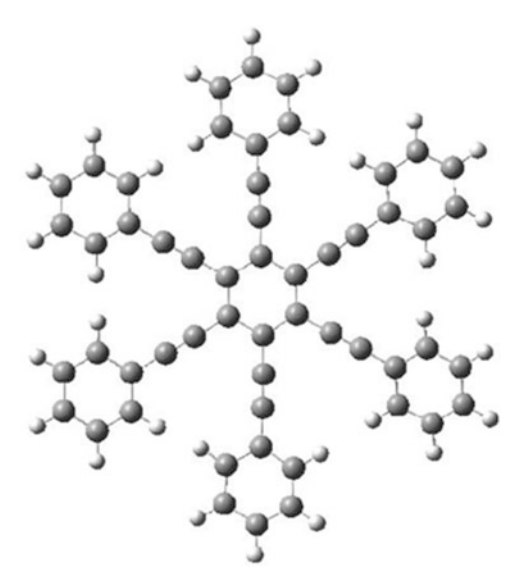


**Fig. 6.41** Hexa-derivative of benzene



#### 6.7 Nanotransducers

A nanotransducer is a device that converts one form of energy into another in the nanoscale range. Note that human sense facilities include the corresponding nanotransducers which convert external influences into neuron (bioelectric and biochemical) signals. Nanotransducers are the necessary parts of nanosensor systems (see Fig. 6.42).

A neuron network communication with the different human brain parts is presented in Fig. 6.43. Using the human brain researches, we can develop various applications for the human body enhancement and prosthetics. Outline the main *goals of human enhancement:* 

6.7 Nanotransducers 179

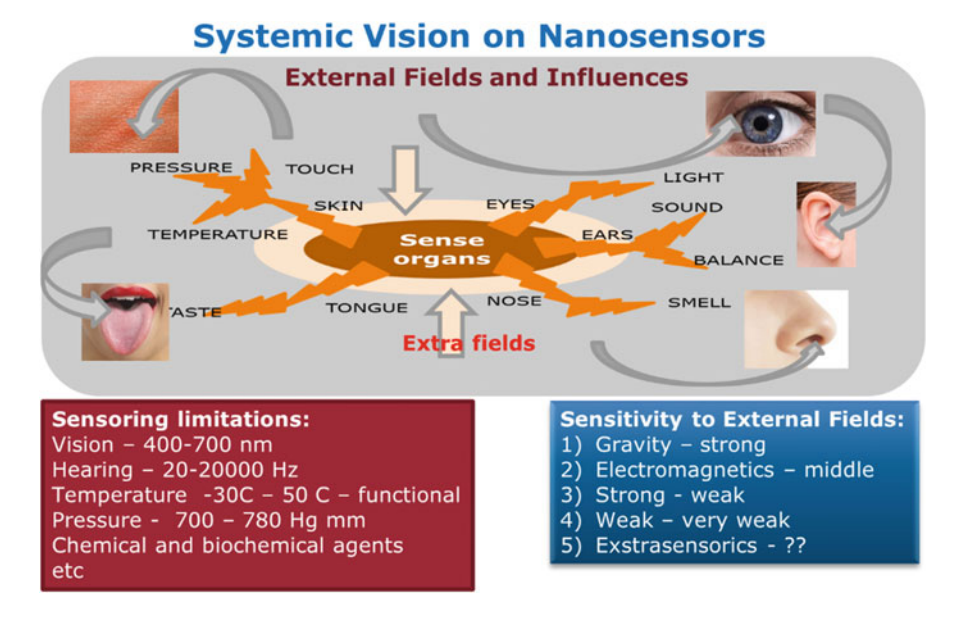


Fig. 6.42 Description of typical external influences on the human body in connection with the human sensing abilities and limitations

## **Neuron network communications**

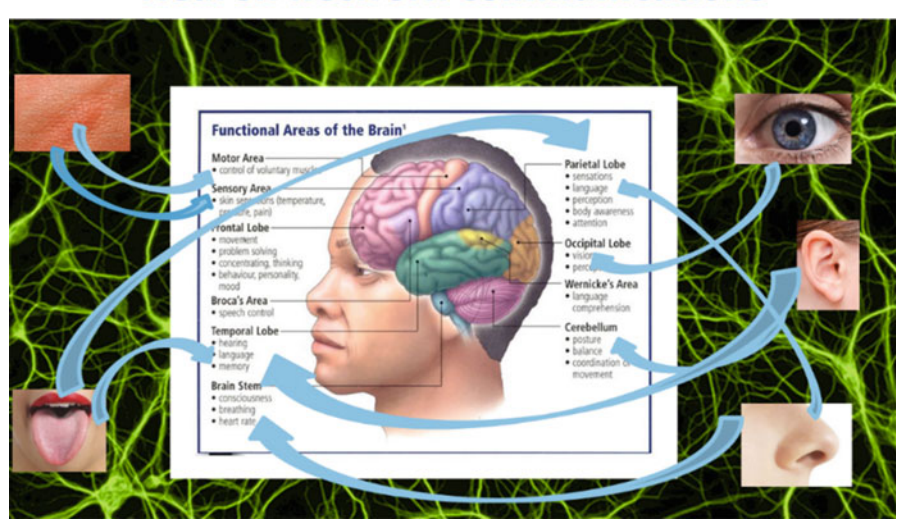


Fig. 6.43 Connections of human sensing with the corresponding human brain areas

Signal transduction	
techniques	Measurements details
Optical sensing and	Luminescence, absorption, surface plasmon resonance
measurements	
Electrochemical sensing and measurements	Redox reactions potentiometric, amperometric, etc.
Electrical sensing and	FET-type devices, nanowires, conductive gels
measurements	
Mass-sensitive sensing and	Surface acoustic wave
measurements	Nanocantilever-based sensing:
	1. Cantilever surface is covered by receptor layer
	(functionalization)
	2. Biomolecular interaction between receptor and target molecules (molecular recognition)
	3. Interaction between adsorbed molecules induces surface
	stress change for cantilever bending.
Magnetic sensing and	Magnetic fields sense magnetic nanoparticles attached with
measurements	biological molecules

Table 6.4 Nanosensoring techniques review

- Enhance cognitive abilities: cognitive stimulants, neurotechnology, neurochips
- Enhance physical abilities: modified biological functions, prosthetics/ exoskeleton
- Modify psychology: stimulants/medication, neurotechnology
- Get non-human abilities [lifespan enhancement]: night-vision technology, prosthetics/implants modified biological functions, genetic engineering, etc.

Some special nanodevices for artificial systems based on nanotransducers can be also created.

Basic and practically essential energy types for transducing include electrical, mechanical, electromagnetic (including light), chemical, acoustic, thermal energies, etc. We can concentrate our attention on a set of particular signal transduction techniques (see Table 6.4).

While the term *transducer* commonly implies the use of a sensor/detector, any device which converts energy can be considered a transducer. Transducers are widely used in measuring instruments. Future sensor systems will incorporate nanoscale transducers that use multiple physical phenomena to sense a broad range of processes to be analysed.

# 6.7.1 Optical Nanotransducers

Optical nanoconverters are nanodevices that measure light and, conversely, convert various impacts into light. Reversibility of transformations of influence signals (e.g. light  $\rightarrow$  chemical reaction and, conversely, chemical reaction  $\rightarrow$  light) is a

6.7 Nanotransducers 181

fundamental property of nanotransducers. This applies, as a rule, to other types of nanotransducers, namely, mechanical, magnetic, electrochemical and so on.

**Chemical Reaction**  $\rightarrow$  **Light.** Optical transduction which utilizes changes in optical properties such as phase, amplitude and frequency is manifested because of the selective binding of an analyte with the biorecognition element; i.e. it converts chemical energy to light. Photometric devices for the light intensity measure the photon output for luminescent or fluorescent processes, which can be detected with photomultiplier tubes or photodiode systems.

 $Light \rightarrow Chemical \ Reaction$ . Colourimetric devices for the colour analysis measure a change in light adsorbed when reactants are converted to products.

Surface Plasmon Resonance. SPR is an optical phenomenon due to a charge density oscillation at the interface of a metal and a dielectric, which has dielectric constants of opposite signs. Some particular research details in the SPR technique are presented by Rupert et al. [72] and Kari et al. [73]. For example, a thin layer of gold on a high refractive index glass surface can absorb laser light, producing electron waves (surface plasmons) on the gold surface. This occurs only at a specific angle and wavelength of incident light and is highly dependent on the surface of the gold, such that binding of a target analyte to a receptor changes the resonant frequency which produces a measurable signal.

**Fluorescence.** Fluorescence is a molecular absorption of light at one wavelength and its instantaneous emission at longer wavelengths. Some molecules fluoresce naturally, and others, such as DNA, can be modified for a fluorescence detection by the attachment of special fluorescent dyes. This process can be considered as nanotransducing.

Light-Induced Actuating Nanotransducers. Ding et al. [74] presented the light-induced actuating nanotransducers (LIAN). Temperature responsive polymers to charged Au nanoparticles, storing elastic energy that can be rapidly released under light control for repeatable isotropic nanoactuation, are developed in [74]. Optically heating above the critical temperature  $T_c = 32\,^{\circ}\mathrm{C}$  using plasmonic absorption of an incident laser causes the coatings to expel water and collapse within a microsecond to the nanoscale, millions of times faster than the base polymer. This leads towards rational design of diverse colloidal nanomachines.

Nanotransducers for Photoactivation Applications. Idris et al. [75] analysed the remote activation of photoactivable therapeutic compounds by light providing a high spatial and temporal control for activating the therapeutic agent. However, photoactivable compounds are mostly responsive towards ultraviolet (UV) or visible light radiation that has poor tissue penetration depth besides being unsafe to the body in the case of UV light. Nanoparticles with energy upconversion hold potential in overcoming this limit by using safe and deeply penetrating near infrared (NIR) light. These upconversion nanoparticles (UCNs) act as versatile nanotransducers. Their highly unusual optical properties to fluoresce with near-

Nanotransducing	Application
DNA sensors	Genetic monitoring, disease (e.g. Schwartz et al. [76]) Immunosensors: HIV, hepatitis, other viral disease, drug testing, environmental monitoring Cell-based sensors: functional sensors, drug testing Point-of-care sensors: blood, urine, electrolytes, gases, steroids, drugs, hormones and proteins Bacteria sensors ( <i>E. coli, Streptococcus</i> , other): food industry, medicine, environmental
O	Enzyme sensors: diabetics, drug testing
Quantum dots	Quantum dots are used as inorganic fluorophores (e.g. Jamieson et al. [77]). QDs have fairly broad excitation spectra – from ultraviolet to red – that can be tuned depending on their size and composition. They are being used in virus tagging and cancer cells imaging for diagnostics purposes
Luciferase luminescence	Nanotransducer is based on luminescence firefly luciferase ( <i>Prototinus</i> -luciferin 4-monooxygenase: ATP-hydrolysing) to detect the presence of bacteria in food or clinical samples [78]. Bacteria are specifically lysed, and the ATP released (roughly proportional to the number of bacteria present) reacted with D-luciferin and oxygen in a reaction which produces yellow light in high quantum yield <i>luciferase</i> $ATP + D-luciferin + O_2 \rightarrow \text{oxyluciferin} + AMP + \text{pyrophosphate} + CO_2 + \text{light (562 nm)}$

Table 6.5 Actual applications of optical nanotransducers

zero photobleaching, photoblinking and background autofluorescence are unique and have an added benefit when used simultaneously as optional imaging agents. Some actual application descriptions are presented in Table 6.5.

#### 6.7.2 Mechanical Nanotransducers

Mechanical nanotransducers detect changes in motions and convert mechanical energy into electrical energy. Mechanical transducers are usually cantilever shaped. The smaller size of mechanical transducers provides an outstanding mass resolution in a single atom, which is an advantage of a quartz crystal. Biomolecules form a monolayer on the upper side of the micro-cantilever that generates a surface stress creating a static mechanical bending with curvature, which causes cantilever to oscillate relative to the equilibrium position [79]. Some actual application descriptions of mechanical nanotransducers are presented in Table 6.6.

#### 6.7.3 Electrochemical Nanotransducers

Electrochemical nanotransducers convert chemical reactions into electrical signals (see also Fig. 6.44).

6.7 Nanotransducers 183

Table 6.6	Actual	applications	of mechan	ical nanotransduce
rabie o.o	Actual	applications	or mechan	icai nanotransuu

Nanotransducing	Application
Biosensors	Biosensors based on mechanical transducers can specifically detect single-base mismatches in oligonucleotide hybridization. Nucleic acids are immobilized on a side of a cantilever (active side). Exposure of the cantilever to a sample containing complementary nucleic acid gives rise to a cantilever bending (deflection) of a few nanometres. Deflection can be measured by an optical system in which a laser beam reflects on cantilever [79]
Boron–carbon–nitride (B–C–N) nanotubes BCN NTs	Nanotube-based materials with piezoelectric properties have been invoked highly valuable tools for next generation transducers [80] Future expectations are mainly focused on nanocomposites with tuneable physical properties, as well as nanotube-based electronic textiles. However, both the high electrical resistivity of BCN NTs and the poor control over bandgap parameters in CNTs can represent shortcomings for their factual application in nanoelectronics. To overcome these limiting factors, ternary boron carbon nitride (B–C–N) nanotubes (BCN NTs), in which boron, nitrogen and carbon atoms are disposed within a honeycomb hexagonal lattice, have recently been proposed as highly sensitive torsional electromechanical nanotransducers [81]

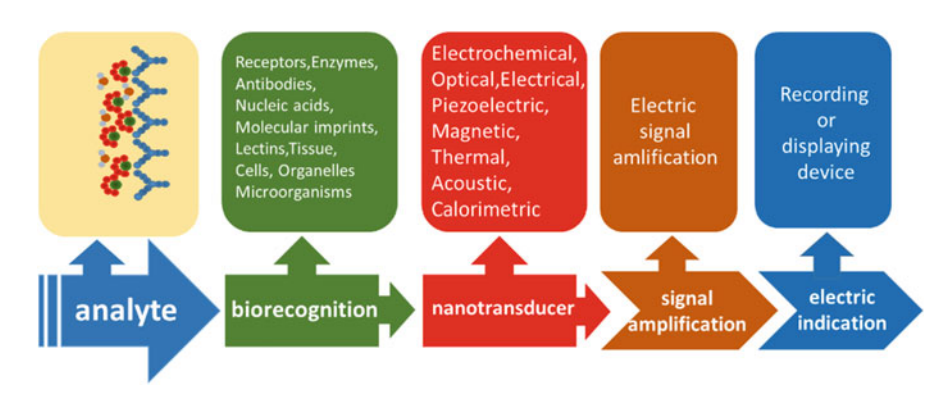


Fig. 6.44 General nanotransduction and nanosensoring scheme using electrochemical techniques

Consider some special techniques of nanotransduction and nanosensoring.

Nanoelectrode Techniques. The development of electrochemical nanosensors in recent years has been of growing interest. The enhanced chemical and physical properties arising from discrete nanoelectrode devices or microelectrodes modified with nanomaterials make these devices an attractive option for the improvement of current electroanalytical applications. Individual electrodes with nanoscale dimensions, which offer fundamental improvements over micro- and macroelectrodes, have been developing at a growing rate. In particular, single gold nanowires

fabricated on silicon substrates using electron-beam (e-beam) lithography have shown to exhibit enhanced mass transport due to radial diffusion. Steady-state currents observed in these electrodes allow the use of increased scanning rates and, as a result, shorter analysis times. The double layer capacitance in these electrodes also shows an improvement over micro-/macroelectrodes due to their very small surface area. The major application fields are health, security, law enforcement, environment and food safety. Nanoelectrode devices offer an attractive option in this field due to their small footprint and the potential for high sensitivity. As a result of the versatility and variety of nanoelectrode devices, they have been employed for the detection of a large range of medically relevant analytes ranging from small molecules such as dopamine and histamine to larger, more complex targets like bacteria or pharmaceutical drugs. Enzyme-based biosensors have long been of interest because of the selectivity of enzymes as biorecognition elements [82–86].

Electrochemical biosensors are some of the most widely used biosensors in the market, mainly due to glucose monitoring. Electrochemical biosensors are easily miniaturized, inherently inexpensive and require simple electronics for conditioning and read-out, making them ideal for point-of-care applications. Amperometric biosensors measure currents due to electroactive species, often using mediators to enhance electron transfer. Electrochemical impedance spectroscopy-based biosensors are some of the most promising electrochemical sensors for systems with well-defined charges, such as DNA. Electrochemical nanobiosensors with extremely low limits of detection are nowadays being developed thanks to the extraordinary properties of nanomaterials such as carbon nanotubes and graphene [87].

Nanoparticle Techniques. An effective detection of biological agents can be realized in the electrochemical impedance spectroscopy (EIS) with the emphasis on using nanoparticles and nanotechnology. Rapid, selective and sensitive detection technologies for biological agents are critical in clinical diagnosis, environmental monitoring and food safety. Recent developments in nanomaterial create many opportunities to advance DNA sensing and gene detection. The fact that gold nanoparticles are able to provide a stable immobilization of biomolecules that retain their bioactivity is a major advantage for the preparation of biosensors. However, there are a lot of researches reporting electrode modification by different nanomaterial to improve the DNA biosensor performance; the preparation of nanomaterial or the electrode modification strategy is often relatively complex. Furthermore, some DNA biosensors based on nanomaterial modification are still very limited for the improvement of DNA biosensor performance [88-92]. The emerging nanotechnology has opened novel opportunities to explore analytical applications of the fabricated nanosized materials. Recent advances in nanobiotechnology have made it possible to realize a variety of enzyme electrodes suitable for sensing application. In coating miniaturized electrodes with biocatalysts, undoubtedly the most of the potential deposition processes suffer from the difficulty in depositing process and reproducible coatings of the active enzyme on the miniature transducer element [93–96].

6.7 Nanotransducers 185

Molecular Imprinting Technique. Molecular imprinting technique (MIT) is a method of preparing polymer scaffolds that function as synthetic receptors [97]. Imprinted polymers that can selectively bind organic compounds have proven useful in developing sensors. Although creating synthetic molecular imprinting polymers that recognize proteins remains challenging, nanodevices and nanomaterials show promise in this area. Molecular imprinting sensors, specific for human ferritin and human papillomavirus-derived E7 protein, have been developed [98]. The molecular imprinting-based nanosensor can also discriminate between Ca<sup>2+</sup>-induced conformational changes in calmodulin. This ultrasensitive, label-free electrochemical detection of proteins offers an alternative to biosensors based on biomolecule recognition [98].

## 6.7.4 Magnetic Nanotransducers

Nanowire Transducers. Magnetic nanotransducers are already central to data storage and sensor devices, and more recently they are penetrating various new areas including life sciences and biomedical applications. Magnetic nanowires offer unique properties, due to a high aspect ratio and shape anisotropy. They are characterized by a single magnetic domain, rendering them nanopermanent magnets. This feature allows energy-efficient and remote operation of the nanowire transducers, i.e. induce motion, produce heat or sense their location [99, 100].

Magnetomotive Nanotransducers. Resonant acoustic spectroscopy of soft tissues using embedded magnetomotive nanotransducers and optical coherence tomography performing dynamic elastography of soft tissue samples is demonstrated in [101]. By sensing nanoscale displacements with optical coherence tomography, a chirped, modulated force is applied to acquire the mechanical spectrum of a tissue sample within a few seconds. This modulated force is applied via magnetic nanoparticles, named 'nanotransducers', which are diffused into the tissue and which contribute negligible inertia to the soft tissue mechanical system. Excised tissues that exhibit mechanical resonance modes which are well described by a linear damped harmonic oscillator have been observed. Results are validated by using cylindrical tissue phantoms of agarose in which resonant frequencies (30-400 Hz) are consistent with longitudinal modes and the sample boundary conditions. Magnetomotive resonant acoustic spectroscopy (MRAS) has been developed. Nanotransducers consist of magnetic nanoparticles (~20 nm diameter iron oxide, -COOH terminated, Ocean NanoTech, LLC) in an aqueous solution that are either diffused into the tissues or premixed into tissue phantoms before gelation. To mechanically drive the nanoparticles, a solenoid is placed 1-2 mm above the tissue to apply a temporally modulated magnetic field from B  $\approx$  0–600 G along its central axis (z). The resulting gradient force on the nanoparticles  $\mathbf{F} \propto \nabla |\mathbf{B}|^2$ is directed primarily towards the solenoid along +z [101–104].

Targeted Magnetic Nanoparticles. Hysteretic heat dissipation by magnetic nanomaterials can be used to remotely trigger activity of neurons expressing heat-sensitive ion channels. Since the alternating magnetic fields in the low radiofrequency range interact minimally with the biological tissues, the magnetic nanoparticles injected into the brain can act as transducers of wireless magnetothermal deep brain stimulation. Similarly, local hysteretic heating allows magnetic nanoparticles to disrupt protein aggregates associated with neurodegenerative disorders [102–104].

Heat-Assisted Magnetic Recording (HAMR). Integrating magnetic thin-film heads with plasmonic nanotransducers has gained importance in magnetic data storage concepts because of its promise to overcome the superparamagnetic limit. Integrated heads offer significant advancement in the performance of hard disc drives by lowering the coercivity of magnetic grains via localized heating of the grains during the recording process. The magnetization of the grains can then be changed by the applied magnetic field of the integrated head, which has paved the way for heat-assisted magnetic recording (HAMR). HAMR is an emerging technology that has increased the areal density of conventional recording techniques for hard disc drives. Integrated heads have enabled this increase through localized heating of the recording media during the recording process. One of the problems in integrating magnetic heads with plasmonic nanotransducers is the resulting losses. In particular, multilayer configurations with gold thin films near magnetic thin films are investigated to minimize radiative and load-induced losses. The effect of loadinduced damping of the magnetic film and evanescent coupling is identified with the intensity enhancement near the magnetic films. A higher intensity enhancement can be obtained by minimizing radiative and load-induced losses through adjusting layer thicknesses in multilayer configurations [105–107].

Magneto-Plasmonic Nanoantennas. Plasmonic nanoantennas are a hot and rapidly expanding research field. Here we overview basic operating principles and applications of novel magneto-plasmonic nanoantennas, which are made of ferromagnetic metals and driven not only by light but also by external magnetic fields. Magneto-plasmonic nanoantennas enhance the magneto-optical effects, which introduces additional degrees of freedom in the control of light at the nanoscale. This property is used in conceptually new devices such as magneto-plasmonic rulers, ultrasensitive biosensors, one-way subwavelength waveguides and extraordinary optical. Magneto-plasmonic nanoantennas may also be used to achieve spectral tuning or enhance nonlinear effects [108]. However, their advantage over nonmagnetic nanoantennas is that they can additionally exhibit nonlinear magnetooptical properties. It was shown that the nonlinear magneto-optical Kerr effect and the SHG effect can be enhanced at the frequencies of plasmon modes supported by arrays of ferromagnetic metal nanorods or magnetic multilayer heterostructures. The inverse magneto-optical effects are important for ultra-fast all-optical control of magnetisation, which may be useful in data storage systems and generation of spin waves with light pulses transmission structures, as well as in novel biomedical imaging modalities.

### 6.8 Nanoaerogels and Nanofoams

### 6.8.1 Introduction to Aerogels

Aerogel is a synthetic porous ultralight material derived from a gel, in which the liquid component of the gel has been replaced by a gas. The result is a solid with extremely low density and thermal conductivity. Nicknames include *frozen smoke*, solid smoke, solid air or blue smoke owing to its translucent nature, and the way light scatters in the material. However, it feels like expanded polystyrene (styrofoam) to the touch.

*Nanofoams* are a class of nanostructured, porous materials (foams) containing a significant population of pores with diameters less than 100 nm. Aerogels are one example of nanofoam.

Table 6.7 presents the evolution of aerogels, steps and stages of the process.

*CNTs and Aerogels*. There are several different ways how nanotubes and aerogels come together:

- Aerogels can be made out of carbon nanotubes.
- Carbon aerogels can be reinforced with embedded carbon nanotubes.
- Metal oxide aerogels can be used as catalysts to grow carbon nanotubes.
- Metal-doped carbon aerogels can act as catalysts for growing carbon nanotubes.

**Remark.** Fluffy masses of nanotubes formed during *nanotube yarn* production and sheets of entangled carbon nanotubes are sometimes incorrectly referred to as aerogels.

Carbon–Carbon Nanotube Aerogels. In 2008, Ted Baumann and Marcus Worsley at Lawrence Livermore National Laboratory developed a composite material made of double-walled carbon nanotubes dispersed uniformly throughout a carbon aerogel. The resulting carbon–carbon nanotube aerogels have improved electrical conductivities over regular carbon aerogels. For 8 wt % nanotube loading and bulk density of  $0.139 \ {\rm g \ cm^{-3}}$ , these aerogels have about twice the conductivity of regular carbon aerogels (5  $\Omega^{-1} \ {\rm cm^{-1}} \ {\rm vs} \ 2 \ \Omega^{-1} \ {\rm cm^{-1}}$ ).

### Graphene Aerogels: Main Properties and Qualities.

- Graphene aerogels demonstrate densities approaching 10 mg/cm<sup>3</sup>.
- Graphene aerogels demonstrate an improvement in bulk electrical conductivity of more than two orders of magnitude  $(1\cdot10^2 \text{ S/m})$  compared to graphene assemblies with physical cross-links alone  $(5\cdot10^{-1} \text{ S/m})$ .
- The graphene aerogels also possess large surface areas (584 m²/g) and pore volumes (2.96 cm³/g), making these materials viable candidates for use in energy storage, catalysis and sensing applications.

Table 6.7 Aerogel evolution and application development

Evolution period	Description
1930s–1940s 1929–1931, Samuel Ste- phens Kistler [109]	A discovery of many different types of aerogels, including transparent silica aerogels with densities as low as $0.030~\rm g \times cm^{-3}$ , alumina aerogels, tungsten oxide aerogels, iron oxide aerogels and tin oxide aerogels
1940s–1970s The early days of aerogels	Aerogels were even commercialized as early as the 1940s by Monsanto Corporation (till 1970s). A powdered silica aerogel product called 'Santocel' for use as a thickening agent for paints, makeup and napalm, as cigarette filters and as insulation for a national line of freezers
1970s–1980s	The 1980s brought forth safer techniques for producing aerogels, ways of making aerogels 30 times lighter than had ever been accomplished before, and a new class of organic and carbon aerogels that would demonstrate aerogels of different substances could do amazing and very different things  In early 1980s, particle physics researchers realized that silica aerogels would be an ideal medium for the production and detection of Cherenkov radiation  In the 1980s, the alkoxide sol-gel process was made less toxic by using a safer alkoxide compound, and the supercritical drying technique was made safer by replacing supercritical alcohol with supercritical carbon dioxide [110]
1980s–1990s	The 1990s was the decade of aerogel increased publicity. More- over, aerogel synthesis evolved to include ways to speed up or even eliminate supercritical drying and to extend aerogels to metal oxides across the periodic table
1990s–2000s Commercialization trends	Mechanically strong aerogels, aerogels of strange new materials and, finally, commercially available aerogels changed the way of thinking for aerogels application from energy transducing to lightweight structures and nanosensors
2000s–2020s The nearest future	Actual and prospective developments trends:  • Mechanically strong aerogels, aerogels of new compositions for sensors and energy production  • Aerogels applications for use as hydrogen storage media  • Metal aerogels  • More advanced supercapacitors that rival today's batteries  • Hydrogen production using cleverly engineered semiconductor aerogels changing the way of thinking about energy and fuel  • Smart materials with the unique combinations of materials properties  There are endless possible applications of aerogel materials

*Ohm's Law and Hooke's Law Analysis* The analysis of graphene/MWCNTs hybrid aerogels [111] is that these materials demonstrate Ohm's law behaviour. It is very important that Hooke's law behaviour also is observed. However, the linearity of *compressive stress* via *compressive strain* is very 'deep' (till 50%). This is larger than for simple elastic materials. This property also gives possibilities to create pressure and force nanosensors.

### 6.8.2 Aerogels Forms and Characterization

Silica Gels. Silica gels are produced through the sol-gel process, in which nanoparticles suspended in a liquid solution (i.e. a sol) are invoked to interconnect and form a continuous, porous, nanostructured network of particles across the volume of the liquid medium (i.e. a gel). Silica aerogels have found a wide array of uses, mostly in high-tech science and engineering, but are beginning to enter the commercial mainstream. Below are a few examples of where silica aerogels have helped out. There are some known applications: Insulation on the Mars Exploration Rovers, Hypervelocity Particle Capture in the Stardust Probe, High-Energy Cherenkov Radiation Particle Counters, Remediating Oil from Water, Transparent Window Insulation and Thermal Insulation Without the Chlorofluorocarbon (CFCs).

Metal Oxide Aerogels. Metal oxide aerogels are the inorganic cousins of the more common silica aerogel – each type with its own unique properties. These aerogels are important, as they can act as catalysts for various chemical transformations, matrices for explosives and precursors for other materials (such as carbon nanotube catalysts), can be magnetic and are often quite colourful. Up until the 1990s, metal oxide aerogels had been historically much more difficult to synthesize than silica aerogels, largely because there were no good synthetic routes for making metal oxide gels. This is mostly due to the difficulty associated with handling metal alkoxide compounds (as they hydrolyse readily), or in some cases simply because of there aren't any or any good metal alkoxides for a particular metal. One of the most notable differences between metal oxide aerogels and silica aerogels is that many metal oxide aerogels are often brilliantly coloured. It is important to remember that the bluish cast characteristic of a silica aerogel is the result of the Rayleigh scattering by nanoparticles (which make up the aerogel backbone) and that silica itself is not blue. There are some colour realizations of metal oxide aerogels (see Table 6.8).

*Organic and Carbon Aerogels*. Organic aerogels have been around as long as any aerogel. In fact, the first aerogel which Samuel Kistler is believed to have prepared was aerogel made from jelly (which is composed of the organic heteropolysaccharide pectin). Kistler also prepared aerogels of gelatin and rubbers,

	e
Metal oxide aerogels	Colour palette
Silica, alumina, titania, zirconia	Clear with Rayleigh scattering blue or white
Iron oxide	Rust red or yellow opaque
Chromia	Deep green or deep blue, opaque
Vandia	Olive green, opaque
Neodymium oxide	Purple, transparent
Samarium oxide	Yellow, transparent
Holmium oxide, erbium oxide	Pink, transparent

Table 6.8 Colour realizations of metal oxide aerogels

both of which are composed of organic polymers. There are numerous examples of organic aerogels which have been prepared in the literature, many of which are biological in nature. Supercritical drying has been used by biologists for many decades to preserve biological specimens or prepare them for electron microscopy – in essence making aeroinsects, aerobacteria and even aeroorgans. Organic aerogels made from polymers of not only resorcinol but also melamine, phlorglucinol and acetic acid are used to prepare carbon aerogels.

Semiconducting Metal Chalcogenide Aerogels. Semiconducting metal chalcogenide aerogels are a new, exciting class of aerogels materials. First prepared in 2002, these aerogels possess a unique combination of porosity, optical translucency and photoluminescence and show great promise for use as chemical sensors (artificial nose) and energy applications such as photovoltaics (solar cells) and extraction of hydrogen from water using sunlight as the energy source. Metal chalcogenide aerogels exhibit a property called photoluminescence, that is, the glow when irradiated with a black light (ultraviolet lamp). In fact, metal chalcogenide aerogels have a bandgap, like other semiconductors, and that bandgap corresponds to the colour of light they will emit under the black light. Bulk CdS has a bandgap around 2.05 eV (meaning the crystal will photoluminesce orange), but nanosized CdS quantum dots can have a very different bandgap depending on their diameter. In general, aerogels made from quantum dots have about the same bandgap as the quantum dots they are made out of, so CdS aerogels made from CdS quantum dots that have a bandgap of 2.73 eV (blue) will photoluminesce blue as well, although a bit greener of a blue (the bandgap of aerogels is usually 'redshifted' compared to quantum dots). Interestingly, if the aerogel is annealed at 300 °C, the aerogel's bandgap decreases to 2.22 eV (green). The main application directions are photocatalysts, photovoltaic cells, chemical and biological sensors and quantum dot metal chalcogenide aerogel.

Nanoporous Metal Foams. There are now a number of ways to make nanoporous metal foams. There are three major approaches: combustion synthesis of metal nanofoams, dealloying of templated Au alloys and nanosmelting of iron aerogels.

One method for making nanoporous metals is called dealloying. In this method, an alloy of gold and a less noble (more reactive) metal is prepared (usually an alloy of copper and gold or silver and gold), where enough less noble metal is present in the alloy that forms a continuous percolating network throughout the gold.

Iron aerogels are made through a nanosmelting process. Fe aerogels are both magnetic and electrically conductive just like iron is. They have surface areas ranging from  $\sim$ 95 to 300 m<sup>2</sup>·g<sup>-1</sup> and densities of about 0.046 g·cm<sup>-3</sup> (about 20 times less dense than water and 172 times less dense than bulk Fe metal).

The main applications are hydrogen storage, antimicrobial scaffolds, irregularly shaped magnetic media and X-ray optics.

**Strong and Flexible Aerogels.** Although it is true that a typical silica aerogel could hold up to 2000 times its weight in applied force, this only holds if the force is gently and uniformly applied. Also, keep in mind that aerogels are also very light,

and 2000 times the weight of an aerogel still might not be very much. Additionally, most aerogels as produced are extremely brittle and friable (i.e. they tend to fragment and pulverize). As a result, structural applications of aerogels were for a long time totally impractical.

There are four general ways to enhance the mechanical properties of aerogels: liquid-phase crosslinking, vapour-phase crosslinking, fibre reinforcing and reduced bonding.

### 6.8.3 Aerogels Commercialization

Mechanically Strong and Flexible Aerogels. If you can dope polymers with nanomaterial fillers, could you dope a filler material with a polymer? [112] – this was a question. It was shown that the lowest density form of silica available is silica aerogel and proceeded to see what kinds of materials you could make if you doped them, that is, crosslinked them, with polymers. Discovered x-aerogels, a new class of flexible, mechanically robust aerogels, have been developed. Diffusing crosslinking agents such as diisocyanates (used in making polyurethane) into the pores of a silica aerogel have been obtained. The hydroxyl groups on the surface of the particles that make up the aerogel framework to create polymer bridges between particles – the structural weak spots in the aerogel structure – have been used. Later, a set of x-aerogels from many more substances than just silica, including most of the transition metal and lanthanide oxides and many organic aerogels, have been prepared.

Quantum Dot Aerogels and Beyond If aerogels of metal oxides could be made, why should other chalcogenides, such as sulphides and selenides be searched for? [113] – this was a question. Gels of cadmium sulphide and selenide have been prepared. The result is a novel class of photoluminescent, semiconducting aerogels with unusual and exciting properties. Many metal sulphides and selenides as well as nitrides and phosphides gels have been prepared, and applications of these types of aerogels in photoelectrolysis of water and chemical sensors have been demonstrated.

Metal Aerogels. The development of a technique for producing monoliths of nanoporous gold was the essential technological step [114, 115]. Cast bimetallic alloys of gold and another metal (such as Cu or Ag) over micron-diameter polystyrene spheres, which served as a template for a foam structure, were created. After dissolving the template, the less noble metal in the alloy was then etched away through a technique called dealloying. The remaining structure was a macroporous foam with nanoporous walls, closely approximating a gold aerogel. The foams had two levels of porosity, micron-diameter pores leftover from the template and nanometre-size pores from dealloying. However, these materials did not exhibit significant mesoporosity, that is, pores between 2 and 50 nm in diameter, which is more typical of aerogels.

Bryce Tappan [116] found that ignition of pressed pellets of these compounds under an inert atmosphere left behind incredibly low-density metallic foams. It was discovered that the foams, although largely macroporous, contained significant mesoporosity as well, approximating the expected structure of a metal aerogel. The group eventually extended the technique to prepare foams of Fe, Co, Ni and Cu, among other metals. The polymer that smelted the iron oxide component of the aerogel, leaving behind an aerogel of 'pig iron' – iron rich in carbon content but magnetic and metallic as characterized by X-ray diffraction [117] was created.

Carbon Nanotube Aerogels. It was shown that carbon nanotubes could be assembled into a gel structure using polyvinyl alcohol as a 'binder' [118]. Then these gels were supercritically dried to prepare carbon nanotube aerogels. The next new technology (Marcus Worsley and Sergei Kucheyev 2008) gave a hybrid of carbon nanotubes and carbon aerogel, with the amazing ability to compress 80% and elastically return undeformed. The materials also showed high electrical conductivity.

Acid-Catalysed Carbon Aerogels. Acid-catalysed carbon aerogels – an intriguing variation on carbon aerogels with incredibly enhanced strength – were developed [119]. Although technically not aerogels because of their primarily macroporous bone-like structure, these materials exhibit compressive strength and stiffness much higher typical of most aerogels and different from any other carbon material. A way to make these materials nanoporous by etching them with  $CO_2$  at high temperatures, resulting in ultrahigh surface area carbon aerogels with promise for hydrogen storage applications, was demonstrated [120].

#### 6.8.4 Functionalization

Functionalization is the process of adding new functions, features, capabilities or properties to a material by changing the surface chemistry of the material. It is a fundamental technique used throughout chemistry, materials science, biological engineering, textile engineering and nanotechnology. Functionalization is performed by attaching molecules or nanoparticles to the surface of a material, sometimes with a chemical bond but sometimes just through adsorption (i.e. the thing you're trying to attach sticks to the surface without forming a covalent or ionic bond).

Functionalization can:

- Make a water-absorbing material waterproof
- · Change the colour of a material
- · Render a surface antibiotic
- Make chemical sensors ('artificial noses')

6.9 Biocomposites 193

- · Make nonmagnetic materials magnetic
- Make sophisticated batteries

Flat surfaces such as silicon wafers or glass are commonly functionalized to make useful and interesting materials and devices. However, aerogels, with ultrahigh surface areas wrapped up inside their porous skeletal frameworks, can also be functionalized to make materials with even more amazing properties than ordinary aerogels (see also Table 6.9).

### 6.9 Biocomposites

### 6.9.1 Biocomposite Concepts and Definitions

Polymer nanocomposites represent a new alternative to conventional polymers. Polymer nanocomposites are materials in which nanoscopic inorganic or organic particles, typically 1–100 nm in at least one dimension, are dispersed in an organic polymer matrix in order to improve the properties of the polymer dramatically.

Owing to the *nm* length scale, which minimizes scattering of light, nanocomposites are usually transparent and exhibit properties that are markedly improved over those of pure polymers or their traditional composites. They have increased modulus and strength, outstanding barrier properties, improved solvency, heat resistance and generally lower flammability, and they do not have detrimental effects on ductility [121]. There are three basic classes of *biopolymers*:

- 1. *Bioresources*: natural biopolymers (plant carbohydrate like starch, cellulose, chitosan, alginate, agar, carrageenan, etc. and animal- or plant-origin proteins like soy protein, corn zein, wheat gluten, gelatin, collagen, whey protein and casein)
- 2. Chemical synthesis: synthetic biodegradable polymers
- 3. Microorganisms: biopolymers produced by microbial fermentation

Table 6.10 demonstrates the evolution biocomposite material concepts from traditional forms till absolutely new and prospective.

Bio-nanocomposites which are obtained from 100% bio-based materials, in which both the fillers and the matrix are obtained from renewable resources. Four different nanofillers are extensively used for the preparation of bio-nanocomposites presented in Table 6.11.

# 6.9.2 Bio-nanocomposites from Renewable Resources

A variety of nanofillers allow the creation of large four classes of bio-nanocomposites.

 Table 6.9
 Aerogels functionalization

Aerogel function	Description
Aerogels are 3D surfaces	While aerogels are generally three-dimensional materials, they contain a tremendous amount of surface area. The surface of each and every nanosized strut that makes up the open porous skeleton of the aerogel can potentially serve as a surface for molecules or particles to be attached to. There is a lot of surface area wrapped inside an aerogel, a typical piece of silica aerogel, say with a density of 0.1 g/cm³, and easily has a surface area of 750 m²/g, which means an ice cube-sized piece having 2.2 cm sides (a little less than a cubic inch) has 750 m²
Aerogels are great things to functionalize	Aerogels offer lots of advantages in functionalization:  Aerogels pack tremendous surface into a small volume (i.e. they have a high surface-to-volume ratio)  Aerogel backbones can be made of many different sub stances, providing tremendous chemical flexibility  Aerogels can frequently made through ambient temperature bench-top processes  The open pore network of aerogels enables movement (mass transport) of stuff through the aerogel, providing avenues for getting things you might want to detect or adsorb to the functional groups that will sense or adsorb them
Waterproof aerogels: an example of functionalization	One classic example of functionalization of aerogels is the making of hydrophobic (waterproof) silica aerogels. Silica aerogels are normally hydrophilic; that is, they readily absorb moisture from the air (which causes them to shrink and become cloudy over time) and wick up liquid water on contact (which causes them to shrivel up and densify). This is because of surface hydroxyl (-OH) groups that cover the struts of the aerogel's skeleton–sticky, polar groups to which water can readily stick by hydrogen bonding. To make a waterproof silica aerogel, we can replace the hydrogen on these sticky -OH groups with a much less sticky, non-polar group called trimethylsilyl (-Si(CH <sub>3</sub> ) <sub>3</sub> ). Transforming just 30% of these -OH groups into -OSi (CH <sub>3</sub> ) <sub>3</sub> groups is enough to make the struts of the aerogel repel water, allowing the aerogel to float in water indefinitely without wicking water into its pore network (which would cause the aerogel to shrivel up).
How to functionalize an aerogel	There are three points in the process of making an aerogel where you can functionalize its surface: during gelation of the precursor gel, after gelation of the precursor gel and after supercritical drying.
Cool stuff using functionalization	Make brittle silica and metal oxide aerogels superstrong and tough by functionalizing the surface with polymers     Make precursors for metallic aerogels by functionalizing metal oxide aerogels with carbon-rich polymers     Make carbon aerogels into battery-like materials by functionalizing with electrochemical coatings such as manganese dioxide

(continued)

Table 6.9 (continued)

Aerogel function	Description	
	<ul> <li>Make silica aerogels into oxygen sensors by functionalizing with oxygen-sensitive fluorophores</li> <li>Make carbon aerogels into efficient catalysts by functionalizing with precious metals</li> <li>Make silica or carbon aerogels into hydrogen storage materials by functionalizing with metals that form hydrides</li> <li>Make aerogels that absorb 20× their weight in oil by functionalizing with oleophilic groups</li> <li>Make aerogels that filter biomolecules like DNA by functionalizing with the complementary DNA sequence</li> </ul>	

 Table 6.10 Bio-nanocomposite concepts evolution [122]

Concept	Definition
Bioplastic	A plastic that is made from biological/renewable resources or degrades by the action of microorganisms/biological activity or both
Bio-based plastic	A plastic that is obtained totally or partially from biological resources, i.e. all the monomers or any of the monomer used in the synthesis is derived from biological resources
Degradable plastic	A plastic, which undergoes major structural changes under prescribed environmental conditions
Biodegradable plastic	A plastic which degrades by the action of microorganisms or undergoes lowering of its molecular weight by biological activity
Compostable plastic	A plastic that undergoes biodegradation in composting environment to yield carbon dioxide, water, inorganic compounds and biomass at a rate equivalent to standard compostable materials and leaves no toxic materials
Biocomposite	Composite that consists of either filler or polymer matrix derived from biological resources
Nanocomposite	Polymer composites that have fillers with at least one dimension in nm
Bio-based nanocomposite	Nanocomposite in which either fillers or polymer matrix has been obtained from biological resources
Bio-nanocomposite	Nanocomposite in which both fillers and polymer matrix obtained from biological resources
Bio-degradable nanocomposite	Nanocomposites that degrades by the action of microorganisms
Bio-compatible	Refers to the ability of a material to carry out its intended function without any adverse reactions or unintended responses

Cellulose Nanocomposites. The importance of cellulose nanocomposites arises from the unique properties of cellulose nanomaterials such as structural stability against various processing windows, excellent mechanical properties in terms of Young's modulus (~138 GPa) compared to other lignocellulosic natural fibres (35–45 GPa for flax fibre) and very low coefficient of thermal expansion in

Table 6.11 Nanofillers for bio-nanocomposites

Nanofillers	Descriptions and characterizations
Cellulose-based nanofillers (CBN)	CBNs are widely available and low-cost material which is both renewable and biodegradable. Cellulose microfibrils and nanocrystalline celluloses or cellulose nanowhiskers (CNW) are the two types of nanoreinforcements obtained from cellulose. Cellulose microfibrils consist of bundles of molecules that are elongated and stabilized through hydrogen bonding [123]. The typical dimensions of these nanofibrils are 2–20 nm in diameters, while lengths in micrometer range
Carbon nanotubes	Carbon nanotubes find many applications that include polymer nanocomposites, electrochemical energy storage/conversion, catalysis, hydrogen storage, health and environmental hygiene products and electronics. In polymer nanocomposites they have been utilized as high-performance functional fillers, which not only improved thermal/mechanical performance but also provided additional functionalities such as fire retardant, moisture resistance, electromagnetic shielding and barrier performances. The field of polymer nanocomposites with carbon nonmaterial has highly diversified; carbon nanotube (CNT)-based polymer composites have been widely explored in many aspects as described elsewhere [124]
Nanoclays	Layered silicates also known as nanoclays are most commonly utilized nanofillers in the synthesis of polymer-layered silicate nanocomposites. Among these layered silicates, phylloscilicates (2:1) are extensively used in preparing clay-based nanocomposites. The crystal arrangement in the silicate layers is made up of two tetrahedrally coordinated atoms amalgamated to edge-shared octahedral sheets. The layers have thickness of 1 nm, and their tangential dimensions range from 30 nm to a few microns. The variation in the dimensions depends on clay source, particulate silicate and preparation technique [125]
Functional nanofillers	A wide range of biocompatible materials such as metal, alloys, ceramics, polymers and composites is used for medical implants. Among them, bio-nanocomposites that are fabricated using the combination of biopolymers and various nanostructured inorganic/ organic functional fillers receive extensive attention due to their diversified biomedical as well as biotechnological application. Nanostructured fillers play an important role in biocomposite fabrication, since they bring various desired functionalities to the composites. Functional nanofillers such as cellulose nanofibres, hydroxyapatite (HAp), layered double hydroxides (LDH), silica nanoparticles and polyhedral oligomeric silsequioxanes (POSS) are most investigated for this proposes [126–128]

longitudinal direction ( $10^{-7} \, \mathrm{K}^{-1}$ ). Structures of cellulose nanofibres are stabilized by hydrogen bonds with high levels of crystallinity, which makes cellulose nanofibres an ideal reinforcing material in polymeric materials. Cellulose nanocomposites made using renewable resource-based biopolymers exhibit superior thermal, mechanical and barrier properties with minimum reinforcement

6.9 Biocomposites 197

( $\sim$ 5 wt %) compared to macro reinforcements with the added advantages of recyclability and biodegradability [129].

CNT Nanocomposites. Carbon nanostructures (including carbon nanotubes, nanofibres and graphene sheets) exhibit a range of properties, such as higher electrical conductivity, enhanced mechanical strength and better thermal behaviour, which make them desirable reinforcing materials for polymer nanocomposites [130]. Especially, carbon nanotubes receive more attention due to their uniqueness in efficient load transfer, which arises from the enormous surface area and high aspect ratio. Mechanical behaviour of carbon nanotubes composites is influenced by carbon nanotubes type, geometry of the carbon nanotubes and polymer nature (amorphous/crystalline/semicrystalline) and the processing method (in situ polymerization/solvent casting/melt processing) [131].

Clay Nanocomposites. Bioplastic—clay nanocomposites have been receiving extensive attention due to their improved thermal, mechanical and barrier properties as well as reduced flammability compared to their respective virgin polymers. Other positive aspect of nanoclay reinforcement is that it does not hamper the biodegradation of biodegradable polymers [132]. These clay materials were classified into many types based on their chemical nature, structure and their unique properties of swelling as well as exfoliation [133].

Functional Nanocomposites. Bio-based polymers with functional fillers such as HAp and LDH found a wide range of applications specially towards tissue engineering, drug deliver and gene therapy due to their compatibility and also non-cytotoxic and noninflammatory towards with biological system [134, 135]. Yamaguchi et al. reported fabrication of chitosan/hydroxyapatite nanocomposites using co-precipitation method. They reported the formation of flexible composites with homogenous dispersion of hydroxyapatite. Heat treatment of this composite caused the formation of hydrogen bonds between chitosan molecules and results in the enhanced mechanical properties [136].

# 6.9.3 Bio-nanocomposite Applications

**Packaging.** Bioplastics suffer from three main disadvantages: performance, processing and cost compared to the petro plastics [137–139].

Food packaging. General requirements for food packaging materials are to ensure gas barrier (O<sub>2</sub>, CO<sub>2</sub>), antimicrobial function, mechanical properties, vapour barrier, optical properties, aroma barrier, thermal properties and environmentally friendly. Bio-nanocomposites open an opportunity for the use of new, high-performance, lightweight green nanocomposite materials making them to replace conventional nonbiodegradable petroleum-based plastic packaging materials. The most studied bio-nanocomposites suitable for packaging applications are starch and cellulose derivatives, polylactic acid (PLA), polycaprolactone (PCL), poly(butylene succinate) (PBS) and polyhydroxybutyrate (PHB). Bio-nanocomposites mostly

use nanoscale fillers being layered silicate nanoclays such as montmorillonite and kaolinite. The main goal is the development of high barrier properties against the diffusion of oxygen, carbon dioxide, flavour compounds and water vapour. Some bio-nanocomposites are useful to provide active and/or smart properties to food packaging systems, as exemplified by antimicrobial properties, oxygen-scavenging ability, enzyme immobilization or indication of the degree of exposure to some detrimental factors such as inadequate temperatures or oxygen levels. An important trend of food packaging applications is the enhancement of packaging performance of the green materials as well as their biodegradability, antimicrobial properties and mechanical and thermal properties [140–142].

*Electronics, Sensor and Energy Applications.* Polymers reinforced with engineered/functional nanostructures provide additional electrical, optical and electromagnetic shielding and magnetic properties and lead to the development of various advanced devices including light emitting, diodes, sensors, solar cells, display panels and other medical devices [143].

**Bio-nanocomposites for Medical Applications.** The versatility and adaptability of bio-nanocomposites enable these materials to be utilized for biomedical applications. An essential characteristic of medical biomaterials is biocompatibility, the ability to function appropriately in the human body to produce the desired clinical outcome, without causing adverse effects [134].

**Bio-nanocomposites for Tissue Engineering.** Bio-nanocomposites are well suited for regeneration of native tissue structures, as nanocomposite materials mimic the natural morphology of the extracellular matrix that surrounds cells. The extracellular matrix exhibits three key characteristics [144]:

- 1. The extracellular matrix is composed of a combination of macromolecules, such as proteins and polysaccharides, and inorganic matter.
- 2. Macromolecules in the extracellular matrix are typically present in a fibre form and possess an axial (length/diameter) ratio greater than 100.
- Macromolecules in the extracellular matrix typically have nanoscale diameters of less than 500 nm.

**Bio-nanocomposites for Drug Delivery.** Bio-nanocomposites designed for implantation and tissue replacement/regeneration can simultaneously serve as reservoirs for drug delivery. A hydroxyapatite/collagen-alginate bio-nanocomposite has been developed as a bone filler and drug delivery vehicle; the composite is loaded with bone morphogenetic protein, a growth factor that stimulates bone formation [145]. Porous hydroxyapatite/collagen scaffolds have additionally been designed as carriers for fibroblast growth factor 2; these drug-releasing scaffolds are efficacious in stimulating both bone regeneration and cartilage regeneration in animal models of large osteochondral defects [146].

**Bio-nanocomposites for Gene Therapy.** Natural nucleic acid biopolymers can be intercalated into layered double hydroxides. Such composite materials can be utilized for gene therapy; for example, an ion exchange method has been used for

intercalation of DNA between the interlayers of LDH, leading to the formation of bio-nanocomposites. The DNA chains are arranged in a double helix conformation, oriented parallel to the basal plane of the LDH [147].

#### References

- Shunin Yu N, Shvarts K K 1989 Atomic and electronic structure of disordered semiconductors Preprint: Institute of Physics Academy of Sciences of Latvia LAFI-154 (Riga-Salaspils: IP) 97 p (in Russian)
- Shunin Yu N, Shvarts K K 1989 Influence of composition on the electronic structure of amorphous As<sub>x</sub>Se<sub>1-x</sub>Phys and tech. semiconductors 23(6) 1049–53 (in Russian)
- 3. Shunin Yu N, Shvarts K K **1990** Modelling of radiation stimulated processes in disordered semiconductors *Izv AN LSSR ser fiz i tehn nauk* No **2** 38–56 (*in Russian*)
- 4. Shunin Yu N, Shvarts K K, Sokol A A **1990** Scattering of electrons in disordered solids: theory and experiment *Izv AN LSSR* No **4** 74–91 (*in Russian*)
- Shunin Yu.N., Zhukovskii Yu.F., Burlutskaya N.Yu., Gopejenko V.I., Bellucci S. 2012 simulation of fundamental properties of CNT- and GNR-metal interconnects for development of new nanosensor systems In: *Nanodevices and Nanomaterials for Ecological Security* Series: NATO Science for Peace Series B - Physics and Biophysics, Springer Verlag 2012 237–62
- Peng L-M, Zhang Zh, Wang Sh 2014 Carbon nanotube electronics: recent advances Materials Today 17(9) 433–4
- 7. Reshma M **2014** Carbon nanotube FET device fabrication, design, modeling, and simulation of cutfet for reconfigurable logic gate design *Asia Pacific Journal of Research* **1**(17) 131–8
- Akyildiz I F, Jornet J M 2010 Electromagnetic wireless nanosensor networks Nano Communication Networks 1 3–19
- 9. Alvi P A, Lal K M, Siddiqui M J and S, Naqvi A H 2005 Carbon nanotubes field effect transistors: A review *Ind. J. of Pure and Appl. Phys.* 43 899–904
- Lima T-Ch, Ramakrishna S 2006 A Conceptual Review of Nanosensors Z. Naturforsch. 61a 402–12
- 11. Hierold Ch, Jungen A, Stampfer Ch, Helbling T **2007** Nano electromechanical sensors based on carbon nanotubes *Sensors and Actuators* A **136** 51–61
- 12. Gruodis A, Ališauskaitė V, Jursenas S, Valkunas L, Muzikante I **2003** Excitonic states in the polar molecular crystals *SPIE Proceedings*. *Advanced optical materials* **5122** 224–31
- 13. Balevicius M, Stumbrys E, Sorokolit B, Gruodis A 1995 Theoretical studies of electronic absorption spectra of dimethylaminobenzylidene 1,3-indandione (DMABI) by means of semiempirical quantum chemical calculations *Lithuanian Journal of Physics* 35(1) 20–6
- 14. Gulbinas V, Kodis G, Jursenas S, Valkunas L, Gruodis A, Mialocq J-C, Pommeret S, Gustavsson T 1999 Charge transfer induced excited state twisting of N, N-Dimethylaminobenzylidene-1,3-indandione in solution *Journal of Physical Chemistry* A 103 3969–80
- Karpicz R, Daskeviciene M, Getautis V, Gruodis A, Gulbinas V 2014 Electronic properties of indan-1,3-dione-carbazole-based compounds revealed by time resolved spectroscopy *Dyes* and *Pigments* 105 208–15
- Valkunas L, Gruodis A, Juodžbalis D, Urbas A 1993 Nonlinear spectral effects in films and crystals of polar molecules Molecular Crystals and Liquid Crystals 230 163–8
- 17. Valkunas L, Juodžbalis D, Urbas A, Gruodis A, Durandin A D, Silinsh E A, Klim-kans A, Larsson S **1993** Visible fluorescence on IR excitation of polar dimethylaminobenzylidene 1,3-indandione crystals *Advanced Materials for Optics and Electronics* **2**(5) 221–32

- Gruodis A, Jursenas S, Aleksa V, Kovalevskij V, Valkunas L 1998 The vibrational spectrum of N,N-dimethylaminobenzylidene-1,3-indandione- *Lithuanian Journal of Physics* 38 (2) 237–43
- Jursenas S, Kodis G, Gruodis A, Valkunas L 1996 Spectroscopy of excitons in the polar molecular crystal DMABI Advanced Materials for Optics and Electronics 6 387–90
- Jursenas S, Gruodis A, Kodis G, Chachisvilis M, Gulbinas V, Silinsh E A, Val-kunas L 1998
   Free and Self-Trapped Charge-Transfer Excitons in Crystals of Dipolar Molecules of N, N-Dimethylaminobenzylidene 1,3-Indandione Journal of Physical Chemistry B 102 1086–94
- Jursenas S, Gulbinas V, Gruodis A, Kodis G, Kovalevskij V, Valkunas L (1999) Spectroscopy of self-trapped charge-transfer excitons in polar films and crystals of N, N-dimethylaminobenzylidene 1,3-indandione (DMABI) *Physical Chemistry Chemical Physics* 1 1715–8
- 22. Kovalevskij V, Gruodis A, Juršėnas S, Balevičius M, Valkunas L **2000** Quantum chemical study of molecular geometry and estimation of the absorption spectrum of indandione-1,3 pyridinium betaine *Environmental and chemical physics* **22**(2) 84–97
- Kovalevskij V, Gruodis A, Juršénas S, Valkunas L 2000 Vibrational Spectra of Indandione-1,3 Pyridinium Betaine Environmental and chemical physics 22(2) 75–83
- Jursenas S, Kovalevskij V, Gulbinas V, Gruodis A, Kodis G, Muzikante I, Gustavsson T, Mialocq J C, Valkunas L 2001 Excitation Dynamics in Solutions, Films and Crystals of Indandione-1,3 Pyridinium Betaine Molecular Crystals and Liquid Crystals 355(1) 105–25
- Baronas P, Kazlauskas K, Gruodis A, Jankauskas V, Tomkeviciene A, Simokaitiene J, Vidas Grazulevicius J, Jursenas S 2016 High-triplet-energy carbazole and fluorene tetrads *Journal* of luminescence Amsterdam: Elsevier BV 169 256–65
- Tomkeviciene A, Grazulevicius J V, Kazlauskas K, Gruodis A, Jursenas S, Ke Tung-Huei, Wu Chung-Chih 2011 Impact of Linking Topology on the Properties of Carbazole Trimers and Dimers J. Phys. Chem. C 115 4887–97
- 27. Gudeika D, Grazulevicius J V, Volyniuk D, Butkute R, Juska G, Miasojedovas A, Gruodis A, Jursenas S 2015 Structure-properties relationship of the derivatives of carbazole and 1,8-naphthalimide: Effects of the substitution and the linking topology *Dyes and Pigments Oxford: Pergamon Press; Elsevier Science LTD* 114 239–52
- Krotkus S, Kazlauskas K, Miasojedovas A, Gruodis A, Tomkeviciene A, Grazulevicius J V, Jursenas S 2012 Pyrenyl-Functionalized Fluorene and Carbazole Derivatives as Blue Light Emitters J. Phys. Chem. C 116 7561–72
- Streckaitė S, Karpič R, Gruodis A, Dehaen W, Van Snick S, Kirkus M, Grigalevičius S, Gražulevičius J V, Gulbinas V 2016 Fluorescence quenching of indolo[3,2-b]carbazole compounds by conformational motions of attached substituents *Dyes and pigments* 133 120–6
- 30. Rimkus R, Tumkevičius S, Serevičius T, Komskis R, Ado-mėnas P, Gruodis A, Jankauskas V, Kazlauskas K, Juršėnas S 2016 Heterocyclic heptacene analogs 8H-16,17-epoxydinaphto[2,3-c:2',3'- g]carbazoles as charge transport materials *Dyes and pigments Oxford: Pergamon Press; Elsevier Science LTD* 124 133–44
- 31. Lambin P, Vigneron J P, Fonseca A, Nagy J B, and Lucas A A 1996 Atomic structure and electronic properties of a bent carbon nanotube *Synthetic Metals* 77 249–52
- 32. Chico L, Crespi V H, Benedict L X, Louie S G, Cohen M L **1996** Pure Carbon Nanoscale Devices: Nanotube Heterojunctions *Phys. Rev. Lett.* **76** 971–4
- 33. Rochefort A, Salahub D R, Avouris P **1998** The effect of structural distortions on the electronic structure of carbon nanotubes *Chem. Phys. Lett.* **297** 45–50
- 34. Prasanna de Silva A, Fox D B, Moody T S, Weir Sh M **2001** Luminescent sensors and photonic switches *Pure Appl. Chem* **73**(3) 503–11
- 35. Collins P G, Bradley K, Ishigami M, Zettl A **2000** Extreme Oxygen Sensitivity of Electronic Properties of Carbon Nanotubes *Science* **287** 1801
- Chopra S, McGuire K, Gothard N, Rao A M 2003 Selective gas detection using a carbon nanotube sensor Appl. Phys. Lett. 83 2280

References 201

37. Suehiro J, Zhou G, Hara M **2003** Fabrication of a carbon nanotube-based gas sensor using dielectrophoresis and its application for ammonia detection by impedance spectroscopy *Journal of Physics D: Applied Physics* **36**(21) L109

- Modi A, Koratkar N, Lass E, Wei B, Ajayan P M 2003 Miniaturized gas ionization sensors using carbon nanotubes Nature 424 171–4
- 39. Grimes C A, Ong K G, Varghese O K, Yang X, Mor G, Paulose M, Dickey E C, Ruan C, Pishko M V, Kendig J W, Mason A J 2003 A Sentinel Sensor Network for Hydrogen Sensing Sensors 3(3) 69–82
- 40. Kong J, Franklin N R, Zhou C, Chapline M G, Peng S, Cho K, Dai H **2000** Nanotube molecular wires as chemical sensors *Science* **287**(5453) 622–5
- 41. Monošik R, Stredansky M, Šturdik E **2012** Biosensors classification, characterization and new trends *Acta Chimica Slovaca* **5**(1) 109–20
- 42. Barone P W, Baik S, Heller D A, Strano M S **2005** Near-infrared optical sensors based on single-walled carbon nanotubes *Nature Materials* **4** 86–92
- Das S, Vikalo H, Hassibi A 2009 On scaling laws of biosensors: a stochastic approach *Journal of Applied Physics* 105 102021
- 44. Wong E W, Sheehan P E, Lieber C.M **1997** Nanobeam Mechanics: Elasticity, Strength, and Toughness of Nanorods and Nanotubes *Science* **277** 1971–5
- 45. Paladugu M C, Maneesh K, Nair P K, Haridoss P **2005** Synthesis of carbon nanotubes by arc discharge in open air *J. Nanoscience and. Nanotechnology* **5** 747–52
- Rochefort A, Avouris P, Lesage F, Salahub D R 1999 Electrical and mechanical properties of distorted carbon nanotubes *Phys. Rev.* B 60 13824–30
- 47. Gajewski S, Maneck H E, Knoll U, Neubert D, Dorfel I, Mach R, Strauss B, Friedrich J F 2003 Purification of single walled carbon nanotubes by thermal gas phase oxidation *Diamond* and Related materials 12 816–20
- 48. Fink D, Klinkovich I, Bukelman O, Marks R S, Kiv A, Fuks D, Fahrner W R, Alfonta L 2009 Glucose determination using a re-usable enzyme-modified ion track membrane sensor *Biosensors and Bioelectronics* 24 2702–6
- Fink D, Kiv A, Shunin Y, Mykytenko N, Lobanova-Shunina T, Mansharipova A, Koycheva T, Muhamediyev R, Gopeyenko V, Burlutskaya N, Zhukovskii Y, Bellucci S
   2015 The nature of oscillations of ion currents in the ion track electronics Computer Modelling and New Technologies 19(6) 7–13
- 50. Fink D, Gerardo Mun~oz H, Alfonta L, Mandabi Y, Dias J F, de Souza C T, Bacakova L E, Vacı'k J, Hnatowicz V, Kiv A E, Fuks D, Papaleo R M 2012 Status and Perspectives of Ion Track Electronics for Advanced Biosensing In: Nanodevices and Nanomaterials for Ecological Security. Series: NATO Science for Peace Series B Physics and Biophysics Eds. Shunin Yu and Kiv A (Springer Verlag:Heidelberg) 269–79
- 51. Fink D, Cruz S A, H Garcia A, G Muñoz H., Kiv A, Alfonta L, Vacik J, Hnatowicz V, Shunin Yu, Bondaruk Yu, Mansharipova A T, Mukhamedyev R I 2017 Improving the design of ion track-based biosensors NATO ADVANCED RESEARCH WORKSHOP, 14-17 AUGUST 2017, KIEV, UKRAINE DETECTION OF CBRN-NANOSTRUCTURED MATERIALS (DCBRN-2017)
- 52. Franckevicius M, Vaišnoras R, Marcos M, Serrano J L, Gruodis A, Galikova N, Gulbinas V 2012 Tautomeric forms of PPI dendrimers functionalized with 4-(40-ethoxybenzoyloxy) salicylaldehyde chromophores *Chemical Physics* 404 2–8
- Kim T-W, Choi H, Oh S-H, Wang G, Kim D-Y, Hwang H, Lee T 2009 Transistor-1 Resistor Devices for Polymer Non-volatile Memory Applications Advanced Materials 21 2497–500
- 54. Zhao E, Liu D, Liu L, Yang X, Kan W, Sun Y 2017 Unipolar nonvolatile memory devices based on the composites of poly(9-vinylcarbazole) and zinc oxide nanoparticles J Mater Sci: Mater Electron 28 11749–54
- 55. Cho B, Kim T-W, Choe M, Wang G, Song S, Lee T 2009 Unipolar nonvolatile memory devices with composites of poly(9-vinylcarbazole) and titanium dioxide nanoparticles Organic Electronics 10 473–7

- 56. Kim T-W, Oh S-H, Choi H, Wang G, Hwang H, Kim D-Y, Lee T 2008 Reliable Organic Nonvolatile Memory Device Using a Polyfluorene-Derivative Single-Layer Film IEEE Electron device letters 29(8) 852–5
- Warren R, Reifenberg J, Goodson K 2008 Compact thermal model for phase change memory nanodevices IEEE Xplore 17 June 2008 doi:https://doi.org/10.1109/ITHERM.2008.4544377
- Peschot A, Qian C, Liu Tsu-Jae King 2015 Nanoelectromechanical Switches for Low-Power Digital Computing *Micromachines* 6 1046–65 doi:https://doi.org/10.3390/mi6081046
- Hwang Ho Jung, Kang Jeong Won 2005 Carbon-nanotube-based nanoelectromechanical switch *Physica E* 27 163–75
- Wang W, Muruganathan M, Kulothungan J, Mizuta H 2017 Study of dynamic contacts for graphene nano-electromechanical switches *Japanese Journal of Applied Physics* 56 04CK05
- Kulothungan J, Muruganathan M, Mizuta H 2016 3D Finite Element Simulation of Graphene Nano-Electro-Mechanical Switches *Micromachines* 7 143 doi: https://doi.org/10.3390/mi7080143
- 62. Kim T-W, Choi H, Oh S-H, Jo M, Wang G, Cho B, Kim D-Y, Hwang H, Lee T 2009 Resistive switching characteristics of polymer non-volatile memory devices in a scalable via-hole structure *Nanotechnology* 20(2) 025201 doi: https://doi.org/10.1088/0957-4484/20/ 2/025201
- 63. Tans S J, Verscheren A R M, Dekker C **1998** Room-temperature transistor based on a single carbon nanotube *Nature* **393** 49
- 64. Ageev O A, Blinov Yu F, Iljin O I, Kolomiitsev A S, Konoplev B G, Rubashkina M V, Smirnov V A, Fedotov A A 2013 Memristor Effect on Bundles of Vertically Aligned Carbon Nanotubes Tested by Scanning Tunnel Microscopy *Technical Physics* 58(12) 1831–6
- 65. Martel R, Schmidt T, Shea H R, Hertel T, Avouris Ph **1998** Single- and multi-wall carbon nanotube field-effect transistors *Appl. Phys. Lett.* **73**(26) 2447–9
- 66. Argall F (1968) Switching phenomena in titanium oxide thin films Solid-State Electronics 11 (5) 535–41
- 67. Alibart F, Pleutin S, Guerin D, Novembre C, Lenfant S, Lmimouni K, Gamrat C, Vuillaume D 2010 An Organic Nanoparticle Transistor Behaving as a Biological Spiking Synapse Adv. Func. Mater. 20 330
- Chanthbouala A, Garcia V, Cherifi R O, Bouzehouane K, Fusil S, Moya X, Xavier S, Yamada H, Deranlot C, Mathur N D, Bibes M, Barthelemy A, Grollier J 2012 A ferroelectric memristor. *Nature Materials* 11 860–4
- 69. Feynman R P (1961) Miniaturisation Editor H. D. Gilber New York: Reinhold 282
- Vicario J, Walko M, Meetsma A, Feringa B L 2006 Fine Tuning of the Rotary Motion by Structural Modification in Light-Driven Unidirectional Molecular Motors *J. Am. Chem. Soc.* 128(15) 5127–35
- 71. Katoono R, Kawai H, Ohkita M, Fujiwara K, Suzuki T 2013 A C3-symmetric chiroptical molecular propeller based on hexakis(phenylethynyl)benzene with a threefold terephthalamide: stereospecific propeller generation through the cooperative transmission of point chiralities on the host and guest upon complexation *Chem. Commun.* 49 10352–4
- 72. Rupert D L M, Shelke G V, Emilsson G, Claudio V, Block S, Lässer C, Dahlin A B, Lötvall J O, Bally M, Zhdanov V P, Höök F 2016 Dual-Wavelength Surface Plasmon Resonance for Determining the Size and Concentration of Sub-Populations of Extracellular Vesicles Analytical Chemistry 88 9980–8
- 73. Kari O K, Rojalin T, Salmaso S, Barattin M, Jarva H, Meri S, Yliperttula M, Viitala T, Urtti A 2017 Multi-parametric surface plasmon resonance platform for studying liposome-serum interactions and protein corona formation *Drug Delivery and Translational Research* 7 228–40
- 74. Ding T, Valev V K, Salmon A R, Forman C J, Smoukov S K, Scherman O A, Frenkel D, Baumberg J J 2016 Light-induced actuating nanotransducers *Proc Nat Acad Sci USA (PNAS)* 113(20) 5503–7

References 203

 Idris N M, Jayakumar M K G, Bansal A, ZhangY 2015 Upconversion nanoparticles as versatile light nanotransducers for photoactivation applications Chem. Soc. Rev. 44 1449–78

- 76. Schwartz J-M, Gaugain C, Nacher J C, de Daruvar A, Kanehisa M **2007** Observing metabolic functions at the genome scale *Genome Biology* **8**(6) R123
- 77. Jamieson T, Bakhshi R, Petrova D, Pocock R, Imani Mo, Seifalian A M **2007** Biological applications of quantum dots *Biomaterials* **28**(31) 4717–32
- 78. Gould S J, Subramani S **1988** Firefly luciferase as a tool in molecular and cell biology *Analytical Biochemistry* **175** (1) 5–13
- Tamayo J, Kosaka P M, Ruz J J, Paulo A S, Calleja M 2013 Biosensors based on nanomechanical systems Chem. Soc. Rev. 42 1287–311
- 80. Jalili N **2010** Piezoelectric-based vibration control In: *Nanomaterial-based piezoelectric actuators and sensor* Ed Jalili N (Berlin: Springer) 419–61
- 81. Garel J, Zhao C, Popovitz-Biro R, Golgberg D, Wang W, Joselevich, E **2014** BCN nanotubes as highly sensible torsional electromechanical transducers *Nano Letters* **14** 6132–7
- 82. Barry S, O'Riordan A **2016** Electrochemical nanosensors: advances and applications *Reports in Electrochemistry* **6** 1–14
- Li Y, Liu Y, Liu J, Liu J, Tang H, Cao C, Zhao D, Ding Yi 2015 Molecularly imprinted polymer decorated nanoporous gold for highly selective and sensitive electrochemical sensors Scientific Reports 5 7699–1–8
- 84. Putzbach W, Ronkainen N J 2013 Immobilization Techniques in the Fabrication of Nanomaterial-Based Electrochemical Biosensors: A Review Sensors 13(4) 4811–40
- Dawson K, Baudequin M, O'Riordan A 2011 Single on-chip gold nanowires for electrochemical biosensing of glucose Analyst 136(21) 4507–13
- Pumera M, Sánchez S, Ichinose I, Tang J 2007 Electrochemical nanobiosensors Sensors and Actuators B: Chemical 123(2) 1195–205
- 87. Hammond J L, Formisano N, Estrela P, Carrara S, Tkac J **2016** Electrochemical biosensors and nanobiosensors *Essays Biochem.* **60**(1) 69–80
- Minaei M E, Saadati M, Najafi M, Honari H 2015 DNA Electrochemical Nanobiosensors for the Detection of Biological Agents *Journal of Applied Biotechnology Reports* 2(1) 175–85
- 89. Liu G, Lin Y **2005** Renewable electrochemical magnetic immunosensor based on gold nanoparticle labels *J. Nanosci. Nanotechnol.* **7** 1060–5
- Liu G, Wu H, Wang J, Lin Y 2006 Electroactive silica nanoparticles for biological labeling Small 2 1139–43
- Liu G, Wang J, Wu H, Lin Y 2006 Versatile apoferritin nanoparticle labels for assay of protein Anal. Chem. 78 7417–23
- 92. Kim B M, Qian S, Bau H H 2005 Filling carbon nanotubes with particles Nano Lett. 5 873–8
- 93. Cabaj J, Sołoducho J **2014** Nano-Sized Elements in Electrochemical Biosensors *Materials Sciences and Applications* **5** 752–66
- 94. Yang G, Yuan R, Chai Y Q 2008 A High-Sensitive Amperometric Hydrogen Peroxide Biosensor Based on the Immobilization of Hemoglobin on Gold Colloid/L-Cysteine/Gold Colloid/Nanoparticles Pt-Chitosan Composite Film-Modified Platinum Disk Electrode Colloids and Surfaces B 61 93–100
- 95. Tang L, Zeng G M, Shen G L, Li Y P, Zhang Y, Huang D L 2008 Rapid Detection of Picloram in Agricultural Field Samples Using a Disposable Immunomembrane-Based Electrochemical Sensor Environmental Science & Technology 42 1207–12
- 96. Turner, M, Golovko V B, Vaughan O P, Abdulkin P, Berenguer-Murcia A, Tikhov M S, Johnson B F, Lambert R M 2008 Selective Oxidation with Dioxygen by Gold Nanoparticle Catalysts Derived from 55-Atom Clusters *Nature* 454 981–3
- 97. Vlatakis G, Anderson L I, Muller R, Mosbach K **1993** Drug assay using antibody mimics made by molecular imprinting *Nature* **361** 645–7
- 98. Cai D, Ren L, Zhao H, Xu Ch, Zhang L, Yu Y, Wang H, Lan Yu, Roberts M F, Chuang J H, Naughton M J, Ren Z, Chiles T C 2010 A molecular-imprint nanosensor for ultrasensitive detection of proteins *Nature Nanotechnology* 5 597–601

- 99. Martínez-Banderas I A I, Aires A, Teran FJ., Perez J E, Cadenas J F, Alsharif N, Ravasi T, Cortajarena A L, Kosel J 2016 Functionalized magnetic nanowires for chemical and magnetomechanical induction of cancer cell death Scientific Reports 6 35786-1-11
- 100. Ivanov Yu P, Alfadhel A, Alnassar M, Perez J E, Vazquez M, Chuvilin A, Kosel J 2016 Tunable magnetic nanowires for biomedical and harsh environment applications Scientific Reports 6 24189-1-10
- 101. Oldenburg A L, Boppart S A 2010 Resonant acoustic spectroscopy of soft tissues using embedded magnetomotive nanotransducers and optical coherence tomography *Phys Med Biol.* 55(4) 1189–201
- 102. Chen R, Romero G, Christiansen M G, Mohr A, Anikeeva P **2015** Wireless magnetothermal deep brain stimulation *Science* **347**(6229) 1477–80
- 103. Romero G, Christiansen M G, Stocche Barbosa L, Garcia F, Anikeeva P 2016 Localized Excitation of Neural Activity via Rapid Magnetothermal Drug Release Advanced Functional Materials 26(35) 6471–8
- 104. Loynachan, C.N., Romero, G., Christiansen, M.G., Chen, R., Ellison, R., O'Malley, T.T., Froriep, U.P., Walsh, D.M., Anikeeva, P 2015 Targeted Magnetic Nanoparticles for Remote Magnetothermal Disruption of Amyloid-β Aggregates. Avanced Healthcare Materials 4 (14) 2100-9
- 105. Ogut E, Menguc M P, Sendur K 2013 Integrating Magnetic Heads With Plasmonic Nanostructures in Multilayer Configurations IEEE Transactions on Magnetics 49(7) 3687–90
- 106. Zhou N, Xu X, Hammack A T, Stipe B C, Gao K, Scholz W, Gage E C 2014 Plasmonic near-field transducer for heat-assisted magnetic recording *Nanophotonics* 3(3) 141–55
- 107. Devarakonda1 S B, Myers M R, Giridhar D, Dibaji S A R, Banerjee R K 2017 Enhanced thermal effect using magnetic nano-particles during high-intensity focused ultrasound *PLoS ONE* 12(4) e0175093-1-17
- 108. Maksymov I S 2016 Magneto-plasmonic nanoantennas: Basics and applications Reviews in Physics 1 36–51
- 109. Kistler S S **1931** Coherent expanded aerogels and jellies *Nature* **127**(3211) 741 http://www.dbc.wroc.pl/dlibra/applet?mimetype=image/x.djvu&sec=false&handler=djvu\_html&content\_url=/Content/31695/Nature\_3211.djvu
- 110. Fricke J 1993 The unbeatable lightness of aerogels: Take 10 parts of metal oxide, 90 parts of air, mix well and watch industry fall upon the product with glee *New Scientist* issue 1858 January <a href="https://www.newscientist.com/issue/1858/">https://www.newscientist.com/issue/1858/</a>
- 111. Sui Zh, Meng Q, Zhang X, Ma R, Cao B 2012 Green synthesis of carbon nanotube–graphene hybrid aerogels and their use as versatile agents for water purification *Journal of Materials* Chemistry 22 8767–71
- 112. Leventis N, Sotiriou-Leventis C, Zhang G, Rawashdeh AMM 2002 Nanoengineering strong silica aerogels Nano Letters 2(9) 957–60
- 113. Mohanan J L, Arachchige I U, Brock S L 2003 Porous semiconductor chalcogenide aerogels Science 307(5708) 397–400
- 114. Biener J, Hodge A M, Hamza A V 2005 Microscopic failure behavior of nanoporous gold Applied Physics Letters 87(12) 121908
- Nyce G W, Hayes J R, Hamza A V, Satcher J H 2007 J Chemistry and Materials Science 19(3) 344–6
- 116. Tappan B C, Steiner S A, Luther E P 2010 Nanoporous metal foams Angewandte Chemie International Edition 49(27) 4544–65
- 117. Leventis N, Chandrasekaran N, Sotiriou-Leventis C, Mumtaz A 2009 Smelting in the age of nano: iron aerogels *Journal of Materials Chemistry* 19(1) 63–5
- 118. Bryning M B, Milkie D E, Islam M F, Hough L A, Kikkawa J M, Yodh A G **2007** Carbon Nanotube *Advanced Materials* **19**(5) 662–4
- 119. Caps R, Heinemann U, Ehrmanntraut M, Fricke J **2001** Evacuated insulation panels filled with pyrogenic silica powders: properties and applications *High Temperatures-High Pressures* **33**(2) 151–6

References 205

120. Worsley M A, Satcher J H, Baumann Jr, Baumann Th F 2008 Synthesis and Characterization of Monolithic Carbon Aerogel Nanocomposites Containing Double-Walled Carbon Nanotubes *Langmuir* 24(17) 9763–6

- 121. Reddy M M, Vivekanandhan S, Misra M, Bhatiac S K, Mohanty A K **2013** Bio-based plastics and bionanocomposites: Current status and future opportunities *Progress in Polymer Science* **38** 1653–89
- 122. Vert M, Doi Y, Hellwich K H, Hess M, Hodge P, Kubisa P, Rinaudo M, Schue F **2012**Terminology for biorelated polymers and applications (IUPAC Recommendations 2012)

  Pure and Applied Chemistry **84** 377–410
- 123. Samir MASA, Alloin F, Dufresne A **2005** Review of recent research into cellulosic whiskers, their properties and their application in nanocomposite field *Biomacromolecules* **6** 612–26
- 124. Moniruzzaman M, Winey K I **2006** Polymer nanocomposites containing carbon nanotubes *Macromolecules* **39** 5194–205
- 125. Sinha Ray S, Okamoto M **2003** Polymer/layered silicate nanocomposites: a review from preparation to processing *Progress in Polymer Science* **28** 1539–641
- 126. Ramakrishna S, Mayer J, Wintermantel E, Leong KW 2001 Biomedical applications of polymer-composite materials: a review *Composites Science and Technology* 61 1189–224
- 127. Hule R A, Pochan D J **2007** Polymer nanocomposites for biomedical applications *MRS Bulletin* **32** 354–8
- 128. Millon L, Wan W 2006 The polyvinyl alcohol-bacterial cellulose system as a new nanocomposite for biomedical applications *Journal of Biomedical Materials Research* B 79 245–53
- 129. Wan Y, Luo H, He F, Liang H, Huang Y, Li X **2009** Mechanical, moisture absorption, and biodegradation behaviors of bacterial cellulose fiber-reinforced starch biocomposites *Composites Science and Technology* **69** 1212–7
- 130. Coleman J N, Khan U, Blau W J, Gun'ko Y K **2006** Small but strong: a review of the mechanical properties of carbon nanotube–polymer composites *Carbon* **44** 1624–52
- 131. Dalmas F, Chazeau L, Gauthier C, Masenelli-Varlot K, Dendievel R, Cavaille J Y, Forro L 2005 Multiwalled carbon nanotube/polymer nanocomposites: processing and properties Journal of Polymer Science B Polymer Physics 43 1186–97
- 132. Nieddu E, Mazzucco L, Gentile P, Benko T, Balbo V, Mandrile R, Ciardelli G 2009 Preparation and biodegradation of clay composites of PLA *Reactive & Functional Polymers* 69 371–9
- 133. Pavlidou S, Papaspyrides C **2008** A review on polymer-layered silicate nanocomposites *Progress in Polymer Science* **33** 1119–98
- 134. Biomaterials Science: An Introduction to Materials in Medicine 2004 Eds Ratner B D, Hoffman A S, Schoeri F J, Lemons J E (London: Elsevier Academic Press) 864 p
- 135. Bhatia S K, Kurian J V 2008 Biological characterization of Sorona polymer from cornderived 1, 3-propanediol Biotechnology Letters 30 619–23
- 136. Yamaguchi I, Tokuchi K, Fukuzaki H, Koyama Y, Takakuda K, Monma H, Tanaka J **2001**Preparation and microstructure analysis of chitosan/hydroxyapatite nanocomposites *Journal*of Biomedical Materials Research **55** 20–7
- 137. Becker O, Varley R J, Simon G P 2004 Thermal stability and water uptake of high performance epoxy layered silicate nanocomposites European Polymer Journal 40 187–95
- 138. Godovsky D **2000** Device applications of polymer-nanocomposites *Advances in Polymer Science* **153** 163–205
- 139. Johannson C **2011** Bio-nanocomposites for food packaging applications In: *Nanocomposites with Biodegradable Polymers* Ed Mittal V (Oxford: Oxford Scholarship) 348–67.
- 140. Rhim J-W, Park H-M, Ha C-S **2013** Bio-nanocomposites for food packaging applications *Progress in Polymer Science* **38** 1629–52
- 141. Sorrentino A, Gorrasi G, Vittoria V 2007 Potential perspectives of bio-nanocomposites for food packaging applications Trends in Food Science & Technology 18 84–95

- 142. Arora A, Padua G W **2010** Review: nanocomposite in food packaging *Journal of Food Science* **75**(1) R43–9
- 143. Kim J Y, Kim M, Kim H M, Joo J, Choi J H 2003 Electrical and optical studies of organic light emitting devices using SWCNTs-polymer nanocomposites *Optical Materials* 21 147–51
- 144. McCullen S D, Ramaswamy S, Clarke L I, Gorga R E **2009** Nanofibrous composites for tissue engineering applications *Wiley Interdisciplinary Reviews: Nanomedicine and Nanobiotechnology* **1** 369–90
- 145. Sotome S, Uemura T, Kikuchi M, Chen J, Itoh S, Tanaka J, Tateishi T, Shinomiya K 2004 Synthesis and in vivo evaluation of a novel hydroxyapatite/collagen–alginate as a bone filler and a drug delivery carrier of bone morphogenetic protein *Materials Science and Engineering* C 24 341–7
- 146. Maehara H, Sotome S, Yoshii T, Torigoe I, Kawasaki Y, Sugata Y, Yuasa M, Hirano M, Mochizuki N, Kikuchi M 2010 Repair of large osteochondral defects in rabbits using porous hydroxyapatite/ collagen (HAp/Col) and fibroblast growth factor-2 (FGF-2) *Journal of Orthopaedic Research* 28 677–86
- 147. Choy J H, Kwak S Y, Jeong Y J, Park J S **2000** Inorganic layered double hydroxides as nonviral vectors *Angewandte Chemie International Edition* **39** 4041–5

# Chapter 7 CNT and Graphene Growth: Growing, Quality Control, Thermal Expansion and Chiral Dispersion

The production of carbon nanotubes (CNTs) and graphene sheets is related to simple manipulation actions similar to production of fullerenes, different carbon allotropes and so on. The arc discharge method can be evaluated as an innovative technique for producing CNTs using graphite evaporation. Unfortunately, this technique requires significant purification and fraction separation routines which are necessary after evaporation.

An alternative CNT production method such as chemical vapour deposition (CVD) allows controlling the quality of production yield on demand. Arc discharge, laser ablation and chemical vapour deposition are three techniques useful for industrial development of CNTs in order to produce a significant amount and the required purity. Depending on the conditions of preparation, single-walled carbon nanotubes (SWCNT) or multiwalled (MWCNT) can be manufactured [1]. High vacuum technologies and magnetic field technologies are also used for purification.

# 7.1 The Iijima Method for Growing CNTs and Graphene

#### 7.1.1 Arc Discharge

Iijima et al. [2] in 1992 reported a novel carbon structure synthesized by arc discharge methods. Iijima characterized it as a carbon derivative which shows complete 'turnaround growth', involving pentagon—heptagon pairs. The main idea was expressed as follows: tubular assemblies are producing MW–CNTs with different morphologies.

In 1994, Iijima and Ichihashi [3] and Bethune [4] synthesized SWCNTs using the same route as producing MWCNTs but adding some metal particles to the carbon electrodes (using transition-metal catalysed arc discharge).

Figure 7.1 represents schematic chart of equipment for producing CNTs in He, Ar or CH4 gas environment (pressure  $20 \div 200$  Torr). The vacuumed arc discharge

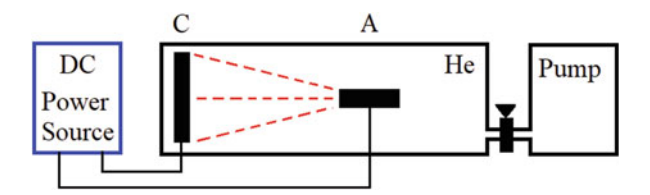


**Fig. 7.1** Schematic diagram of arc discharge chamber for producing of CNT in He surrounding. Closed electric circuit includes two graphite electrodes: cathode (C) and anode (A) – both stabile. Face-to-face orientation of electrodes, traces of plasma particles are depicted in red (Adapted according to Ref. [5])

chamber contains two graphite electrodes: cathode (C) and anode (A). Direct current up to 100 A is the reason for a high discharge temperature and the following carbon evaporation. In this case, cathode sublimation occurs.

To carry out the described experiment, several conditions must be fulfilled:

- 1. The distance between cathode and anode up to 2 mm
- 2. The orientation of surfaces of electrodes from face-to-face up to a sharp angle
- 3. The voltage between cathode and anode up to 25 V
- 4. The current up to  $50 \div 100 \text{ A}$
- 5. The density of the current up to  $100 \text{ A cm}^{-2}$

MWCNTs were grown in the cathode deposits of soot. Ando et al. [5] reviewed different arc techniques. For SWCNTs synthesis, incorporation of metallic particles in the graphite anode is necessary. Using another technique, the so-called *arc plasma jet* method, two electrodes are placed at a sharp angle. In this case, the amount of cathode deposits decreases, the amount of soot including SWCNT increases. Ando et al. [6] described the usage of the mentioned technique to get three kinds of allotropes of carbon: CNTs, disordered polyhedra and graphene sheets. The length of CNTs exceeds 50 μm, diameter up to 30 nm. Somu et al. [7] reviewed some of the important developments in the processing of CNT.

In addition to the well-known classical techniques by Iijima et al. [2–6] where direct current (DC) operates the CNT yielding, additional technique was invented in order to solve the problems of purity, homogeneity, quality, etc. Alternating current (AC) arc discharge method was reported as more effective than DC one for synthesis of SWCNT [8, 9].

Sugai et al. [10] reported the possibility of synthesis of high-quality double-walled carbon nanotubes (DWCNT). High-temperature pulsed arc discharge method was used with Y/Ni alloy catalysts at 1250 °C. Using described technique, inner and outer diameter of DWCNTs was obtained as  $0.8 \div 1.2$  and  $1.6 \div 2.0$  nm, respectively.

The task to increase the reaction yield by producing SWCNTs and DWCNTs was partially solved by means of plasma rotating in arc discharge technique. Cassel et al. [11] reported plasma rotating arc discharge technique. Figure 7.2 represents arc discharge chamber where anode (A) is rotating at a high velocity along the long axis. Cathode stays stabile. The rotation of the anode stabilizes the plasma. Due to

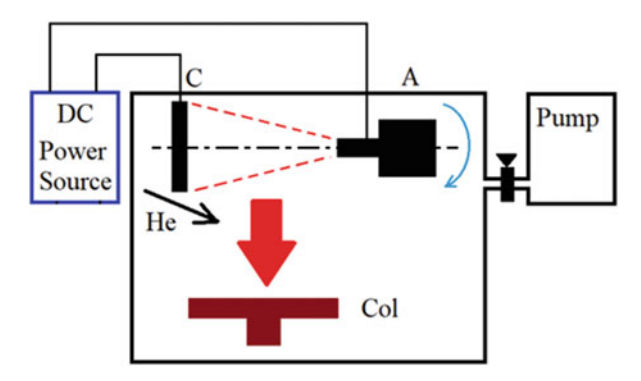


Fig. 7.2 Schematic diagram of arc discharge chamber for producing of CNT in He surrounding. Closed electric circuit includes two graphite electrodes: stable cathode (C) and anode (A), which are rotating at a high velocity along the long axis. Deposition of carbon particles occurs on graphite collector (Col) (Adapted according to [11])

centrifugal rotation forces, turbulence accelerates the particles of carbon vapour perpendicular to the anode.

Carbon vapour is collected on the collector at the periphery of the plasma. CNT increases with the increasing of rotational speed.

#### 7.1.2 Purification

Using the arc discharge method, CNT yield exceeds 50%. The deposit on cathode also contains additional amount of fullerenes, graphene sheets, disordered polyhedra, etc.

Three operations are necessary for the cleaning purposes:

- 1. The mixture of deposit and methanol must be dispersed by ultrasound until some suspension occurs.
- 2. The dispersed suspension must be diluted by water. Centrifuging separates diluted suspension into large agglomerates (deposited on the wall of centrifuge) and CNT (in suspension).
- 3. The suspension including CNT must be influenced by pure nitric acid (HNO3) and afterward must be dried by gaseous mixture containing 20% O2 and 80% H2 at temperature  $\approx$ 750 °C.

The mentioned purification technique allows getting a mixture of CNT of diameter in average 20 nm. The use of nitric acid HNO3 is related to the structure of impurities. The reactivity of hexagonal layer is much lower in comparison to pentagonal one. Pentagonal rings are involved in fullerenes, etc. Oxidizer reacts with spherical derivatives. CNTs, as ordered hexagonal structures, are inert in reaction path. The purification of DWCNTs can be achieved by oxidation in air at 500 °C [10].

#### 7.2 Arc Discharge and Induced Non-regularities

The arc discharge technique initially was invented for the synthesis of fullerenes. Direct current up to 100 A generates a high discharge temperature. The arc discharge is a rather unstable process. The current flow contains certain discontinuities, which is related to the inhomogeneity of the electric field. The spatial density of current is determined by the rapid processes of graphite particle evaporation from electrode surface. Actually, it is a time-dependent and gradient-dependent process which is impossible to control by current stabilization.

CNTs and graphene sheets were obtained in product soot as the additional product to fullerenes. As Ando et al. [5] claimed this method represents the easiest way to synthesize the CNT. Several disadvantages of the arc method occur in practice:

- (a) The pure quality of CNTs (quality is strongly dependent on the uniformity of the plasma arc).
- (b) The selection of filling gases (He, Ar, etc.) influences the growth of CNTs.
- (c) The reaction product always contains a mixture of different types of CNTs.
- (d) To remove fullerenes and amorphous carbon, several purification processes are necessary.

Eftekhari et al. [12] probed to estimate different aspects of damages in graphene structure. They told that in a sense, ideal defect less flat graphene is an analogy to diamond. The chemical reactivity decreases for an ideally ordered hexagonal structure in comparison with the damaged one. Practical interest in applications increases with increasing reactivity due to certain damages so-called crystallographic defects.

The Stone–Wales defect is related to the change of connectivity between two  $\pi$ -bonded carbon atoms with changing orientation [13]. Stone and Wales described these phenomena in 1986 on the isomerization of fullerenes [14]. Figure 7.3 represents conversion from naphthalene to fulvene with following redistribution of carbon atoms in the centrum part when two hexagons are converted into two pentagons. The previous central [..C = C..] junction changes orientation by 90° with respect to the midpoint of their bond. Reaction of this type is typical for CNT,

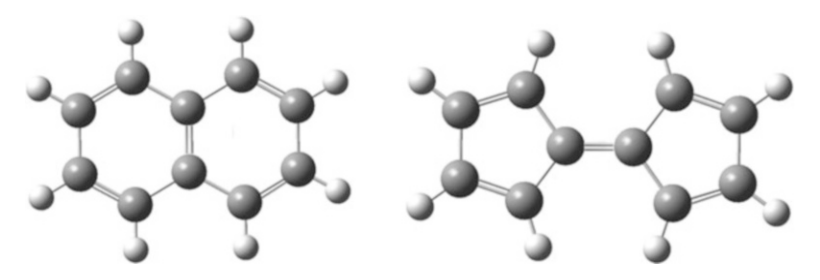


**Fig. 7.3** The Stone–Wales defect. Conversion from naphthalene to fulvene. Two hexagons are converted into two pentagons. [..C = C..] junction changes orientation by  $90^{\circ}$ 

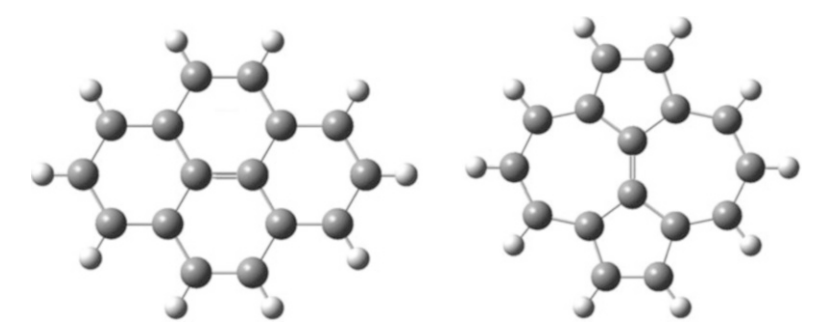


Fig. 7.4 The Stone-Wales defect in pyrene with formation of pentagon-heptagon pair

Fig. 7.5 The Stone–Wales defect in graphene sheet with the formation of pentagon–heptagon alternating pairs (green–red) (Adapted according to [16])



graphene, etc. Figure 7.4 represents Stone–Wales defect in pyrene with formation of pentagon–heptagon pair.

Figures 7.3 and 7.4 represent two structures when rearrangement structure contains a region with greater chemical reactivity. Due to large surface area, high affinity of such type defects increases the possibility of hydrogen adsorption. Letardi et al. [15] proposed to solve atomic hydrogen storing problem using graphene defects of the Stone–Wales type.

Meyer et al. [16] presented transmission electron microscopy investigation of graphene membranes. Figure 7.5 represents Stone–Wales (SW) defect with formation of pentagon–heptagon alternating pairs. Such defects, consisting of pentagon–heptagon pairs, play a key role in bonding by transformation of sp<sup>2</sup> hybridization. Figure 7.6 represents defects in a graphene sheet – an open vacancy is presented.

Figure 7.7 represents a set of non-aligned pentagon—heptagon pairs (four pentagons and four heptagons) in a graphene sheet. Meyer et al. [16] stated that in the study of defects, the vacancies are important for basic understanding of potential electronic and thermal applications.

Side effects described by Eftekhari et al. [12] are also important for analysing electronic properties of graphene sheets as well as CNT. Figure 7.8 represents a

**Fig. 7.6** A defect in a graphene sheet (Adapted according to [16])

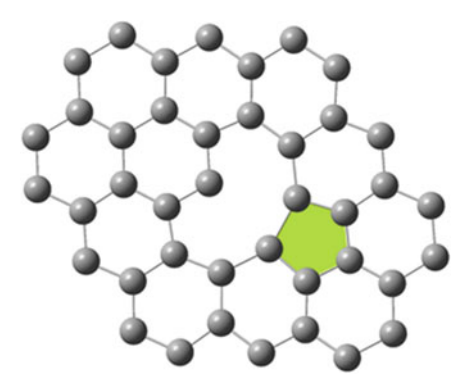
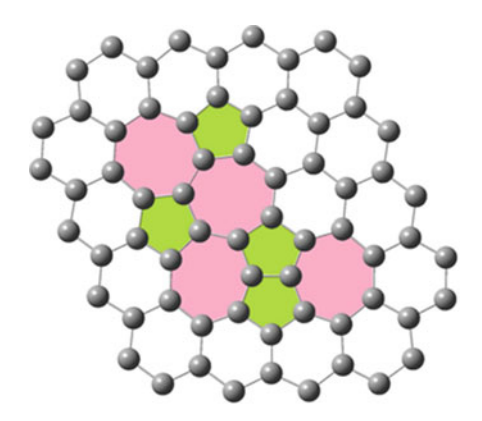


Fig. 7.7 A set of nonaligned pentagon–heptagon pairs (green–red) in a graphene sheet (Adapted according to [16])



schematic chart of graphene edge cuts. Corners (yellow), armchair (red) and zigzag (blue) arrangements are the places of interest due to increased electronic reactivity.

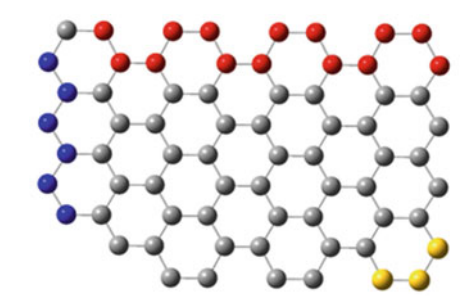
# 7.3 Laser Ablation and Self-Organization of Matter

#### 7.3.1 Laser Ablation

Laser ablation belongs to one of the most prominent techniques to manufacture CNTs and was first used by Smalley et al. [17, 18] in 1995. The main idea of this method is to use the radiation of high power laser to distinguish the high temperature at a local place of a graphite target. Vapourization from a carbon target starts immediately. The quality of the produced CNTs depends on the environment factors such as type of inert gas, temperature, pressure, type of catalysts as well as on laser power and frequency.

Figure 7.9 represents a schematic chart of the equipment for laser ablation. Radiation of YAG:Nd laser (300 mJ/pulse at 532 nm wavelength, second harmonic)

Fig. 7.8 A schematic chart of graphene edge cuts. Corners (yellow), armchair (red) and zigzag (blue) arrangements are the places of interest (Adapted according to [12])



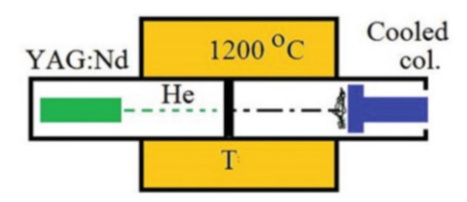


Fig. 7.9 Schematic chart of equipment for laser ablation. Radiation of YAG:Nd laser is pointed to carbon target (T). Evaporated carbon particles are collected on cooled collector (col). Environment of inertial gas (Ar or He), furnace heated until 1200  $^{\circ}$ C

is focused on carbon target (T). After focusing, the density of energy must exceed the value of 3 J/cm², when pulse duration is 8 ns. The carbon target is placed in a quartz tube furnace heated until about 1200 °C. The environment of the target consists of inertial gas at 500 Torr pressure (Ar or He). The evaporated carbon particles and the reaction products including CNTs are collected on a cooled collector (col) (self-assembling technique). The vapour condensation process on the cooled collector finishes with layer-to-layer covering as well as formation of CNT due to the influence of catalyst particles.

Using the laser ablation technique, MWCNTs can be produced from the pure graphite and SWCNTs from a composite consisting of graphite and any transition metal (nickel, cobalt, etc.). As in the case of the arc discharge technique, the graphite target must be enriched by metal particles as catalysts. The standard composition of the carbon target contains 98.8% of graphite and 1.2% of cobalt/ nickel. Using this equipment, SWCNT can be manufactured with a diameter in the range of about  $1.0 \div 1.6$  nm.

The laser ablation method allows receiving high purity of CNTs (up to 90%) in comparison to the arc discharge one. Moreover, very narrow distribution of diameters can be achieved.

Van de Burgt [19] presented a review of the current situation in the use of the laser ablation technique. Physical parameters, which influence nanotube growth (gas type, selection of catalyst and exchange of thermal energy), were commented and argued from the position of industrial manufacturing.

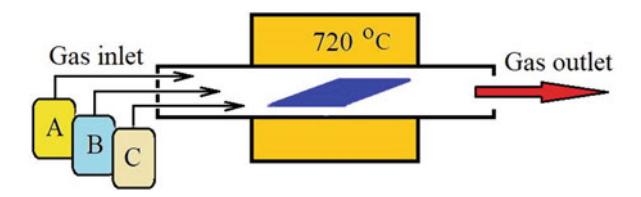


**Fig. 7.10** Schematic chart of equipment for chemical vapour deposition (CVD). Quartz tube for flow of hydrocarbons in furnace. Catalyst reactions from metal substrate Fe, Ni and Co (blue). Reservoirs A, B and C are designed for gaseous hydrocarbons (CO, C<sub>2</sub>H<sub>2</sub>, CH<sub>4</sub>) as well as for flow gases (Ar)

One of the most important factors in the laser-assisted synthesis of CNT is the possibility to employ the thermal energy of laser radiation. A great number of CW gaseous lasers such as CO<sub>2</sub>, Ar-ion, YAG:Nd,YVO<sub>4</sub>:Nd as well as diode lasers could be used.

A special case arises when the resonance frequency of the catalyst nanoparticles is equal to the laser frequency. Conditions of the surface plasmon resonance become excellent. In that case, laser light is efficiently converted into heat inside the catalyst particles. Cao et al. [20] reported the usage of low-power 532 nm CW-laser radiation for local induction of surface plasmon reaction on nanoparticles. Quick heating allows to synthesize the CNTs on nickel and gold particles.

# 7.3.2 Chemical Vapour Deposition

The catalytic chemical vapour deposition (CVD) method to produce MWCNTs was described by Endo et al. [21]. After several years, Dai et al. [22] announced CVD method to produce SWCNTs adapted CO-based CVD to produce SWNTs. CVD is the most promising method to produce CNT on industrial scale [23].

Figure 7.10 represents a schematic chart of the equipment for CVD. Carbon sources are hydrocarbon gases such as carbon monoxide (CO), acetylene ( $C_2H_2$ ), methane (CH<sub>4</sub>) and benzene ( $C_6H_6$ ). Quartz tube is designed for the flow of hydrocarbons with heating to  $600 \div 1200$  °C inside the furnace. Inertial gases such as Ar could be used as flow gases. Passing the hydrocarbon vapour through a quartz tube occurs in 60 min. The vapour of hydrocarbons is thermally decomposed at sufficiently high temperature. The presence of the metal catalyst outside the furnace initiates self-organization processes of carbon. Fe, Ni and Co as transition metals are suitable for such purposes. Catalyst material (also in liquid or gaseous form) can be placed inside the furnace. Atomized carbon is condensed by creating certain form of CNT (growing processes). Depending on the temperature, SWCNTs and MWCNTs can be produced.

Cassell et al. [24] reported the semi-continuous system for commercial production of highly crystalline and pure CNTs. Combination of the classical CVD method and the subsequent high-temperature thermal treatment takes place. Takeuuchi et al. [25] estimated the CVD method as a unique for industrial usage for large-scale production of CNT. Inami et al. [26] reported applications of alcohol catalytic CVD for growth of SWCNTs using Co catalyst film. Three types of heat treatment were investigated.

The advantages of the CVD method are the following: (1) relatively high purity in comparison to arc discharge, (2) lower temperature range and (3) low power input.

#### 7.4 Simulations of Growth: Sporadic and Stimulated

#### 7.4.1 CNT Growth Mechanism

Since the discovery of CNTs in the 1990s, their growth has been treated as an unresolved task so far. Since the demand for CNTs growth remains as the purpose for the future, industrial production of several fixed parameters for CNTs is outspread. The control of quantity and quality is connected with fundamental questions about the growth mechanism of CNTs – sporadic and stimulated. Because of the large gradients in the energy exchange processes and the difficulties that arise as a result of surface microcontrol and nanocontrol, the laser ablation method, as well as the arc discharge method, relates to sporadic methods.

Otherwise, the chemical vapour deposition (CVD) method belongs to stimulated methods (driving the experiment due to the contribution of the catalysis).

Firstly, catalysed decomposition of hydrocarbon as an exothermic process occurs at a high temperature:

$$CH_4 \to C + 2H_2O + Q. \tag{7.1}$$

The reaction begins when the hydrocarbon of the reagent enters a short contact with the catalyst. Reaction products such as atomic and/or molecular hydrogen are not involved in following reactions: they remain in the near surrounding as pollutants. After decomposition, carbon atoms cover the catalyst surface creating an amorphous film (some sort of 'dissolving' of the catalyst particle occurs).

Secondly, the coating of the metal surface with carbon is a temperature-limited and diffusely limited process. Due to that, some limit of metal covering by carbon could be achieved. By overstepping this limit, carbon starts to crystallize (endothermic process) to pass to a more energetically stable form. Now it is necessary to estimate how the substrate interacts with the catalyst. Due to the interaction strength, two types of CNT growth mechanisms are present: the tip-growth mechanism and the base-growth mechanism [27].

#### 7.4.2 The Tip-Growth Mechanism

The surface of the substrate is covered with a catalyst. Let us assume the catalyst as surface structured – spherical metal nanoparticles which could be placed on the substrate surface without forming a strong contact. Van der Waals forces keep the catalyst particle fixed using a small surface of the interconnect area. In that case, the substrate weakly interacts with the catalyst. Figure 7.11 represents several stages of reaction path, when the interaction of catalyst to substrate is weak. Hydrocarbon decomposes on the top of the nanoparticle, carbon atoms begin covering the surface of the nanoparticle starting from the top to the bottom. In such conditions, the formation of the inhomogeneous amorphous layer begins (Fig. 7.11a). Deposition continues until the top of nanoparticle is fully covered by carbons.

Due to the temperature and concentration gradients of the deposited carbon on the surface, carbon starts crystallizing to form pentagons and hexagons (fragments of fullerene) on the top (Fig. 7.11b). The process of crystallization continues from the top particle to the side particle with the formation of the fullerene hemisphere. After that, a tubular form of the carbon (CNT) starts growing. Due to interactions in the hemisphere zone, the nanoparticle is attracted to the fullerene network. Filling X area (between nanoparticle and substrate) by crystallized carbon stimulates the process of CNT growth which is related to pushing the nanoparticle off the surface of the substrate (Fig. 7.11c).

The growth of CNTs continues until a metal nanoparticle is fully covered by carbons. In this case, the catalytic activity of a metal nanoparticle decreases to zero, following crystallization interrupts. At this step, CNT growth terminates (Fig. 7.11d). This type of CNT growth from top to bottom is called the tip-growth mechanism.

#### 7.4.3 The Base-Growth Mechanism

The substrate surface is coated with a catalyst. Let's assume that the catalyst as metal nanoparticles of hemispheric type (surface structured) can be placed on the substrate surface forming a strong contact. Van der Waals forces keep the catalyst particle fixed using a large interconnect surface area. In that case, the substrate strongly interacts with the catalyst.

Figure 7.12 represents several stages of the reaction path, when the interaction of the catalyst and substrate is strong. Hydrocarbon decomposes on the top of the nanoparticle and, carbon atoms begin covering the surface of the nanoparticle starting from top to bottom.

Due to the surface properties, X zone in that case is absent. Any force to push the nanoparticle from the bottom could be organized. Crystallization starts from bottom with development of a tubular structure at the bottom (Fig. 7.12a) and continues with development of a hemisphere at the top (Fig. 7.12b). The growth of the

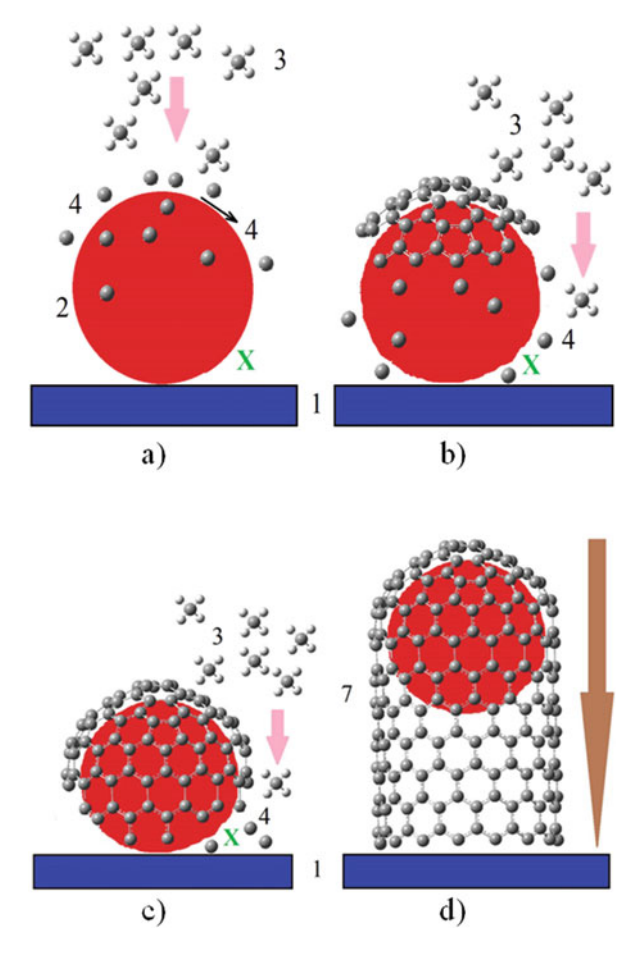


**Fig. 7.11** Tip-growth mechanism for CNTs, weak interactions between catalyst and substrate. The direction of growth (from top to bottom) is pointed by a brown arrow: (a) hydrocarbon decomposes at the surface of nanoparticle, carbon atoms cover the catalyst, formation of amorphous layer; (b) crystallization starts, part of fullerene at the top; (c) crystallization is continuing, fullerene and CNTs start growing; (d) catalyst particle is fully covered, crystallization stops. X area (area between spherical nanoparticle and substrate) is denoted as X (green). 1 – substrate (blue); 2 – catalyst as surface structured metal nanoparticle (red); 3 – hot hydrocarbon (in that case methane) is pointed to catalyst; 4 – carbon atoms (adsorbate) are covering the surface of catalyst; 5 – carbon starts to crystallize, and hemisphere of fullerene starts to form; 6 – tubular derivative starts to grow; 7 – CNT with hemisphere of fullerene, CNT growth terminates

hemisphere transforms into the growth of the tubular structure (Fig. 7.12c). The growth of CNTs continues until the metal nanoparticle is fully covered by carbons as in the previous case. At this stage, the growth of CNTs terminates (Fig. 7.12d). This type of CNT growth from bottom to top is called the base-growth mechanism.

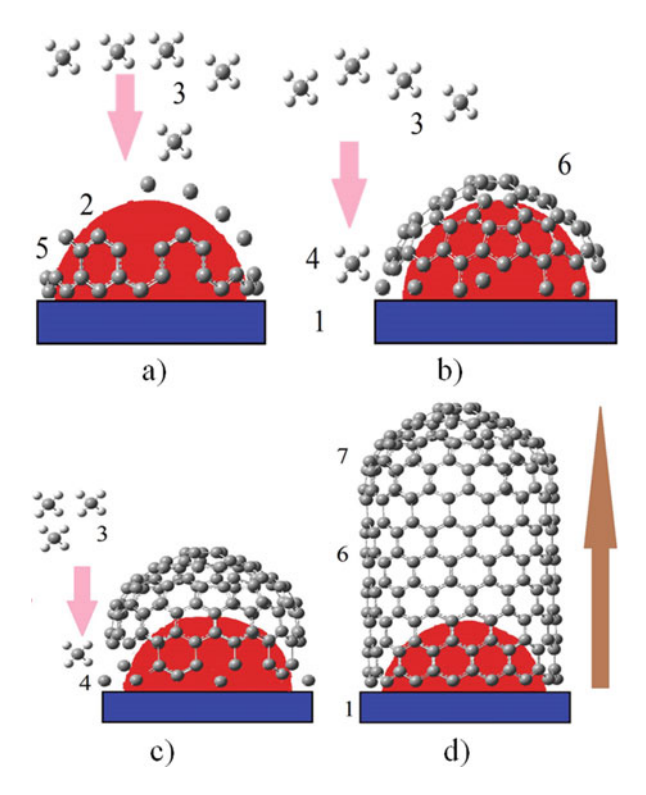


Fig. 7.12 The base-growth mechanism for CNTs, strong interactions between catalyst and substrate. Direction of growth (from bottom to top) is pointed by a brown arrow: (a) crystallization starts from bottom with generation of tubular structure; (b) crystallization continues with generation of hemisphere of fullerene on the top; (c) CNT growing from bottom continues; (d) catalyst particle at the bottom is fully covered, crystallization stops. 1 – substrate (blue); 2 – catalyst as surface structured metal nanoparticle (red); 3 – hot hydrocarbon (in that case methane) is pointed to catalyst; 4 – carbon atoms (adsorbate) are covering the surface of catalyst; 5 – carbon starts to crystallize; tubular fragments start to form; 6 – CNT starts to grow from bottom with formation of hemisphere of fullerene; 7 – CNT growth terminates

# 7.4.4 Several Control Strategies

Liu et al. [28] declared that the controlled growth of SWCNT with predefined and uniform structures remains a big challenge. Liu observed several strategies of the controlled synthesis of SWCNTs by CVD method.

The laser ablation technique is one of the most prominent in the industrial production of CNTs. Reinhardt et al. [29] described the novel equipment consisting of a nanosecond pulsed laser for the generation of transition metal oxide precursors. The catalysed growth of CNTs is ensured in gaseous species (5%  $\rm H_2$  and 95%  $\rm N_2$ ) at 800 °C. The presented technique is automated for large-scale production of CNTs on demand.

Neyts [30] reviewed a big number of techniques allowing the CNT growth: electric arc discharges, laser ablation, fullerene recrystallization, catalysed CVD (C-CVD) and plasma-enhanced CVD (PE-CVD). Neyts claimed that plasma-enhanced growth can be strongly beneficial. Several advantages of PE-CVD are present for CNT industrial producing.

- 1. Low-temperature growth. Decreasing the temperature allows excluding of generation of additional fragments which damage the tubular structure. Hofmann et al. reported MWCNT growth at 393 K temperature in DC plasma. PE-CVD experiment was organized using a Ni catalysed acetylene and ammonia system. Comparing the energy of thermal CVD (up to 1.5 eV), the PE-CVD activation energy for the growth rate was found to be 0.23 eV, six times less. Surface diffusion of carbon on nickel could be estimated as condition for growth [31].
- 2. *Effect of electric field*. Electric fields effects are useful in CNT production due to the possibility to make an alignment on demand.
- 3. Effect of plasma on the catalyst during the growth. To understand the processes of covering of catalyst surface by carbon is an interesting task in order to control the reaction pathway. Chiang et al. [32] reported the development of chirality pure SWCNTs in microplasma (pressure 10<sup>5</sup> Pa). By varying the composition of Ni<sub>x</sub>Fe<sub>1-x</sub>, nanocatalysts, chirality distribution of SWCNTs can be altered. At lower temperature, catalyst of this type may adopt a different surface structure resulting in epitaxial growth. This reference could be estimated as one possible route for chirality-selective synthesis.
- 4. Plasma chemistry effects on the catalyst during the growth. Bogaerts et al. [33] analysed plasma-enhanced growth mechanisms of CNT. In plasma chemistry, the problem of atomic hydrogen is related to the growth control. Atomic hydrogen reacts to methane molecules, creating radicals. Recombination of radicals into C<sub>1</sub>H<sub>4</sub>, C<sub>2</sub>H<sub>2</sub>, C<sub>2</sub>H<sub>4</sub>, C<sub>3</sub>H<sub>6</sub>, etc. creates inhomogeneity of the flow. Concentrations of the set of hydrocarbons in the gas phase are temperature dependent. Strong temperature regime and absence of temperature gradients allow controlling of product growth parameters on demand.

# 7.4.5 Quality Control

Raman spectroscopy belongs to the group of non-invasive non-destructive techniques for identifying the low-frequency vibrational modes in a system. Molecular systems or small clusters could be recognized by characteristic frequencies (so-called fingerprints) which occur as normal vibrations. Due to interaction between external electric field and electronic subsystem of molecule, induced dipole moment will be created. Vibrational (Raman) frequencies depend on behaviour of chemical bonds and symmetry of molecule.

Raman microspectrometry can be used to analyse structural parameters (diameter, chirality) as well as adsorption parameters (presence of adsorbates). Table 7.1 represents Raman modes which are useful for non-invasive identification of structure.

Mode	Structure	Wave number $\nu$ (cm <sup>-1</sup> )	Formula	Intensity (I)	Source
RB	SWCNT	100 ÷ 350	Eq. (7.2)	Strong	[34, 35]
	DWCNT	100 ÷ 350	Eq. (7.3)	Strong	[34, 35]
G	Graphite	1580		Strong	[36]
	SWCNT	<1580		Strong	[36]
D	Graphite	1330 ÷ 1360		Weak	[36, 37]
	SWCNT	1280 ÷ 1350		Weak	[36, 37]

Table 7.1 CNT and graphite: Raman modes

Table 7.2 Parameters of RB mode function

		A (cm <sup>-1</sup>		C (cm <sup>-1</sup>		
CNT type	Formula	·nm)	B (cm <sup>-1</sup> )	·nm)	D (cm <sup>-1</sup> )	Source
SW-RBM	Eq. (7.2)	234	10	_	_	[34, 35]
DW-RBM	Eq. (7.3)	248	0	_	_	[34, 35]
CNT metallic	Eq. (7.4)	227	$11.8 \pm 1.0$	$-2.7 \pm 1.2$	$-2.7 \pm 0.8$	[38]
CNT	Eq. (7.4)	227	$7.3 \pm 0.3$	$-1.1 \pm 0.3$	$-0.9 \pm 0.2$	[38]
semicond.						

Motion of radial contraction and following expansion represents the radial breathing mode (RB mode) of CNT [34, 35]. Wave number of RBM mode  $\nu$  is different for SWCNT and DWCNT and depends on the nanotube diameter d:

$$\nu_{\text{RBM}}^{\text{SW}} = \frac{A}{d} + B,\tag{7.2}$$

$$\nu_{\text{RBM}}^{\text{DW}} = \frac{A}{d}.\tag{7.3}$$

Jorio et al. [38] presented revised function for RB mode wave number definition where chiral angle  $\theta$  is included:

$$\nu_{\text{RBM}} = \frac{A}{d} + B + \frac{C + D(\cos 3\theta)^2}{d^2}.$$
 (7.4)

Table 7.2 represents parameters of RB mode function. Planar vibrations of carbon atoms (so-called G mode, graphite mode) are present in most graphite-like materials including CNT [36]. All graphite-like carbons which contain any structural defects could be identified by the presence of so-called D mode, disorder-induced mode [36, 37]. For high-quality nanotubes, Q > 100:

$$Q = \frac{I_G}{I_D}. (7.5)$$

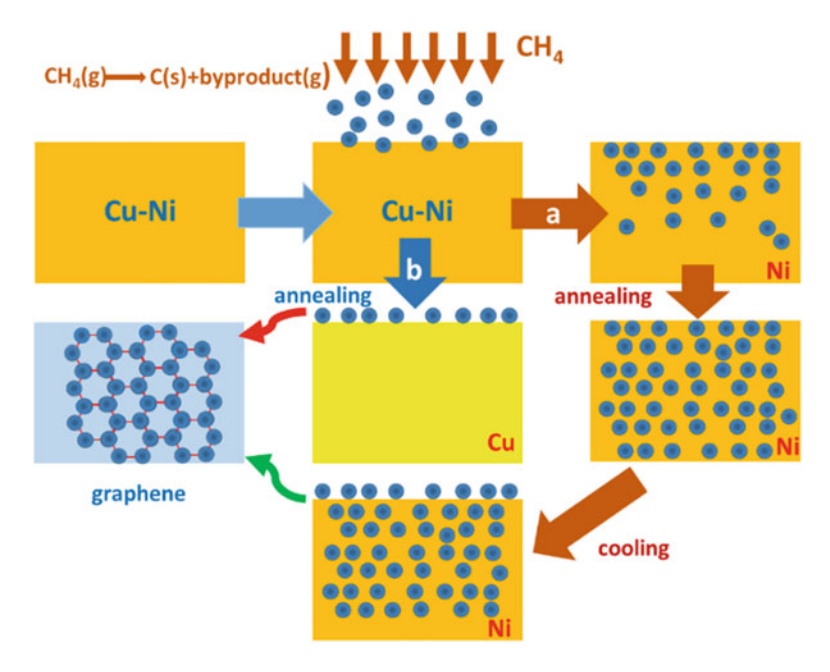


**Fig. 7.13** Graphene growth mechanisms. (a) The mechanism of dissolution–precipitation graphene growth. (b) The mechanism of direct deposition graphene growth

#### 7.5 Graphene Growth and Technological Defects

Recently, graphene has become the focus of research due to its properties. The most traditional and technologically popular technique for the synthesis of graphene is the method of chemical vapour deposition [39]. Two basic CVD graphene growth mechanisms have been proposed (see Fig. 7.13) [6, 40]:

- (a) Segregation of surface carbon atoms: It is proposed here that decomposed carbon atoms diffuse into the bulk catalyst (e.g. Ni) during the annealing stage at a high temperature. Then, carbon atoms precipitate on the catalyst during the cooling period.
- (b) Surface deposition of carbon atoms: Carbon atoms here are directly deposited on the catalyst surface (e.g. Cu) without segregation resulting in a graphene layer.

The quality and continuity of the graphene film could be affected by numerous CVD parameters such as temperature, hydrocarbon (e.g. CH<sub>4</sub>) concentration, hydrocarbon pressure and cooling rate. The graphene growth mechanism is significantly affected by catalyst type, structure, quality and carbon solubility [41]. Typical catalysts using for graphene growth are polycrystalline Co, Ni, Cu, Pt, Ir and Ru [42–44].

#### 7.5.1 Defects in Graphene

However, there are some physical and chemical conditions during CVD processes when we can observe graphene defects formation. In particular, if graphene films are synthesized by copper-catalysed atmospheric pressure chemical vapour deposition (APCVD) method using a mixture of Ar, H<sub>2</sub> and CH<sub>4</sub> gases, it was found that variations in the reaction parameters, such as reaction temperature, annealing time and growth time, affected the size of the growing graphene domain. Moreover, the reaction parameters influenced the number of layers, degree of defects and uniformity of the graphene films. The increase in growth temperature and annealing time tends to accelerate the graphene growth rate and increase the diffusion length, respectively, thereby increasing the average size of graphene domains [45].

It was experimentally found that the number of pinholes reduced with increase in the growth time. Micro-Raman analysis of the as-grown graphene films confirmed that the continuous graphene monolayer film with low defects and high uniformity can be obtained with prolonged reaction time, under the appropriate annealing time and growth temperature.

The real problem of nanoelectronics is the formation of various interconnects and direct contacts, e.g. graphene—metal, which is an actual technological task for novel electronic nanodevices. It is known that graphene—metal interconnects are characterized by the increased concentration of morphological defects (dangling bonds, spatial disordering). It is necessary to investigate and evaluate the influence of contact architecture and the density of graphene defects on the specific resistance of graphene—metal contacts to forecast electrical properties of prospective nanodevices [46].

Graphene is one of the most promising materials in nanotechnology. The electronic and mechanical properties of graphene samples with high perfection of the atomic lattice are outstanding, but structural defects, which may appear during growth or processing, deteriorate the performance of graphene-based devices. However, deviations from perfection can be useful in some applications, as they make it possible to tailor the local properties of graphene and to achieve new functionalities. In this article, the present knowledge about point and line defects in graphene is reviewed. Particular emphasis is put on the unique ability of graphene to reconstruct its lattice around intrinsic defects, leading to interesting effects and potential applications. Extrinsic defects such as foreign atoms which are of equally high importance for designing graphene-based devices with dedicated properties should be analysed. A short review of typical defects of graphene in connection with technological details is presented in Table 7.3.

 Table 7.3
 Graphene defects types

Defect type	Defect description
Point defects. Single vacancies. Stone–Wales defect	One of the unique properties of the graphene lattice is its ability to reconstruct by forming non-hexagonal rings. The simplest example is the Stone–Wales (SW) defect, which does not involve any removed or added atoms. Four hexagons are transformed into two pentagons and two heptagons by rotating one of the C_C bonds by 90° [48]
Single vacancies	The simplest defect in any material is the missing lattice atom. Single vacancies (SV) in graphene (or in the outermost layer of graphite) have been experimentally observed by TEM and STM [49]
Multiple vacancies	Double vacancies (DV) can be created either by the coalescence of two SVs or by removing two neighbouring atoms. No dangling bond is presented in a fully reconstructed DV so that two pentagons and one octagon appear instead of four hexagons in perfect graphene. The atomic network remains coherent with minor perturbations in the bond lengths around the defect [50]
Carbon adatoms	Interstitial atoms, as they appear in 3D crystals, do not exist in graphene. This is because placing an atom to any in-plane position, for example, in the centre of a hexagon, would require a prohibitively high energy. Rather than straining the local structure in two dimensions, additional atoms use the third dimension. The energetically favoured position is the bridge configuration [51]
Foreign adatoms	The effect of a foreign (noncarbon) atom on the properties of graphene depends on the bonding between the atom and graphene [52]. If the bond is weak, only physisorption due to van der Waals interaction occurs. If the interaction is stronger, covalent bonding between the foreign atom and the nearest carbon atoms leads to chemisorption
Substitution impurities	Foreign atoms can also be incorporated into graphene as substitutional impurities. In this case, the impurity atom replaces one or two carbon atoms. Boron or nitrogen serve as the natural dopants in carbon structures since they have one electron less or more, respectively, but roughly the same atomic radius. [47, 53]
Topology of defective graphene	It has been known (from the 1980s) that non-hexagonal rings induce local Gaussian curvature in a graphene sheet. In defective graphene, the arrangement of defects determines the local deviation from planarity. Defect domains might be created to induce hillocks or trenches in graphene[54]
1D Defects. Dislocation-like defects	1D defects have been observed in several experimental studies of graphene [55]. Such defects can be thought of as a line of reconstructed point defects with or without dangling bonds [55]
Defects at the edges of a graphene layer	Each graphene layer is terminated by edges with the edge atom being either free or passivated with hydrogen atoms.
	(continued

(continued)

Defect type	Defect description		
	The simplest edge structures are the armchair and the zigzag orientation [56]		
Defects in bilayer graphene	Bilayer graphene consists of two stacked monolayers which may or may not be shifted with respect to each other. Similar to graphite, the interlayer distance in bilayer graphene is approximately 3.35 Å, as dictated by the weak van der Waals interaction between the layers. [57].		
Electronic structure of graphene in the presence of defects	The electronic structure of graphene with point and line defects was studied in a considerable number of papers [58, 59]		

Table 7.3 (continued)

# 7.6 Simulation of Magnetically Stimulated CVD CNT Growth

CNTs of various chiralities open new wide possibilities for modern nanoelectronics as promising candidates for nanointerconnects in high-speed electronic nanosensoring and nanomemory devices [60–66]. We focus our current study on the implementation of advanced simulation models for a proper description of the fundamental electromagnetic properties (electrical resistance, capacitances and impedances) in contacts between carbon nanotubes of different morphologies and metallic substrates of different nature. We also present the model of magnetically stimulated CNT growth for a special case of Fe–Pt metallic nanoparticles, which have unique magnetic properties. We expect that in the presence of magnetic field, the CNTs growth will be more determined from the point of view of possible CNTs morphologies. Moreover, the creation of a CNT forest based on Pt–Fe nanoparticles provides the possibilities to consider this kind of structure as the basic fragment of nanomemory devices, where information bits are located in nanoparticles and the CNT forest provides the necessary spin transport for reading and recording information.

Thus, in our simulations, we expect to reproduce not only a CNT forest with the predefined morphology but also to develop a prototype of a nanomemory device. The adequate description of CNT chirality [61] is one of the key points for a proper simulation on electric properties of CNT-based nanoelectronic devices. Further development of the cluster approach allowed us to formulate the 'effective bonds' model [64] and to carry out a cycle of simulations on electromagnetic properties in various CNT- and graphene (GNRs – graphene nanoribbons)-based metal interconnects (Me = Fe, Cu, Ag, Pt, Au, Pd, Ni) [62, 67]. We consider that this model serves as a tool for understanding the process of CNT growth adequate to the CVD process.

#### 7.6.1 Research Motivation

The main goal of the current research is to understand if there is a relationship between the use of magnetic catalysts and the CVD growth of CNTs, taking into account that most commonly used materials for the growth of CNTs are just Fe, Co and Ni nanoparticles. The nanoparticles of these catalysts are magnetically isotropic. The key question arises: What would happen if one used, instead of Fe, Co and Ni nanoparticles, magnetically anisotropic nanoparticles such as those in the alloy Fe-Pt? The anisotropy of Fe-Pt alloy is due to a spin-orbit coupling of Fe and Pt orbitals. This coupling takes place only if the alloy is formed of alternating planes of Fe and Pt. This particular structure is called L10. In this way, because of the different sizes of the atoms of Fe and Pt, the structure is crushed, and atoms of Fe and Pt are close forming a centred tetragonal phase (fct). This approach allows for the coupling and then the magnetic anisotropy with the magnetization axis perpendicular to such planes. It is essential in this case to find conditions to control the growing CNT chirality. We also should take into account a possible substitutional disorder of Fe<sub>x</sub>Pt<sub>1-x</sub> alloy, when the stoichiometry number 'x' becomes an additional parameter of CNT growth. No doubt, the diameter of the grown CNTs is also an essential parameter, which is evidently predefined by the created nanoparticle diameter. But again, we should discuss some limitations in the creation of Fe-Pt nanoparticle sizes in connection with the Fe-Pt melting point. However, Fe-Pt nanoparticles demonstrate an extremely strong coercing field, and this promises definite hopes for the controlled CNT growth in the CVD process. We also consider the CVD process of CNT growth as a more predictable one from the point of view of the expected growing CNT parameters (diameter, chirality, morphology of SW or MWCNTs).

Our experience with the nanotubes synthesis by means of the arc discharge brought about large doubts in the possibilities of CNTs growth control. Two cathodes of pure graphite (99.7%) were taken  $\phi=6$  mm (cathode) and  $\phi=10$  mm (anode) in diameter. Carbon black was added to iron–platinum powder, and after which the mixture was introduced to complete the filling of the hole. At this point the whole mass was placed in the room. The synthesis was carried out according to the parameters presented here: current 90 A, voltage ~18  $\div$  20 V DC, vacuum ~2  $\times$   $10^{-4}$  mbar, gas: He, work pressure 600 mbar and arc duration ~15 min.

Some filaments also exit from the outer wall of the cathode but in smaller quantities than found on the anode. The residue of the deposit formed on the upper part of the synthesis chamber was collected. It appeared to be quite little compared to other discharges with other catalysts (Figs. 7.14 and 7.15).

Figure 7.15 shows that filaments are of different nature – some formats are created from these spheres, and others have very fine structures of a few nanometers, probably single-walled nanotubes, covered by these spheres, partly or totally. The question is *what percentage of nanoparticles was originally made or how much* 

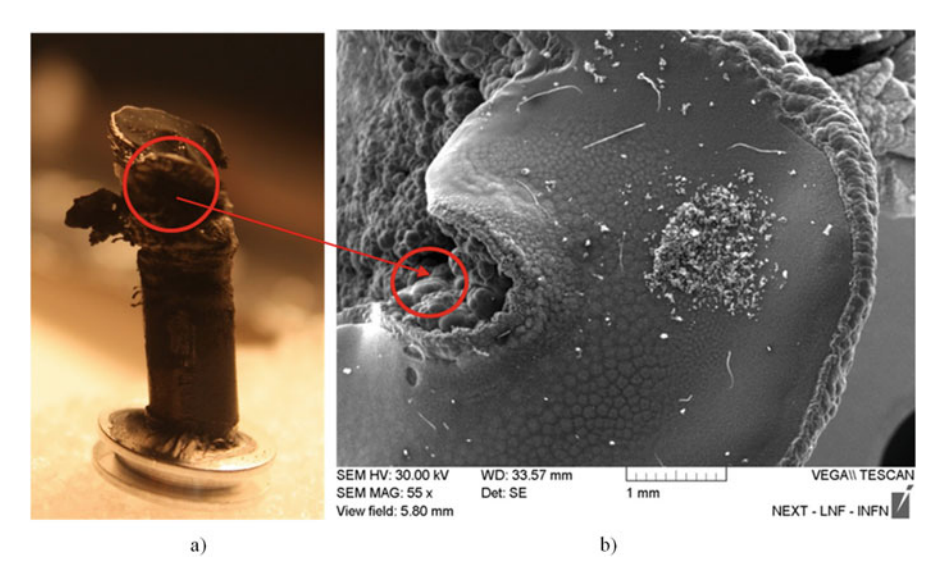


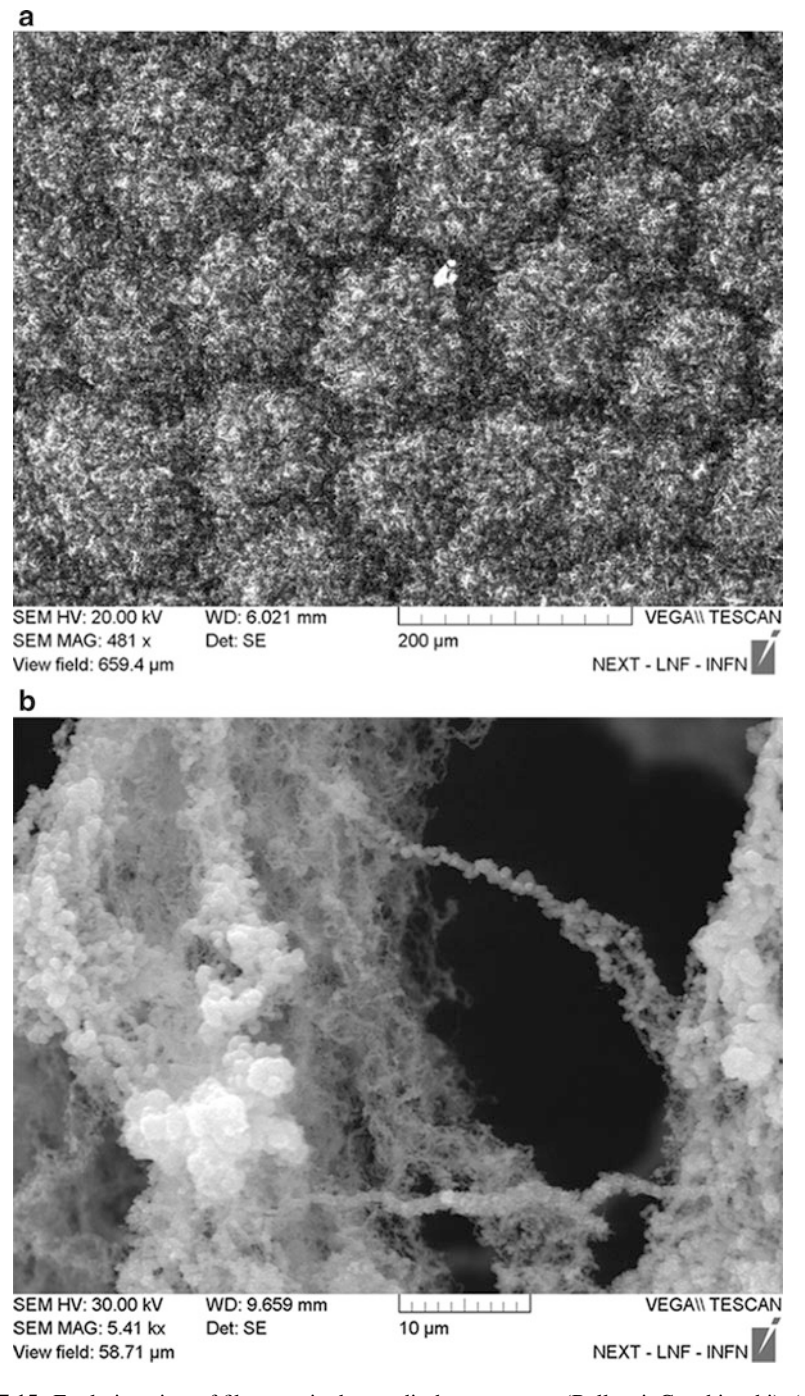
Fig. 7.14 (a) Photo of the cathode filaments exiting out after the synthesis, (b) SEM photo of the cathode surface

iron and platinum and how this underwent a change, during the arc discharge process?

We also take into account the extremely marginal parameters of the Fe–Pt system: Pt has the melting point at  $T=2041.4~\rm K~(1768.2~^\circ C)$  and the boiling point at  $T=4098~\rm K~(3825~^\circ C)$ .

There are four major crystal structure modifications for Fe: below 769 °C (Curie temperature), it is  $\alpha$ -Fe ( $\alpha$ -ferrite) with a body-centred cubic crystal structure and ferromagnetic properties. Ferrite above the critical temperature (769–917 °C) is beta-ferrite ( $\beta$ -Fe) where it is paramagnetic rather than ferromagnetic, and it is crystallographically identical to  $\alpha$ -Fe. Within the interval of 917–1394 °C, it is  $\gamma$ -Fe (austenite) with acicular cubic crystal structure. At temperatures between 1394 °C and 1538 °C, the body-centred cubic crystal structure is a more stable form of delta-ferrite ( $\delta$ -Fe), the melting point 1538 °C (1811 K) and the boiling point at T=3273 K (3000 °C).

Our earlier research proved that close to the arc, the temperature ranges between 4000 and 6000 K and there is a subsequent rapid temperature gradient decrease with the distance from it. Filaments are found nearby the arc itself, more precisely, upstream of it. Taking into account the essentially nonsteady character of the arc discharge process and very high working temperatures, the CNT growth control is practically impossible, and CNT morphologies are nonpredictable.



 $\begin{tabular}{ll} Fig. 7.15 & Evolution view of filaments in the arc discharge process (Bellucci-Capobianchi): (a-c) \\ [68-71] & \end{tabular}$ 

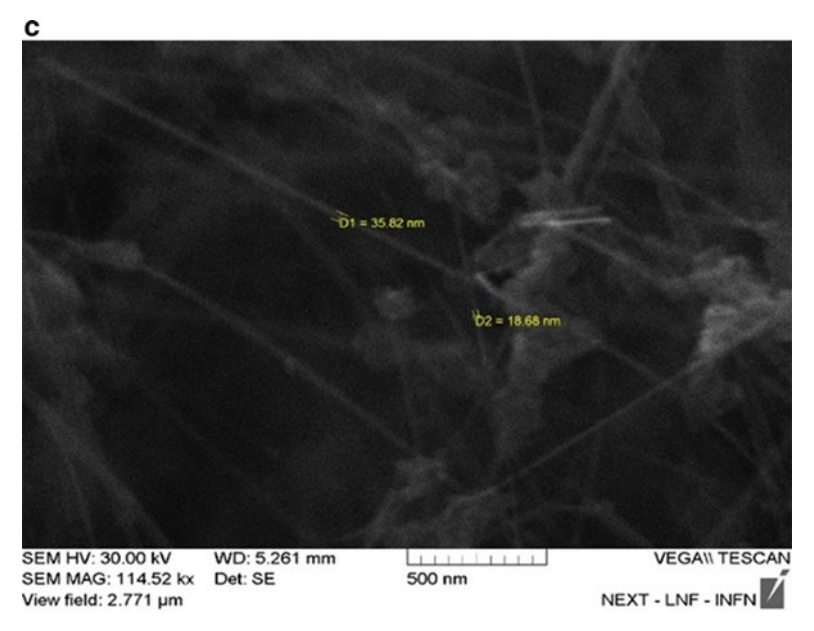


Fig. 7.15 (continued)

# 7.6.2 CNT Growth in the Chemical Vapour Deposition Process Based on Metal Nanoparticles

The CVD (chemical vapour deposition) is a highly versatile approach to producing nanotubes and is, perhaps, the most commonly published technique for nanotube growth often used to synthesize CNTs for commercial applications. The process involves decomposition of a carbonaceous precursor at high temperatures under oxygen-free conditions and reduced atmosphere to produce nanotubes.

CVD process begins with previously made supported catalyst material placed in a furnace. A flow of gaseous carbon precursor is introduced for a given time period follows the heating of the furnace till the appropriate reaction temperature. Heating periods can reach several hours. The reaction product is collected from the reactor walls and support surfaces after cooling. There are various experimental conditions for CVD realization in SWCNTs production procedure. Catalyst and carbon precursors, flow rates, reaction temperatures and batch run times together with support materials are presented when available. There are two growth mechanisms in the CVD process: root (base) and tip growth. In root growth, the catalyst particle stays pinned at the support surface and the support – particle interaction must be taken into consideration. In the tip growth, the catalyst is lifted off from the support surface during CNT growth due to weak support – catalyst interaction. Evaporation of the catalyst metal may take place during CVD synthesis due to the physical

properties of nanosized catalyst particles (nanodrops). The vapourized metal may nucleate and form secondary metal particles away from the surface. The catalytic decomposition reaction may then take place in the gas phase on the surface of the newly formed particles. This product is eventually deposited on the reactor walls.

#### 7.6.3 CVD Process Analysis

The chemical vapour deposition (CVD) process involves decomposition of a carbonaceous precursor at high temperatures. The carbonaceous precursor may be a carbon gas, methane or ethylene, for instance, or it can be in the form of a volatile hydrocarbon solvent such as ethanol, which is generally fed into the reactor with some inert carrier gas. In the reaction chamber, the precursor is decomposed in the presence of a catalyst – usually a transition metal such as iron, cobalt or some similar combination of metals. The catalyst can be introduced in a number of different ways.

The substrate needs to have catalyst nanoparticles providing the growth of CNTs where nanoparticles present the place from which nanotubes start growing. Nanoparticles can be composed of lots of different substances (usually, a metal like Fe, Co, Ni Co, Mo, Mn, Pd, etc.) [72].

The substrate is then heated to the temperature of about 700–800  $^{\circ}$ C under  $H_2$ . As the nanoparticles heat up, the hydrogen pulls oxygen out from the nanoparticles, leaving behind metallic nanoparticles.

At the target temperature, a carbon-containing gas such as ethylene (or some others, e.g. alcohol vapour) is introduced. At these temperatures, the gas partly decomposes, giving carbon-containing fragments and other molecules. These fragments and molecules then work their way onto the catalyst nanoparticles, where they stick and then break down into carbon. The carbon dissolves with some probability into or on the nanoparticle. When a critical concentration of carbon is reached in the nanoparticle, the addition of just a little bit more carbon from the vapour causes carbon to precipitate as a crystal.

When carbon crystallizes under the atmospheric pressure (like in CVD), it crystallizes into flat sheets of hexagonally patterned carbon. But because the nanoparticle is so small and has such a high curvature, when the carbon crystallizes out, it is constrained into a cylindrical shape in the form of a carbon nanotube.

Additional carbon atoms on the nanoparticle provide further nanotube growth, which stops when the carbon-containing gas is turned off if the substrates cool down or for a number of other reasons that can influence the nanotube or catalyst nanoparticles.

Tuning the appropriate parameters, it is possible to obtain a huge amount of CNTs in a cheap and quick way. Also it is the technique enabling the growth of CNTs with specific characteristics: particular diameter, length and orientation (alignment) and family (multi- or single wall).

Catalys			Temperature (°C)	Carbon source
Metal	Catalyst type	Preparation method	Temperature ( C)	source
Fe	Ultrafine particle	Decomposition of metallocene	1,060	Benzene
	Silica support	Pore impregnation	700	Acetylene
	Zeolite or clay support	Ion exchange	700	Acetylene
	Graphite support	Impregnation	700	Acetylene
	Ultrafine particle	Decomposition metal of carbonyl	800	Acetylene
	Silica support	Sol-gel process	700	Acetylene
Co	Ultrafine particle	Laser etching of Co thin film	1,000	Triazine
	Ultrafine particle	Decomposition metal of carbonyl	800	Acetylene
	Silica support	Pore impregnation	700	Acetylene
	Zeolite or clay support	Ion exchange	700	Acetylene
	Graphite support	Impregnation	700	Acetylene
Ni	Graphite support	Impregnation	700	Acetylene
	Ultrafine particle	Decomposition of Ni (C <sub>8</sub> H <sub>12</sub> ) <sub>2</sub>	800	Acetylene
Mo	Ultrafine particle	Decomposition of Mo*a	800	Acetylene
Mn	Ultrafine particle	Decomposition metal of carbonyl	800	Acetylene
Pd	Ultrafine particle	Decomposition metal of carbonyl	800	Acetylene

**Table 7.4** Most commonly used catalyst metals for the CVD method [73, 75]

It has been well known for a long time that carbon nanotubes are synthesized by catalytic decomposition of hydrocarbon [73] in the reactor, where metal nanoparticles are presented as a catalyst on a substrate. Catalyst metals mostly used for these purposes are listed in the following Table 7.4. Hydrocarbon such as methane adsorbed on the catalytic particle surface releases carbon during decomposition, which dissolves and diffuses into a metal particle. When a supersaturated state is reached, carbon precipitates in a crystalline tubular form.

It is necessary to emphasize that it will be possible to grow CNTs using a gas, both as a catalyst and as hydrocarbon. If a stream of catalyst particles can be injected into the flowing feedstock, it is possible to produce nanotubes in the gas phase. This approach is amenable for scale-up to large-scale production. Sen et al. [74] first reported such a possibility when they used ferrocene or nickelocene as a source of the transition metal and benzene as a carbon source.

This approach yielded MWNTs, whereas their later work [76] with gas-phase pyrolysis of acetylene using a metallocene yielded SWNTs with diameters around 1 nm [75]. CVD-produced CNTs are curved and have high amount of defects,

 $<sup>{}^{</sup>a}Mo^{*} = (NH_{4})_{25 \pm 5}[Mo_{154}(NO)_{14}O_{420}(OH)_{28}(H_{2}O)_{70}] 350H_{2}O$ 

mainly after the purification in the acid bath; it is needed to remove metal nanoparticles inside of tubes.

The main interests related to iron-containing nanoparticles are focused on their potential applications as high-quality magnetic materials. Thus, a new generation of iron-metal nanoparticles is studied to be used as a catalyst in growing CNTs, with a magnetic nanomaterial inside, making it possible to design a precise carbon nanomagnetic device for drug delivery diagnostics.

For example, iron nanoparticles have been widely used as a catalyst for CVD synthesis of multiwalled carbon nanotubes, [77] while iron–molybdenum can act as a very efficient catalyst for the synthesis of either single-walled or multiwalled carbon nanotubes with the CVD method [78–83].

To prevent the magnetic behaviour of these iron nanocompounds, it is necessary to grow carbon nanotubes of nanocompounds below the Curie temperature. Typically, the growth temperature is around 600–700 °C at the atmospheric pressure [84].

The potential applications of carbon nanotubes grown for semiconductor and sensor devices are presented for CMOS industrial applications [85]. The low-temperature growth of vertically aligned carbon nanotubes (CNTs) at high growth rates by a photothermal chemical vapour deposition (PTCVD) technique using a Ti/Fe bilayer film as a catalyst is presented in [86]. The bulk growth temperature of the substrate is as low as 370 °C, and the growth rate is up to 1.3 μmmin<sup>-1</sup>, at least eight times faster than the values reported by traditional thermal CVD methods. It should be recognized that the mechanism of CNTs growth is not obvious enough. Technological growth characteristics may differ in detail, although the concept remains the same. The mechanism of carbon atom deposition on metal catalyst nanoparticles with the subsequent nucleation of CNTs can be considered one of the most effective and practically important. Crystal (e.g. Si) nanoparticles with a set diameter created on a substrate give a high probability of producing CNTs with the regulated diameter. However, the problem of controlling the chirality of CNTs remains a pressing one. Among more effective catalysts, it is possible to distinguish Pt, Pd, Cu, Ag, Au, Si, SiC, Ge and Al<sub>2</sub>O<sub>3</sub> [87] in addition to the earlier investigated Mg, Ti, Cr, Mn, Fe, Co, Ni, Sn and Pb [88–90](see also Table 7.5).

# 7.6.4 Advantages of CVD

Compared to the discharge and laser ablation methods, CVD is a simple and economic technique for synthesizing CNTs at low temperatures and ambient pressures. Arc- and laser-grown CNTs are superior to the CVD-grown ones. In yield and purity, CVD has advantages over the arc and laser methods. Considering CNTs in relation to structure or architecture control, CVD is the only answer. CVD is versatile in the sense that it offers harnessing plenty of hydrocarbons in any state (solid, liquid or gas), enables the use of various substrates and allows CNT growth

		SWCNT size	Catalysis for	Carbon	Growth temperature for	Growth
Type	State	for growth (nm)	cracking	solubility	ethanol (°C)	rate
Fe, Co, Ni	Liquid/ solid	<10	Yes	High	600–950	High
Pt, Pd	Liquid/ solid	<5	No?	High	850–950	High
Au, Ag, Cu	Liquid/ solid	<5	No	Low	850–950	High
Ge	Liquid/ solid	<5	No	Low?	850–950	Low?
Si, SiC	Solid	<5	No	No?	850–950	Low
$Al_2O_3$	Solid	<5	No	No	850-950	Low

**Table 7.5** Comparison of catalysts for SWCNTs growth [88–90]

in a variety of forms, such as powder, thin or thick films, aligned or entangled, straight or coiled nanotubes or a desired architecture of nanotubes on predefined sites of a patterned substrate. It also offers better control over the growth parameters zone, while carbon crystallization (being an endothermic process) absorbs some heat from the metal precipitation zone. This precise thermal gradient inside the metal particle keeps the process going on. This last advantage is the most essential one [87]. Taking only two main CNT parameters, namely, CNT diameter and chirality, the problem cannot be solved well enough. There are two marginal cases of CVD growth.

Tip-growth model – the catalyst–substrate interaction is weak (metal has an acute contact angle with the substrate); hydrocarbon decomposes on the top surface of the metal; carbon diffuses down through the metal, and CNT precipitates out across the metal bottom, pushing the whole metal particle off the substrate; as long as the top of the metal is open for fresh hydrocarbon decomposition, CNT continues to grow longer and longer; the metal is fully covered with the excess carbon and its catalytic activity ceases and the CNT growth stops.

Base-growth model – the catalyst–substrate interaction is strong; initial hydrocarbon decomposition and carbon diffusion take place similar to that in the tip-growth case; the CNT precipitation fails to push the metal particle up, so the precipitation is compelled to emerge out of the metal apex; carbon crystallizes out as a hemispherical dome, which then extends up in the form of seamless graphitic cylinder; subsequent hydrocarbon deposition takes place on the lower peripheral surface of the metal, and a dissolved carbon diffuses upward; CNT grows up on the catalyst nanoparticle base.

#### 7.6.5 CNT Precursors

Most commonly used CNT precursors are methane [91, 92], ethylene [76, 78] acetylene [93], benzene [78] xylene [94] and carbon monoxide [95].

SWCNTs were first produced from the disproportionation of carbon monoxide at 1200 °C, in the presence of molybdenum nanoparticles [22], and later they were produced from benzene [96], acetylene [76], ethylene [97], methane [98], cyclohexane [99] and fullerene [100] by using various catalysts. It means that the working temperature and pressure of the CVD process can be changed in a wide range of ways and the kinetics of carbon atoms deposition can also be widely varied.

In 2002 the low-temperature synthesis of high-purity SWCNTs from alcohol on Fe–Co-impregnated zeolite support was carried out [101], and since then, ethanol has become the most popular CNT precursor in the CVD method worldwide [102–104].

A special interest in binary catalysts becomes principal now. The unique feature of ethanol is explained by the fact that ethanol-grown CNTs are almost free from amorphous carbon, owing to the etching effect of OH radical [105]. Later, vertically aligned SWCNTs were also grown on Mo–Co-coated quartz and silicon substrates [106, 107]. It has been shown that intermittent supply of acetylene in ethanol CVD significantly assists ethanol in preserving the catalyst activity, thus, enhancing the CNT growth rate [108].

Generally, low-temperature CVD (600–900 °C) yields MWCNTs, whereas high-temperature (900–1200 °C) reaction favours SWCNT growth. It means that SWCNTs have a higher energy of formation (presumably owing to small diameters and the fact that high curvature bears high strain energy). Probably, this is the reason that MWCNTs are easier to grow than SWCNTs.

Recent developments in the nanomaterials synthesis and characterization have enabled many new catalysts for the CNTs growth. Apart from popularly used transition metals (Fe, Co, Ni), a range of other metals (Cu, Pt, Pd, Mn, Mo, Cr, Sn, Au, Mg, Al) have also been successfully used for horizontally aligned SWCNT growth on quartz substrates [109]. It has been also proposed that the active catalyst is Au–Si alloy with about 80 at% Au [110].

#### 7.6.6 CNT Growth Control

It is a general experience that the catalyst particle size dictates the tube diameter. The particle size dependence and a model for iron-catalysed growth of CNTs have been reported in [111]. Metal nanoparticles of the controlled size, pre-synthesized by other reliable techniques, can be used to grow CNTs of the controlled diameter [112].

*Influence of a catalyst material and concentration.* The additional advantage of using the bimetallic catalyst is that CNTs can be grown at a much lower

temperature  $-550\,^{\circ}$ C. For example, the melting point of the mixture of Fe and Co is lower than their individual melting points. Moreover, alloys are known to be better catalysts than pure metals. These trends suggest that tri-metallic catalysts should also give interesting results, though the interpretation of the results would be more complicated.

Influence of temperature. There are investigations of the temperature effect on camphor CVD in a wide range of temperatures 500-1000 °C [113]. It was noticed that camphor did not decompose below 500 °C. At 550 °C very shortlength tubes emerged from the zeolite pores suggesting that the catalyst activity, and hence the CNT growth rate, was quite low at 550 °C. However, the CNT growth abruptly increased at 600 °C, and a profound growth was observed all around the zeolite pores. At 650 °C and above, the growth rate was so enormous that hardly a zeolite particle could be located amid nanotubes. The CNT diameter is increased with the growth temperature increase. Very pure CNTs, almost free from metallic impurity, were produced up to 750 °C. From 750 °C onward, both the diameter and the diameter distribution range increased drastically. It is supposed that at high temperature, the metal atoms agglomerate into bigger clusters leading to thick CNTs. At 850 °C and above, SWCNTs began to take shape alongside with MWCNTs, and the volume of SWCNTs increased with the increasing temperature. For instance, at 900 °C, samples of large bundles of SWNTs can be observed. The CVD temperature plays the central role in CNT growth. For a fixed metal concentration, the increasing CVD temperature enlarges the diameter distribution. It should also be noted that MWCNTs and SWCNTs can be selectively grown as a function of CVD temperature if the catalyst concentration is properly optimized [113, 114].

Influence of pressure. For the controlled growth of CNTs by CVD, the vapour pressure of the hydrocarbon in the reaction zone is another very important parameter. For gaseous hydrocarbons, a desired vapour pressure in the CVD reactor can be maintained by a limited gas flow rate and the controlled suction with a rotary pump [115]. In the case of a liquid hydrocarbon, its vapour pressure is controlled by its heating temperature before it enters the reactor [116]. However, for a solid hydrocarbon such as camphor, it is quite problematic to control its vapour pressure. It becomes a function of three parameters: camphor mass, its vapourization temperature and the flow rate of argon – the carrier gas. By proper optimization of these three parameters, the influx of camphor vapour to the zeolite bed and its decomposition rate were balanced to a great extent, and a record growth of MWCNTs was achieved at atmospheric pressure by CVD. Pure SWCNTs (free from MWCNTs) have been selectively obtained from camphor CVD at low pressures (10–40 Torr) where the camphor vapour pressure is quite in tune with the low metal concentration [117]. It is important to note that the melting point of nanoparticles below 10 nm falls abruptly, e.g. 5 nm Fe and Co particles can melt at about 850 °C and 640 °C, respectively. It leads to essential limitations in the CVD process of small diameter (< 5 nm) CNTs growth.

Schematic representation of the basic steps of SWCNT growth on a metal catalyst is usually simulated in three steps [118]:

- 1. The diffusion of single C atoms on the surface of a catalyst.
- 2. The formation of an  $sp^2$  graphene sheet floating on the catalyst surface with edge atoms covalently bonded to the metal.
- 3. The root incorporation of diffusing single C atoms. It has been shown that carbon atoms diffuse only on the outer surface of the metal cluster. At first, a graphene cap is formed which floats over the metal, while the border atoms of the cap remain anchored to the metal. Subsequently, more C atoms join the border atoms pushing the cap up and, thus, constituting a cylindrical wall.

# 7.6.7 Magnetically Stimulated CNT CVD Growth on Fe-Pt Catalysts

The key question for a CVD process of CNTs growth is the formation of initial interconnects between substrates (catalyst nanodrops). This step predefines the future morphology of the created CNTs. Computer simulation of CNT-metal interconnects is an effective way in formulation of technological recommendations. Our systemic theoretical approach in a wide scale simulations and modelling is based on multiple scattering theory and effective media approximation [119]. This is a reasonable and constructive way to solve a set of marginal condensed media problems in cases of essential structural disordering.

### 7.6.8 Effective Bonds Model for CNT-Fe-Pt Interconnect Electromagnetic Properties

CNT-Fe-Pt interconnect atomistic structures are in compliance with the proposed 'effective bonds' model. The 'effective bonds' are responsible for mechanical, electronic, magnetic and electrical properties of interconnects. The common consideration of two marginal carbon structures (CNTs and GNRs) is induced by the similar technological problems in respect of these materials for the modern nanoelectronics [120].

We have developed structural models for CNT–Me and GNR–Me junctions, based on their precise atomistic structures of clusters, which take into account the CNT chirality effect and its influence on the interconnect resistance for Me (= Fe, Ni, Cu, Ag, Pd, Pt, Au) as well as the predefined CNT (or GNR) geometry. These atomistic structures are in compliance with the proposed 'effective bonds' model.

Our main interest in this particular case is focused entirely on CNT-Me interconnects, when the modelling of CNT growth on metal surfaces is combined with the controlled electromagnetic properties in the interconnect area. To ensure a predictable interconnect morphology, the permanent magnetic field is used that accompanies the growth, and magnetic drops are used as growth catalysts that provide for the special composition of Fe-Pt with unique magnetic properties. The results of our simulations show that interconnects resistance and the number of effective bonds can be considered as indicators of chirality. Figures 7.16, 7.17, 7.18, 7.19 and 7.20 demonstrate the numbers of effective bonds via CNT diameters, chirality angles and CNT–Me interconnect resistances and impedances. It means that resistances and the number of effective bonds in the interconnect space are indicators of CNTs morphology.

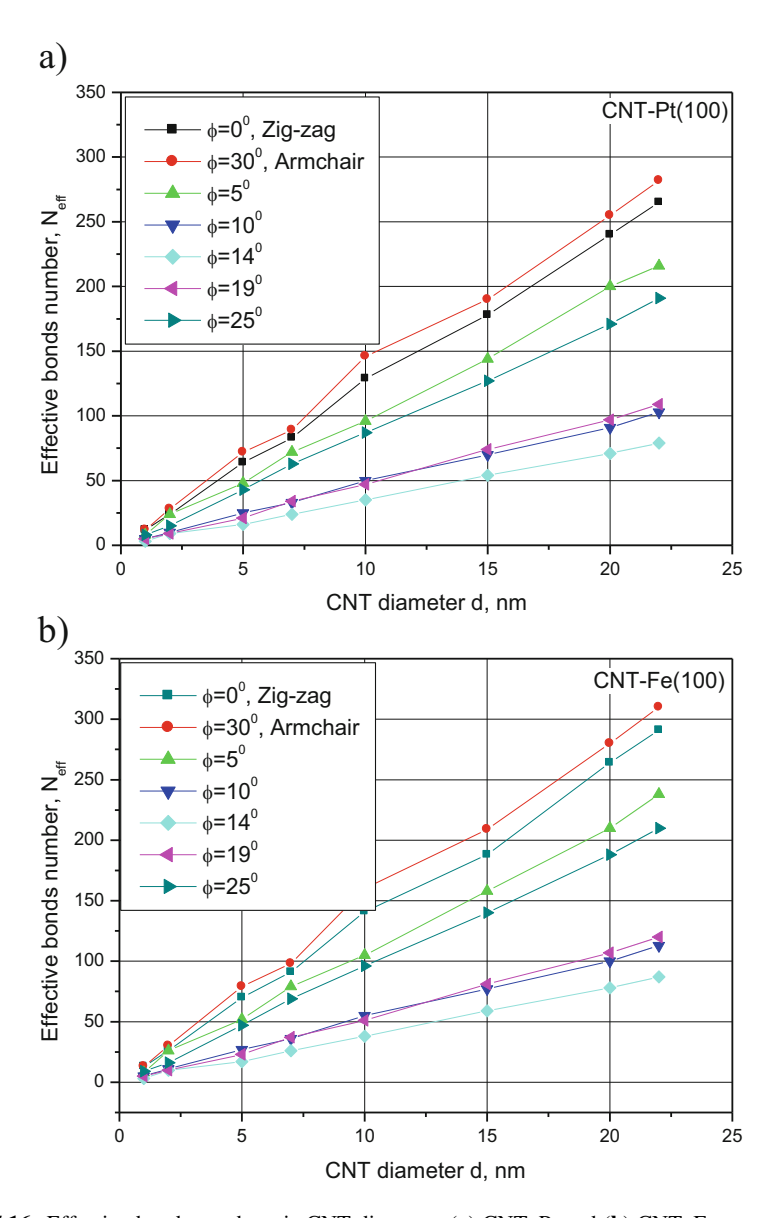


Fig. 7.16 Effective bonds number via CNT diameter: (a) CNT-Pt and (b) CNT-Fe

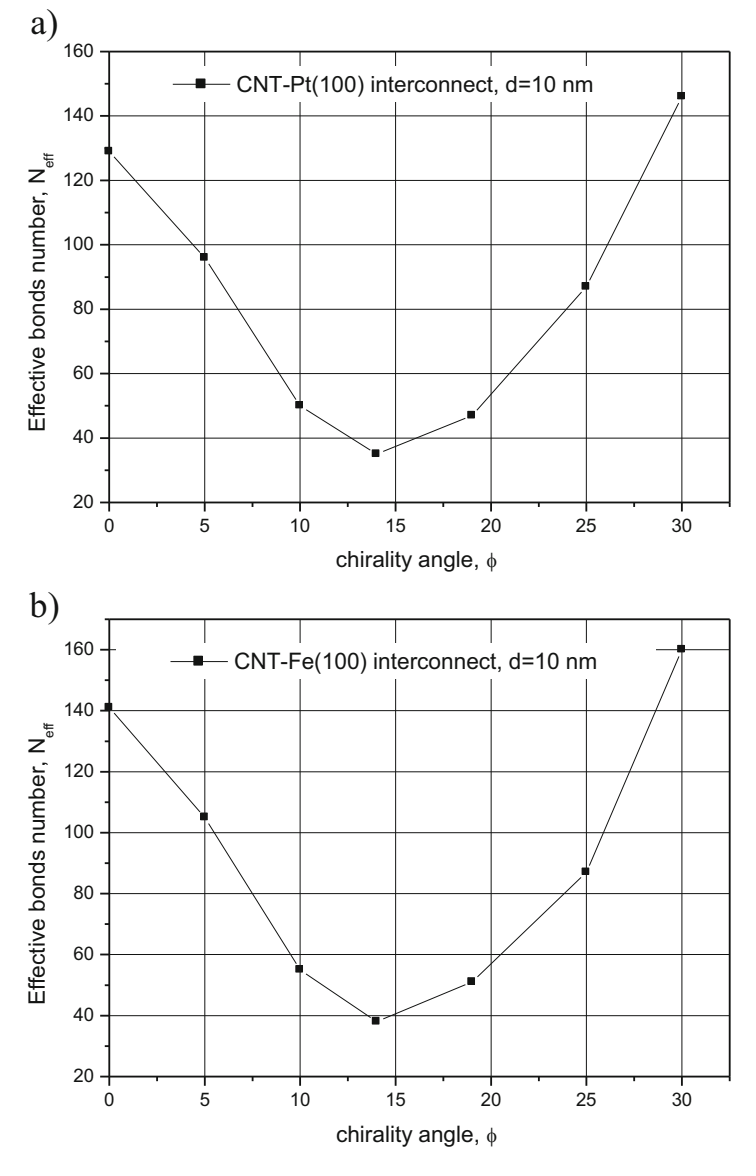


Fig. 7.17 Effective bonds number via CNT chirality for the diameter d=10 nm: (a) CNT–Pt and (b) CNT–Fe

#### 7.6.9 CNT- $Fe_xPt_{1-x}$ Interconnect Formation

There is a relation between the use of magnetic catalysts and the CVD growth of CNTs determining the most commonly used materials for the CNT growth – Fe, Co and Ni. The nanoparticles of the latter catalysts are magnetically isotropic. Magnetism of the particles of catalysts brings order into the process of CVD growth.

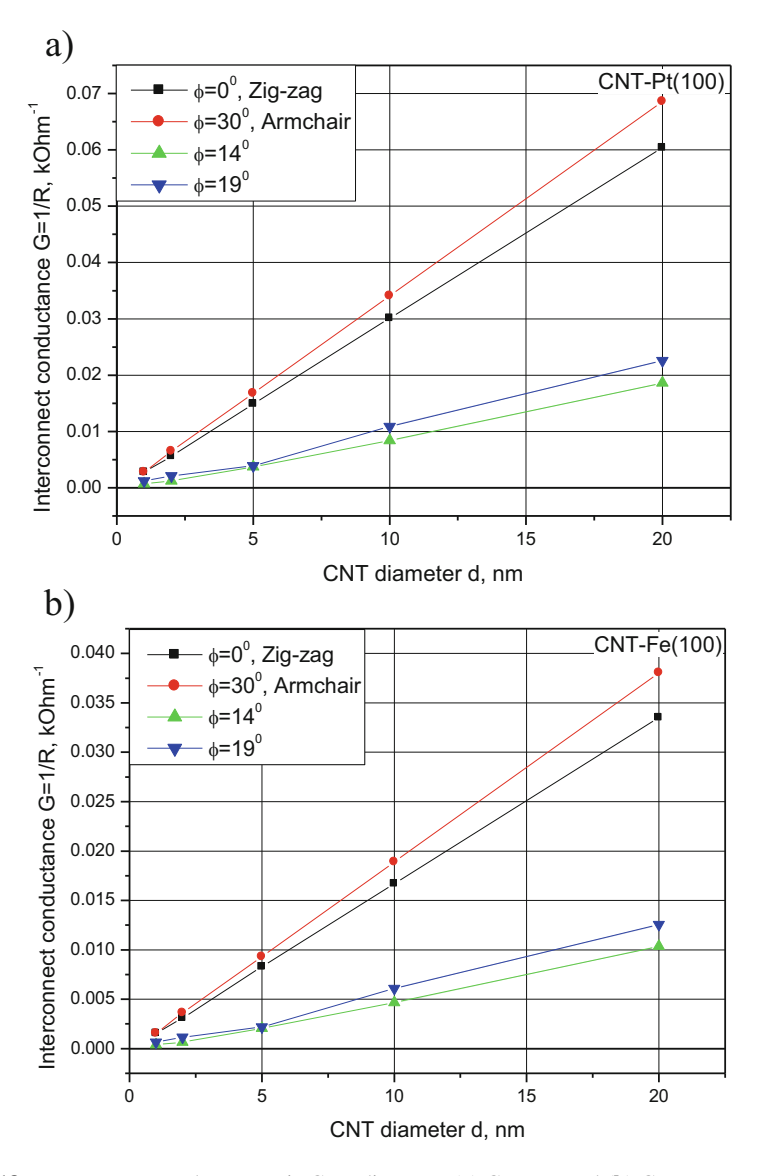
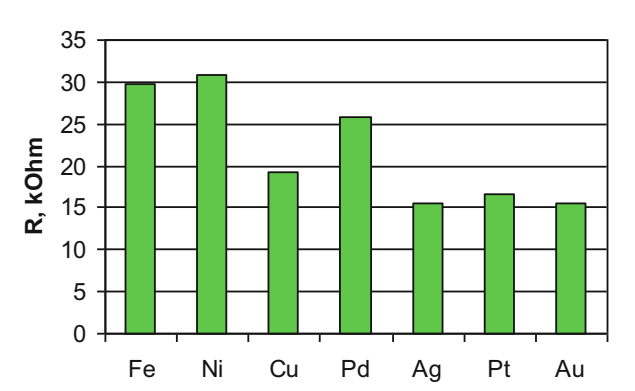


Fig. 7.18 Interconnect conductance via CNT diameter: (a) CNT-Pt and (b) CNT-Fe

Actual class of Fe–Pt nanodrops as possible catalysts in a CVD process has the diameter ranging from 5 to 30 nm. The stable and predictable creation of definite sizes of nanodrops is a basis for the output growth of CNTs with the expected morphology. Their magnetic properties are essentially changed in dependence on their size. Magnetization orientation of nanodrops in a Fe–Pt system is regulated in competition of the heat factor and collective magnetization of the nanodrop

**Fig. 7.19** Resistances of zigzag SWCNT–metal interconnects in comparison

#### **Resistance of SWCNT-Metal Interconnects**



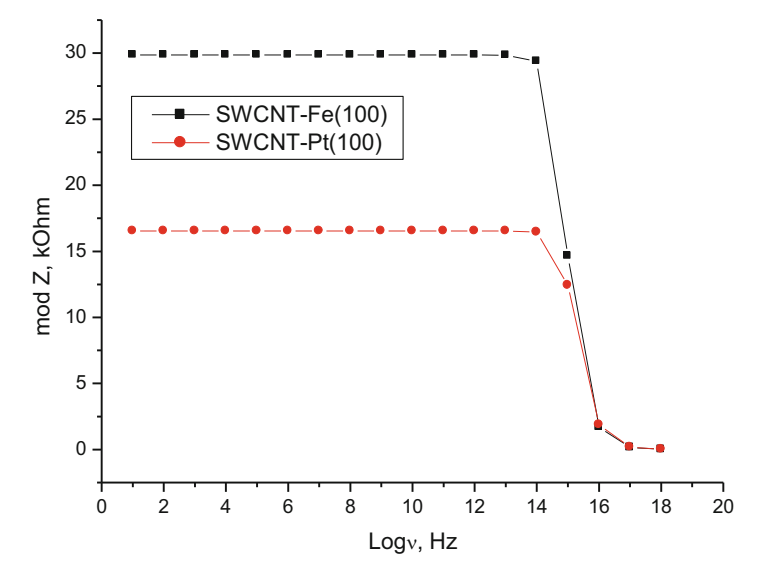


Fig. 7.20 Impedances of SWCNT-Fe and Pt interconnects in comparison

ferromagnetic state. Magnetization of nanodrops becomes non-stable for small sizes. This also means additional technological complications in magnetically controlled CMTs CVD growth. Fe—Pt nanoparticles containing a near-equal atomic percentage of Fe and Pt are an important class of magnetic nanomaterials. They are known to have a chemically disordered face-centred cubic (fcc) structure or a chemically ordered face-centred tetragonal (fct) structure.

Additional possibilities in controlling the process of CVD growth open up the ways to use magnetically anisotropic nanoparticles such as those in the alloys with a different substitutional disorder (e.g.  $Fe_xPt_{1-x}$ ), to manage the CVD process with the formation of the predefined CNT chiralities. Besides, the stimulation of the

process by means of the external magnetic field activates magnetic moments of the catalyst and the deposited carbon atoms. This also means that we can control the number of effective bonds inside interconnects. We pay a special attention to Pt and Fe substrates as possible elements for nanoelectronic and nanomagnetic devices considering interconnect fundamental properties and magnetically stimulated nanoprocesses on Fe–Pt L1<sub>0</sub> nanoparticles [59–61, 121].

#### 7.6.10 Magnetic Properties of Fe-Pt Alloys

The unique magnetic properties of Fe–Pt alloys are an open field for research to correlate different CNT techniques in terms of the catalyst role in entirely different range of temperatures and pressures. Carbon nanotubes grow using bimetallic nanoparticle Fe–Pt as a catalyst [122–125]. Since the mid-1930s, Fe–Pt alloys have been known to exhibit high coercivities due to high magnetocrystalline anisotropy of the L1<sub>0</sub> FePt phase, but their high cost prevented these alloys from widespread applications in the past. In Fe–Pt alloys, both Fe and Pt atoms carry a magnetic moment: the induced magnetic moment on the Pt sites and the enhanced magnetic moment on the Fe sites. A wide variety of the magnetic structure types in the Fe–Pt alloys is evidently the consequence of various atomic configurations around Fe atoms, which, in turn, has a considerable effect on the electronic structure of these alloys (see Fig. 7.21, Table 7.6 and eutectic phase diagram of Fe–Pt alloy (http://www.himikatus.ru/art/phase-diagr1/Fe-Pt.php)).

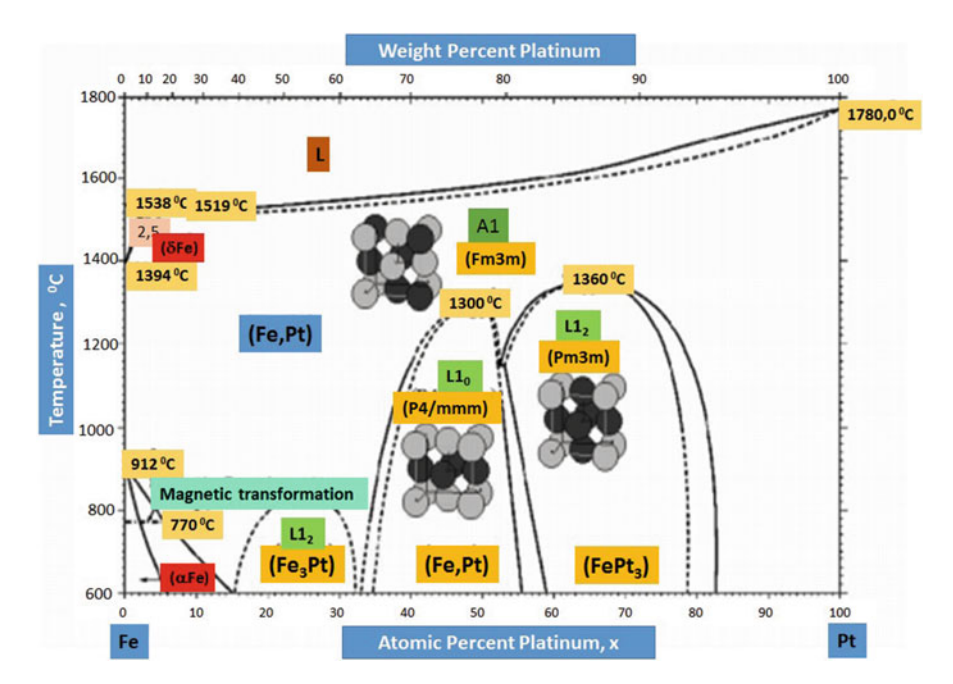


**Fig. 7.21** Eutectic phase diagram of Fe–Pt alloy (http://www.himikatus.ru/art/phase-diagr1/Fe-Pt.php)

Magnetic structure	Behaviour	Curie temperature (K)
L1 <sub>2</sub> Fe <sub>3</sub> Pt	Ferromagnetic	410
L1 <sub>0</sub> FePt	Ferromagnetic	750
L1 <sub>2</sub> FePt <sub>3</sub>	Paramagnetic	273

Table 7.6 Specific magnetic structures of Fe-Pt systems

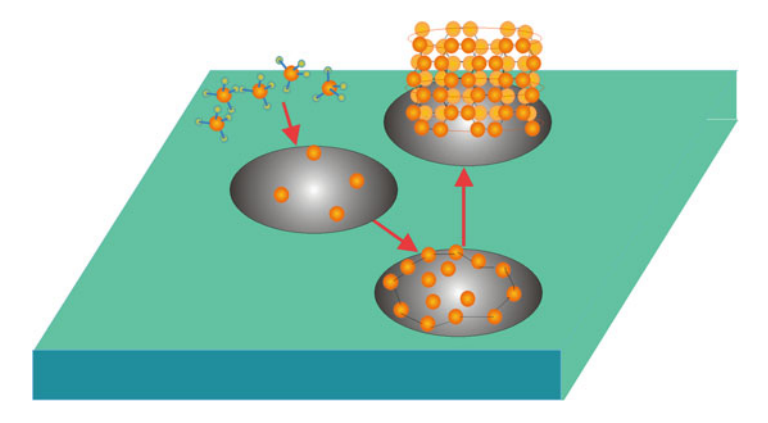


Fig. 7.22 A fragment of the CNT CVD process growth on nanoparticle surfaces

To obtain the Fe–Pt alloy in  $L1_0$  phase, we use a new chemical synthesis strategy reported in detail in our previous works [59–61, 121]. By planetary ball milling of nanocrystals of a particular precursor, [Fe(H<sub>2</sub>O)<sub>6</sub>]PtCl<sub>6</sub> and NaCl were grounded and then annealed at 400 °C (300 °C – less than typically used temperature) in reductive atmosphere. After washing, we obtain FePt  $L1_0$  NPs with selected size as a function of the fraction [Fe(H<sub>2</sub>O)<sub>6</sub>]PtCl<sub>6</sub> and NaCl used. By varying the precursor ratio, we are able to avoid the coalescence phenomena and obtain single-crystal NPs with the size around 6 nm, not agglomerated.

# 7.6.11 Magnetically Stimulated CNT Growth

The formation of the initial optimal perimeter for carbon–metal (Fe–Pt) bonds is a synergetic process with a minimal free energy (see Fig. 7.22).

The nanoparticle diameter determines with a certain error the diameter of a CNT. The number of effective bonds defines the morphology of the future CNT (see Fig. 7.23, armchair, chiral, zigzag CNTs,) in terms of chirality. Obviously, there is a considerable uncertainty in the morphology of the future CNTs, owing to sporadic thermal dynamics of the deposited carbon atoms.

According to our model, the process can be considerably streamlined using even minor diamagnetic properties of carbon atoms at the expense of magnetic field and strong induced ferromagnetism of the nanoparticle. It becomes evident that the

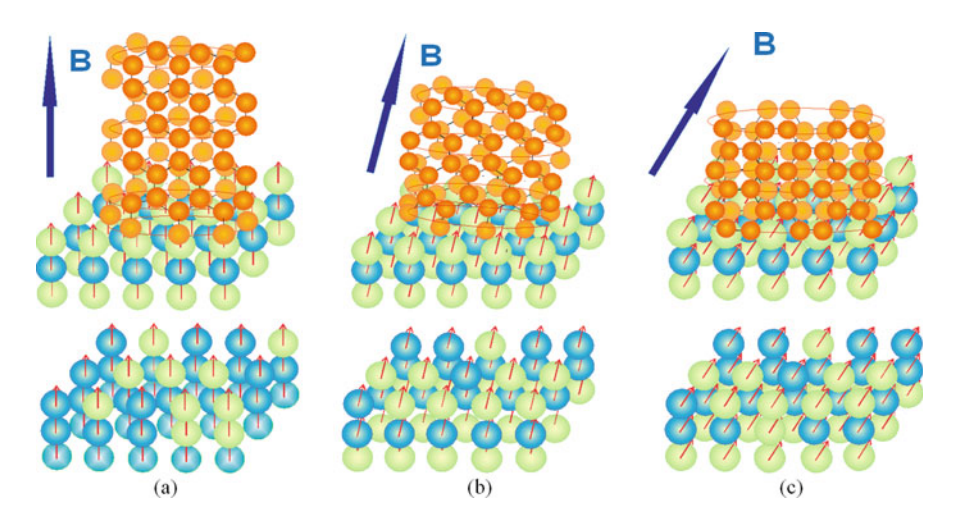


**Fig. 7.23** Magnetically stimulated orientation of magnetic moments of atoms in model interconnects during the CNT controlled growth with the expected chiralities under the directed magnetic field *B* with the orientation angle  $\phi = \Theta_B$ : (a) armchair CNT, magnetic field *B* with the orientation angle  $\Theta_B$ , where *B* is the magnetic induction and the chirality angle is  $\phi = 0^\circ$ ; (b) chiral CNT  $0 < \phi < 30^\circ$  and (c) zigzag CNT, $\phi = 30^\circ$ 

nanoparticle composition Fe–Pt and its atomic structure (including the short-range order) play a primary role in the process of CNT growth stimulated by the magnetic field of CVD.

Nucleation in the process of CNT growth in cases of the ordered Fe–Pt nanoparticles is more stable and has principal advantages in relation to the CNT controlled growth compared with the cases of any kind of anisotropic Fe–Pt nanocatalysts [126].

The availability of substitutional disorder and anisotropy in Fe–Pt nanodrops used for CNT CVD controlled growth is a negative factor for the production of CNTs with predictable morphologies. There are some essential negative features of disorder in Fe–Pt nanodrops for the CVD process:

- 1. C atoms chemical binding preferences (C–Fe bonds are stronger than C–Pt ones).
- 2. A higher structural anisotropy leads to higher relaxation times of a nanodrop structure [127].
- 3. Disordering effects in Fe–Pt lead to sporadic magnetization phenomena.

Thus, it is important to control the process of formation of nanodrop structures corresponding to L1<sub>0</sub> (Fe–Pt) and L1<sub>2</sub> (Fe<sub>3</sub>Pt) systems with reliable magnetism and adequate cooling rates, when relaxation processes in nanodrops are accomplished.

As it has already been mentioned, Fe–Pt nanoparticles containing a near-equal atomic percentage of Fe and Pt are an important class of magnetic nanomaterials. They are known to have a chemically disordered face-centred cubic (fcc) structure or a chemically ordered face-centred tetragonal (fct) structure.

# 7.6.12 Model of CVD CNT Growth with the Probabilistically Predefined Morphology

Magnetically stimulated CNT CVD model formulation looks as follows (see Figs. 7.22 and 7.23):

- Effective bonds are responsible for the future chirality of CNT in the CVD processes.
- The permanent magnetic field provides the alignment of CVD growth.
- The binding with the Fe–Pt nanoparticle has a probabilistic character; the probability of binding of C atoms with Fe atoms is preferable as compared to Pt atoms.
- The composition of Fe–Pt atoms in a nanoparticle and the atomic structure ordering are essential for chirality of the obtained CNTs.
- The diameter of the future CNT is correlated with the nanoparticle size.
- The direction of the magnetic field stabilizes the direction of CNT forest growth and is a tool of the growth control.
- The ordering of a nanoparticle atomic structure, as well as a substitutional disorder or arbitrary disorder of a nanoparticle, is responsible for the magnetic state of the nanoparticle, which is essential for the possible future nanomemory devices.

Even a very strong magnetic field is not able to suppress thermal fluctuations of magnetic moments in carbon atoms. It is a different thing when carbon diamagnetic atoms appear on the surface of a catalyst in the ferromagnetic condition where magnetism induced by the external field can be very strong and is able to correct the behaviour of carbon atoms by suppressing thermal fluctuations.

At the same time, the growth control over chiral and non-chiral nanotubes essentially depends on stoichiometric composition of Fe–Pt nanoparticles. The beginning of the nucleation process with the growth of nanotubes might be connected with stochastic fluctuations of the magnetic moment in a carbon atom relative to the direction of the local magnetic field in a nanoparticle. Distribution of the fluctuation angle obeys the Gaussian law (see Fig. 7.24):

$$f(\theta) = \frac{1}{\sigma\sqrt{2\pi}} \cdot \exp\left(-\frac{(\theta - \theta_B)^2}{2\sigma^2}\right),\tag{7.6}$$

where  $\sigma^2$  is the angular dispersion of thermal fluctuations of the magnetic moment angle of a carbon atom. To evaluate this dispersion, the potential energy change of the magnetic moment under the influence of the thermal energy should be evaluated:  $\mu_C B(1-\cos\theta_T)\approx k_B T_{\rm CVD}$ , where  $\mu_C$  is the induced magnetic moment of a carbon atom  $\mu_C=1.25\mu_B$  (see evaluations in [125],  $\mu_B=5.788\cdot 10^{-5}\,{\rm eV/T}$ , B is the magnetic induction of the catalyst surface,  $\theta_T=\theta-\theta_B$ ,  $T_{\rm CVD}$ - is the operating temperature of the CVD process,  $k_B=8617\,3324(78)\cdot 10^{-5}\,{\rm eV/K}$ - is the Boltzmann constant. Hence,  $2\sin\frac{2\theta_T}{2}\approx\frac{k_B T_{\rm CVD}}{\mu_C B}$ . Taking into consideration one of the main

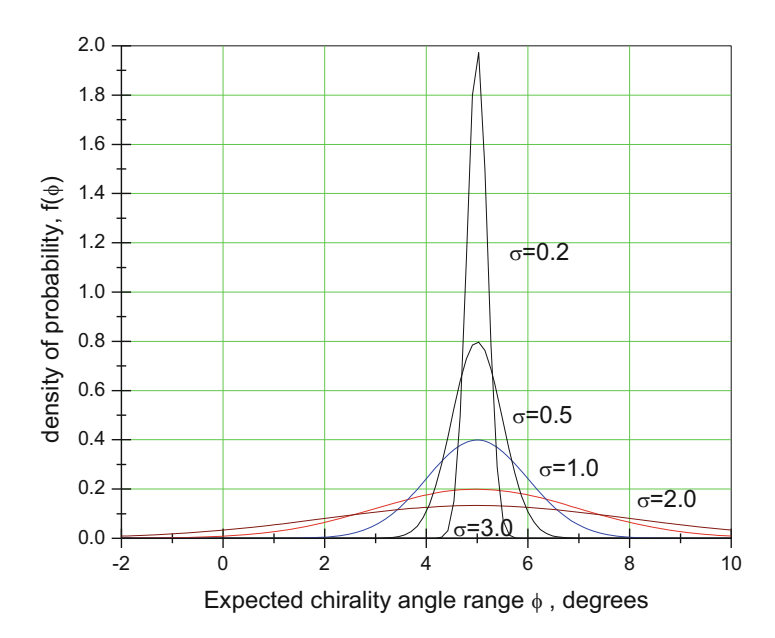


Fig. 7.24 The predictable scattering of chiralities for nanotubes of approximately similar diameters

problems of the nanotubes growth control – the chirality control – it is necessary to seek for the small fluctuation angle  $\theta$ . Then,  $\sigma^2 = \theta_T^2 = \frac{2k_B T_{\rm CVD}}{\mu_C B}$ .

The condition of the small fluctuation angle (e.g. $\theta < 10^{\circ}$ ) at a certain temperature of the CVD process imposes limitations on the values of the demanded magnetic induction B.

Taking into account the ratio between the chirality angle and the direction of the magnetic field  $\phi = \theta_B$ , Fig. 7.24 displays the predictable scattering of chiralities for nanotubes of approximately the same diameter.

We are also able to evaluate the necessary value of the magnetic field *B* providing the expected chirality angles scattering, e.g.  $\sigma = 0.2$ (appr. 12°) leads to the *B* evaluation for the CVD process temperature  $T_{\text{CVD}} = 700 \,^{\circ}\text{C}$  as  $B = \frac{2k_B T_{\text{CVD}}}{\sigma^2 \mu_C} \approx \frac{16755}{\sigma^2 \mu_C} \approx 57895 \approx 6 \cdot 10^4 \, Tesla$ . For small angle dispersions  $\sigma^2 = \theta_T^2 = \frac{2k_B T_{\text{CVD}}}{\mu_C B}$ 

the high local magnetic field on the nanoparticle surface is necessary. The result also strongly depends on the carbon atom magnetic moment $\mu_C$ .

Speaking about the possible errors in diameters of growing nanotubes, their evaluation from beneath is defined by the minimal variations in parameters of the chirality vector  $\vec{c} = (n, m) \Delta n$  and  $\Delta m$ , which are equal 1.

Taking into consideration the formula for calculating the diameter of CNT:

$$d = \frac{\sqrt{3}a}{\pi}\sqrt{m^2 + n^2 + mn},$$

where a = 0.142 nm is the distance between the neighbouring carbon atoms in the graphite plane.

The relationship between chirality indices (n and m) and the angle  $\phi$  is given by the ratio:

$$\sin \phi = \frac{m\sqrt{3}}{2\sqrt{m^2 + n^2 + mn}}. (7.7)$$

Then the minimum relative error in the diameter of CNT is possible to define as:

$$\varepsilon_d = \frac{\Delta d}{d} \approx \frac{\sqrt{5m^2 + 5n^2 + 8mn}}{2(m^2 + n^2 + mn)}.$$
(7.8)

Particularly, in the case of armchair CNT  $(m=0) \varepsilon_d \approx \sqrt{5}/2n$ , and in the case of zigzag CNT (m=n),  $\varepsilon_d \approx 1/(2\sqrt{2}n)$ .

Thus, errors in the diameter of growing CNTs are incorporated in discrete morphological properties. But these minimum estimates are only reinforced, given the obvious errors in the size of catalyst nanoparticles are taken into consideration.

#### References

- Li Y H, Wang S, Wei J, Zhang X, Xu C, Luan Z, Wu D, Wei B 2002 Lead adsorption on carbon nanotubes Chemical Physics Letters 357(3-4) 263-6
- Iijima S, Ajayan P M, Ichihashi T 1992 Growth Model for Carbon Nanotubes Physical Review Letters 69(21) 3100–3
- 3. Iijima S, Ichihashi T 1993 Single-shell carbon nanotubes of 1-nm diameter Nature 363 603-5
- Bethune D S, Kiang C H, De Vries M S, Gorman G, Savoy R, Vazquez J, Beyers R 1993
   Cobalt-catalysed growth of carbon nanotubes with single-atomic-layer walls *Nature* 363 605–7
- Ando Y, Zhao X 2006 Synthesis of Carbon Nanotubes by Arc-discharge method New Diamond and Frontier Carbon Technology 16(3) 123–37
- Ando Y, Iijima S 1993 Preparation of Carbon Nanotubes by Arc-Discharge Evaporation Japanese Journal of Applied Physics 32(2) L107–9
- Somu C, Karthi A, Sing S, Karthikeyan R, Dinesh S, Ganesh N 2017 Synthesis of various forms of carbon nanotubes by arc discharge methods - comprehensive review *International Research Journal of Engineering and Technology* (IRJET) 04(01) 344–54
- Maria K H, Mieno T 2015 Synthesis of single walled carbon nanotubes by low-frequency bipolar pulsed arc discharge method Vacuum 113 11–8
- Berkmans J A, Jagannatham M, Reddy R D, Haridoss P 2015 Synthesis of thin bundled single walled carbon nanotubes and nanohorn hybrids by arc discharge technique in open air atmosphere *Diamond and Related Materials* 55 12–5
- Sugai T, Yoshida H, Shimada T, Okazaki T, Shinohara H. 2003 New synthesis of highquality double-walled carbon nanotubes by high temperature pulsed arc discharge Nano Letters 3(6) 769–73

- 11. Jong Lee S, Koo Baik H, Yoo J, Hoon Han J **2002** Large scale synthesis of carbon nanotubes by plasma rotating arc discharge technique *Diamond and Related Materials* **11** 914–7
- 12. Eftekhari A, Garcia H 2017 The necessity of structural irregularities for the chemical applications of graphene *Materials Today Chemistry* 4 1–16
- Brayfindley E, Irace E E, Castro C, Karney W L 2015 Stone–Wales Rearrangements in Polycyclic Aromatic Hydrocarbons: A Computational Study J. Org. Chem. 80(8) 3825–31
- 14. Stone A J, Wales D J **1986** Theoretical studies of icosahedral C60 and some related structures *Chemical Physics Letters* **128**(5–6) 501–3
- Letardi S, Celino M, Cleri F, Rosato V 2002 Atomic hydrogen adsorption on a Stone–Wales defect in graphite Surface Science 496 33–8
- Meyer J C, Kisielowski C, Erni R, Rossell M D, Crommie M F, Zettl A 2008 Direct Imaging of Lattice Atoms and Topological Defects in Graphene Membranes Nano Letters 8 (11) 3582–6
- 17. Guo T, Nikolaev P, Rinzler A G, Tomanek D, Colbert D T, Smalley R E **1995** Self-Assembly of Tubular Fullerenes *J. Phys. Chem.* **99** 10694–7
- 18. Guo T, Nikolaev P, Thess A, Colbert D T Smalley R E 1995 Catalytic growth of single-walled nanotubes by laser vaporization *Chem. Phys. Lett.* 243 49–54
- van de Burgt Y 2014 Laser-assisted growth of carbon nanotubes A review Journal of Laser Applications 26(3) 032001–18
- Cao L, Barsic D N, Guichard A R, Brongersma M L 2007 Plasmon-Assisted Local Temperature Control to Pattern Individual Semiconductor Nanowires and Carbon Nanotubes Nano Letters 7(1) 3523–7
- 21. Endo M, Takeuchi K, Igarashi S, Kobori K, Shiraishi M, Kroto H W **1993** The production and structure of pyrolytic carbon nanotubes *J. Phys. Chem. Solids* **54** 1841–8
- Dai H, Rinzler A G, Nikolaev P, Thess A, Colbert D T, Smalley R E 1996 Single-wall nanotubes produced by metal-catalyzed disproportionation of carbon monoxide *Chem. Phys. Lett.* 260 471–5
- Karthikey S, Mahalingam P, Kartnik M 2009 Large Scale Synthesis of Carbon Nanotubes E-Journal of Chemistry 6(1) 1–12
- Cassell A M, Raymakers J A, Kong J, Dai H 1999 Large Scale CVD Synthesis of Single-Walled Carbon Nanotubes *Journal of Physical Chemistry B* 103(31) 6484–92
- Takeuchi K, Hayashi T, Kim Y A, Fujisawa K, Endo M 2014 The state-of-art science and app-lications of carbon nanotubes *Nanosystems: Physics, Chemistry, Mathematics* 5 (1) 15–24
- Inami N, Mohamed M A, Shikoh E, Fujiwara A 2007 Synthesis-condition dependence of carbon nanotube growth by alcohol catalytic chemical vapor deposition method Science and Technology of Advanced Materials 8 292–5
- 27. Kumar M 2011 Nanotube synthesis and growth mechanism In: InTech Carbon Nanotubes -Synthesis, Characterization, Applications Sery Nanotechnology and Nanomaterials Ed by Yellampalli S Ch 8
- 28. Liu C, Cheng H M **2013** Carbon nanotubes: controlled growth and application *Materials Today* **16**(1/2) 19–28
- Reinhardt H, Hellmann C, Nürnberger P, Kachel S, Hampp N 2017 Free Form Growth of Carbon Nanotube Microarchitectures on Stainless Steel Controlled via Laser-Stimulated Catalyst Formation Adv. Mater. Interfaces 4 1700508–1–7.
- 30. Neyts E 2012 PECVD growth of carbon nanotubes: From experiment to simulation *Journal* of Vacuum Science & Technology B, Nanotechnology and Microelectronics: Materials, Processing, Measurement, and Phenomena 30 030803
- 31. Hofmann S, Ducati C, Robertson J **2003** Low-temperature growth of carbon nanotubes by plasma-enhanced chemical vapor deposition *Applied Physics letters* **83** 135–7
- Chiang W H, Sankaran R M 2009 Linking catalyst composition to chirality distributions of as-grown single-walled carbon nanotubes by tuning Ni(x)Fe(1-x) nanoparticles Nature Materials 8 882–6

33. Bogaerts A, Eckert M, Mao M, Neyts E **2010** Computer modelling of the plasma chemistry and plasma-based growth mechanisms for nanostructured materials *J. Phys. D: Appl. Phys.* **44** 174030

- 34. Fantini C, Jorio A, Souza M, Strano M S, Dresselhaus M S, Pimenta M A **2004** Optical Transition Energies for Carbon Nanotubes from Resonant Raman Spectroscopy: Environment and Temperature Effects *Phys. Rev. Lett.* **93** 147406
- 35. Souza Filho A G, Chou S G, Samsonidze Ge G, Dresselhaus G, Dresselhaus M S, An Lei, Liu J, Swan Anna K, Unlu M S, Goldberg B B, Jorio A, Grüneis A, Saito R 2004 Stokes and Anti-Stokes Raman Spectra of Small-Diameter Isolated Carbon Nanotubes *Physical Review B*, 69(11) 115428
- Eklund P C, Holden J M, Jishi R A 1995 Vibrational modes of carbon nanotubes; Spectroscopy and theory Carbon 33 959–72
- Hennrich F, Krupke R, Lebedkin S, Arnold K, Fischer R, Resasco D E, Kappes M M 2005
   Raman Spectroscopy of Individual Single-Walled Carbon Nanotubes from Various Sources J. Phys. Chem. B 109 10567–73
- 38. Jorio A, Fantini C, Pimenta M A, Capaz R B, Samsonidze G G, Dresselhaus G, Dresselhaus M S, Jiang J, Kobayashi N, Gruneis A, Saito R 2005 Resonance Raman spectroscopy (n,m)-dependent effects in small-diameter single-wall carbon nanotubes *Phys. Rev. B* 71 075401
- 39. Seah Ch-M, Chai S-P, Mohamed A R **2014** Mechanisms of graphene growth by chemical vapour deposition on transition metals *Carbon* **70** 1–21
- 40. Li X, Cai W, Colombo L, Ruoff R S **2009** Evolution of graphene growth on Ni and Cu by carbon isotope labelling. *Nano Letters* **9**(12) 4268–72
- Baraton L, He Z, Lee C, Cojocaru C, Châtelet M, Maurice J, Lee Y, Pribat D 2011 On the mechanisms of precipitation of graphene on nickel thin films *Europhysics Letters* 96 (4) 46003–1–6
- Cabrero-Vilatela A, Weatherup R S, Braeuninger-Weimer P, Caneva S, Hofmann S 2016
   Towards a general growth model for graphene CVD on transition metal catalysts *Nanoscale* 8

   (4) 2149–58
- 43. Sun J, Nam Y, Lindvall N, Cole M T, Teo K B K, Park Y W, Yurgens A **2014** Growth mechanism of graphene on platinum: Surface catalysis and carbon segregation *Appl. Phys. Lett.* **104** 152107
- 44. Li X, Cai W, Colombo L, Ruoff R S **2009** Evolution of Graphene Growth on Ni and Cu by Carbon Isotope *Nano Lett.* **9** (12), 4268–72
- 45. Kang C, Jung D H, Nam J E, Lee J S **2014** Correlating defect density with growth time in continuous graphene films *J Nanosci Nanotechnol.* **14**(12) 9169–73
- 46. Krishna Bharadwaj B, Nath D, Pratap R, Raghavan S 2016 Making consistent contacts to graphene: effect of architecture and growth induced defects Nanotechnology 27 (20) 205705-1-6
- Banhart F, Kotakoski J, Krasheninnikov A V 2011 Structural Defects in Graphene ACS Nano 5(1) 26–41
- 48. Stone A J, Wales D J 1986 Theoretical Studies of Icosahedral C60 and Some Related Species *Chem. Phys. Lett.* 128 501–3
- Ugeda M M, Brihuega I, Guinea F Gomez-Rodriguez, J M 2010 Missing Atom as a Source of Carbon Magnetism *Phys. Rev. Lett.* 104 096804
- 50. El-Barbary A A, Telling R H, Ewels C P, Heggie M I, Briddon P R 2003 Structure and Energetics of the Vacancy in Graphite *Phys. Rev. B* 68 144107
- Lehtinen P O, Foster A S, Ayuela A, Krasheninnikov A V, Nordlund K, Nieminen R M 2003
   Magnetic Properties and Diffusion of Adatoms on a Graphene Sheet *Phys. Rev. Lett.* 91 017202
- 52. Banhart F **2009** Interactions between Metals and Carbon Nanotubes: At the Interface between Old and New Materials *Nanoscale* **1** 201–13
- 53. Krasheninnikov A V, Lehtinen P O, Foster A S, Pyykkö P, Nieminen R M 2009 Embedding Transition-Metal Atoms in Graphene: Structure, Bonding, and Magnetism *Phys. Rev. Lett.* 102 126807

- 54. Lusk M T, Wu D T, Car L D 2010 Graphene Nanoengineering and the Inverse StoneThrowerWales Defect Phys. Rev. B 81 155444
- 55. Lahiri J, Lin Y, Bozkurt P, Oleynik I I, Batzill M **2010** An Extended Defect in Graphene as a Metallic Wire *Nat. Nanotechnol.* **5** 326–9
- Koskinen P, Malola S, Häkkinen H 2009 Evidence for Graphene Edges Beyond Zigzag and Armchair Phys. Rev. B 80 073401
- Xia F, Farmer, D. B.; Lin, Y.; Avouris, Ph. 2010 Graphene Field-Effect Transistors with High On/Off Current Ratio and Large Transport Band Gap at Room Temperature Nano Lett. 10 715–8
- 58. Pedersen T G, Flindt C, Pedersen J, Mortensen N A, Jauho A-P, Pedersen K **2008** Graphene Antidot Lattices: Designed Defects and Spin Qubits. *Phys. Rev. Lett.* **100** 136804
- Yazyev O V, Louie S G 2010 Electronic Transport in Polycrystalline Graphene Nat. Mater.
   9 806–9
- Shunin Yu and Kiv A (Eds) Nanodevices and Nanomaterials for Ecological Security 2012
   Series: NATO Science for Peace Series B Physics and Biophysics (Heidelberg: Springer Verlag) 363p
- 61. Shunin Yu N, Zhukovskii Yu F, Burlutskaya N Yu, Gopejenko V I, Bellucci S 2012 Properties of CNT- and GNR-Metal Interconnects for Development of New Nanosensor Systems In: *Nanodevices and Nanomaterials for Ecological Security* Series: NATO Science for Peace Series B - Physics and Biophysics Eds Yu Shunin and A Kiv (Heidelberg: Springer Verlag) 237–62
- 62. Shunin Yu N, Zhukovskii Yu F, Gopejenko V I, Burlutskaya N, Lobanova-Shunina T, Bellucci S **2012** Simulation of Electromagnetic Properties in CNT and Graphene Based Nanostructures *Journal of Nanophotonics* **6**(1) 061706–1-16
- 63. Shunin Yu N, Schwartz K K 1997 Correlation between electronic structure and atomic configurations in disordered solids In: Computer Modelling of Electronic and Atomic Processes in Solids Eds R C Tennyson and A E Kiv. Kluwer Academic Publisher: Dodrecht/Boston/London 241–57
- 64. Shunin Yu N, Zhukovskii Yu F, Gopejenko V I, Burlutskaya N, Bellucci S **2011** *Ab Initio* Simulations on Electric Properties for Junctions Between Carbon Nanotubes and Metal Electrodes *Nanoscience and Nanotechnology Letters* **3(6)** 816–825
- Economou, E L 2006 Green's Functions in Quantum Physics Solid State 7 (Berlin/Heidelberg: Springer Verlag)
- 66. Ziman J M **1979** *Models of Disorder* (New York-London: Cambridge University Press) Chapter 10
- 67. Shunin, Yu N, Zhukovskii Yu F, Burlutskaya N, Bellucci S. **2012** Journal of Nanoelectronics and Optoelectronics **7**(1) 3–11
- 68. Capobianchi A, Colapietro M, Fiorani D, Foglia S, Imperatori P, Laureti S, Palange E 2009 General strategy for direct synthesis of L1<sub>0</sub> nanoparticle alloys from layered precursor: the case of FePt Chem. Mater. 21(10) 2007–9
- Capobianchi A, Campi, G, Camalli M, Veroli C Z 2009 Crystal and molecular structure of the saline complex hexaaquairon(II) hexachloroplatinate, [Fe(H 2 O) 6] [PtCl 6] Kristallogr 224 (8) 384–8
- Faustini M, Capobianchi A, Varvaro G, Grosso D 2012 Bifunctional FePt@MWCNTs/Ru Nanoarchitectures: Synthesis and Characterization Chem. Mater. 24 1072–9
- 71. Bellucci S Carbon nanotubes: physics and applications **2005** *Physica Status Solidi* (c) **2** (1) 34–47
- 72. Moisala A, Nasibulin A G, Kauppinen E I **2003** The role of metal nanoparticles in the catalytic production of single-walled carbon nanotubes a review *J. Phys. Condens. Mater.* **15** S3011–35
- 73. Baker R T K, Hams P S **1978** *Chemistry and Physics of Carbon* **14** Eds P L Walker Jr and P A Thrower (New York: Marcel Dekker) 83p
- Sen R, Govindaraj A, Rao C N R 1997 Metal-filled and hollow carbon nanotubes obtained by the decomposition of metal-containing free precursor molecules *Chem. Phys. Lett.* 267 (3) 276–80

75. Carbon Nanotubes Science and Applications 2005 Ed Meyyappan (Florida: CRC Press LLC Google e-Book)

- Satishkumar B C, Govindraj A, Sen R, Rao C N R 1998 B–C–N, C–N and B–N nanotubes produced by the pyrolysis of precursor molecules over Co catalysts *Chem. Phys. Lett.* 293 (1) 47–52
- Xie S., Chang B, Li W, Pan Z, Sun L, Mao J, X. H. Chen, L. X. Qian, W. Y. Zhou 1999
   Synthesis and Characterization of Aligned Carbon Nanotube Arrays Adv. Mater. 11 1135–9
- Cassell A M, Raymakers J A, Kong J, Dai H J 1999 Large Scale CVD Synthesis of Single-Walled Carbon Nanotubes *Phys. Chem. B* 103 6484–9
- 79. Su M, Zheng B, Liu J **2000** A scalable CVD method for the synthesis of single-walled carbon nanotubes with high catalyst productivity *Chem. Phys. Lett.* **322** 32–6
- Su M, Li Y, Maynor B, Buldam A, Lu J P, Liu J J 2000 Lattice-Oriented Growth of Single-Walled Carbon Nanotubes *Phys. Chem. B* 104 6505–12.
- 81. Fan S S, Chapline M G, Franklin N R, Tombler T W, Cassell A M, Dai H 1999 Self-oriented regular arrays of carbon nanotubes and their field emission properties *Science* 283 512–4
- 82. Cheng H M, Li F, Su G, Pan H Y, He L L, Sun X, Dresselhaus M S 1998. Large-scale and low-cost synthesis of single-walled carbon nanotubes by the catalytic pyrolysis of hydrocarbons *Appl. Phys. Lett.* 72 3282–4
- 83. Li Y, Liu J Z. Wang Z **2001** Preparation of monodispersed Fe-Mo nanoparticles as the catalyst for CVD synthesis of carbon nanotubes *Chem. Mater.* **13** 1008–14
- Lee D C, Mikulec F V, Korgel B A 2004 Carbon nanotube synthesis in supercritical toluene Amer. Chem. Soc. 126(15) 4951–7
- 85. Chen G Y, Jensen B, Stolojan V, Silva S R P **2011** Growth of carbon nanotubes at temperatures compatible with integrated circuit technologies *Carbon* **49**(1) 280–5
- 86. Shang N G, Tan Y Y, Stolojan V, Papakonstantinou P, Silva S R P 2010 High-rate low-temperature growth of vertically aligned carbon nanotubes *Nanotechnology* 21 (50) 505604
- 87. Kumar M, Ando Yo 2010 Chemical vapor deposition of carbon nanotubes: a review on growth mechanism and mass production *Journal of Nanoscience and Nanotechnology* 10 (6) 3739–58
- 88. Takagi D, Hibino H, Suzuki S, Kobayashi Y, Homma Y **2007** Carbon Nanotube Growth from Semiconductor Nanoparticles *Nano Lett.* **7** 2272–5
- 89. Takagi D, Homma Y, Hibino H, Suzuki S, Kobayashi Y **2006** Single-Walled Carbon Nanotube Growth from Highly Activated Metal Nanoparticles *Nano Lett.* **6** 2642–5
- Liu H, Takagi D, Ohno H, Chiashi Sh, Chokan T, Homma Yo 2008 Growth of Single-Walled Carbon Nanotubes from Ceramic Particles by Alcohol Chemical Vapor Deposition Appl. Phys. Express 1 014001–3
- 91. Hernadi K, Fonseca A, Nagy J B, Bernaerts D, Lucas A A **1996** Fe-catalyzed carbon nanotube formation *Carbon* **34**(10) 1249–57
- 92. Kong J, Cassell A M, Dai H **1998** Chemical vapor deposition of methane for single-walled carbon nanotubes *Chem. Phys. Lett.* **292**(4) 567–74
- 93. Li W Z, Xie S, Qian L X, Chang B H, Zou B S, Zhou W Y, Zhao R A, Wang G **1996** Large-scale synthesis of aligned carbon nanotubes *Science* **274** 1701–3
- 94. Wei B Q, Vajtai R, Jung Y, Ward J, Zhang R, Ramanath G, Ajayan P M 2002 Microfabrication technology; organized assembly of carbon nanotubes *Nature* 416 495–6
- 95. Nikolaev P, Bronikowski M J, Bradley R K, Rohmund F, Colbert D T, Smith K A, Smalley R E **1999** Gas-phase catalytic growth of single-walled carbon nanotubes from carbon monoxide *Chem. Phys. Lett.* **313** 91–7
- 96. Cheng H M, Li F, Sun X., Brown S D M., Pimenta M A., Marucci A, Dresselhaus G, Dresselhaus M S 1998 Bulk morphology and diameter distribution of single-walled carbon nanotubes synthesized by catalytic decomposition of hydrocarbons *Chem. Phys. Lett.* 289 602–10
- 97. Hafner J H, Bronikowski M J, Azamian B R, Nikolaev P, Rinzler A G, Colbert D T, Smith K A, Smalley R E **1998** Catalytic growth of single-wall carbon nanotubes from metal particles *Chem. Phys. Lett.* **296** 195–202

- 98. Flahaut E, Govindaraj A, Peigney A, Laurent C, Rao C N R **1999** Synthesis of single-walled carbon nanotubes using binary (Fe, Co, Ni) alloy nanoparticles prepared in situ by the reduction of oxide solid solutions *Chem. Phys. Lett.* **300**(1–2) 236–42
- 99. Gruneis A, Rummeli M H, Kramberger C, Grimm D, Gemming T, Barreiro A, Ayala P, Pichler T, Kuzmany H, Schamann C, Pfeiffer R, Schumann J, Buchner B 2006 Novel catalysts for low temperature synthesis of single wall carbon nanotubes. *Physica Status Solidi* (b) 243 3054–7
- 100. Maruyama S, Miyauchi Y, Edamura T, Igarashi Y, Chiashi S and Murakami Y 2003 Single-walled carbon nanotubes catalytically grown from mesoporous silica thin film *Chem. Phys. Lett.* 375 553–9
- 101. Maruyama S, Kojima R, Miyauchi Y, Chiashi S, Kohno M 2002 Low-temperature synthesis of high-purity single-walled carbon nanotubes from alcohol Chem. Phys. Lett. 360(3) 229–34
- 102. Okubo S, Sekine T, Suzuki S, Achiba Y, Tsukagoshi K, Aoyagi Y and Kataura H 2004 Purification of Single-Wall Carbon Nanotubes synthesized from Alcohol by Catalytic Chemical Vapor Deposition *Jpn. J. Appl. Phys.* 43 L396–8
- 103. Gruneis A, Rummeli M H, Kramberger C, Barreiro A, Pichler T, Pfeiffer R, Kuzmany H, Gemming T, Buchner B 2006 High quality double-wall carbon nanotubes with a defined diameter distribution by chemical vapor deposition from alcohol Carbon 44 3177–82
- 104. Nasibulin A G, Moisala A, Jiang H, Kauppinen E I 2006 Carbon nanotube synthesis from alcohols by a novel aerosol method J. Nanopart. Res. 8 465–75
- 105. Murakami Y, Miyauchi Y, Chiashi S, Maruyama S 2003 Direct synthesis of high-quality single-walled carbon nanotubes on silicon and quartz substrates *Chem. Phys. Lett.* 377 (1) 49–54
- 106. Murakami Y, Chiashi S, Miyauchi Y, Hu M, Ogura M, Okubo T, Maruyama S 2004 Growth of vertically aligned single-walled carbon nanotube films on quartz substrates and their optical anisotropy Chem. Phys. Lett. 385(1) 298–303
- 107. Maruyama S, Einarsson E, Murakami Y, Edamura T **2005** Growth process of vertically aligned single-walled carbon nanotubes *Chem. Phys. Lett.* **403**(4–6) 320–3
- 108. Xiang R, Einarsson E, Okawa J, Miyauchi Y and Maruyama S 2009 Acetylene-Accelerated Alcohol Catalytic Chemical Vapor Deposition Growth of Vertically Aligned Single-Walled Carbon Nanotubes J. Phys. Chem. C 113 7511–5
- 109. Yuan D, Ding L, Chu H, Feng Y, McNicholas T P, Liu J 2008 Horizontally Aligned Single-Walled Carbon Nanotube on Quartz from a Large Variety of Metal Catalysts Nano Lett. 8 (8) 2576–9
- 110. Ward J, Wei B Q, Ajayan P M **2003** Chem. Phys. Lett. **376**(5–6) 717–25
- 111. Morjan R E, Nerushev O A, Sveningsson M, Rohmund F, Falk L K L, Campbell E E B **2004** Growth of carbon nanotubes from C 60 *Appl. Phys. A* **78**(3) 253–61
- 112. Ago H, Komatsu T, Ohshima S, Kuriki Y, Yumura M **2000** Dispersion of metal nanoparticles for aligned carbon nanotube arrays *Appl. Phys. Lett.* **77**(1) 79–81
- 113. Kumar M, Ando Y 2005 Controlling the diameter distribution of carbon nanotubes grown from camphor on a zeolite support Carbon 43(3) 533–40
- 114. Li W Z, Wen J G, Ren Z F **2002** Effect of temperature on growth and structure of carbon nanotubes by chemical vapor deposition *Appl. Phys. A* **74**(3) 397–402
- 115. Li W Z, Wen J G,, Tu Y, Ren Z F **2001** Effect of gas pressure on the growth and structure of carbon nanotubes by chemical vapor deposition *Appl. Phys. A* **73**(2) 259–264
- 116. Maruyama S, Murakami Y, Shibuta Y, Miyauchi Y, Chiashi S 2004 Generation of single-walled carbon nanotubes from alcohol and generation mechanism by molecular dynamics simulations. J. Nanosci. Nanotechnol. 4 360–7
- 117. Kumar M and Ando Y 2008 Gigas growth of carbon nanotubes Defence Sci. Journal 58 (4) 496–503
- 118. Raty J-Y, Gygi F, Galli G 2005 Growth of Carbon Nanotubes on Metal Nanoparticles: A Microscopic Mechanism from Ab Initio Molecular Dynamics Simulations. Phys. Rev. Lett. 95 096103–7
- 119. Bellucci S, Micciulla F, Shunin Yu, Zhukovskii Yu, Gopejenko V, Burlutskaya N 2015 Memory Nanodevices Based on Carbon Nanotube-Fe-Pt Interconnects: Electromagnetic

- Simulations and Magnetically Stimulated Nanotube Growth Journal of Materials Science and Engineering B 5 (3-4) 120-34
- 120. Shunin Yu **2015** Spintronic *Nanomemory and Nanosensor Devices Based on Carbon Nanotube-Fe-Pt Interconnects: Models and Simulations* LAP LAMBERT Academic Publishing
- 121. Bellucci S., Zhukovskii Yu F, Gopejenko V I, Burlutskaya N, Shunin Yu N **2012** Interconnects fundamental properties and magnetically stimulated nanoprocesses on Fe-Pt substrates *CIMTEC2012 Theses* June 10–14 Montecatini Terme Tuscany Italy 78
- 122. Sun A C, Kuo P C, Chen S C, Chou C Y, Huang H L, Hsu J H **2004** Magnetic properties and microstructure of low ordering temperature L10L10 FePt thin films *J. Appl. Phys.* **95** (11) 7264–6
- 123. Elkins K, Li D, Poudyal N, Nandwana V, Jin Zh, Chen K, Liu J P 2005 J. Phys. D 38 2306-9
- 124. Yan M L, Sabirianov R F , Xu Y F , Li X Z , Sellmyer D J 2004 <code>IEEE Trans.on Magnetics 40 (4) 2470–2</code>
- 125. Kim Y-H , Choi J, Chang K J, Tománek D **2003** Defective fullerenes and nanotubes as molecular magnets: An *ab initio* study *Phys. Rev. B* **68** 125420
- 126. Medwal R., Sehdev N, Annapoorni S J **2012** Order–disorder investigation of hard magnetic nanostructured FePt alloy *J Phys. D Appl. Phys.* **45** 055001–7
- 127. Arabshahi H, Hematabadi A, Bakhshayeshi A, Ghazi M **2012** Temperature Dependence and Magnetic Properties of FePt Nanoparticles via Monte Carlo Simulation *World Applied Programming* **2**(8) 415–20

# Chapter 8 Graphene, Fullerenes, Carbon Nanotubes: Electronic Subsystem

#### 8.1 Carbon: Allotropic Forms

The non-metallic tetravalent carbon element C belongs to the list of the most abundant elements due to the possibility to form organic compounds. Life on Earth is based on organic materials built up using various carbon molecular derivatives. Electronic configuration  $1s^22s^22p^2$  determines the unique possibility of carbon atoms to create the interatomic bonds and also to create structural chains and cyclic compounds. Well-expressed chemical bonding in different ways predetermines existence of various allotropes of carbon with different physical properties. Carbon is also important in various technological applications – from drugs to synthetic materials. This is due to the carbon's ability to create chemical bond with almost any item in various ways. The result is a variety of structural organic compounds with strong expressed physical and chemical properties as pointed by Hirsch [1].

Formation of the main allotropic forms is determined thermodynamically as presented in Fig. 8.1. Sublimation occurs at temperature about 3900 K. Triple point is present at pressure of  $[10.8 \pm 0.2]$  MPa and temperature of  $[4600 \pm 300]$  K [2].

Generally, carbon could form a great number of chemical compounds (molecular derivatives up to several millions). This fact could be explained by the existence of the unique electronic structure formed after sp hybridization (single–double–triple bonding, formation of  $\pi$ -conjugated system) which finally determines certain macromolecular physical properties – such as hardness, specific thermal conductivity, electrical conductivity, etc. [3]. Cambridge Structural Database [4] represents covalent radii of carbon for different hybridization, sp3, 76 pm; sp2, 73 pm; and sp, 69 pm, when van der Waals radius is equal to 170 pm.

Table 8.1 represents several typical carbon allotropes and molecular derivatives. The simplest plain molecular forms are known as benzene (one hexagonal ring), naphthalene (two rings), anthracene (three rings), etc. Carbon atoms can form

Fig. 8.1 Phase diagram of carbon near triple point at 10.8 MPa and 4600 K. Area 1 – phase of metastable graphite and diamond, and 2 – phase of graphite and metastable diamond

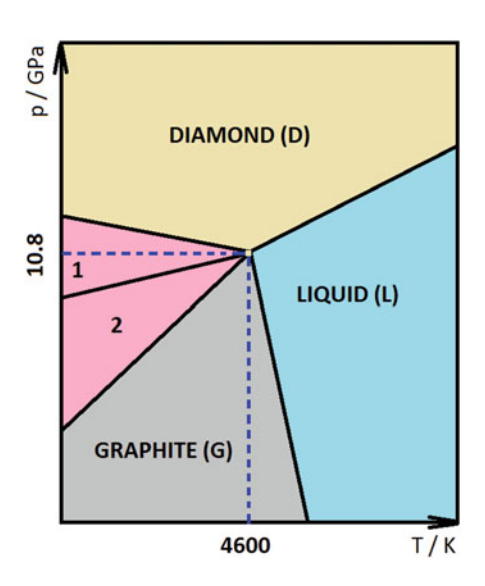


**Table 8.1** Different structures of carbon

Allotropic forms	Molecular derivatives	
Diamond	Benzene	
Graphene	Naphthalene	
Graphite	Anthracene	
Fullerene		
Nanotubes	Coronene	

regular tetrahedral structures (diamonds, etc.), closed spatial loops (fullerene, etc.) or plane loops (graphite, etc.).

Two allotropic forms of carbon – diamond and graphite – are known as the classical crystallographic samples. The difference between the phases is 0.02 eV per atom. In order to make the phase transformation, due to the high activation barrier >0.4 eV per atom, a very high temperature and pressure are required.

Diamond represents one of the best known metastable allotropes of carbon. Figures 8.2 and 8.3 represent two projections of the diamond lattice, face-oriented and isometric, respectively. Structure parameters were obtained from Crystallography Open Database [5]; crystallographic parameters of diamond data were published by Straumanis et al. [6]. Cubic lattice parameters are the following: a=0.35667 nm,  $\alpha=90^\circ$  and 8 atoms per cell: 1 atom at the corner, 3 atoms in the faces and 4 internal atoms on diagonals.

Three geometric figures are organized in a diamond lattice: cube, octahedron and tetrahedron. Eight external atoms (placed at the corners of lattice, denoted by C) create a cube. Six external atoms (placed in the faces of lattice, denoted by F) create an octahedron. Four internal atoms (placed at 1/4 of the distance along diagonal, denoted by I) create a tetrahedron. All bond lengths are equal to 0.154 nm, all bond angles – 109.5°. Diamond lattice *fcc* (face-centred cubic crystal structure) warrants

**Fig. 8.2** Diamond lattice, face-oriented projection. *C* corner atom, *F* face-centred atom, *I* internal atom

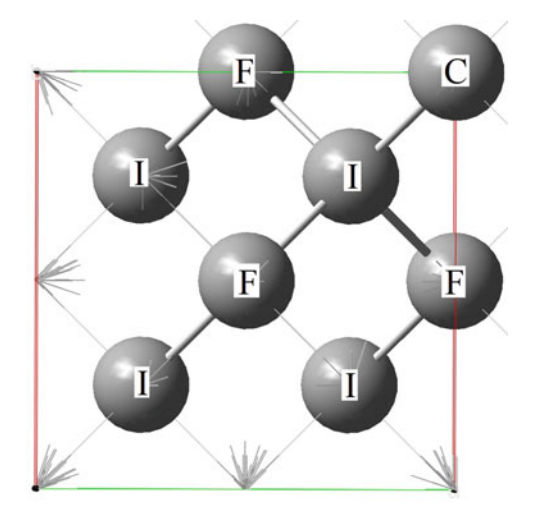
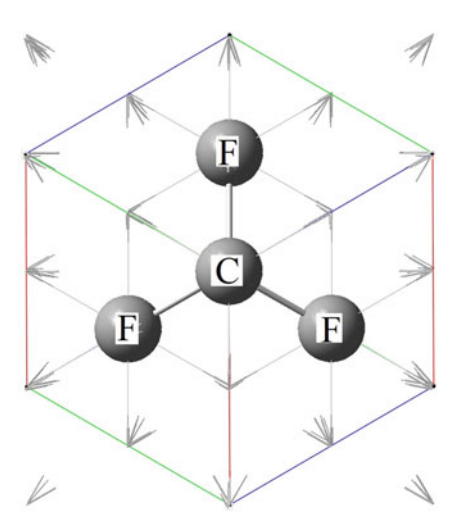


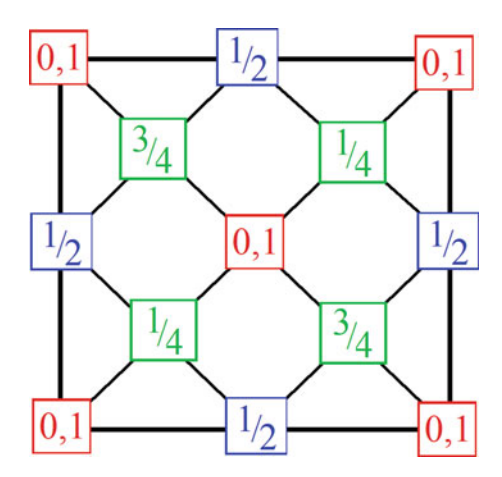
Fig. 8.3 Diamond lattice, isometric projection. Atom labels according to Fig. 8.2. Internal atoms are covered



superlative physical qualities due to strong covalent bonding between atoms  $-sp^3$  hybridization. Every atom is surrounded by four neighbouring atoms situated at the corners of tetrahedron (regular).

Figure 8.4 represents formal diamond cubic structure as a combination of two interpenetrating sub-lattices of face-centred cubic type. Both sub-lattices are displaced along the body diagonal of the cubic cell by 1/4 length of that diagonal. Origins of two face-centred cubic sub-lattices are placed at points (0, 0, 0) and (1/4,1/4,1/4). The points at 0 and 1/2 are on the face-centred cubic lattice; those at 1/4 and 3/4 are on a similar fcc lattice displaced along the body diagonal by 1/4 of its length.





Graphene represents two-dimensional planar structure (so-called layer) where carbon atoms are bonded covalently making honeycomb hexagonal lattice (six atoms per one ring,  $sp^2$  hybridization) (Fig. 8.5a). Graphene is also a basic element for another allotrope such as graphite, CNT and fullerenes. Looking from another point of view, graphene could be treated as infinite alternant polycyclic aromatic hydrocarbon [7]. In the hexagonal lattice, the interatomic distance is equal to 0.142 nm. Graphene belongs to the class of zero-gap semiconductors, and surprisingly, valence band and conduction band start at the same Dirac point. It means that the delocalized  $\pi$ -system realizes electron migration only in the plane but not between the planes. The practical usage of graphene includes light-emitting diodes (LED), solar cells, touch panels for displays and so on.

Graphite is known as the most stable allotrope of carbon under standard conditions. Several stacked graphene sheets (when the distance between planes is 0.335 nm) could form graphite. In the hexagonal lattice, interatomic distance is equal to 0.142 nm [8]. Graphite is more stable thermodynamically in comparison with diamond, and graphite is much more electronically reactive due to the properties of delocalized  $\pi$ -system.

Two types of graphite – amorphous and crystalline (including  $\alpha$ (hexagonal) and  $\beta$ (rhombohedral) crystalline forms, also bilayer graphene) – represent semimetal derivatives of a layered planar structure, with the distance between planes of 0.335 nm (in case of graphene, two-dimensional planar structure represents one sheet only). In a layer, atoms are bonded covalently making a honeycomb hexagonal lattice (six atoms per one ring). The bonding between layers is realized through the van der Waals bonds.

**Fullerenes.** Fullerenes represent a carbon derivative class of spherical or ellipsoidal form (Fig. 8.5b). The most stable and best-known form is Buckminster  $C_{60}$  fullerene [9] which is composed as a network containing 60 carbon atoms. Geometrically, this structure could be titled as a truncated icosahedron with 60 vertices and 32 faces. Carbon atoms are placed only at vertices. 12 pentagons and

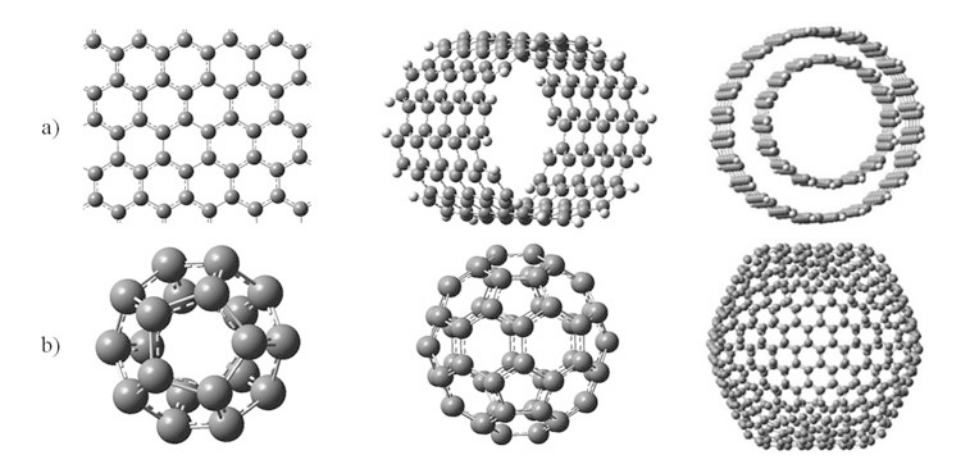


Fig. 8.5 Carbon allotropes: (a) graphene, single-walled carbon nanotube (SWCNT) and multi-walled carbon nanotube (MWCNT); (b)  $C_{20}$ ,  $C_{60}$ ,  $C_{540}$ 

20 hexagons create a pseudosphere, the so-called ball. The van der Waals diameter is equal to 1.01 nm, and the radius of molecule is 0.357 nm [10]. The electronic structure is of  $sp^2$  hybridization.

Figure 8.6 represents a nonplanar fragment of the fullerene  $C_{60}$  – the so-called hat of a fullerene. The pentagon in the centre is surrounded by five hexagons. The bond length is different for the pentagon (0.143 nm) and hexagon (0.139 nm).

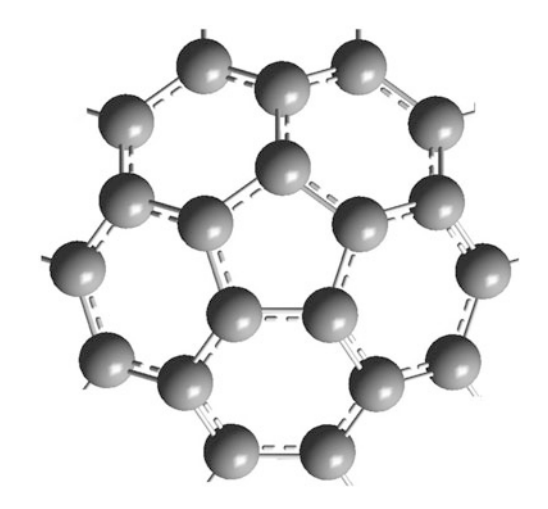
Fullerene  $C_{60}$  is quite stabile up to 1700 K in the surrounding argon and up to 500 K in the surrounding oxygen. The barrier of photoreaction is quite low: at room temperature -0.55 eV (IR region).

Figure 8.7 represents a fragment of fullerene  $C_{180}$  as half of the spherical structure. All fullerenes with the atom number <60 are unstable due to unrealized bonding properties on a plane surface. The smallest possible fullerene is dodecahedra  $C_{20}$  with the biggest sphere curvature. Instability of fullerenes with the atom number >60 arises from topological aspects – the sphere radius increases, for series  $C_{70}$ ,  $C_{76}$ ,  $C_{84}$ ,  $C_{164}$ ,  $C_{192}$ ,  $C_{216}$ ,  $C_{540}$ , and the curvature decreases. For big structures, starting from  $C_{180}$ , the sphere reforms into several islands of pseudo plane surface – see, for example,  $C_{540}$  in Fig. 8.5b.

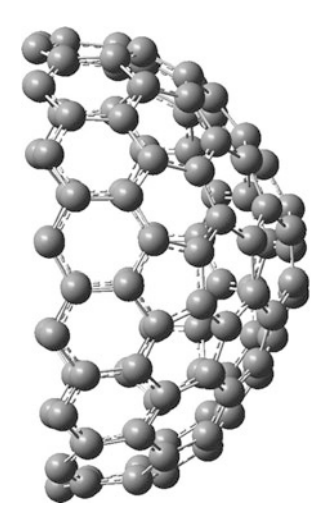
This factor (the reformation of the sphere) increases the aromatic properties only on the local surface, but not on all derivatives.

Carbon Nanotubes (CNTs). Derivatives of the tubular structure, considered as single, rolled graphite sheets, are called carbon nanotubes (CNTs) (see Fig. 8.5a). CNTs can be formed by stranded filaments that intersect with atoms of the  $sp^2$  hybridization atom, usually several nanometres in length, in a particular case up to several mm. Eatemadi et al. [11] described different forms of CNTs. The authors claimed that physical parameters such as size distribution, structure, surface area, surface charge, agglomeration state and purity of the samples have a considerable impact on the reactivity of CNTs.

**Fig. 8.6** Fragment of fullerene  $C_{60}$ . Pentagon is environed by five hexagons



**Fig. 8.7** Fragment of fullerene  $C_{180}$ . One half of spherical structure



The structure mathematically could be described by periodicity through the chiral vector  $\mathbf{C}_h$ :

$$\mathbf{C}_h = \left| \vec{\mathrm{OA}} \rightarrow \right| = n\mathbf{a}_1 + m\mathbf{a}_2 \rightarrow (n, m), \tag{8.1}$$

where (n, m) are integers,  $0 \le m \le n$ ; the so-called pair of indices,  $\mathbf{a}_1$  and  $\mathbf{a}_2$ , are the base cell vectors of graphene. Each hexagonal ring could be enumerated (n, m) as a numeric pair. Figure 8.8 represents a graphene sheet for manufacturing CNTs. The formation of CNTs can be achieved by bonding together various parts of the graphene sheet. To establish the chiral vector, two atoms in the graphene sheet must be selected: zero-point O and any point A. The main idea for this realization is to connect the points O and A by covalent junction. The vector  $\overrightarrow{OA} \rightarrow$  (between

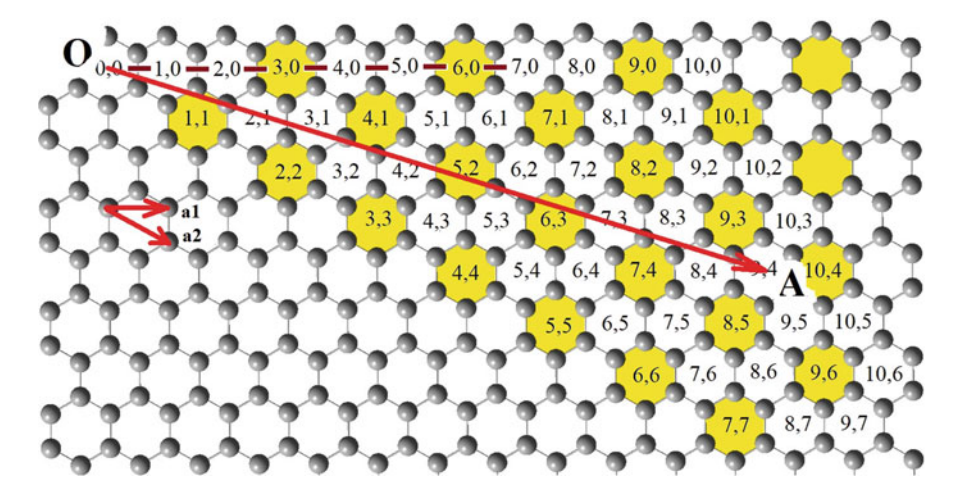


Fig. 8.8 Graphene sheet for manufacturing of CNT. Vector  $\overrightarrow{OA} \rightarrow$  for CNT(9,4). Hexagons with indices if (n-m) is divisible by 3 are yellow (for manufacturing of metallic CNT)

hexagonal rings (0,0) and (9,4)) and 0-th vector (between hexagonal rings (0,0) and (10,0)) describe the chiral angle  $\theta$ . Graphene represents the plane surface constructed from identical hexagonal rings. Let us assume that  $a_0$  is the shortest distance between two atoms in graphene plane surface,  $a_0 = 0.142$  nm; a corresponds to the lattice constant (hexagon is constructed from six triangles):

$$a = a_0 \sqrt{3} = 0.24595$$
, nm. (8.2)

Length of chiral vector *l* and diameter *d* of CNT are determined by formulas:

$$l = a\sqrt{n^2 + nm + m^2} = 0.24595, nm$$
 (8.3)

$$d = \frac{L}{\pi} = \frac{a\sqrt{n^2 + nm + m^2}}{\pi} = 0.24395, nm$$

$$d = \frac{L}{\pi} = \frac{a\sqrt{n^2 + nm + m^2}}{\pi} = 0.07828\sqrt{n^2 + nm + m^2}.$$
(8.4)

Chiral angle  $\theta$  is very important from the structural aspects – allows relating the geometrical properties to the electronic ones:

$$\vartheta = \arccos \frac{2n+m}{2\sqrt{n^2+nm+m^2}}.$$
 (8.5)

Manipulating by indices (n, m) (according to condition  $0 \le m \le n$ ) allows to generate a great number of different CNTs. Three different types of CNT are named 'zigzag' with indices (n,0) (when m=0 in any case), 'armchair' (n,n) (when n=m in any case) and 'chiral' (any n and m). These structural variations result in differences in mechanical strength and electronic properties.

Figure 8.9 represents two bending directions of graphene sheet for manufacturing CNTs. The type of CNT depends on the rolling direction.

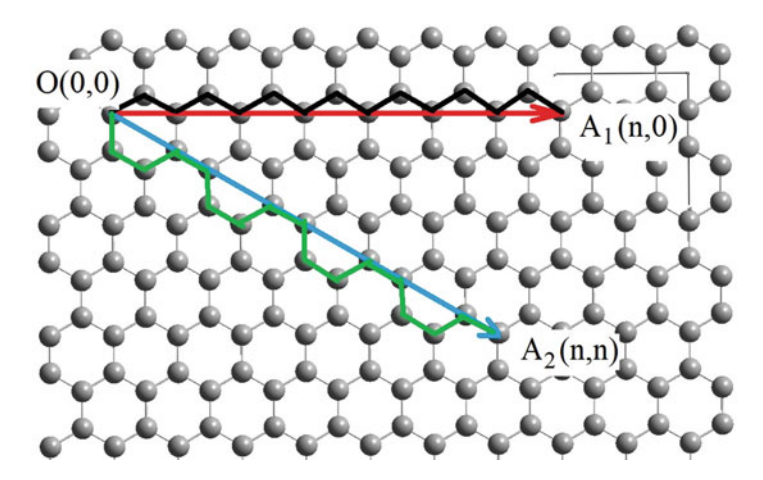


Fig. 8.9 CNT structure: zigzag type, vector  $A_1$  (n,0), and armchair type, vector  $A_2$  (n,n). Black and green figures represent zigzag and armchair, respectively

The zigzag type is determined by the vector  $\mathbf{A}_1$  (n,0), also (0,m), the chiral angle  $\theta = 0^{\circ}$ .

The armchair type is determined by the vector  $A_2(n,n)$ , also (2n,-n), the chiral angle  $\theta = 30^{\circ}$ .

Chiral type (intermediate) is determined by the vector  $\mathbf{A}(n,m)$ , where indices n and m are selected according to the condition  $0 \le m \le n$  only. In that case, chiral angle  $\theta$  is present in the range  $[0 \div 30]^{\circ}$ .

For CNTs, the difference of indices n and m could be related to the electronic properties. In the case if (n-m) is exactly divisible by 3, the structure is called metallic (with band gap 0 eV). Figure 8.8 represents a set of hexagons coloured by yellow for metallic CNTs. In the case if (n-m) is not divisible by 3, the structure is called as semiconducting (with band gap approximately 0.5 eV). The index Ims – metallic/semiconductor - plays an important role of establishing electronic properties from the structure definition:

$$I_S = (n - m) \bmod 3 = 0,$$
 (8.6)

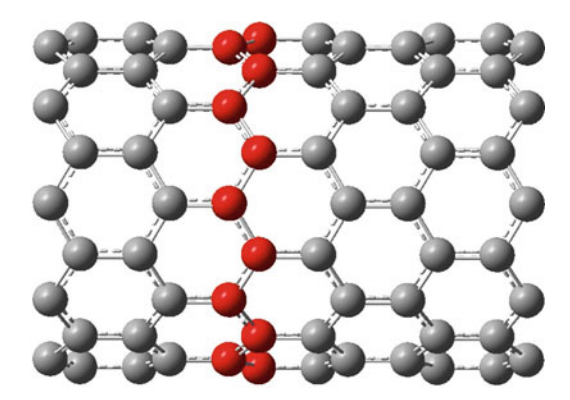
$$I_S = (n - m) \mod 3 = 0,$$
 (8.6)  
 $I_S = (n - m) \mod 3 = \pm 1.$  (8.7)

The diameter of CNTs is not limited by any physical or chemical law, but with the increase of the diameter, the mechanical stability of CNTs decreases. Tersoff et al. [12] established the relation between CNT diameter and structural properties. CNTs with the diameter of 1 nm and less behave as rigid cylinders. For diameters over 2.5 nm, CNTs flatten against each other under the van der Waals attraction, forming a honeycomb structure. This structure exhibits an anomalous rigidity, which does not decrease with increasing the CNT diameter. With decreasing the CNT diameter, the surface tension increases rapidly. The equilibrium point between such two conditions could be achieved at diameter of 1.6 nm. According to

**Table 8.2** Approximate values of diameter for CNT (n,0) of zigzag type

	Diameter, nm	n
Biggest, max	2.5	≈32
Optimal	1.6	≈20
Smallest, min	0.31	≈4

**Fig. 8.10** CNT(10,0) structure of zigzag type



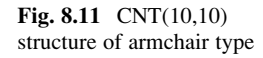
Eq. (8.4), it would be possible to estimate d and n relations for CNT of (n,0) type, when D is the biggest, optimal and smallest, respectively (see Table 8.2).

Figure 8.10 represents semiconductor CNT(10,0) of zigzag type; Figs. 8.11 and 8.12 represent metallic structures: CNT(12,3) of chiral type and CNT(10,10) of armchair type, respectively. Track atoms are coloured in red. Mentioned structures of CNT were generated using carbon nanotube generation applet, written by Veiga et al. [13].

CNT of single-wall type (SW-CNT) could be described as the long tube of diameter 1÷1.6 nm, as presented in Figs. 8.10, 8.11 and 8.12. The ends of CNT are capped by hemispheres of corresponding fullerene – see Fig. 8.7. Due to the construction properties (CNT + hemisphere of fullerene), chemical activity of such structure will be much higher at the top (with hemisphere) in comparison to the body (regular CNT). This phenomenon could be explained as follows. CNT is constructed as the rolled sheet where all carbon atoms are placed in hexagons. Hemisphere of fullerene of corresponding diameter contains pentagons with vacant valences which significantly increase the chemical activity.

Figure 8.13 represents real structure, when the ends of CNT(15,0) are connected to two hemispheres of fullerene  $C_{180}$ .

Due to the extraordinary construction (multiple oriented bonding), mechanical properties of CNTs are extreme in comparison to another molecular compound. Ternones [14] compares physical properties of CNTs and several metals (see Table 8.3). The Young's modulus of SWNT is four times greater in comparison to steel, and thermal conductivity is five times greater in comparison to copper.



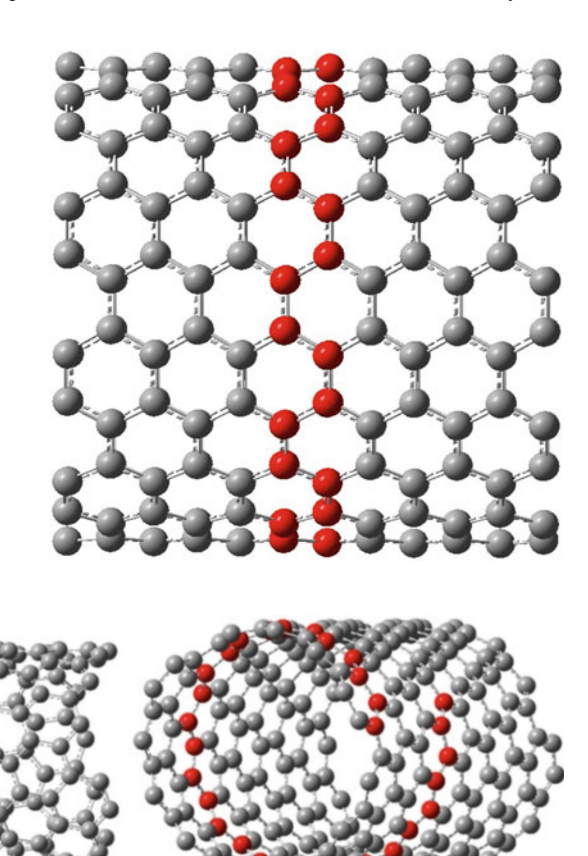
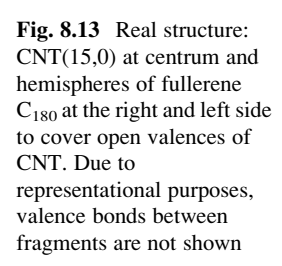
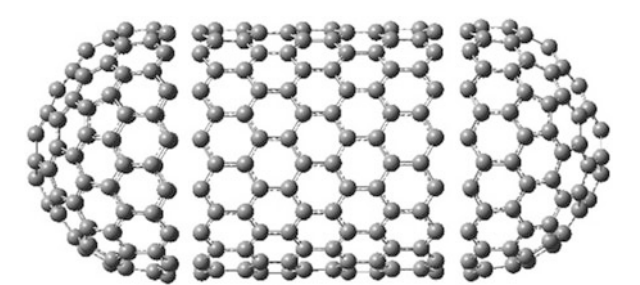


Fig. 8.12 CNT(12,3) structure of chiral type. Two projections





Multiwalled CNT (MWCNT) represents another type of CNT as the assemblies of SWCNT, which could be concentrically aligned. It means that several SWCNTs of different diameters could be aggregated in one derivative. Due to different dimensions, MWCNTs express different electronic properties.

Property	SW-CNT	Steel	Copper
Young's modulus, GPa	1000	230	117
Density, kg/m <sup>3</sup>	1300	7850	8940
Thermal conductivity, W/(m·K)	2000	50	380

 Table 8.3 Physical properties of CNT and several metals

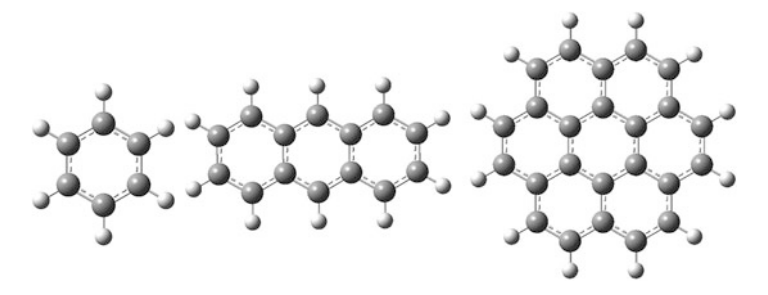


Fig. 8.14 Carbon: molecular derivatives – benzene, anthracene, coronene

#### 8.2 Carbon Derivatives: Formation of Electronic System

The simplest carbon molecular derivative of hexagonal type is benzene (see Fig. 8.14). Planar molecule consists of six carbon atoms and six hydrogen atoms. All C–C bonds are of the same length  $a_l$  = 0.140nm. Due to similar electron delocalization between each of all C atoms,  $a_l$  is intermediate in comparison to the distance between atoms while creating single bond [H<sub>3</sub>C-CH<sub>3</sub>] and double bond [H<sub>2</sub>C = CH<sub>2</sub>].

Anthracene and coronene are the polycyclic aromatic hydrocarbons consisting of three and six fused benzene rings, respectively (see Fig. 8.14).

In the framework of molecular orbitals (MO), formation of three delocalized  $\pi$ -orbitals (in space of all six carbon atoms) warrants the stability of benzene molecule (condition of aromaticity).

Maps of electronic charge redistribution were depicted according to quantum chemistry simulations using *Gaussian09 package* [15]. Optimization of ground state energy was provided using DFT B3LYP method at 6-31G(d) basis including polarization functions. Excited electronic states were simulated by TD method (for singlets only).

Wang [16] presented large review of different simulation methods, which are applicable for predicting CNT properties: atomistic and molecular dynamics.

Figure 8.15 represents electronic charge redistribution of benzene molecule. Two one-particle transitions [HOMO-1]  $\rightarrow$  [LUMO] and [HOMO]  $\rightarrow$  [LUMO + 1] of the same probability populate the first excited electronic state. The presented two MO are of great importance in the optical excitation; the last third MO (not depicted here) plays a significant role in high-energy photoelectron excitation only. Bonding orbitals [HOMO-1] and [HOMO] are constructed from three on the left and three on

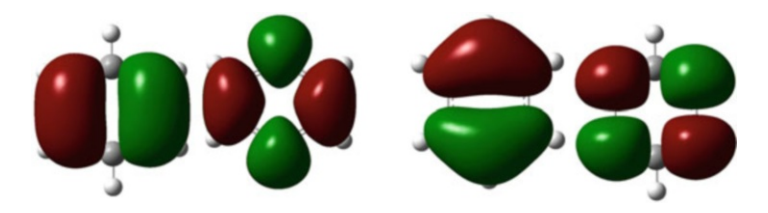


**Fig. 8.15** Benzene. Maps of electronic charge redistribution related to the transition  $S_0 \to S_I$ 

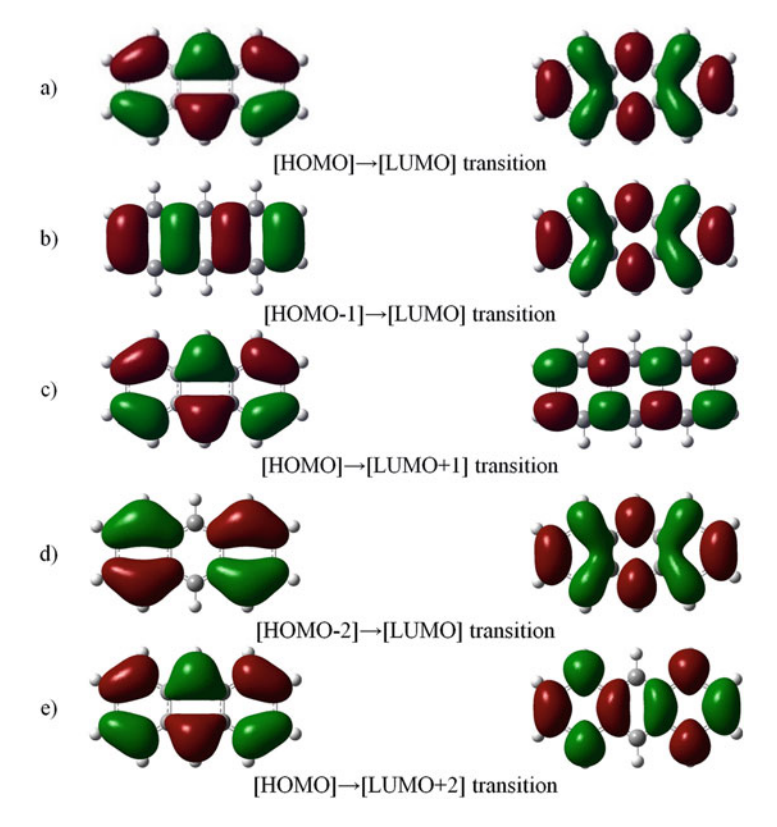


**Fig. 8.16** Anthracene. Maps of electronic charge redistribution related to the transitions: (a)  $S_0 \rightarrow S_1$ ; (b, c)  $S_0 \rightarrow S_2$ ; (d, e)  $S_0 \rightarrow S_3$ 

the right atomic orbitals (AO) when symmetry axis is vertical and horizontal, respectively (localized on three atoms). Antibonding orbitals [LUMO] and [LUMO + 1] keep the two-axis symmetry, but essential charge redistribution takes place. Atomic charge is delocalized along one of symmetry axis.

Figure 8.16 represents the electronic charge redistribution of the anthracene molecule. Two one-particle transitions are devoted to population of excited electronic states  $S_1$ ,  $S_2$  and  $S_3$ . Anthracene contains three benzene rings distributed

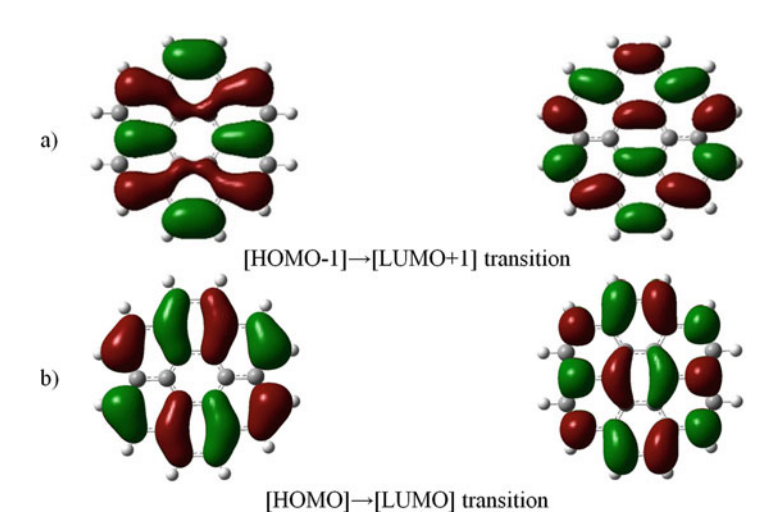


**Fig. 8.17** Coronene. Maps of electronic charge redistribution related to the transition  $S_0 \to S_I$ 

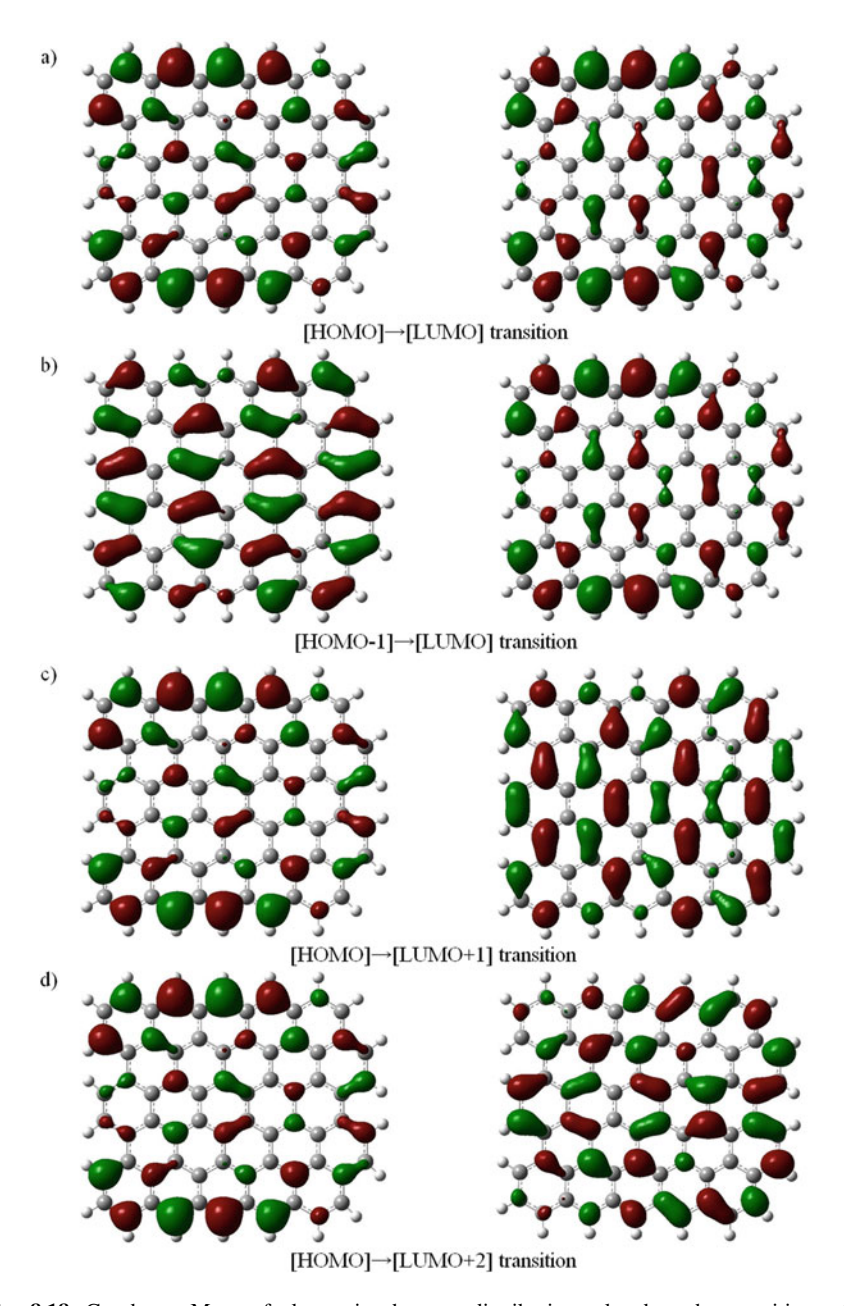
along the long axis. According to that, several bonding orbitals such as [HOMO-1] and [HOMO-2] are similar to benzene ones. [HOMO] bonding orbital contains three types of charge distributions: central parts and two axial symmetric outside parts. Antibonding orbital [LUMO] expresses specific type of charge redistribution (so-called 'big X' type – symmetric cross at the centrum). The antibonding orbital [LUMO + 1] expresses the charge redistribution on carbon atoms belonging to the neighbouring rings (and also on the outside atoms). It is necessary to point out that several MO contain substructure along the long axis for each ring (e.g. [HOMO-1]). Other molecular orbitals (e.g. [HOMO-2]) express axial symmetry properties.

Figure 8.17 represents electronic charge redistribution of the coronene molecule. Two one-particle transitions are devoted to population of excited electronic states  $S_I$ . Due to molecular geometry (hexagonal rings are placed around, but not in the straight line as in the case of anthracene), new tendencies related to charge distribution occur.

Bonding orbitals [HOMO-1] and [HOMO] are constructed from a large number of atomic orbitals (AO), where the main part of electronic charge is depopulated outside the centrum of coronene. The antibonding orbitals [LUMO + 1] and [LUMO] express the charge concentration in the centre of the coronene. For antibonding orbitals [LUMO + 1] and [LUMO], the charge delocalization outside the coronene takes place.

## 8.3 Graphene Electronic Structure

Graphene represents infinite two-dimensional structure of  $sp^2$  hybridization, where each carbon atom has four bonds, one  $\sigma$ -bond with each of its three neighbours and one  $\pi$ -bond that is oriented out of plane.



**Fig. 8.18** Graphene. Maps of electronic charge redistribution related to the transitions: (a)  $S_0 \to S_1$ ; (b)  $S_0 \to S_2$ ; (c)  $S_0 \to S_3$ ; (d)  $S_0 \to S_4$ 

Figure 8.18 represents the maps of electronic charge redistribution of graphene-25 structure. Due to the technical troubles to simulate infinite structure, graphene has been presented here as a sheet with dimensions  $5 \times 5$  with 25 hexagons (one array is created by five hexagons in the row; three arrays are bonded to each other

by covalent junction). To exclude the ionic states, free outside valences of carbons are filled by hydrogens (as in case of molecules).

Several one-particle transitions are devoted to population of excited electronic states  $S_1$ ,  $S_2$ ,  $S_3$  and  $S_4$ . As in the case of coronene, several equivalent maps or sub-maps could be observed.

Bonding orbitals [HOMO] and [HOMO-1] are constructed from a very big number of atomic orbitals (AO), when the main part of electronic charge is depopulated outside the centrum of graphene-25. Wave functions for expressing charge distribution outside the substructure are not typical for graphene. Their occurrence could be estimated as outside effect (free outside valences of carbons are filled by hydrogens).

The bonding orbital [HOMO] contains the charge localization on two atoms as well as one atom. Otherwise, bonding orbital [HOMO-1] contains charge localization on three atoms as in the case of [HOMO] benzene or [HOMO-2] of anthracene.

The antibonding orbitals [LUMO] and [LUMO + 1] express the charge redistribution in the range of one hexagonal ring with changing the localization atoms.

Usage of 25 hexagons for simulation of graphene electronic properties is sufficient but not complete. Due to the outside effect, several MO could not be mapped in formally correct form. Otherwise, the main tendencies related to charge distribution could be perceived.

Graphene as the material could be characterized by two features: (1) zerooverlap semiconductor and (2) very high electronic mobility when holes as well as electrons are charge carriers.

The chemical bonding in graphene is organized using four outer shell electrons (in each carbon atom). Each carbon atom is connected to three neighbouring atoms due to the two-dimensional structure of the carbon net. One last electron, which is not included in the valence junction, could take part in electronic conduction (occurring of  $\pi$ -orbitals). Due to the overlapping of  $\pi$ -orbitals of bonding and antibonding types, the following formation of valence and conduction bands warrants the lability of the electronic system.

The electronic mobility of graphene  $\mu$  is very high. Bolotin et al. [17] reported the maximum allowed value  $\mu = 2 \cdot 10^5 \text{ cm}^2 \cdot \text{V}^{-1} \cdot \text{s}^{-1}$  with electron densities of  $\rho = 2 \cdot 10^{11} \text{ cm}^{-2}$  which is limited by the scattering of acoustic photons of graphene.

The experiments show the lower value:  $\mu = 1.5 \cdot 10^4 \, \mathrm{cm^2 \cdot V^{-1} \cdot s^{-1}}$ . High mobility could be explained by the assumption related to the planar distribution of the graphene sheet. Due to the ballistic transport phenomenon, graphene electrons could move long distances in hundreds nm without scattering. Due to their lack of mass, motions of graphene electrons and acoustic photons are similar.

Novoselov et al. [18] reported the quantum Hall effect in graphene at room temperature. The effect is due to the magnetic energy of the electrons in graphene, which is 1000 times greater than in other materials. Novoselov claimed that electronic quality of graphene could be estimated by mentioned phenomenon.

#### 8.4 Π-Zones for Nanotubes (n,0), Nanotubes (n,n)

The geometrical form of CNTs is very important to estimate their electronic properties. All carbon atoms are distributed in space as points of hexagon apexes. Due to the curvature of CNTs, dihedral angles between hexagonal rings are not zero (different plane surfaces). It means that pure sp<sup>2</sup> hybridization (as in the case of graphene) is broken; with decreasing diameter of CNTs, the influence of sp<sup>3</sup> hybridization increases. This phenomenon is known as the factor of more active surface in comparison with plane graphene.

Saito et al. [19] studied electronic structure CNT and established the function of the diameter and helicity of the constituent CNT. Differences between metallic CNTs and semiconducting CNTs are discussed.

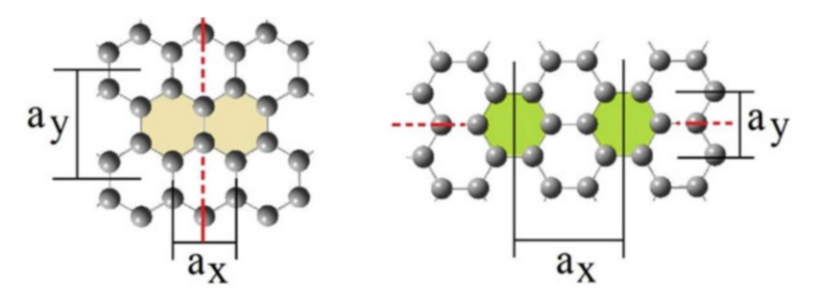
**Primitive Cell.** The task of establishing the electronic states of CNTs could be solved by several assumptions of solid-state physics. The Schrödinger equation allows estimating the system ground state energy due to several simple assumptions concerning the interaction conditions.

Let us assume the CNT is very long (in comparison to diameter) and the effects of open valences at the ends are negligible. Let us assume the existence of translational symmetry along the long axis.

As in the case of plane graphene, interactions are realized only through the  $\pi$ -orbital. For CNTs, let us assume the absence of interactions between  $\pi$  and  $\sigma$  orbitals due to different symmetry. These conditions are true only for graphene (plane surface structure). For CNTs, neglecting of the mentioned condition is allowed as the first assumption.

First of all it is necessary to define a primitive cell as a rectangle in order to define the first Brillouin zone. Figure 8.19 represents the primitive cells of CNT (n,0) and CNT(n,n).

Due to different rolling directions of the graphene sheet, primitive cells differ essentially. For the zigzag type CNT(n,0), two hexagons are connected through the side of polygon, and this side coincides with the symmetry axis (in the chart, oriented vertically). For the armchair type CNT(n,n), two hexagons are connected



 $\textbf{Fig. 8.19} \ \ \text{Primitive cells of zigzag type CNT} (n,0) \ (\text{left}) \ \text{and armchair type CNT} (n,n). \ \text{Symmetric axes are depicted in red}$ 

**Table 8.4** Parameters of primitive cells of CNT(n,0) and CNT(n,n)

Туре	$a_x$	$a_{y}$
CNT(n,0)	a	$a\sqrt{3}$
CNT(n,n)	$a\sqrt{3}$	a

via [>CC<] bond, which coincides with the symmetry axis (in the chart, oriented horizontally). For CNTs (also graphene), a side of hexagon or [..C-C..] distance is equal to  $a_0 = 0.142$  nm. The distance between opposite edges of the hexagon is equal to a = 0.2457 nm. Parameters of primitive cells are presented in Table 8.4.

Saito et al. [20] presented one-dimensional electronic band-structure model of CNTs. In both cases, a primitive cell contains 4n atoms and also 4n pi-orbitals. Due to the translational symmetry of the system, the 4n basis Bloch functions will describe the system. The rotating symmetry (about long axis) allows decreasing the dimensionality of the secular equation.

**CNT** (n,0). Several features are significant due to CNT structure. According to the assignments of the primitive cell,  $a_x = a$ ,  $a_y = a\sqrt{3}$ . Such two factors determine phase factor ka. The translational wave vector k could vary at k-space:

$$-\frac{\pi}{\sqrt{3}a} < \mathbf{k} < \frac{\pi}{\sqrt{3}a},\tag{8.8}$$

$$-\frac{\pi}{\sqrt{3}} < ka < \frac{\pi}{\sqrt{3}}.\tag{8.9}$$

After solving the Schrödinger Eq. (8.16), the dispersion of  $\pi$  bands energy on the phase factor ka is expressed by Eq. (8.3):

$$E_{n\,m}^{\pm} = \alpha \pm \beta S_I,\tag{8.10}$$

where  $\alpha$  and  $\beta$  are the Coulomb and exchange integrals, respectively, and  $S_I$  represents the so-called phase factor for CNT(n,0):

$$S_I = \sqrt{1 + 4\cos\frac{\sqrt{3}ka}{2}\cos\frac{\pi m}{n} + 4\cos^2\frac{\pi m}{n}}.$$
 (8.11)

The integer number m represents behaviour of rotational symmetry:

$$m = 1, \dots, n. \tag{8.12}$$

Let us divide Eq. (8.10) by value of the exchange integral  $\beta$ . Energy  $\gamma$ , normalized by value ( $\alpha/\beta$ ), will be used for estimations:

$$\frac{E_{n,m}^{\pm}}{\beta} = \frac{\alpha}{\beta} \pm S_I, \tag{8.13}$$

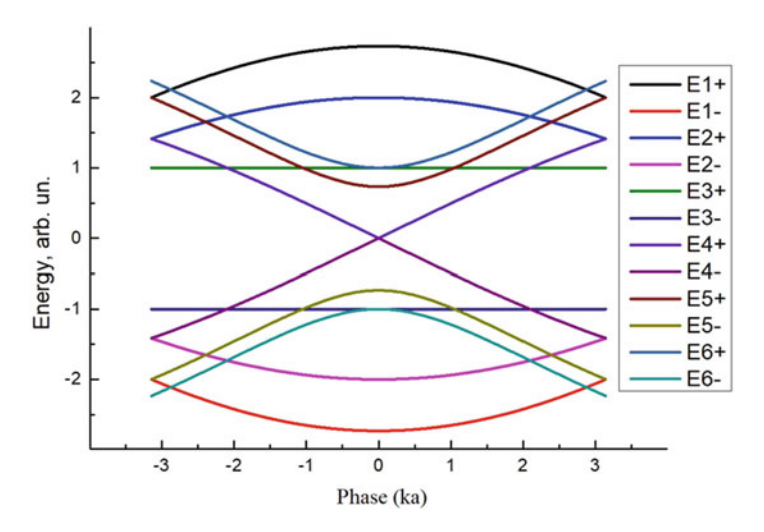


Fig. 8.20 Π-zones of metallic CNT(6,0). Fermi level is set at zero

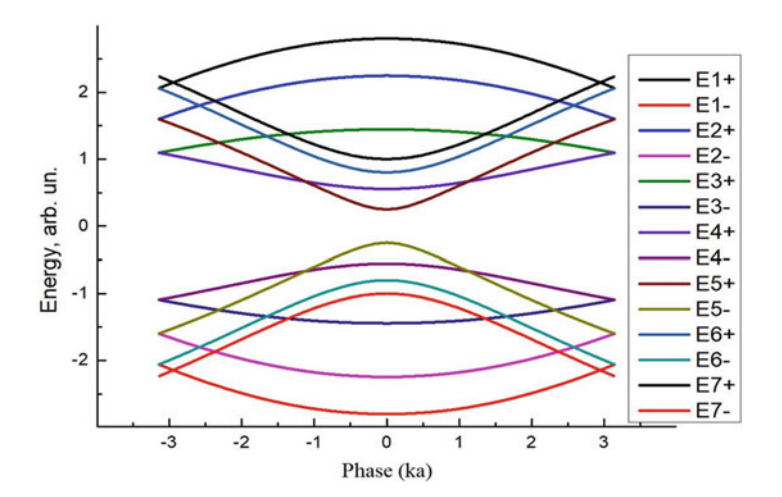


Fig. 8.21 Π-zones of semiconductor CNT(7,0). Fermi level is set at zero

$$\gamma = \frac{E_{n,m}^{\pm}}{\beta} = \pm S_I. \tag{8.14}$$

Figures 8.20 and 8.21 represent  $\Pi$ -zones of metallic CNT (6,0) and semiconductor CNT(7,0), respectively. The dispersion of  $\pi$  bands energy  $\gamma$  on the phase factor ka was calculated according to Eq. (8.14). Due to the energy normalization by value  $(\alpha/\beta)$ , the energy dependency is shifted down when zero corresponds to the Fermi level.

The solution of the Schrödinger equation contains  $(\pm)$  factor (see Eq. (8.10)). It is easy to check that the symmetry of the energy band distribution is defined by the mentioned factor.

Axis of symmetry is distributed at the position of the Fermi level. The valence bands (below Fermi level) correspond to HOMO, and lower states in molecular structures and conductive bands (before Fermi level) correspond to LUMO and higher states. The number of bands corresponds to the number 2n (due to  $(\pm)$  factor, minus for valence, plus for conductive). At a certain position of the phase ka, some values of  $\gamma$  coincide.

For CNT (6,0), the gap between zones is absent – two state curves of the valence zone and conducting zone intersect only in the centre of the Brillouin zone (see Fig. 8.21), when k = 0.

Due to the absence of gaps, CNT (6,0) expresses the metallic properties. Another CNT such as CNT (9,0), CNT (15,0), etc. will be also of the metallic type.

For CNT (7,0), the gap between zones is present in the centre of the Brillouin zone, when k = 0. Due to any intersections between the curves of the valence zone and conducting zone (see Fig. 8.22), CNT(7,0) is called semiconducting with the optical gap. Graphene belongs to zero-gap semiconductors.

*CNT* (n,n). According to the assignments of the primitive cell,  $a_x = a\sqrt{3}$  and  $a_y = a$ . Such two factors determine the phase factor ka. The translational wave vector k could vary at k-space:

$$-\frac{\pi}{a} < \mathbf{k} < \frac{\pi}{a},\tag{8.15}$$

$$-\pi < ka < \pi. \tag{8.16}$$

After solving the Schrödinger Eq. (8.16), the dispersion of  $\pi$  bands energy on the phase factor ka is expressed by Eq. (8.17):

$$E_{n\ m}^{\pm} = \alpha \pm \beta S_2,\tag{8.17}$$

where  $S_2$  represents the so-called phase factor for CNT(n,n):

$$S_2 = \sqrt{1 + 4\cos\frac{ka}{2}\cos\frac{\pi m}{2} + 4\cos^2\frac{ka}{2}}.$$
 (8.18)

Integer number m represents behaviour of rotational symmetry:

$$m = 1, \dots, n. \tag{8.19}$$

As in the previous case, energy normalization routine takes place:

$$\gamma = \frac{E_{n,m}^{\pm}}{\beta} = \pm S_2. \tag{8.20}$$

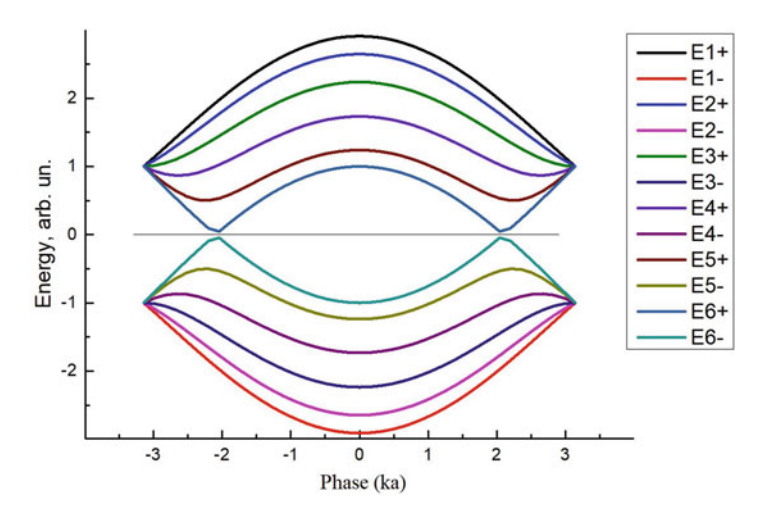


Fig. 8.22 Π-zones of metallic CNT (6,6). Fermi level is set at zero

Figure 8.22 represents  $\Pi$ -zones of CNT (6,6). The dispersion of  $\pi$  bands energy  $\gamma$  on the phase factor ka was calculated according to Eq. (8.13). All curves representing valence and conducting bands start from two points  $\gamma = 1$  and  $\gamma = -1$ , respectively, when  $ka = \pi$ . Such two values could be obtained by the absence of the second and third factor in Eq. (8.11) due to  $\cos(\pi/2) = 0$ .

A gap between zones is absent – state curves of the valence zone and conducting zone intersect at the cross value phase:

$$(ka)_{\rm C} = \frac{2\pi}{3}. (8.21)$$

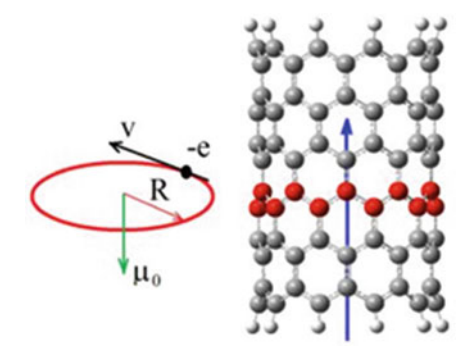
Due to the absence of the gap, CNT (6,6) expresses the metallic properties. Another CNT such as CNT (7,7), CNT (10,10), etc. will be also of the metallic type.

## 8.5 Nanotubes: Electronic Angular Momentum and Spin-Dependent Properties

A model of the hydrogen atom (a heavy proton in the centre and an electron in the orbital motion) is a classic example for explaining the orbital magnetic moment  $\mu_{\text{ORB}}$  (see Fig. 8.23). A negative charged particle e performs a motion with a velocity v with a radius R, which acts as a current loop:

$$\mu_{\text{ORB}} = \frac{evR}{2}.\tag{8.22}$$

Fig. 8.23 Classical orbital magnetic moment for electron and CNT in magnetic field directed along the long axis (blue arrow)



Let us assume a CNT in the magnetic field, directed along the long axis (blue arrow). For a metallic CNT (diameter D), the transition of the conducting electron along the long axis as well as around the circumference of the CNT is allowed. The orbital magnetic moment  $\mu_{\text{ORB}}$  could be created when electrons are moving around the tube (according to the mechanistic model similar to a hydrogen atom).

The potential energy E is proportional to the external magnetic field B, which is directed along the long axis:

$$\Delta E = -\mu_{\text{ORB}}B = \pm \frac{evDB}{4}.$$
 (8.23)

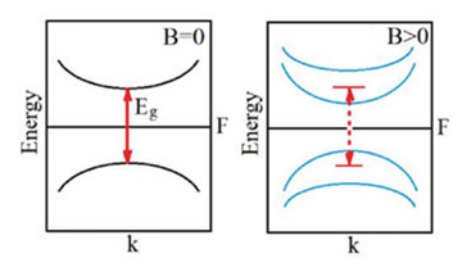
The influence of the magnetic field into the structure of the  $\Pi$ -zone is evident. Figure 8.24 represents a simplified chart of one CNT  $\pi$ -zone in the absence and presence of the magnetic field oriented along the long axis. Two serious phenomena occur. Firstly, the degenerated zone splits into two zones in the valence as well as conductance regions. Secondly, a significant decrease of the gap occurs in the presence of the oriented magnetic field. Minot et al. [21] announced the occurrence of  $\mu_{\rm ORB}$  for states near the energy gap. Minot found that the orbital magnetic moment (due to the motion around the circumference of CNT) is much larger than the Bohr magneton.

The orbital magnetic moment plays the main role in the magnetic susceptibility of CNTs [22]. It means that the electronic properties of CNTs can be modulated by a magnetic field. Oscillations of the energy band structure could realize the reversible switch of CNT properties between a metal and a semiconductor.

Several spin-dependent properties which are most promising in spintronics are presented as follows: chirality-dependent spin polarization, gate-dependent spin-orbit coupling and spin filtering.

Wang et al. [23] analysed chirality-dependent spin polarization through the spin density of a chiral CNT (9, m), which decreases gradually with the increase of m. Wang established that the spin of the ground state for the armchair CNT (9, m) mainly comes from the contributions of the frontier molecular orbitals and the energy gap decreases gradually with the spin density for chiral CNTs.

Fig. 8.24 Simplified chart of CNT  $\pi$ -zone in absence and presence of magnetic field along the long axis. Split of degenerated zone into two zones and following decreasing of gap



Analysing the interactions of orbital motions of electrons with the spin in the nanoscale systems, Jespersen et al. [24] reported systematic dependence of the spin—orbit coupling on the electron occupation of the CNT quantum dot. Jespersen confirmed that the spin—orbit coupling is a general property of CNT quantum dots.

Wang et al. [25] analysed transport of graphene nanoribbons through a longitudinal unzipped carbon nanotube in the longitudinal direction. Wang established the variation of the Fermi energy from (a) an insulator to a spin-down half metal and (b) an insulator to a spin-up half metal. He guessed that a spin-filter device can be realized using graphene nanoribbons.

# 8.6 Nanotubes of the Metal Type and of the Semiconductor Type

By estimating the electronic structure for different types of CNTs, it is necessary to analyse the inhomogeneous energy distribution on the one-dimensional density of states (DOS). Three-dimensional crystals have continuous DOS; otherwise, one-dimensional crystals are of another type. A characteristic evidence of the distribution is a gradual descend of energy followed by a fast increase (a sharp spike form). For one-dimensional crystals, sharp peaks in the energy distribution are called the van Hove singularities.

Figure 8.25 represents energy diagram of semiconducting and metallic SWCNT. The valence zone (green) and conducting zone (dark yellow) are separated by a gap (semiconducting CNT) or are joined at a contact level – the Fermi level (metallic CNT).

Transition from the valence zone to the conduction zone (absorption) for both semiconducting and metallic SWCNTs is dipole-allowed with the high oscillator strength:  $V_1 \rightarrow C_1$ ,  $V_2 \rightarrow C_2$ , etc. The crossover transitions  $C_2 \rightarrow V_1$ ,  $C_1 \rightarrow V_2$  are dipole-forbidden with the low oscillator strength. Using the cross-polarized optical geometry, Miyauchi et al. [26] reported the presence of significant anisotropy from polarized photoluminescence measurements of the mentioned dipole-forbidden transitions.

The type of CNTs (metallic or semiconducting) could be recognized from the absorption spectrum in VIS and near-IR region.

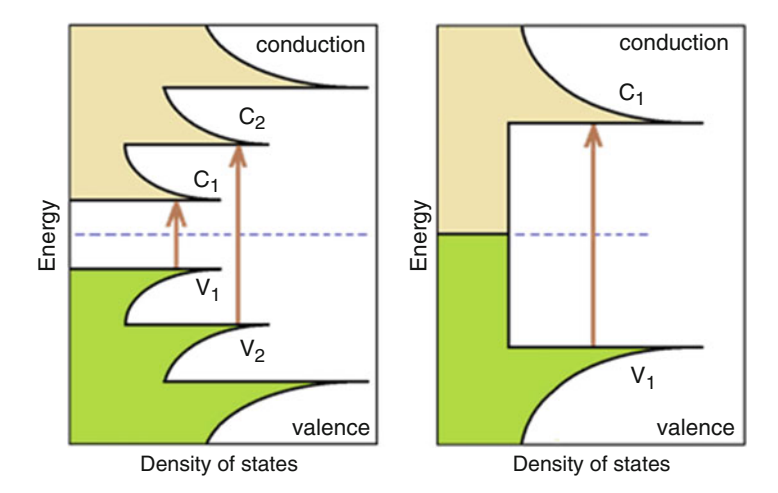


Fig. 8.25 Energy diagram of semiconducting (left) and metallic SW-CNT

A selective excitation of CNTs with indices (n, m) could be realized by exact absorption in the selected band restricted by the van Hove singularities. By varying the structure of CNTs, it is possible to tune optoelectronic properties of CNTs selected on demand. Iakoubovskii et al. [27] demonstrated that even weak UV light 1 mW cm<sup>-2</sup> can irreversibly alter the SWCNT structure. These UV-induced changes are attributed to the creation of mid-gap PL centres.

Figures 8.26 and 8.27 represent the maps of electronic charge redistribution related to the transition  $S_0 \rightarrow S_1$  for CNT (14,14) and CNT (24,24) of armchair type, respectively.

Both maps are devoted to the HOMO  $\rightarrow$  LUMO transition. Electronic clouds distributed over the whole surface of the derivative are absent in both cases. The distribution of molecular orbitals is localized on the atom groups. For CNT (14,14), the HOMO state corresponds to a cloud localized on two atoms on the edge, and two neighbouring clouds create a pair of V-type. The LUMO state corresponds to clouds localized on two atoms and parallel aligned around the circumference. For CNT(24,24), the HOMO state corresponds to the cloud localized on two atoms parallel aligned around the circumference. For the LUMO state, localization decreases up to one atom.

As Wildoer et al. [28] and Odom et al. [29] stated, the electronic properties of CNTs depend sensitively on the tube diameter. Increasing the diameter of CNTs, the curvature of the tube becomes flatter, and the reorientation of the junctions changes the dihedral angles.

Molecules consisting of only one element (carbon) may have very different electronic behaviours – a shift from a metallic to a semiconducting state.

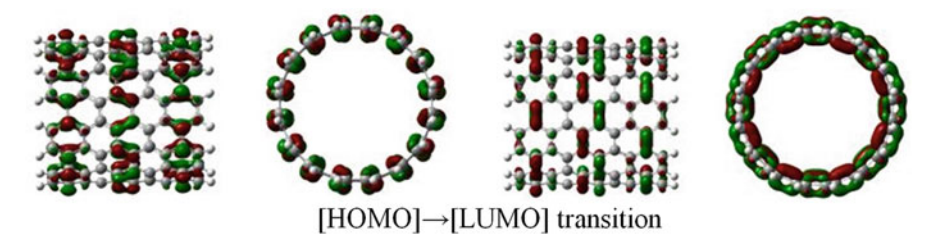


Fig. 8.26 CNT (14,14) of armchair type. Maps of electronic charge redistribution related to the transition  $S_0 \rightarrow S_1$ 

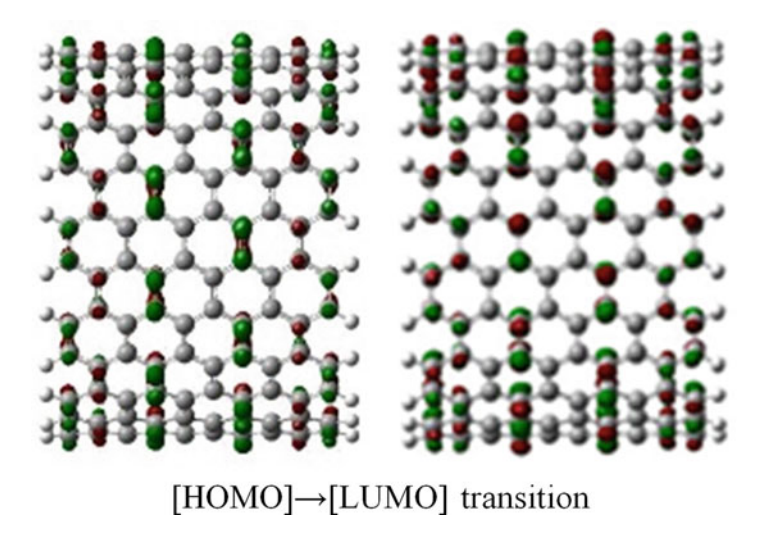


Fig. 8.27 CNT (24,24) of armchair type. Maps of electronic charge redistribution related to the transition  $S_0 \rightarrow S_1$ 

### 8.7 Chemistry of Nanotubes: Catalysis and Toxicity

A CNT is a well-known active catalyst material due to several unique properties.

Firstly, CNT is a consistent material with an extra high thermal and mechanical stability. Without participating in any permanent chemical changes, CNT only increases the rate of chemical reaction and the subsequent yield of the product. Secondly, the choice of CNTs due to helicity and diameter (from 1 nm to 10s of nm) allows to control the surface impact. Due to that, CNTs sometimes are called a catalyst on demand. The use of large tubular surfaces allows the organization of efficient heterogeneous catalysts [14].

Thirdly, the geometrically fixed tubular surface of CNTs avoids high purity in the molecular environment with low dipole activity. This factor guarantees a high resistance to oxidation, called chemical inertness [19].

Fourth, the catalytic reaction can be carried out by controlling the electrical and thermal conductivity of CNTs. Depending on their helicity and diameter, metallic or semiconducting CNTs can obtain different parameters related to the charge transfer processes [11].

Fifthly, because of the high thermal conductivity of CNTs, preventing the agglomeration of the product and the subsequent separation of product phases can be organized as an additional stage in the reaction. The inhomogeneity of the annealing can be guaranteed with a very low gradient.

Luo et al. [30] observed the application of CNTs in fuel cells. The use of CNTs for such purposes can decrease the need for noble metals which are used as catalysts and improve the performance of fuel cells. In addition, the interaction between catalysts and carriers of CNTs and the conditions for the synthesis of a catalyst based on CNTs were discussed and evaluated.

Girishkumar et al. [31] reported the use of CNT-based electrodes that demonstrate an order of magnitude less reactivity of the charge transfer reaction for the hydrogen evolution reaction compared to commercial carbon black-based electrodes.

According to the constitution of CNTs, the electronic activity is very low. The electronic excitation of single CNTs is related to the charge redistribution localized in the framework of several atoms (or in the framework of primitive cell) (see Figs. 8.26 and 8.27). Otherwise, the environment effects can significantly change the behaviour of the charge redistribution and the following electronic activity.

As active material with well-expressed  $\pi$ - and n-electronic systems, indandione-related compounds were selected [32]. Figure 8.28 represents M66 merocyanine compound containing spiropyran and indan-1,3-dician-dione fragments, which are connected via the [..C = C..] bridge. The derivative of merocyanine expresses one of the biggest molecular nonlinear optical (NLO) coefficient  $\beta$  which is proportional to the oscillator energy and depends on the transition dipole moment. In addition, for the M66 merocyanine compound, high value of  $\beta$  could be limited by the molecular structure when the  $\pi$ -electronic system could be supplemented by the impact of the n-electron from fragments (cyano and carbonyl fragments). Due to the connection via [..C = C..] bridge, a big lability of the molecule delimits several forms of conformers.

Figure 8.29 represents a M66 merocyanine compound in the near surrounding of CNT (14,14). Due to well-expressed donor–acceptor properties for the pair [M66.. CNT], the intermolecular charge redistribution takes place. It is interesting that intermolecular distances are too big in order to establish the valence function. For an excited state, the charge redistribution in CNTs could be titled as hemi tubular (divided into two parts). It is the influence of the M66 molecule, which could play a role of donor on *n*-electrons.

The toxicity of CNTs is related to the environment interactions. The presence of any material and subsequent deposition on the CNT surface dramatically changes the electronic properties of the molecule both in the ground and in the lowest excited states. In this case, it is necessary to emphasize a new field of use: CNT-mediated cytotoxicity (toxicity in the cell structure). Madani et al. [33]

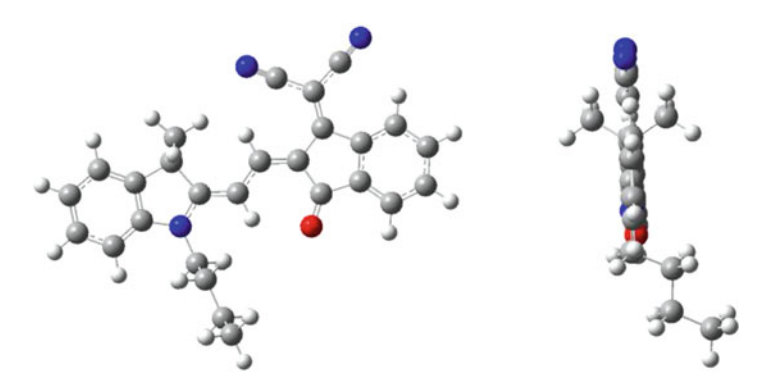


Fig. 8.28 M66: merocyanine compound containing spiropyran and indan-1,3-dician-dione fragments

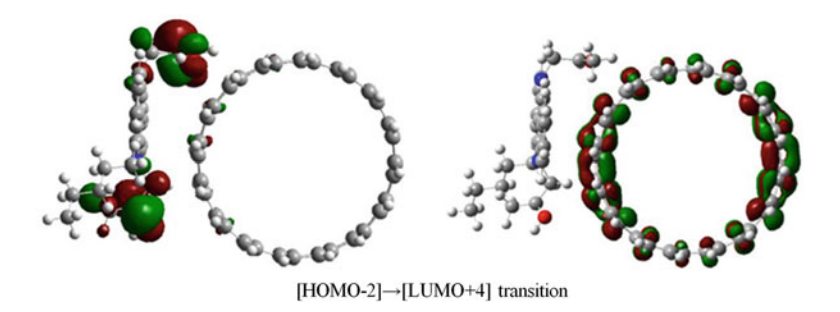


Fig. 8.29 M66 merocyanine compound in near surrounding of CNT (14,14). Maps of electronic charge redistribution related to the transition  $S_0 \rightarrow S_6$ 

observed the potential use of CNTs as agents for cancer treatment and drug delivery. The ability of CNTs to absorb NIR light and generate heat can be considered as possible ways of intrusion into the cellular space. Madani et al. [33] described four factors, which are significant for CNT cytotoxicity: (1) the presence of impurities, (2) the shape, (3) functionalization and (4) the size.

The impurities of transition metals, such as iron, cobalt and nickel after deposition on the surface of CNTs, disrupt the electronic system to create additional activated centres. The following deposition on the additional activated surface can be realized using the materials surrounding the cells. Transit through the cell membrane of a large CNT should be considered as a mechanical action. Because of the certain shape (rod or fibrous), CNTs can damage the cell membrane as bilayer of phospholipids [11].

The functionalization of CNTs can be increased or decreased by changing the environmental parameters by adding/extracting certain acids, polymer chains, cations/anions, etc. With increasing diameter, the mobility of CNT through cell membrane decreases.

**Table 8.5** Typical fundamental properties of graphene [36–48]

Property	Value
Young's modulus	1.0 TPa
Fracture strength	130 GPa
Tensile strength	100 GPa
Thermal conductivity	5000 w/mK
Shear modulus	280 GPa
Longitudinal sound velocity	20 km/s
Melting temperature	4900 K
Specific surface area	2630 m <sup>2</sup> /g
Optical transmittance	97.70%
High electron mobility	250,000 cm <sup>2</sup> /vs

# 8.8 The Influence of Defects on Electrical, Mechanical and Thermal Properties of Graphene

Defect types in graphene were considered in a number of papers. See, for example, Rajasekaran et al. [34] and Krasheninnikov et al. [35]. Table 8.5 demonstrates typical values of fundamental graphene characteristics, which usually are the subject of scientific and technological interest. However, in 2009 Taghioskoui [49] and Geim [50] paid attention to graphene nanofillers as some new trend of graphene technology development. This new research resulted in opening the defective states of graphene. Most of the research on nanofillers is usually concentrated on the pristine graphene. It was shown that the structural defects which are inevitable during the production process affect the mechanical properties as well as thermal and electrical conductivities of graphene and graphene-based nanocomposites [51, 52] (Table 8.6).

Stone-Thrower-Wales (STW) Defects. Robertson and Warner [55] analysed one of the unique properties of the graphene lattice. It is its ability to reconstruct by forming non-hexagonal rings. The STW defect is the 90° rotation of two carbon atoms connected by short-ranged covalent bond with respect to the midpoint of the bond. Transformation of four adjacent hexagonal unit cells into two pentagonal and two heptagonal unit cells, due to two pentagon and two heptagon transformation STW defects, is also known as 5-7-7-5 defects [55].

*Vacancy Defects.* Vacancies in graphene were considered in a set of papers (see, e.g., [65, 71, 74]). The absence of atoms from the lattice of graphene is usually termed as vacancy defects, which can be further subclassified as mono-vacancy, di-vacancy and multi-vacancy defects based on a number of atoms absent from the lattice of graphene. The absence of single carbon atom from the graphene lattice yields a mono-vacancy, which left the graphene lattice with three under coordinated edge carbon atoms; each of them possesses a single dangling bond. There are some typical graphene defects which arise from vacancies in a pristine graphene structure after relaxation of dangling bonds: stable 5-8-5 structure, 555-777 structure and 5555-6-7777 structure [34].

Graphene defect engineering	Research direction
Controlled distributions of topological defects [53, 54]	Mechanical properties, thermal and electrical conductivities of graphene
Atomic resolution imaging of graphene [55, 56]	Mechanical and fracture properties of graphene
Graphene sheets [57, 58]	Mechanical properties of graphene
Defect engineering of graphene for effective hydrogen storage [59]	Stone–Thrower–Wales (STW) and vacancy defects for improved hydrogen storage
Defect control engineering [60]	Defect control engineering-based tailoring of graphene's electronic, chemical, mechanical and magnetic properties
Graphene doping [61]	Dopant and STW defects to improve gas-sensing properties of graphene
Intrinsic defects of bilayer graphene [62]	Mechanical properties and strength of pristine graphene in the frame of molecular dynamics (MD), finite element and experimental work

**Table 8.6** Graphene defects research in the field of nanofillers

Dislocations and Grain Boundaries. Some particular investigations of Bitzek and Gumbsch ([63]) have shown a special class of defects such as dislocations and grain boundaries. It is known that the fracture toughness critically depends on the microstructures of the materials and, in particular, on how the dislocations are generated or multiplied at the tip of the crack [63]. This fundamental defect is of great interest to materials scientists. It is the form of defects where the excess half of the plane of the atoms can destroy the strength of graphene [64]. Due to the two-dimensional (2D) nature of graphene, only edge dislocations have been studied. Talking about the so-called grain boundaries, we define them as line defects (composed of dislocation), separating graphene grains (domains/crystallites) with different crystal lattice orientations. Namely, each grain boundary in a 2D graphene separates two grains whose crystal lattices are rotated/tilted relative to each other by a tilt misorientation angle  $\theta$ , with the rotation axis being perpendicular to the sheet plane [65].

Following the general concept of atomic and electronic structure correlations, any local and distributed defects in graphene will generate new electronic states and change the conductivity and optical properties.

# 8.9 Defected Nanocarbon Systems

Carbon-based nanomaterials such as CNTs, graphene, mesoporous nanocarbon, carbon quantum dots and other nanocarbon formations due to their large *surface-to-volume ratio* possess good electrical and thermal conductivity and mechanical strength. These unique properties make them suitable for application in different

Carbon application	Technological comments
A glassy carbon electrode modified with mesoporous carbon [75]	Direct electrocatalytic and simultaneous determination of four DNA bases
Modified mesoporous carbon composite [76]	NADH sensor based on gold nanoparticle
Electrode modified with CeO <sub>2</sub> -embedded ordered mesoporous carbon [77]	Strong electrocatalytic effect towards the oxidation of hydrazine
Mesoporous carbon with controllable defect density [66]	Electrochemical activity of synthesized materials, cyclic voltammetry and electrochemical impedance spectroscopy

**Table 8.7** Mesoporous carbon nanostructure applications

fields, including energy storage [68]; chemical, biochemical and electrochemical sensing [69]; water purification [67]; catalysis [70]; and many more.

Structural defects have a crucial influence on the properties of carbon nanostructures and inevitably generate during production processes or intentionally induced by chemical treatments and ion irradiation [52]. The availability of defects in nanocarbon structures significantly affects the mechanical strength, electrical and thermal conductivity and optical properties [52, 71].

Various experimental techniques which are responsible for defect creation in nanocarbon structures (porous nanocarbons, nanofoams, defect graphene, heavy ion-based nanotrack structures, nanocarbon interfaces with dangling bonds, etc.) give many variants for design of nanosensors and nanotransducers.

*Electrochemical Sensing.* The essential impact of structural defect on the electrochemical activity has been proved by the study of heterogeneous electrochemical reactions, e.g. oxygen [72] and nitrate [74] and ferrocenemethanol [73] at the surface of nanocarbon-based electrodes. Some particular applications of electrochemical nanosensoring application details are presented in Table 8.7.

Synthesis and Gas Sorption, Storage and Separation. Achievements and challenges in the syntheses of graphene-based materials with hierarchical pore structures, tuneable high surface area, chemical doping and surface functionalization for gas (NH<sub>3</sub>, NO<sub>2</sub>, H<sub>2</sub>S, SO<sub>2</sub>, H<sub>2</sub>, CH<sub>4</sub>, CO<sub>2</sub>, N<sub>2</sub>, etc.) sorption, storage and separation are based on graphene structure defect forms and states. This is a reason of intensive researches of various graphene modifications [78].

Hydrogen Storage: Expanded and Pillared Graphene Layers. The planar sheet of graphene with its inherent specific surface area of 2630 m<sup>2</sup>/g in the ideal case has further motivated theoretical calculations for gas adsorption from the well-established carbon nanotubes and graphitic structures. The adsorption of a monolayer of  $H_2$  on a single side of graphene sheet can lead to about 3 wt% of  $H_2$  [79].

*Hydrogen Storage: Pillared Graphene Oxide Structures.* The loosely stacked layers in GO similar to graphite, but with a much wider interlayer spacing (0.6–0.9) nm, would be more convenient to store H<sub>2</sub> [80].

**Doped, Functionalised and Metal-Dispersed Graphenes.** Simple graphene-based nanostructures show weak binding energy thus low H<sub>2</sub> adsorption capacity at ambient conditions [81].

*Graphene-Based Materials.* Grafane is nothing but graphene with alternately covalent bond hydrogen atoms on each carbon atom on both sides of the graphene sheet. Structurally graphene is crumpled, rather than planar, because each hydrogen atom bonded to carbon pulls it a small distance out of the plane [82].

**Hydrogen Spillover.** The  $H_2$  adsorption by hydrogen spillover is a hydrogen dissociative atomic adsorption, and it has been found to be another alternative to enhance  $H_2$  adsorption in the carbonaceous materials. The spillover is expected in some of the graphene-based materials with functionalized/doped structures [83].

*CH*<sub>4</sub>*and CO*<sub>2</sub>: *Sorption, Storage and Separation.* Similar to H<sub>2</sub> adsorption, graphenes with ripples, defects, pores, functional groups, metal dispersion or doping and pillaring also show favourable CH<sub>4</sub> and CO<sub>2</sub> adsorptions [84].

Gas Separation Membranes Pristine and porous 2D graphene membranes with and without functionalization have been investigated for gas purification. The pristine graphene is impermeable to He and  $H_2$  [85, 86].

#### References

- 1. Hirsch A **2010** The era of carbon allotropes *Nature materials* **4** 868–70
- 2. Greenville Whittaker A **1978** The controversial carbon solid-liquid-vapour triple point *Nature* **276**(5689) 695–6
- Shenderova O A, Zhirno V V, Brenner D W 2002 Carbon Nanostructures Critical Reviews in Solid State and Materials Sciences 27(3/4) 227–356
- Cambridge Structural Database 2016 https://www.ccdc.cam.ac.uk/structures-beta/, retrieved 2016–10-14
- 5. Crystallography Open Database 2016 http://www.crystallography.net, accessed 2016 10 02
- Straumanis M E, Aka E Z 1951 Precision determination of lattice parameter, coefficient of thermal expansion and atomic weight of carbon in diamond J. Am. Chem. Soc. 73 5643–6
- Simpson C D, Brand J D, Berresheim A J, Przybilla L, Räder H J, Müllen K 2002 Synthesis of a Giant 222 Carbon Graphite Sheet *Chemistry* 6(6) 1424–9
- Cooper D R, D'Anjou B, Ghattamaneni N, Harack B, Hilke M, Horth A, Majlis N, Massicotte M, Vandsburger L, Whiteway E, Yu V 2012 Experimental Review of Graphene ISRN Condensed Matter Physics International Scholarly Research Network 2012 1–56
- 9. Singh S B, Singh A 2002 The Third Allotrope of Carbon: Fullerene an Update *International Journal of ChemTech Research* **5**(1) 167–71
- Qiao R, Roberts A P, Mount A S, Klaine S, J, Ke P C 2007 Translocation of C60 and Its Derivatives Across a Lipid Bilayer Nano Letters 7(3) 614–9
- Eatemadi A, Daraee H, Karimkhanloo H, Kouhi M, Zarghami N, Akbarzadeh A, Abasi M, Ha-nifehpour Y, Joo S W 2014 Carbon nanotubes: properties, synthesis, purification, and medical applications *Nanoscale Research Letters* 9 393
- Tersoff J, Ruoff R S 1994 Structural Properties of a Carbon-Nanotube Crystal Physical Review Letters 73(5) 676–9

13. Veiga R G A, Tomanek D, Frederick N **2008** Carbon nanotube generation applet, http://www.nanotube.msu.edu/tubeASP/, accessed 2016 08 16

- 14. Terrones M 2003 Science and technology of the twenty-first century: synthesis, proper types, and applications of carbon nanotubes Annu. Rev. Mater. Res. 33 419–501
- 15. Gaussian 09, Revision D.01 2013 Frisch M J, Trucks G W, Schlegel H B, Scuseria G E, Robb M A, Cheeseman J R, Scalmani G, Barone V, Mennucci B, Petersson G A, Nakatsuji H, Caricato M, Li X, Hratchian H P, Izmaylov A F, Bloino J, Zheng G, Sonnenberg J L, Hada M, Ehara M, Toyota K, Fukuda R, Hasegawa J, Ishida M, Nakajima T, Honda Y, Kitao O, Nakai H, Vreven T, Montgomery J A Jr, Peralta J E, Ogliaro F, Bearpark M, Heyd J J, Brothers E, Kudin K N, Staroverov V N, Keith T, Kobayashi R, Normand J, Raghavachari K, Rendell A, Burant J C, Iyengar S S, Tomasi J, Cossi M, Rega N, Millam J M, Klene M, Knox J E, Cross J B, Bakken V, Adamo C, Jaramillo J, Gomperts R, Stratmann R E, Yazyev O, Austin A J, Cammi R, Pomelli C, Ochterski J W, Martin R L, Morokuma K, Zakrzewski V G, Voth G A, Salvador P, Dannenberg J J, Dapprich S, Daniels A D, Farkas O, Foresman J B, Ortiz J V, Cioslowski J, Fox D J, Gaussian, Inc., Wallingford CT.
- Wang C M, Zhang Y Y, Xiang Y, Reddy J N 2010 Recent Studies on Buckling of Carbon Nanotubes Appl. Mech. Rev. 63(3) 030804
- Bolotin K I, Sikes K J, Jiang Z, Klima M, Fudenberg G, Hone J, Kim P, Stormer H L 2008 Ultrahigh electron mobility in suspended graphene Solid State Communications 146 351–5
- Novoselov K S, McCann E, Morozov S V, Falko V I, Katsnelson M I, Zeitler U, Jiang D, Schedin F, Geim A K 2006 Unconventional quantum Hall effect and Berry's phase of 2pi in bilayer graphene *Nature Physics* 2 177–80
- 19. Saito R, Fujita M, Dresselhaus G, Dresselhaus M S 1992 Electronic structure of chiral graphene tubules *Appl. Phys. Lett.* 60 2204–6
- Saito R, Fujita M, Dresselhaus G, Dresselhaus M S 1992 Electronic structure of graphene tubules based on C60 Phys. Rev. B 46 1804–11
- Minot E D, Yaish Y, Sazonova V, McEuen P L 2004 Determination of electron orbital magnetic moments in carbon nanotubes *Nature* 428 536–9
- Ramirez A P, Haddon R C, Zhou O, Fleming R M, Zhang J, McClure S M, Smalley R E 1994
   Magnetic susceptibility of molecular carbon: nanotubes and fullerite Science 265 84–6
- 23. Wang J, Jiang W, Wang B, Gao Y, Wang Z, Zhang R Q **2016** Chirality dependent spin polarization of carbon nanotubes *New J. Phys.* **18** 023029
- 24. Jespersen T S, Grove-Rasmussen K, Paaske J, Muraki K, Fujisawa T, Nygard J, Flensberg K 2011 Gate-dependent spin-orbit coupling in multielectron carbon nanotubes *Nature Physics* 7 348–53
- Wang B, Wang J 2010 First-principles investigation of transport properties through longitudinal unzipped carbon nanotubes *Physical Review B* 81 045425
- Miyauchi Y, Oba M, Maruyama S 2006 Cross-polarized optical absorption of single-walled nanotubes by polarized photoluminescence excitation spectroscopy *Physical Review B* 74 205440
- Iakoubovskii N, Minami N, Kim Y, Miyashita K, Kazaoui S, Nalini B 2006 Midgap luminescen-ce centers in single-wall carbon nanotubes created by ultraviolet illumination Applied physics letters 89 173108
- 28. Wildoer J W G, Venema L C, Rinzler A G, Smalley R E, Dekker C 1998 Electronic structure of atomically resolved carbon nanotubes *Nature* 391 59–62
- Odom T W, Huang J L, Kim P, Lieber C M 1998 Atomic structure and electronic properties of single-walled carbon nanotubes *Nature* 391 62–4
- Luo C, Xie H, Wang Q, Luo G, Liu C 2015 A Review of the Application and Performance of Carbon Nanotubes in Fuel Cells *Journal of Nanomaterials* 2015 560392
- Girishkumar G, Rettker M, Underhile R, Binz D, Vinodgopal K, McGinn P, Kamat P 2005 Single-wall carbon nanotube-based proton exchange membrane assembly for hydrogen fuel cells Langmuir 21(18) 8487–94

- Berkovic G, Krongauz V, Weiss V 2000 Spiropyrans and Spirooxazines for Memories and Swi-tches Chem. Rev. 100 1741–53
- 33. Madani S Y, Mandel A, Seifalian A A 2013 A concise review of carbon nanotube's toxicology *Nano Rev.* 4(10) 21521(1–14)
- 34. Rajasekaran G, Narayanan P, Parashar A 2016 Effect of Point and Line Defects on Mechanical and Thermal Properties of Graphene: A Review Critical Reviews in Solid State and Materials Sciences 41(1) 47–71
- Krasheninnikov A V, Lehtinen P O, Foster A S, Pyykkö P, Nieminen R M 2009 Embedding Transition-Metal Atoms in Graphene: Structure, Bonding, and Magnetism *Phys. Rev. Lett.* 102 12680
- Wang M C, Yan C, Ma L, Hu N, Chen M W 2012 Effect of defects on fracture strength of graphene sheets Comput. Mater. Sci. 54 236–9
- 37. Zandiatashbar A, Lee G H, An S J, Lee S, Mathew N, Terroness M, Hayashi T, Picu C R, Hone J, Koratkar N 2014 Effect of defects on the intrinsic strength and stiffness of graphene Nat. Commun. 5 3186
- 38. Wang M C, Yan C, Galpaya D, Zheng B L, Ma L, Hu N, Yuan Q, Bai R, Zhou L **2013** Molecular dynamics simulation of fracture strength and morphology of defective graphene *J. Nano Res.* **23** 43–9
- 39. Balandin A A, Ghosh S, Bao W, Calizo I, Teweldebrhan D, Feng M, Lau C N 2008 Superior thermal conductivity of single-layer graphene *Nano Lett.* 8, 902–7
- 40. Baimova J A, Bo L, Dmitriev S V, Zhou K, Nazarov A A **2013** Effect of Stone-Thrower-Wales defect on structural stability of graphene at zero and finite temperature *EPL* **103** 46001
- 41. Xiao L, Thomas H M, Robinson J T, Houston B H, Scarpa F **2012** Shear modulus of monolayer graphene prepared by chemical vapor deposition *Nano Lett.* **12** 1013–7
- 42. Gillen R, Mohr M, Maultzsch J **2010** Raman-active modes in graphene nanoribbons *Phys. Status Solidi* B **247** 2941–4
- 43. Bosak A, Krisch M, Mohr M, Maultzsch J, Thomsen C **2007** Elasticity of single-crystalline graphite: Inelastic x-ray scattering study *Phys. Rev.* B *Condens. Matter* **75** 153408
- 44. Dmitrriev S V, Baimoya J A, Savin A V, Kivshar Y S 2012 Ultimate strength, ripples, sound velocities, and density of phonon states of strained graphene *Comput. Mater. Sci.* 53 194–203
- Zakharchenko K V, Los J H, Katsnelson M I, Fasolino A 2010 Atomistic simulations of structural and thermodynamic properties of bilayer graphene *Phys. Rev. B Condens. Matter* 81 235439(1–6)
- 46. Zhu Y, Murali S, Cai W, Li X, Suk J W, Potts J R, Ruoff R S **2010** Graphene and graphene oxide: synthesis, properties and applications *Adv. Mater.* **22** 3906–24
- 47. Edwards R S, Coleman K S **2013** Graphene synthesis: relationship to applications *Nanoscale* **5** 38–51
- 48. Bolotin K I, Sikes K J, Jiang Z, Klima M, Fudenberg G, Hone J, Kim P, Stormer H L **2008** Ultrahigh electron mobility in suspended graphene *Solid State Commun.* **146** 351–5
- 49. Taghioskoui M 2009 Trends in graphene research Mater. Today 12 34-7
- 50. Geim K 2009 Graphene: status and prospects Science 324 1530-4
- 51. Garg R, Dutta N K, Choudhuri N R **2014** Work function engineering of graphene *Nanomaterials* **4** 267–300
- 52. Araujo P T, Terrones M, Dresselhaus M S **2012** Defects and impurities in graphene-like materials *Mater. Today* **15**(3) 98–109
- 53. Liu L, Qing M, Wang Y, Chen S **2015** Defects in graphene: generation, healing, and their effects on the properties of graphene: a review *J. Mater. Sci. Technol.* **31** 599–606
- 54. Zhang T, Li X, Gao H 2014 Designing graphene structure with controlled distributions of topological defects: A case study of toughness enhancement in graphene ruga Extreme Mech. Lett. 1 3–8
- 55. Robertson W, Warner J H **2013** Atomic resolution imaging of graphene by transmission electron microscopy *Nanoscale Res. Lett.* **5** 4079–93

References 285

56. Xu L, Wei N, Zheng Y **2013** Mechanical properties of highly defective graphene: from brittle rupture to ductile fracture *Nanotechnology* **24** 505703

- 57. Sun S, Wang C, Chen M, Zheng J **2013** A novel method to control atomic defects in graphene sheets, by selective surface reactions *Appl. Surf. Sci.* **283** 566–70
- 58. Liu J, Liu Z, Barrow C J, Yang W **2015** Molecularly engineered graphene surfaces for sensing applications: A review *Anal. Chim. Acta* **859** 1–19
- Yadav S, Zhu Z, Singh C V 2014 Defect engineering of graphene for effective hydrogen storage Int. J. Hydrog. Ener. 39 4981–95
- 60. Terrones M, Botello-Mendez A R, Campos-Delgado J, Lopez-Urias F, Vega-Cantu Y I, Rodriguez-Macias F J, Elias A. L, Munoz-Sandoval E, Cano-Marquez A G, Charlier J C, Terrones H 2010 Graphene and graphite nanoribbons: Morphology, properties, synthesis, defects and applications, *Nano Today* 5 351–72
- 61. Liu X Y, Zhang J M, Xu K W, Ji V **2014** Improving SO<sub>2</sub> gas sensing properties of graphene by introducing dopant and defect: A first-principles study *Appl. Surf. Sci.* **313** 405–10
- 62. Li T, Tang X, Liu Z, Zhang P **2011** Effect of intrinsic defects on electronic structure of bilayer graphene: First-principles calculations *Physica* E **43** 1597–601
- Bitzek E, Gumbsch P 2013 Mechanisms of dislocation multiplication at crack tips Acta Mater.
   61 1394–403
- 64. Bonilla L L, Carpio A 2012 Driving dislocations in graphene Science 337 161-2
- 65. Yazyev O V, Louie S G **2010** Topological defects in graphene: Dislocations and grain boundaries *Phys. Rev. B Condens. Matter* **81** 195420
- 66. Mohammadi N, Adeh N B, Najafi M 2016 Synthesis and characterization of highly defective mesoporous carbon and its potential use in electrochemical sensors RSC Adv. 6(40) 33419–25
- 67. Huang H, Ying Y, Peng X **2014** Graphene oxide nanosheet: an emerging star material for novel separation membranes *J. Mater. Chem.* A **2** 13772–82
- Nishihara H, Kyotani T Templated nanocarbons for energy storage 2012 Adv. Mater. 24, 4473–98
- Zhou M, Guo S 2015 Electrocatalytic Interface Based on Novel Carbon Nanomaterials for Advanced Electrochemical Sensors ChemCatChem 7(18) 2744

  –64
- Zhai Y, Zhu Z, Dong S 2015 Carbon-Based Nanostructures for Advanced Catalysis ChemCatChem 7 2806–15
- 71. Vicarelli L, Heerema S J, Dekker C, Zandbergen H W **2015** Controlling Defects in Graphene for Optimizing the Electrical Properties of Graphene Nanodevices *AcsNano* **9** 3428–35
- Lim D H, Wilcox J 2012 Mechanisms of the Oxygen Reduction Reaction on Defective Graphene-Supported Pt Nanoparticles from First-Principles J. Phys. Chem. C 116 3653–60
- 73. Zhong J H, Zhang J, Jin X, Liu J Y, Li Q, Li M H, Cai W, Wu D Y, Zhan D, Ren B 2014 Quantitative Correlation between Defect Density and Heterogeneous Electron Transfer Rate of Single Layer Graphene J.Am Chem. Soc 136 16609–17
- 74. Kamiya K, Hashimoto K, Nakanishi S 2014 Graphene Defects as Active Catalytic Sites that are Superior to Platinum Catalysts in Electrochemical Nitrate Reduction *ChemElectroChem* 1 858–62
- 75. Ren T Z, Liu L, Zhang Y, Yuan Z Y 2013 Direct electrocatalytic and simultaneous determination of purine and pyrimidine DNA bases using novel mesoporous carbon fibers as electrocatalyst *J Solid State Electrochem* **17** 927–35
- 76. Hosseinia H, Behbahania M, Mahyaria M, Kazeroonib H, Bagheria A, Shaabania A 2014 Ordered carbohydrate-derived porous carbons immobilized gold nanoparticles as a new electrode material for electrocatalytical oxidation and determination of nicotinamide adenine dinucleotide *Biosensors and Bioelectronics* 59 412–7
- 77. Liu Y, Lia Y, He X **2014** In situ synthesis of ceria nanoparticles in the ordered mesoporous carbon as a novel electrochemical sensor for the determination of hydrazine *Anal. Chim. Acta* **819** 26–33
- 78. Gadipelli S, Guo Z X **2015** Graphene-based materials: Synthesis and gas sorption, storage and separation *Progress in Materials Science* **69** 1–60

- Zuttel A, Sudan P, Mauron P, Wenger P 2004 Model for the hydrogen adsorption on carbon nanostructures Appl Phys A 78 941–6
- Burress J W, Gadipelli S, Ford J, Simmons J M, Zhou W, Yildirim T 2010 Graphene oxide framework materials: theoretical predictions and experimental results Angew Chem Int Ed 49 8902–4
- 81. Kubas J 2001 Metal-dihydrogen and r-bond coordination: the consummate extension of the Dewar-Chatt-Duncanson model for metal-olefin p bonding J Organomet Chem 635 37–68
- 82. Hussain T, Pathak B, Ramzan M, Maark TA, Ahuja R **2012** Calcium doped graphane as a hydrogen storage material *Appl Phys Lett* **100** 183902
- 83. Miura Y, Kasai H, Dino W, Nakanishi H, Sugimoto T **2003** First principles studies for the dissociative adsorption of H<sub>2</sub> on graphene *J Appl Phys* **93** 3395–400
- 84. Chen J J, Li W W, Li X L, Yu H Q **2012** Improving biogas separation and methane storage with multilayer graphene nanostructure via layer spacing optimization and lithium doping: a molecular simulation investigation *Environ Sci Technol* **46** 10341–8
- 85. Katsnelson M I, Fasolino A **2013** Graphene as a prototype crystalline membrane. *Acc Chem Res* **46** 97–105
- Leenaerts O, Partoens B, Peeters F M Graphene: a perfect nanoballoon 2008 Appl Phys Lett 93 193107

# **Chapter 9 Spintronics and Nanomemory Systems**

CNTs forest can be considered as a prototype of the magnetic memory, where ferromagnetic nanoparticles serve as cells of the magnetic memory – that is, ferromagnetic contacts are controlled by spin pulses, the transport of which is provided by nanotubes (see Fig. 9.1) [1]. This CNTs forest morphology can be obtained as a result of CVD growth using FM (ferromagnetic) nanodrops of predefined diameters and magnetism. In particular, we analyse Fe–Pt nanoparticle ability as nanomemory elements. Spin transport between magnetic cells is essential for nanomemory device operation.

There are similar spin valve structures formed from arrays of aligned carbon nanotubes. These devices require only one deposited ferromagnetic layer with the embedded iron catalyst nanoparticle serving as the other magnetic electrode [2]. Device magnetoresistance ratios are estimated about 25%. Spin valve structures include Au with Fe-catalyst drops, grown CNT array, Fe–Co layer, Cr–Au layer and glass substrate.

Spin-polarized transport over 5 µm long carbon nanotubes (CNTs) is observed in magnetically assembled spin valves with electrochemically deposited ferromagnetic (FM) electrodes. FM/CNT/FM devices as Co/CMT/Ni interfaces were considered. An annealing procedure is developed to produce stable devices with highly transmissive FM/CNT contacts [3].

## 9.1 Spin Transport Fundamentals

It has been found that carbon nanotubes can acquire magnetic properties when brought into contact with ferromagnetic materials. This property of carbon nanotubes has previously been predicted theoretically by M Ferreira and S Santivo. The effect is based on the exchange of polarized electrons between the ferromagnetic material and nanotubes. The main difficulty of the experiment was in detecting the weak magnetic moment of the nanotubes on the background of a

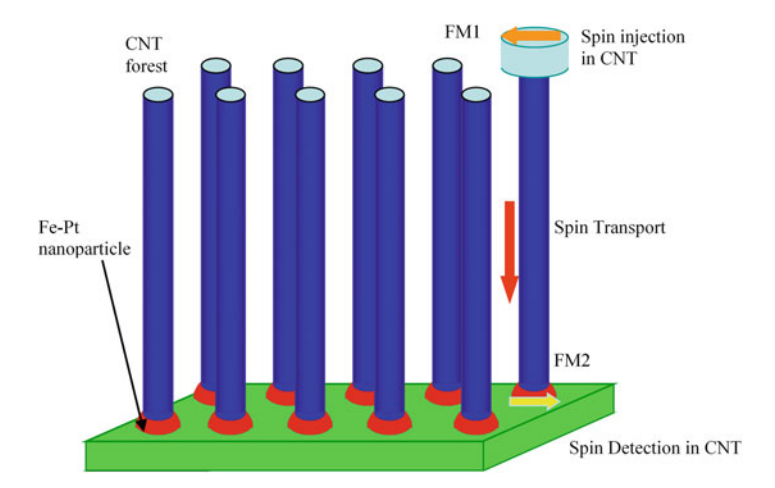


**Fig. 9.1** CNT forest is grown on the Fe–Pt nanoparticles of the predefined radius as a fragment of magnetic nanomemory device, which can be realized if spin injection, spin transport and spin detection (spin recording) are provided

strong magnetic moment of the ferromagnetic sample. The sample used in the experiment was a thin film of cobalt or iron oxide and was uniformly magnetized strictly in one direction.

With the help of a magnetic force microscope, weak perturbing magnetic fields were revealed produced by nanotubes on the surface of the sample. According to the measurements, the magnetization of nanotubes is 0.1 Bohr magneton per one carbon atom, which is in contact with the film. The control experiments demonstrated that carbon nanotubes in contact with nonmagnetic materials such as Si or Au do not possess magnetism [4].

The general approach is to examine the chain of weakly interacting CNT spins in contact with the two ferromagnetic (FM) metals. Let us consider Hamiltonian  $\mathcal{H}$  of the system of localized spins whose interaction is described by the model of Ising or Heisenberg:

$$\mathcal{H} = -\frac{1}{2} \sum_{\mathbf{l},\mathbf{l}'} J_{\mathbf{l},\mathbf{l}'} \left[ \alpha \left( S_{\mathbf{l}}^{x} S_{\mathbf{l}'}^{x} + S_{\mathbf{l}}^{y} S_{\mathbf{l}'}^{y} \right) + S_{\mathbf{l}}^{z} S_{\mathbf{l}'}^{z} \right] - \mu \sum_{\mathbf{l}} \mathbf{S}_{\mathbf{l}} \mathbf{H} =$$

$$= -\frac{1}{2} \sum_{\mathbf{l},\mathbf{l}'} J_{\mathbf{l},\mathbf{l}'} \left[ \alpha \left( S_{\mathbf{l}}^{x} S_{\mathbf{l}'}^{x} + S_{\mathbf{l}}^{y} S_{\mathbf{l}'}^{y} \right) + S_{\mathbf{l}}^{z} S_{\mathbf{l}'}^{z} \right] - \mu H \sum_{\mathbf{l}} S_{\mathbf{l}}^{z},$$
(9.1)

where  $\mathbf{S}_l$  is the spin localized in the lattice site l, H is the external magnetic field,  $\mu$  is the effective magneton and  $J_{l,\Gamma} = J(\mathbf{R}_{l,\Gamma})$  is the energy of the exchange interaction (the exchange integral) of the nearest neighbours in the lattice. If  $\alpha = 1$ , Hamiltonian corresponds to the Heisenberg model, with  $\alpha = 0$  – to the Ising model. The magnetic disordering in the system of CNT type is due to the weak magnetism of diamagnetic carbon atoms, where the only essential thing is the level

of magnetic interaction of the short-range order. In this case, a regular atomic structure of CNT is accompanied by a magnetic disorder of diamagnetic-liquids type. The correlation of the magnetic moments of CNTs can be ensured by a spin injection at the expense of the controlled magnetic field in the area of ferromagnetic contacts. At the same time, the initial values  $J_{l,r}$  of the energy of the magnetic interaction till the controlled magnetic pulse have random values. The weak correlation between adjacent carbon atoms in the atomic structure of CNT is also supported by the excitation of FM-CMT-FM. Accordingly, in Eq. (9.1) summation is assumed only considering the efficiency degree of unbroken bonds.

In the Heisenberg model, the node approximation with the l-th node of the ideal crystal is associated with a localized magnetic moment proportional to the localized spin variable  $S_l$ .

In the case of paramagnetic materials, in the absence of an external magnetic field,  $S_l$  is oriented randomly from node to node and forms a system with magnetic disorder. Diamagnetic materials exhibit their magnetic properties due to the induced magnetic moments in the presence of a magnetic field. However, the magnetic moments are very small, and their correlated behaviour is characterized only by a short-range order. Therefore, in terms of spin transfer, paramagnetic and diamagnetic materials are quite similar.

In the case of cooperative spin interactions at low temperatures, magnetic order appears. It is characteristic for ferromagnets, antiferromagnets and ferrites. However, the order disappears at high temperatures and magnetic system itself is transformed into a paramagnetic with a certain level of magnetic disorder. Considering that  $S_l$  is a vector quantity, the types of disorder may be different. Of course, the thermal fluctuations significantly stimulate spin disordering.

Using the Ising model in its pure form (when  $S_z = \pm 1$ ) for the systems such as FM–CMT–FM is not correct, because each node has three spin variables –  $S_x$ ,  $S_y$  and  $S_z$ , which can take random values and are connected by the relation  $S^2 = S_x^2 + S_y^2 + S_z^2$  and quantized by being inherently quasi-continuous. This is due to the boundary conditions on the FM–CNT interconnects. Really used constructive models of spin coupling (Ising model, classical and quantum Heisenberg model) for the system under investigation require further modifications. For example, in the near-field approximation, it is possible to use one parameter of the exchange interaction J in the model Hamiltonian:

$$\mathcal{H} = -\frac{1}{2} \sum_{\mathbf{l}, \mathbf{l}'} J \mathbf{S}_{\mathbf{l}} \mathbf{S}_{\mathbf{l}'} - \mu \mathbf{H} \sum_{\mathbf{l}} \mathbf{S}_{\mathbf{l}}.$$
 (9.2)

Further steps may be associated with a version of Heisenberg magnetic system and the corresponding Hamiltonian:

$$\mathcal{H} = -\frac{1}{2} \sum_{\mathbf{l},\mathbf{l}'} \xi_{\mathbf{l}} \xi_{\mathbf{l}'} J(\mathbf{R}_{\mathbf{l}\mathbf{l}'}) \mathbf{S}_{\mathbf{l}} \mathbf{S}_{\mathbf{l}'} - \mu \sum_{\mathbf{l}} \xi_{\mathbf{l}} \mathbf{S}_{\mathbf{l}} \mathbf{H}, \tag{9.3}$$

where  $\xi_l$  is the random value from 0 to 1, which can be adjusted by the temperature factor, that is  $\xi_l \sim \exp(-W/kT)$ , where W is m the magnetic interaction energy of the induced magnetic dipole with an external magnetic field.

Obviously, this type of complex Hamiltonian needs to be simplified. For example, we can neglect the spin deviations along the z axis and consider only the transverse deviations introducing spin variables such as  $S^{\pm} = S_I^x \pm i S_I^y$ .

The linearized equations of motion look as follows:

$$i\hbar \frac{dS_k^-}{dt} = 2SJ \sum_{k'} \left[ S_k^-(t) - S_{k'}^-(t) \right],$$
 (9.4)

where  $S^2 = (S_I^x)^2 + (S_I^y)^2$ .

Then, the approximate system of equations defining the dispersion of the model spin system will be as follows:

$$\left[ \left\{ 2S \sum_{k} [J - \hbar \omega] S_{k}^{-} - 2S \sum_{k'} J S_{k'}^{-} = 0. \right.$$
 (9.5)

This conceptual analysis allows us to imagine the complexity of the theoretical description of spin transport in the considered FM-CNT-FM systems and the amount of computational work.

## 9.2 Magnetoresistance Nanodevices

# 9.2.1 Spin Valve Concepts

Nanocarbon-based (e.g. CNT or graphene) spintronics is well-predicted theoretically. The main point of technological problem is the spin current injection efficiency into carbon nanotubes by using ferromagnetic electrodes. The next point of attention is spin transport experiments to obtain evaluations of digital information processing rates. A typical spintronic device is the so-called spin valve. The typical spin valve device contains two ferromagnetic electrodes (one ferromagnetic electrode for spin current injection and another for spin signal detection) and nonmagnetic material responsible for spin transport. For practical implementation, the spin signal should be large enough. A large spin signal can be obtained in a weak spin relaxation system, where spin can travel a long distance without being scattered in ballistic regimes. Nanocarbon-based materials (e.g. CMTs) due to long spin relaxation distances look as the best candidates in comparison with the nonmagnetic metals and semiconductors. The spin current is propagated for long

macroscopic distances due to some spin correlation. These nanocarbon-based materials are expected to be beneficial for implementation of large-scale spintronic logic circuits, quantum computing, fast data processing, magnetic hard disc drivers and dynamical nanomemory devices.

Electron transfer in spintronic devices depends on the spin polarization of the current. Such devices include a method of generating a spin-polarized current based on interconnects of nonmagnetic materials with ferromagnetic ones. In our case, these are Fe–Pt compositions.

EDOS spin splitting on the Fermi level defines the efficiency of spintronic devices. In accordance with Stoner model, the band structure of transition metals depends on spin orientation (up and down) [5]. The theoretical basis for considering spintronic devices is a magnetoresistance phenomenon. Namely, there are two variants of magnetoresistance – giant magnetoresistance (GMR) and tunnelling magnetoresistance (TMR).

Electronic transport through CNTs depends on the contacts with electrodes. For short CNTs at low temperatures, we should also pay attention to Kondo effect – the formation of a many-body dynamical singlet between a localized spin and delocalized conduction electrons of electrodes [6]. It should be borne in mind that carbon nanotubes possess in addition to spin also orbital degeneracy. The increase of degeneracy corresponds to the enhancement of Kondo temperature, which is important for potential applications.

Giant magnetoresistance is a quantum mechanical effect observed in thin metal films consisting of alternating ferromagnetic and nonmagnetic conductive layers. The effect is a substantial change in the electrical resistance of such a structure when changing the relative direction of magnetization of adjacent magnetic layers. The direction of magnetization can be controlled, for example, by applying an external magnetic field. The effect is based on the scattering of electrons depending on the spin direction.

The GMR was discovered in 1988 (2007 Nobel Prize, Albert Fert and Peter Grünberg) as a large change in resistance of magnetic Fe/Cr multilayer in the presence of an applied magnetic field [7]. Soon after GMR was discovered in Fe/Cr/Fe trilayers [8]. As it was shown later, the effect can be obtained in trilayers having other magnetic materials such as Co [9].

Such trilayer structures, i.e. sandwiches of two ferromagnetic metals separated by a thin spacer layer of normal metal (Fig. 9.2), are of great industrial importance. They are called spin valves and are used as magnetic field sensors. The resistance of the device is dependent on the relative magnetization orientation of the ferromagnets. It is  $R_P$  when the magnetizations are parallel and  $R_A$  when they are antiparallel. The GMR ratio is defined as  $GMR = \frac{R_A - R_P}{R_P}$ .

The TMR is a quantum mechanical effect manifests itself when a current flows between the two ferromagnetic layers separated by a thin (about 1 nm) dielectric layer. The total resistance of the device, the current which flows due to the tunnelling effect, depends on the relative orientation of the two fields, the magnetization of the magnetic layers and resistance above at the perpendicular

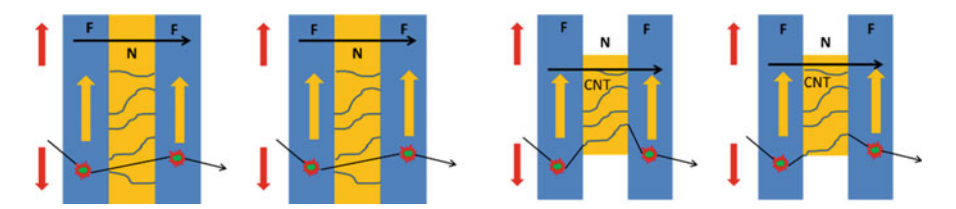


Fig. 9.2 Giant magnetoresistance (GMR) device. A thin normal metal spacer (N) separates two ferromagnets (F), the current flows perpendicular to the plane of the sample and N space can be filled by introduced (or grown) CNT, e.g. metal-like

magnetization layer. The effect of the tunnel magnetic resistance is similar to the effect of a giant magnetic resistance, except for the use of insulating layer of the tunnel barrier instead of a nonmagnetic metal layer.

The TMR was discovered in 1975 by Jullière [10] in a device that consisted of two Fe films separated by Ge. It was first in 1995 when room temperature TMR was discovered by Moodera [11] and caused a great interest in spintronics after GMR was discovered in 1988 [6]. Our idea is that the same effect can be reached by introducing into the N space semiconductor CNTs.

The TMR signal operates in the same way as the GMR  $TMR = \frac{R_A - R_P}{R_P}$ , where  $R_P = (1/G_P)$  and  $R_A = (1/G_A)$  are the resistances (conductances) of the device for parallel and antiparallel orientations, respectively, of the ferromagnet magnetization. However, the nature of TMR is different than that of the GMR.

The resistance for the antiparallel magnetization is normally higher than for the parallel one. At the applied zero magnetic field, the relative orientation of the magnetization is governed by the exchange coupling between the ferromagnetic layers. The sign and size of the interlayer exchange coupling is dependent on the thickness of the nonmagnetic spacer. The coupling can thus be ferromagnetic and antiferromagnetic dependent on the spacer thickness [12, 13].

# 9.2.2 Spintronic Device Descriptions

The first two-terminal CNT spin valve device was presented in [14], where spin-dependent transport was demonstrated for MWCNTs with 9% magnetoresistance ratio (MR) at 4.2 K.

The device shown in Fig. 9.2 is the so-called current perpendicular to the plane (CPP) geometry. The resistance of such geometry is very low and difficult to detect. For practical applications, structures with the current in the plane (CIP) are used because they have higher resistance and thus higher difference with the magnetic field [9].

The GMR can be understood through the Mott's two-current model [15]. According to that model, the electrical conductivity of metal can be described by two more or less independent channels, one for majority spins and the other for

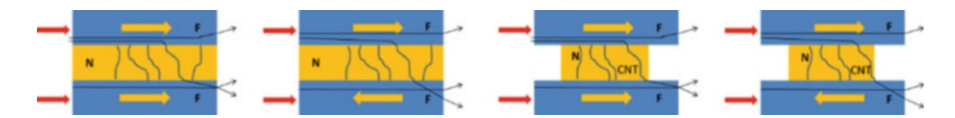


Fig. 9.3 Current in plane (CIP) spin valve and equivalent resistor mode, separate channels are for minority and majority spins, the electrons scatter from one F layer to the other on the way through the sandwich

minority spins. Scattering processes that conserve spin states are much more probable than the processes that flip spins. Another view proposed by Mott is that the scattering probability of spin up and spin down is quite different, independent on the nature of the scattering process [16]. This is shown schematically in Fig. 9.2.

The difference in the resistance of ferromagnets can be explained by the exchange split band structure. The scattering of the electrons depends on where the electron band crosses the Fermi level [9].

As mentioned above, commercial spin valves have normally the current in plane (CIP) geometry. This gives higher resistance and thus higher resistance difference between parallel and antiparallel spin orientations. Having the current in plane of the sandwich will qualitatively give the same effect as in CPP devices. This situation is shown schematically in Fig. 9.3. Electrons with minority and majority spins are treated separately. When the electrons flow through the sandwich, they will scatter back and forth from the upper F layer to the lower one.

We consider a possibility for the creation of magnetic memory devices on the magnetoresistance phenomenon (GMR or TMR) consisting of sandwiches of two ferromagnetic metals separated by a thin spacer layer of *normal metal* (see, e.g. Fig. 9.3) or semiconductor. Spin valves are of great industrial importance and are used as magnetic field sensors. The resistance of the device is dependent on the relative magnetization orientation of the ferromagnets. The TMR signal operates in the same way as the GMR, where  $R_P$  and  $R_A$  are the resistances of the device for parallel and antiparallel orientations, respectively, of the ferromagnets magnetization (Figs. 9.2 and 9.3) [17]. The main idea is to reach the same effect by introducing metal or semiconductor-like CNTs into the N space after magnetically controlled CVD CNTs growth [1, 17].

# 9.3 Magnetic Disorder and Spin Transport

We outline two main problems of spintronics, namely, spin states of localized Fe–Pt ferromagnetic spaces and spin transport efficiency provided by CNTs system.

#### 9.3.1 Magnetic Disorder in Fe-Pt Nanodrops

Consider ferromagnets with localized magnetic moments in which the magnetic atoms are randomly distributed at the sites of the crystal lattice. It is also advisable to consider structurally non-regular metal alloys such as metal glasses  $A_x B_{1-x}$ , on which magnetic (spin) disorder is superimposed. This can affect the additional contributions to the exchange integrals of the spin interaction. Such ferromagnetic systems are technologically important, in particular for the CVD magnetically controlled CNTs growth, when nanodrops of ferromagnetic binary metallic glass are used. This is essential also for creating prototypes of magnetic nanomemory systems. The consideration of two possible opposite situations for magnetic properties  $A_x B_{1-x}$  metal glasses is essential and should be carried out.

The First Model Only the nearest lattice neighbours interact. In this case, the magnetic order exists only if the concentration of magnetic atoms x exceeds the critical value  $x_c$  (percolation threshold), i.e. in addition to the temperature phase transition, a concentration phase transition at  $x > x_c$  occurs at zero temperature.

The Second Model The exchange interaction is non-zero for any distance between magnetic atoms. In this case, ferromagnetism exists for any arbitrarily small concentration x. We will assume that the exchange potential decreases with distance exponentially  $V(r) \sim \exp(-r/R)$ , where r is the average distance between magnetic atoms and R is the radius of the exchange potential.

The magnetism of such systems can strongly differ from the properties of ordinary ordered ferromagnets. The behaviour of such model spin systems at various concentrations x is of interest.

#### 9.3.1.1 Diluted Ferromagnets with the Nearest Neighbour Interaction

Consider a system of localized spins, the interaction of which is described by the Ising or Heisenberg model (see Eq. 9.1). The disorder in this system is most easily created in two ways. First, it is possible randomly replace magnetic atoms in the lattice sites by nonmagnetic atoms. In this case,  $J_{ij} = V_0 p_i p_j$ , where  $p_i = 1$ , if the node is occupied by a magnetic atom, and  $p_i = 0$ , if it is nonmagnetic. Secondly, it is possible to break sites in a random way, i.e. consider some  $J_{ij}$  to be zero. Such a situation can in principle be realized in ferromagnets with indirect exchange through nonmagnetic ions. Removing the latter or replacing them with ions that do not take part in indirect exchange corresponds to a rupture of the connection between the spins.

At T = 0 K, all spins, bound by the exchange interaction, are oriented in parallel. If the concentration x of magnetic atoms or unbroken bonds is small, the magnetic atoms form clusters isolated from each other. The dimensions of them do not change with increasing of the crystal volume. We call such clusters finite.

The average magnetic moment of the whole crystal is zero in this case. With increasing x, the characteristic size of finite clusters increases, and at a certain critical concentration,  $x_c$  arises a cluster, in which the number of particles is proportional to the volume of the system. We shall henceforth call such a cluster infinite.

The magnetic moment of the crystal M(x) is different from zero at  $x > x_c$  and equals M(x) = M(1)P(x), where M(1) is the moment of the ordered crystal and P(x) is the concentration of magnetic atoms (per lattice site) included in an infinite cluster. Thus, in a disordered ferromagnet at T = 0 K, a phase transition occurs from the paramagnetic state to the ferromagnetic state when the concentration  $x = x_c$ . The problem of the concentration phase transition, or, the problem of the origin of an infinite cluster, is studied in percolation theory (see, e.g. [18, 19]). In accordance with the above two methods of creating disorder in the lattice, it is customary to distinguish between the *site problem* and the *node problem*. The critical concentration is called the *percolation threshold*. The values depend on the type of lattice and are different for the *site problem* and the *node problem*.

They were obtained as a result of computer modelling. For cubic lattices in the site problem model  $x_c = 0.243$  (body-centred cubic-bcc) and 0.195 (face-centred cubic-fcc); in the node problem model  $x_c = 0.178$  (bcc) and 0.120 (fcc). The detailed table containing  $x_c$  for different lattices is given in the review of Essam [19]. The value P(x) changes from 0 at  $x = x_c$  to 1 at x = 1. Results of typical simulation of behaviour are presented in Fig. 9.4.

The next problem is to determine the concentration dependence of the *rigidity* of the magnons D. It is convenient to use the coupling that exists between the concentration dependences and the conductivity of an equivalent resistance lattice (see Kirkpatrick [18]):  $\frac{D(x)}{D(1)} = \frac{\sigma(x)}{P(x)\sigma(1)}$ .

The equivalent resistance network is constructed from a magnetic lattice in the following way: the magnetic bonds  $V_{ij}$  correspond to conductivities distributed according to the same law as  $\sigma_{ij}$ . According to Kirchhoff's laws, the time dependence of the potential  $V_i(t)$  at the i-th node is determined by the following equation:

$$\frac{dV_i(t)}{dt} = -\left(\frac{\sigma_0}{C}\right) \sum_{i'} \{V_i(t) - V_{i'}(t)\},\tag{9.6}$$

where C is the magnet assembly capacity and  $\sigma_0$  is the conductivity of each connecting link. This equation is similar to the equation for magnon modes:

$$i\hbar \frac{dS_i^-(t)}{dt} = 2SJ \sum_{i'} \left\{ S_i^-(t) - S_{i'}^-(t) \right\}.$$
 (9.7)

Thus, the solution of the conductivity problem with respect to a random resistance network can be related to the properties of the eigenfunctions  $|\alpha\rangle$  of the residual matrix:

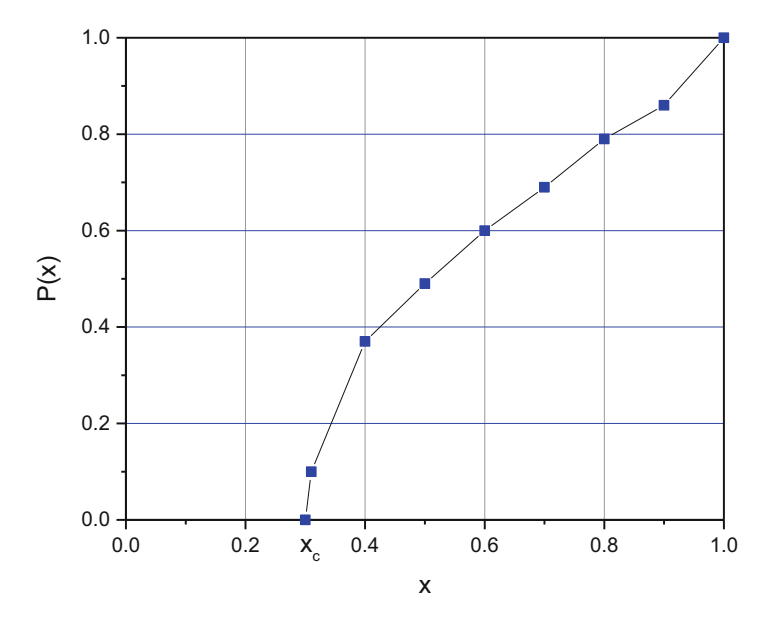


Fig. 9.4 Typical behaviour of P(x) simulation for simple cubic lattice

$$\Delta = \sum_{i,i'} \{|i\rangle\langle i| - \} \{|i\rangle\langle i'|\}. \tag{9.8}$$

The macroscopic static conductivity  $\sigma(p)$  of the network should be equal the limiting value of the dissipative part of the response function to the external field for zero frequency and infinitely long waves. The classical analogue of the fluctuation-dissipative theorem directly leads us to an expression equivalent to the Kubo–Greenwood formula [20–23]:

$$\sigma(x) = \lim_{\omega \to +0} \left\{ \lim \left[ \left( \frac{\omega^2 C^2}{q^2} \right) \sum_{\alpha} |\langle \mathbf{q} | \alpha \rangle|^2 \frac{\lambda_{\alpha}}{\lambda_{\alpha}^2 + \omega^2 C^2} \right] \right\}. \tag{9.9}$$

In the limiting case of long waves, the Fourier transform  $\langle \mathbf{q} | \alpha \rangle$  of the eigenfunction of the matrix  $\Delta$  reduces to the Fourier transform of the plane wave corresponding to the momentum  $\mathbf{q}_{\alpha} = \langle \alpha; \mathbf{R} | (\hbar/i) \nabla | \mathbf{R}; \alpha \rangle$ , and  $\mathbf{R}$  is the position of the *i-th* node. In the continuum approximation (see [18]), the eigenvalues of the matrix are estimated as  $\lambda_{\alpha} \approx a^2 q_{\alpha}^2 D(x)$ , where D(x) characterizes the concentration of the magnetic nodes of the system and  $\alpha$  is the lattice constant.

Using the relationship  $\lambda_{\alpha} \approx a^2 q_{\alpha}^2 D(p)$  can be found [18]:  $\sigma(x) = \sigma_0 a^2 D(x) P(x)$ .

It expresses the relationship between the rigidity parameter of spin waves in a dilute ferromagnet D(x) and the volume conductivity of the corresponding network

 $\sigma(x)$ . Mobility percolation  $\mu(x) = \sigma(x)/P(x)$  is not constant but decreases to zero at  $p \to p_c$  (see [24]).

Note that the magnetic ordering in a dilute Heisenberg ferromagnet becomes unstable with respect to the excitation of long-wave magnons exactly at the percolation threshold  $p_c$ . This confirms the well-founded hypothesis that under these conditions, the value really determines the point of the magnetic transition in the system at  $T_C \rightarrow 0$  [25].

#### 9.3.1.2 Bethe Lattice of the Spin System

The system of spins randomly located in the Bethe lattice is an exactly solvable model of a disordered ferromagnet. The Bethe lattice is a convenient topological model of atomic structures of a certain connectivity. In this case, the lattice sites and connections can be associated with certain local physical characteristics.

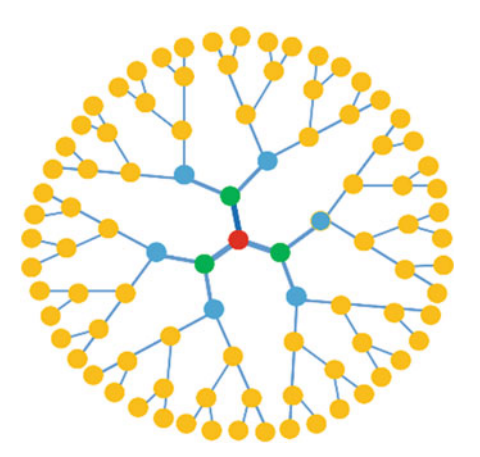
The Bethe lattice is a convenient topological model of atomic structures of a certain connectivity. In this case, the lattice sites and connections can be associated with certain local physical characteristics (see Fig. 9.5). In the Bethe lattice, z sites emerge from each node, giving rise to disjoint branches (see Fig. 9.5). Suppose, that at the sites of the Bethe lattice, the magnetic atoms are randomly distributed, whose concentration (calculated on the lattice site) is equal x and whose interaction is described by the Hamiltonian (9.1).

Let us find the expression for the mean magnetic moment of the lattice at  $T \ll V_0$ . Let R be the probability that a branch originating from some fixed node (node 0 in Fig. 9.5) is finite, i.e. the magnetic atoms in it do not form an infinite cluster. The branch can be finite if the node adjacent to the null (node 0) in the given branch (node I) is not occupied (probability (1-x)) or if this node is busy, but the outgoing branches z-1 are finite (probability). Consequently, R satisfies Eq. [28–33]:  $R = 1 - x + xR^{z-1}$ . The simplicity of this equation is due to the main property of the Bethe lattice is a non-intersection of branches. The average moment is  $M(x) \sim P(x) = 1 - R^z$ . The equation  $R = 1 - x + xR^{z-1}$  always has a trivial solution R = 1 corresponding to M = 0. A nontrivial solution  $R \neq 1$  appears at  $R \neq 1$ , R = 1 is the percolation threshold in the Bethe lattice. Near the threshold  $(x - x_c)/x_c \ll 1$ , from we have:

$$\frac{M(x)}{M(1)} = \frac{2z}{z - 2} \frac{x - x_c}{x_c}.$$
 (9.10)

Stinchcombe was the first who studied spin waves in the Bethe lattice [26, 27]. He used the relationship  $\frac{D(x)}{D(1)} = \frac{\sigma(x)}{P(x)\sigma(1)}$ . He determined the conductivity by fixing the potential difference between the beginning (point 0, Fig. 9.5, Bethe tree) and the boundary. It was shown that for the Bethe lattice the effective medium method is valid with respect to the  $z^{-1}$  parameter everywhere, except for the region near the threshold, for which the conductivity is proportional  $(x - x_c)^2$ . de Gennes

**Fig. 9.5** Bethe lattice with z = 3



payed attention to the fact that macroscopic conductivity should be determined for a fixed external field in the entire sample [30]. In this case, near the threshold, the conductivity varies according to the law [28–30]:  $\sigma \sim (x-x_c)^3$  (the Bethe lattice with the index z=3). It then follows that  $D \sim (x-x_c)^2$ . We see that the exact results for the Bethe lattice are completely consistent with the similarity hypothesis near the percolation threshold.

#### **9.3.1.3** Spin Waves

Crangle and Boszort et al. [34, 35, 37] discovered an astonishing phenomenon: the paramagnetic Pd metal becomes ferromagnetic with little Fe or Co doping. Later it was shown that the spontaneous moment arises even at concentrations x of Fe and Co of the order of  $10^{-4}$  [36], as well as in alloys  $Pd_{1-x}Mn_x$  [38].

The properties of the investigated magnetic system are completely determined by the ratio of two characteristic lengths: the radius R of the potential and the average distance between the impurities  $r_c \approx n^{-1/3}$ , where n is the number of spins per unit volume. If  $R \gg r_c$ , then a large number of magnetic atoms  $\nu_R = (4/3)\pi nR^3$ ≫1 effectively interact with this spin. Therefore, the energy of the exchange interaction of each spin with the environment depends little on the specific configuration. In this case, naturally, is proportional to the average energy of the exchange interaction, i.e.  $T_C \sim x$  [39]. A completely different situation arises when  $R \ll r_c$ , i.e.  $\nu_R \ll 1$ . Now the energy of the exchange interaction of a given spin with the remaining spins depends very strongly on the specific configuration. In fact, for most spins, the nearest neighbour is located at a distance of order  $r_c$ . In this case, even insignificant fluctuations in the arrangement of the spins lead to a significant change in the energy of the exchange interaction [40]. In a system of randomly located points, all connections between points that are separated by a distance  $r < r_{\text{max}}$  are included. When  $r_{\text{max}} \ll n^{-1/3}$ , there are only finite clusters of connected atoms in the system. For almost all atoms are connected in an infinite cluster. At

what value  $r_{\rm max}$  does the infinite cluster first appear? According to [41], the critical value  $r_{\rm max}$  is equal to  $r_0 = (0, 87 \pm 0, 01) n^{-1/3}$ . At high temperatures  $r(T) < r_0$  and the system is paramagnetic. The temperature of the ferromagnetic transition is determined from the condition  $r(T) = r_0$ . Then,  $T_C \approx V_0 S^2 \exp\left(-\frac{0.87}{Rn^{1/3}}\right) = V_C \exp\left(-\frac{0.87}{Rn^{1/3}}\right)$ , where S is the spin of the system,  $r(T) = R \ln \frac{V_0}{T}$  and  $V(T) = V_0 \exp(-r/R)$  [40].

Rigidity coefficient of spin waves. To determine the concentration dependence of the rigidity D for small concentrations of magnetic atoms, it is convenient to use the coupling between D and the conductivity  $\sigma$  of an equivalent resistance network. The generalization of the formula  $\frac{D(x)}{D(1)} = \frac{\sigma(x)}{P(x)\sigma(1)}$  to a disordered ferromagnet in which the spin interaction potential depends on the distance r according to the law  $V_{\text{ferro}}(r) = U_0 \frac{R}{r} \exp(-r/R)$  consists in the fact that the probability P(x) should be replaced by the number of magnetic atoms whose binding energy exceeds the energy of the spin wave. Consequently, in the low-frequency limit [40]  $D^{\sim \sigma}_{n}$ .

Here  $\sigma$  can be regarded as the conductivity of electrons in a system of chaotically located centres, in which the probability of electron hopping between centres is determined by the formula  $V_{\text{ferro}} = U_0 \frac{R}{r} \exp(-r/R)$ , where  $U_0 = J^2 N(\varepsilon_F) \frac{\Omega_0}{2\pi a^2 R}$  [40]. Its dependence on concentration is known:  $\sigma^{\sim} r_0^{-(2+\nu)} \exp\left(\frac{0,87}{Rn^{1/3}}\right)$  [42], where  $\nu$  is the index of the correlation radius and  $r_0 = 0,87n^{-1/3}$ . Then follows  $D^{\sim} n^{-(1-\nu)/3} \exp\left(\frac{0,87}{Rn^{1/3}}\right)$  [40]. It should be noted  $D/T_C$  that the concentration dependence is determined only by the index of the correlation radius  $\nu$ :  $(D/T_C) \sim n^{-(2-\nu)/3}$ , where  $\nu \approx 0.70 - 0.85$  (for  $\text{Pt}_{1-x}\text{Fe}_x$ ). Assuming  $n \sim (x-x_c)$  for small concentrations, we obtain  $\frac{T_C}{D} \sim x^{(2-\nu)/3}$ . Further, we get  $\ln\left(\frac{T_C}{D}\right) \approx A \frac{(2-\nu)}{3} x$  where A is the proportionality coefficient (see Fig. 9.6).

Magnetic atoms are randomly distributed at the lattice sites. Their concentration is low  $(x \ll 1)$ . Their exchange interaction is described by the Heisenberg Hamiltonian.

*Spin Transport Mechanisms* There are mainly two kinds of geometries for CNTs spin valve devices: local geometry and non-local geometry. The local geometry has two ferromagnetic electrodes; the spin current is injected from one electrode, then transported through CNTs and detected by another electrode.

The spin current is mixed with the charge current. The spin signal is detected as the difference in resistance between the parallel state and antiparallel state of two magnetic electrodes. Generally, it can be expressed as magnetoresistance (MR) as  $MR = (R_A - R_P)/R_P$ . Usually, the two magnetic electrodes should be different in geometric aspect ratios to obtain different coercive fields; thus the two electrodes can be aligned to antiparallel or parallel states by sweeping the magnetic field.

Tsukagoshi et al. fabricated the first two-terminal CNT spin valve device. Spin-dependent transport was demonstrated through MWNTs, and MR = 0.09 at 4.2 K was observed [14].

Spin waves transport can be tested experimentally using corresponding schemes.

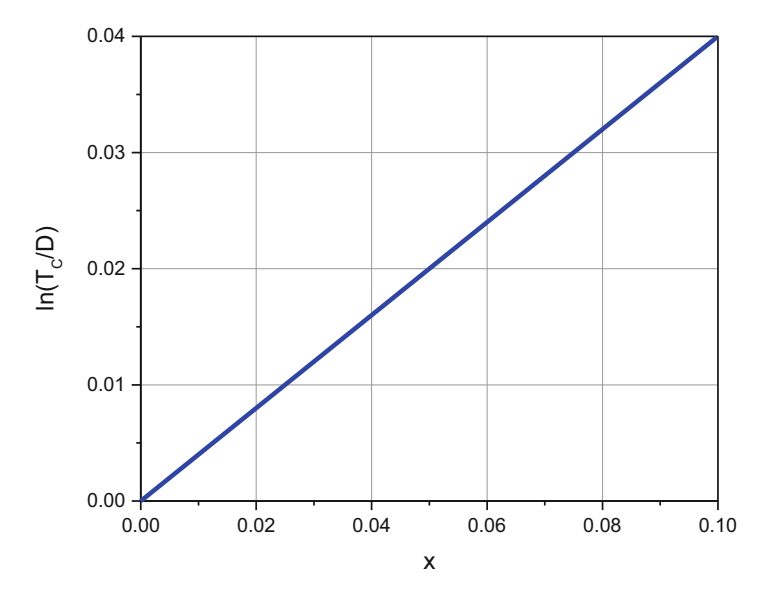


**Fig. 9.6** Typical model dependence  $\ln(T_C/D)$  via the concentration x alloys for  $\operatorname{Pt}_{1-x}\operatorname{Fe}_x(\nu=0.8, x \ll 1)$ 

The simplest measurement scheme is a local spin valve (see Fig. 9.7a). However, the non-local scheme is more correct (see Fig. 9.7b, c). The first variant of the schematic diagram of non-local spin valve device FM1, FM2, FM3 and FM4 denotes the four electrodes, respectively. Current *I* is injected into CNT from FM3 and extracted from electrode FM4. The voltage is detected between electrode FM1 and FM2 (see Fig. 9.7b). The second variant of schematic diagram of non-local spin valve device FM1, FM2, FM3 and FM4 denotes the four electrodes, respectively. Current *I* is injected into CNT from FM1 and extracted from electrode FM4. The voltage is detected between electrode FM2 and FM3 (see Fig. 9.7c). We also can consider end-type FM–CNT contacts taking into account a set of end-type schemes in Fig. 9.8, which corresponds to spin transport in the case of CNT forest (see Fig. 9.1).

#### 9.3.1.4 Spin Injection and Detection

Consider the mechanism of electrical spin injection and detection in a nonmagnetic material. We pay attention to traditional conventional two probe spin valve and the non-local four probe techniques.

Electrical Spin Injection and Detection A current which moves through a diffusive conductor can be considered to be carried in parallel by two independent spin channels, a channel for the spin-up electrons and one for the spin-down electrons [43]. This holds when most scattering events preserve the spin orientation;

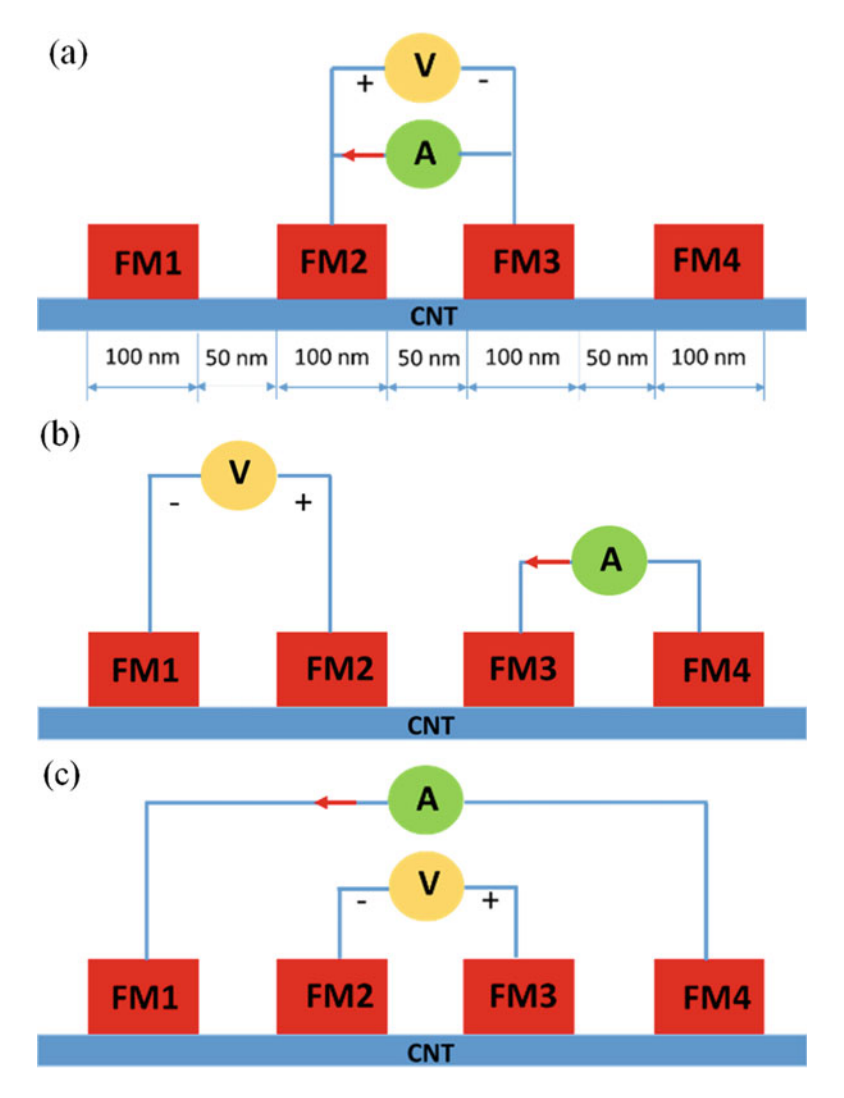


**Fig. 9.7** (a) Local side-type CNT spin valve device; (b) non-local side-type CNT spin valve device, the first scheme; (c) non-local side-type CNT spin valve device, the second scheme

otherwise, the two channels become strongly coupled and are not independent anymore. The spin current density  $j_{\uparrow\downarrow}$  of the spin-up  $\uparrow$  or spin-down  $\downarrow$  channel is proportional to the gradient of the electrochemical potential of one of the two spin species and is given by the relation  $j_{\uparrow\downarrow} = \frac{\sigma_{\uparrow\downarrow}\partial\mu_{\uparrow\downarrow}}{e\partial x}$ , where  $\sigma_{\uparrow\downarrow}$  is the conductivity,  $\mu_{\uparrow\downarrow}$  is the chemical potential of the two spin channels and e is the electron charge. The total charge current is given by  $j=j_{\uparrow}+j_{\downarrow}$ , and the spin current  $j_s$  is given by  $j_s=j_{\uparrow}-j_{\downarrow}$ . Looking now into a ferromagnet in which  $\sigma_{\uparrow}\neq\sigma_{\downarrow}$ , we can define a spin polarization P given by the relation  $P=\frac{j_{\uparrow}-j_{\downarrow}}{j_{\uparrow}+j_{\downarrow}}=\frac{\sigma_{1}-\sigma_{\downarrow}}{\sigma_{\uparrow}+\sigma_{\downarrow}}$ ; using  $\sigma=\sigma_{\uparrow}+\sigma_{\downarrow}$  which

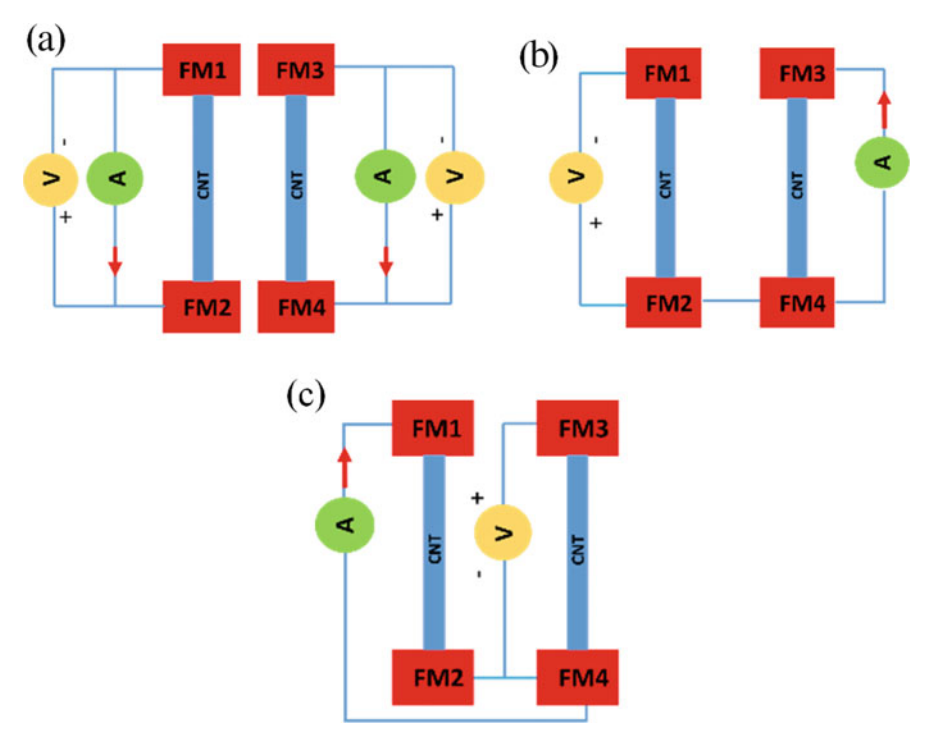


Fig. 9.8 (a) Local end-type CNT spin valve device; (b) non-local end-type CNT spin valve device, the first scheme; (c) non-local end-type CNT spin valve device, the second scheme

is the total conductivity in the system we obtain  $j_{\uparrow}=(1+P)\frac{\sigma\partial\mu_{\uparrow}}{e\partial x}$  and  $j_{\downarrow}=(1+P)\frac{\sigma\partial\mu_{\downarrow}}{e\partial x}$ .

We can use the ferromagnet as a spin source, because  $j_{\uparrow} \neq j_{\downarrow}$ . In practice, ferromagnets are used in conventional two-terminal spin valve device. A spin valve device contains two ferromagnetic electrodes, the injector and the detector, which make contact to a nonmagnetic material. Sending an electrical current through the ferromagnetic injector creates a spin accumulation in the nonmagnetic material. In a diffusive material, this accumulation decays exponentially with distance from the spin injector following the differential equation  $\frac{\partial^2 \Delta \mu}{\partial x^2} = \frac{\Delta \mu}{\lambda_s^2},$  where  $\lambda_s = \sqrt{D_s \tau_s}$  is the spin relaxation length,  $D_s$  is the diffusion constant,  $\tau_s$  is the spin relaxation time and  $\Delta \mu = \mu_{\uparrow} - \mu_{\downarrow}$ . If the spins relax fast, such as to reach a uniform distribution over spin direction before arriving at the spin injector, then the spin detector measures the average chemical potential which is zero. In this case, switching the magnetization of the ferromagnets from parallel to antiparallel gives no change in the total resistance of the spin valve. However, in the situation in which the detector is set within a distance  $\lambda_s$  from the spin injector, a switching of the magnetization of the ferromagnets from parallel to antiparallel produces a

change in the spin valve resistance. The reason for this is that when the magnetization of injector and detector are parallel, the spins can enter easily the spin detector, corresponding to a low resistance of the spin valve. However, when the magnetization of the detector is antiparallel to the injector, then the spins first have to flip their magnetization before they can enter the detector; this results to an increase in resistance.

Spin Injection and Detection, the Non-local Technique The conventional two-terminal spin valve geometry can be used to extract the spin relaxation length  $\lambda_s$ . However, this technique is not so reliable in respect of pure spin transport detection. Really we can observe mixed signals (e.g. Hall effects, anisotropic magnetoresistance interference effects, magneto-coulomb effects). A four-terminal non-local spin valve geometry [44, 45] is able to completely separate the spin current path from the charge current path. Hence, the signal measured is due to spin transport only. To determine spin accumulation in the non-local geometry, one needs to contact the system under investigation (metal, semiconductor, carbon nanotube) with four electrodes. At least two of these should be ferromagnetic. They act as spin injector and spin detector, respectively [44, 45].

As shown in Fig. 9.7b, two of the ferromagnetic electrodes are connected to a current demonstrates the spin transport in a four-terminal CNT-based spin valve device using the non-local spin valve geometry: a current I is injected from electrode FM3 through the contact barrier into CNT and is extracted at contact FM4. The voltage difference is measured between contact FM2 and FM1. The non-local resistance is  $R_{\text{non-local}} = (V_+ - V_-)/I$ . Injection of up spins by contact FM3 results in an accumulation of spin-up electrons underneath contact FM3, with a corresponding deficit of spin-down electrons. Due to spin relaxation the spin density decays on a scale given by the spin relaxation length. The electric voltage is measured by contact FM1 and FM2 in the ideal case of 100% spin selectivity. A positive non-local resistance is measured. In cases of spin injection and spin diffusion for antiparallel magnetizations the voltage contacts probe in opposite spin directions gives a negative non-local resistance.

#### 9.3.1.5 Spin Precession

In the non-local geometry but also in the conventional geometry, the effectiveness of spin injection and detection strongly depends on the relative magnitude of the contact resistance of the ferromagnetic electrodes compared to the resistance of the nonmagnetic material. A small contact resistance with respect to the nonmagnetic material, unavoidably, results in the so-called conductivity mismatch and also provides an extra path for spin relaxation at the ferromagnetic contacts [46]. This has to be taken into account in fitting of the spin precession measurements by solving the one-dimensional Bloch Eqs. [45]. The Bloch equations describe the

combined effect of diffusion, precession and spin relaxation in the system  $D_s \frac{d^2 \vec{\mu}}{dx^2} - \frac{\vec{\mu}}{\tau} + \frac{g\mu_B}{\hbar} (\vec{B} \times \vec{\mu}) = 0$ , where  $D_s$  is the diffusion constant,  $\vec{\mu}$  is the chemical potential vector of the spin species,  $\tau$  is the spin relaxation time, g is the g-factor,  $\vec{B}$  is the magnetic field,  $\hbar$  is Planck's constant and  $\mu_B$  is the Bohr magneton.

#### 9.3.1.6 Spin Relaxation

Consider possible spin relaxation mechanisms in a nonmagnetic material, for example, in a single wall nanotube. Spin relaxation in a nonmagnetic material is an unavoidable process which brings a non-equilibrium population of spins (found at the spin injector interface to the nonmagnetic system) into a uniform distribution over spin directions [47]. This description is also adequate for corresponding graphene-based systems. Four important mechanisms of spin relaxation in semi-conductors should be analysed (see, Fig. 9.9, [47]).

Elliott–Yafet Mechanism Conduction electron spins can relax via ordinary momentum scattering from impurities, boundaries and phonons if the lattice ions induce spin-orbit coupling in the system ([47], Fig. 9.9a). Spin-orbit interaction mixes spin-up and spin-down states, and therefore the Bloch states (momentum eigenstates) are not eigenstates anymore. The result is that the longitudinal time,  $T_1$ , is proportional to the momentum scattering time,  $\tau_p$ . Therefore, the spin flip length  $\lambda_s = \sqrt{D_s T_1}$  is proportional to the mean free, since the diffusion constant is proportional to  $\tau_p$ .

Dyakonov–Perel Mechanism Spin dephasing occurs because electrons feel an effective magnetic field, resulting from the lack of inversion symmetry and from the spin-orbit interaction, which changes in random directions every time the electron scatters to a different momentum state (Fig. 9.9b, [47]).

*Bir*, *Aronov and Pikus Mechanism* The electron–hole exchange scattering can lead to efficient electron spin relaxation in p-type semiconductors [48, 49]. According to the electron–hole exchange interaction, within the elastic scattering approximation, the spin lifetime limited by the Bir–Aronov–Pikus mechanism is given by the Fermi Golden Rule [50].

Hyperfine Interaction Mechanism The hyperfine interaction is the interaction between the magnetic moments of the electrons and the nuclear magnetic moment (Fig. 9.9d, [47]). This mechanism dominates in the case of localized electrons, for example, in quantum wells and quantum dots.

References 305

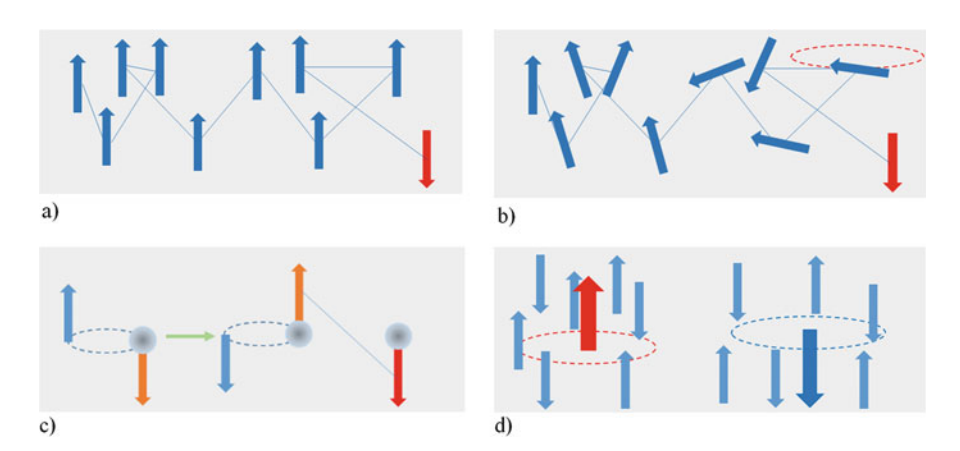


**Fig. 9.9** Four important mechanisms of spin relaxation in semiconductors. (a) Elliott-Yafet mechanism. (b) Dyakonov-Perel mechanism. (c) Bir-Aronov-Pikus mechanism. (d) Hyperfine interaction

### 9.4 Concluding Remarks

CNTs are expected to be good candidates for spintronic devices. The first organic spintronic device was reported by Tsukagoshi et al. in 1999 [51], and remarkably, it consisted of a multiwalled carbon nanotube contacted by Co contacts. Many other spintronic experiments on multi- and single-walled carbon nanotubes followed up. Unfortunately, the experiment of Tsukagoshi and all other experiments performed after his work have made use of the conventional two- terminal spin valve geometry. Magnetoresistance phenomenon (GMR and TMR) for nanomemory devices based on CNTs of various morphologies (i.e. various chiralities, diameters) including metal- and semiconductor-like ones and ferromagnetic Fe–Pt contacts can be potentially viewed as an alternative for electromagnetic nanosensoring and magnetic nanomemory.

#### References

- 1. Shunin Yu **2015** Spintronic Nanomemory and Nanosensor Devices Based on Carbon Nanotube-Fe-Pt Interconnects: Models and Simulations LAP (Saarbrücken-Germany: Lambert Academic Publishing) 50 p
- Bergeson J D, Etzkorn S J, Murphey M B, Qu L, Yang J Dai L, Epstein A J 2008 Iron nanoparticle driven spin-valve behavior in aligned carbon nanotube arrays Appl. Phys. Lett. 93 172505-1-3
- 3. Thamankar R, Niyogi S, Yoo B Y, Rheem Y W, Myung N V, Haddon R C, Kawakamia R K **2006** Spin-polarized transport in magnetically assembled carbon nanotube spin valves *Appl. Phys. Lett.* **89** 033119-1-3

- 4. Céspedes O, Ferreira M S, Sanvito S, Kociak M, Coey J M D **2004** Contact induced magnetism in carbon nanotubes *Journal of Physics: Condensed Matter* **16**(10) L155–61
- Barth'el'emy A, Fert A, Contour J-P, Bowen M, Cros V, De Teresa J M, Hamzic A, Faini J C, George J M, Grollier J, Montaigne F, Pailloux F, Petroff F, Vouille C 2002 Magnetoresistance and spin electronics *Journal of Magnetism and Magnetic Materials* 242–245(1) 68–76
- 6. Hewson A C **1993** *The Kondo problem to heavy fermions* (Cambridge: Cambridge University Press)
- Baibich M N, Broto J M, Fert A, van Dau F N, Petroff, F, Etienne P, Creuzet G, Friederich A, Chazelas J 1988 Giant Magnetoresistance of (001)Fe/(001)Cr Magnetic Superlattices *Phys. Rev. Lett.* 61 2472–5
- 8. Binasch G, Grünberg P, Saurenbach F, Zinn W **1989** Enhanced magnetoresistance in layered magnetic structures with antiferromagnetic interlayer exchange *Phys. Rev. B* **39** 4828–30
- Tsymbal E Y, Pettifor D G 2001 Perspectives of Giant Magnetoresistance In: Solid State Physics 56 Eds H Ehrenreich and F Spaepen (Oxford: Academic Press) 113–237
- 10. Julliére M 1975 Tunneling between ferromagnetic films Phys. Lett. A 54 225-6
- 11. Moodera J S, Kinder L R, Wong T M, Meservey R 1995 Large magnetoresistance at room temperature in ferromagnetic thin-film tunnel junction *Phys. Rev. Lett.* 74 3273–6
- 12. Parkin S S P, More N, Roche K P 1990 Oscillations in exchange coupling and magnetoresistance in metallic superlattice structures: Co/Ru, Co/Cr, and Fe/Cr Phys. Rev. Lett. 64 2304–7
- 13. Parkin S S P, Bhadra R, Roche K P **1991** Oscillatory magnetic exchange coupling through thin copper layers *Phys. Rev. Lett.* **66** 2152–5
- Tsukagoshi K, Alphenaar B W, Ago H. 1999 Coherent transport of electron spin in a ferromagnetically contacted carbon nanotube *Nature* 401(6753) 572–574
- Mott N F 1936 The Electrical Conductivity of Transition Metals Proc. Royal. Soc. 153 699–726
- Mott N F 1936 Resistance and thermoelectric properties of the transition metals *Proc. Royal.* Soc. 156 368–82
- 17. Shunin Yu N, Zhukovskii Yu F, Gopeyenko V I, Burlutskaya N Yu, Lobanova-Shunina T D, Bellucci S 2015 CNTs- and GNRs-based electromagnetic and spintronic devices: models and simulations In: Proc Int Conf NANOMEETING-2015 PHYSICS, CHEMISTRY AND APPLICATION OF NANOSTRUCTURES, 2015 Eds V E Borisenko, S V Gaponenko, V S Gurin, C H Kam (New-Jersey-London-Singapore-Beijing-Hong Kong-Taipei, Chennai: World Scientific) 207–10
- 18. Kirkpatrick S 1973 Percolation and Conduction Rev. Mod. Phys. 45 574–88
- 19. Essam J M **1972** Phase Transition and Critical Phenomena (London-N.-Y.: Academic Press) 197 p
- 20. Brenig W, Döhler G, Wölfle P **1971** Theory of thermally assisted electron hopping in amorphous solids *Z. Physik* **246** 1–12
- 21. Greenwood D A **1958** The Boltzmann equation in the theory of electrical conduction in metals *Proc. Phys. Soc.* **71** 585–96
- 22. Kubo R 1966 The fluctuation-dissipation theorem Rep. Prog. Phys.29 255-84
- 23. Kubo R 1956 A general expression for the conductivity tensor Can. J. Phys. 34 1274–7
- 24. Butcher P N **1974** Stochastic interpretation of the rate equation formulation of hopping transport theory: III. DC hopping analogues and their application to percolative conductance networks and spin systems *J. Phys. C* **7** 3533–40
- Last B J 1972 Percolation theory and the critical concentration of a dilute Heisenberg ferromagnet J Phys. C 5 2805–12
- 26. Stinchcombe R B **1973** The branching model for percolation theory and electrical conductivity *J. Phys. C* **6**(1) L1–5
- 27. Stinchcombe R B **1974** Conductivity and spin-wave stiffness in disordered systems-an exactly soluble model *J Phys. C* **7**(1) 179–203
- de Gennes P.-G. 1979 Scaling Concepts in Polymer Physics (Ithaca and London: Cornell University Press) 38–43

References 307

29. de Gennes P.-G. **1976** On a relation between percolation theory and the elasticity of gels *J de Phys. Lett.* **37** L1–2

- 30. de Gennes P.-G. 1976 Scaling theory of polymer adsorption J de Phys. Lett. 37 1445-52
- 31. Fisher M E, Essam J W **1961** Some cluster size and percolation problems *J Math. Phys.* **2** 609–19
- 32. Young A P **1976** The critical behaviour of disordered magnetic systems-an exactly solvable model *J. Phys. C* **9** 2103–20
- 33. Essam J W, Gwilym K W, Loveluck J M 1976 Thermodynamic scaling laws for a dilute ferromagnet in the percolation limit by series methods *J Phys. C* 9 365–78
- 34. Crangle J 1960 Ferromagnetism in Pd-rich palladium-iron alloys *Phil. Mag.* 5 335–42
- 35. Bozorth R M, Wolf P A, Devis D D, Compton V B, Wernik J **1961** Ferromagnetism in Dilute Solutions of Cobalt in Palladium *Phys. Rev.* **122** 1157–60
- 36. Parfenova V P, Alekseevskii N E, Erzinkyan A L, Shpinel' V S 1968 Measurement of the effective magnetic fields acting on Co<sup>60</sup> nuclei in dilute solid solutions of Co in Pd Soviet Physics JETP 26(2) 324–7
- 37. Sarachik M P, Shaltiel D **1967** Low-Temperature Resistivity and the Sign of the Exchange Integral *J Appl. Phys.* **38** 1155–6
- 38. Crangle C, Scott W R 1965 Dilute Ferromagnetic Alloys J Appl. Phys. 36 921-7
- Ginzburg S. L, Korenblit I Ya, Shender E F 1973 Spin waves and density of states in disordered ferromagnetic substances Zh. Eksp. Teor. Fiz. 64 2255–68; Sov. Phys. JETP 37 (6) 1141–7
- 40. Korenblit I Ya, Shender E F **1978** Ferromagnetism of disordered systems *Uspekhi fizicheskikh nauk* **126** 233–68 (in Russian)
- 41. Kurkijärvi J **1974** Conductivity in random systems. II. Finite-size-system percolation *Phys. Rev. B* **9** 770–4
- 42. Ambegaokar V, Cochran S, and Kurkijärvi J **1973** Conduction in Random Systems *Phys. Rev. B* **8** 3682–8
- 43. Wohlfarth E P **1982** *Transport properties of ferromagnets* In *Ferromagnetic materials* (North Holland, 1982) Ch.9 Eds I A Campbell and A Fert 747 p
- 44. Jedema F J, Filip A T, van Wees B J **2001** Electrical spin injection and accumulation at room temperature in an all-metal mesoscopic spin valve *Nature* **410** 345–8
- 45. Jedema F J, Heersche H B, Filip A T, Baselmans J J A, van Wees B J **2002** Electrical detection of spin precession in a metallic mesoscopic spin valve *Nature* **416** 713–6
- 46. Schmidt G, Ferrand D, Molenkamp L W, Filip A T, van Wees B J 2000 Fundamental obstacle for electrical spin injection from a ferromagnetic metal into a diffusive semiconductor *Phys. Rev.* B 62 4790–4
- Žutić I, Fabian J, and Das Sarma S 2004 Spintronics: Fundamentals and applications Rev. Mod. Phys. 76 323–410
- 48. Bir G L, Aronov A G, Pikus G E **1975** Spin relaxation of electrons scattered by holes, *Zh. Eksp. Teor. Fiz.* **69** 1382–97
- 49. Aronov A G , Pikus G E, Titkov A N **1983** Spin relaxation of conduction electrons in p-type III–V compounds *Zh. Eksp. Teor. Fiz.* **84** 1170–84
- Wu M W, Jiang J H, Weng M Q 2010 Spin dynamics in semiconductors *Physics Reports* 493 61–236
- Tsukagoshi K, Alphenaar B W, Ago H 1999 Coherent transport of electron spin in a ferromagnetically contacted carbon nanotube Nature 401 572–4

# **Chapter 10 Nanosensor Systems Simulations**

We focus our research on two important directions of real-time control nanosystems addressed to ecological monitoring and medical applications, both of which provide environmental security for the human society and every individual. Ecological monitoring has been widely presented in [1]. For individual application, it is necessary to develop nanodevices with various functions for the human body, particularly for the control of health parameters, the enhancement of human abilities and prosthetics. Another course of development of nanosensors, nanoactuators, nanotransducers, etc. is the creation of artificial systems such as artificial intelligence or artificial individual [2, 3].

There are some successful schemes of nanosensors based on FET-type devices where induced conductivity changes in included nanocarbon elements (e.g. CNT or GNR) are indicators of external influence intensities. For chemical and biological agents, nanocarbon elements should be purposely functionalized [2].

We pay attention to the development of bio-nanosensors based on polymer nanoporous structures (nanotracks) with various enzymes, which provide the corresponding biocatalytic reactions and give reliably controlled ion currents [4, 5]. In particular, we describe a concept for a glucose biosensor based on the enzyme glucose oxidase (GOx) covalently linked to nanopores of etched nuclear track membranes. Using the simulation of chemical kinetics glucose oxidation with glucose oxidase, we have obtained theoretical calibration dependences, when the concentration of H<sup>+</sup> is proportional to the concentration of the detected glucose. Experimental and theoretical calibration dependences demonstrate similar trends. The proposed device can serve to detect physiologically relevant glucose concentrations. The catalytic sensor can be made reusable due to the production of diffusible products from the oxidative biomolecular recognition event. Moreover, we can develop a multi-agent packet nanosensor, which can be used for human breathing analyser in relation to cancer detection, hepatitis and so on.

We consider physical nanosensors (pressure and temperature) based on functionalized CNT and GNR nanostructures. The model of nanocomposite materials based on carbon nanocluster suspension (CNTs and GNRs) in dielectric polymer environments (e.g. epoxy resins) is regarded as a disordered system of fragments of nanocarbon inclusions with different morphologies (chirality and geometry) in relation to a high electrical conductivity in a continuous dielectric environment. The electrical conductivity of a nanocomposite material depends on the concentration of nanocarbon inclusions (in fact, carbon macromolecules). The basic conductivity mechanism for the considered nanocomposites is the hopping conductivity. This mechanism can usually be observed, for example, in amorphous semiconductors or some disordered solids. Various nanocomposite morphologies are considered, and computer simulation results for pressure and temperature nanosensor models are discussed in comparison with the experimental nanodevice prototype.

The sensitivity of the considered nanosensors in this case depends on percolation ability of a nanocomposite subdued to the changes of physical factors (pressure or temperature). Attention should be paid to the nanoscaled quantum mechanical phenomenon of percolation ability among the neighbouring nanocarbon 'islands' within a nanocomposite. Integrated 'micro'- or 'mesoscale' conductivity effects should also be evaluated as a goal for calibration of a nanocomposite material as a measurement tool for pressure or temperature [3–5].

#### 10.1 Physical and Chemical Nanosensors

Nanosensor systems constitute an essential functional part of any modern device that provides information processing for information systems, engineering interfaces, healthcare and many others. The talk is about nanosensor systems for various aspects of ecological monitoring and security.

The fundamental electronic devices are nanocarbon-based FET transistors capable of providing high sensitivity to various external influences of different nature. In particular, changes of local electronic density of states correlate with corresponding physical, chemical and biochemical influences and lead to FET-device conductivity changes. Conventional schemes of nanosensoring systems are based on nano-FET-type devices [1–5].

However, these types of nanosensors are oriented on local external influences at atomic or molecular levels, when the external agent has a direct contact with nanocarbon surface atoms, like in FET-type nanosensors (see Fig. 10.1).

## 10.1.1 Conductivity as a Tool of Nanosensor Systems

The calculations of conductivity are usually performed using Kubo-Greenwood formula [1, 2, 34]:

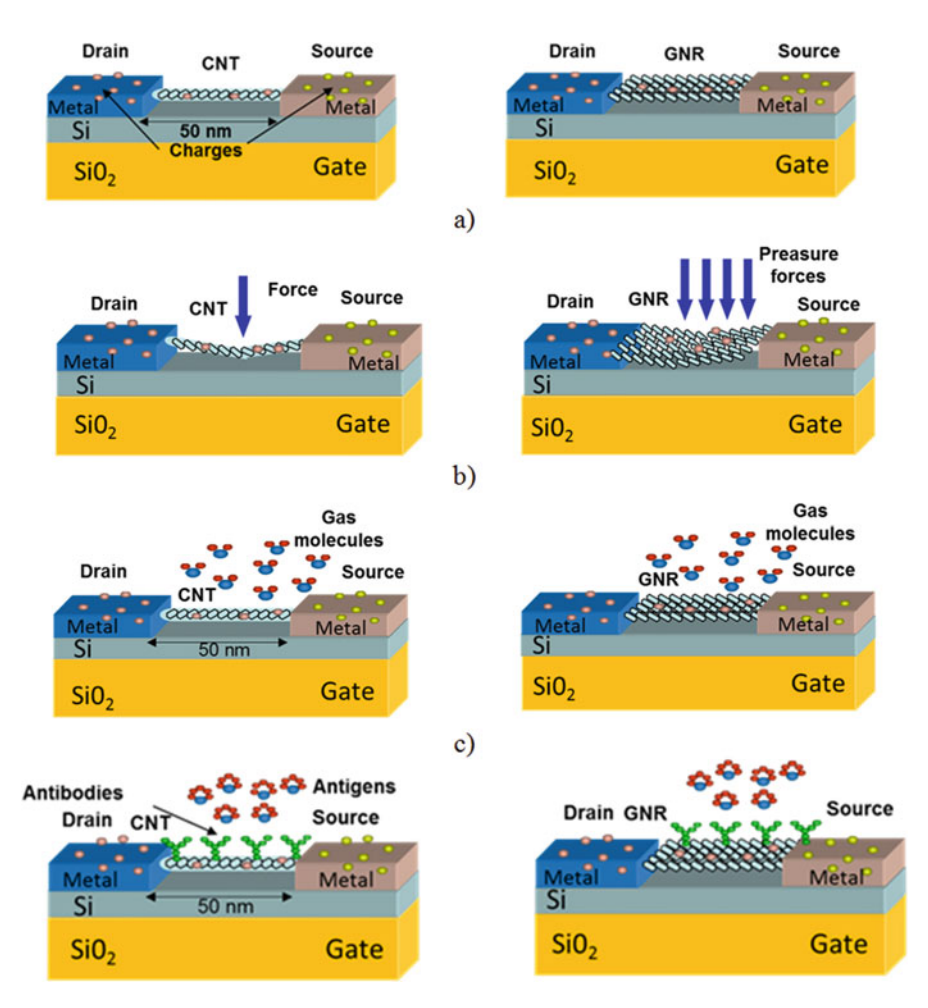


**Fig. 10.1** Models of FET-type nanosensors as a prototypes of novel nanodevices: (**a**) *the unperturbed field-effect transistors* based on CNT or GNR elements; (**b**) *physical nanosensors*, a conducting threshold can be altered when the tube or graphene ribbon is bent; (**c**) *chemical nanosensors*, a conducting threshold can be altered when the amount of free charges on the tube of graphene ribbon surface is increased or decreased by the presence of donor or acceptor molecules of specific gases or composites, (**d**) *biological nanosensors*, monitoring of biomolecular processes such as antibody/antigen interactions, DNA interactions, enzymatic interactions or cellular communication processes, among others

$$\sigma_{E}(\omega) = \frac{\pi \Omega}{4\omega} \int [f(E) - f(E + \hbar \omega)] |D_{E}|^{2} \rho(E) \rho(E + \hbar \omega) dE, \qquad (10.1)$$

where  $\omega$  is a real frequency parameter of Fourier transform for the time-dependent functions; f(E) is Fermi–Dirac distribution function;  $D_{E,E'} = \int_{\Omega} \Psi_{E'}^* \nabla \Psi_E d\mathbf{r}$ , where

 $\Psi_{E(\mathbf{K})} = A \exp(i\mathbf{K}\mathbf{r})$ ; and  $\mathbf{K}$  is the complex wave vector of the effective medium. The dispersion function  $E(\mathbf{K})$  determines the properties of the wave function  $\Psi_{E(\mathbf{K})}$  upon the isoenergy surface in  $\mathbf{K}$ -space.

Usually two basic electron conductivity mechanisms in CNT-based structures are considered. The ballistic mechanism is engaged in electron transport within CNTs, while the collisional mechanism is a characteristic of CNT-substrate interconnects. The general conductivity  $\sigma_{\rm gen}$  is evaluated as follows:  $\sigma_{\rm gen}^{-1} = \sigma_{\rm coll}^{-1} + \sigma_{\rm ball}^{-1}$ .

For pure CNTs, we clearly observe that  $\sigma_{ball}\gg\sigma_{coll}$ . But Kubo-Greenwood formalism is free from this division on ballistic and collisional mechanisms and seems to be more objective. The analysis of Kubo-Greenwood's conditions in respect of CNT morphology has been presented taking into account both dc ( $\omega=0$ ) and ac ( $\omega\neq0$ ) regimes as well as the temperature factor of electron transport.

We use in this research the results of ab initio electronic structure calculations of D'yachkov et al. [6] based on the linear augmented cylindrical wave (LACW) theory of the perfect SWCNT band structure. The developed generalization of this method allows one to treat the electronic structure of various defects in the SWCNTs. The method combines the advantages of density functional ab initio theory with the Green's function approach to the point defects electronic structure.

The main aim of our research is a simulation on sensitivity of SWCNTs to various defects which evidently change the local EDOS and then, as a result, give the changes of conductivity. The detailed properties of EDOS at the vicinity of Fermi level are essential for expected conductivity values.

Figure 10.2 shows the parametric simulations of *ac*-conductivity for *armchair* (m,m) CNTs, where the essential sensitivity to the radius of SWCNT for energies more than 0.5 eV is shown.

But, there is no essential dependence on chirality number m for THz-range, excluding m = 4. Figures 10.3 and 10.4 demonstrate the comparison of conductivity calculations for pure perfect and doped (B or N) CNTs (5,5) and (7,7) in the case of noninteracting defects.

Numerical simulations of conductivity have been carried out for zigzag (m,0), armchair (m,m) and chiral (m,n) CNTs, where the sensitivity of conductivity has been demonstrated to the local electronic density of states in CNTs with local impurities (N and B atoms). In particular, this sensitivity means that the potential possibility of CNT-based nanodevices is to be used as nanosensor systems. This means that the calibration of such nanosensors on current is possible.

Similar calculations for graphene-based structures on the basis of EDOS [9] (graphene, CO-graphene, Al-doped, Al-graphene and Al-CO-graphene) are shown in Fig. 10.5.

Doping technology of graphene is problematic [7]. However, taking into account that edges of GNRs can be considered as an extended topological defect, we pay attention to these regions as possible tools of nanosensoring. Extended defects in

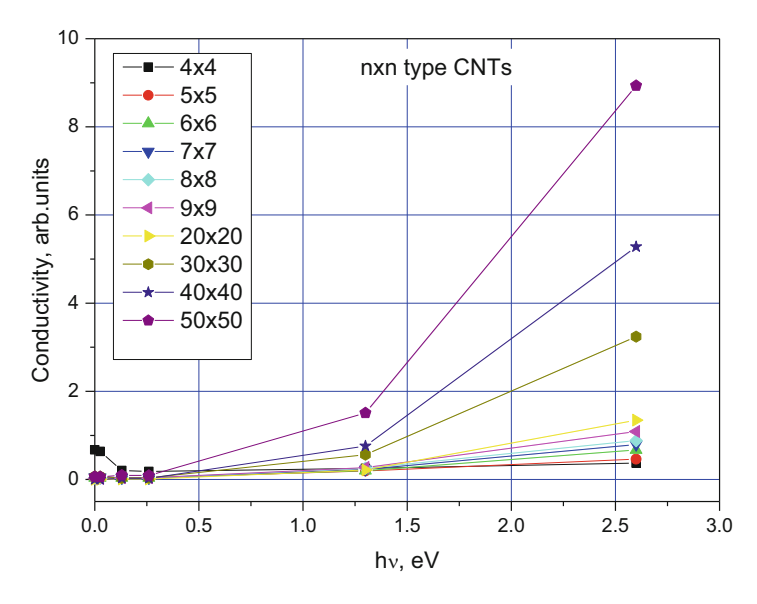


**Fig. 10.2** Conductivities of perfect *armchair* SWCNTs of various morphologies. *Note:* the critical frequency of about 0.25 eV corresponds to 60 THz

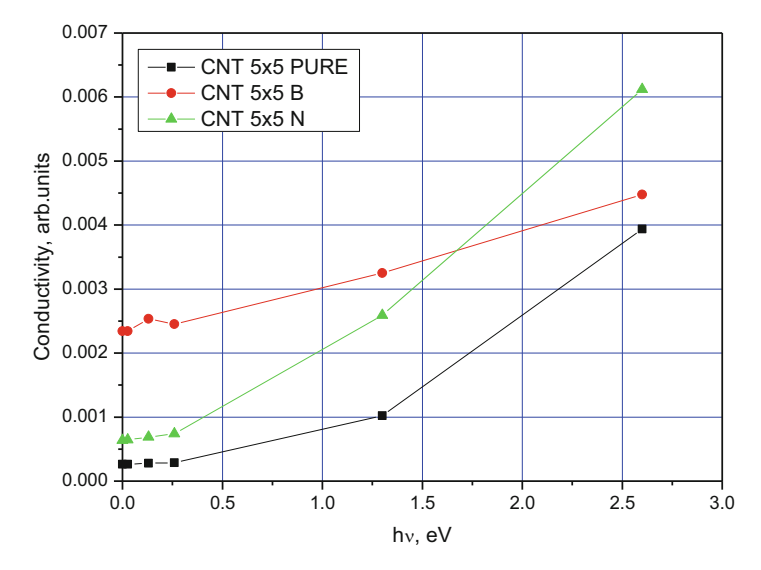


Fig. 10.3 Conductivities of pure perfect and doped (B or N) CNTs (5,5) in the limit of noninteracting defects

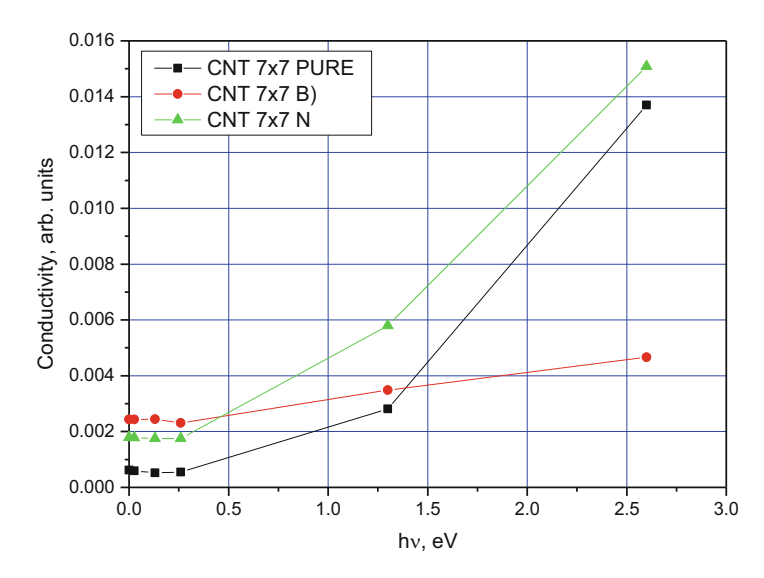


Fig. 10.4 Conductivities of pure perfect and doped (B or N) CNTs (7,7) in the limit of noninteracting defects

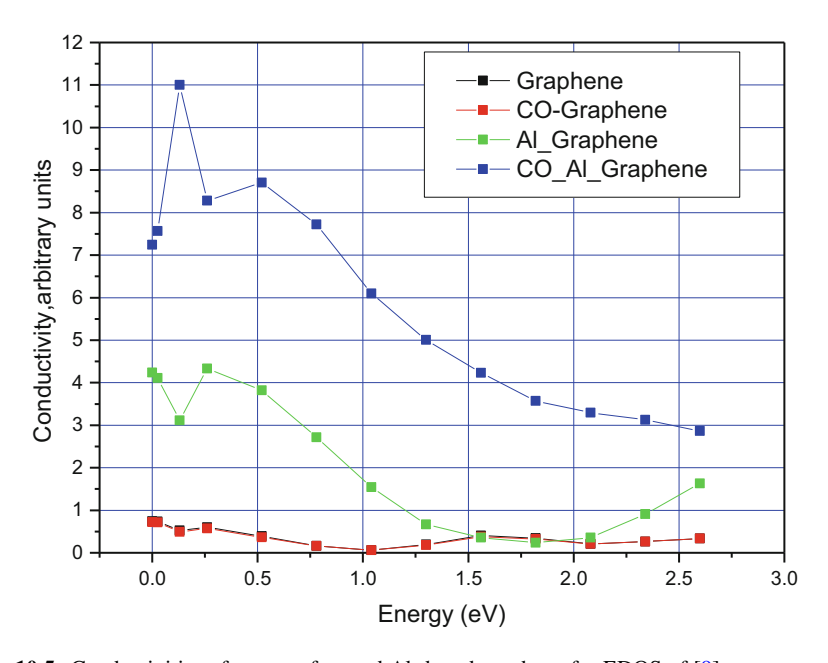


Fig. 10.5 Conductivities of pure perfect and Al-doped graphene for EDOS of [9]

graphene sheets, such as grain boundary (GB) defects, have been observed in some experimental investigations [8, 9]. Our calculations for pure and N- and B-doped GB on the basis of EDOS given in [10] are presented in Fig. 10.6.

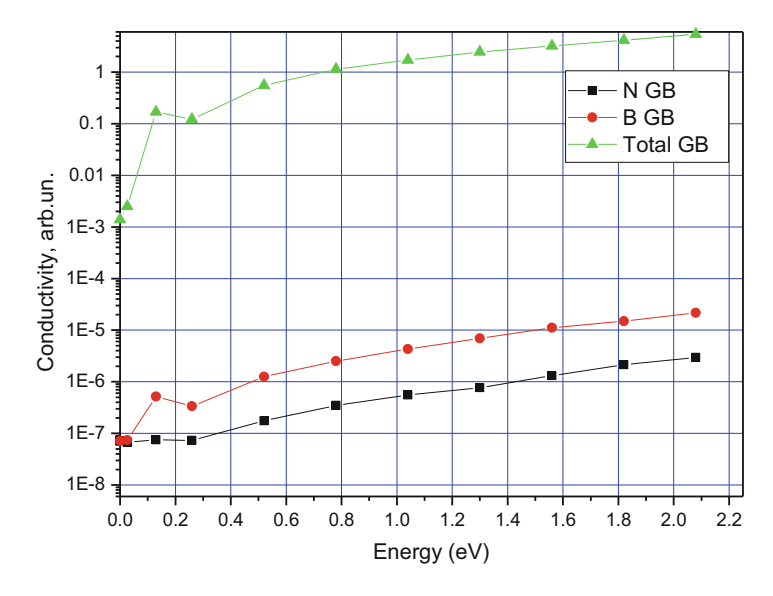


Fig. 10.6 Conductivities of pure and N- and B-doped GB on the basis of EDOS in [10]

# 10.2 Bio-nanosensors: Polymer Nanoporous Model Structures

Since the 1960s, it has been known that energetic (with tens of MeV or more) heavy (with atomic masses being usually larger than that of Ar) ion irradiation ('swift heavy ions', SHI) introduces very narrow (~ some nm) but long (typically  $10{\text -}100~\mu\text{m}$ ) parallel trails of damage in irradiated polymer foils, the so-called latent ion tracks. The damage shows up primarily by the formation of radiochemical reaction products. Whereas the smaller ones readily escape from the irradiated zone, thus leaving behind themselves nanoscopic voids, the larger ones tend to aggregate towards carbonaceous clusters. Thus, emerging structural disorder along the tracks modifies their electronic behaviour (see Fig. 10.7).

Description of the sensing reaction of glucose with the enzyme GOx looks as follows:

- (a) The overall net reaction is glucose  $(C_6H_{12}O_6) + O_2$  (due to enzyme-induced oxidation) gluconic acid  $(C_6H_{12}O_7) + O$ .
- (b) This remaining O attaches to some  $H_2O$  to form peroxide  $H_2O_2$ .
- (c) The product, gluconic acid, dissociates around pH = 7. Thus, the conductivity of the liquid changes (essentially if the product is enriched in the track's confinement); this is what is measured by the sensor [11, 35].

In particular, a complicated biochemical kinetics of basic reaction of glucose detection depends on track qualities (e.g. track creation mechanism, foil material properties), enzyme (GOx) distribution on the track surface, geometry of the etched

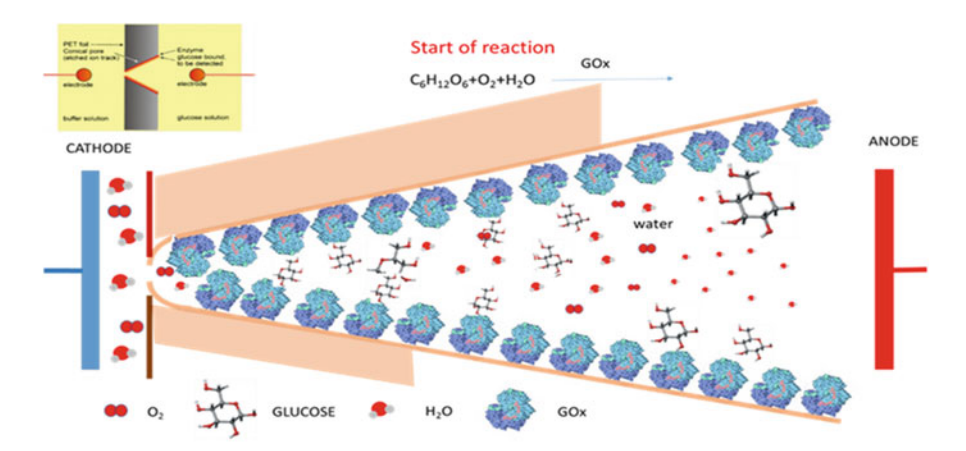


**Fig. 10.7** General scheme describing the detection scheme and modified polymer. Principle arrangement of experimental setup to study current-voltage dependences in ion track-containing foils embedded in electrolytes

track, etc. All these factors are the subject for the nearest special research. Moreover, the detailed kinetics of reaction is the object of 3D-modelling to design the optimal geometry of nanosensor active space. This allows creating optimal nanosensors with the increased efficiency.

The newly created intrinsic free volume enables electrolytes to penetrate into the polymer, thus forming parallel liquid nanowires. In case of tracks penetration through all the foil, the conducting connections emerge between the front and back sides of the foil. The ion track technology is particularly intended to biosensing applications. In this case, the ion tracks are functionalized directly by attaching organic or bioactive compounds (such as enzymes) to their walls.

#### 10.2.1 Biosensor Model Testing and Experimental Results

Experimental and theoretical calibration dependences demonstrate similar trends. The proposed device can serve to detect physiologically relevant glucose concentrations. The catalytic sensor can be made reusable due to the formation of diffusible products from the oxidative biomolecular recognition event. Moreover, we can develop a multi-agent packet nanosensor, suitable for application as a human breathing analyser in relation to cancer detection, hepatitis and so on [11–15].

The recent advancements in the field of nanosensor design allow monitoring and tracking biomolecules in such areas as the environment, food quality and healthcare. The presently developed ion track-based nanosensors provide high sensitivity, reliable calibration (see Fig. 10.8), small power and low cost.

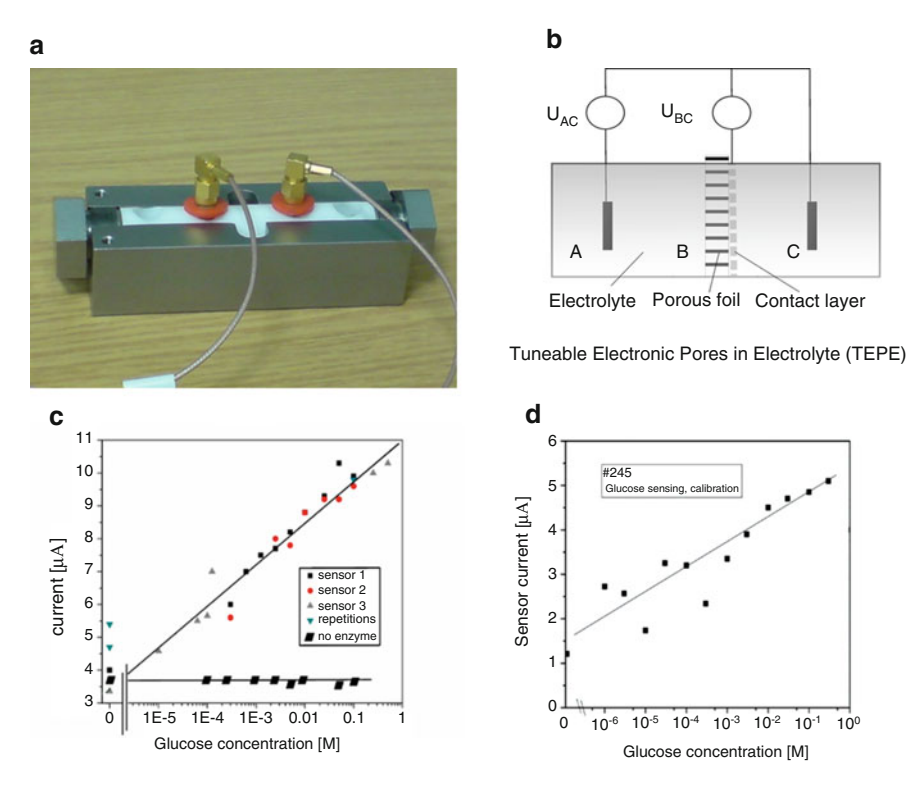
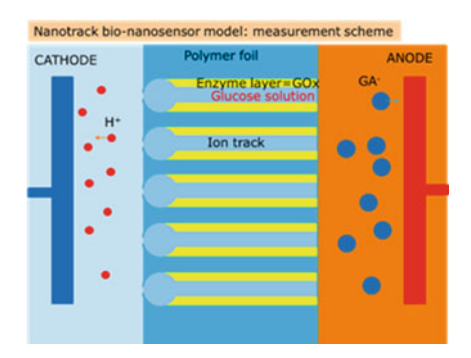


**Fig. 10.8** Favourable platform for measuring enrichment of chemical reaction products via electrical current transmitted through the nanopores: (a) nanosensor system prototype [11]; (b) principal electrical scheme of sensor current [11]; (c) experimental calibration curves on 2007 year glucose testing series [11], experimental calibration dependence performance comparison of three identically produced track-based glucose detectors against a calibration curve I (+5 V) vs glucose concentration; (d) similar experimental calibration curve on 2016 year glucose testing series [16]

Using simulation of chemical kinetics glucose oxidation with glucose oxidase (see Fig. 10.9), we have obtained theoretical calibration dependences, when the concentration of H<sup>+</sup> is proportional to the concentration of the detected glucose.

Simulation schemes are directed on concentrations of  $H^+$  which are equal to glucose concentrations. In cases of stable of glucose, inputs we obtain can write typical simulation equations which lead to the saturated values of  $H^+$  ions concentrations (see Fig. 10.10):

$$\begin{cases} \frac{d}{dt} [C_6 H_{12} O_6] = -w_1 \\ \frac{d}{dt} [H_2 O_2] = w_1 - w_2 \\ \frac{d}{dt} [O_2] = -w_1 + w_2 \\ \frac{d}{dt} [H^+] = 2w_1 \end{cases}$$
(10.2)



Basic chemical reactions of Glucose detection: and simulation equations are:

$$\begin{split} &C_{6}H_{12}O_{6}+O_{2} \xrightarrow{GOx} C_{6}H_{12}O_{7}+O \\ &O+H_{2}O\to H_{2}O_{2}, H_{2}O_{2} \xrightarrow{catalaza} \frac{1}{2}O_{2}+H_{2}O \\ &C_{6}H_{12}O_{7}\to C_{6}H_{12}O_{7}^{-}+H^{+} \\ &Anode: H_{2}O\to \frac{1}{2}O_{2}+2H^{+}+2e^{-} \\ &Cathode: 2H^{+}+2e^{-}\to H_{2} \\ &Ultimate \ \ reaction: C_{6}H_{12}O_{6}+H_{2}O\to C_{6}H_{12}O_{7}+H_{2}. \end{split}$$

Fig. 10.9 General model of glucose detection process on the ion track-containing foils embedded in electrolyte and basic set of biochemical reaction [11, 12, 15]

where  $w_1 = k_1[C_6H_{12}O_6][O_2][GOx]$  and  $w_2 = k_2[H_2O_2]$  are the reactions rates and  $k_1$  and  $k_2$  are simulation parameters.

We can point out that theoretical simulation results demonstrate similar linear trend in comparison to experimental data (see Fig. 10.8c, d).

Taking into account the probable process of  $H^+$  ions recombination, we can modify simulation Eq. (10.3) as:

$$\begin{cases} \frac{d}{dt}[C_{6}H_{12}O_{6}] = -w_{1} \\ \frac{d}{dt}[H_{2}O_{2}] = w_{1} - w_{2} \\ \frac{d}{dt}[O_{2}] = -w_{1} + w_{2} \\ \frac{d}{dt}[H^{+}] = 2w_{2} - 2w_{3} \end{cases}$$
(10.3)

where  $w_1 = k_1[C_6H_{12}O_6][O_2][GOx]$ ,  $w_2 = k_2[H_2O_2]$  and  $w_3 = k_3[2H^+][2e^-]$  are the reactions rates and  $k_1$ ,  $k_2$  and  $k_3$  are again simulation parameters (Fig. 10.11).

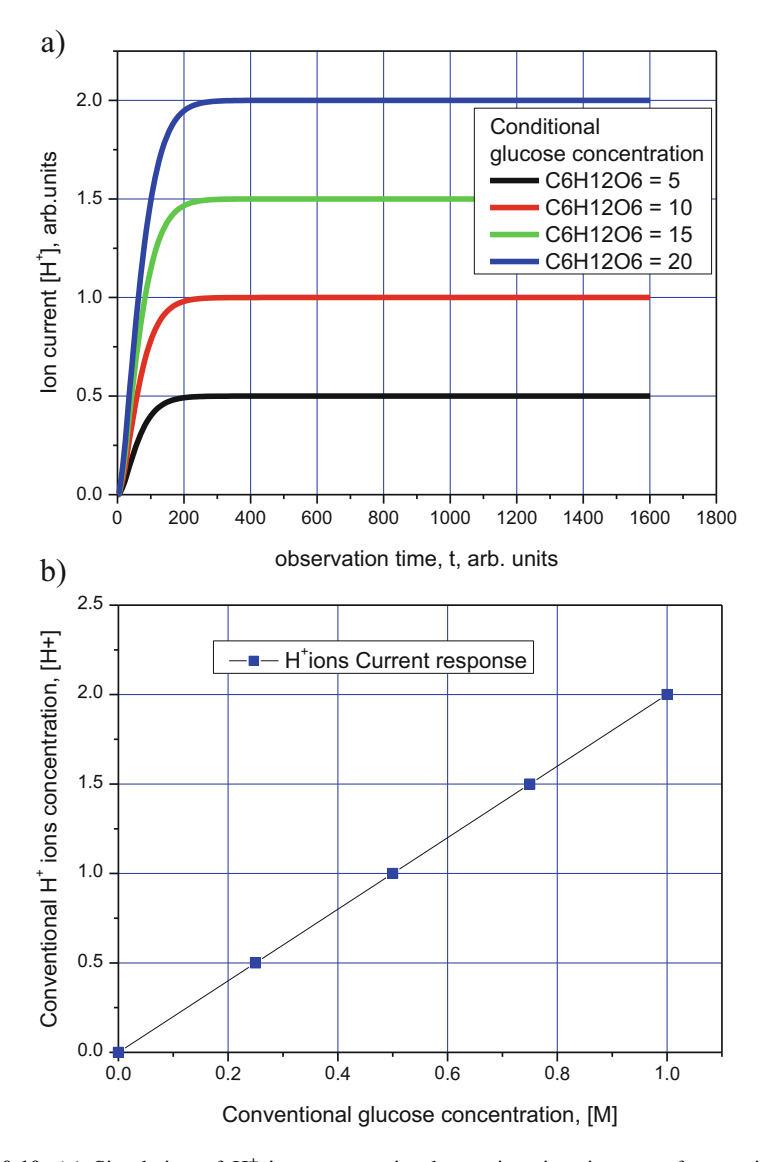


Fig. 10.10 (a) Simulation of  $H^+$  ion current via observation time in case of saturation; (b) theoretical model of typical calibration dependence based on chemical kinetics results: simulation of induced  $H^+$  ion current via glucose concentration

The creation of novel biosensors and their further improvement requires a careful study of the mechanisms of electrolytes passing through the tracks. Experimental and theoretical calibration dependences demonstrate similar trends. The proposed device can serve to detect physiologically relevant glucose concentrations. The catalytic sensor can be made reusable due to the formation of diffusible

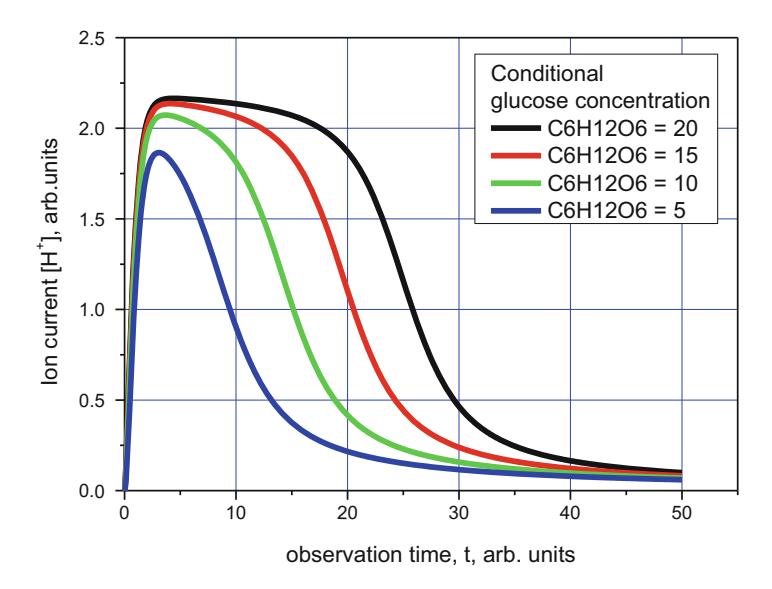


Fig. 10.11 Simulation of H<sup>+</sup> ion current via observation time in case of H<sup>+</sup> ions recombination

products from the oxidative biomolecular recognition event. Moreover, we can develop a multi-agent packet nanosensor, which can be used as a human breathing analyser in relation to cancer detection, hepatitis and so on (Fig. 10.12c).

Every nanocell (Fig. 10.12b) has an independent electrical metrology scheme. Moreover, sensitive cells for particular bioagent can be distributed along the sensitive surface of multi-agents flux. All electrical responses corresponding to a particular bioagent accumulated digitally as calibrated medical data on the special integrated screen.

#### 10.3 Nanocomposite-Based Nanosensoring Devices

### 10.3.1 Real-Time Polymer Nanocomposite-Based Physical Nanosensors

#### 10.3.1.1 Methods and Models

We consider physical nanosensors (pressure and temperature) based on functionalized CNT and GNR nanostructures. The model of nanocomposite materials based on carbon nanocluster suspension (CNTs and GNRs) in dielectric polymer environments (e.g. epoxy resins) is regarded as a disordered system of fragments of nanocarbon inclusions with different morphologies (chirality and geometry) in relation to a high electrical conductivity in a continuous dielectric

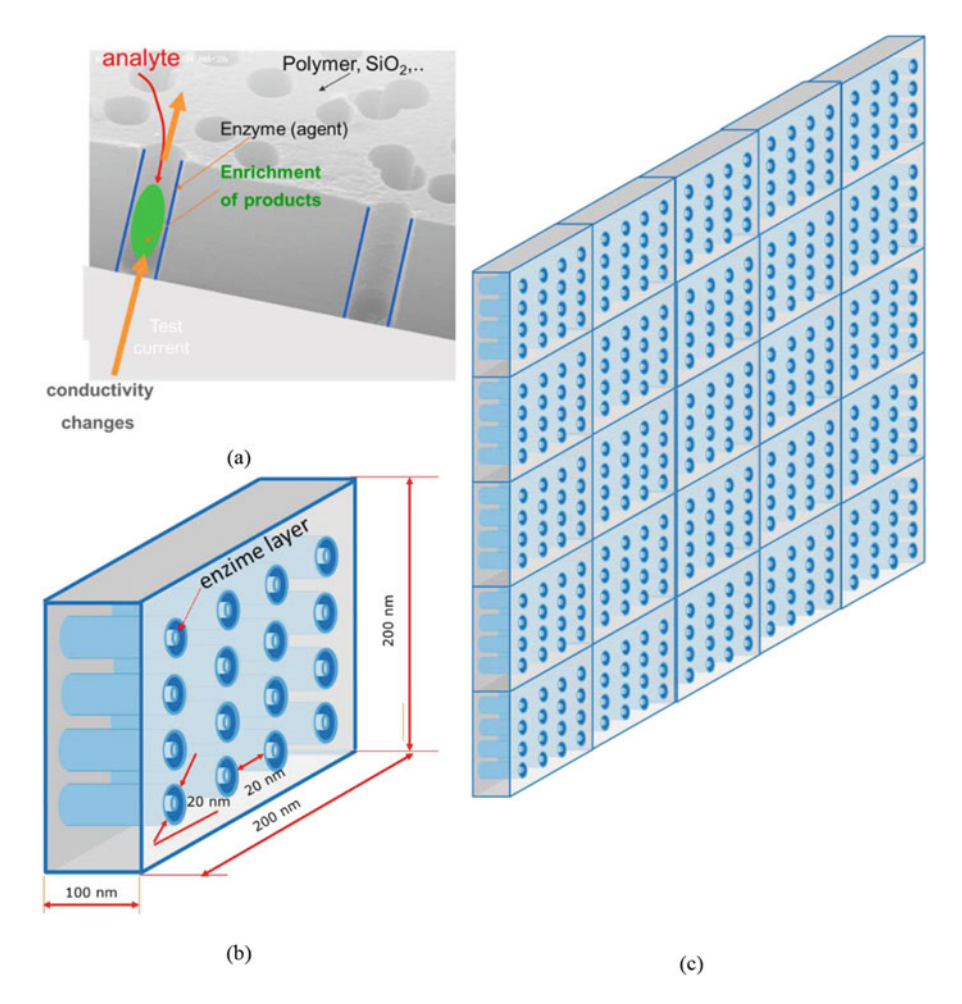


**Fig. 10.12** Sensing of chemical reaction products of an analyte with a specific enzyme via the track conductivity: (a) nanotracks in the foil, (b) model of nanocell with nanotracks including to corresponding tested bioagent, (c) multi-agent testing nanocell matrix  $(5 \times 5)$ , where the matrix any cell element independently oriented on particular bioagent

environment. The electrical conductivity of a nanocomposite material depends on the concentration of nanocarbon inclusions (in fact, carbon macromolecules) and corresponding morphologies. We should evaluate the role of particular local conductivity mechanisms in nanocomposites using the cluster approach based on the multiple scattering theory formalism, realistic analytical and coherent potentials, as well as effective medium approximation (EMA-CPA) which we have effectively used for modelling of nanosized systems, especially for various nanointerconnect problems [17, 18]. We have found during conductivity calculations in CNT-metal and GNR-metal interconnects that the conductivity mechanism is very sensitive to local morphological disordering [19–21].

#### 10.3.1.2 Conductivity Mechanisms

Considering models of physical nanosensors using CNT- and GNR-based nanocomposites, we should discuss conductivity mechanisms. In particular, in a medium with practically essential conductivity, it is useful to consider the phenomenon through the contributions of scattering effects that can take place in nanocomposite materials. We focus our attention on the four possible ways (see Fig. 10.13) trying to find the best description, in particular, for functionalized nanocomposites.

The key parameter for the analysis is the mean scattering length  $\ell_{e-\text{gen}}$  of an electron in the conductive matter. In general,  $\ell_{e-\text{gen}}$  includes various contributions in accordance with the well-known Matthiessen's rule, chapeau stating:

$$\frac{1}{\ell_{e-\text{gen}}} = \frac{1}{\ell_{e-e}} + \frac{1}{\ell_{e-a/\text{phon}}} + \frac{1}{\ell_{e-o/\text{phon}}} + \frac{1}{\ell_{e-o/\text{phot}}} + \frac{1}{\ell_{e-o/\text{phot}}} + \frac{1}{\ell_{e-\text{boundary}}} + \cdots,$$
(10.4)

where  $\ell_{e-e}$  is the electron–electron scattering length;  $\ell_{e-a/\text{phon}}$  is the acoustic phonon (emission and absorption) scattering length;  $\ell_{e-o/\text{phon}}$  is the optical phonon emission scattering length, is the optical phonon absorption scattering length and is the electron-impurity scattering length;  $\ell_{e-o/\text{phot}}$  is the electron-defect scattering length; and  $\ell_{e-\text{impurity}}$  is the electron scattering length with the boundary.

Hydrodynamical character of electric conductivity is the fundamental property of certain metals at low temperatures [22, 23]. This quality can be observed for such cases, when the length of electron mean free path is the order of the sample character size, namely,  $\ell_{e-\text{boundary}} \propto L$  and  $\ell_{e-e} \ll L$ .

The last relation should be precise in cases of collisional and non-collisional electronic plasma with concentrations less than  $10^{17}$  cm<sup>-3</sup>. Hydrodynamical behaviour of electron liquid is possible to observe in some critical spaces of metal-like graphene-based electronic devices [24].

Collisional mechanism is a more expanded conductivity mechanism and takes place in most cases of typical normal conditions, e.g. for metals and semiconductors. In this case  $\ell_{e-\text{phon}} \propto a \ll L$ , where a is the character distance between 'scatterers' – atoms. This mechanism for DC conductivity is described by the classical Drude model [25, 26]:  $\sigma = \frac{ne^2\tau_{e-\text{phon}}}{m^*}$ , where n is the electron concentration, e is the electron charge,  $\tau_{e-\text{phon}}$  is the time electron–phonon scattering and  $m^*$  is the effective mass of electron.

Ballistic character of conductivity is characterized by transport of electrons in a medium having negligible electrical resistivity caused by scattering. Moreover, the scattering character is essentially elastic, and the medium should be considered ideally regular. The time of electro–phonon interaction is negligible. This mechanism is observed, for example, in GNRs and CNTs included in FET-type devices. The most popular description of ballistic mechanism was given by Rolf Landauer and is known now as Landauer–Büttiker formalism [27]. Landauer formula

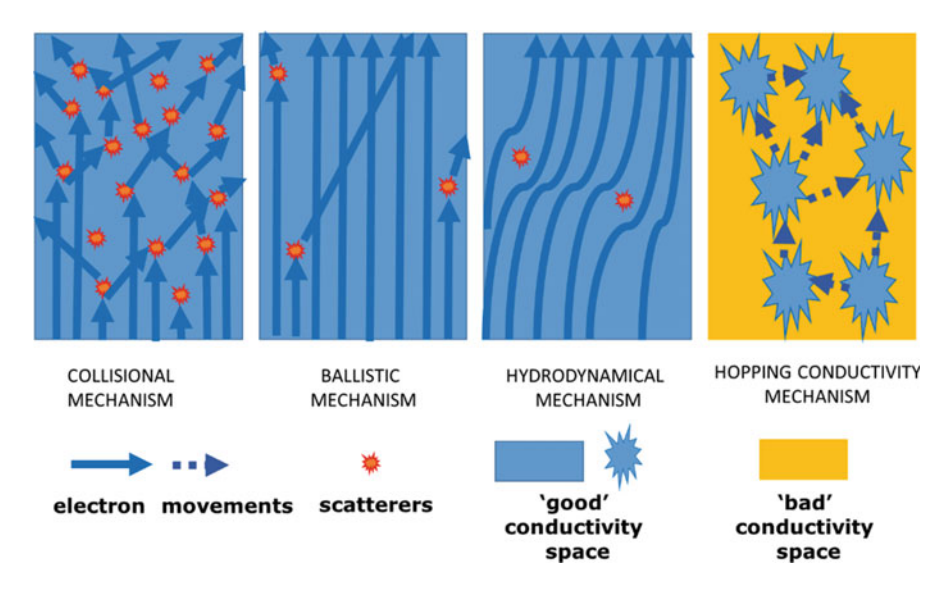


Fig. 10.13 Review of general mechanisms of electron DC conductivity

 $G(\mu) = G_0 \sum_n T_n(\mu)$ , where G is the electrical conductance,  $G_0 = e^2/(\pi\hbar) \approx 7.75 \cdot 10^{-5}$  Ohm is the conductance quantum,  $T_n(\mu)$  is the transmission eigenvalues of the channels and the sum runs over all transport channels in the conductor. The conductance can be calculated as the sum of all the transmission possibilities that an electron has when propagating with an energy E equal to the chemical potential  $\mu$ . In fact, the phenomenon is similar to optical thin films effect, when the transparency is achieved due to the quantization of the wave length. However, it is impossible to realize the remarkable conductivity property of GNRs and CNTs without any contacts. Appropriate nanocarbon–metal interconnects are characterized as disordered regions with essentially scattering mechanism of conductivity.

Hopping conductivity mechanism was proposed for disordered condensed systems (e.g. for composite amorphous semiconductors and dielectrics) for the explanation of the metal-insulator transition [28]. The talk is about the existence of the electron hopping between the conductive clusters in the dielectric or between the impurity centres of localization. In this model, the medium (insulator-metal) is represented by the following pattern: there is a random distribution of the nodal points related to each other by 'conductivities' exponentially dependent on the interstitial distances. The hopping conductivity model with a variable 'jump' length can be considered the most general one  $\ell_{e-\text{impurity}} \propto a$ :

$$\sigma = A \exp\left(-\frac{4}{3} \left(\frac{4\alpha r_s}{a}\right)^{3/4} \left(\frac{W}{\kappa T}\right)^{1/4},\tag{10.5}\right)$$

where a is the characteristic borous radius of the considered 'doping' centre,  $r_s$  is the characteristic radius of the doping centre or conductive region, W is the characteristic potential barrier for electron tunnelling, k is the Boltzmann constant, T is the sample temperature,  $\alpha \approx 0.70$  is the empirical constant which can be evaluated only using Monte-Carlo numerical simulations [29] and  $\sigma_0$  is the pre-exponential factor that is calculated taking into account the character of localization centre distribution.

#### 10.3.2 Models of CNT- and GNR-Based Nanocomposites

We develop a set of prospective models of nanocarbon-based nanomaterials and nanodevices having various interconnects and interfaces. In particular, nanoporous and nanocomposite systems are considered as complicated ensembles of basic nanocarbon interconnected elements (e.g. CNTs or GNRs with possible defects and dangling boundary bonds) within the effective media type environment. Interconnects are essentially local quantum objects and are evaluated in the framework of the developed cluster approach based on the multiple scattering theory formalism as well as effective medium approximation [3, 4, 30].

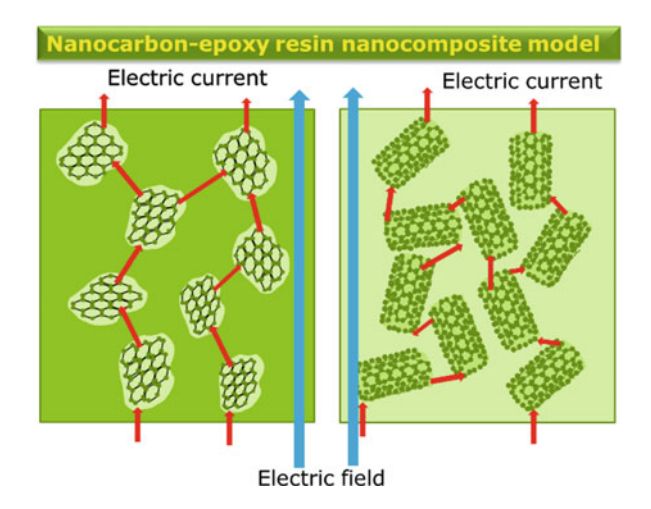
In cases when nanocarbon clusters are embedded in high resistance media (instead of vacuum), we come to a nanocomposite material. The utilization of polymeric composite materials (e.g. epoxy resins) supplemented with various morphological nanocarbon groups of carbon nanotube type (CNTs) and graphene nanoribbons (GNRs) allows us to create effective pressure and temperature sensors. Application of such nanocomposites as coatings can provide continuous monitoring of the mechanical strains in piping systems (e.g. in aircraft or automotive applications), when the critical pressure values can indicate malfunctions of the engine. The analysis of possible medical instruments for real-time measuring human body temperature and blood pressure can also be realized.

The interest in CNT- and GNR-based polymer nanocomposites as prospective pressure and temperature nanosensor materials is based on the observed electric percolation phenomena via the nanocarbon inclusions concentration. In particular, the electrical conductivity of a nanocomposite increases with the increasing CNT loading up to a critical filler concentration, where a dramatic increase in conductivity is observed. This critical filler concentration is called electrical percolation threshold concentration. At percolation threshold concentration, a filler forms a three-dimensional conductive network within the matrix; hence electron can tunnel from one filler to another, and, in doing so, it overcomes the high resistance offered by insulating polymer matrix.

Consider the model of composite material with carbon nanocluster inclusions of CNT and GNR types (see Fig. 10.14).

The host material is a flexible dielectric medium of epoxy resin type with high resistance [5]. However, a low concentration of nanocarbon inclusions cannot change the mechanical properties of the host material. At the same time, high

**Fig. 10.14** Model of composite polymer material with carbon nanocluster inclusions of GNR and CNT types



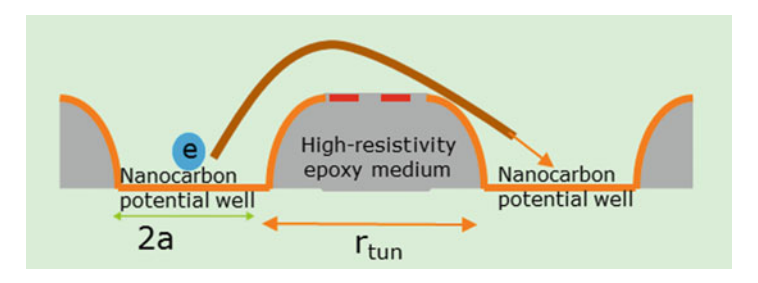


Fig. 10.15 Potential wells model for hopping in polymer nanocomposites, where 2a is the characteristic size of nanocarbon inclusion and  $r_{\text{tun}}$  is the length of the tunnel 'jump' of the electron

electrical conductivity of CNTs and GNRs incorporated in the host material can significantly affect the total conductivity of the nanocomposite material. According to our model, the mechanism of these changes is related to the effects of percolation through the hopping conductivity (see Fig. 10.15). This is the only mechanism that takes into account the compliance with our analysis-induced morphological changes in the whole nanocomposite matrix. This is a single mechanism which takes into account accordance with our analysis-induced morphological changes in the whole nanocomposite matrix.

Thus, the model of nanocomposite materials based on carbon nanocluster suspension (CNTs and GNRs) in dielectric polymer environments (e.g. epoxy resins) is considered as a disordered system of fragments of nanocarbon inclusions with different morphology (chirality and geometry) in relation to a high electrical conductivity in a continuous dielectric environment. Presumably, the electrical conductivity of a nanocomposite material will depend on the concentration of nanocarbon inclusions (in fact, carbon macromolecules). Isolated nanocarbon inclusions will provide conductivity due to the hopping conductivity mechanism

through dangling bonds up to the percolation threshold, when at high concentrations (some mass %) a sustainable ballistic regime appears, which is characteristic of pure carbon systems. The hopping mechanism is regulated by the electron hopping between 'nanocarbon macromolecules' (see Eq. (10.2) and [3, 28, 30]:

$$\sigma = A\sigma_0 \exp\left(-\frac{4}{3} \left(\frac{4\alpha r_{\text{tun}}}{a}\right)^{3/4} \left(\frac{W_0}{\kappa T}\right)^{1/4},\tag{10.6}$$

where  $r_{\rm tun}$  is the length of the tunnel 'jump' of the electron equal to the distance between 'nanocarbon' clusters and  $\sigma_0$  is the pre-exponential normalization factor, which means the conductivity of monolithic dielectric medium. This factor can be evaluated following the relationship:  $\sigma_0 = \frac{16e^2r_{\rm tun}^3N}{\pi\hbar a_0}$ , where N is the concentration of localization centres, in our case, nanocarbon inclusions concentration. For arbitrary distribution of localization centres,  $r_{\rm tun}^3N=0.24$  [33].

Added to this is the effect of intrinsic nanocarbon cluster conductivity, which is dependent on its morphology. The electric conductivity will also depend on the spatial orientation of nanocarbon inclusions. It will be greater for the longitudinal electric field orientations and lower for the transverse ones. Of course, any spatial orientations are technologically possible. If we introduce the volume part as an indicator of the nanocarbon inclusions concentration,  $\eta = \left(\frac{R_0}{R_0 + r_{\text{turn}}}\right)^3$ , where  $R_0$  is the average nanocarbon macromolecule radius and  $r_{\text{turn}}$  is the statistically averaged width of the potential barrier between the nearest nanoclusters, which is responsible for the percolation ability of the model nanocomposite. We should also diminish the hopping phenomena and percolation probability taking into account the nanocarbon macromolecule orientation within a hypothetical sphere embedded into high resistance dielectric medium. Based on this definition, we can obtain a contribution of potential nanocarbon clusters to nanocomposite conductivity as follows (see also Fig. 10.16):

$$\ln\left(\frac{\sigma}{\sigma_0}\right) = -\frac{4}{3} \left(\frac{4\alpha}{3} R_0 \left(\eta^{-1/3} - 1\right)\right)^{3/4} \left(\frac{W_0}{\kappa T}\right)^{1/4}.$$
 (10.7)

The overall conductance of nanocomposite material is evaluated using equivalent electric scheme (see Fig. 10.17 and [5]):

$$\Sigma \approx \Sigma_D + \Sigma_{NC}, \ \Sigma_{NC} = \sum_{i=1}^{N} (R_i)^{-1},$$

$$R_i = A \sum_{k=1}^{N_i} \left( \sigma_{\text{nano},ik}^{-1} + \sum_{k=0}^{N_i} \left( N_{\text{eff},ik\sigma} \sigma_{\text{jump},ik} \right)^{-1} \right), \tag{10.8}$$

where N is the number of conductivity channels,  $N_i$  is the number of nanocarbon clusters in the conductivity channel,  $N_{\text{eff}}$  is the number of effective tunnelling bonds

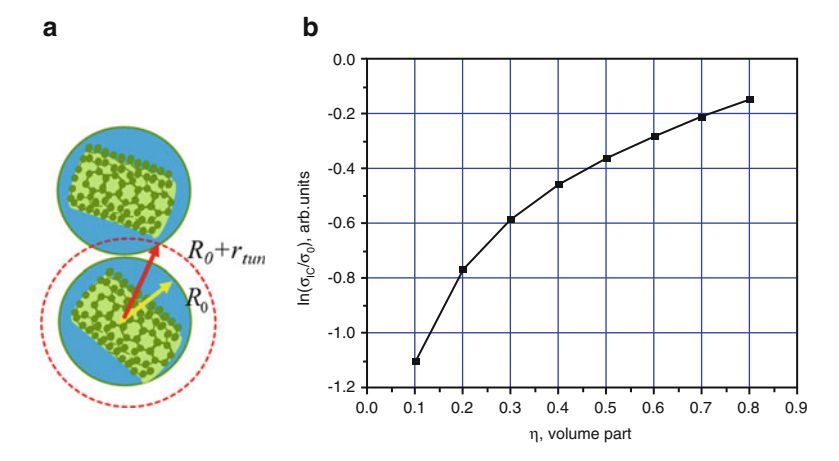
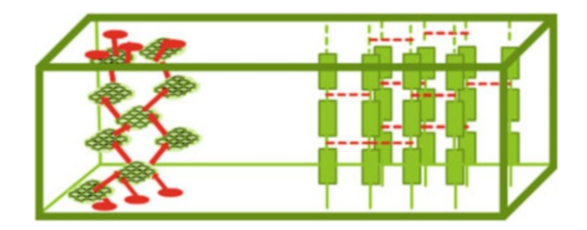


Fig. 10.16 Typical statistically averaged morphology of CNT-polymer nanocomposite: (a) structural model and (b) the hopping conductivity correlation via the average nanocarbon macromolecules volume part within continuous dielectric medium

Fig. 10.17 Principle equivalent scheme of nanocomposite model for resistance calculation



including the contact region,  $\Sigma_D = (R_D)^{-1}$  is the conductance of dielectric medium,  $\sigma_{\rm nano}$  is the conductivity nanocluster and  $\sigma_{\rm jump}$  is the hopping conductivity of the effective bond, which creates interconnect for large nanocarbon inclusion concentrations.

Basic nanocomposite models for simulation are presented in Fig. 10.18.

#### 10.3.3 Simulation of Stress- and Temperature-Induced Resistance of Carbon-Based Nanocomposite Sensors: Results and Discussions

The basic dimensions of nanocarbon clusters (CNTs and GNRs) are as follows: the diameter of the CNT, 5 nm; the height, 10 nm, and the width of the expanded CNT, i.e. the width of the GNR  $=\pi \cdot 5 \approx 15,6$  nm. The total height of model sensor is accepted as 100 nm.

The average statistical distance between nanocarbon clusters is 5 nm. This is the key distance for the mechanism of hopping conductivity. Nanocarbon cluster is

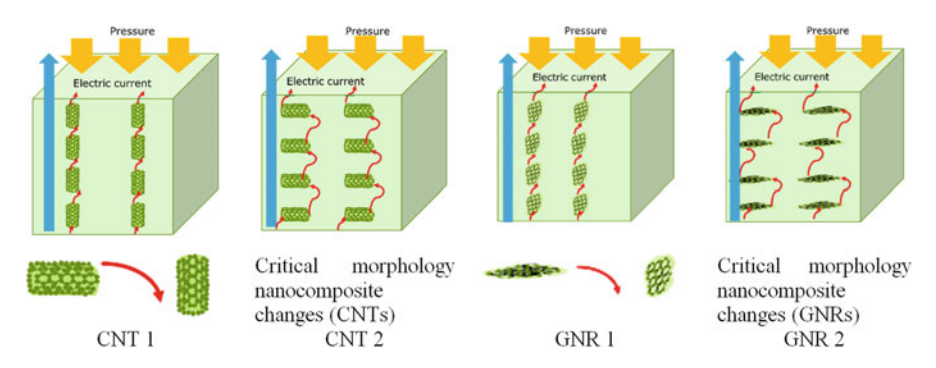


**Fig. 10.18** Models of nanocarbon-based functionalized polymer nanocomposites: CNT configuration 1, CNT configuration 2, GNR configuration 1, GNR configuration 2, — electric field direction

considered as a potential well with a typical size 2a. Neighbouring potential wells are separated by a distance  $r_{\text{tun}}$ . These two parameters ultimately determine the morphology of the nanocomposite material. For modelling it is also necessary to recalculate a microscopical parameter of relative jumping length to macroscopic strain parameter  $\varepsilon = \Delta L/L$  in Hooke's law  $\sigma = E\varepsilon$ , where L is the total sample length. In cases of longitudinal orientation of CNTs (configuration CNT 1), the recalculation looks as:

$$\varepsilon = \frac{\Delta L}{L} \approx \frac{\Delta r}{r} \cdot \frac{1}{1 + \frac{1}{1 + (1/n)} \cdot \frac{l}{r}},$$

where l is the CNT length (close to 2a) and n is the number of CNT inclusions along the line (current direction). For transversal CNT orientations (configuration CNT 2), the similar recalculation looks as:

$$\varepsilon = \frac{\Delta L}{L} \approx \frac{\Delta r}{r} \cdot \frac{1}{1 + \frac{1}{1 + (1/n)} \cdot \frac{d}{r}},$$

where *d* is the diameter of the CNT. The proposed model of hopping conductivity for current percolation in carbon-based epoxy resin nanocomposite takes into account basically the percolations along the nanocluster sets which are located along the stress direction. Interactions between the neighbouring sets are not considered for a low general concentration of nanocarbon inclusions.

In cases of longitudinal orientation of GNRs (configuration GNR 1), the recalculation looks as:

$$\varepsilon = \frac{\Delta L}{L} \approx \frac{\Delta r}{r} \cdot \frac{1}{1 + \frac{1}{1 + (1/n)} \cdot \frac{h}{r}},$$

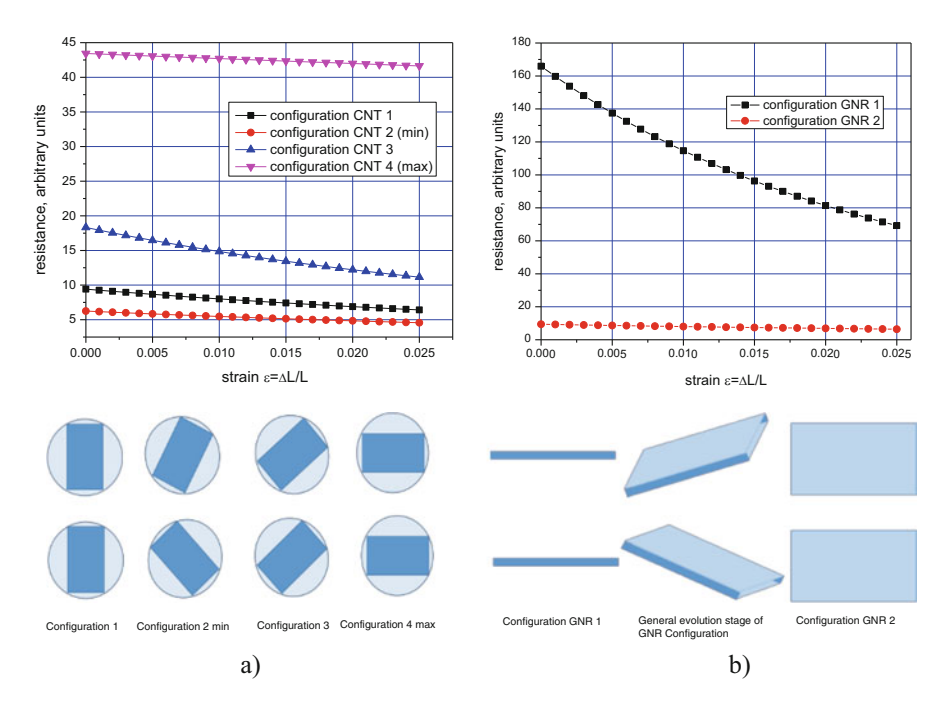


Fig. 10.19 Simulation of nanocarbon composites resistances via strain: (a) CNT configurations and (b) GNR configurations

where h is the GNR height (close to 2a) and n is the number of GNR inclusions along the line (current direction).

For transversal GNR s orientations (configuration GNR 2), the similar recalculation looks as:

$$\varepsilon = \frac{\Delta L}{L} \approx \frac{\Delta r}{r},$$

where d is the diameter of the GNR.

Figure 10.19 demonstrates resistance correlations via static stresses for ideal morphologies of a nanocomposite when CNTs and GNRs are oriented pure longitudinally, pure transversely. Configurations CNT 2(min) and CNT 4(max) correspond to the minimal and maximal tunnelling (jumping) distances due to the angle deviation of CNTs relatively longitudinal orientation.

From the technological point of view, it is not so simple to provide such ideal orientations for host polymer materials similar to epoxy resins. The first problem of the nanocomposite morphology is the selection of CNTs and GNRs with identical parameters. The second problem is the polymer–nanocarbon mixture creation when we evidently should expect a homogenous random distribution of nanocarbon orientations. Figure 10.20 demonstrates the marginal rotational disordering of CNTs inclusions from 'ideal' longitudinal orientation. Deviations of orientations

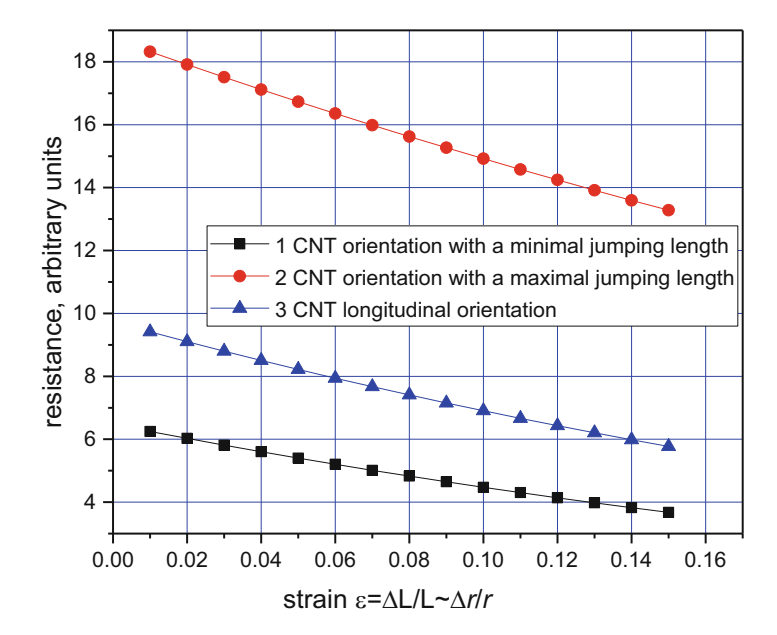


Fig. 10.20 Simulation of nanocarbon composites resistances via strain for rotational deviations of CNT inclusions

give the characteristic intercluster distances of 3.82 nm (see Fig. 10.19a, Configurations 2,3) and 7.02 nm (see Fig. 10.19a, Configurations 4) taking into account basic 5 nm in the ideal case.

Figures 10.19 and 10.20 present the full-scale simulation of CNT orientation deviations within a host material. The results show various sensitivity of the model nanocomposite as a potential pressure nanosensor in dependence of its morphology. Configurations of the fourth type (see Fig. 10.18) are more sensitive and, evidently, more practically preferable.

The model uses morphologically compatible carbon nanoconfigurations with the same number of carbon atoms, the same surface area of model CNTs and GNRs, and the same chirality. In this way, the model CNTs and GNRs are interconnected by a simple topological transformation from a cylinder to a rectangular fragment.

#### 10.3.3.1 Modelling and Experimental Results

In this section, we will discuss the correlation of simulation results for pressure and temperature nanosensors with the experimental data of the particular prototype of similar devices [30, 36], where the developed technology of functionalized nanocomposite based on epoxy resin (ED-20, GOST 10587–84. epoxy-diane resins uncured, elasticity modulus E=3.05 GPa, mass density  $\rho_m=1.16-1.25$  g/cm³) with multiwalled CNT inclusions was applied. The testing of the mentioned

nanosensors with various CNTs morphologies and mass concentrations (1%, 2%, 3%) was carried out for temperatures ranging from 27 till 90 °C and the pressure ranging from 1 till 30 Bars. The pressure test was carried out on a machine Instron 5942.

When testing the pressure sensor, the load ranged from 0 to 500 N, which corresponds to the change in pressure from 0 to 30 Bars. The temperature test was carried out using a Brookfield TC-502 water bath. The sensor sample was protected with a waterproof bag and placed in a water bath. The typical dependence of the sensor resistance on the pressure changes, as compared with the simulation results, is shown in Fig. 10.21a. Small deviations are connected with technological problems in the reproduction of perfect morphology, which reduces the percolation limit of the nanocomposite.

The typical dependence of the temperature sensor in the temperature range of 27–90 °C compared with the simulation results is shown in Fig. 10.21b. The discrepancy in behaviour between the experimental and theoretical dependencies is associated with morphological imperfections of the real sensor induced the orientation dispersion of CNTs. This effect can diminish the hopping mechanism efficiency, especially, for the higher temperatures.

Modelling of resistivity dependence via weight fraction of CNTs is presented in Fig. 10.22, where the sharp changes of resistivity within the weight fraction interval (0.08–0.12) are observed.

Evidently, this phenomenon can be explained by the increase in the percolation processes under the growing CNT weight fraction.

#### 10.4 Concluding Remarks

Simulation of sensitivities of CNTs and GNRs to doping in FET-type devices demonstrates the efficiency of functionalization of nanocarbon elements in the process of creation FET-based nanosensors.

Our work has demonstrated that ion track-based glucose sensors can be effectively created. Furthermore, they show good sensitivity, they cover a wide range of medical applications, and they can be re-used at least ten times. This study also proves that track-based biosensors with other enzymes can be similarly developed.

The prototypes of nanocomposite pressure and temperature nanosensors have been simulated. The hopping conductivity mechanism gives the adequate description of possible nanosensor qualities. An important problem in manufacturing sensors based on CNTs and GRNs is nanocarbon inclusions orientation, which determines the electrical properties of the future nanosensors. Various nanocomposite morphologies are considered, and computer simulation results for pressure and temperature nanosensor models are presented in comparison with the experimental nanodevice prototype. A good correlation between the proposed

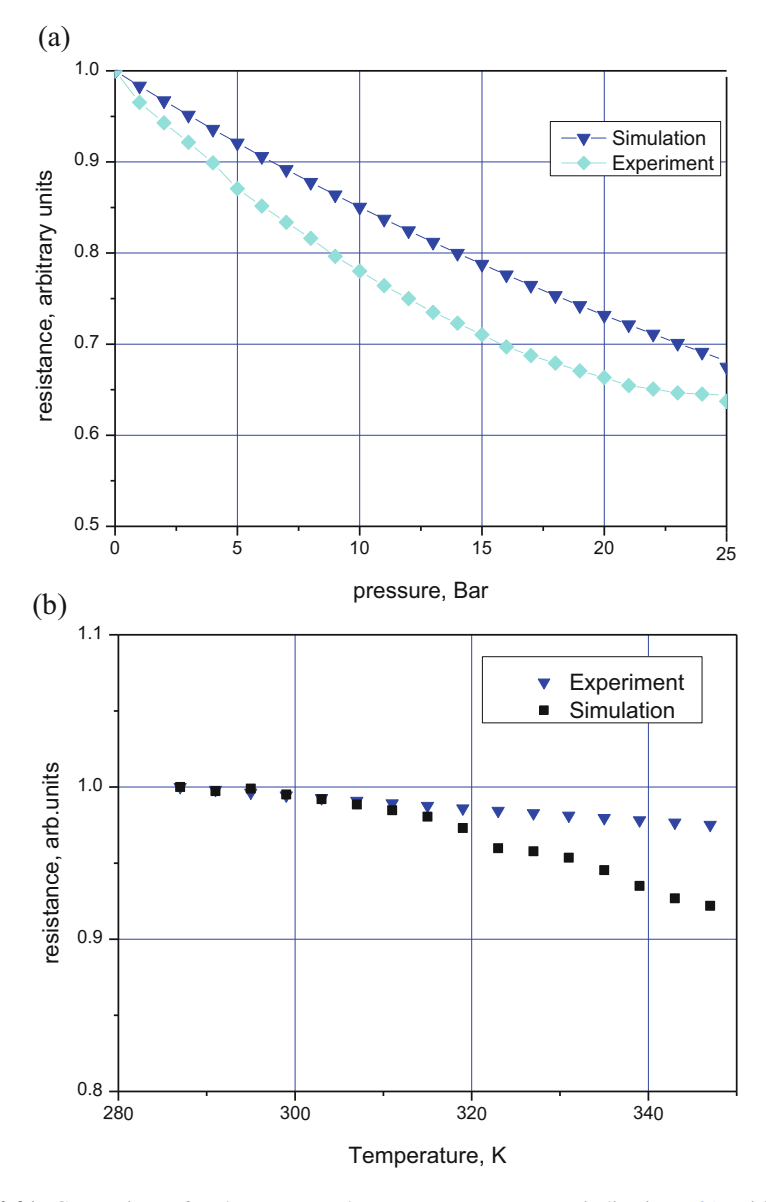
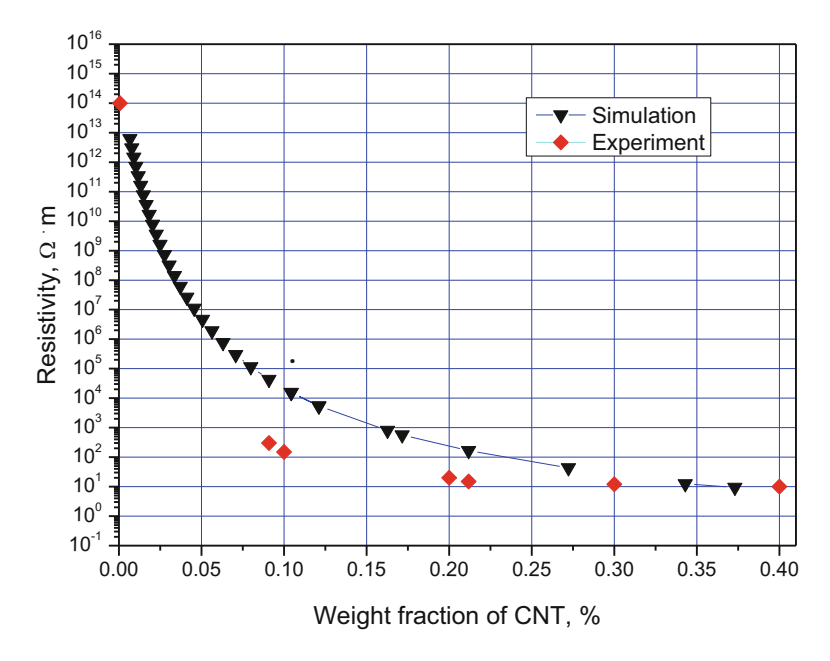


Fig. 10.21 Comparison of real pressure and temperature nanosensor indications [31] with more adequate models morphologies simulation: (a) pressure nanosensor and (b) temperature nanosensor

nanocomposite-based sensor model and the experimental one was shown. The developed mathematical model can be applied to polymer nanocomposites with inclusions of different types. Various morphologies of resistive network models can be realized for evaluation of the total resistance in different nanosensor prototypes.

References 333



**Fig. 10.22** Comparison of resistivity of developed model CNT-based nanocomposite via weight fraction of CNT with the experimental data [32]

#### References

- Shunin Yu, Kiv A (Eds) 2012 Nanodevices and Nanomaterials for Ecological Security. Series: NATO Science for Peace Series B – Physics and Biophysics (Heidelberg: Springer Verlag) 363 p.
- 2. Shunin Yu N, Zhukovskii Yu F, Gopeyenko V I, Burlutskaya N Yu, Bellucci S 2012 Properties of CNT- and GNR-Metal Interconnects for Development of New Nanosensor Systems In: Nanodevices and Nanomaterials for Ecological Security. Series NATO Science for Peace Series B Physics and Biophysics Eds Shunin Yu, Kiv A (Heidelberg: Springer Verlag) 237–62
- Shunin Y, Bellucci S, Zhukovskii Y, Lobanova-Shunina T, Burlutskaya N, Gopeyenko V 2015
   Modelling and simulation of CNTs- and GNRs-based nanocomposites for nanosensor devices
   Computer Modelling and New Technologies 19(5) 14–20
- 4. Shunin Yu N, Gopeyenko V I, Burlutskaya N, Lobanova-Shunina T, Bellucci S 2013 Electromagnetic properties of CNTs and GNRs based nanostructures for nanosensor systems In: Proc. Int.. Conf. "Physics, Chemistry and Application of Nanostructures-Nanomeeting-2013, Minsk, Belarus Eds. Borisenko V E, Gaponenko S V, Gurin V S, Kam C H (New-Jersey, London, Singapore: World Scientific) 250–3
- Shunin Yu, Bellucci S, Zhukovskii Yu, Gopeyenko V, Burlutskaya N, Lobanova-Shunina T 2015 Nanocarbon electromagnetics in CNT-, GNR- and aerogel-based nanodevices: models and simulations Computer Modelling and New Technologies 19(1A) 35–42
- 6. D'yachkov P N, Kutlubaev D Z, Makaev D V 2010 Linear augmented cylindrical wave Green's function method for electronic structure of nanotubes with substitutional impurities Phys. Rev. B: Condens. Matter Mater. Phys. 82 035426-1-15

- 7. Ao Zh, Yang J, Li S **2011** Applications of Al Modified Graphene on Gas Sensors and Hydrogen Storage In: *Physics and Applications of Graphene-Theory* Ed Mikhailov S (InTech: Rijeka-Shanghai) 534 p
- Huang P Y, Ruiz-Vargas C S, van der Zande A M, Whitney W S, Levendorf M P, Kevek J W, Garg S, Alden J S, Hustedt C J, Zhu Y, Park J, McEuen P L, Muller D A 2011 Grains and grain boundaries in single-layer graphene atomic patchwork quilts *Nature* (London) 469 389–92
- 9. Lahiri J, Lin Y, Bozkurt P, Oleynik I L, Batzill M **2010** An extended defect in graphene as a metallic wire *Nature Nanotechnology* **5** 326–9
- Brito W H, Kagimura R, Miwa R H 2012 B and N doping in graphene ruled by grain boundary defects Phys. Rev. B 85 035404-1-6
- 11. Fink D, Klinkovich I, Bukelman O, Marks R S, Kiv A, Fuks D, Fahrner W R, Alfonta L 2009 Glucose determination using a re-usable enzyme-modified ion track membrane sensor *Biosensors and Bioelectronics* 24 2702–6
- Fink D, Kiv A, Shunin Y, Mykytenko N, Lobanova-Shunina T, Mansharipova A, Koycheva T, Muhamediyev R, Gopeyenko V, Burlutskaya N, Zhukovskii Y, Bellucci S 2015 The nature of oscillations of ion currents in the ion track electronics Computer Modelling and New Technologies 19(6) 7–13
- 13. Fink D, Gerardo Mun~oz H, Alfonta L, Mandabi Y, Dias J F, de Souza C T, Bacakova L E, Vacı'k J, Hnatowicz V, Kiv A E, Fuks D, Papaleo R M 2012 Status and Perspectives of Ion Track Electronics for Advanced Biosensing In: Nanodevices and Nanomaterials for Ecological Security. Series: NATO Science for Peace Series B Physics and Biophysics Eds. Shunin Yu and Kiv A (Springer Verlag: Heidelberg) 269–79
- 14. Shunin Yu, Alfonta L, Fink D, Kiv A, Mansharipova A, Muhamediyev R, Zhukovskii Yu, Lobanova-Shunina T, Burlutskaya N, Gopeyenko V, Bellucci S 2016 Modelling and simulation of electric response of nanocarbon nanocomposites and nanoporous polymer based structures for nanosensor devices In: Theses of the 14th Int. scientific conference Information Technologies and Management 2016 April 14–15, 2016 ISMA University Riga Latvia 2016 11–4 http://isma.lv/FILES/SCIENCE/IT&M2016\_THESES/NN/01\_IT&M2016\_Shunin.pdf
- Shunin, Yu, Fink D, Kiv A, Alfonta L, Mansharipova A, Muhamediyev R, Zhukovskii Yu, Lobanova-Shunina T, Burlutskaya N, Gopeyenko V, Bellucci S 2016 Theory and modelling of physical and bio-nanosensor systems In: *Proceedings of the 5th Int Workshop Nanocarbon Photonics and Optoelectronics*. 1–6 August 2016, Holiday Club Saimaa, Lappeeranta, Finland 2016 101 http://www.npo.fi/documents/409792/994899/Yury\_Shunin.pdf/08431866-6f2c-4624-a4c9-9614dea5f747
- Fink D, Cruz S A, H Garcia A, G Muñoz H., Kiv A, Alfonta L, Vacik J, Hnatowicz V, Shunin Yu, Bondaruk Yu, Mansharipova A T, Mukhamedyev R I 2017 Improving the design of ion track-based biosensors NATO ADVANCED RESEARCH WORKSHOP, 14–17 AUGUST 2017, KIEV, UKRAINE DETECTION OF CBRN-NANOSTRUCTURED MATERIALS (DCBRN-2017)
- 17. Shunin Yu N, Schwartz K K 1997 Correlation between electronic structure and atomic configurations in disordered solids In: Computer Modelling of Electronic and Atomic Processes in Solids Eds Tennyson R C and Kiv A E (Dordrecht/Boston/London: Kluwer Acad. Publisher) 241–57
- Shunin Yu N, Shvarts K K 1986 Calculation of the electronic structure in disordered semiconductors *Physica Status Solidi (b)* 135(1) 15–36
- Shunin Yu N, Zhukovskii Yu F, Gopeyenko V I, Burlutskaya N, Lobanova-Shunina T, Bellucci S 2012 Simulation of electromagnetic properties in carbon nanotubes and graphene-based nanostructures. J Nanophotonics 6 061706-1-16
- Shunin Yu N, Zhukovskii Yu F, Gopejenko V I, Burlutskaya N, Bellucci S 2011 Ab initio simulations on electric properties for junctions between carbon nanotubes and metal electrodes *Nanosci. Nanotech. Lett.* 3(6), 816–25, https://doi.org/10.1166/nnl.2011.1249

References 335

Shunin Yu N, Zhukovskii Yu F, Burlutskaya N, Bellucci S 2011 Resistance simulations for junctions of SW and MW carbon nanotubes with various metal substrates *Central Eur. J. Phys.* 9(2) 519–29 https://doi.org/10.2478/s11534-010-0086-9

- 22. Landau L D 1957 The theory of a Fermi liquid Soviet Physics JETP 3(6), 920–5; Exp. Theoret. Phys. (U.S.S.R.) 1956 30 1058–64
- 23. Gurzhi R P, Shevchenko S I **1968** Hydrodynamic mechanism of electric conductivity of metals in a magnetic field *Soviet Physics JETP* **27**(6) 1019–22
- 24. Mendoza M, Herrmann H J, Succi S **2013** Hydrodynamic model for conductivity in graphene *Scientific Reports* **3** 1052 1–6 doi: https://doi.org/10.1038/.srep01052
- 25. Drude P **1900** Zur Elektronentheorie der metalle *Annalen der Physik* **306**(3) 566 Bibcode:1900AnP 306..566 D. doi:https://doi.org/10.1002/andp.19003060312
- Drude P 1900 Zür Elektronentheorie der Metalle; II. Teil. Galvanomagnetische und thermomagnetische Effekte Annalen der Physik 308(11) 369 Bibcode:1900AnP...308..369D. doi:https://doi.org/10.1002/andp.19003081102
- Landauer R 1957 Spatial Variation of Currents and Fields Due to Localized Scatterers in Metallic Conduction IBM Journal of Research and Development 1 223–31
- 28. Mott N F 1968 Metal-Insulator Transition Rev. Mod. Phys. 40 677-83
- Seager C H, Pike G E 1974 Percolation and conductivity: A computer study. II. Phys. Rev. B 10 1435–46
- Shunin, Yu N, Gopeyenko V I, Burlutskaya N Yu, Lobanova-Shunina T D, Bellucci S 2015
   Electromechanical properties of carbon-based nanocomposites for pressure and temperature
   nanosensors EuroNanoForum 2015, 1–12 June 2015 http://euronanoforum2015.eu/wp-con
   tent/uploads/2015/03/Abstract\_Shunin.pdf
- Abdrakhimov R R, Sapozhnikov S B, Sinitsin V V 2013 Pressure and temperature sensors basis of ordered structures of carbon nanotubes in an epoxy resin *Bulletin of the South Ural State University Series "Computer Technologies, Automatic Control, Radio Electronics* 13 (4) 16–23
- 32. Zhou Y X, Wu P X, Cheng Z Y, Ingram J, Jeelani S **2008** Improvement in electrical, thermal and mechanical properties of epoxy by filling carbon nanotube *EXPRESS Polymer Letters* **2** (1) 40–8 http://www.expresspolymlett.com/articles/EPL-0000490\_article.pdf
- Shklovski B I, Efros A L 1979 Electronic properties of doped semiconductor (Moscow: Nauka) ) (in Russian); Shklovski B I, Efros A L 1984 Electronic properties of doped semiconductors (Heidelberg: Springer)
- 34. Kubo R 1957 Statistical mechanical theory of irreversible processes. I. General theory and simple applications to magnetic and conduction problems *J. Phys. Soc. Jpn.* 12 570–86
- 35. Wang J 2008 Electrochemical Glucose Biosensors Chem. Rev. 108 814-25
- Bellucci S, Shunin Yu, Gopeyenko V, Lobanova-Shunina T, Burlutskaya N, Zhukovskii Yu
   2017 Real time polymer nanocomposites-based physical nanosensors: theory and modelling Nanotechnology 28 355502 (9p)

# Chapter 11 Nanotechnology Application Challenges: Nanomanagement, Nanorisks and Consumer Rehaviour

# 11.1 Consumer Insights into Nanotechnology: Introduction to Rational Consumerism and Consumer Behaviour

The map of the globe does not show a place called Techno Union, yet in many ways we are already its citizens and consumers. And, as consumers, our lives and behaviours are strongly influenced and shaped by an ever-increasing system of modern technology, transcending national boundaries to create a vast technological synergy grounded in complex applications in industrial production, logistics, electronic communications, agribusiness, medicine and science. We begin to realize, whether we like it or not, that we have become a part of technoculture.

The term 'consumption' is usually defined as 'the using up of goods and services' to satisfy man's needs. In neoclassical economics, an individual tends to gain more than he can personally consume. The economic theory deals with the behaviour of the 'economic human' and his relationships with the environment.

The rational choice theory [1] presents individuals as rational beings acting to realize their interests, having all available information, taking account of probabilities of events and potential costs and benefits in determining preferences and acting consistently in choosing the self-determined best choice of action and the reasoning required to make objective decisions in order to maximize their personal gain. The concept of rationality used in the rational choice theory is different from the colloquial and most philosophical use of the word.

Colloquially, 'rational' behaviour typically means 'well-thought', 'sensible', 'predictable' or in a 'clear-headed manner'. Rational choice theory uses a narrower definition of rationality: behaviour is considered rational if it is goal-oriented, evaluative/reflective, well informed and consistent (across time and different choice situations), which is in contrast with impulsive, uninformed, non-evaluative and random behaviour. In reality, the latest studies in behavioural economics demonstrate that man does *not* behave rationally.

Professor Dan Ariely, an international expert in behavioural economics, describes in his book, *Predictably Irrational: The Hidden Forces That Shape Our Decisions*, many incidents of such irrational behaviour. One example deals with a person who was willing to make a 15-minute drive to save seven dollars on a pen that cost \$25, but would not drive 15 min to save the same seven dollars for a \$455 suit [2].

Our ambitions have grown alongside with technological and industrial achievements. Over time, people have adopted the 'culture of consumption', otherwise known as 'consumerism'. This implies acquisition of goods and services *not* for satisfying fundamental needs but for obtaining social status. Thus, the product has become a symbol of one's social status, and the product itself and its worthiness have very little value. Buying the product may well bring more pleasure to the buyer than its actual use.

In the modern, technologically saturated consumer society, happiness has become a function of an individual's level of consumption, while consumption itself has become the essence of our lives. Barbara Kruger, an American conceptual artist, memorialized the consumer society with her piece in the Museum of Modern Art – a paper shopping bag with the words 'I shop, therefore I am' – paraphrasing Descartes' famous words describing the essence of man: 'I think, therefore I am'. Man has become an avid consumer with a new pastime – shopping. With the advent of new technologies constantly penetrating all spheres of our life, excessive consumption has become a culture in the modern society – as a 'vending machine' – and its primary characteristic.

In our high-tech time, even the human body is sometimes metaphorically referred to as a machine. We 'fill our tanks' while eating to 'oil our bearings' and to 'keep our motors running'. Our hearts beat like 'clockwork'. A complex problem sets our 'gears turning'. Can we view ourselves as a machine with replaceable 'parts'? Today the answer will sooner be 'not'. However, the future might be promising. Human is not a simple machine but an amazingly complex system that is perfectly ordered. Looking at ourselves from the systemic point of view, we can classify our human system as open, developing, non-regular and dissipative. It means that the system can exist physically, mentally and spiritually only provided there is a continuous exchange of substance, energy and information with the external environment (nutrition, breathing, heat exchange, excretion, reproduction, cognition, production of utilitarian and spiritual values, communication, etc.). However, according to the conventional medical wisdom, too much external loads result in illnesses and ageing of the human system. In other words, loads reduce the degree of ordering, causing unstable reactions or disrupting the normal periodic rhythms of the processes in the body. Hence, there is a need of awareness in everything that we consume – what we eat, what we dress, what we breathe and what we do for the environment we live in.

The industrialized world has developed into a production and consumption global community with a highly advanced level of technologies. Technological advancements have led to markedly increased demands for a standard of living and consumption. However, the current economic crisis has provoked a growing

consensus that the twenty-first-century consumer society is on a path that cannot promise its citizens a hope for sustainable future. The prevailing forms of political economy are failing to guarantee the consumers economic stability, preserve ecological resources and services, reduce social inequality, maintain cultural diversity and protect physical and mental health of citizens. We face related crises of political, social, cultural, educational and personal sustainability.

Moreover, current developments in scientific and technological research raise a number of ethical questions comprising responsibility. Areas of research as nanotechnology and biotechnology, regarding food, healthcare and environmental issues, elicit complex and undeniable debates within society today. Sometimes, scientific—technological research and investments in different areas do not advocate a common good as their overall aim but serve the interests of those who finance the research itself while forcing those who use these products into commercial traps, often without enough research and information regarding the effects they may have on consumers' health.

Striking developments of new technologies, particularly nanotechnologies, are finding applications in all spheres of life and producing rapid, systemic and far-reaching effects in the business, government, society and environment, along-side with the challenges they pose to the society. Furthermore, rapid technological changes are forcing organizations to embrace new technologies and change the way they work and interface with suppliers and consumers, thus leading to changes in many behaviour patterns based on the great expectations for nanotechnologies promising tremendous benefits in the future.

Unfortunately, there is no one-way-fit-all strategy to guarantee a brighter tomorrow for everyone. Nor can the separate efforts of businesses, governments, organizations and individuals cope with the tasks imposed by advanced technologies without complementary contributions of others. Yet everyone can benefit from the insights of reasonable research into the nature of change in rational consumption stipulated by the advent of nanotechnologies and innovations.

# 11.2 Nanoscience and Nanotechnology: What Is Special About 'Nano' and Why Should Consumers Be Informed?

Consciously or unconsciously, the term 'nanotechnology' is firmly entering the life of every consumer-citizen of the global community. It designates both relatively simple nanomaterials and goods such as plastic bags and containers and very complex technologies that are supposed to change radically the future of humanity such as prosthetic implants that look, feel, move, have a sense of touch like real ones and are controlled by the brain. However, the general public often lacks awareness and understanding of the basic properties and sometimes even the existence of nanotechnologies and their implications linked to the consumption of

nanoproducts. Moreover, a generally sceptical attitude within the society prevails towards new technologies.

The general lack of public knowledge about nanoproducts that are already on the market in full swing is likely to bring irrational and erroneous, potentially harmful results. Therefore, modern technology requires educated workforce and responsible consumers and hence imperative for educated population. Education should begin with a clear understanding of what nanotechnology is.

Nanotechnology is not really anything absolutely new. In one sense, it is the natural continuation of the miniaturization revolution that we have witnessed over the last decades, where millionth of a metre  $(10^{-6} \text{ m})$  admittance in engineered products has become commonplace. A good example of the application of nanotechnology is a mobile phone, which has changed dramatically in a few years – becoming smaller and smaller, while paradoxically growing cleverer and faster and cheaper! The same is true about the computer industry and many clever gadgets we use today that have *nano* features – such as cameras, flash memory, computer processor chips, car airbag pressure sensors, inkjet printers and many others, simplifying many things in our life.

What is new about nanotechnologies, though, is the multidisciplinary approach, the convergence of various sciences and technologies making it possible not just to 'see' these tiny entities – atoms and molecules – but also to manage them. Although scientists have manipulated matter at the nanoscale for centuries, calling it physics or chemistry, it was not until a new generation of microscopes were invented in IBM, Switzerland, in the late 1980s that the world of atoms and molecules could be visualized and managed. Now biologists can discuss steric effects of cell membranes with chemists, while physicists provide the tools to watch the interaction in vivo – infrared microscopes to study molecules and X-ray microscopes to study atomic structures and even to handle single atoms. What is really breathtaking is the unprecedented degree of control over materials at the molecular and atomic levels. This may not capture the imagination as much as a tiny machine that precisely assembles materials atom by atom, but it is an extraordinarily interesting and useful phenomenon and is, ultimately, why nanotechnology is kicking up such a fuss.

Nanotechnology is an advanced and exciting area of scientific research and development that is truly multidisciplinary, bringing to the agenda the convergence of technical sciences (technosciences) and even humanitarian sciences (humanosciences). None of the separate disciplines would be able to study all aspects of this tiny world.

It is noteworthy that the prefix 'nano' originates from the Greek word meaning 'dwarf' and in modern science means 'a one billionth part'  $(10^{-9})$  of a metre. It seems next to impossible to draw a picture of one billionth of a metre in our imagination. To imagine it more vividly, let us take a 'metre' – the unit of length. Now let us imagine a person of medium height – about 1 m 70 cm. Reducing this size by 100 times, we will get the diameter of the iris (a round coloured part of the eye). Further reducing it by ten times, it will make the diameter of the pupil (a black movable opening in the middle of the eye through which light passes). But if once again we decrease it by 1000 times, it will turn out a micron – an extremely small

unit; our red blood cell is five times bigger. And if we divide it by 1000 times more, we will get a nanoparticle – the size of molecules and atoms. Consequently, the talk is about researches of the world at the scale of atoms and molecules, which is one billionth of a metre in size, the nanometre (or one millionth of a millimetre), which is tiny and unseen. A sheet of paper is about 100,000 nanometres thick, a single human hair is about 80,000 nm wide, a red blood cell is approximately 7000 nm wide, a DNA molecule is 2–2.5 nm, a single gold atom is about a third of a nanometre in diameter, and a water molecule is almost 0.3 nm. The important thing is that size matters!

On a nanoscale (dimensions between approximately 1 and 100 nm), the properties of materials can be very different from those in bulk matter. *Nanoscience* can be defined as 'the study of phenomena and manipulation of materials at atomic, molecular and macromolecular scales, in order to understand and exploit properties that differ significantly from those on a larger scale' [3]. The question arises — why do the properties of materials become different on a nanoscale? There are two main reasons for it.

First, nanomaterials have, relatively, a larger surface area than the same materials in bulk matter (e.g. sugar powder and sugar cubes). And, consequently, they become more chemically reactive, showing very useful physical and chemical properties (e.g. copper which is opaque at a macroscale and becomes transparent at a nanoscale). They become many times stronger than steel and, at the same time, hundreds of times lighter. They demonstrate exceptional electric conductivity and resistivity, a high capacity for storing and transmitting heat. This is confirmed by the fine-grained materials that we use in our daily lives, such as flour, which can become explosive in some circumstances. Nanomaterials can even modify their biological properties (silver that becomes bactericide at a nanoscale, nanogold kills cancer cells, nanotitanium kills influenza viruses – nanoparticles of these metals are very active).

Second, below 50 nm, the laws of classical physics give way to quantum effects, causing different optical, magnetic and electrical behaviours of nanomaterials like gold, for instance, which has different optical absorption properties [7] and demonstrates a wide range of colours depending on the size of nanogold particles (see Fig. 11.1).

These properties, however, can be difficult to control. For example, when nanoparticles touch each other, they can fuse, losing both their shape and those unusual properties – as magnetism – that scientists hope to exploit for a new generation of nano(bio)sensors and devices. Therefore, *nanotechnology* can be defined as the 'understanding, modeling, design, engineering, production and application of structures, devices and systems by controlling shape and size on a nanometer scale' [3]. Specific functionalities, therefore, can be achieved by reducing the size of the particles to 1–100 nm.

A concise definition is given by the US National Nanotechnology Initiative: 'Nanotechnology is concerned with materials and systems whose structures and components exhibit novel and significantly improved physical, chemical, and biological properties, phenomena, and processes due to their nanoscale size. The goal is to exploit these properties by gaining control of structures and devices at



Fig. 11.1 Picture of solution containing gold nanoparticles

atomic, molecular and supramolecular levels and to learn to efficiently manufacture and use these devices' [4]. This term can be applied to many areas of research and development – from medicine to manufacturing, renewable energy, transport, computing and even textiles and cosmetics.

Using nanotechnology, materials can effectively be made to be stronger, lighter, more durable, biocompatible, more reactive, more sieve-like or better electrical conductors, among many other characteristics due to the fact that it is possible to set the required essential structures of materials at the nanoscale to achieve the desired specific properties.

Most commonly discussed nanomaterials – basic building blocks – are *nanoparticles* which are below the wavelength of visible light and therefore cannot be seen, *carbon nanotubes* (single-walled and multiwalled) which are thin cylinders of atomic layers of graphite and *quantum dots* which are fluorescent nanoparticles like 'artificial atoms' made of silicon and are invisible until lit up with ultraviolet light.

Nanoparticles are not new. Nanoparticulate carbon black has been used in vehicle tyres for decades, currently at a rate of six million tons per year. Nanoparticles can be found in nature, ranging from milk products (containing nanoparticulate casein) to the burning candles or almost anything that burns and creates nanoparticulate material. We live surrounded by nanoparticles: a normal room can contain from 10,000 to 20,000 nanoparticles per cm<sup>3</sup>, in a forest 50,000 nanoparticles per cm<sup>3</sup> and 100,000 nanoparticles per cm<sup>3</sup> in city streets. The bright colours on a butterfly's wings are due to the light reflected from nanoscale layers in the structure of the wings. The red and yellow colours seen at sunset are also due to nanoparticles.

But nanoparticles behave like neither solids, liquids nor gases and exist in the topsy-turvy world of quantum physics, which governs those denizens small enough to have escaped the laws of Newtonian physics. This allows them to perform their almost magical feats of conductivity, reactivity and optical sensitivity, among others. 'That's why nanomaterials are useful and interesting and so hot right now', says Kristen Kulinowski, executive director for education and policy at the Rice University Centre for Biological and Environmental Nanotechnology (CBEN). 'Being in this quantum regime enables new properties to emerge that are not possible or not exhibited by those same chemicals when they're much

smaller or much larger. These include different colours, electronic properties, magnetic properties, mechanical properties – depending on the particle, any or all of these can be altered at the nanoscale. That's the power of nanotech' [6].

However, there is a distinction between *incidental* and *manufactured* nanoparticles [5]. Incidental nanoparticles are those which are not manufactured deliberately, but either occur in nature (as produced by forest fires and volcanoes) or as a by-product of high-temperature industrial processes (such as combustion, welding, grinding and exhaust fumes of cars, trucks and aircraft). Incidental particles are comparatively less chemically reactive and bioactive than manufactured nanoparticles. They do not have the same bioavailability as manufactured nanoparticles, and they cannot be taken up by individual cells. Still, the exposure to large levels of incidental nanoparticles in urban air pollution causes increased incidences of disease and even death [5].

Manufactured nanomaterials are those which are produced deliberately. They include nanoparticles (e.g. metal oxides such as zinc oxide (ZnO) or titanium dioxide (TiO<sub>2</sub>)), as well as structures created through nanotechnology such as nanotubes, nanowires, quantum dots, carbon fullerenes (buckyballs), etc. Pathology studies suggest that manufactured nanoparticles are taken up through the human gastrointestinal tract, translocated through the body and accumulated in organs where they can have serious long-term health effects, leading to chronic inflammation and even cancer [5].

Therefore, since the market offers nano-enhanced goods manufactured with engineered nanoparticles, the question goes beyond 'to buy or not to buy'. There is something far more fundamental at play. Consumers should have the right to know what is in the goods they buy – and know how they were produced. Full transparency and easy access to detailed information are key to gaining and retaining public confidence in nanotechnologies. It is not enough to just say to someone they should buy organic or natural if they seek such a guarantee – not everyone can afford to do so. The consumer right to information about nanoproducts must revoke debate about pros and cons of these. If some people wish (as some really do) to avoid nanogoods – for whatever reason – they should have the information at hand on the labelling to allow them to do so. Benjamin Franklin was absolutely right saying that sometimes things are difficult to see, but it is even more difficult to foresee things and to predict what impact they might have on us. Invisible nanoparticles quite meet these words.

## 11.3 Basic Categories of Nanotechnology-Based Consumer Products on the Market and Consumer Awareness

Advancements in the fields of nanoscience and nanotechnology have resulted in thousands of consumer products that have already migrated from laboratory benches onto store shelves and e-commerce websites. While much of nanotechnology's potential has yet to be realized, and research is still ongoing on its effects to the environment and human health, products that incorporate nanotechnology have already flooded the market, and after more than 25 years of basic and applied research, they are gaining in commercial use. The estimation for a nanoproduct value of \$1 trillion in 2015, about \$800 billion of which was in the USA, appears to hold true [31]. The market is doubling every 3 years as a result of successive introduction of new consumer products incorporating engineered nanoparticles, but very few of general public realize that the foods we eat, the clothes we wear, the medicines we take, the cosmetics we use and many other consumer products are manufactured with the use of nanotechnologies. Only a small number of consumers or business executives realize the extent to which nanotechnology is going to change the products they use every day.

Owing to their unique properties, nanomaterials are increasingly used in commercial applications in a variety of fields including optics, electronics, magnetics, mechanics, catalysis, energy science, agri-food sector, nanobiotechnology and nanomedicine. Nanomaterials are used to manufacture lightweight, strong functional details, parts and systems for applications in marine and aerospace equipment and automotive parts. They are also widely used in foods – diet milkshakes, cooking oil, tea and beverages, soft drinks, dairy products, food additives in processed meats and cheeses – as well as in electric home appliances, antibacterial kitchenware, touchscreens (iPhone), computer memory, clothing, coatings, wound dressings, dental fillers, toothpastes and toothbrushes, sporting goods and equipment, cosmetics and many other applications and processes. Because of the high demand, more than a trillion dollars' worth of nanotechnology-based products is expected on the market in the near future [9].

There already exist over 1800+ everyday commercial products that rely on nanoscale materials and processes [8]. At least 400 nanofoods and agricultural products and 300–400 nanofood packagings containing nano-ingredients are now on sale internationally. However, it has been difficult to find out how many exactly 'nano' consumer products are on the market and which merchandise could be called 'nano'. To document the penetration of nanotechnology in the consumer market-place, the Woodrow Wilson International Center for Scholars and the Project on Emerging Nanotechnology created the Nanotechnology Consumer Product Inventory (CPI) in 2005, listing 54 products [9]. This first-of-its-kind inventory has become one of the most frequently cited resources showcasing the widespread applications of nanotechnology in consumer products. In 2010, the CPI listed 1012 products from 409 companies in 24 countries. Even though it did not go through substantial updates in the period between 2010 and 2013, it continued being heavily cited in government reports and the scientific literature.

The new total of 1800+ products as of March 2015 represents more than a 30-fold increase over the 54 products originally listed in 2005 – which is not a complete representation of the growth of this market. While not comprehensive, this inventory gives the public the best available look at the 1800+ manufacturer-identified nanotechnology-based accepted consumer products [10]. They are grouped under eight generally accepted consumer goods categories and subcategories:

- Appliances (heating, cooling and air conditioning; large kitchen appliances; laundry and clothing care)
- Automotive (exterior, maintenance and accessories)
- Goods for children (basics, toys and games)
- Electronics and computers (audio, cameras and film, computer hardware, display, mobile devices and communications, television, video)
- Food and beverage (cooking, food, packaging, storage, supplements)
- Health and fitness (clothing, cosmetics, filtration, personal care, sporting goods, sunscreen)
- Home and garden (cleaning, construction materials, home furnishings, luxury, paint)
- Cross-cutting (coatings)

For us, as consumers, the most important categories are food and beverages, health and fitness and home and garden. As we can see from the pie chart (Fig. 11.2), the health and fitness category includes the largest listing of products in the CPI, comprising 42% of listed products. Within the health and fitness category, personal care products (e.g. toothpastes and toothbrushes, lotions and hairstyling tools and products) comprise the largest subcategory (39% of products). The next biggest category is home and garden that accounts for 20% of the total. The food and beverage category is further subdivided as food, cooking, storage and supplements accounting for 11% of the total. The nanofood products include a canola oil, a chocolate slim shake drink and a nanosized beverage – Nanotea. The nanoproduct Slim Shake Chocolate is pitched at health-conscious consumers. The product is described as being 'low in fat and calories', 'no artificial sweeteners' and 'tastes delicious'. The promotional text advises that this chocolate drink contains 'CocoaClusters'.' - 'The natural benefits of cocoa have now been combined with modern technology to create CocoaClusters'.

These so-called nanoclusters are tiny particles, 100,000th the size of a single grain of sand, and they are designed to 'carry nutrition into your cells'. This nanofood product is available for ordering via the Internet from a US address [11].

The contribution of nanoscience research in food science and technology is extensively developing in such major sectors as food safety and biosecurity, materials science and food processing and product development. According to a definition in a recent book *Nanotechnology in Agriculture and Food*, food is considered nanofood when nanoparticles and nanotechnology techniques or tools are used during cultivation, production, processing or packaging of the food. It does not mean atomically modified food or food produced by nanomachines [12].

Nanotechnology has begun to find extensive applications in the area of functional food by engineering biological molecules with functions very different from those they have in nature, opening up a new area of research and development. Of course, there seems to be no limit to what food technologists are prepared to do to our food (Fig. 11.3).

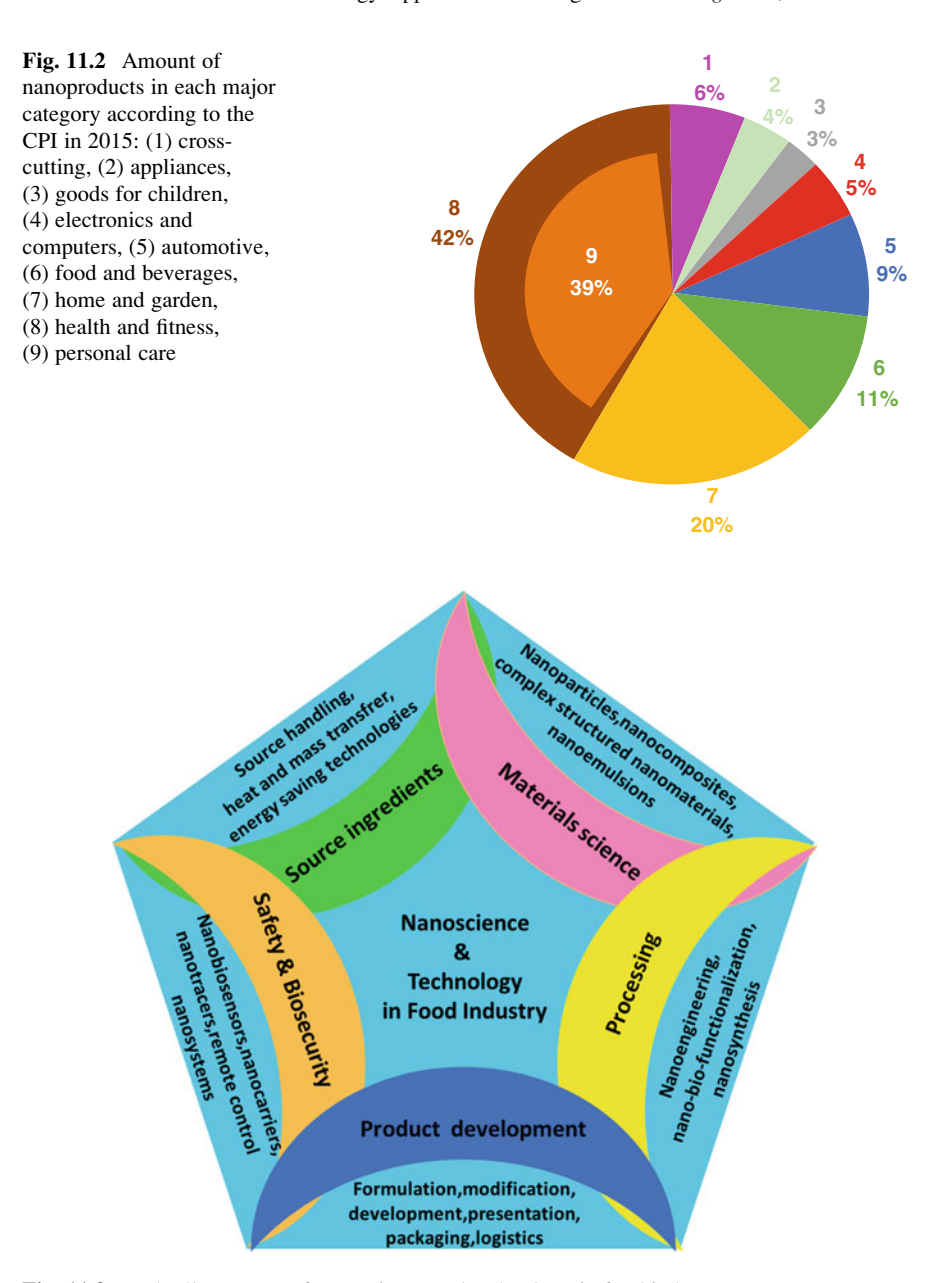


Fig. 11.3 Umbrella concept of nanoscience and technology in food industry

Nanotechnology will give them a whole new range of tools to attain new extremes in the industry, moving out of the laboratory and into every sector of food production.

The development of foods is capable of changing their colour, flavour or nutritional properties according to a person's dietary needs, allergies or taste preferences, such as soft drinks, ice cream, chocolate or chips to be marketed as 'health' foods. Packaging increases food shelf life by detecting spoilage, bacteria or the loss of food nutrient and releases antimicrobials, flavours, colours or nutritional supplements in response.

A significant portion of such products in the CPI (31% of products analysed) utilize nanomaterials – mostly silver nanoparticles but also titanium dioxide and others – to confer antimicrobial protection. Nanomaterials such as titanium dioxide and silicon dioxide are used to provide protective coatings (15%) and for environmental treatment (to protect products against environmental damage or to treat air and water in the home, 15%). Cosmetic products (12%) are advertised to contain a variety of nanomaterials such as silver nanoparticles, titanium dioxide, nanoorganics, gold and others. A wide variety of nanomaterial compositions (silver, nano-organics, calcium, gold, silicon dioxide, magnesium, ceramics, etc.) are also advertised to be used for health applications, such as dietary supplements (11%).

Dairy products, cereals, breads and beverages are now fortified with vitamins; minerals such as iron, magnesium or zinc; probiotics; bioactive peptides; antioxidants; plant sterols; and soy. Some of these active ingredients are now being added to foods as nanoparticles or particles having a few hundred nanometres in size. Nanoparticles are added intentionally to many foods for processing and preservation of beverages, meats, cheese and other foods to improve properties: for example, titanium dioxide (TiO<sub>2</sub>) is a common food whitener and brightener additive, used in confectionery, some cheeses and sauces [13, 14].

German company Aquanova has developed a nanotechnology-based carrier system (using 30 nm micelles) to nano-encapsulate active ingredients such as vitamins C and E, preservatives and enzymes like coenzyme Q10 or omega 3 and fatty acids. They market 'Nova Sol' and claim that the system increases the potency and bioavailability of active ingredients. They offer considerable advantages for meat processors, sausages and cured meat production, to speed up the production process, to stabilize colour and to 'improve' taste.

The Daewoo refrigerator claims: 'Nano silver presents strong disinfection, deodorant and storage power. It also maintains balance of hormone within our body and intercepts electromagnetic waves significantly' [11]. Nestlé and Unilever are developing a nanoemulsion-based ice cream with a lower fat content that retains a fatty texture and flavour. However, the greater potential for cellular uptake of nanomaterials, coupled with their greater chemical reactivity, could also introduce new health risks.

Most of us are familiar with the waxy coatings often used on apples. Now nanotechnology is enabling the development of nanoscale edible coatings as thin as 5 nm wide, which are invisible to the human eye. An edible coating material can be defined as a thin layer of a selected formulation, which is applied directly over food in liquid form by using different techniques, such as immersion, spraying, etc. In addition, an edible film is defined as a packaging material, which is a thin layer placed on or between food components, used as wraps or separation layers [15]. The

edibility of films and coatings is only possible when all components including biopolymers, plasticizers and other additives are food-grade ingredients, while all of the involved processes and equipment should be also acceptable for food processing. Edible nanocoatings can be used on meats, cheese, fruits and vegetables, confectionery, bakery goods and fast food. They can provide a barrier to moisture and gas exchange; act as a vehicle to deliver colours, flavours, antioxidants, enzymes and anti-browning agents; and can also increase the shelf life of manufactured foods, even after the packaging is opened [16, 17].

Storage includes plastic beer bottles, Miracle Food Storage plastic bags and containers, plastic food wrap and baby's mugs and milk bottles. There is no need to tap or shake mayonnaise or ketchup bottles now to remove the last of their contents. Several German research institutes, industry partners and the Munich University of Technology have joined forces to develop non-stick nanofood packaging. The researchers have applied thin films that measure less than 20 nm to the inside surface of food packaging. The researchers promote their product as an environmentally friendly solution to reduce leftover traces of condiments in bottles [18].

Nano-CareTM fabrics, sold in Eddie Bauer chinos and other clothing since November 2001, incorporate 'nanowhiskers' into the fabric to make it stain-resistant to water-based liquids such as coffee and wine. PPG Industries produces SunCleanTM self-cleaning glass, which harnesses the sun's energy to break down dirt and spreads water smoothly over the surface to rinse the dirt away without beading or streaking. Various sunscreens (Wild Child, Wet Dreams and Bare Zone) incorporate ZinClearTM, a transparent suspension of nanoscopic zinc oxide particles that are too small to scatter visible light as do products containing microscopic particles. Nanotechnology creates added value to these products through a variety of properties – impermeability to gas, water-repellence and transparency – that manifest only or optimally at the nanoscale.

However, there are concerns that manufactured nanomaterials are released into the environment from waste streams or during recycling. This may present a new range of serious ecological risks. Therefore, it is possible that such packaging may introduce more pollution problems than it solves [14, 18].

Of the 1800+ products listed in the CPI, 47% (846 products) advertise the composition of at least one nanomaterial component, and 62 of those products list more than one nanomaterial component (e.g. a product comprised of both silver and titanium dioxide nanomaterials) [10].

Nominally, metals and metal oxides comprise the largest nanomaterial composition group listed in 37% of products (Table 11.1). Titanium dioxide (TiO<sub>2</sub>), silicon dioxide (SiO<sub>2</sub>) and zinc oxide (ZnO) are the most produced nanomaterials worldwide.

However, silver nanoparticles (AgNPs) are the most popular advertised nanomaterial, present in 438 products (24%). Silver and titanium dioxide are the nanomaterial components most likely to be combined with other nanomaterials in consumer products, with 35 and 30 product combinations, respectively. Silver and titanium dioxide are paired with each other in 10+ products (cosmetics and electronics). Titanium dioxide and zinc oxide are paired in 10+ products

Table 11.1 Types of nanoparticles used in the food production chain

Type of nanoparticles	Application	Function
Nanosized nutrients (powders, sprays, emulsions)	Food additives/supplements/ nutraceuticals	Greater uptake, increased absorption of nutrients, better bioavailability and dispersion of nutrients
Metal nanoparticles and metal oxides (silver, gold, platinum, copper, magnesium, iron, iron oxide, zinc oxide, aluminium oxide, titanium dioxide, silicon dioxide, etc.)	Food additives/supplements, drugs, cosmetics, sunscreens	Better uptake; increase reactivity and bioavailability of vitamins and minerals, protein, antioxidants, fibre, enzymes (coenzyme Q10), prebiotics and omega 3 (DHA); ensure preservation, improve properties; and provide protective coatings
	Packaging materials/storage (plastic bags, containers, bot- tles, food wrap, baby mugs and milk bottles)	Improving quality, extending property limits and durability of contents.
	Equipment for food preparation (antibacterial utensils, cutlery, chopsticks, cookware)	Antibacterial, self-cleaning surfaces rinsing the dirt away without beading or streaking
	Fridges, storage equipment	Antibacterial coating of equipment extend storage power, disinfection, deodorant
	Sprays for healthcare	Antibacterial properties, better uptake, increase bioavailability
Colloidal metal nanoparticles	Food additives/supplements	Enhance gastrointestinal uptake, prevent caking, deliver nutrients and prevent bacterial growth
Complex nanostructures and nanodevices	Nanobiosensors/nanochips in packaging	Detection of food spoilage, detection of pathogens; iden- tity preservation and tracking
	Biodegradable nanosensors	Temperature, moisture and time monitoring/storage conditions
	Handheld equipment	Detection of contaminants
Incorporated active nanoparticles	Packaging materials, edible nanocoatings	Provide a barrier to moisture and gas exchange; deliver colours, flavours, antioxi- dants, enzymes and anti- browning agents; increase the shelf life of foods, even after the packaging is opened; pre- vent pathogen growth
Filters with nanopores	Water treatment, purification	Removal of pathogens and contaminants or catalysing/oxidation of contaminants

(continued)

Type of nanoparticles	Application	Function
	Monodisperse emulsions	Product development
Nano-encapsulated carrier systems, nanoclusters	Food additive/supplement	Targeted delivery of vitamins and minerals, preservatives and enzymes like coenzyme Q10 or omega 3 and fatty acids; increase potency, absorption and bioavailability; stabilize colour and 'improve' taste
Nanoparticle-biomolecule corona	Nanomedicine	NP-based targeted drug deliv- ery – better cellular uptake, drug release and biodistribution profiles

Table 11.1 (continued)

(sunscreens, cosmetics and paints), whereas the European Commission's Cosmetics Regulation has permitted the use of nanoscale titanium dioxide in sunscreens, but not zinc oxide [19].

Since 2012, consumer products advertising to contain metal and metal oxide nanomaterials, silicon-based nanomaterials (mostly  $SiO_2$  nanoparticles) and a variety of other nanomaterial components (organics, ceramics, polymers, clays, nanocellulose, liposomes, nano micelles, carnauba wax, etc.) have been growing in popularity. Meanwhile, carbonaceous nanomaterials have remained stable at around 50 products available on the market [10].

CPI is a resource for consumers, citizens, policymakers and others who are interested in learning about how nanotechnology is entering the marketplace. When used as food additives, drugs or cosmetics, nanomaterials are regulated under the Federal Food, Drug, and Cosmetic Act (FFDCA). In the European Union, nanomaterials are regulated under the concern of the Registration, Evaluation, Authorization and Restriction of Chemicals (REACH) and the Classification, Labelling and Packaging (CLP) regulations when those are classified by the commission as hazardous chemical substances [20].

However, the CPI reports only the numbers of different consumer products and product lines available on the market, so there is no implication on mass, volume or concentration of nanomaterials incorporated into products or the production volume of each product. Of carbonaceous nanomaterials (89 products), the majority of products listed contain carbon nanoparticles (sometimes described as carbon black, 39 products) and single- or multiwalled carbon nanotubes (CNT, 38 products). Unfortunately, 891 (49%) of the products included in the CPI do not present the composition or a detailed description of the nanomaterial used [10].

Claimed composition of nanomaterials listed in the CPI is grouped into five major categories: not advertised, metal (including metals and metal oxides), carbonaceous nanomaterials (carbon black, carbon nanotubes, fullerenes, graphene), silicon-based nanomaterials (silicon and silica) and others (organics, polymers, ceramics, etc.). Claimed elemental composition of nanomaterials listed in the

metals category includes silver, titanium, zinc, gold and other metals (magnesium, aluminium oxide, copper, platinum, iron and iron oxides, etc.). Claimed carbonaceous nanomaterials (include CNT = carbon nanotubes).

The fundamental factor driving most nanotechnology applications in foods is the promise for new or improved functionalities of materials and a possible reduction in the use of conventional chemical additives. On an equivalent weight basis, engineered nanoparticles (ENPs) have a much larger surface area due to their very small size and the ability to change their biological and chemical properties. Thus, a much smaller amount of ENPs may be needed to provide the necessary functionality to a material compared to conventional substances. For example, nanosized water-insoluble substances can ensure their uniform dispersion in aqueous compositions. This makes it possible to reduce the use of solvents in certain applications such as cosmetics, food packaging coatings and paints and allows the dispersion of food additives such as water-insoluble flavours, colours and preservatives in low-fat products.

Nanosized nutrients and supplements are also claimed to have a greater uptake, absorption and bioavailability in the body than their bulk equivalents. This fact has evoked a great commercial interest in the use of nanosized ingredients, nutraceuticals and supplements in food and healthcare applications. Moreover, consumer health has become a marketed commodity – it is everywhere – whatever we buy or consume.

Often, a failure to address even one component can decimate an entire industry. A lack of concern for food security, for example, led to enormous outbreaks of mad cow and hoof and mouth disease. What might have seemed frugal and prudent cost management at the time ended up crippling meat producers.

Safe food is a prerequisite for food security and paramount to the industry. The production, marketing and consumption of safe food are non-negotiable requirements that all partners along the food chain must adhere to, regardless of their place from farm to fork [21, 22].

One of the most promising applications of nanotechnology, known as *nanomedicine*, involves the development of nanoscale tools and devices designed to monitor health, deliver drugs, cure diseases and repair damaged tissues, all within the molecular factories of living cells and organelles (small, specialized structures in cells which operate like organs by carrying out specific tasks).

Medical applications of nanoparticles (NPs) are wide-reaching as evidenced by their rapid development as therapeutic and diagnostic agents. In particular, significant advances have been made in cancer therapy by pursuing NPs as drug delivery systems. One of the most important challenges affecting NP-based drug delivery is the formation of the 'biomolecule' or 'protein' corona [23]. As NPs enter physiological fluids, proteins and other biomolecules such as lipids adsorb to their surfaces with various exchange rates leading to the formation of the biomolecular corona. As a consequence, the 'synthetic identity' of the NP is lost, and a distinct 'biological identity' is acquired. This new identity governs how the NP is 'seen' by cells and subsequently alters the way in which NPs interact with cells. The biomolecular corona has been demonstrated to have a major impact on the biological behaviours

of nanoparticles. Nanoparticles functionalized with disease-specific targeting ligands are positioned to revolutionize the treatment of debilitating diseases such as cancer by achieving targeted and selective cellular interactions [23–25].

Notwithstanding the fact that no one has yet invented a little machine that will swim through our body and mechanically strip away plaque from our inner arterial walls, nanotechnology is poised to have an enormous impact on the diagnosis and treatment of disease. Nanotechnology has the real potential to revolutionize a wide array of medical and health applications, tools and procedures so that they are more personalized, portable, cheaper, safer and easier to apply. In order to understand better how nanotechnology could revolutionize such diverse areas, we need to review a bit of fundamental physics.

Two sets of theories relate to this question: classical mechanics, which governs the world of our immediate perception (e.g. an apple falling from a tree to hit Newton on the head), and quantum mechanics, which governs the world of atoms and molecules (e.g. electrons tunnelling through seemingly impenetrable barriers). Given enough information about the initial position of an object and the forces acting upon it, classical mechanics allows us to determine with certainty where that object was at some time in the past and where it will be at some time in the future. This is useful because it allows us, for example, to track a basketball to where it will drop from centre field – get into the basket or successfully fly past (at least in theory).

Quantum mechanics does not provide such comforting predictability but does a far better job explaining the strange behaviour of atoms and molecules and allows us to make (at best) probabilistic assessments of where an electron is and what it might do if we poke it with a light probe. The classical world and the quantum world seem miles apart. However, as we move along the scale – from the largest to the smallest – the classical rules eventually give way to the quantum rules. The murky, middle ground in between the two domains is the province of nanotechnology. Moreover, in this transitional regime, a material often exhibits a different behaviour than it does in the bulk, where it is governed by classical mechanics, or as a single atom, where quantum mechanics dominates.

For example, quantum dots, which are semiconducting nanocrystals, can enhance biological imaging for medical diagnostics. When illuminated with ultraviolet light, they emit a wide spectrum of bright colours that can be used to locate and identify specific kinds of cells and biological activities. These crystals offer optical detection up to 1000 times better than conventional dyes used in many biological tests, such as MRIs, and render significantly more information [8]. Gold nanoparticles can be used to detect early-stage Alzheimer's disease.

Molecular imaging for the early detection where sensitive biosensors constructed of nanoscale components (e.g. nanocantilevers, nanowires and nanochannels) can recognize genetic and molecular events and have reporting capabilities, thereby offering the potential to detect rare molecular signals associated with malignancy. Nanotechnology enables multifunctional therapeutics where a nanoparticle serves as a platform to facilitate its specific targeting to cancer cells and delivery of a potent treatment, minimizing the risk to normal tissues. The ability

to create unusual nanostructures such as bundles, sheets and tubes holds promise for new and powerful drug delivery systems [26].

Research enablers such as microfluidic chip-based nanolabs are capable of monitoring and manipulating individual cells and nanoscale probes to track the movements of cells and individual molecules as they move about in their environments. Research is underway to use nanotechnology to spur the growth of nerve cells, e.g. in damaged spinal cord or brain cells when a nanostructured gel fills the space between existing cells and encourages new cells to grow [27].

Nanoceramics are used in some dental implants to fill holes in diseased bones, because their mechanical and chemical properties can be 'tuned' to attract bone cells from the surrounding tissue to make a new bone. Some pharmaceutical products have been reformulated with nanosized particles to improve their absorption and make them easier to manage. Opticians apply nanocoatings to eyeglasses to make them easier to keep clean and harder to scratch. With nano-enabled drugs that destroy diseased cells and enable tissue repair, doctors may one day extend life expectancy far beyond our current capabilities – at least in countries wealthy enough to afford the technology.

Diabetes treatment could be improved by injecting a nanoparticle into the blood that was programmed to deliver a dose of insulin automatically upon sensing an imbalance in blood glucose level. Cancer may be treated someday soon with an injection of nanoparticles that latch onto cancerous tissue and cook it to death upon external application of a light source that poses no threat to healthy tissue.

People have always tried to use technological benefits, particularly, to overcome limitations of the human body, compensating the missing parts by artificial means. Still, cyber-ware is going into the past, because nanotechnologies really offer amazing benefits. Thanks to a new nano-surgical technology which opens up the possibility that a prosthetic hand looks, moves and feels like the real one, has a sense of touch and is controlled by the brain. Tiny, invisible brain cell implants can enhance memory, change mood and control artificial arms, legs and other parts; they can store information equal to several big libraries. An eye implant makes it possible for a blind person who has never seen sunlight to read books and help himself in everyday life. An invisible cochlear nano-implant (a spiral-shape tube-like part of the inner ear) is introduced into the ear that allows deaf people, who have never heard the birds singing, to hear music and to distinguish a range of sounds. Molecular-size nanorobots can search for and destroy cancer cells, and, being inhaled, they can clean lungs and remove tumour [28–30].

In the light of scientific and technologic advances, it is not surprising that many people are beginning to think that health can be purchased. The health marketplace abounds in products of every description to satisfy people's desires. It is overcrowded with nanoproducts, many of which are questionable. The vast majority of mail-order health products are fakes. The common ones include weight-loss products (mostly diet pills), hair restorers, wrinkle removers and alleged sex aids. Many worthless devices are claimed to synchronize brain waves, relieve pain, improve eyesight, relieve stress, detoxify the body, boost the immune system and prevent diseases.

Our market abounds in products offering magic effects – being able to prevent ageing, boost energy and enhance physical performance. Thousands of supplements are marketed with false claims that they can improve vision and joint flexibility, synchronize heart rhythms, relieve stress or treat numerous health problems including cancer. The media have a tremendous influence. Radio stations and television channels broadcast health-related news, commercials, commentaries, infomercials and talk shows. Advertising should also be regarded with caution. Some of them just attempt to exploit common hopes, fears and feelings of inadequacy, hopelessness and despair [31].

Consumer health goes far beyond the decision to buy or not to buy. The everincreasing perplexity of the healthcare delivery system; the prevalence of myths and misconceptions about health, disease and remediation; the widespread usage of unproven health products and services; and the rapidly escalating costs of healthcare show evidence of the need to educate people in the proficient, judicious and economical utilization of health information, products and services [31].

Consumer health encompasses all aspects of the marketplace related to the purchase of health products and services and has both positive and negative aspects. Positive aspects include knowledge and understanding that enable people to make medically, scientifically and economically responsible choices, while negative aspects comprise unwise decisions based on lack of knowledge, deception, quackery, misinformation or other factors leading to unpredictable effects.

Thousands of self-instructional products and programs are marketed with false claims that they can help people lose weight, stop smoking, quit drinking, think creatively, raise IQ, restore hearing, cure acne, relieve depression, enlarge breasts, enhance athletic performance and do many other things. Magnets embedded in clothing, mattresses or other products are falsely claimed to relieve pain, regulate blood flow, strengthen immunity and provide other health benefits [31].

Nanoparticles in sunscreens are another problem that raises questions of safety. Two increasingly popular sunscreen ingredients are zinc oxide (ZnO) and titanium dioxide (TiO<sub>2</sub>) which block UV light, making them suitable for use in sunscreens. Large bulks of these particles in sunscreen reflect light and appear white on the skin, and so they are not popular with consumers. Nanoparticles do not reflect sunlight, making the lotion appear transparent when rubbed into the skin. Studies now demonstrate that skin penetration of ingredients can occur: small amounts of zinc from sunscreen were found in the blood and urine of human trial participants. New research shows that zinc from the sunscreens reaches the bloodstream and has the potential to cause damage to DNA and cells. The European Union's high-level Scientific Committee on Consumer Products has warned that existing research into skin penetration by nano-ingredients is inadequate and that further studies taking into account effects on skin penetration need to be undertaken [32].

Such a seemingly useful and friendly material as silver, in its nanosize, (AgNPs) causes worries because of a very extensive use, just to support the idea that the very best thing reduced to absurdity can become dangerous. Since silver nanoparticles have unique biological properties and possess dimensions below the critical wavelength of light, it renders them transparent, which makes them very useful and

significant for consumer products, food technology (e.g. food processing equipment, packaging materials, food storage), textiles/fabrics (e.g. antimicrobial clothing) and medical applications (e.g. wound care products, implantable medical devices). In addition, nano-silver has unique optical and physical properties that are not present in bulk silver and which are claimed to have great potential for medical applications (e.g. diagnostics, drug delivery and imaging).

Today, about 370 tons/year of AgNPs are produced and used worldwide in industrial products [66, 67], and it is reported that an estimate of 1150 tons of AgNPs were used in 2015. Researchers also reported that the number of products that contain AgNPs has increased from 30 in 2010 to over 500 at the beginning of 2015 [32, 33].

Silver nanoparticles are extensively used for the production of catheters, electric home appliances and biomedical implants [5]. Because of their well-known antiseptic activities, silver compounds are used in clinical settings to prevent skin infections, such as in the treatment of burns (e.g. silver sulfadiazine) and as coatings on various surfaces such as catheters [5]. Metallic silver appears to pose minimal risk to health, whereas soluble silver compounds are more readily absorbed and have the potential to produce adverse effects [34].

Millions of people die each year from infections picked up in hospitals. This is a shocking loss of life. Overuse of antibiotics has contributed to the problem, by promoting the development of more powerful bacteria that are resistant to antibiotics. Now, leading microbiologists have warned that the rapid rise in household antibacterial products containing nano-silver could put more lives at risk. Dozens of socks, shoe pads, sports clothing, towels and bedding now marketed as 'antibacterial' or 'odour controlling' use nanoparticles of silver to kill the bacteria that cause odour. Similarly, antibacterial soaps, acne treatments, toothbrushes, hairbrushes, mattresses and cots, computer keyboards, refrigerators and other appliances, pet products and even water flasks contain nano-silver [35, 36].

The current and former presidents of the Society for Microbiology have told that overuse of nano-silver in consumer products could breed bacterial resistance to antibiotics and other drugs undermining the immune system. If we start using nano-silver quite broadly in the environment, then we will have bacteria that are not only resistant to nano-silver but also multidrug [antibiotic] resistant. Our immune system will degrade, and no medicine to withstand viruses will be available [35, 36].

Although research and development of environmental applications is still a relatively smaller area of nanotechnology work compared to other directions of R&D, it is growing rapidly, and nanomaterials promise just as dazzling an array of benefits here as they do in other fields. Nanotechnology will be applied to both sides of the environmental spectrum, to clean up the existing pollution and to prevent its generation. It is also expected to contribute to significant advancements in the environmental monitoring and environmental health science in the near future [36, 37].

Contaminated soil and groundwater are among the most urgent issues, and there has been considerable progress in nanotechnology-based remediation methods. With one of dozens of nanoremediation methods, the iron nanoparticles, for

example, contaminants can be neutralized into benign compounds in a few days. It takes much less time to achieve remediation goals than with conventional technology, which can take years using biological processes. The implementation is very simple; the nanoparticles are suspended in a slurry and are basically pumped directly into the heart of a contaminated site, while current methods often involve digging up the soil and treating it [36, 37].

Population growth, urban migration and the effects of extreme events associated with climate change make water availability an increasingly pressing issue. In environmental remediation applications, nanotechnology could help to meet the need for affordable, clean drinking water quantity and quality through rapid, low-cost detection of impurities in it as well as filtration and purification of water. For example, researchers have discovered unexpected magnetic interactions between ultrasmall specks of rust, which can help remove arsenic or carbon tetrachloride from water; they are developing nanostructured filters that can remove virus cells from water.

Over 96% of the water on earth is seawater, and desalination offers an opportunity to convert previously unusable saline water to fresh water, so researchers are investigating a deionization method using nanosized fibre electrodes to reduce the cost and energy requirements of removing salts from water.

Nanoparticles are planned to be used to clean industrial water pollutants in groundwater through chemical reactions that render them harmless, at much lower cost than methods that require pumping the water out of the ground for treatment. Researchers have developed a nanofabric 'paper towel' woven from tiny wires of potassium manganese oxide that can absorb 20 times its weight in oil for clean-up applications.

New nanotechnology-enabled sensors and solutions are developed to be able to detect, identify and filter out and/or neutralize harmful chemical or biological agents in the air and soil with much higher sensitivity than is possible today. Researchers around the world are investigating carbon nanotube 'scrubbers' and membranes to separate carbon dioxide from power plant exhaust. Researchers are also investigating particles such as self-assembled monolayers on mesoporous supports (SAMMS<sup>TM</sup>), dendrimers, carbon nanotubes and metalloporphyrinogens to determine how to apply their unique chemical and physical properties for various kinds of toxic site remediation.

There is really an opportunity with this new technology, to make nanoparticles without waste, in an environmentally friendly way, so that we do not have to worry about the emissions and we don't have to worry about the clean-up afterwards.

There are diverging opinions in the nanotechnology industry with regard to labelling nano-engaged products, ranging from 'If it's a nano-scale material, people should know, hands down' to not supporting labelling because 'it wouldn't accurately inform consumers of anything and would be bad for business because it would scare consumers' [38].

Appropriate nanomaterial labelling containing sufficient technical information (i.e. at a minimum, nanomaterial composition, concentration and average particle size) would better inform consumers and highly benefit researchers interested in

understanding consumers' exposure and nanomaterial fate and transport in the environment.

The positive attitude to nanotechnology is based not on knowledge but on hope and fascination. The perceived risk is low because of a lack of vivid and frightening images of possible hazards. If news flashes were to link nanotechnology to concrete hazards or actual harm to people, attitudes might suddenly change [39]. In the case of nanotechnology, there is currently only limited knowledge available regarding the potential health, safety and environmental impacts of this technology.

## 11.4 Towards an Open Dialogue with Consumers on the Benefits and Risks of Nanotechnology-Engaged Products

Since applications of nanotechnology will quickly penetrate all sectors of life and affect our social, economic, ethical and ecological activities, the general public's acceptance is compulsory for further developments in the field of nanotechnology and its applications. This acceptance will be influenced by the degree of public awareness of many innovations in science and, particularly, in nanotechnologies.

Still, scepticism might occur mainly due to the unpredictability of their properties at the nanoscale and the fragile public confidence in technological innovation and regulatory systems.

Food occupies a privileged position in all cultures and all considerations. The food and beverages sector is a global multi-trillion dollar industry. Leading food corporations are investing billions and billions of dollars with the ultimate goal of gaining competitive advantage and market share. For the industry where competition is tough and innovations are vital, nanotechnologies have emerged with the potential to advance the production of improved quality food with functionalized properties.

As in other sectors, nanotechnology is promising to revolutionize the food industry from targeted crop pesticides, food production, processing, packaging, transportation and storage to the development of new food tastes, textures, flavours, colours, peculiar properties and innovative food packaging applications. As a converging technology, nanotechnology through integration with biotechnology, chemistry and information technology is enabling the development of miniaturized devices, such as nanobiosensors, to detect pathogens and contaminants during food processing, packaging, transportation and storage, which is supposed to enhance safety and security of food products.

There is an opportunity, as well as a risk, in the application of nanotechnology to food and healthcare products. Currently, nanotechnologies are being incorporated into commercial products at a faster rate than the development of knowledge and regulations; hence, it is important to mitigate potential health and environmental risks associated with their manufacturing, application and disposal. Although

plenty of studies have been conducted on the influence of nanomaterials on food and healthcare product quality, it is a highly complex question, and a huge gap in knowledge still remains.

Since hundreds of products containing nanomaterials are currently available commercially, this situation clearly necessitates investigation of the exposure and toxicity of these materials. Scientific data compiled to date demonstrate that adverse effects due to exposure to nanoparticles cannot be excluded. Much more information is required to be able to estimate the potential risks of exposure to nanoparticles to both man and the environment. The focus is on free, nondegradable and insoluble nanoparticles found in medical applications, food, consumer products and the environment. Filling these gaps will help with the development of safe products and simplify the consumption of nano-enhanced goods.

Nanomaterials in food and healthcare products are often listed in combination (e.g. calcium and magnesium in dietary supplements, nanoceramics and silver in water filtration products, cosmetics and humidifiers), which demonstrates the use of nanohybrids [40] in consumer products. It also indicates that the use of nanotechnology-based consumer products at home may, in some cases, lead to multiple exposures from a combination of nanomaterial compositions. These instances suggest the need to examine nanomaterial toxicity effects that could be synergistic, additive or even antagonistic.

A recent study in *Environmental Science & Technology* showed that zinc oxide nanoparticles were toxic to human lung cells in lab tests even at low concentrations. Other studies have shown that tiny silver particles (15 nm) killed liver and brain cells from rats. These particles are more chemically reactive and more bioactive because of their size, which allows them to easily penetrate organs and cells. Products should be at least labelled so consumers can choose whether they want to be part of this experiment [41].

Since metals and metal oxides are the most common nanomaterial compositions in consumer products, they are also the most likely materials to which consumers will be exposed during the normal use of product via dermal, ingestion and inhalation routes. Products containing nanomaterials of unknown composition are most likely to lead to exposure via the dermal route.

The assessment of food or food ingredients includes details of the composition, nutritional value, metabolism, intended use and the level of microbiological and chemical contaminants. Where appropriate, this might also include studies into the potential for toxic, nutritional and allergenic effects. Details of the manufacturing process used to process the food or food ingredients are also considered, because novel food production processes can render a food 'novel' if it alters the final composition of the food [22].

For most of us, the notion of quality of life is closely connected with the notion of quality of food, healthcare and the environment we live in. The European Union (EU) Parliament's Environment Committee voted on March 4, 2015, to prohibit foods and supplements containing nanomaterials until they undergo validated new risk assessment and are proven safe for the human health and subjected to obligatory labelling on products. Foods and nutritional supplements produced using

nanotechnology should undergo specific risk assessment, with possible health effects determined, before being put on the European market, claimed the European Parliament's environment committee. Foods for which production processes require risk assessments – including nanomaterials – should therefore not be authorized until they are approved by the European Food Safety Authority (EFSA), say MEPs. Special attention should also be paid to food packaging containing nanomaterials, to prevent them from migrating into food. And in line with the precautionary principle, all novel food should also be subject to post-market monitoring, they add. They call for severe controls including the principle 'no data, no market' [22].

Since then, scientists have gathered more and more evidence that nanomaterials now in use in foods, agricultural products, supplements, healthcare products and other consumer goods – like CNTs, nano titanium dioxide  $(TiO_2)$ , nano zinc (ZnO), silicon dioxide  $(SiO_2)$ , cerium dioxide  $(CeO_2)$  and nano-silver (Ag) — can be highly toxic and bring new risks to human health and the environment. While the effects of physiochemical properties on toxicity of nanoparticles appear unclear, the results of a recent in vitro cytotoxicity study suggest that single-walled carbon nanotubes (SWCNTs) are more toxic than multiwalled carbon nanotubes (MWCNTs).

It has been well demonstrated that carbon nanotubes (*CNTs*) are indirect genotoxins. They primarily cause DNA/chromosomal breaks via reactive oxygen formation. In addition, CNTs can directly interact with the centrosome structure of dividing cells and induce DNA damage. The primary properties of CNTs associated with their toxicological mode of action are currently being investigated, which may help with predicting their toxicity or workplace classification banding based on associations between the properties and biological responses.

A number of organizations established by authorities or industry for engineered nanomaterials (ENMs) have recently established exposure standards for CNTs (e.g. workplace exposure standards (WES)). Using different studies and different adjustment factors to account for uncertainty, the derived standards for long-term exposures have been established in the range from 0.0003 to 0.034 mg/m<sup>3</sup> [42].

A number of in vitro and in vivo investigations have shown that *titanium dioxide* (nano-TiO<sub>2</sub>) has genotoxic potential manifested primarily as DNA strand breaks in the comet assay (this is the single-cell gel electrophoresis assay (SCGE), an uncomplicated and sensitive technique for the detection of DNA damage. The term 'comet' refers to the pattern of DNA migration through the electrophoresis gel, which often resembles a comet. This has been concluded to occur through secondary genotoxic mechanisms (oxidative stress) and not direct interaction with the genome. Current opinion remains that TiO<sub>2</sub> carcinogenicity is related to pulmonary overload. A two-stage skin carcinogenicity assay showed nano-TiO<sub>2</sub> does not have tumour promotion potential. A number of agencies have derived provisional health-based workplace exposure standards (WESs or similar standards) for TiO<sub>2</sub> NPs. They range in value from 0.017 to 0.3 mg/m<sup>3</sup> [42].

The toxicological database of *zinc oxide* (*nano-ZnO*) is not as extensive as some other nano-metal oxides (nMeOs). As with other nMeOs, nano-ZnO in in vitro cell culture systems is able to cause cytotoxicity (being toxic to cells) and indirect DNA

damage via oxidative stress. This appears to be mediated by zinc ions within the cell after the nano-oxide has been translocated from the media into the cell. Toxicity information for workplace assessment has proved that at high concentrations the expected lung inflammation and cytotoxic responses are observed [42].

While the available astute studies with nano-ZnO show increased metal concentration in various tissues, plus or minus indications of tissue damage, their usefulness is diminished by lack of evidence that the nano-ZnO has actually been absorbed from the gastrointestinal tract. In this milieu nano-ZnO is likely to be extensively solubilized. The studies of the use of nano-ZnO in sunscreens have been able to show small fractions (<0.001%) of the dermally applied zinc (either in nano- or submicron form) absorbed into the blood. Furthermore, the absorption continues for some days after the repeat applications stop and the skin has been washed. It cannot be determined whether the increased blood zinc is the result of zinc ion or nano-zinc absorption [42].

When silicon binds with oxygen, it creates a compound called *silicon dioxide*  $(SiO_2)$ . Another name for silicon dioxide is *silica*, which includes its various compositions, both natural and synthetic. Silica has three broad categorizations: crystalline, amorphous and synthetic amorphous. The most common form of crystalline silica is called quartz, which is found in the rocks and sand that make up 90% of the Earth's crust. Silica, or silicon dioxide, is found in a variety of forms in our environment, as it is ubiquitous. It is naturally found in the earth, in our body tissues and in our food [43].

Silica nanoparticles are used by many industries including drug, cosmetic and food industries. Most commercially used silica is created by crushing or milling it from natural sources. Depending on its form, amorphous silica has a wide range of physicochemical properties. Just as it appears in multiple forms, it has a variety of uses and can be found in many products. Its appearance in food can be due to multiple reasons. Amorphous silica is used as a supplement additive as an anticaking agent, since silica absorbs excess moisture and prevents ingredients from sticking together when supplements are exposed to moist or humid conditions without interfering with the active ingredients. It can also be used as a food additive as a carrier of flavours and fragrances. Silicon dioxide and silica gel are used as pesticides, so it may be found in food due to exposure to crops, food handling and food preparation.

Various products contain silicon dioxide due to its uses in multiple industries. They can be found in drugs (such as alprazolam by Actavis, oxycodone hydrochloride by Actavis and Xanax by Pfizer). They are also used in supplements (such as silica complex and cosmetics including toothpaste, insecticides and biomedical applications) [43].

The health risks associated with silicon dioxide vary and are dependent on many factors, especially the form of silica. Additional factors include qualities such as the size, specific surface area, coating, number of particles, concentration and duration of exposure. One of the concerns about the silica nanoparticles is that they are able to pass the blood–brain barrier, which usually keeps harmful substances from getting into the brain [43].

Those most at risk for adverse health outcomes correlated with silicon dioxide exposure are occupational industry workers in fields that breathe in large amounts of crystalline silica dust, particularly in the crystalline forms of quartz and cristobalite, as these have been deemed carcinogenic. Although the mechanisms of this toxicity are not clear, there is a lot of work that demonstrates this correlation. Crystalline silicon is associated with silicosis, which is a lung disease caused by inhaling tiny bits of silica over a long amount of time [43].

Silica exposure has also been associated with rheumatoid arthritis, small vessel vasculitis, autoimmune diseases and kidney damage, but there have been contradicting studies about kidney damage. A 2012 study published in the journal *Renal Failure* found a positive and consistent association between silica exposure and chronic kidney disease (CKD). This study found that occupational exposure to silica is associated with about a third of an increased risk in CKD, and with the duration of the exposure, the risk for CKD increased [43].

Despite many reports and research studies, there is inconsistent and contradictory research on silicon dioxide's safety. This may be due to the fact that it appears in various versions and most of the research conducted has been on crystalline forms and just recently started on amorphous forms. There is not enough evidence yet to conclude that amorphous silica is correlated with the health risks that crystalline silica appears to have. According to the Food and Drug Administration, silicon dioxide and silica gel as food additives are generally recognized as safe (GRAS), meaning that the average consumer will only ingest small amounts without adverse health effects.

Cerium dioxide (CeO<sub>2</sub>) nanoparticles have low solubility and are potentially retained in the lungs. High inhalation exposures have resulted in pathology changes in the lung typical of particulates. Biokinetic studies have been performed by measuring the fate of cerium, rather than the nanoparticle per se. However, because they are poorly soluble and stable, it is presumed by investigators that tissue cerium concentrations are associated with particulates. Soon after inhalation of moderate amounts of nanoceria, approximately 25% is excreted in faeces; of this more than 90% is in the first 24 h. This indicates the clearance from the lungs is rapid, and gastrointestinal absorption is limited [42].

Once in the systemic circulation, CeO<sub>2</sub> nanoparticles may be widely distributed with the highest tissue concentrations found in the reticuloendothelial system (a part of the immune system). Inhalation and intra-tracheal investigations indicate a typical oxidative stress and inflammatory response associated with bio-persistent particulates, including formation of pulmonary granulomas. It is not surprising for a particle producing oxidative stress after entering cells that nanoceria can cause DNA strand breaks in in vitro systems [42].

Intravenous studies with *silver nanoparticles* (*Ag-NPs*) show silver accumulating in the liver, spleen and kidneys, but increased concentrations in other organs are also noted. There is a growing body of evidence indicating that the toxicological effects of Ag-NPs may be influenced more by silver ions than their nanoform. For Ag-NPs there are a number of short-term (10, 28 and 90 days) repeated exposure inhalation studies available. Some of these have been conducted according to

OECD inhalation guidelines designed to generate safety data for chemicals. While there are clear dose-related increases in blood and tissue silver concentrations, it appears significant effects (alveoli inflammation and alterations in lung function) that only occur in the lungs. Silver ions and Ag-NPs can form DNA adducts (by-products) and micronuclei in a concentration-dependent manner, with silver ions being more potent.

We do not yet know how nanoparticles will affect the way they are transported and hence their biological and environmental fate. The risk, therefore, is that these materials will have as yet unanticipated impacts on human health and the environment. Preliminary studies in the field of nanotoxicology (an emerging science which looks at the potential for nanotechnology to cause adverse effects) have indicated that some nanomaterials may have toxic effects. In particular, a number of studies have noted the potential for carbon nanotubes (cylindrical nanoforms of carbon which are characterized by their extraordinary strength and unique electrical properties) to exhibit toxic effects in the lung comparable to those of asbestos (UK RS-RAE 2004). Such studies have raised serious concerns as well as recent calls for a moratorium (FoE Australia 2008).

To date, there have been no documented cases of adverse health or environmental effects directly attributable to nanotechnology [3]. However, numerous concerns have been raised by scientists, advocacy groups and the general public alike that the specific properties of nanomaterials arising from their small size – the same properties associated with their tremendous potential and numerous possible applications and benefits – may lead to different interactions in humans at the cellular level and with the environment.

The assessment of nanomaterials will follow the guidance issued by the European Food Safety Authority (EFSA) in May 2015. The FSA carried out research into consumer awareness and attitudes to nanotechnologies in the food sector. The research revealed that consumer awareness about nanotechnologies in relation to food was generally low. Consumers were concerned about safety, particularly long-term safety, and impacts on the environment. There was a greater acceptance of certain types of potential applications than others and a general scepticism about industry's motives for developing these technologies. Overall, consumers wanted more information and transparency [21].

In 2016 a EC-funded project 'Europeans and Nanotechnologies' bringing together 17 partners from 11 countries was undertaken by *NanOpinion* with the aim of monitoring public opinion on what Europeans expect from innovation with nanotechnologies (NT). In order to carry out this study, different modes of public participation have been organized. The project is aimed at citizens with a special focus on hard-to-reach target groups, i.e. people who do not actively show interest in science [44].

*NanOpinion* used an innovative outreach approach, focusing on dialogue, to monitor Europeans' opinions on NT across Europe. It included surveys, social media, discussions, street labs, events in public and semipublic spaces, etc. A total of 8,330 people filled in the questionnaire, and approximately 15,000 citizens were engaged in more than 20 live events, including activities in the streets, debates

and workshops. Besides, a total of 1,556 students were engaged in school activities, and NanOpinion contents on social media reached thousands of users too. In parallel, the media partners published 6 supplements and 161 articles, on blogs and microsites, reaching hundreds of thousands of visitors. The research has demonstrated that less than 50% of Europeans are informed about nano and about 60% heard about it. The majority of the population (88%) consider that labelling of nanoproducts is important. In general, Europeans have a positive attitude to nanotechnology (about 70%) but do not feel themselves competent to discuss it [44]. There is certainly an evidence to suggest that some dimensions of nanotechnology may pose potential risks to human health, worker safety and the environment. However, at this time, we cannot yet fully appreciate the precise nature, magnitude or frequency of such risks. The burgeoning field of nanotoxicology has begun to address these questions; however there remains a substantial gap between this field of academic research and the research that is of relevance to risk regulators and policymakers.

As nanomaterials are finding new applications every day, care should be taken about their potential toxic effects. Yet in some countries (Australia, USA), laws do not require food companies to conduct new safety tests on nano-ingredients before putting them in foods or to label nano-ingredients. Therefore, it is impossible to know how many nanofoods are now on sale, and which foods contain nano, or for consumers to choose whether or not to buy nanoproducts or to eat nanofoods.

## 11.5 New Technologies and Responsible Scientific Consumption in Constructing Consumer Identity

A prominent feature of the modern society is the pervasiveness of the consumer culture. People's behaviours, activities and possessions are organized around their consumer identities – the multifaceted labels by which their 'self' is recognized by themselves and members of society. Marketing professionals strive to influence consumers towards choosing and purchasing a particular brand of their product, at a particular time and place. To succeed, they have to have a clear understanding about what makes people want to buy and consume. However, the modern consumer is not an isolated individual making purchases in a vacuum. Rather, we are all part of a contemporary phenomenon that is often referred to as a global consumer society where all people have become increasingly interconnected and interdependent due to the fast scientific and technological advancements in all spheres of life including such areas as information and communications technology.

The growing use of communication devices brings a number of challenges to making information disclosures effective (e.g. on the screens), which can either facilitate or constrain the advancement of any innovation by consumers. The dynamic and innovative character of modern consumption enables consumers to gather, compare, analyse, review and share information about goods and services

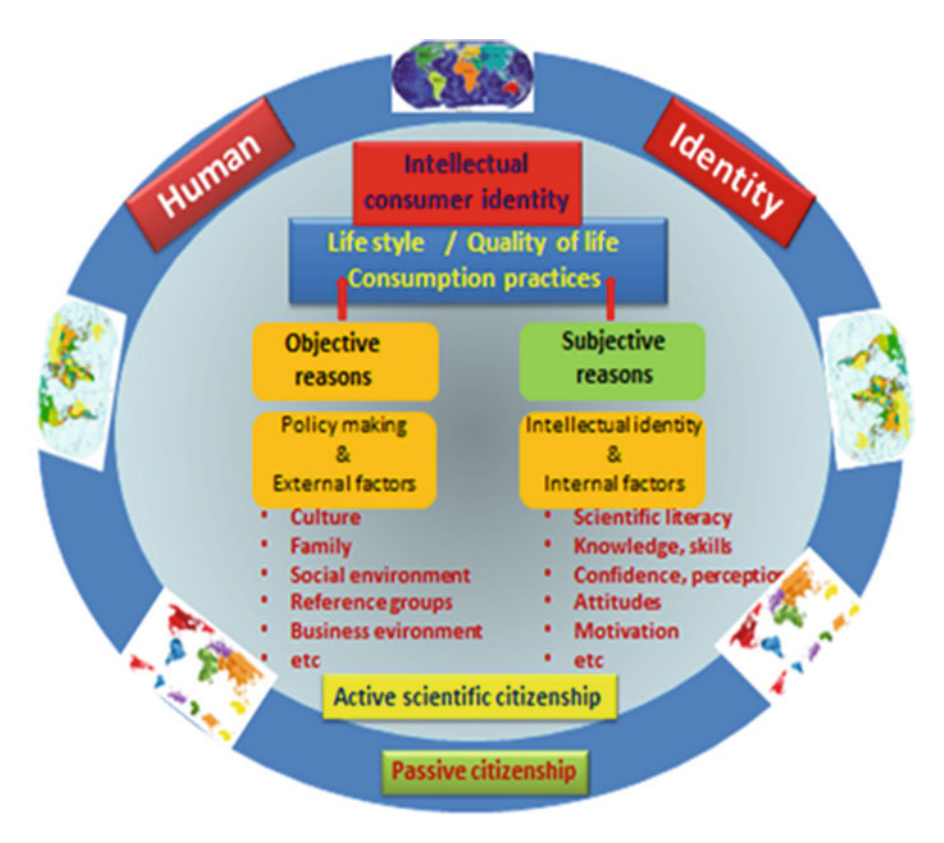


Fig. 11.4 Constructing responsible scientific consumption practices

and fosters the development of new business entities, some of which promote goods manufactured with the use of innovative technologies (e.g. a huge market of nanotechnology-enhanced products). This aspect could potentially raise greater awareness of the fact that we are all part of a single global community that shares a common consumer identity as a background and destiny [45]. Yet, in a contemporary consumer culture, people no longer consume for merely functional satisfaction, but consumption becomes meaning-based, and a person's consumption culture is often perceived as a symbolic resource for the construction and maintenance of consumer identity.

All of us are consumers: we consume goods, services and natural resources; hence, our consumer identity is a major factor making up our human commonality and the most essential factor that unites all people of the world into a global consumer society (Fig. 11.4). But against the background of this commonality, we develop different consumption practices, and we have different living standards due to various reasons – both objective and subjective. Objectively, we are all exposed to approximately similar conditions. Still, on the subjective side, it is to a

great extent our intellectual power that shapes our decision-making, our consumption choices and our life styles and contributes to the quality of life [45].

It means that today, in a highly technological business world, we need to have enough scientific literacy, knowledge, skills and confidence to effectively construct our responsible scientific consumption practices with the intention to contribute to innovations, new technology admission, sound business practices and facilitation of responsible and informed policymaking to satisfy the requirements of individual consumers as well as to contribute to the improvement of the quality of life in general.

In the past, a nation's quality of life and competitive power were mostly determined by its geographical position and the size of population. The advent of technological age has changed the balance of power among nations, and today even a small nation can achieve abundance, economic strength and high standards of living through its industrial and technological achievements. The rise of consumer culture, the creativity of public and the increased scientific literacy can move ahead the development and manufacturing of new products through the use of and commercializing new advanced technologies, since a scientifically literate public can better contribute to the potential for achieving a more affluent society by introducing technology and developing added value in manufactured goods.

Technology does not stay at the idea stage; it is converted into marketable products. The fast scientific and technological advancements in all spheres of human activity, including biomedical engineering, computer and communications technology, biotechnology and nanotechnology, call for fresh reflections on what it means, in the twenty-first century, to be a consumer and for ethical judgements on how we might shape our scientific responsible consumption on the way to sustainable future consumer society.

What is important for a contemporary consumer to be able to cope with all the tasks imposed by new technologies and scientific advancements in order to make independent knowledgeable decisions? But what if those decisions are influenced by producers and aggressive marketing of businesses?

Education, as a major catalyst, has to help people become effective, scientifically literate, knowledgeable decision-makers and responsible consumer-citizens. The cost is much greater if it does not.

We want our students to leave university with a clear understanding of the scientific, political, legal, economic and ethical functions of the society they live in and with the moral awareness and social responsibility to thrive in it. Social responsibility is an ethical framework and suggests sustaining the equilibrium between the welfare of the society and the environment. Responsible consumption remains a crucial way of organizing people's place in the contemporary technological consumer society. It will undoubtedly continue to change the quality of life across space and time in the twenty-first century.

New technologies and, particularly, nanotechnologies have emerged on the market with the changing of consumer status from passive to active and the coming out of the new 'intellectual consumer'. The new intellectual consumer expresses a responsible behaviour towards his consumption practices and develops a

knowledgeable and thoughtful approach to his consumption. A new consumer is perceived as intellectual because he possesses different kinds of knowledge and knows how to select, organize, combine and integrate this set of knowledge within his environment – which can be defined as a contextualized know-how. A new consumer is intellectual, competent and technologically and scientifically empowered, which is fundamental to both the future sustainable global society and the quality of life of every individual [45].

This is why we need to consider the role of new technologies in students' daily lives, in shaping responsible attitude to the consumption practices, and their implications for classroom performances. How closely, for example, should students' worlds outside the classroom match what occurs in the classroom? Why is it important to develop intellectual, responsible attitude to consumption? Intellectual, responsible consumers are people showing power of the mind to reason and apply knowledge, who are capable of choosing through connecting, of buying through thinking, of consuming through awareness and of changing through understanding [45].

## 11.6 Knowledge Management as a Means of Social Change: Who Needs Nanotechnology Education?

According to Petrides and Nodine (2003), knowledge management (KM) brings together three organizational resources – people, processes and technologies – to use and share information more effectively. Knowledge has become the most valuable resource concerning the use of technology as a tool for achieving an improved standard of living for all people.

However, there is no monolithic thing called technology. Rather there are various technologies that converge or compete to fit into what can be called an ecosystem of technological and societal arrangements. Societal and technological arrangements co-evolve. This co-evolution happens most favourably in an educated, intellectual and affluent society that is tolerant of change and divergent views. By fostering an educated, intellectual society, it creates conditions that foster responsible moral and social behaviour of the individual and contributes to shaping intellectual humankind [46].

Important questions have been raised about nanotechnology's potential economic, social and environmental implications by prominent technology leaders, nanotechnology boosters, scientists, policy officials and environmental organizations. But there is very little knowledge in wider European society about what nanotechnologies are and what impact they might have on how we live. Many experts acknowledge that uncertainties prevail about this.

Nanotechnology based on multidisciplinary research provides an abundance of potential applications. While advocates preach a revolution, e.g. in chemical production methods, medicine, materials science and energy systems, critics warn

about unknown side-effects, e.g. allergies, and deliberate misuse of the technological solutions developed. Higher education has to be at the heart of these processes, ensuring accessible information that will allow people to better understand what nanotechnology is and how it will be applied and its implications for society [47].

The central question on nanotechnology education is 'Do we need nanoeducation?' To answer this question, we should first find out who needs nanoeducation. What is the interest in nanoeducation from those who have expressed the need? What kind of education is needed – expertise, skills or level? For what kind of jobs are skills and knowledge of nanotechnology needed?

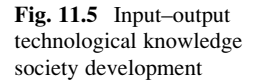
Nanotechnology has shaken the world, and the advanced countries are investing billions of dollars for its R&D and industrial applications. For example, US cumulative investments in nanotechnology-related research since 2001 now total over 24 billion dollars (including the 2017 request) [48]. This support reflects the continued importance of investments to significantly improve our fundamental understanding and control of matter at the nanoscale and to translate that knowledge into solutions for critical societal needs. Environmental, health and safety research since 2005 now total nearly \$575 million; education and research on ethical, legal and other societal dimensions of nanotechnology since 2005 total more than \$416 million [49]. Similar amounts are being spent on nanotechnology by Japan, Russia, China and European Union. Nanotechnology has therefore been taken up in these countries as an important national requirement.

Nanotechnology is already evolving towards becoming a general-purpose technology by 2020 [50]. The National Science Foundation (NSF) has estimated that by 2017, the world will require about 2,000,000 multidisciplinary trained nanotechnologists, including Europe with about 3–400,000 nano-specialists with 10 million new jobs. Therefore, modern technology requires educated workforce and responsible consumers and hence imperative for educated population. The needs of new emerging technologies and a beneficial state of consumer society are compatible in this case.

The basis of any reflection, whether personal or social, rests on an enlightened and critical intellect. Given its ubiquitous nature, nanotechnology is an essential component of multidisciplinary education on the way to intellectual global society. It motivates the young adult to shape his thought process, to favour opportunities that refine his critical judgement and to allow him to look upon the society of which he is a full member with a clear and constructive eye. He will then be ready to play his role as a knowledgeable citizen and contribute to the on-going intellectual growth and wellbeing of his community.

Sustainability is defined as a long-term maintenance of responsibility, which has environmental, economic and social dimensions, and encompasses the concept of responsible management. In its turn, responsible management rests on knowledge and understanding of new technologies and scientific advancements fostering the societal development.

To create a sustainable, democratic, technologically empowered and intellectual global society, higher education has to be at the heart of these processes and play a double role. First of all, it has to provide a top-level multidisciplinary education to





produce a highly educated workforce and, secondly, to educate the general public by ensuring accessible information that will allow people to better understand what nanotechnology is, how it will be applied and its implications for the society and personal life.

Society belongs to all of us. What we put into it creates what we get out of it (Fig. 11.5). Society is best when we all join in and when we all bring our knowledge, energy, inquisitiveness, creativity and judgement to it [51].

But if we, as citizens and consumers, are ignorant and scientifically illiterate, what kind of input can we provide and how can we affect policymaking and expect a dignified output? Here another question arises: does higher education today fulfils its role as a major catalyst to provide the necessary knowledge and relevant skill mix for our students to be prepared to join the highly technological global economy to ensure sustainable society development and be able to manage innovations for the improvement of the quality of life [51]?

Universities play a crucial role in generating new ideas, in reflecting on new technologies and in accumulating and transmitting knowledge, thus, creating knowledge-added value. Knowledge-added value refers to the contribution of educational factors (e.g. innovative courses, new technologies, foreign languages to be able to work in multicultural organizations) used in raising the intellectual capital, thus, increasing the value of a person.

Outside of economics, added value refers to 'extra features' of a person that go beyond the standard expectations and provide something 'more' while adding intellectual capital to the cost of a person. Value-added features (in fact, professional competences) give competitive advantage to outperform others due to the raised intellectual capital and personality features that include multidisciplinary convergent knowledge, cognitive abilities and strategies, practical research skills and professional aptitude, entrepreneurship, personal responsibility, flexibility, positive attitudes, emotions, ethics and motivations [51].

However, unless fundamental changes are made in the educational models, curricular and infrastructure to institutionalize the convergent education; to reverse the general erosion of science, technology, engineering and math (STEM); and to address the specific growing need for the convergence with humanitarian education, there will not be a counterbalance of technosciences and humanosciences in the society. The convergence does not suggest the creation of a kind of education where literary intellectuals understand quantum theory or the nature of neutron stars and scientists in lab overalls spend their free time reading John Ashbery or Dostoevsky. It would be unwise to expect the creation of such a culture.

The talk is about convergence that is essential for the modern society consisting of people who live and work in a knowledge economy forced to confront diverse kinds of knowledge from unrelated fields in their everyday work. Even today, we feel the mistakes and failures of education with a sharp divide into humanities and hard sciences, which has threatened by the prospect that engineering spreads from biology up through the human sciences and arts. Computer technologies serve as a bridge to join the concepts of physics, mathematics and logics with the classical world. Yet it can also serve to carry philosophical and artistic thinking into the scientific community.

Nanotechnology is inherently interdisciplinary, touching upon just about every field of science and engineering, and provides many points of entry for students in non-technical fields, who will find plenty of opportunities to debate its social, moral, ethical, legal and economic impacts. Finally, nanotechnology is now, and it is bound to become a major factor in the world's economy and part of our everyday lives in the near future. The science of the very small is going to be very big, very soon. Therefore, there is an opportunity to equip students with the background and perspectives that will prove useful as they pave their way into the future abundance in nanotechnologies. Given its potential impact on society, and the growing public debate over nanotechnology's benefits and risks, both science and non-science majors alike should have at least a passing understanding of what nanotechnology is.

Thus, higher education must, in one way or another, come to terms with new emerging technologies and identify the paramount place that nanotechnologies have taken in the society. It will offer an opportunity for students from a wide range of disciplines to learn about nanoscience and nanotechnology, to explore these questions and to reflect on the place of the technology in the spheres of their major, their personal life and in the global society. Therefore, the presence of new technologies – as *means* (sources of information), *object* (area of cognition and activity) and *context* (the environment where education/training takes place) – in the sphere of contemporary higher education is undeniable (Fig. 11.6).

The learning context of nanotechnologies could be presented as the 'Nanotechnology Education Tree' with at least four main branches – comprising ecological, health and medical, consumer goods and information and communications technologies – they touch everyone's life, and they are understandable and contextually accessible. It would provide an introduction to nanotechnology and how it can be

Fig. 11.6 New technology as means, object and context of contemporary higher education



applied in different business and industry sectors. It would also convey information on societal aspects, potential risks, the need for standards, some of the myths surrounding nanotechnology and a timeline of some of the key developments. Contemporary top-notch education presupposes the engagement of all students into the research of the nanoworld, irrespective of their major. There is a special merit in such a research – that is a high degree of task authenticity, globality, integration with other subjects and involvement of all the aspects of the individual's personality, previous experience and knowledge [52].

Responsible consumption is based on the understanding of advantages and threats of new technologies [45]. The European Commission highlights the need to promote the interdisciplinary education and training together with a strong entrepreneurial mindset. It is emphasized that the need for nanotechnologists will not only be confined to the industrial and R&D sectors but will be needed practically in all spheres of life [50].

Experts have estimated that marketing of nano-based industrial products will have risen to some two to three trillion dollars by 2017, and nanotechnology is going to dominate the socio-economic life of the world for the next 40–50 years [50]. It requires a lot of resources on the consumer side (intellectual, psychological, economic, etc.) to adjust to the rapid changes in the social and business environment by bridging the gap between the change in attitude to new technologies and the change in consumer behaviour. To a great extent, bridging this attitude-intention behaviour gap is stipulated by the increase of consumer awareness and the raise of the knowledge level.

Therefore, shaping intellectual, responsible consumption practices based on knowledge and awareness is viewed today as the development of civic skills contributing to the sustainable future by enabling people to make their own informed decisions about highly complex technological problems of the day, to take responsibility for their health and their own lives and to contribute to the wellbeing of their communities.

To fulfil the task, it is the job of our higher educational systems of the twenty-first century to prepare young citizens for the challenges and controversies of the rapidly changing and diverse consumer societies and highly technologically empowered business world. It is the role of higher education to develop skills and values required to enhance democratic life for everyone and to make their informed consumer voices heard in policy decision-making. Democracies need knowledgeable problem-solvers and responsible decision-makers on the way to social justice — as the fair way in which human rights are manifested in the everyday lives of people at every level of society. Social justice may be broadly understood as the fair and generous distribution of the results of economic growth. Although maximizing economic growth appears to be the primary objective for the adoption of new technologies, it is also essential 'to ensure that this growth is sustainable, that the integrity of the natural environment is respected, that the use of non-renewable resources is rationalized, and that future generations will be able to inherit a beautiful, flourishing and prosperous planet from our hands' [53].

The conception of social justice must integrate numerous dimensions, starting with the right of all human beings to benefit from a safe and comfortable environment, from the achievements of new advanced technologies and from knowledgeable decisions in policymaking. This entails the fair distribution among countries and social groups of the cost of protecting the environment and of developing safe technologies for production and safe products for consumption, ensuring everyone a decent standard of living, which is an inseparable part of the notions of a knowledge society and knowledge economy.

All these tasks cannot be fulfilled based on separate areas of discovery, technological inventions or scientific disciplines. There is an emergent need for the system convergence of multidisciplinary knowledge and new technology for the benefit of society, which is the core opportunity for the progress in the twenty-first century.

### 11.7 Convergence of Science, Technology and Society: Nano-Bio-Info-Cogno-Socio-Humanosciences and Technologies – A Way to NBICSH Society

Higher education today is not seeking the ability to perceive hidden connections between disciplines. It seems, thus, unrealistic to think of nanotechnologies as a single technology and to consider nanoeducation totally the privilege of natural or technical sciences. Alexandersson [54] argues about the division of education on theoretical and practical subjects and emphasizes that the ultimate goal of higher education for sustainable development is to empower citizens with the perspectives, knowledge, skills and understanding of new sciences and technologies for helping them adjust and live in democratic sustainable societies. A growing gap between technology use and technology understanding in a consumer society creates a need to educate students and the general public about new emerging technologies – the backbone of a strong economy.

A frequent topic in scientific and scholarly discourses today is the *convergence* related to technical sciences (or technosciences) and humanitarian sciences (or humanosciences). The examples of such rapidly developing valuable convergences in knowledge–science–technology–engineering–society are manifested in the creation of universal databases, cloud computing, unmanned vehicles, human-robotics systems, mind–cyber-physical systems, research programmes on space and fundamental particles. A familiar example of such a convergence is the development of a cell phone. A wide range of technologies including high-frequency communications and packet-switching protocols (for connections to global networks), materials science and nanotechnology (for CPUs, data storage, touchscreens, antennas, etc.) and cognitive science and human–computer interface technologies (for the user interface) converged to create a 'smart phone' [55].

Another simple example is the creation of educational programmes where computer technologies/robotics converge with humanitarian/linguistic

technologies to entertain, nurture and shape societal knowledge. Entirely new disciplines have appeared – synthetic biology, nanophotonics and quantum communication. However, the concept of convergence is also used to describe the integration of scientific disciplines to solve common problems through interdisciplinary cooperation (e.g. nanobiotechnology), the solution of which separate sciences cannot resolve. The integration of biomedicine with physics and engineering has already affected human healthcare systems. In order to advance faster, these sciences have to converge, complementing each other, to form new sciences, based on the teachings of each constituent part, but serving innovatory purposes [56].

At the core of the new concept are interrelations, interconnections, synergies or syntheses between broad fields of disciplines and research and development, such as nanoscience and nanotechnology, biotechnology and the life sciences, information and communications technologies, cognitive sciences, neurotechnologies and even humanities, fostering social responsibility. Robotics, artificial intelligence and other fields of research and development are also taken into account. Innovative and converging technologies have therefore been characterized as a platform for exploring the future impact of all sciences, technologies and engineering on the sustainability of the society.

The notions of the future knowledge society and knowledge economy, which are inseparable from the concept of innovation, pervade science, engineering, technology, social spheres and humanitarian areas and appear repeatedly, whether we consider an ancient civilization, the human body or a comet. The concepts are directed to establishing and developing innovative bonds and interconnections among multiple disciplines from contributions based on smart technologies, on the convergence of technosciences and humanosciences (Fig. 11.7) [52, 56].

The problem really demands a scrupulous consideration. Products are made for consumption, and as other complete technical solutions, they are to be evaluated

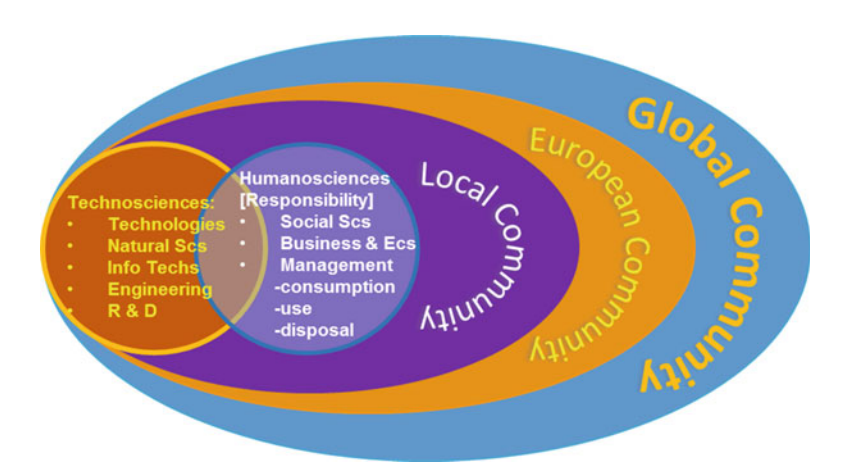


Fig. 11.7 Convergence of technosciences and humanosciences for sustainable knowledge global society

and analysed: possible improvements, strengths and weaknesses and benefits and risks are to be identified and considered. And in these processes, scientific knowledge integrating both technosciences and humanosciences is of paramount importance. The development of new products and the relevant technologies are inherent in the natural sciences – technosciences – while all the processes relating to the economic management, consumption and disposal of these products link with economic and management sciences, i.e. humanosciences. To put it simply, technologies do the right things, and humanities do the things right! [53].

Contemporary higher education model should be directed to the convergent knowledge through an extensive review of technosciences and humanosciences. At the beginning of the educational process, these two domains operate with near independence (Fig. 11.7). However, as a person reaches the stage of high level of technoscientific proficiency combined with sociocultural and ethical knowledge, the overlap area approaches totality, so that both future technoscientists and humanoscientists develop a common language and common understanding to deal with complex technical, social, ethical, legal, political, business and other life support problems on the local level, transcending to European and global levels.

In the model (Fig. 11.7), the citizen is not a mere consumer of scientific knowledge but a person whose voice and knowledgeable opinions are heard and valued in policymaking and governance. The aim is at developing not only scientific competence but also at the global personality development of the student through the experience of interdisciplinary learning (attitudinal change to new emerging technologies, to nanoproducts, to intercultural cooperation, to global societal problems, to each other and to the process of learning – i.e. motivation, awareness and social scientific responsibility). And if the educational process is strategically targeted, we can view education as a contribution to a scientifically literate, knowledgeable society (*local–European–global*) where younger generations are able to take responsibility for its sustainable development [52].

Nanoscience and nanotechnologies in their application contexts affect medicine and healthcare, the environment, working conditions, food production, agriculture, industrial production, social interactions and law enforcement and have a huge impact on other major areas of life, thus, significantly shaping society and social systems. In fact, these areas, to a great extent, touch the humanitarian side of life (i.e. concerned with or seeking to promote human welfare). Therefore, non-technical students who are not engaged in in-depth study of mathematics or technical courses should get the general knowledge of nanoscience, nanotechnologies and their implications in the society as a result of integration of the humanities with technosciences. At the same time, nanoscientists, students and nanoproduct developers with a technical background possess the knowledge about the technologies they are working on but seldom address ethical, legal or social implications. Therefore, the ability of nanoscientists, students and engineers to comprehend societal demands and expectations, to recognize the moral responsibility for their fulfilments and to understand the economic and environmental contexts of their work is of crucial importance.

In many scientific fields, much of the most exciting discovery potential is located between the boundaries of traditional disciplines. Already today, a great deal of novel multifunctional nanomaterials, advanced nanodevices, new nano-based products and processes are designed and developed by team efforts of materials' scientists working with chemists, biologists, physicists, information technology experts, geologists, physicians, environmentalists, sociologists and engineers. It is thus apparent that we need to create new types of universities, which have 'departments without walls' to explore convergence as a way of enhancing the impact that nanotechnology can have on scientific discovery and solving critical problems [9, 52].

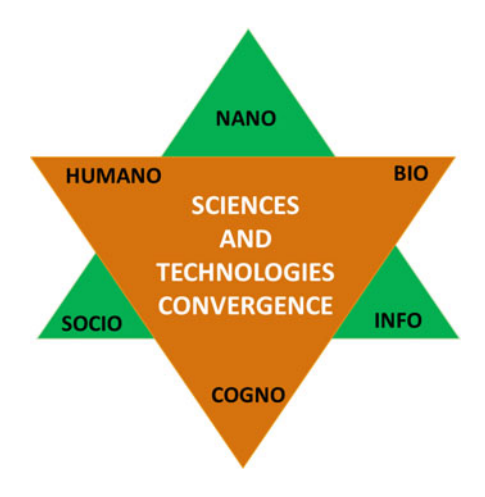
The perspective of a new technological revolution and the formation of a knowledge society imply transformative convergence among seemingly separate scientific disciplines, technologies and social areas of human activity as a holistic system providing the clue for societal challenges and resolving problems that isolated disciplines cannot. This process is associated with the convergent development of nano-, bio-, info-, cogno-, socio- and humanosciences and technologies – ultimately resulting in NBICSH society (Fig. 11.8).

This convergence would allow us to create a counterbalance, based on which it is only possible to anticipate future challenges and adequately respond to them, making responsible decisions. Without that counterbalance, we risk getting scientists without conscience, technicians without taste and policymakers without responsibility. Without that convergence there will be no robust workforce with the potential to change the society for the better [51].

The convergence of NBICSH sciences and technologies envisions a number of radical transformations in human endeavours:

 Empower people with the multidisciplinary knowledge providing added value through the convergence of NBICSH technologies and create new sciences, industries and jobs at their frontiers and interfaces.

Fig. 11.8 Convergence of nano-bio-info-cogno-socio-humano- (NBICSH) Sciences and technologies



- Expand human physical and cognitive potential, significantly improving lifelong wellness (nanomedicine, nanoprosthetics).
- Improve manufacturing technologies for higher productivity, healthier goods and economic efficiency.
- Ensure dignified quality of life for all, providing fair access to natural resources, food, healthcare, knowledge, safety and security.
- Advance the new participative democracy of the society through the convergence of technosciences and humanosciences, engaging general public in educated problem-solving forums and responsible decision-making legislatures to improve the efficiency of societal governance.

The convergence places an emphasis on humanitarian applications of new technologies by focusing on the role of nanotechnologies in tackling society's grand challenges such as safety, health and the environment. This new approach to teaching about technologies will also engage and inspire those students who have typically been excluded from the process by the traditional educational experience.

Additionally, there is a hope that such an approach will better prepare a new generation of specialists to address major societal problems in the future, maintaining, at the same time, an awareness of political, economic, ethical and social constraints on technologies. Undoubtedly, education in this case is to be guided by teams of teachers from a diverse array of disciplines. Science and technology teachers will have to learn humanities and social sciences. Humanities and social science teachers will have to learn sciences and technologies, promoting interdisciplinarity [52].

The European Union is stimulating the development of nanoscience education in universities to address complex issues and to solve multidisciplinary problems. From a practical stance, nanotechnology is widely considered to be 'the next big thing' and is well worth learning more about, in order to get a knowledgeable understanding of what place for nanotechnology might be allocated in our lives.

The values and ethical imperatives of the modern society in relation to advances in science and technologies, including information, self-organization, integrity, security, ecology and the formation of new priorities, take place under the influence of a new – synergistic – methodology and the implementation of high technologies and social transformations under conditions of global information accessibility, international cooperation and expanded global educational environment.

Nanotechnology can bring substantial changes to the sustainable development and social culture of the society through the NBICSH sciences and technologies, at the same time manipulating the way people communicate and think. Higher education and new technologies have to be synergistically interwoven. The concept of the role of higher education in the creation of new technological and cultural synergies to change human understanding of the new technologies and social practices is the problem of developing an innovative culture implying 'global citizenship competence' (GCC) (see Fig. 11.9).

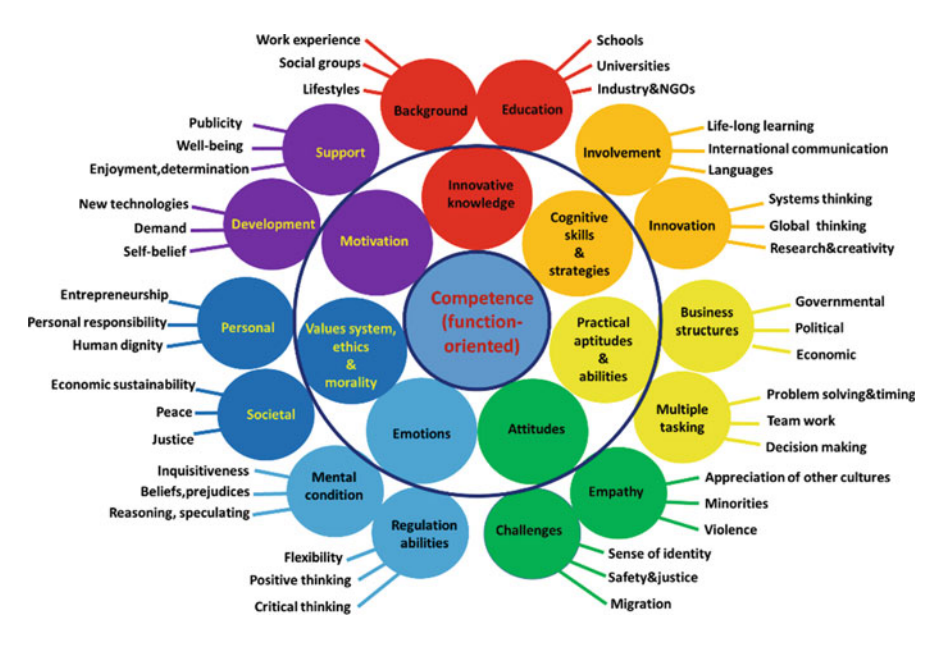


Fig. 11.9 Global citizenship competence (GCC) model [34]

## 11.8 Global Citizenship Competence: The Vision for Educational Change

Our world has become a global interdependent community. Since nanotechnology is starting to play an extremely important role in the socio-economic development of all countries, it is imperative for higher education that emphasis be placed on producing a properly educated, qualified and trained manpower possessing competences that would allow them to cope with challenges in their professional and personal lives encouraging both greater self-sufficiency and more deliberative decision-making.

Most of today's higher educational institutions are awash in technology, but the outcomes for students remain little changed from 20 years ago. The problems are not in our technology but in our universities, including the issues of what we teach and how we teach. Today the educational outputs and the performance are crucial factors to be in demand. Business companies want to have the best – those who are talented and those who have innovative ideas and creative thinking. Yet this will not be developed by chance but by strategic, targeted education. The necessity to reconsider the academic outcomes in higher education has stimulated the development of 'global citizenship competence' (GCC) model to provide the vision for educational change. It is a student-centred and world-minded concept from the perspective of NBICSH sciences and technologies and global citizenship and the implementation of which can contribute to the formation of a scientifically grounded structure of contemporary higher education (Fig. 11.9) [57].

Based on the EU definition of the concept of competence and taking into account external and internal factors, personal qualities and features and context as an essential condition for competence implementation, it is possible to define the concept of global citizenship competence as an objective characteristic determined by the integrated personal system of mental structures and abilities. It assumes mobilization of interdisciplinary convergent knowledge, cognitive skills and strategies, advanced practical abilities and aptitudes based on new technology application, as well as social and behavioural components comprising responsible attitudes, regulated emotions, values, ethics, morality and motivation, all of which are functionally directed towards a positive result achievement in a particular context [57].

As we can see from the model, the functional orientation of GCC (need, demand of certain qualities for a particular activity) and context (the environment in which a person fulfils his activity) can change. However, the inner structure (comprising innovative knowledge, cognitive skills and strategies, advanced practical abilities based on new technology application, responsible attitudes, regulated emotions, motivation, values and ethics) remains constant.

The model encompasses the principle of 'bearings' driven by the need for enhancement and knowledge added value – that is the core of the human thinking and behaviour, which is also reflected in lifelong learning and social activities. The focus is on producing students who are broad-minded and technologically empowered and possessing global system thinking, critical thinking and contextual thinking (learning transfer), as well as organization and communication skills and problem-solving and decision-making abilities, thus, contributing to the convergent/interdisciplinary skill development [57–59]. It prepares them to follow the evolution of knowledge and technologies, to be active responsible citizens today and speak knowingly on questions dealing with quality of life within their local communities and the global society.

Global citizenship competence is directed to an active interdisciplinary learning process based on the convergent NBICSH science and technology education addressing the values of welfare for all, equality, inclusion and cooperation. It presents people with an opportunity to set on an educational voyage that starts from a basic awareness of sustainable human development, the priorities of international cooperation, passes through the understanding of the causes and effects of global issues and of the new possibilities offered by new emerging sciences and technologies and ends with a personal dedication through informed decision-making. It encourages a full participation of all citizens against exclusion and towards the influence on economic, social and environmental policies at both national and international levels, so that they are fair, sustainable and based on respect for human rights. It is the concept that supports a new model of interdisciplinary education based on the full awareness of the dignity, which is inherent in every human being, on the belonging to a local and global community and on the active commitment to contribute to the society that is more just and sustainable.

Education and personality development are closely interdependent and have very much in common, although pedagogical science distinguishes between these two notions. Educational content includes knowledge and awareness of its place in the scientific environment, as well as learning strategies and metacognitive strategies.

Developmental content deals with the awareness of moral values, norms, rules, laws and ideals. Education has to do mostly with the intellect, whereas personality development appeals to motivational and needs spheres of an individual. Both processes influence consciousness, behaviour and emotions and determine the development of a personality. Furthermore, the entity of the process, the unity of education and personality development, constitutes the main methodological principle of education, which is especially topical at present. Hence, global citizenship competence (GCC) cannot be restricted to a separate subject. It has to be pervasive – to constitute an integral part of all education and it has to be lifelong – continuing throughout life.

# 11.9 Nanochallenges: Nanomanagement, Nanoeducation, Nanothinking and Public Participatory Technology Assessment (pTA)

One decade into the twenty-first century, people and governments worldwide face decisions involving complex scientific considerations or innovations in technology. The new participatory democracy demands that citizens be asked to make judgements, and even vote, on subjects about which they know very little – the desirability of cloning animals and human beings, creating novel biological organisms, manipulating matter at an atomic scale, eugenics, genetic engineering, GM foods and nanoproducts and other great moral and economic questions of the day. But the technologies that so radically redefine our standards of living, health and mortality will also profoundly challenge our social support systems and cultural values.

Therefore, educational systems have to produce a steep increase in students' and general public's intellectual potential in order to provide responsible answers to such complex questions, previously the domain of university researchers.

The world has gone through historical processes that are dramatically and rapidly transforming our social, educational and business environment, producing far-reaching effects on our life styles and our habitat. People all over the world have become increasingly interconnected and interdependent. Educational environment is becoming a new supercomplex system with a constantly expanding and changing intellectual pattern.

In addition, the society has gone through many experiences and technological advancements which are taking us away from 'the world we live in' towards 'the world we want to live in'. Technological progress, especially related directly to basic human rights, needs to be accessible for all consumers and given priority over economic interests, thus contributing to equal opportunities.

On the other hand, current developments in scientific and technological research raise a number of ethical questions comprising responsibility. Areas of research as nanotechnology and biotechnology, regarding food, healthcare and environmental issues, elicit complex and undeniable debates within society today.

Despite steadily increasing dependency of modern consumer societies on nanotechnology, society-wide understanding of these new emerging technologies necessary for informed and critical decision-making is usually lacking. The implications of these processes are critical because the consumption behaviour in technologically empowered societies has a profound effect on the present quality of life and that of the future generations. Higher education is the primary agent of transformation towards sustainable development and future knowledge society.

It has been predicted that today school-leavers will have many careers – not just jobs, over their lifetimes – and that more than 50% of the jobs they will be doing do not exist yet. However, one thing is certain – they will be doing knowledge jobs, intellectually more demanding and almost certainly involving interaction with technologies far more sophisticated compared to those existing at present [60, 61].

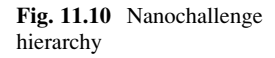
It is regrettable to recognize that the structure of our universities has changed very little in the past 50 years. What we witness today is that higher education is not about understanding reality but about accumulating knowledge through individual subjects which are disconnected from each other and decontextualized. If we want higher education to become an intellectual engagement that goes beyond the study of specific issues inserted in a single subject within the broader context of compulsory curricula, it needs to adopt the systemic approach based on NBICSH science and technology education, which corresponds to the educational demands of today and the nearest future.

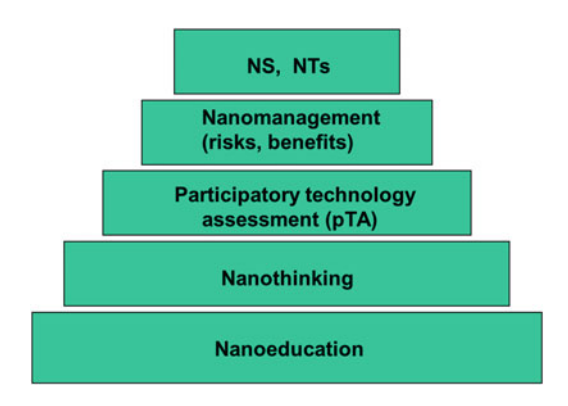
In fact, this situation has led to a number of important considerations related to the principles of interdependence in nature and society as a holistic system demanding solutions for key educational and societal challenges, which is only possible based on the convergence of multiple knowledge and technology. Convergence is as essential to our future knowledge society as engines were to the industrial revolution [60].

By 2050 UN and other demographic experts estimate that the global population will have reached approximately nine billion people. New advanced technologies and, particularly, nanotechnologies will be critical to feed, dress and house this number of people living in the environment stressed by climate change, global economic recession, exponential population growth, widespread fuel and raw material shortages, environmental deterioration and societal problems [61].

Some experts point out that the demographic decline in Europe, combined with the lack of vocation in youngsters for hard sciences, will generate a dramatic shortage of qualified workers in less than a generation. This will jeopardize the standard of living of Europeans in key areas such as medical research, healthcare, information technologies, food and knowledge-intensive industries [56].

Nanotechnology – the creation, manipulation and application of materials at the nanoscale – involves the ability to engineer, control and exploit the unique chemical, physical and electrical properties that emerge from the infinitesimally tiny





man-made particles, but the areas where nanotechnologies are set to make a tremendous difference are expanding alongside with the challenges they pose to society. Challenges in nanotechnologies can be presented in their hierarchical priorities (Fig. 11.10).

Nanochallenges comprise such basic areas as *nanoeducation*, *nanothinking*, *participatory technology assessment (pTA)* and *nanomanagement (incorporating risks and benefits)* to contribute to the creation of new branches of *nanosciences* and *nanotechnologies* [47].

### 11.9.1 Nanomanagement: Risks Versus Benefits

There is irony in the reasoning of some 'smarties', who turn a critical eye towards the term 'nanomanagement' that they correlate with tiny dimensions by analogy with 'micro' and 'macro' instead of implying the direction of activities. Without further much ado about nothing, it should be noted that the term 'nano' (as an abbreviation or scientific slang) is applied to everything that is associated with nanotechnology – nanoscience, nanotechnology, nanoengineering, nanomedicine, nanoproducts, nanoeducation, nanothinking, etc. – which, definitely, does not imply that all these phenomena are minute. On the contrary, they promise huge possibilities to capture imagination!

Since nanotechnology is an inherently interdisciplinary field, *nanomanagement* suggests the organization and coordination of the activities in multiple areas of science, technology and engineering to create a vast technological synergy with educational institutions, R&D, industry, governmental structures and public authorities in order to achieve defined innovative objectives [4].

Awareness of nanotechnology has dramatically risen in recent years among lawmakers, regulators and environmental activists alike. However, the question of how best to regulate nanotechnology is not new. It was first raised in March 1989 by David Forrest in a paper originally written for a course on law, technology and public policy at the Massachusetts Institute of Technology. As Forrest so elegantly

stated almost three decades ago: 'The emergence of new technologies continually forces us to ask whether our laws provide the proper balance between protecting us from potentially harmful consequences of those technologies, and allowing us to reap the benefits. The development of nanotechnology, a molecular-precision manufacturing technology which is surprisingly close to realization, will seriously challenge the ability of our regulatory system to respond quickly and to maintain the critical balance between dangers and benefits' (Forrest 1989).

Forrest demonstrates an uncanny degree of foresight, especially given that nanotechnology was at a very early stage of development at the time it was written. Almost 30 years after the publication of Forrest's 1989 paper, there is still much that we do not know about the potential impacts of nanotechnology, and this raises a number of regulatory issues. Questions arise as to which regulatory or policy instruments or approaches are most effective and appropriate for managing the categories of potential risks associated with nanotechnology. For example, should the applications of nanotechnology, either in whole or in part, rely solely on premarket regulatory risk assessments? Should nanotechnology-enhanced products be subject to obligatory reporting or labelling requirements? On one extreme: should regulatory authorities adopt a wait-and-see reaction, until further information regarding toxicity and exposure becomes available? On the other extreme: should regulators impose product restrictions or even a moratorium until a full assessment of risk becomes possible?

Regulatory regimes designed to protect human health, consumer safety and the environment in many countries, including the USA and the EU, were accepted long before the prospect of nanotechnology was yet on the horizon. Given the state of knowledge at the time, regulatory requirements were designed to assess the toxicity of bulk (macro and micro), not nano, materials. The issue is that the risk assessment criteria, regulatory oversight triggers, toxicity parameters and threshold minimums outlined in health, safety and environmental regulations are no longer applicable in the context of nanotechnology-enhanced products.

The broader issues associated with nanotechnology relate to risk governance, which goes beyond the scope of risk assessment and risk management. The term risk management refers to the decision-making process regarding acceptable levels of risk. Traditionally, such decision-making relies heavily on technical evidence obtained through science-based risk assessments.

In the area of environmental regulation, one of the key questions to be addressed pertains to the establishment of a regulatory definition for engineered nanomaterials. In other words, should nanoforms of well-characterized materials, for example, carbon or silver, be defined as 'new' or 'existing' chemicals? Individual jurisdictions' chemical management frameworks are generally structured in such a way that health and environmental risk assessments must be conducted for any chemical with a new Chemical Abstract Service number (i.e. one, which is not already included in the jurisdiction's chemical inventory). By this standard, a large number of engineered nanomaterials may be exempted from regulatory scrutiny, even though they may possess distinct properties that could have health, safety and potential environmental impacts. One issue therefore becomes the challenge of

defining under which circumstances a nanomaterial should be considered, in regulatory terms, a new chemical, and then determining how such a chemical should be administratively handled [22].

Nanotechnology presents both an unprecedented challenge and unparalleled opportunity for risk management. The challenge arises because nanotechnology does not fit traditional risk management models, thereby hampering efforts to manage its risks using existing approaches. The opportunity arises because nanotechnology will force risk managers to develop innovative risk management approaches that may be applicable to future emerging technologies. As nanotechnology has emerged from the laboratory into industrial manufacture and commercial distribution, the potential for human and environmental exposure, and hence risk, has become both reality and priority. Nanotechnology risk is dependent upon toxicity and exposure:  $RISK = EXPOSURE \times TOXICITY$  [42, 47].

Nanotechnology risks associated with health hazards can be eliminated, or at least greatly reduced, by minimizing exposure to nanoparticles. Nanoparticle toxicity is complex and multifactorial, regulated by a variety of physicochemical properties, such as size, chemical composition and shape, as well as surface properties such as charge, area and reactivity [62]. As the size of particles decreases, a resulting larger surface-to-volume ratio correlates with increased toxicity as compared with bulk material toxicity. Also, as a result of their smaller size, nanoparticles can pass into cells directly through cell membranes or penetrate the skin and distribute throughout the body. While the effects of shape on toxicity of nanoparticles appear unclear, the results of a recent study suggest that single-walled carbon nanotubes are more toxic than multiwalled carbon nanotubes. Therefore, with respect to nanoparticles, there is concern for systemic effects (e.g. target organs, cardiovascular and neurological toxicities) in addition to portal of entry (e.g. lung, skin, intestine toxicity).

Risk management of nanotechnology is challenged by enormous uncertainties about the properties, risks, benefits and future direction of nanotechnology applications. Moreover, traditional risk management principles such as acceptable risk, cost-benefit analysis and feasibility (or best available technology) as well as a more recent precautionary principle are all inadequate to the risk management that nanotechnology challenges present due to the pervasive uncertainty and great dynamism of this rapidly developing technology. Yet simply to expect that these ambiguities were resolved by themselves, before attempting to manage nanotechnology risks, would not be reasonable, in particular, because of the growing public concerns driven by risk perception incomprehension concerning exposure, affect and availability.

However, there is an innovative the so-called responsive regulation approach – a complex regulatory system incorporating several levels of responsibility:

- 1. Self-regulation (persuasion, warnings) 'soft law'
- 2. Enforced self-regulation (civil penalties)
- 3. Command regulation with discretionary punishment (licensure penalties)

4. Command regulation with nondiscretionary punishment (criminal penalties) – 'hard law'

This system is incremental, flexible and decentralized to fill the risk management gap [63]. Still, the fate of humankind is not a spectator sport. The health implications of nanoparticlesNanotechnology: are unknown, the ramifications may be profound, and only lengthy and extensive research efforts can assess the safety implications with any certainty. A more reliable, comprehensive and cooperative approach is required. Such an approach will not only help manage threatening risks from nanotechnology but will also serve as a model for managing future emerging technologies.

Public policy has to be grounded on understanding the risks and benefits of new technologies. Uncertainties surround nanotechnology and reinforce the doubts of consumers [64].

#### 11.9.2 Nanoeducation and the Global Consciousness

During the past 10 years, we have seeded many ideas into the global consciousness to stimulate preparing our students and the general public for their future. The world is changing, but our education matrix remains in the industrial version of reality. We are not even close to understanding nor preparing our students for these major changes they will face in the next few decades. Education must be transformed in the twenty-first century due to the higher level of knowledge reached by the world societies, accelerating progress in foundational emerging technologies and the creation of new industries and jobs at their frontiers and interfaces, developing information exchange and interaction, improving lifelong wellness and human potential and advancing a cognitive society. Knowledgeable citizens in a diverse democratic society should be reflective, moral, responsible and active citizens showing enough knowledge, skills and commitment needed to make the world safe and well-secured habitat for all.

Nanoeducation is the new foundation for the integration of all disciplines for the next generation to expand our student's knowledge base and prepare them for a very different future in a global society enhanced by all of the integrated science research now in process [47]. Nanoeducation concept envisions launching a broad-based integration of nanoscale science and engineering (NSE) concepts into the classrooms starting already from the secondary school. As scientists develop the ability to work at levels thousands of times smaller than a human hair, a new world of possibilities – and critical concerns – opens up. Nanoeducation explores the social, ethical and personal implications of advances in nanotechnology. The program should be directed to ask policymakers, researchers and activists to wrestle with difficult but essential issues that will impact the environment, human health, public safety and individual privacy.

The contribution of nanoeducation courses to the development of the student's personality as a citizen and his intellect as a consumer of the twenty-first century has to be reflected in the purpose of the courses. The main objectives are to explore the nanotechnology potential benefits and possible risks for human health, safety and security and the environment, to work internationally with fellow citizens to identify common values and institutions that will protect these values and to make them active.

To fuel students' reflections and curiosity and allow them to cultivate their own citizenship personality, nanoeducation acts as a compass to help them position themselves within the whole of humanity. It is up to them to decide what kind of human being they want to be today, in their own immediate environment. Nanoeducation envisions developing *intellectual attitude to life* in our students.

From this standpoint, students can establish with others a meaningful, fulfilling and humane relationship. Such activities as creating a forum, for instance, where students can pursue their reflections and discussions with colleagues, as social players and not as mere spectators to discussions about nanotechnology realities of which they know little or nothing, are a good measure of the contribution that nanoeducation courses bring to the development of citizenship awareness among students.

Many companies throughout Europe and the world report problems in recruiting the types of graduates they need, as many graduates lack the skills to work in a modern economy. For Europe, to continue to compete alongside prestigious international institutions and programmes on nanomaterials, it is important to create educational institutions, which would provide a top-level education and the relevant skill mix and would cover education, training, sciences and technologies for research and have strong involvement by European industry. The elements for such a top-notch education are:

- Multidisciplinary skills.
- Top expertise in nanomaterials science and engineering.
- Literacy in complementary fields (physics, chemistry, biology).
- Exposure to advanced research projects.
- Literacy in key technological aspects; exposure to real technological problems.
- Basic knowledge in social sciences, culture, management, ethics and foreign languages.
- Literacy in neighbouring disciplines: international business, law, IT, etc.
- Interlinkages between education, research and industrial innovation: students will be ready for what research and development will provide.
- Sharing of post-docs, master's and PhD students to foster the mobility of permanent researchers and professors between different institutions to create 'team spirit' [47].

Companies, universities, governments, research organizations and technical societies must all strive to define their roles in this partnership. The 'output' will be graduates with a new way of thinking, skilful manipulators, synthesizers and

creators of new knowledge excellently equipped to solve future complex problems and to work collaboratively.

Nanoeducation is an integrated skills project built around active learning methods to promote an active discussion-based approach to developing responsible scientific citizenship and new emerging consumption practices. It offers an opportunity for students from a wide range of disciplines to learn about nanotechnologies, to explore their risks and benefits and to reflect on the place of nanotechnologies in their personal life, in their future professional practices and the modern consumer society.

The teaching objective of these academic activities is to create an openness of mind and criticism of thought in students for a very broad range of knowledge. This will help them position themselves within the vastness of current scientific knowledge and technological development that is shaping our modern society – scientific knowledge and development that could have major consequences on the fundamental way we see intellectual consumption, scientific citizenship and the sustainable development of the society we live in.

Nanoeducation envisions teaching students to move with the times and stay abreast of the fundamental knowledge of the day in order to understand what is at stake and participate in key social debates and informed decision-making. The option offered by a new era of emerging technologies to all of us on the planet today can be spelled out in the words: nanoeducation can be considered a privileged discipline for supporting the development of responsible intellectual citizenship in the twenty-first-century technologically empowered global society.

### 11.9.3 Nanothinking as an Educational Concept of the Twenty-First Century

Data saturation that accompanies our new technologies' age has fostered an everincreasing feeling of dependency among people. The pace of expected adaptation is accelerated to a pace that exceeds individuals' abilities to accommodate. Being on the receiving end of technologies, torrent serves to undermine people's confidence and sense of personal responsibility, giving rise to the sense of helplessness that many people feel as the world enters the age of global 'technologization'.

Nanothinking can serve as the antidote to the sense of helplessness since it is a concept for seeing the 'structures' that underlie complex processes, for a much better understanding how our organism correlates with the outside world and for discerning how to foster health, safety and the surrounding environment. Our life is reduced due to ignorance and neglect of the elementary things concerning our health. If we do not understand ourselves, we will not be able to change our life for the better.

Nanothinking is a comprehensive system thinking which offers a language that begins by restructuring the way how we think. It is a dynamic concept where

practitioners continually engage in a process of 'seeing wholes' – a perspective that pays attention to the interrelationships and patterns of influence among constituent parts to foster the dissolution of compartmentalization of science and the corresponding compartmentalization of the mind [65].

Contemporary top-notch education envisions causing students think systemically – integrating not only macro- and micro- but also the nanoscale. *Nanothinking* can be defined as *visualizing matter*, *structures* and *processes at the nanoscale*. *Nanothinking* can be viewed as *the understanding of nanophenomena within the context of a larger whole*. To think nanoscalely means to put things into a nanoscale context and to establish the nature of their relationships within larger contexts [65].

Nanoscientists are now enthusiastically examining how the 'living world works' in order to find solutions to long-standing problems in the 'nonliving world'. The way marine organisms build 'strength' into their shells or insects create the most amazing structures has lessons on how to engineer lightweight, tough materials for vehicles and other applications or to improve the design and create even better structures for buildings and the environment. The way a leaf photosynthesizes can lead to techniques for efficiently generating, converting and storing renewable energy. Even how a nettle delivers its sting can suggest better vaccination techniques.

Natural systems provide us with solutions, but solutions are usually package solutions with concepts strongly interconnected one with the other. The problem is that too much of our thinking today in business is poor business based on poor competence. We have one knowledge and we have one market. The time has come to rethink the system. And if we are prepared to rethink (probably due to the crisis) the business world, we will be able to rethink how to put innovative structures and systems into the production process for the benefit of the whole society and every individual.

Education in this highly technological global economy has to play a double role. First, it has to provide a top-level, systemic, multidisciplinary education to graduates able to think innovatively and creatively and, second, to educate the general public, thus, shaping public consciousness.

Public thinking can be formed and expanded through sustained and carefully crafted dialogue, which has to be integrated into educational communication practice. Educational communication has to contribute to developing a new way of thinking – the systemic thinking, with the main strategy – 'how to think' rather than 'what to think'. It is the privilege only of liberal universities not to give the right answers to students but to put the right questions [65].

The development of a new way of thinking envisions bringing the practice of participatory technology assessment (pTA) into alignment with the realities of the twenty-first-century technology – to create a twenty-first-century public consciousness model.

## 11.9.4 Public Participatory Technology Assessment (pTA) in Risk Management

New developments in technology usually start out with strong public support, as the potential benefits to the economy, human health or quality of life are proclaimed. The ability to create novel biological organisms, manipulate matter at an atomic scale or intervene significantly (and possibly irreversibly) in the earth's climate system raises a lot of ethical, social, legal and environmental questions that will require broad public discourse and debate. Any technology that promises so much change is bound to generate controversy, because with such awesome power comes the capacity to penetrate beyond boundaries that society has deemed acceptable.

Societal and ethical concerns can rapidly turn any technological philosophy to oblivion. These concerns are often focused on fundamental moral and social perceptions of being human and humanity's relationship with the natural world. The debates surrounding many of the emergent technologies that preceded nanotechnology can help us predict a likely future path for the controversy surrounding nanotechnology. One such example is provided by the debate over GM foods. Genetic engineering promised a revolution in medical care, including the ability to cure or prevent diseases with a genetic basis such as Huntington's disease, haemophilia, cystic fibrosis and some breast cancers. Manipulation of plant genomes promised a revolution on how food is produced, by engineering crops with increased yield, nutritional content and shelf life.

Not all potential impacts of nanotechnology will be social in nature. After all, the technology is based on the production and use of materials. Therefore, issues of environmental and toxicological effects must also be addressed. History is replete with examples of technologies or materials that were enthusiastically embraced by society and then found years later to cause environmental contamination or disease. The chemical DDT killed disease-bearing mosquitoes, thus allowing areas with tropical and subtropical climates to be more safely populated and developed, yet was ultimately banned in the USA after it was linked to destruction of animal life. CFC-based refrigerants allowed for affordable air conditioning yet were ultimately banned after they were linked to destruction of the ozone hole. Asbestos was used as a fire retardant and insulator in many buildings until it was found to cause a deadly lung disease. Some materials, such as semiconductors, are not in themselves known to be harmful but are produced through environmentally burdensome processes.

Nanotechnology has tremendous potential to improve human health and the environment. However, it could also have unintended impacts. Nanoparticles' ability to penetrate into living cells could be exploited to produce a new life-saving drug, or it could result in toxicity. Nanomaterials could be used to produce cheap and energy-efficient filters that improve drinking water quality, or they could become environmental contaminants. Given the breadth of materials and devices that fall under the broad umbrella of nanotechnology, all of these outcomes may result to one extent or another.

Scientists and researchers engaged in nanoscience and nanotechnology research and development constitute a relatively small group compared to the general public. However, the outcomes of their work – innovative materials, systems, devices and technologies – have a strong impact on the life of every citizen and the whole human society.

The research into health, safety and the environmental implications of nanotechnology lacks universal strategic direction and coordination. As a result, researchers are unsure about how to work safely with new nanomaterials, nanobusinesses are uncertain about how to develop safe products, and public confidence in the emerging applications is in danger of being undermined.

In light of these developments, it is important that the relations between science, technology and society be given proper attention in nanoeducation of general public. It is about ensuring that everyone has the knowledge and skills to *understand*, *engage with* and *challenge* the main pillars of nanoeducation – *society*, *technology* and *processes*.

However, public capacities do not develop unaided. They have to be learnt. If citizens are to become genuinely involved in public life and affairs, a more explicit approach to public education and involvement is required to deal responsibly with new technologies.

In the first place, public concerns include the ensuring of peoples' physical integrity and safety (as the condition of being protected against physical, social, financial, political, emotional, occupational, psychological, educational or other types or consequences of threats).

Technology assessment (TA) is a practice intended to enhance societal understanding of the broad implications of science and technology. This creates the possibility for citizens of the world to influence constructively technology developments to ensure better outcomes. Participatory technology assessment (pTA) enables the general public/laypeople, who are otherwise minimally represented in the politics of science and technology, to develop and express informed judgements concerning complex topics, as well as to make informed choices. It addresses the context of social desirability of innovations looking into processes of technical modernization, changes in the interface between humans and machines/products and ethical issues concerned with the boundaries of intervention into the environment and the human body [65].

Therefore, citizens' acceptance is compulsory for further developments in the field of nanotechnology and its applications. Consequently, it is of the utmost importance to educate citizens and to disseminate the results of nanotechnology development in an accurate and open way so that the general public will eventually transform their way of thinking to accept nanotechnology. In this endeavour, educational institutions have a pivotal role in developing pTA practices by:

- Educating citizens (including pupils, students) about science and technology
- Informing the public about the benefits and risks of nanomaterials and nanoproducts

- Evaluating, minimizing and eliminating risks associated with the manufacturing and use of nanomaterials and nanotechnology enabled products (risk assessment)
- Exchanging with public authorities for the risk management of nanotechnologies

In the process, pTA deepens the social and ethical analysis of nanotechnology, complementing the expert-analytic and stakeholder-advised approaches. The Internet and interactive TV capabilities can help pTA be more effective and cost-efficient and would also align with the policymakers' initiatives to make them more transparent, accessible and responsive to citizens' concerns.

## 11.10 Concluding Remarks

People are collaborative creatures – it is how we are. We are driven by the need to think for ourselves – it is how we survive. If we remember that, we can have everything that we need to deal with the problems facing the global society. It is our world to shape, not just to take! The time to start shaping the future is always in the present. Yet the future is not just new technologies: health issues, economic trends, population growth and environmental problems – just a few to name. However, to become future-ready, it is worth noting that new technologies are not everything, but everything without new technologies is nothing!

Nanotechnology creates massive challenges and massive opportunities in the years to come. It is expected to have a significant impact on every sector of the economy. The ability to create unusual nanostructures such as bundles, sheets and tubes holds promise for new and powerful drug delivery systems, electronic circuits, catalysts and light-harvesting materials. As manufacturing methods are perfected and scaled up, nanotechnology is expected to soon pervade and often revolutionize, virtually every sector of industrial activity, from electronics to textiles, from medicine to agriculture and from the energy we use to drive our cars and light our homes to the water we drink and the food we eat. Nanotechnology is today's version of the space race, and countries around the globe are enthusiastically investing billions of dollars into support of research, development and commercialization. Today, the long-term goals of nanotechnology development might sound like scenarios straight out of science fiction. However, science fiction may soon become science fact.

In terms of human health and the environment, nanotechnology also presents the same enigma as past major technological advances: there may be enormous benefits in terms of benign applications, but there are inherent risks as well. What will happen when nanomaterials and nanoparticles get into our soil, water and air, as they most assuredly will, whether deliberately or accidentally? What will happen when they inevitably get into our bodies, whether through environmental exposures or targeted applications? The answers to those vital questions remain largely unanswered, although some latest findings are less than reassuring.

Questions of another sort also need to be answered. Is anyone looking at these health and safety issues? And can enough solid, reliable risk assessment knowledge be gained in time to ensure that the public will be comfortable with the proliferation of the technology? Or will issues of safety and trust, surrounding nanotechnology with controversy, hinder its potential as happened in the past with such achievements as genetically modified organisms (GMOs)? To ensure that nanotechnology is striding confidently and responsibly, with strong public support, it is very important to identify and collect risk data so that questions can be answered and problems addressed early enough on the way of the technology development.

On another level, at the intersection of technology and society, there is a new angle to think of some timeless issues. Is nanotechnology good? What is progress? How much risk are we willing to take? How does politics and society drive technology and vice versa? Why should we care about the societal implications of nanotechnology? These are profoundly important questions, the answers to which are to be found on the counterbalance of technologies and humanities. Without that counterbalance, society risks scientists without conscience, technicians without taste and policymakers without responsibility.

Values reflect and shape the ongoing social development, and debates surrounding nanotechnology should be guided by public participation. The world is undergoing fundamental change that goes to the heart of the individual – society relationship on which the concept of sustainability is founded. Understanding the impact of a new technology on society is vital to ensuring that development takes place in a responsible manner. Scientific knowledge is expected to play some role in educating citizens about their powers and responsibilities. In this case, the citizen is not a mere consumer but a person whose opinions are valued.

Education should help students and general public to develop thoughtful and technologically knowledgeable identifications with their cultural communities, nation-states and the global community. It also should enable them to acquire a clear understanding, attitudes and skills needed to act to make the nation and the world more scientifically literate and just. It is of the utmost importance to educate the general public and to disseminate the results of nanotechnology development in an accurate and open way so that people will eventually accept nanotechnology.

Convergence of the humanities with technosciences envisages the development of systemic, multidisciplinary knowledge instilling that:

- Knowledge should have a social purpose to improve life conditions based on the abilities to cope with and perhaps anticipate changes imposed by technoscientific developments.
- Learning should comprise the acquisition of advanced practical skills and the abilities to forecast the socio-ethical values of technoscientific developments.
- Learning requires an action scale in order to develop skills and abilities to assess
  the significance of new technoscientific developments and thus be engaged in
  educated problem-solving and responsible legislative decision-making.
- Education has to be emotive as well as cognitive promoting systems, global consciousness.

- Education should recognize pluralism and diversity developing perspective consciousness.
- Education should have a global perspective and involve the study of major technological global challenges, as well as to promote environmental awareness.
- Education should have a futuristic range and process mindedness, implying that learning and personal development are continuous and with no fixed destination.

A democracy needs an educated citizenry. To participate in a democracy influenced by technology, not only do citizens need to know how to understand the multiple technological perspectives that they encounter, they need to feel an obligation to explore multiple perspectives to fully understand the society they live in and make informed decisions. When we do not pay close attention to the decisions we make, when we fail to educate ourselves about the major issues of the day and when we choose not to make our voices and opinions heard, that is when democracy breaks down.

Nanotechnology is expected to have a significant impact on every sector of the economy through the use of nanostructured materials in medicine; the enhancement of consumer products; the means of soil and water purification; the production of clean energy and reduction in energy consumption; the creation of nanobiosensors; the new materials for optics, photonics and nanoscopic magnets; the development of new techniques for the fabrication of large-scale structures; the replacement of silicon-based technology for electronics and computing; etc.

We are facing unprecedented global challenges such as the depletion of natural resources and climate change, pollution, scarcity of clean water and providing food and energy to a growing world population and poverty. These problems are directly linked to the current development of nanotechnologies for manufacturing products and producing energy. The exploitation of nanotechnology and nanomaterials is the key development that can significantly address these global problems by changing both the products and the means of their production and addressing pressing needs in welfare, healthcare, security, safety, communications and electronics.

Nanotechnology is a double-edged sword – on the one side, there are benefits and, on the other side, risks. Still, we have to weigh all pros and cons of this technology. We all have learned how to cope with television, mobile phones and even airplanes in a safe way because we need their benefits. A synonym for uncertainty is ignorance. We face risk because we are ignorant about the future. If we were omniscient, there would be no risk. Because ignorance is a personal experience, risk is necessarily subjective. When we put a number on risk, this number says as much about us – how little we know – as it says about the world around us.

Unfortunately, the nanotechnology questions to be answered are so numerous that it will take years to compile the relevant data. Key concepts in the coming years include expanding our knowledge of nanoparticles and making this knowledge readily transparent and available, identifying and where necessary taking appropriate risk management measures and contributing to this field by supporting research and development and promoting cooperation between governments and NGOs, scientific communities and educational institutions and manufacturing and trade industries.

## References

- 1. Scott J **2000** Rational Choice Theory In: Contemporary Society: Theories of The Present Eds G Browning, A Halcli, F Webster Understanding (UK: Sage Publications) http://www.soc.iastate.edu/sapp/soc401rationalchoice.pdf
- 2. Ariely D **2008** Predictably Irrational: The Hidden Forces That Shape Our Decisions (NY: Harper Collins Publishers) 20p
- 3. Opportunities and risks of Nanotechnologies 2010 Report in cooperation with the OECD International Futures Programme Allianz Center for Technology OECD http://www.oecd.org/science/nanosafety/44108334.pdf
- 4. EPA 2009 Nanotechnology White Paper (US Environmental Protection Agency (EPA)-Washington: Science Policy Council Nanotechnology Workgroup
- Viswanath B, Kim S 2016 Influence of Nanotoxicity on Human Health and Environment: The Alternative Strategies Ed P de Voogt Reviews of Environmental Contamination and Toxicology 242 Springer International Publishing Switzerland doi https://doi.org/10.1007/398\_2016\_ 12
- Kulinowski K M, Johnson D R, Baker J 2007 Nanotechnology & environmental professionals *EnviroMentor* 6(3)
- https://commons.wikimedia.org/wiki/File:Gold255.jpg Acc Aug 29, 2017 Picture of solution containing gold nanoparticles Source=kondinski.webs.com /Author=Aleksandar Kondinski / Date=2.01.2010
- 8. Vance M E, Kuiken T, Vejerano E P, McGinnis S P, Hochella M F Jr, Rejeski, D, Hull M S **2015** Nanotechnology in the real world: Redeveloping the nanomaterial consumer products inventory *Beilstein Journal of Nanotechnology* **6** 1769–80 https://doi.org/10.3762/bjnano.6. 181
- National Nanotechnology Initiative Strategic Plan, National Science and Technology Council Committee on Technology (CoT) 2016 Subcommittee on Nanoscale Science, Engineering, and Technology (NSET) http://www.nano.gov/sites/default/files/2016\_nni\_strategic\_plan\_public\_ comment draft.pdf
- The Project on Emerging Nanotechnologies. Consumer Products Inventory 2015 http://www.nanotechproject.org/cpi
- Paull J, Lyons K 2008 Nanotechnology: the next challenge for organics Journal of Organic Systems 3(1) 3–22
- 12. Nanowerk 2017 http://www.nanowerk.com/nanotechnology-in-food.php (Acc Aug 14 2017)
- 13. Dudefoi W, Terrisse H, Richard-Plouet M, Gautron E, Popa F, Humbert B, Ropers M H 2017 Criteria to define a more relevant reference sample of titanium dioxide in the context of food: a multiscale approach *Food Additives & Contaminants:* Part A 34(5) 653–65
- 14. Miller G, Senjen R **2008** Out of the Laboratory and onto our Plates: Nanotechnology in Food & Agriculture. A report prepared for Friends of the Earth Australia Friends of the Earth Europe and Friends of the Earth United States and supported by Friends of the Earth Germany Friends of the Earth Australia Nanotechnology Project, Australia; **2008** Out of the Laboratory and on to Our Plates: Nanotechnology in Food & Agriculture (Washington, DC: Friends of the Earth) http://libcloud.s3.amazonaws.com/93/b5/4/547/Nanotechnology\_in\_food\_and\_agriculture\_-\_web\_resolution.pdf
- 15. Mellinas C, Valdés A, Ramos M, Burgos N, Garrigós M C, Jiménez A **2016** Active edible films: Current state and future trends *Journal of Applied Polymer Science* **133**(2) 1–15
- Sekhon B S 2010 Food nanotechnology an overview Nanotechnology, Science and Applications 3 1–15
- Janjarasskul T, Krochta J M 2010 Edible packaging materials Annual Review of Food Science and Technology 1 415–48
- 18. Bumbudsanpharoke N, Ko S **2015** Nano-food packaging: an overview of market, migration research, and safety regulations *Journal of Food Science* **80**(5) R910–23

19. European Commission. Nanomaterials in Cosmetics 2017 http://ec.europa.eu/growth/sectors/cosmetics/products/nanomaterials/index\_en.htm (Acc. Aug 14, 2017)

- 20. European Commission. Nanomaterials Chemicals Enterprise and Industry 2017 http://ec.europa.eu/enterprise/sectors/chemicals/reach/nanomaterials/index\_en.htm (Acc. Aug 14, 2017)
- Safe Food for European Consumers. European Food Safety Authority EurActiv.com 2017 www.euractiv.com/topics/european-food-safety-authority/ (Acc. Aug 14, 2017)
- European Parliament Committee on Environment, Public Health and Food Safety 2017 http://www.nanowerk.com/nanotechnology-in-food.php (Acc. Aug 14, 2017)
- Hadjidemetriou M, Kostarelos K 2017 Nanomedicine: Evolution of the nanoparticle corona Nature Nanotechnology 12 288–90
- 24. Chen F, Wang G, Griffin J I, Brenneman B, Banda N K, Holers V M, Backos D S, Wu L P, Moghimi S M, Simberget D 2017 Complement proteins bind to nanoparticle protein corona and undergo dynamic exchange in vivo Nature Nanotechnology 12 387–93
- 25. Saptarshi S R, Duschl A, Lopata A L **2013** Interaction of nanoparticles with proteins: relation to bio-reactivity of the nanoparticle *J. Nanobiotechnol.* **11**(26) 1–12 https://jnanobiotechnology.biomedcentral.com/track/pdf/10.1186/1477-3155-11-26? site=jnanobiotechnology.biomedcentral.com
- 26. Ke Changhong **2011** Recent Advances in Nanotechnology CRS Press-Apple Academic Press 306p
- 27. Mobasser Sh, Firoozi A A **2016** Review of Nanotechnology Applications in Science and Engineering *J. Civil Eng. Urban.* **6**(4) 84–93
- 28. Rojahn S Y **2013** What It's Like to See Again with an Artificial Retina MIT Technology Review https://www.technologyreview.com/s/514081/can-artificial-retinas-restore-natural-sight/
- Saha M 2009 Nanomedicine: Promising Tiny Machine for the Healthcare in Future-A Review Oman Med J. 24(4) 242–7
- 30. Talbot D **2013** *An Artificial Hand with Real Feelings* MIT Technology Review https://www.technologyreview.com/s/522086/an-artificial-hand-with-real-feelings/
- Schwitzer G 2010 The future of health journalism Public Health Forum 18(3) 19e1–3 http:// www.chsourcebook.com/01.pdf
- 32. Cook A **2010** Nanoparticles in sunscreens raise questions of safety. Cosmos-The science of Everything http://archive.cosmosmagazine.com/news/nanoparticles-sunscreens-still-raising-safety-questions/
- 33. Lem K W Hsu S-H, Lee D S, Iqbal Z, Sund S, Curran S, Brumlik C, Choudhury A, Hu D. S-G, Chiu N, Lem R C, Haw J R 2012 Waste minimization for the safe use of nanosilver in consumer products-Its impact on the eco-product design for public health In: J Public Health Methodology, Environmental and Systems Issues Ed J Maddock Publishing Process Manager Ch10 217–48 https://www.intechopen.com/books/public-health-methodology-environmental-and-systems-issues
- 34. Chaudhari S P, Damahe A, Kumbhar P **2016** Silver Nanoparticles A Review with Focus on Green Synthesis *International Journal of Pharma Research & Review* **5**(3) 14–28 http://www.rroij.com/open-access/silver-nanoparticles--a-review-with-focus-on-green-synthesis.pdf
- 35. Crocetti G, Miller G (2011) Nano-silver: policy failure puts public health at risk Friends of the Earth Australia http://emergingtech.foe.org.au/wp-content/uploads/2011/10/Nano-silver\_2011.pdf
- 36. Opinion on Nanosilver: safety, health and environmental effects and role in antimicrobial resistance 2014 European Commission Scientific Committee on Emerging and Newly Identified Health Risks SCENIHR http://ec.europa.eu/health/scientific\_committees/emerging/docs/scenihr\_o\_039.pdf
- 37. Hood E **2004** Nanotechnology: Looking As We Leap *Environ Health Perspect*. **112** (13) A740–9

- 38. Becker S **2013** Nanotechnology in the marketplace: how the nanotechnology industry views risk *J. Nanopart. Res.* **15**(1426) https://doi.org/10.1007/s11051-013-1426-7
- 39. Ho S S, Scheufele D A, Corley E A (2013) Factors influencing public risk-benefit considerations of nanotechnology: Assessing the effects of mass media, interpersonal communication, and elaborative processing *Public Underst. Sci.* 22(5) 606–23
- 40. Saleh N B, Aich N, Plazas-Tuttle J, Lead J R, Lowry G V 2015 Research strategy to determine when novel nanohybrids pose unique environmental risks Environmental Science: Nano 2 11–8
- 41. OECD **2016** Nanomaterials in Waste Streams: Current Knowledge on Risks and Impacts (OECD Publishing:Paris) https://doi.org/10.1787/9789264249752-en
- 42. Drew R, Hagen T **2009** Engineered Nanomaterials: An Update on the Toxicology and Work Health Hazards Safe Work Australia https://www.safeworkaustralia.gov.au/system/files/documents/1702/engineerednanomaterials review toxicologyhealthhazards 2009 pdf.pdf
- 43. Cash L **2015** What Is Silicon Dioxide in Supplements? LIVESTRONG.COM http://www.livestrong.com/article/520897-what-is-silicon-dioxide-in-supplements/
- 44. What do people really think about nanotechnologies? How do we imagine our future with nanotechnologies? **2016** *NanOpinion* http://nanopinion.archiv.zsi.at/
- 45. Lobanova-Shunina T, Shunin Y **2013** Consumer insights into nanotechnologies: responsible consumption management *Changes in social and business environment*, CISABE'13 (KTU: Panevežys, Lithuania) 1–7
- 46. Langdon W **2010** The Whale and the Reactor: A Search for Limits in an Age of High Technology (Chicago: University of Chicago Press)
- 47. Lobanova-Shunina T, Shunin Y 2011 Nanothinking as a concept of Citizenship Education for 21st Century Europe *In: Europe's Future: Citizenship in a Changing World* Eds Cunningham P and Fretwell N (London: CiCe) 345–55
- 48. The national nanotechnology initiative. Supplement to the president's budget for fiscal year **2017** Subcommittee on Nanoscale Science, Engineering, and Technology Committee on Technology National Science and Technology Council https://www.whitehouse.gov/sites/default/files/microsites/ostp/nni fy17 budget supplement.pdf
- NATIONAL NANOTECHNOLOGY INITIATIVE (NNI) 2016 Total Funding for NNI https://www.nsf.gov/about/budget/fy2016/pdf/50\_fy2016.pdf
- Roco M C 2011 The long view of nanotechnology development: the National Nanotechnology Initiative at 10 years Springer Science+Business Media https://www.nsf.gov/crssprgm/nano/ reports/MCR\_11-0201\_JNR13\_NNI+at+10+years\_11051\_2010\_192\_print.pdf
- 51. Lobanova-Shunina T, Shunin Y 2014 Innovation management in higher education: Nano sciences and technologies for scientific citizenship In: Innovative Practice and Research Trends in Identity, Citizenship and Education Eds Cunningham P and Fretwell N (London: CiCe) 56–66
- 52. Lobanova-Shunina T, Shunin Y 2012 Nanoeducation for developing responsible scientific citizenship and creating a sustainable intellectual global community In: Creating Communities: Local, National and Global Eds Cunningham P and Fretwell N (London: CiCe) 316–26
- 53. Lobanova-Shunina T Shunin Yu 2016 Convergence of Nano-Bio-Info-Cogno-Socio-Humano Sciences and Technologies for societal benefit and justice *The 14th International Scientific Conference Information Technologies and Management 14–15 April 2016* (ISMA University: Riga) 15–16
- 54. Alexandersson M, Dimenäs J 2012 Crossing Disciplinary Borders: Perspectives on Learning about Sustainable Development. *Journal of Teacher Education for Sustainability* 14(1) 5–19
- 55. Roco M C, Bainbridge W S, Tonn B, Whitesides G 2013 Convergence of knowledge, technology, and society: Beyond Convergence of Nano-Bio-Info-Cognitive Technologies World Technology Evaluation Center (WTEC)
- 56. Lobanova-Shunina T, Shunin Y 2013 Nanotechnologies: challenges and controversy on the way to scientific citizenship, new emerging identities and intellectual consumption In: *Identities and Citizenship Education: Controversy, crisis and challenges* Ed. Cunningham P (London: CiCe) 182–93

References 395

57. Lobanova-Shunina T, Shunin Y 2016 Smart technologies: Nanoeducation and nanothinking as triggering factors on the way to social justice In: Education, Citizenship and Social Justice: Innovation Practices and Research Eds Cunningham P and Fretwell N (London: CiCe) 79–89

- 58. Lobanova T, Shunin Y **2007** Communicative Competences as an Instrument for European Identity *In: Citizenship Education in Society* Ed Ross, A. (London: CiCe) 251–60
- Lobanova T 2006 Teaching Technologies in Profile Education, In: Consumer Citizenship Network: CCN Eds D Tangen and V Thoresen (Hamar Norway: CiCe) 215–26
- 60. Luhmann N 1982 The Differentiation of Society (New York: Columbia University Press)
- 61. Enhancing employability **2016** Report prepared for the G20 Employment Working Group with inputs from The International Monetary Fund https://www.oecd.org/g20/topics/employment-and-social-policy/Enhancing-Employability-G20-Report-2016.pdf
- Vasilevska Nikodinovska V, Mladenovska K, Grozdanov A 2015 Risks and health effects from exposure to engineered nanostructures: a critical review *Journal of Chemical Technology* and Metallurgy 50(2) 117–34
- Braithwaite V 2007 Responsive Regulation and Taxation: Introduction Law & Policy 29

   (1) 3–10
- 64. Falkner R, Jaspers N **2012** Regulating nanotechnologies: risk, uncertainty and the global governance gap *Global environmental politics* **12**(1) 30–55 http://eprints.lse.ac.uk/41579/1/Regulating%20nanotechnologies%20(lsero).pdf
- 65. Lobanova-Shunina T, Shunin, Yu N 2011 Nanothinking as an Essential Component of Scientific Competence and Social Responsibility in the 21st Century Society Computer Modelling and New Technologies 15(1) 58–68
- 66. Nowack B, Baalousha, M, Bornhöft N, Chaudhry Q, Cornelis G, Cotterill J, Gondikas A, Hassellöv M, Lead J, Mitrano D M, von der Kammer F, Wontner-Smith T **2015** Progress towards the validation of modeled environmental concentrations of engineered nanomaterials by analytical measurements *Environ. Sci.: Nano* **2** 421–8
- 67. Stensberg M C, Madangopal R, Yale G, Wei Q, Ochoa-Acuña H, Wei A, Mclamore E S, Rickus J, Porterfield D Marshall, Sepúlveda M S 2014 Silver nanoparticle-specific mitotoxicity in Daphnia magna Nanotoxicology 8(8) 833–42

A	crystalline and noncrystalline materials, 11
Acid-catalyzed carbon aerogels, 192	energy gap and the interatomic distance, 12
Adiabatic approximation, 33	high-pressure compressions, 11
Aerogels, 25	nano-faults, 10
acid-catalyzed carbon, 192	photoinduced changes, 12
CNTs, 187, 192	relaxation time, 10
definition, 187	semi-quantitative model, 11
evolution, 187, 188	short-range structures, 13
functionalization, 192-195	statistical approach, 10
graphene, 187	temperature dependence, 13
Hooke's law, 188	theoretical models, 12
metal, 191, 192	Atomic force microscopy (AFM), 21
metal oxide, 189	Atomic nanostructures
nanoporous metal foams, 190	broken topology, 19
Ohm's law, 188	condensed materials, 18, 19
organic and carbon, 189, 190	concepts of disorder, 19, 20
quantum dot, 191	continual disorder, 20
semiconducting metal chalcogenide, 190	magnetic disorder, 18
silica gels, 189	methods, 21, 22
strong and flexible, 190, 191	nano-, micro- and macrophysical
Allotropic form, 253–262	properties, 18
Analcime, 24	nanoporous and nanocomposite
Angular momentum, 272–274	materials, 20
Anthracene, 253, 263–265, 267	nanoscale materials, 21
Antibonding orbitals, 267	production, 22
Armchair GNR–Me end-type interconnect	RDCA, 22
formation, 91	topological disorder, 20
Atmospheric pressure chemical vapour	Atomic potential functions
deposition (APCVD), 222	differential equations, 35
Atomic-electron correlation	electron gas density, 36
absorption coefficient, 12	exchange-correlation correction, 38
amorphous semiconductors, 13	exchange-correlation potential, 37
Bloch theorem, 10	Fermi hole, 36
chalcogenides, 11-13	Hartree approach, 34
characteristics, 10	Hartree method, 37

Atomic potential functions ( <i>cont.</i> ) Hartree–Fock equation, 35–37	Brookfield TC-502 water bath, 331 Brunauer–Emmett–Teller (BET) adsorption
Hartree–Fock–Slater type, 35	isotherm, 129–131, 133
Herman–Skillman potentials, 38, 39	Buckminster C <sub>60</sub> fullerene, 4, 256
isolated neutral atoms, 33	Buckyballs, 9
Poisson equation, 37	zuenjemis, y
pseudopotential, 34	
scattering problems, 34	C
Schrödinger equation, 35	Capacitances
statistical exchange-correlation	ML GNR–Me interconnects, 108
potential, 37	SL GNR–Me interconnects, 108
total charge density, 35	Carbon
wave functions, 34	allotropes, 257
Wigner correlation radius, 37	different structures, 254
Auger electron spectroscopy (AES), 21	molecular derivatives, 263
Auger emission spectroscopy, 3	Carbon nanotubes (CNTs), 1, 3, 4, 20, 27, 257
ruger emission speed escopy, s	342, 350, 351, 356, 359, 362, 382
	and aerogels, 187
B	atomic and molecular hydrogen, 215
Ballistic mechanism, 82, 88	base-growth mechanism, 216–218
Ballistic conductivity, 322	endothermic process, 215
Benzene, 253, 263–265, 267	energy exchange processes, 215
Bethe lattice, 297, 298	exothermic process, 215
Bio-chemical nanosensors, 165–167	industrial production, 215
Bio-hybrid approach, 26	laser ablation, 212–214
Biological nanosensors, 79, 80	nanocomposites, 197
Biomolecular rotary machines, 177	PE-CVD advantages, 219
Biomolecules, 9, 10	plasma effect, 219
Bio-nanocomposites	tip-growth mechanism, 216, 217
biopolymers, 193	Catalysed CVD (C-CVD), 219
cellulose, 195	Cellulose nanocomposites, 195
clay, 197	Centre for Biological and Environmental
CNT, 197	Nanotechnology (CBEN), 342
drug delivery, 198	Ceramic-matrix nanocomposites (CNC), 9
electronics, sensor and energy	Cerium dioxide (CeO <sub>2</sub> ), 359, 361
applications, 198	Chabazite, 24
evolution, 193, 195	Chalcogenides, 11–13, 41, 42
functional, 197	Charged defects
gene therapy, 198	chalcogenides, 41, 42
medical applications, 198	general scheme, 44
nanofillers, 193, 196	Phillips–Thorpe constraint theory, 42
packaging, 197	photo and radiation-induced changes, 42
tissue engineering, 198	radial densities, electron charge, 43
Bio-nanosensors	spin-paired electrons, 42
experimental and theoretical calibration,	Chemical nanosensors, 79, 80, 163–165, 311
316–318, 320	Chemical vapour deposition (CVD), 4,
polymer nanoporous model, 315–320	224–245
Bir, Aronov and Pikus mechanism, 304	advantages, 215
Black carbon, 4	carbon sources, 214
Bogoliubov–Born–Green–Kirkwood–Yvon	catalyst material, 214
(BBGKY) approximation, 16	CNT growth
Bonding orbitals, 267	acetylene, 230
Bottom-up approach, 26	arc discharge, 226, 227
ar artanama, an	

base-growth model, 232	defects, 222, 223
carbon atoms, 243	growth mechanisms, 221
carbonaceous precursor, 229	Iijima method
carbon-containing gas, 229	arc discharge, 207–209
catalyst material and concentration, 233	purification, 209
catalyst metals, 230	radial breathing mode, 220
cathodes, 225	Raman vibration modes, 219, 220
characteristics, 229	CNTs-Ni case, 86-88
chiralities, 243–245	CNTs-polymer nanocomposite, 327
CNT–Fe–Pt interconnects, 235–240	CNT structure
crystal structure, Fe, 226	armchair type, 262
discharge and laser ablation	chiral type, 262
methods, 231	SW-CNT, 261
effective bonds, 241, 242	zigzag type, 261
electromagnetic properties, 224	Coherent potential approximation (CPA), 2,
ethylene, 229	52–55, 58, 60, 62, 80
Fe–Pt alloys, 240, 241	Collisional conductivity, 88, 312
Fe_Pt catalysts, 235	Convergent advantion 368
Fe–Pt nanodrops, 241, 242	Convergent education, 368
Fe–Pt nanoparticles, 225	Coronene, 254, 263, 265
iron nanoparticles, 231	Crystalline potentials
magnetic catalysts, 225	exchange-correlation correction, 41
metal nanoparticles, 228, 229, 233	liquids, 39
nanoelectronics, 224	superposition principle, 39
nanomemory device, 224	Cubic crystal lattice, 136
precursors, 233	Current perpendicular to the plane (CPP)
pressure, 234	geometry, 292
semiconductor and sensor devices, 231	CVD, see Chemical vapour deposition (CVD)
Si nanoparticles, 231	Cytotoxicity, 277, 278
SWCNTs, 232, 234	
temperatures, 229, 234	_
tip-growth model, 232	D
crystalline, 215	Decomposed fuel, 132
equipment, 214	Defected nanocarbon system, 4
MWCNTs, 214	Diamond, 4, 254, 255
Chemisorption, 121, 125, 129	Diamond lattice
Chirality, 77, 80, 81, 88, 89, 93–96, 106, 110,	cubic structure, 256
111, 310, 312, 320, 325, 330	face-oriented projection, 255
Chronic kidney disease (CKD), 361	isometric projection, 255
Classification, labelling and packaging	Diffractive elements, 42
(CLP), 350	Diluted ferromagnets, 294–297
Clausius–Chaperon equation, 123	N,N-dimethylamine benzylidene indan-
Clay nanocomposites, 197	1,3-dione (DMABI), 153–156
Clinoptilolite, 24	Drude model, 322
Cluster approach, non-regular material, 59, 60	Drug delivery, 198
CNTs and graphene, 207–212	Dyakonov-Perel mechanism, 304
arc discharge	
chemical reactivity, 210	
disadvantages, 210	E
non-aligned pentagon-heptagon pairs,	Economic human, 337
211, 212	Effective bonds model, 88–90, 96, 100,
side effects, 211	106, 110
Stone-Wales defect, 210, 211	Effective media approximation (EMA), 2,
temperature, 210	51–54, 80, 85
- · · · · · · · · · · · · · · · · · · ·	

Electrochemical nanotransducers	F
electrical signals, 182, 183	Federal Food, Drug, and Cosmetic Act
MIT, 185	(FFDCA), 350
nanoelectrodes, 183, 184	Fe-Pt alloys, 240, 241
nanoparticles, 184	Fe–Pt catalysts, 235
Electron scattering, general type potential,	Fe-Pt nanoparticle, 290-304
60–62	ferromagnetic, 305
Electronic density of states (EDOS), 80	iron catalyst nanoparticle, 287
Electronic nanosystems, 28	magnetic disorder (see Magnetic disorder)
Electronic structure	magnetic memory, 287, 288
non-regular condensed system	magnetoresistance nanodevices (see
average T-matrix approximation, 52	Magnetoresistance nanodevices)
band calculation of crystals, 53	spin transport, 287–290
calculation methods, 53, 54	Fermi electron wave, 95
CPA, 53	Fermi hole, 36
Green's functions, 51–53	Fermi–Dirac distribution function, 311
MT-approximation, 54, 55	Ferroelectric nanodevices, 176
single-site approximation, 52	FET-type devices, 322, 331
virtual crystal approximation, 52, 53	FET-type nanosensors, 311
and total energy	Field-effect transistors (FETs), 78, 149, 161,
atomic structure, 47	162, 165, 166
cohesive energy, 44	Flash memory nanodevices, 175
electron charge density, 44, 46, 47	Fluorescence, 181
electron gas, 45	Food packaging, 197
exchange-correlation potential, 46	Freundlich adsorption isotherm, 128, 129
fundamental characteristic, 44	Fullerene C <sub>60</sub> , Pentagon, 4, 258
ground states of atoms, 47	Fullerenes, 8, 9, 13, 20, 256
interstitial space, 48	
kinetic energy, 45	
local and total phase transitions, 44	G
local density approximation, 45	Gas separation, 25
MT-approximation, 48	Gaspar potential, 37
nanoclusters, 47	Gene therapy, 198, 199
one-electron equations, 45	Geometry, 310, 315, 316, 320, 325
self-consistent calculations, 44	Giant magnetoresistance (GMR), 291–293, 305
statistical approximation, 46	Gibbs adsorption isotherms, 126–131
Electronic subsystem	Gibbs dividing surface (GDS), 118
carbon, 253–262	Gibbs free energy, 126
catalysis and toxicity, 276–278	Gibbs model, 116
formation of, 263–265	Gibbs vs. Guggenheim interface, 116
graphene, 265–267	Gibbs–Duhem equation, 119
mechanical and thermal properties,	Global citizenship competence (GCC),
graphene, 279, 280	375–378
nanocarbon systems, 280–282	Glucose oxidase (GOx), 309, 315
nanotubes, 268–272	GNR–Me side-type interconnect, 91
semiconductor, 274, 275	Graphene, 256, 266
and spin-dependent properties, 272–274	fundamental properties, 279
Elliott–Yafet mechanism, 304	nanofillers, 280
Engineered nanoparticles (ENPs), 343,	Graphene–nanoflakes (GNFs), 1, 77
344, 351	Graphene–nanoribbons (GNRs), 1, 77–80,
Epoxy resins, 310, 320, 324, 325, 329	85, 111, 324
Erionite, 24	Graphene-based materials, 282
European Food Safety Authority (EFSA), 362	Graphite, 4, 254, 256
Exchange-correlation, 33, 36–39, 41, 45–47	Guggenheim model, 116

Н	K
Halogens, 42	Kohn-Sham (KS) procedure, 49
Hamilton operator, 133	Kondo temperature, 291
HAMR, see Heat-assisted magnetic recording	Korringa-Kohn-Rostoker (KKR) method, 54
(HAMR)	Kubo-Greenwood formula, 85, 296, 310, 312
Hartree approach, 34	
Hartree–Fock equation, 35–37	
Hartree–Fock–Slater (HFS) method, 35, 37, 45	L
Heat-assisted magnetic recording	Landauer-Büttiker formalism, 322
(HAMR), 186	Langmuir adsorption isotherm, 121, 129, 130
Heisenberg model, 288, 289, 294	Laser ablation method (LAM), 3, 212–214
Heulandite, 24	Laser microprobe analysis (LMA), 21
Highest occupied molecular orbital	Laumontite, 24
(HOMO), 134	Le Chatelier's principle, 125
High-resolution transmission electron	Light-emitting diodes (LED), 256
microscopy (HRTEM), 21	Light-induced actuating nanotransducers
Holography, 42	(LIAN), 181
Hopping conductivity, 310, 323, 325, 327,	Linear augmented cylindrical wave
328, 331	(LACW), 312
Humanosciences, 340, 368, 371–373, 375	Linear combination of the atomic orbital
Hydrodynamical conductivity, 322	(LCAO), 134
Hydrogen adsorption	Liposomes, 9
advantages, 132	Liquid metal model, 54–59, 86–88
CNT, 132	Local density approximation (LDA), 82
decomposition, 132	Long-range order (LRO), 14
metal hydrides, 132	Lowest unoccupied molecular orbital
metal surface, 133	(LUMO), 134
microporous, 133	
molecular hydrogen, 132	
physical storage, 132	M
solid-state materials, 132	M66 merocyanine compound, 277, 278
storage, 132	Magnetic disorder
Hydrogen spillover, 282	Bethe lattice, 297, 298
Hydrogen storage, 281	diluted ferromagnets, 294–297
Hydrolysed fuel, 132	Fe-Pt nanodrops, 294-304
Hyperfine interaction mechanism, 304	spin precession, 303, 304
	spin relaxation, 304
	spin waves, 298–301, 303
I	Magnetic force microscope (MFM), 21
Iljima method, 3	Magnetomotive nanotransducers, 185
Indan-1,3-dione pyridine betaine (IPB),	Magneto-plasmonic nanoantennas, 186
157, 158	Magnetoresistance, 4
Integral optics, 42	Matissien rule, 82
Interatomic interaction potentials and force	Mechanical nanotransducers, 182, 183
calculations	Medium-range order (MRO), 14
dynamic properties of solids, 49	Memory nanodevices
electron-ion system, 49	bistable system, 168
general rules, potential modelling, 49	characteristics, 167
Schrödinger equation, 49	ferroelectric, 176
Ion separation, 25	flash memory, 175
Ising model, 288, 289	macro-realization, 168
<b>○</b>	, = **

Memory nanodevices (cont.)	CNT-Me and GNR-Me junctions,
memristor, 175, 176	88–91, 111
molecular based, 169-172	CNT-Me interconnect resistances, 78, 96,
NEM switch, 173, 174	97, 100–111
phase change, 172, 173	CNT-Ni case, 86-88
potential energy, 168	disadvantages, microtechnology, 77
sandwich-type structure, 169	electrical resistance, 77
Schmitt trigger, 168	FET, 78, 80
spintronic, 176	inter-shell interaction, MWCNTs, 111
Memristor-type nanodevice, 175, 176	Landauer relationship, 110
Mesolite, 24	nanosensor devices, 111
Mesoporous carbon nanostructure, 281	non-regularities, 78–81
Metal aerogels, 191, 192	physical nanosensors, 80
Metal matrix nanocomposites (MNC), 9, 27	scattering processes, 80–85
Metal oxide aerogels, 189	SWCNT and SL and ML GNR simulations,
Metal particles (MP), 142	89–96
Metallic CNT, 259, 260, 268, 270, 272	Nano-CareTM fabrics, 348
Metallic nanoshell, 144	Nanochalcogenides
Method of localized MT-orbitals (LMTO), 54	atomic structure, 69
Magnetoresistance nanodevices	chalcogenides, 69, 71–74
spin valve, 290–292	cluster model, 69
spintronic device, 292, 293	structural configuration, 69
Micelles, 9	Nanochallenges, 378–389
Molecular based nanodevices, 169	Nanoclusters, 8, 9, 11, 22
Molecular electronics, 28	Nanocomposites, 2, 26, 27
Molecular imprinting technique (MIT), 185	Nanoconsumers, 5
Molecular motors, 177, 178	Nanocrystalline materials, 9
Molecular system, 133	Nanocrystaline materials, 9 Nanocrystals, 8, 9, 21
Muffin-tin approximation (MTA), 82	Nanodevices, 3, 7, 8, 10, 26, 28
Multiple scattering theory (MST), 2, 78, 83, 85 Multi-walled carbon nanotube (MWCNT),	Nanodispersions, 9
	Nanoeducation, 4, 367, 371, 378–389
165, 257, 262 MWCNT Majuration 06	Nanoelectrode techniques, 183, 184
MWCNT–Me junction, 96	Nano-electromechanical (NEM) switching
	devices, 173, 174
N	Nanoelectromechanics, 28
N Name and the O	Nanoelectronics, 28
Nanoaerogels, 9	Nanoemulsions, 9
Nanoaerosols, 10	Nano-FET-type devices, 310
Nano-bio-info-cogno-socio- and	Nanofoams, 187
humanosciences and technologies	Nanointerfaces, 10
(NBICSH), 371–377, 379	Nanomagnetics, 4
Nanocarbon clusters, 326	Nanomanagement, 4, 378–389
Nanocarbon composites resistances	Nanomechanics, 28
CNT configurations, 329	Nanomedicine, 344, 351, 375, 380
CNT inclusions, 330	Nanoobjects, 7, 8, 12, 13
GNR configurations, 329	Nanooptics, 28
Nanocarbon macromolecules, 326	Nanooptoelectronics, 28
Nanocarbon systems, 7	Nanoparticle approach, 142
Nanocarbon-based nanointerconnects	Nanoparticle techniques, 184
and metallic catalytic substrate, 77	Nanoparticles, food production chain, 349
biological nanosensors, 80	Nanophotonics, 28
chemical nanosensors, 80	NanOpinion, 362
CNT-/GNR-based FET, 79	Nanoporous materials, 2, 9, 23–25

Nanoporous metal foams, 190	human health and environment, 389
Nanopowders, 9	humanities with technosciences, 390, 391
Nanorisk, 4	in medicine, 391
Nanoscience	individual-society relationship, 390
in food industry, 346	knowledge management, 366–371
and nanotechnology, 339–343, 373, 380	nanochallenges, 378–389
Nano-selenium	nanoeducation, 383-385
electronic structure, 68–69	nanomanagement, 380-383
environment, 67, 68	and nanoscience, 339-343
health effects, 68	nanothinking, 385, 386
selenium (Se) applications, 67	NBICSH society, 371–375
Nanosensorics, 28	pTA, 387–389
Nanosensors (NS), 80	rational consumerism and consumer
classification, 151, 152	behaviour, 337–339
cubic and spherical models, 151	scientific consumption, 363-366
description, 150	unusual nanostructures, 389
micro- and nanotechnologies, 152	Nanotechnology Consumer Product
nanocrystalline and nanostructured, 152	Inventory, 344
nanoparticles, 150	Nanothinking, 4, 378–389
photons, 150	Nanotracks, 4, 309, 321
recognition mechanism, 152	Nanotransducers, 3, 182–185
sensitivity, 150	description, 178, 179
surface/volume ratio, 151	electrochemical (see Electrochemical
types, 151	nanotransducers)
Nanosensor systems, 315–324	human brain, 178, 179
bio-nanosensors (see Bio-nanosensors)	magnetic, 185, 186
carbon-based nanocomposite sensors,	mechanical, 182, 183
327–331	nanosensoring techniques, 180
CNT- and GNR-based nanocomposites,	optical, 180–182
324–328	Nanotubes, 9, 10, 12, 13, 20
ecological monitoring, 309	Nanowire transducers, 185
FET-type devices, 309	Naphthalene, 253
ion track-based glucose sensors, 331	Near-field scanning optical microscopy
nanocomposite material, 310	(NFSOM), 21
physical and chemical, 309–314	Nearly free electron approximation (NFEA), 51
polymer nanoporous structures, 309	Node problem, 295
prototypes of, 331	Non-regular materials, 147–149
physical nanosensors ( <i>see</i> Real-time	atomic and electronic structure, 147
PNC-based physical nanosensors)	CNT-based FET and GNR-based FET
tool of, 310–314	nanodevices, 149
Nanoshell, 144	electron and phonon factors, 148
Nanosilicon	general scheme of modelling, 147
applications, 63, 64	Non-regular nanosystems, 7
cluster models, 64	atomic structures, 2
EDOS curves, 64, 65	carbon-based macromolecule, 1
electronic structure, 64–66	characterization, 1
nanopowders, 62	CNTs and graphene growth, 3
plasma-chemical synthesis, 62	electronic structure, 2
Nanotechnology	graphene, fullerenes and carbon
benefits and risks of, 357–363	nanotubes, 4
consumer products, 343–357	macro-, meso-, micro- and
double-edged sword, 391	nanoapproaches, 2
exploitation of, 391	
global citizenship competence, 376–378	nanoagents, 2 nanodevices, 3
health and safety issues 390	nanoeducation and nanothinking 4

Non-regular nanosystems (cont.)	Porous 2D graphene memoranes, 282
nanomaterials, 13	Positional disorder, 20
nanophysics, 2	Pristine 2D graphene membranes, 282
nanoproducts, 5	Pseudopotential, 34, 59
nanosensor systems simulations, 4	
and regularity, 1	
spintronics and nanomemory systems, 4	Q
technological interfaces, 1	Quantitative disorder, 20
	Quantum dot aerogels, 191
	Quantum dots, 342, 343, 352
0	Quasi-crystalline approximation (QCA), 54, 55
Optical nanotransducers, 180–182	Quasi erjoumne approximation (Qerr), e i, ee
Organic aerogels, 189, 190	
Organic–nonorganic interfaces, 145	R
Organic-nonorganic interfaces, 143	Radial distribution curves of atoms (RDCA), 22
	· · · · · · · · · · · · · · · · · · ·
n	Raman microspectrometry, 219
P	Raman scattering (RS), 3
Participatory technology assessment (pTA),	Raman spectroscopy, 219
378–389	Real-time PNC-based physical nanosensors
Percolation threshold, 294, 295, 297, 298	conductivity mechanisms, 322–324
Perfect order (PO)	methods and models, 320–321
amorphous materials, 15	Registration, Evaluation, Authorization
correlation function, 15	and Restriction of Chemicals
entropy evaluation, 18	(REACH), 350
mass densities, 17	Regular nanosystems, 1, 7
over-superposition, 16	Resistances
pair correlation function, 16	ML GNR-Me interconnects, 106, 107
pair distribution function, 17	MWCNT-Me interconnects, 105
particle distribution functions, 16	SL GNR–Me interconnects, 107
temperatures, 15	Rigidity coefficient of spin waves, 299
Phase change nanodevices, 172, 173	Rigidity coefficient of spin waves, 299
Photoacoustic spectroscopy (PA), 21	S
Photoactivation applications, 181	
Photoinduced transformation, 73	Scanning electron microscopy (SEM), 21
Photonic crystals, 9, 42	Scanning probe microscopy (SPM), 21
Photoresist, 42	Scanning tunneling microscopy (STM), 21
Physical nanosensors, 79, 80, 320, 322	Schrödinger equation, 33, 35, 49, 55, 56, 62,
carbazole and fluorene derivatives,	134–136, 138
158–161	Scolecite, 24
CNTs and GNRs, 161, 163	Secondary ion mass spectrometry (SIMS), 21
DMABI, 153–156	Self-assembled monolayers on mesoporous
electromagnetic radiation, 153	supports (SAMMS <sup>™</sup> ), 356
FET, 161	Self-consistent quasi-crystalline approximation
IPB, 157, 158	(SQCA), 54
low-cost mass production, 153	Self-consistent single-site approximation
near IR radiation, 153	(SSSA), 54, 55
Physisorption, 121, 129, 131	Semiconducting metal chalcogenide
Plasma-enhanced CVD (PE-CVD), 219	aerogels, 190
Pnictogens, 42	Semiconductor CNT, 261, 270
PO, see Perfect order (PO)	Shockley states, 139
Polymer ion track-based bio-nanosensors, 167	Short-range order (SRO), 14
•	
Polymer nanocomposites (PNC), 9, 193	Side-type contact, 88, 106, 109
Polymer-matrix, 27	Silica gels, 189

Silicon dioxide (SiO2), 348, 350, 359, 360	Targeted magnetic nanoparticles, 186
Silver nanoparticles (Ag-NPs), 348, 354, 355,	Technosciences, 340, 368, 371–373, 375, 390
361, 362	Tetragens, 42
Single-cell gel electrophoresis assay (SCGE),	Thermoplastic recording, 42
359	Thorpe disorder, 20
Single wall CNT (SWCNT), 89–96,	Thorpe model
164–166, 257	amorphous solid, 20
Site problem, 295	polymer glass, 20
Spin detection, 288	Tight-binding approximation (TBA), 51
Spin injection, 288, 289, 300, 303	Tissue engineering, 198
Spin precession, 303, 304	Titanium dioxide (TiO <sub>2</sub> ), 343, 347
Spin relaxation, 290, 302–305	Top-down approach, 26
Spin transport, 287, 288, 290, 293, 300, 303	Topological disorder, 20
Spin-valve, 287, 290, 292, 293, 299–303, 305	Tunnelling magnetoresistance (TMR),
Spintronic nanodevices, 176	291–293, 305
Spintronics, 28, 290, 292, 293	
Stilbite, 24	
Stone-Thrower-Wales (STW) defects, 279	$\mathbf{U}$
Supermolecules, 9	Urbach's empirical rule, 12
Superposition approximation, 16	
Surface control of nanosurfaces, 21	
Surface nanointeractions, 7	V
Surface nanophysics, 132–133	van der Waals adsorption, 121
adsorption kinetics, 120–126	van der Waals diameter, 257
electronic structure, 133-139	van Hove singularities, 274, 275
Gibbs adsorption isotherms, 126–131	Variational principle, 37
hydrogen adsorption (see Hydrogen	
adsorption)	
light and nanoparticle, 141–144	$\mathbf{W}$
in materials science, 120	Wigner lattice, 36
nanoshells, 144, 145	Workplace exposure standards (WES), 359
organic-nonorganic interfaces, 145	
phases, 117	
plasmon resonance, 140, 141	X
processes, 116, 117, 124	Xerography, 42
silica (Si) surface, 124	X-ray phase analysis, 21
thermodynamics and anisotropy, 115-120	X-ray structural analysis, 21
Surface plasmon resonance (SPR), 3, 140, 141, 144, 181	$X\alpha$ -approximation, 37
Surface states, 137, 139	
Surface tension anisotropy, 3	Z
1 4 /	Zeolites, 23, 24
	Ziman model, 80
T	Zinc oxide (ZnO), 343
Tamm states, 138, 139	